Examining the role of Novel Thienopyridines as anti-cancer agents

Christopher Paul Broughton

Doctor of Philosophy (PhD)

2023

Examining the role of Novel Thienopyridines as anti-cancer agents

Christopher Paul Broughton

A thesis submitted in partial fulfilment of the requirements of Manchester Metropolitan University for the degree of Doctor of Philosophy

Department of Life Sciences

Manchester Metropolitan University

2023

TABLE OF CONTENTS

LIST OF ABBREVIATIONS

ABC DLBCL - Activated B-cell DLBCL

ABL1 - ABL proto-oncogene 1

ACTB – Actin Beta

ADCC - Antibody-dependent cellular cytotoxicity

AIHA - Autoimmune Haemolytic Anaemia

alloSCT - Allogeneic stem cell transplant

APC/C - Anaphase Promoting Complex/Cyclosome

ATM - Ataxia-telangiectasia-mutated

ATR - Ataxia telangiectasia and Rad3-related

Aur A – Aurora kinase A

Aur B – Aurora kinase B

B2M - Beta-2-microglobulin

Bax -Apoptosis regulator BAX

BCA - Bicinchoninic acid

BCL- 2 - B-cell lymphoma 2

BCL2i - B-cell lymphoma-2 inhibitor

BCL-XL – BCL2 extra large

BH3 – BH3 interacting-domain death agonist

Bim -Bcl-2 Interacting Mediator of cell death

BCR – B-cell receptor

BTK - Bruton's tyrosine kinase

BTKi - Bruton Tyrosine Kinase inhibitor

BR - Bendamustine and rituximab

BSH - British Society of Haematology

BUB - Budding uninhibited by benzimidazoles

Bub1 - Mitotic checkpoint serine/threonine-protein kinase BUB1

Bub3 - Mitotic checkpoint protein BUB3

BubR1 - Mitotic checkpoint serine/threonine-protein kinase BUBR1

Ca^{2+} - Calcium

CBSI - The Colchicine binding site inhibitor

CD19 – B-lymphocyte antigen CD19

CD20 - B-lymphocyte antigen CD20

CDC - Complement-dependent cytotoxicity

CDK - cyclin dependent kinases

cdc - Cell division cycle

cdc20 - Cell division cycle 20

CHK1 – Checkpoint kinase 1

CHK2 – Checkpoint kinase 2

CIRS - Cumulative Illness Rating Scale

CIT – Chemoimmunotherapy

Clb - Chlorambucil alone

CLL – Chronic Lymphocytic Leukaemia

CO –Chlorambucil with Obinutuzumab

CR - Rituximab plus chlorambucil

Ct – Cycle Threshold

DAG -Diacylglycerol

DLBCL – Diffuse large B-cell lymphoma

DLBCL ABC - Activated B-cell DLBCL

DLBCL GCB - Germinal centre B-cell DLBCL

DLBCL NOS - DLBCL, not otherwise specified

DPBS - Dulbecco's Phosphate Buffered Saline

ECACC - European Collection of Authenticated Cell Cultures

EDTA - Ethylenediaminetetraacetic Acid

EIF2B1 - Eukaryotic translation initiation factor 2B subunit alpha

Emi1 - Early mitotic inhibitor 1

ERK - Extracellular signal-regulated kinase

ER – Endoplasmic reticulum

FBS - Foetal Bovine Serum

FC –Fludarabine with chlorambucil

FCR –Fludarabine, cyclophosphamide and rituximab

FCS - Flow Cytometry Standard

FL - Follicular lymphoma

FL2-A - FL2-Area

FL2-W - FL2-Width

FLIPI - Follicular Lymphoma International Staging Index

FOXM1 - Forkhead box protein M1

FSC-H - Forward Scatter Height

GAPDH - Glyceraldehyde-3-phosphate dehydrogenase

GCs - Glucocorticoids

GCB DLBCL - Germinal centre B-cell DLBCL

GEP - Gene expression profiling

GOI - Gene of Interest

G-PEM – PEM buffer plus GTP

GR - Glucocorticoid receptor

Gsk3β - Glycogen synthase kinase-3 beta

GTP - Guanosine triphosphate

GUSB - Glucuronidase beta

HMBS - Hydroxymethylbilane synthase

HPRT1 - Hypoxanthine phosphoribosyltransferase 1

IGVH-M - IGVH mutatation.

IP_3 –Inositol trisphosphate

IWCLL - International Workshop on Chronic Lymphocytic Leukaemia

LN - Lymph nodes

Lyn – Lyn tyrosine kinase

mAB - Monoclonal antibody

Mad1 - Mitotic arrest deficient 1

Mad2 - Mitotic arrest deficient 2

MAPs - Microtubule-associated proteins

MAPKs - Mitogen-activated protein kinases

MBL - Monoclonal B-cell lymphocytosis

MCC - Mitotic Checkpoint Complex

MCL – Mantle cell lymphoma

MDAs - Microtubule destabilising agents

Mdm2 - Mouse double minute 2 homolog

MEK - Mitogen-activated protein kinase kinase

MGUS - Monoclonal gammopathy of undetermined significance

MIPI - MCL International Prognostic Index

MPF - Mitosis Promoting Factor

Mps1 - Monopolar spindle 1 kinase

MRPL19 - mitochondrial ribosomal protein L19

MSAs - Microtubule stabilising agents

MTS – 3-(4,5-dimethylthiazol-2-yl)-5-(3-carboxymethoxyphenyl)-2-(4-sulfophenyl)-2H-tetrazolium

NADPH - Reduced Nicotinamide adenine dinucleotide phosphate

NCBI - National Center for Biotechnology Information

NEKs - NIMA (Never-in-mitosis *Aspergillus*)-related kinases

NF - Normalisation factor

NF-κB - Nuclear factor kappa B

NHL – Non-Hodgkin lymphoma

NICE - National Institute for Health & Care Excellence

NIH - National Institutes for Health

NIMA - Never-in-mitosis *Aspergillus*

NK - Natural killer cells

NTC - No Template Control

OC - Obinutuzumab plus chlorambucil

PABPC4 - poly(A) binding protein cytoplasmic 4

PCM – Plasma cell myeloma

PEM - General tubulin buffer

PFS - Progression free survival

PI3K - Phosphoinositide 3-OH kinase (PI3K)

PI3Kδ - Phosphoinositide 3-OH kinase delta

PI3Ki - Phosphatidylinositol-3 kinase inhibitor

PIP_2 – Phosphatidylinositol 4,5-bisphosphate

PIP_3 - Phosphatidylinositol 3,4,5-triphosphate

PLC - Phospholipase C

PLK - Polo-like kinase

PLCγ2 - Phospholipase C gamma 2

PKC – Protein kinase C

POLR2A - RNA polymerase II subunit A

PP1 - Protein Phosphatase 1

(PP2A)-B56 - Protein Phosphatase 2

PPIA - Peptidylprolyl isomerase A

PRISMA-P - Preferred reporting items for systematic review and meta-analysis protocols

PSMC4 - Proteasome 26S subunit, ATPase 4

RAS – Ras GTPase

Raf – RAF kinase

Rb - Retinoblastoma protein

R-CHOP – Rituximab, cyclophosphamide, doxorubicin, vincristine and prednisolone

RCS - Reduced Chi Squared

RNA18SN1 - RNA, 18S ribosomal N1

ROS - Reactive oxygen species

RPL4 - Ribosomal protein L4

RPL13A - Ribosomal protein L13a

RPL19 - Ribosomal protein L19

RPLP0 - Ribosomal protein lateral stalk subunit P0

RPS17 - Ribosomal protein S17

RT-qPCR - Reverse Transcription Quantitative Polymerase Chain Reaction

SAC - Spindle Assembly Checkpoint

SD - Standard deviation

SDS - Sodium Dodecyl Sulfate

SEM - Standard error of mean

Skp2 - S-phase kinase-associated protein 2

SSC-H - Side Scatter Height

SYK - Spleen tyrosine kinase

TBP - TATA-box binding protein

TBS – Tris-buffered Saline

TBS-T - TBS-Tween

TEMED – tetramethylethylenediamine

Tm - Temperature gradient plates

UBC - Ubiquitin C

UBE2D2 - Ubiquitin conjugating enzyme E2 D2

Ven-mono - Single agent continuous venetoclax

VenO – Venetoclax with Obinutuzumab

Ven-R - Venetoclax and Rituximab

VR-CAP –Rituximab, cyclophosphamide, doxorubicin, prednisolone and bortezomib

YWHAZ - Tyrosine 3-monooxygenase/tryptophan 5-monooxygenase activation protein zeta

% CV - % coefficient of variance

%E - Percentage efficiency

ΔCt - Relative change in Ct value

ABSTRACT

Despite extensive research and significant advances, particularly over the past two decades, the treatment of mature B-cell malignancies remains a challenge. Drug resistance and disease relapse continue to occur and B-cell malignancies such as Chronic Lymphocytic Leukaemia (CLL), Follicular Lymphoma (FL) and Mantle Cell Lymphoma (MCL) largely remain incurable.

This thesis focused on the application of a group of agents known as Thienopyridines in the treatment of mature B-cell malignancies. These novel molecules were developed by virtual screening followed by chemical synthesis at the University of Auckland, New Zealand. The ten compounds tested in this thesis are classed by their chemical structure into Cyclooctanes, Cycloheptanes and Cyclohexanones. The first experimental chapter explored the overall mode of effect of these compounds on the mature B-cell cell line, DAUDI, by identifying cytostatic and cytotoxic properties of the different compounds and relating the mode of action to the chemical structures. The effect of each of these compounds on the cell cycle was also investigated. After identifying that these compounds were inducing cell cycle arrest in the G_2/M phase and inducing apoptosis, the second experimental chapter hypothesised, and demonstrated, that the G_2/M arrest could be caused by effects on Tubulin polymerisation during spindle formation. The effect of these compounds on genes and proteins involved in (1) regulation of the Mitotic Checkpoint Complex (MCC) and Spindle Assembly Checkpoint, (2) mediators of the G_2/M cell cycle checkpoint, and also (3) components of the B cell receptor signalling cascade was then specifically tested. The thesis was able to identify a group of the original ten Thienopyridines that show significant anti-neoplastic effects against the DAUDI cell line, mediated via tubulin destabilisation/stabilisation and activation of the SAC.

As an aside, prior to any work investigating the effects of these compounds on gene regulation in this cell model, it was important to establish a robust set of reference genes for data normalisation. Chapter 5 reports on a systematic review

of the literature that revealed a distinct lack of robust published data concerning reference genes in B-cell models and therefore went on to design primers for a panel of candidate reference genes and test these candidates in the experimental conditions for which they are required, thereby providing new data on a set of stable reference genes for use in RT-qPCR data normalisation. Overall, the data presented here define the Thienopyridines as a novel class of compounds that induce B-cell cytostasis or apoptosis via perturbation of microtubule polymerization and could be further developed as a new class of drug for the treatment of mature B-cell malignancies.

Keywords: B-cell malignancies; Thienopyridines; Mitosis; Cell Cycle; Spindle Assembly Checkpoint; Tubulin; DAUDI.

.

Declaration and Copyright Statements

Declaration

No portion of the work referred to in this thesis has been submitted in support of an application for another degree or qualification of this or any other university or institute of learning.

Signed……(candidate) Date…….

Statement 1

This thesis is being submitted in partial fulfilment of the requirements for the degree of PhD.

Signed……(candidate) Date…….

Statement 2

This thesis is the result of my own independent work/investigation, except where otherwise stated. Other sources are acknowledged by explicit references.

Signed……(candidate) Date…….

Statement 3

I hereby give consent for my thesis, if accepted, to be available for photocopying and for interlibrary loan, and for the title and summary to be made available to outside organisations.

Signed……(candidate) Date…….

ACKNOWLEDGEMENTS

"Many years ago the great British explorer George Mallory, who was to die on Mount Everest, was asked why did he want to climb it. He said "Because it is there."

John F. Kennedy

I have listened to that quote many, many times during this project. Mainly because it's at the start of 'The Race for Space' album by Public Service Broadcasting, which has been the soundtrack to large sections of my data collection and write up. But it sums up my sentiments quite well really. This PhD has felt like that sometimes. That I've carried on doing it 'because it is there'. One giant puzzle to chip away at, one assay and figure at a time. And with part-time study, it's taken me nearly as long as to finish it as the time it took from Yuri Gagarin being the first man sent into space to Neil Armstrong and Buzz Aldrin walking on the moon. But as I'm now writing this acknowledgment, it means I must nearly be finished and this would be an appropriate time to say thank you to everyone who has contributed, big or small to this chapter in my life.

My first acknowledgement goes to Dr Nina Dempsey, my director of studies, without whom this thesis would not have been possible. Thank you for all your wisdom, guidance, and support throughout this process and for the unending amount of patience and understanding you've shown when I turned up to meetings with data half-finished because I'd been given a load of last-minute teaching to do. Thank you for giving me this opportunity to do my own research, I hope I can repay your faith in me in the future.

My thanks also go to my other supervisors, Professor Kathryn Whitehead, particularly for the well-timed kicks to the posterior or kind words when I needed both of them, and for setting up the cell culture lab where the bulk of my data collection took place, and to Dr Ciaren Graham, who, even in the short time we shared a lab together,

impressed upon me that cell culture was a serious task, and to always leave flasks the way you found them.

I am also indebted to Professor David Barker, Dr Jóhannes Reynisson, Dr Euphemia Leung and all of the researchers at School of Chemical Sciences, University of Auckland, New Zealand who identified and synthesised of the novel compounds I have used throughout this PhD. It has been a privilege to have worked on this project and it would not have been possible without the years of prior research and development from your group.

My biggest and most wholehearted thank you goes to my partner Pippa Bulger, who has put up with me for the duration of this rollercoaster of a PhD, supported me emotionally, financially and missed out on numerous potential holidays we could have had together while I suffered on my post-graduate teaching assistant wages. Pippa also successfully studied for a Master's during lockdown and provided me with inspiration that I would eventually finish too if I applied the same level of hard work and dedication to my own studies. I owe you everything.

Thank you also goes to my parents, Margaret Broughton-Smith and Steve Smith, for telling me I can "only do my best" and that anything was achievable if you work hard for it. Apologies to them and my wider family for all the visits and occasions that I have missed because of these studies. Particular gratitude goes to my Uncle Robert Broughton and his dog Hugo, who housed myself and Pippa for 18 months when we needed help the most.

My next thanks go to my PhD brothers, Dr Lewis Mattin and Dr Tony Scimone, who were with me for almost every step of this journey until they both buggered off to do bigger and better things! Thank you for all the ill-advised weekday pints, the wild post-teaching rants and for showing me that there is life after MMU when you graduate. Also along on this journey were my lab mates Dr Mohamed El Mohtadi and Dr Niall Hickey, you are both my inspiration of what 'proper' scientists should be, and the most productive time I had was when I shared T4.08B with you both. I'm sorry it took me 18 months to come to Friday Football, it's never been the same without you.

I am also indebted to all the people I have shared office E231 with. In chronological order: to Dr Devine Akhidime, the captain of the ship and custodian of numerous PhDs to pass through E231, thank you for being a calming presence when we were often losing our heads; to Dr Louise Melling, for showing me how mad MMU was early on and the passing conversations on corridors about the latest Star Wars projects; to Dr Liam Bagley for (almost) convincing me that I'm a physiologist hiding in a molecular biologist's body; to Dr Rhiannon Parkhouse for being 'one of us' and telling me "you just have to get your thesis done Chris" at least once per week in the final stages of my PhD; to (soon to be Dr) Matteo Scorcelletti, vielen dank for finishing your thesis and giving me the push to finish mine and for making me unable to use a cafetiere without saying "soot"; to Dr Paul Hendrickse for showing me how much data you can analyse around your teaching if you're dedicated; and to (also soon to be Dr) Lauren McNeill for understanding what being a part-time postgrad teaching assistant does to a person and for always being a positive about me finishing this PhD at some point. You are all tremendous people.

Next, I need to send monumental thanks to the peerless technicians Dr Stuart Fielding and (another soon to be Dr) Glenn Ferris, who are probably the most mentioned acknowledgements in the MMU thesis repository, for a very good reason. Thank you for excellent support with lab assays and for the consistently patient responses to "can I just ask you…?" questions when I already knew the answer would be "no, you can't do that" but you still helped anyway.

My final thanks go to my friends, who I have equally neglected during completing this degree. To the Thread (Paul Hayton, Barry Ryan, Gareth Kemp, Chris Hindle, Ryan Kershaw, Dominic Kinsey, Luke Wenmouth and Adam Ashworth) and to the Parrs Wood Bells and Chai Latte Social Club (Simon Blood, Imran Dewan, Peter Atkinson, Stephen Tierney, and Michael Thomas): I wouldn't have kept my sanity during lockdown without you. Thank you for keeping me grounded and forever making me either terrified or elated to open Messenger or WhatsApp in public.

In the duration of this PhD project, I have seen the elections of three US presidents and five UK Prime Ministers, and have lived through a global pandemic and several

states of lockdown. I have been evicted, moved house three times and have bought my own home with Pippa. I have scrapped two cars and held three different teaching positions at MMU. I have seen my brother Louis get married, my brother Robert get on the property market before me, my cousin Rachel had baby Emily and I've watched my friends build families of their own. And we suffered the tragic losses of Pippa's mum Nikki and my grandparents Bob and Margaret Broughton. I want to dedicate this thesis to their memories. In particular, I doubt I would be writing this if my grandad hadn't told me that I "should do something with my brain" when all I wanted to be was a glazier like him as a child. Much of my thesis has been written at my grandparents' old kitchen table that I use as a desk, so they have been with me along the way. I hope I have made them proud.

1. INTRODUCTION

1 INTRODUCTION

1.1 Mature B-cell Malignancies

The category of mature B-cell malignancies is an umbrella term for a diverse group of B-cell neoplasms, which ranges from precursor conditions such as monoclonal B-cell lymphocytosis (MBL) and monoclonal gammopathy of undetermined significance (MGUS) to more overtly malignant conditions such as chronic lymphocytic leukaemia (CLL), diffuse large B-cell lymphoma (DLBCL), mantle cell lymphoma (MCL) and plasma cell myeloma (PCM) (Swerdlow et al., 2016).

They are categorised as mature B-cell malignancies due to the morphologic stage of development of the B-cell lymphocytes from which they have arisen, that is cells that have progressed from haematopoietic stem cells, through the stages of pro-B cells, pre-B cells and immature B cells in the bone marrow to lymphocyte release into the peripheral blood (Burger and Wiestner, 2018). Further development of B-cells takes place in the extramedullary organs of the lymph nodes (LN), particularly in the germinal centres of LN, and spleen, and the location of maturation informs what type of neoplasm develops (Swerdlow et al., 2016; Burger and Wiestner, 2018).

The B-cell receptor (BCR) is essential to B-cell maturation, the role of the B-cell in immunological response to foreign antigens and also its interaction with the microenvironment of lymphatic tissues that is necessary for B-cell survival (Burger and Chiorazzi, 2013; Burger and Wiestner, 2018). The BCR is a transmembrane receptor, comprising an extracellular ligand binding moiety coupled to a signal transducer complex (CD79a and CD79b) (Burger and Chiorazzi, 2013). Activation of the BCR via antigen binding triggers a signalling kinase cascade involving Src family kinases (Lyn, Fyn and Blk) that in turn activate spleen tyrosine kinase (SYK), Bruton's tyrosine kinase (BTK) and phosphoinositide 3-OH kinase (PI3K) and trigger numerous downstream signalling pathways including phospholipase C gamma 2 (PLCγ2), mitogen-activated protein kinases (MAPKs), RAS activation, AKT signalling and NF-κB signalling (Burger and Chiorazzi, 2013; Burger and Wiestner, 2018) see Figure 1-1. BCR signalling exists in two forms, tonic signalling, that is signalling in the absence of an antigen derived signal (also referred to as background signalling), and signalling in

response to the BCR antigen stimulation (Burger and Wiestner, 2018). Many of these pathways contribute to B-cell proliferation and survival, and as such mutations affecting the BCR can lead to malignancies including CLL, DLBCL, MCL and follicular lymphoma (FL) (Burger and Chiorazzi, 2013; Burger and Wiestner, 2018). It is vital that the events involved in BCR signalling are fully elucidated in order to continue to identify targets for therapy across a wide range of mature B-cell malignancies.

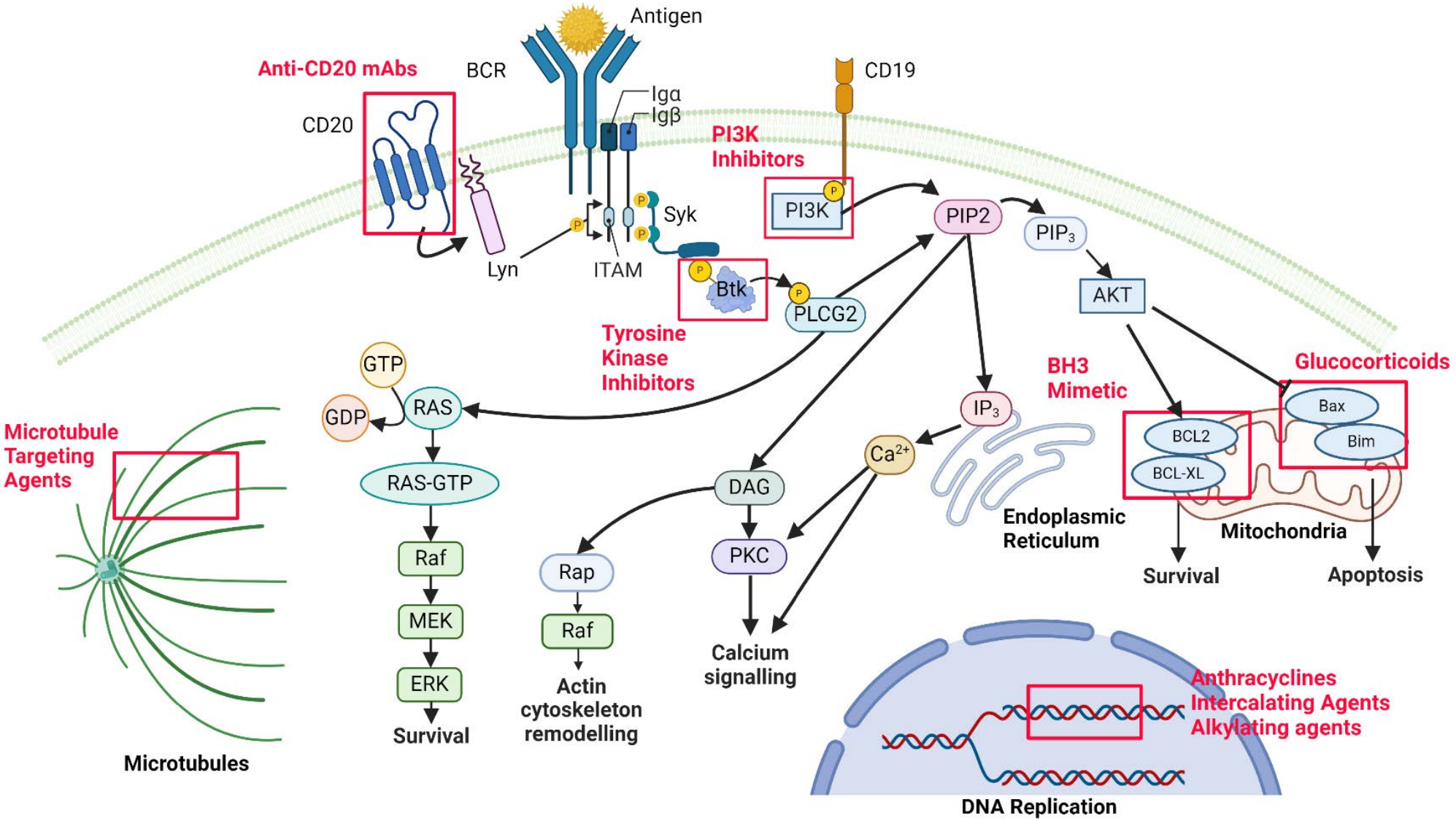
Antigen
Anti-CD20 mAbs
BCR
CD20
Igα
Igβ
CD19
PI3K Inhibitors
PI3K
PIP2
PIP3
Syk
Lyn
ITAM
Btk
PLCG2
AKT
Tyrosine Kinase Inhibitors
GTP
GDP
RAS
RAS-GTP
Raf
MEK
ERK
Survival
Microtubule Targeting Agents
Microtubules
Rap
Raf
Actin cytoskeleton remodelling
DAG
PKC
IP3
Ca2+
Calcium signalling
BH3 Mimetic
Endoplasmic Reticulum
BCL2
BCL-XL
Bax
Bim
Mitochondria
Survival
Apoptosis
Glucocorticoids
Anthracyclines
Intercalating Agents
Alkylating agents
DNA Replication

Figure 1-1: B-Cell Receptor Signalling and existing drug targets in B cell malignancies. Cell surface receptors and their associated intracellular signalling pathways allow for numerous routes for treatment of B cell leukaemias and lymphomas. Key pathways activated as a result of antigen binding include the Ras-MAPK pathway which results in cell survival, Rap-Raf signalling which is associated with actin cytoskeleton remodelling, PI3K-Akt signalling which offers further anti-apoptotic resistance and the Btk-PLCG2-Protein Kinase C pathway of calcium signalling.

Traditional chemotherapeutics targeted DNA replication and microtubules often with global side effects in the patient. More targeted treatments specific for cell surface markers or signalling pathways specific for the cell of origin with anti-CD20 monoclonal antibodies, tyrosine kinase inhibitors, PI3K and BH3 mimetic drugs. Created with BioRender.com and based on information in (Routledge and Bloor, 2016; Burger and Wiestner, 2018; Dunleavy et al., 2018).

Bax -Apoptosis regulator BAX, BCL-XL – BCL2 extra large, BCL2 - B-cell lymphoma 2, BCR – B cell receptor, BH3 – BH3 interacting-domain death agonist, Bim -Bcl-2 Interacting Mediator of cell death, Btk – Bruton's kinase, Ca^{2+} - Calcium, CD19 – B-lymphocyte antigen CD19, CD20 - B-lymphocyte antigen CD20, DAG -Diacylglycerol, ERK - extracellular signal-regulated kinases, IP_3 –Inositol trisphosphate -Lyn – Lyn tyrosine kinase, MEK - Mitogen-activated protein kinase kinase, PKC – protein kinase C, PIP_2 – Phosphatidylinositol 4,5-bisphosphate, PIP_3 - Phosphatidylinositol 3,4,5-triphosphate, RAS – Ras GTPase, Raf – RAF kinase, Syk- Spleen tyrosine kinase.

1.2 Diffuse Large B-cell Lymphoma

Classed as a mature B-cell malignancy, DLBCL is the most common form of non-Hodgkin lymphoma (NHL), with an incidence of 3.8/100000/year in Europe and accounts for more than 30 % of all cases of NHL (Tilly et al., 2015; Chaganti et al., 2016). It has been subdivided into two distinct subtypes via gene expression profiling (GEP) which identified the cell of origin that the malignancy has developed from; either germinal centre B-cells DLBCL (DLBCL GCB), activated B-cell DLBCL (DLBCL ABC) as well as those where the cell of origin cannot be determined classified as DLBCL, not otherwise specified (DLBCL NOS) (Tilly et al., 2015; Chaganti et al., 2016; Swerdlow et al., 2016). Each categorisation of DLBCL has an impact on the prognostic factors for the disease, with DLBCL ABC having a worse prognosis compared to DLBCL GCB, with 40 % compared to 75 % progression free survival (PFS) at 3 years (Chaganti et al., 2016). Other poor prognostic markers include gene rearrangements affecting *MYC, BCL2* and *BCL6*, which lead to a median survival of < 12 months (Chaganti et al., 2016). Treatment for DLBCL is stratified by Ann Arbor stage at presentation (Carbone et al., 1971; Lister et al., 1989) and international prognostic index score (Project, 1993), with factors including age at presentation, fitness for treatment (number of comorbidities), baseline LDH levels and the number of involved lymph nodes/extramedullary lymphatic organs taken into consideration (Tilly et al., 2015). All treatment regimens include a version of the R-CHOP treatment regime (rituximab, cyclophosphamide, doxorubicin, vincristine and prednisolone) irrespective of staging, with modifications made to the number of cycles and the intensity of the treatment dose given (Chaganti et al., 2016). However, with relapse rates at 20-30 % post R-CHOP treatment, 10-15 % of patients being refractory to first line treatment and a survival rate of 10 % at 1-3 years for refractory patients following salvage therapy (Chaganti et al., 2016), there is a requirement for the development of alternative treatments for this disease.

1.3 Follicular Lymphoma

Another mature B-cell malignancy, Follicular lymphoma is the most common low-grade lymphoma is the United Kingdom and the second most common nodal lymphoid malignancy in Western Europe, with an incidence of 5/100000/year and a median age of onset between 60 and 65 years (McNamara et al., 2012; Dreyling et al., 2016). In line with DCLBL, FL is also staged using the Ann Arbor system (Carbone et al., 1971; Lister et al., 1989) while its prognosis is predicted using the Follicular Lymphoma International Staging Index (FLIPI) (Solal-Céligny et al., 2004). FL is a chronic, relapsing disorder, which is considered incurable, despite improvements in treatment leading to overall response rates of 85 % and overall survival at 10 years being 73 % (McNamara et al., 2012; Sorigue and Sancho, 2018). FL is characterised by the presence of translocation between chromosome 14 and 18, leading to gene rearrangement and the overexpression of BCL2 protein, which provides anti-apoptotic protection to FL B-cells, although t(14;18) is not exclusively required for the development of FL (Sorigue and Sancho, 2018). Treatment for FL ranges from 'watch and wait' strategies to rituximab based regimes, with more intensive chemo- and immunotherapy reserved for high risk disease patients (Dreyling et al., 2016). However, around 15-20 % of patients show a poorer response to treatment or show progression following treatment within 2 years, meaning further treatment options are required for FL (Dreyling et al., 2016).

1.4 Mantle Cell Lymphoma

Mantle cell lymphoma (MCL) is a relatively rare type of non-Hodgkin lymphoma, with an incidence rate of 3-10 % (of total NHL cases) in the UK, and 5-7 % (of total malignant lymphoma cases) in Western Europe (1-2/100000/year), with a median age of onset of 60-65 years and a higher rate of presentation in males compared to females (3:1) (McKay et al., 2012; Dreyling et al., 2017). Despite advances in treatment options, MCL is still classed as an incurable neoplasm, with median survival of 4-5 years, and an overall survival of up to 12 years (McKay et al., 2012). MCL presents as a mixture of high and low grade NHLs, showing features of relapsing

disease combined with an aggressive phenotype of development (McKay et al., 2012). It is classified by the cytogenetic marker translocation between chromosomes 11 and 14 leading to an overexpression of the cell cycle regulator protein, cyclin D1, which plays an important role in regulating the transition from G1 to S phase during mitosis, however MCL can present with the absence of t(11;14) (McKay et al., 2012; Dreyling et al., 2017). MCL is staged using the modified Ann Arbor scale (Lugano Classification) (Cheson et al., 2014) with prognosis predicted using the MCL International Prognostic Index (MIPI) (Hoster et al., 2008) with treatment stratified by age, fitness and tumour burden (Dreyling et al., 2017). In common with other variants of NHL, treatment regimens heavily feature the anti-CD20 antibody rituximab, in combination with chemotherapy treatments including R-CHOP, BR (bendamustine and rituximab), VR-CAP (rituximab, cyclophosphamide, doxorubicin, prednisolone and bortezomib), with younger fitter patients also offered cytarabine at induction (Dreyling et al., 2017). Early phase clinical trials focus on targeting the B-cell receptor pathway, such as ibrutinib, in a relapsed MCL setting and there is potential for other novel compounds which target the BCR in the treatment of MCL in the future (Dreyling et al., 2017).

1.5 Chronic Lymphocytic Leukaemia

Chronic Lymphocytic Leukaemia is the most common leukaemia, with an incidence of 4.2:100000/year in the Western World. The median age at diagnosis is 72 years and the disease remains largely incurable (Eichhorst et al., 2015). It is arguably one of the most difficult mature B-cell neoplasms to manage, given the heterogeneity in terms of the patient population and in terms of disease progression. It is characterised by the presence of greater than 5000/µl peripheral blood monoclonal, mature-appearing B lymphocytes which co-express the cell surface antigen CD5 and B-cell surface antigens CD19, CD20 and CD23 (Eichhorst et al., 2015). In some patients, the disease remains indolent for many years, and patients at this stage will not benefit from treatment. The approach in such cases is to continue to monitor the patient (the so-called “watch & wait approach”) for changes in disease status and to refrain from chemotherapeutic intervention. However, some patients progress very

quickly, suffering a wide range of symptoms synonymous with bone marrow infiltration, ineffective production of other cell lineages (consequent anaemia and thrombocytopenia) and circulating lymphocytes that are unable to fight infection. In these patients, treatment is necessary, yet the best course of treatment remains to be fully determined.

There is a large body of literature, dating back to the early 2000s, focussing on the identification of prognostic markers that can help better stratify patients for effective treatment and management. Presence of cytogenetic abnormalities have long been shown to provide useful prognostic information (Juliusson and Gahrton, 1993), while the presence or absence of specific gene mutations are also of paramount importance (Hallek et al., 2018). In patients with later stage CLL a decision must be made on whether to treat and what to treat with and consideration of prognostic factors is critical. In 2008, the International Workshop on Chronic Lymphocytic Leukaemia (IWCLL) published (updated) recommendations for the management of CLL in clinical trials and general practice (Hallek et al., 2008), taking into account the age, fitness (co-morbidities), presence of important cytogenetic abnormalities (del(17p), del(11q), trisomy 12), presence of specific gene mutations (*TP53* mutation, IGVH mutation) and Binet/Rai staging (presence of palpable lymph nodes and/or enlarged liver and spleen; results of full blood count – lymphocyte count, haemoglobin levels, thrombocyte count) (Eichhorst et al., 2015).

In 2014, the German CLL Cooperative Group proposed a simplified classification of fitness status which defined patients as 'go-go' (i.e., fit), 'slow-go' (i.e., unfit) and 'no-go' (i.e., frail) (Table 1.1). This assessment was based on three criteria; (1) the physical condition (fitness and co-morbidity) of the patient, which is independent of calendar age, (2) the individual prognostic risk, as determined by genetic and other prognostic factors (e.g., del(17p), del(11q), trisomy 12, *TP53* mutation, IGVH mutation), and (3) the Rai or Binet stage of the disease. Patients with symptomatic disease who possess del(17p) or *TP53* mutations were managed as a distinct subgroup of patients due to defective cell-death pathways and hence drug-resistance. Low risk patients (Binet stage A/Rai stage 0) typically have a median survival following treatment of greater

than 10 years, while intermediate risk (Binet stage B/Rai stage I/II) have median survival of 8 years and high risk (Binet stage C/Rai stage III/IV) have reduced median survival of 6.5 years (Eichhorst et al., 2015). The presence of unfavourable cytogenetic markers (del(17p) or *TP53* mutation) is synonymous with poorer prognosis with median survival of 2-5 years. (Eichhorst et al., 2015).

Table 1-1: A historical rational approach to treating CLL patients (Ghia and Hallek, 2014).

Rational approach	Disease stage	Patient fitness
go go	Rai stage III-IV or Binet stage C	Young patients, adequate fitness. Normal creatinine clearance and a low score on the Cumulative Illness Rating Scale (CIRS)
slow go	Rai stage III-IV or Binet stage C	Old patients, inadequate fitness with a relevant co-morbidity
no go	Rai stage III-IV or Binet stage C	Unfit, Frail

Combination therapies have been the main treatment approach in CLL, with fludarabine-cyclophosphamide-rituximab (FCR), the frontline treatment for 'fit' patients (Fischer et al., 2016) . However, relapse rates are high and second- and even third-line treatments are often required. More recently, the British Society of Haematology (BSH) published updated guidelines for the treatment of CLL (Walewska et al., 2022). This has been largely in response to a surge in the availability of target pathway inhibitors, which have been demonstrated to provide effective therapy for older patients for whom palliative treatment was previously the only option. According to these BSH 2022 guidelines, the decision to treat a patient still requires consideration of several factors, including patient-related factors such as age, presence of other comorbidities, concomitant medication as well as disease-related factors such as speed of progression and presence of prognostic markers. A patient's response to previous therapies, both in terms of tolerability and disease resistance must also be considered.

As research has progressed, the importance of *TP53* gene mutation status and IVGH mutation status has continued to be extensively evidenced, and both are considered in the most up-to-date treatment decision models. Indeed, screening for *TP53* disruption (i.e. del 17p13.1 and/or *TP53* mutation) prior to each line of treatment is recommended in the current guidelines, since these patients are

considered a high-risk group, refractory to most chemoimmunotherapy (CIT) regimes and with a much shorter overall survival (Y.-C. Liu et al., 2020). IGHV gene mutation analysis is also important for prognostication and is recommended to be performed at diagnosis. IGHV-M identifies a subgroup of patients with good prognosis and are likely to be functionally cured with more basic (and less costly) CIT regimes such as FCR, for fit, younger patients, or the BCL-2 inhibitor venetoclax combined with the anti-CD20 monoclonal antibody, obinutuzumab (collectively termed VenO), for older patients.

Given that CLL is most often a disease of the elderly, the majority of patients fall into a category of 'less fit', with almost 90% presenting with comorbidities. Prior to the approval of targeted agents, the alkylating agent chlorambucil in combination with the anti-CD20 monoclonal antibody, obinutuzumab (collectively known as CO therapy) was used as an international standard of care for this patient cohort (Goede et al., 2013). However, several randomised clinical trials in 'unfit' patients have since shown improved prognosis following the use of targeted inhibitors (either inhibitors of BTK (e.g., acalabrutinib) or inhibitors of BCL2 (e.g., ventoclax)) in combination with obinutuzumab, compared to CO (Moreno et al., 2019; Al-Sawaf et al., 2020; Sharman et al., 2020). The current (BSH 2022) approaches to treatment of CLL are shown in Figure 1-2 and evidence the wide treatment options available for this notoriously resistant disease.

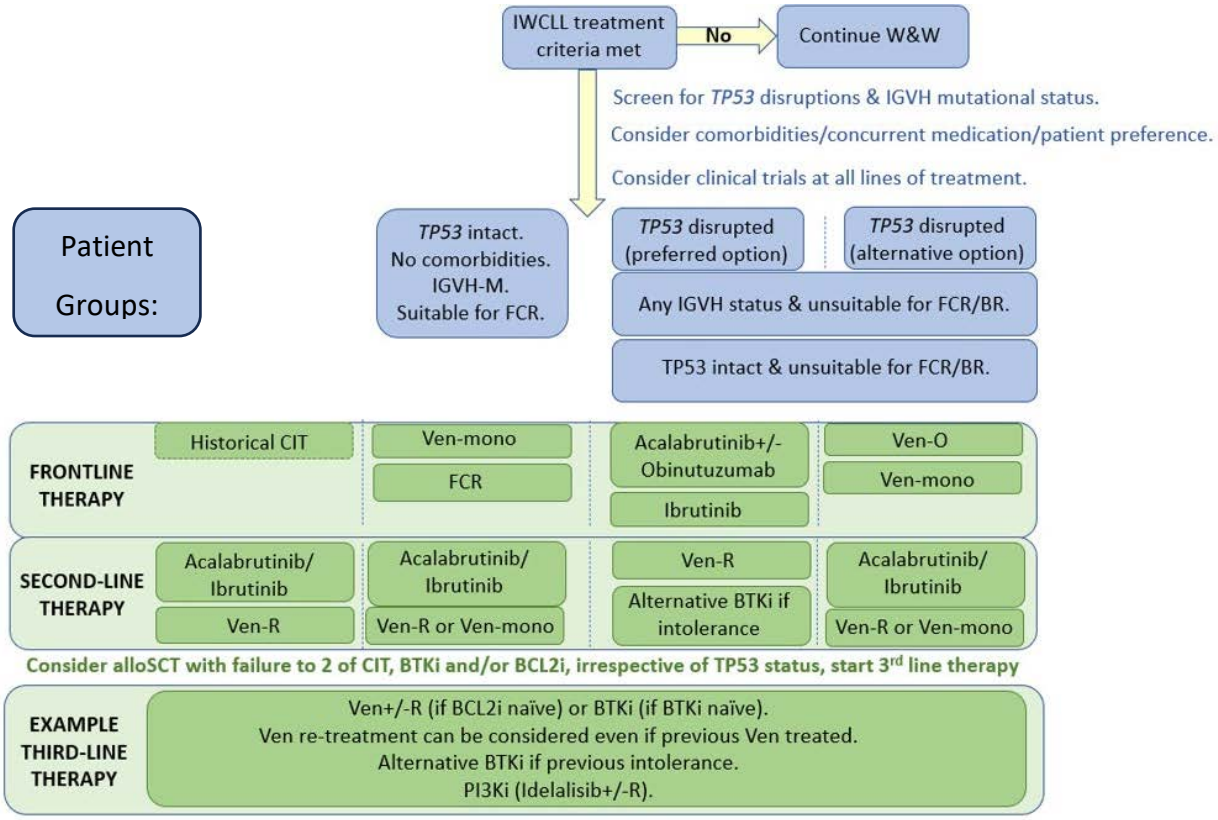

Figure 1-2: The BSH (2022) treatment decision tool (adapted from Walewska et al. 2022)

The flowchart summarises the treatment strategy for newly diagnosed CLL patients. Following diagnosis, if a patient has asymptomatic early-stage disease (Binet stage A/Rai stage 0) can be monitored without therapy (Watch and wait) until their disease progresses (blue boxes). Upon progression to intermediate-risk (Rai stages I and II) and high-risk (Rai stages III and IV) disease (or if a patient presents at this stage), treatment is recommended and is stratified by patient fitness (see Table 1-1), TP53 and IVGH mutation status and co morbidities (green boxes). Frontline treatment historically consisted of Chemoimmunotherapy using FCR for younger fitter patient, however, newer targeted treatment options (BTKi, BCL2i, PI3Ki) alone or in combination with anti-CD20 monoclonal antibodies offer chemotherapy free options, with recommended treatments listed in the columns under each patient group. For Second-Line and Third-Line treatments (following disease resistance or progression), patients can be switched to an alternative targeted therapy, or be re-treated the venetoclax. Allogeneic stem cell transplant (alloSCT) is considered for patients with high-risk disease following failure of two previous lines of CIT or BTKi/BCL2i therapy who are fit for transplant. Access to newer treatments, particularly for those patients with relapsed disease is gained through enrolment on clinical trials.

IWCLL – International Workshop on CLL. W&W – Watch and wait. IGVH-M = IGVH mutatation. FCR = fludarabine, cyclophosphamide & rituximab. BR = bendamustine and rituximab. CIT = Chemoimmunotherapy. Ven-mono = Single agent continuous venetoclax. Ven-O = Venetoclax and Obinotuzumab, 12 months. Ven-R = venetoclax and rituximab, 24 months. BTKi = Bruton Tyrosine Kinase inhibitor. alloSCT = allogeneic stem cell transplant. BCL2i = B-cell lymphoma-2 inhibitor. PI3Ki = Phosphatidylinositol-3 kinase inhibitor.

1.6 Cell Cycle Checkpoints as treatment targets

The molecular control of cell division via the cell cycle (see Figure 1-3) is often dysregulated in cancer, including in B cell malignancies, where DNA mutations or chromosomal alterations can allow cells to rapidly proliferate or bypass the cell cycle checkpoints which maintain ordered cell division cycles that are linked to mitogen stimulation or adaptive immune responses (Malumbres and Barbacid, 2009; Hallek and Al-Sawaf, 2021).

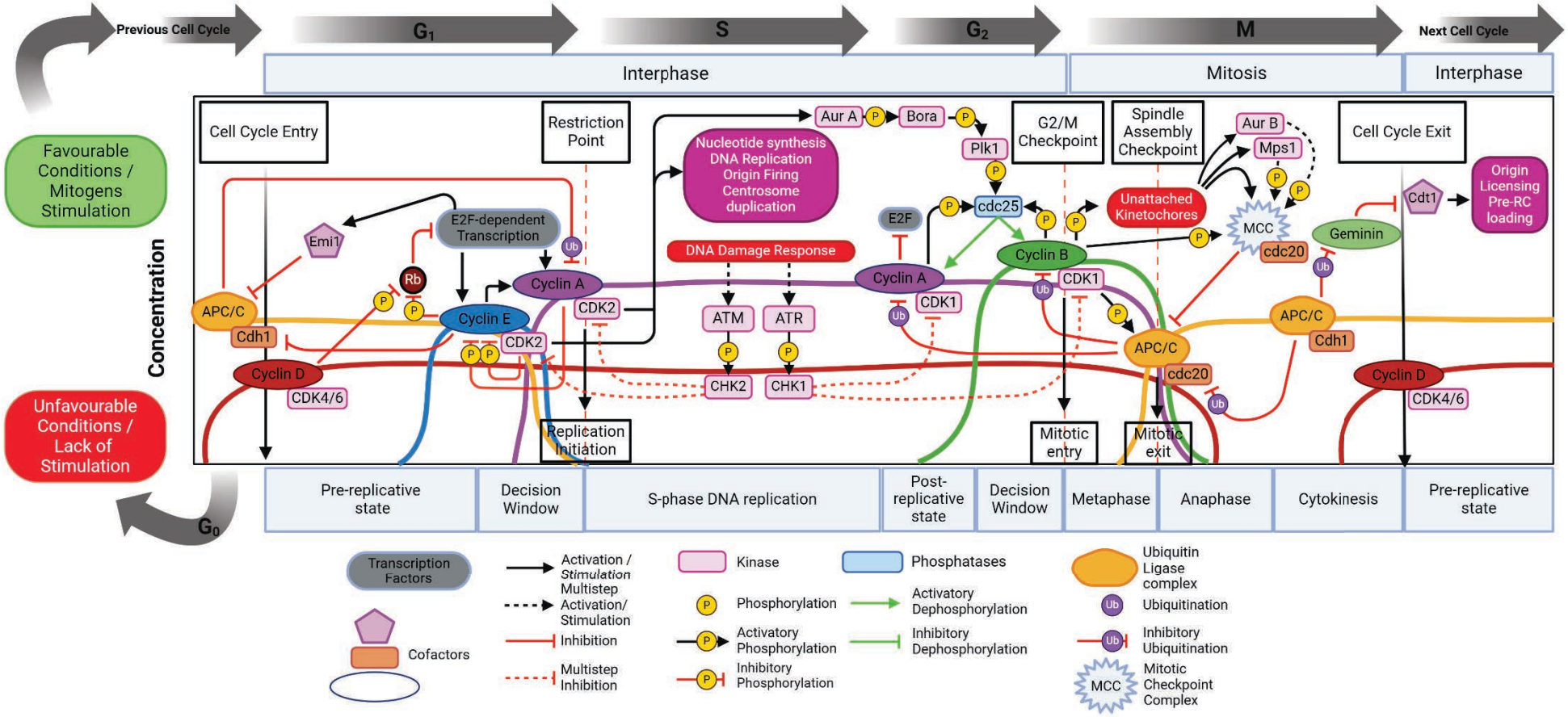
Previous Cell Cycle
G1
S
G2
M
Next Cell Cycle
Interphase
Mitosis
Interphase
Favourable Conditions / Mitogens Stimulation
Unfavourable Conditions / Lack of Stimulation
Concentration
G0
Cell Cycle Entry
Restriction Point
Nucleotide synthesis DNA Replication Origin Firing Centrosome duplication
Aur A
Bora
Plk1
G2/M Checkpoint
Spindle Assembly Checkpoint
Aur B
Mps1
Cell Cycle Exit
Origin Licensing Pre-RC loading
Cdt1
Geminin
Unattached Kinetochores
MCC
cdc20
Emi1
E2F-dependent Transcription
Rb
APC/C
Cdh1
Cyclin D
CDK4/6
Cyclin E
CDK2
Cyclin A
DNA Damage Response
ATM
ATR
CHK2
CHK1
E2F
cdc25
Cyclin B
CDK1
Replication Initiation
Mitotic entry
Mitotic exit
Pre-replicative state
Decision Window
S-phase DNA replication
Post-replicative state
Decision Window
Metaphase
Anaphase
Cytokinesis
Pre-replicative state
Transcription Factors
Cofactors
Activation / Stimulation
Multistep Activation/ Stimulation
Inhibition
Multistep Inhibition
Kinase
Phosphorylation
Activatory Phosphorylation
Inhibitory Phosphorylation
Phosphatases
Activatory Dephosphorylation
Inhibitory Dephosphorylation
Ubiquitin Ligase complex
Ubiquitination
Inhibitory Ubiquitination
Mitotic Checkpoint Complex

Figure 1-3 The regulation of cyclin dependent kinase activation via cyclins, cell cycle checkpoints and ubiquitination. Fluctuating levels of cyclins and activation of CDKs regulate ordered cell division cycles in mammalian cells. Preparation for re-entry into the cell cycle begins at the end of the previous cell division where APC/C_{Cdh1} ubiquitinated Geminin, which allows Cdt1 to bind to pre-replication (Pre-RC) complexes ready for activation during origin firing to ensure the once only duplication of DNA during S-phase.

*Mitogen stimulation leads to transcription and accumulation of Cyclin D, its activation of CDK4/6 and phosphorylation inhibition of retinoblastoma protein (Rb) which partially frees the E2F-dependent family of transcription factors allowing for the transcription of Cyclin E genes and activation of CDK2. CDK2-Cyclin E further phosphorylates Rb, allowing for the accumulation of Cyclin A and further CDK2 upregulation. In the absence of mitogen stimulation or in unfavourable cell conditions, cells can exit the cell cycle into G_0 phase, which can pause cell division until condition become favourable or induce senescence. APC/C_{Cdh1} targets Cyclin A and Cyclin B for destruction via ubiquitination from metaphase in the previous cell cycle and this inhibition of Cyclin A is present during G_1 phase until APC/C_{Cdh1} is itself inhibited by the production of Emi1 by E2F related transcription. This step allows the rapid accumulation of Cyclin A and in a positive feedback loop decouples the cell from mitogen stimulation and progresses through the first cell cycle checkpoint, the **Restriction Point**. CDK2-Cyclin A also phosphorylates Cyclin E (with CDK2-Cyclin E also undergoing autophosphorylation) leading to its destruction via SCF mediated Ubiquitin ligation. Inhibition of APC/C_{Cdh1} also allows Geminin levels to rise and bind to free Cdt1 and therefore ensure that origin licensing only occurs once per cell cycle.*

CDK2-Cyclin A then phosphorylates hundreds of targets, becoming the dominant CDK during S-phase and triggering nucleotide synthesis, origin firing and ordered DNA and organelle duplication. During late S-phase and following the E2F-driven accumulation of CDK1, Cyclin A switches its CDK partner and then drives the cell through G_2 and the start of M-phase where it inhibits E2F transcription in another positive feedback mechanism. Activation of CDK1 is promoted by the upstream activation of Aurora A (Aur A), Bora and Plk1, which in turn activates the phosphatase cdc25 which removed inhibitory phosphorylation of CDK1 by Wee1 and Myt1.

*The fidelity of DNA is protected through G_1, S, and G_2 phases by the **DNA Damage Response** cell cycle checkpoint, which responds to DNA double and single strand breaks and stalled origin forks via the activation of ATM/ATR kinases, to halt cell cycle progression until the underlying damage has been corrected, or to trigger apoptosis in the event of catastrophic DNA damage. ATM activate the CHK2 kinase to inhibit the activity CDK2 while ATR activates CHK1 kinase (in turn activating Wee1 and Myt1) to inhibit CDK1.*

*CDK1-Cyclin A primes the cell for mitosis, but it is CDK1 partnered with Cyclin B (the mitosis promoting factor) which phosphorylates thousands of targets to prepare the cell for mitosis (including nuclear envelop breakdown, spindle assembly and chromosome alignment) until metaphase of mitosis prior to chromosome separation. At the metaphase to anaphase transition, the **Spindle Assembly Checkpoint** commits the cell to mitosis only when chromosomes are correctly aligned and attached to microtubules originating at the spindle poles. In the absence of fully attached chromosome kinetochores, CDK1-Cyclin B together with Aurora B kinase (Aur B) and Mps1 (monopolar spindle 1 kinase) promote the formation of the Mitotic Checkpoint Complex (MCC) which sequesters the APC/C cofactor cdc20 (cell division cycle 20), preventing the formation of APC/C_{cdc20} and the separation of sister chromosomes at anaphase until all chromosome pairs are attached to the spindle poles. On attachment at the kinetochores, the MCC is disassembled, allowing APC/C_{cdc20} to ubiquitinate securin, freeing the enzyme separase to cleave the cohesion complexes which secure the sister chromatids at the kinetochores and allowing their separation. APC/C_{cdc20} also ubiquitinates both Cyclin B and Cyclin A to ensure mitotic signals are extinguished and the phosphatase families PP1 (protein phosphatase 1) and PP2A (protein phosphatase 2A) dephosphorylate targets of CDK1 to prevent unscheduled re-entry to mitosis (not shown). APC/C subsequently binds to its cofactor Cdh1 (cdc20 homolog 1), targets cdc20 for destruction and ensures the continued proteosome degradation of Cyclin A and B until the cell commits to a new cell division cycle.*

Created with BioRender.com and based on information in (Deshpande et al., 2005; Kops et al., 2005; Musacchio and Salmon, 2007; Malumbres and Barbacid, 2009; Reinhardt and Yaffe, 2009; Johnson and Skotheim, 2013; Fragkos et al., 2015; Musacchio, 2015; Techer et al., 2017; Crncec and Hochegger, 2019; Hayward et al., 2019; Holder et al., 2019; Lara-Gonzalez et al., 2019; Rubin et al., 2020; Neizer-Ashun and Bhattacharya, 2021; Greil et al., 2022; Matthews et al., 2022; Milletti et al., 2023).

1.6.1 Cell cycle control

In non-cancerous, non-senescent cells, the decision to undergo cell division is normally stimulated by external mitogenic signalling or conditions in the microenvironment that support proliferation and is regulated by cyclin dependent kinases (CDKs) and their interaction between their cofactors, the cyclins (Malumbres and Barbacid, 2007; 2009; Malumbres, 2014; Martinez-Alonso and Malumbres, 2020). Both interphase (containing the cell cycle Gap (G_1 and G_2) and synthesis (S) phases) and mitosis (M phase) are regulated by the phosphorylation events driven by specific CDKs that are activated by cyclin partners (Martinez-Alonso and Malumbres, 2020). As their name suggests, cyclins have a tightly regulated, cyclical pattern of gene transcription and protein destruction via ubiquitination (see Figure 1-3), which ensures that the key processes of DNA replication and chromosome separation occur in a controlled manner and without errors that could have potentially fatal consequences for the cell (Matthews et al., 2022).

1.6.1.1 Cell cycle initiation

A cell's decision to redivide is intrinsically linked to both the external conditions of the cell microenvironment and key regulators of G_1 phase that ensure there is a gap between the end of mitosis and the start of a new cell division cycle. Following the previous cell mitosis and cytokinesis (from the anaphase to metaphase transition onwards), the activity of the mitotic cyclin dependent kinase, CDK1, is silenced via proteosome degradation of cyclins A and B by the ubiquitin E3 ligase APC/C (Anaphase-promoting complex/Cyclosome) in complex with its cofactor Cdh1 (cdc20 homolog 1) (see Figure 1-3), which ensures that the cell cannot re-enter mitosis and prevents unscheduled proliferation until DNA and cell organelles have been duplicated (Kernan et al., 2018; Rubin et al., 2020; Matthews et al., 2022). APC/C-Cdh1 also primes the cell for DNA duplication via degradation of Geminin, which frees the DNA replication factor Cdt1 (Cdc10-dependent transcript 1) to prime replication origins (origin licensing) which become activated during S-phase (Fragkos et al., 2015).

1.6.1.2 Mitogen stimulation, transcription of Cyclins D, E and A in G_1 phase and the Restriction Point cell cycle checkpoint

As shown in Figure 1-4, the external stimulation of a cell via the Mitogen-activated protein kinase pathway (MAPK) via RAS-Raf-MEK-ERK leads to accumulation of Cyclin D and activation of CDK4/6 to trigger the first stages of a new cell cycle (Martinez-Alonso and Malumbres, 2020), with each subsequent stage forming a positive feedback loop which promotes accumulation of both Cyclin E and Cyclin A. Both of these cyclins are essential to the cell passing through the restriction point and proceeding to DNA duplication in S-phase, and their activation of CDK2 ensure inhibition of their own inhibitors via phosphorylation of p21 and p27 (Rubin et al., 2020; Matthews et al., 2022). Commitment to the cell cycle relies on a series of sequential inhibitory phosphorylation events to the pocket protein Rb (retinoblastoma protein) which repress the E2F transcription factor family via directly coupling, with E2F not just promoting the transcription of Cyclin E and A, but also CDK1 which drives the cell through G_2 and mitosis (Rubin et al., 2020). Several models are proposed for how Rb phosphorylation is achieved, with consensus that initial phosphorylation by CDK4/6-Cyclin D releases E2F to transcribe Cyclin E and its complex with CDK2 leads to further Rb phosphorylation until Cyclin A production is initiated (Deshpande et al., 2005; Pennycook and Barr, 2020; Rubin et al., 2020; Milletti et al., 2023). The activity of CDK2 in complex with Cyclin E and A can be downregulated by the Cyclin Dependent Kinase inhibitors (CIP/KIP family) proteins p21 and p27, with p21 upregulated by the DNA Damage Response cell cycle checkpoint downstream of p53, providing a link between G_1 and later cell cycle phases (Deshpande et al., 2005; Johnson and Skotheim, 2013). However, as Cyclin E and A accumulate, the activity of CDK2 promotes the phosphorylation of P21 and p27, providing a positive feedback mechanism that promotes progression through the restriction point and commitment to S-phase and DNA replication, with both E2F and FOXM1 transcription factors upregulating the production of essential proteins required for the rest of the cell cycle including the Aurora kinases, Cyclin B, Polo-like kinase 1 (Plk1) and cdc25 phosphatases (Kalathil et al., 2020; Rubin et al., 2020; Matthews et al., 2022).

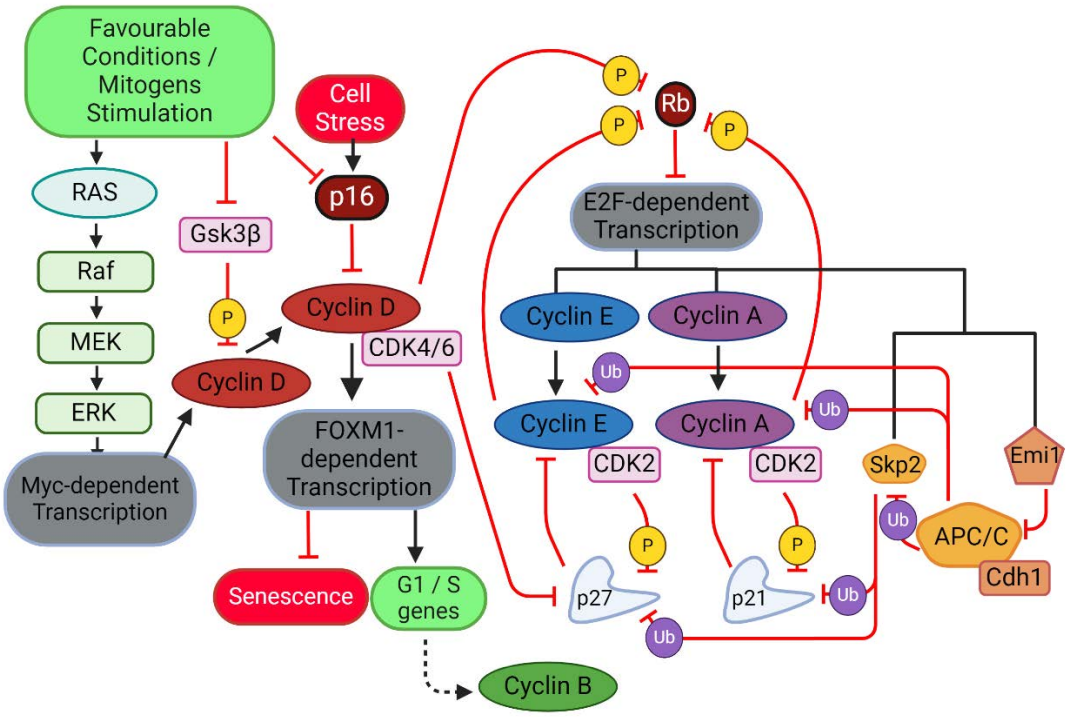

Figure 1-4 Cell cycle initiation is triggered by external mitogen stimulation and an absence of cell stress via the RAS-Raf-MEK-ERK pathway and the Myc-transcription factor dependent increase in Cyclin D production.Mitogen stimulation also inhibits key regulators of Cyclin D and CDK4/6-Cyclin D activation including Gsk3β (Glycogen synthase kinase-3 beta) and p16 which are upregulated in the absence of mitogens and via cell stress respectively.

CDK4/6-Cyclin D triggers transcription of genes necessary for G_1, S, G_2 and M phase via activation of FOXM1 (Forkhead box protein M1) and E2F family of transcription factors. E2F activation is achieved by the dual mechanism of inhibitory phosphorylation of Rb (retinoblastoma protein) which triggers production of Cyclin E and activation of its partner CDK2, and the sequestering of the CDK inhibitor protein p27 by CDK4/6-Cyclin D, with p27 a key inhibitor of CDK2-Cyclin E. CDK2-Cyclin E further phosphorylates Rb, upregulating the production of Cyclin A via E2F transcription, which allows Cyclin A to complex with CDK2 and complete the inhibitory phosphorylation of Rb, fully releasing the E2F family transcription factors from inhibition.

E2F also triggers the production of the production of the APC/C_{Cdh1} inhibitory protein Emi1 (Early mitotic inhibitor 1) and Skp2 (S-phase kinase-associated protein 2), part of the Skp, Cullin, F-box containing complex (or SCF complex) Ubiquitin E3 ligase which targets p21 and p27 for ubiquitination and proteasomal degradation. This step effectively inhibits the inhibitors of Cyclin E and Cyclin A, allowing their rapid accumulation and pushes the cell towards the first cell cycle checkpoint, the restriction point, after which the cell no longer requires mitogenic stimulation to continue with the cell cycle.

Created with BioRender.com and based on information in (Deshpande et al., 2005; Johnson and Skotheim, 2013; Kernan et al., 2018; Martinez-Alonso and Malumbres, 2020; Pennycook and Barr, 2020; Rubin et al., 2020; Milletti et al., 2023)

1.6.1.3 S-phase, G_2 and the DNA damage response

As shown in Figure 1-3, Cyclin A becomes the dominant activator of the CDKs from the end of G_1 phase through S, G_2 and M phase where it allows CDK1 to prime the cell for mitosis. During S-phase, CDK2-Cyclin A triggers hundreds of events required for DNA replication, including origin firing, following the completion of origin licensing and the loading of pre-replication complexes (Pre-RC complex) to DNA by CDk2-Cyclin E prior to S-phase (Kastan and Bartek, 2004; Limas and Cook, 2019; Fagundes and Teixeira, 2021). DNA damage during the replication process or due to environmental factors such as UV, radiation, reactive oxygen species can lead to double strand or single strand DNA breaks, or the stalling of replication forks with potentially deleterious effects on cell replication and the generation of aneuploid cells with incorrect chromosome numbers or generation of mutations leading to cancer (Ciccia and Elledge, 2010; Lanz et al., 2019). There are two key mechanisms to detect DNA damage (collectively the DNA Damage Response or DDR, see Figure 1-3), which halt cell cycle progression and trigger downstream repair mechanisms or trigger programmed cell death via apoptosis are active through G_1, S and G_2 phase (Kastan and Bartek, 2004; Bartek and Lukas, 2007).

1.6.1.3.1 ATM and response to double strand DNA breaks

Ataxia-telangiectasia mutated kinase (ATM) mediates the response to double strand DNA breaks (DNA DSBs) throughout interphase (see Figure 1-3 and Figure 1-5). Its recruitment to the site of DNA DSBs by the MRN complex (Mre11, Rad50 and Nbs1) leads to activation of monomeric ATM and the downstream phosphorylation of targets to both halt the progression of the cell cycle and trigger DNA repair mechanisms to fix the damaged DNA strands (Neizer-Ashun and Bhattacharya, 2021; Matthews et al., 2022). ATM phosphorylation of Checkpoint Kinase 2 (CHK2) leads to its activation and the dual effects of activation of the transcription factor p53 and upregulation of p21 to directly inhibit CDK2-Cyclin E/A complexes, and the inhibition of the phosphatase cdc25 (cell division cycle 25) removes inhibitory phosphorylation of CDK1 when bound to Cyclin A and B in late G_2 and M phase (Reinhardt and Yaffe, 2009; Matthews et al., 2022).

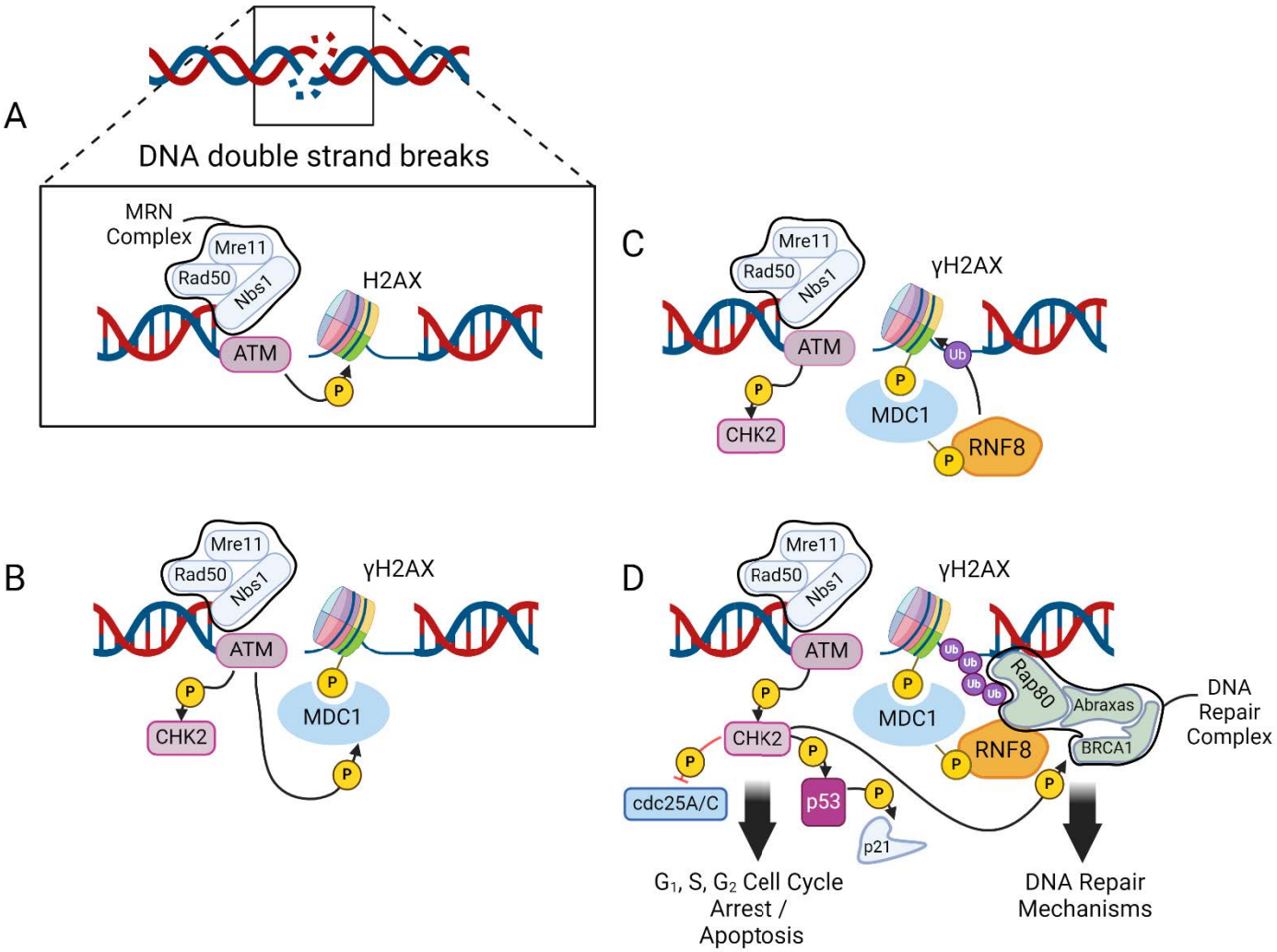

Figure 1-5 The DNA Damage Response following double strand DNA breaks.

***(A)** DNA double strand breaks are detected by the MRN complex (Mre11, Rad50 and Nbs1) which binds to the site of damage and recruits Ataxia-telangiectasia mutated kinase (ATM) allowing ATM to phosphorylate Histone H2AX to produce γH2AX. **(B)** The phosphorylation site on γH2AX acts as a binding site for Mediator of DNA damage checkpoint protein 1 (MDC1) which is then phosphorylated by ATM, with ATM also phosphorylating Checkpoint Kinase 2 (CHK2). **(C)** The E3 Ubiquitin ligase RNF8 (Ring Finger Protein 8) binds to the phosphor-sites on MDC1, brings RNF8 into proximity to the site of DNA damage whereby it ubiquitinates γH2AX. **(D)** Ubiquitinated γH2AX is recognised by the Rap80 subunit of the DNA repair complex (Rap80, Abraxas and BRCA1), which triggers BRCA-linked DNA repair mechanisms while activated CHK2 promotes cell cycle arrest mediated via activation of p53 and p21, and inhibition of cdc25A/C which in turn removes an activation pathway for CDK2 and CDK1. Failure to repair the DNA damage can lead to p53 mediated cell apoptosis.*

Created with BioRender.com and based on information in (Kastan and Bartek, 2004; Reinhardt and Yaffe, 2009; Ciccia and Elledge, 2010)

1.6.1.3.2 ATR and response to single strand DNA breaks, replicative stress and stalled replication

As shown in Figure 1-6, ataxia telangiectasia and Rad3-related (ATR) kinase is the central hub of a series of protein interactions and phosphorylation events that result in a cell's response to the prolonged exposure of single strand DNA, either due to stalled replicative machinery or genotoxic stress (Gaillard et al., 2015; Saldivar et al., 2017; Techer et al., 2017).

Checkpoint Kinase 1 (CHK1) is the key mediator of the replicative stress response to single strand DNA (Figure 1-6D), which via the dual inhibition of CDK2 and CDK1 at tyrosine residue-15 (the site of inhibitory phosphorylation by Wee1 and the target for activatory dephosphorylation by cdc25A/C) provides the final G_2/M cell cycle checkpoint before a cell commits to mitosis (Reinhardt and Yaffe, 2009; Matthews et al., 2022).

To trigger DNA repair mechanisms, ATR recruits Fanconi anaemia complementation group D2 (FANCD2) via a series of phosphorylation events, to help stabilise the replication fork and prevent double strand breaks, (Saldivar et al., 2017; Techer et al., 2017). However, in the event of DSB DNA the ATM-mediated response is also activated allowing cross over of both DNA damage response processes (Bartek and Lukas, 2007; Gaillard et al., 2015).

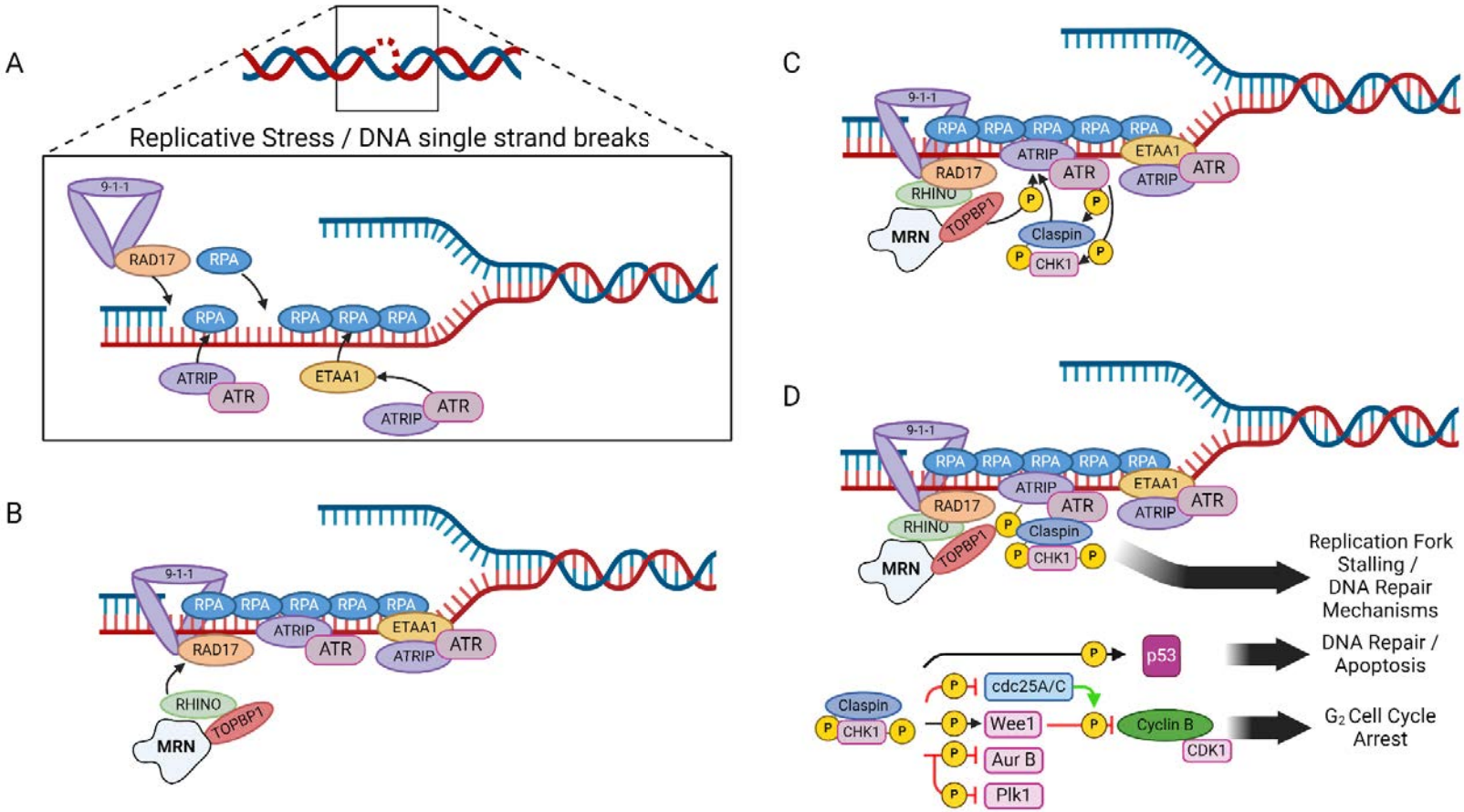

Figure 1-6 DNA Damage Response checkpoint following single strand breaks or replicative stress. ***(A)*** *Exposed single strand DNA, either as a result of stalled replication forks or via genotoxic stress, is rapidly bound by replication protein A (RPA), which provides a platform for ATR-interacting protein (ATRIP) and ataxia telangiectasia and Rad3-related (ATR) kinase to bind. Ewing tumour-associated antigen 1 (ETAA1) can also bind to RPA and recruit ATR-ATRIP. In parallel RAD17 helps to load the 9-1-1 complex (RAD9–RAD1–HUS1) to the junction between single and double stranded DNA.* ***(B)*** *The 9-1-1 clamp the recruits a further complex consisting of MRN (*Mre11, Rad50 and Nbs1*), RHINO and topoisomerase II binding protein 1 (TOPBP1), which serves as an activator of ATR.* ***(C)*** *TOPBP1 phosphorylates ATRIP which in turn provides a binding site for Claspin. This brings Claspin into proximity to ATR where it is phosphorylated to create a binding site for Checkpoint Kinase 1 (CHK1). CHK1 is then itself phosphorylated by ATR and the activated CHK1-Claspin complex can dissociate away from the site of DNA damage to phosphorylate multiple targets.* ***(D)*** *ATR at the site of damage continues to phosphorylate target which mediate DNA repair or re-initiation of stalled replication forks. CHK1-Claspin phosphorylates targets which promote inhibition of kinases essential to cell cycle progression, including direct inhibition of Aurora B and Plk1, and indirect inhibition of CDK1 via activation of Wee1 and inhibition of cdc25A/C. CHK1 also phosphorylates p53 to activate further DNA repair mechanisms and trigger apoptosis in the absence of successful repair of DNA. Created with BioRender.com and based on information in (Gaillard et al., 2015; Saldivar et al., 2017; Techer et al., 2017)*

1.6.1.4 Mitosis and the Spindle Assembly Checkpoint

The final checkpoint in the cell cycle occurs at the metaphase to anaphase transition, immediately prior to chromosome segregation to the bipolar spindle pores. Known as the Spindle Assembly Checkpoint (SAC) (see Figure 1-7), it is the checkpoint which protects the cells against disordered chromosome division and generation of daughter cells with irregular chromosome copy numbers (Musacchio, 2015). At unattached kinetochores, formation of the Mitotic Checkpoint Complex (comprising Bub3, BubR1, Mad2 and cdc20) inhibits the Anaphase Promoting Complex/Cyclosome, with just one unattached kinetochore producing sufficient MCC signal to prevent chromosome separation until the final centromere has been attached to the spindle (Greil et al., 2022).

Fulfilment of the SAC leads rapidly to activation of APC/C_{cdc20} followed by APC/C_{Cdh1} which commits the cell to mitosis, cell division and returns the cell back to interphase via the degradation of Cyclin A and B and the inactivation of CDK1 ready for a new cell cycle (Malumbres and Barbacid, 2009; Matthews et al., 2022).

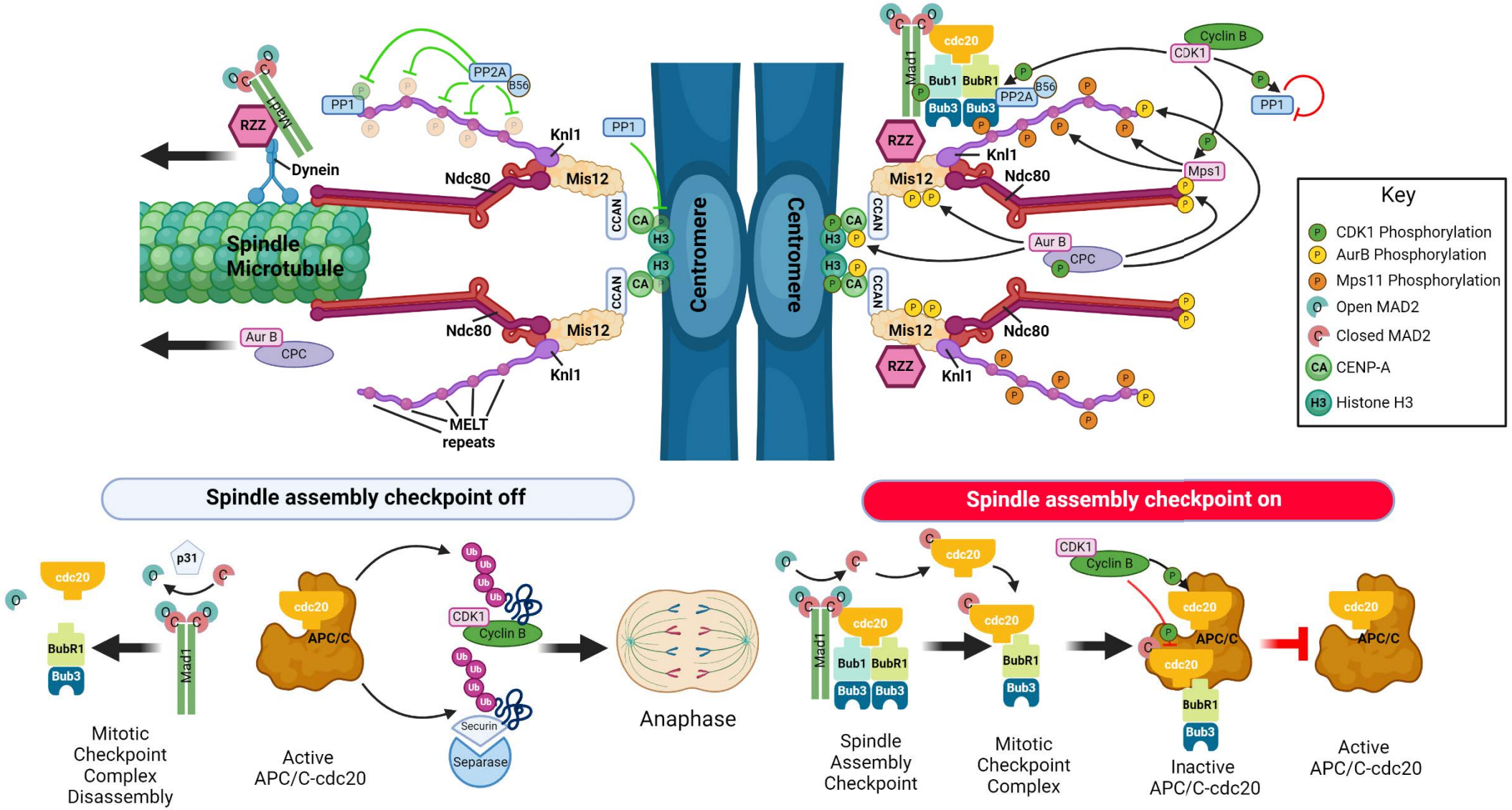
Spindle Microtubule
Dynein
RZZ
Mad1
PP1
PP2A
B56
Knl1
Ndc80
Mis12
MELT repeats
Aur B
CPC
CCAN
CA
H3
Centromere
cdc20
Bub1
BubR1
Bub3
Cyclin B
CDK1
Mps1
Key
CDK1 Phosphorylation
AurB Phosphorylation
Mps11 Phosphorylation
Open MAD2
Closed MAD2
CENP-A
Histone H3
Spindle assembly checkpoint off
Spindle assembly checkpoint on
p31
APC/C
Ub
Securin
Separase
Anaphase
Mitotic Checkpoint Complex Disassembly
Active APC/C-cdc20
Spindle Assembly Checkpoint
Mitotic Checkpoint Complex
Inactive APC/C-cdc20
Active APC/C-cdc20

Figure 1-7 The Spindle Assembly Checkpoint (SAC) is the last cell cycle checkpoint before a cell commits to mitosis and cell division and the final opportunity for a cell to rescue itself from chromosomal instability via the incorrect separation of sister chromatids prior to cytokinesis. The SAC responds to absence of chromosome attachment at the kinetochores during alignment and mitotic spindle formation during metaphase and prevents passage through to anaphase and chromatid separation until kinetochores are attached to both poles of the mitotic spindle.

***Spindle Assembly Checkpoint on (righthand side of figure)**: At the outer kinetochore region of the centromere (which connects the duplicate sister chromatids prior to cleavage at anaphase), a number of protein complexes prepare the kinetochore for microtubule attachment and generate the SAC signal until proper connection is established. The ROD (rough deal)–ZW10 (zeste white-10)–ZWILCH (RZZ) complex forms part of the fibrous corona at outer kinetochore (single unit shown for clarity) and recruits/localised the mitotic arrest deficient 1 and 2 (Mad 1 and Mad2) complex to the unattached kinetochore prior to SAC activation. The Knl1 (kinetochore scaffold 1)-Mis12 (Mis12 complex)-Ndc80 (Ndc80 complex) (together the KMN complex) connects to the inner kinetochore via the constitutive centromere associate network (CCAN), another complex of repeated centromere protein (CENP) subunits that are anchored to chromatin via the centromere protein A (CENP-A) and histone H3.*

The KMN complexes then provides the scaffold upon which the SAC is formed at unattached kinetochores. The kinase Aurora B is also localised to the kinetochore by the chromosomal passenger complex (CPC, containing the subunits survivin, borealin and INCENP) where it phosphorylates sites on CENP-A, Mis12 and Ndc80 (yellow circles) with the latter promoting the binding of monopolar spindle 1 (Mps1) kinase (also promoted by phosphorylation of Ncd80 by CDK1-Cyclin B1, green circles). Mps1 then phosphorylates MELT repeats on Knl1 (orange circles) that provide binding sites for the components of the SAC itself. Mitotic checkpoint protein BUB3 (Bub3) which forms dimers with Bub1 and BubR1 (Mitotic checkpoint serine/threonine-protein kinase BUB1 and BUBR1 respectively) binds to the phosphorylated MELT repeats and is brought into proximity to Mad1-Mad2 anchored to RZZ. CDK1-Cyclin B and Mps1 phosphorylation of Bub1 promotes binding to Mad1, with Mad2 bound to Mad1 undergoing a conformation change from open Mad2 (O-Mad2) to closed Mad2 (C-Mad2). Cell division cycle protein 20 (cdc20) is also localised at the kinetochore and is recruited to the SAC by both Bub1 and BubR1, where Mad1 catalyses free O-Mad2 to C-Mad2 which binds to cdc20. The Mitotic Checkpoint Complex (MCC) is then formed of BubR1, Bub3, cdc20 and C-Mad which can dissociate from Ndc80 whereby it binds to APC/C, blocking its substrate recognition (and thus the ubiquitination of securin, Cyclin B1 to promote mitotic exit) and holding the cell cycle at metaphase until microtubule attachment at the kinetochore. CDK1-Cyclin B also plays a dual role in activating the APC/C and inhibiting cdc20 via phosphorylation as well as promoting the binding of phosphatase PP2A-B56 (protein phosphatase 2A, regulatory subunit B56) to BubR1 to prime the reversal of mitotic signalling after the chromosomes have divided and allow the cell to return to G_1. High levels of Cyclin B also tip the balance of kinase/phosphatase activity towards phosphorylation, with CDK1-Cyclin B also directly inhibiting PP1.

***Spindle Assembly Checkpoint off (lefthand side of figure):** SAC silencing is achieved by several mechanisms upon microtubule binding to the outer kinetochore via Ndc80. The tension applied by the spindle is thought to mechanically removed Mps1 away from Knl1 and leads to a reduction in phosphorylation of MELT repeats and therefore inactivation of the MCC. PP2A-B56, located at Knl1 through interaction with BubR1, acts to further dephosphorylate targets of Aurora B and CDK1. Cyclin B degradation by APC/C_{cdc20} frees PP1 from inhibition and tips the balance of kinase/phosphatase activity in the direction of dephosphorylation, with PP1 binding to Knl1 and further reversing Mps1 activity. The cytosolic inhibitor of C-Mad2, $p31^{comet}$-TRIP13 complex is also thought to block the conversion of O-Mad2 to C-Mad2, aiding to disassemble the MCC. The motor protein dynein(via adapter protein Spindly attachment to RZZ) mechanically strips the RZZ and Mad1-Mad2 complexes from the kinetochore at microtubule attachment, physically removing the MCC away from its site of activation to fully extinguish MCC activity. Finally, APC/C_{cdc20} is freed from MCC inhibition and swiftly ubiquitinates its targets including Cyclin B and securin to promote metaphase and the separation of chromatid pairs.*

Created with BioRender.com and based on information in (Kops et al., 2005; Musacchio and Salmon, 2007; Malumbres and Barbacid, 2009; Musacchio, 2015; Hayward et al., 2019; Holder et al., 2019; Lara-Gonzalez et al., 2019; Lara-Gonzalez et al., 2021).

1.6.1.5 Targeting cell cycle checkpoints for disease

Many of the current treatments for B cell malignancies aim to use the cell cycle checkpoints to halt the uncontrolled proliferation, with combinations of treatments aimed at either causing irreversible DNA damage or mitotic spindle dysfunction in order to cause cell death via apoptosis still an option for less fit patients (Walewska et al., 2022) and more target treatments showing great effects in patients with disease driven by oncogene mutations such as p53 (Furstenau and Eichhorst, 2021; Eichhorst et al., 2023).

1.7 Mechanisms of action of currently available treatments

Mature B-cell malignancies remain a treatment challenge, as many patients develop resistance and become treatment-refractory. It is essential that the precise mechanism of action of each agent is fully understood to determine how future novel therapies may be introduced or even added to more established combination therapy regimes.

1.7.1 Chemotherapy

Chemotherapeutic agents which selectively target rapidly dividing cells have long since been the basis of many combination-therapies for mature B-cell malignancies. CHOP (cyclophosphamide, hydroxydoxorubicin, vincristine and prednisolone) chemotherapy has been an established treatment of NHL since the late 1970s (Jones et al., 1979), while the combination of fludarabine and chlorambucil (FC) has long been an established treatment for CLL (Routledge and Bloor, 2016). These regimens feature drugs from distinctive drug classes, each of which trigger apoptosis, cell death or cell cycle arrest by a different mechanism, with the idea that by targeting cells via multiple mechanisms, development of drug resistance may be reduced (See Figure 1-1).

1.7.1.1 Microtubule Targeting Agents

MTAs exert their effects by binding to tubulins at specific binding sites interrupting alignment of chromosomes before the metaphase-anaphase transition, triggering the SAC (see section 1.6.1.4 and Figure 1-7) and leading to mitotic arrest or apoptotic cell death (Jordan et al., 1991; Kavallaris, 2010). An extended period of mitotic arrest can lead to mitotic slippage, where cells exit mitosis in a state of tetraploidy, with four copies of each chromosome following duplication during S-phase (Kavallaris, 2010) Apoptotic cell death is mediated by members of the Bcl-2 family of pro- and anti-apoptotic proteins, including pro-apoptotic Bim which triggers mitochondrial induced apoptosis (Kavallaris, 2010). In addition to mitotic spindle formation, microtubules are also involved in several other key cell functions, including control of cell shape, motility, and intracellular trafficking, meaning that targeting of microtubules has multiple effects on the cell (Fanale et al., 2015).

The MTAs can be broadly divided into two categories: The first is the microtubule stabilising agents (MSAs) such as members of the Taxane family that bind to the taxane-binding site within the microtubules. The second is the microtubule destabilising agents (MDAs), such as members of the Vinca Alkaloid family (of which Vincristine and Vinblastine are the most well-known and bind to the vinca alkaloid binding site). The Colchicine binding site inhibitor (CBSI) family also fit into this second group, although at present, CBSIs have yet to reach the commercial phase as anti-cancer drugs due to toxicity issues (Wang et al., 2016). MSAs work by binding to the tubulin polymer and stabilizing the microtubules, while MDAs bind to tubulin dimers causing destabilisation. Irrespective of the mode of action, both MSAs and MDAs result in disruption of the mitotic spindle, activation of the spindle assembly checkpoint, resultant cell cycle arrest at the metaphase-anaphase transition, and ultimately cell death (Fanale et al., 2015; Pérez-Pérez et al., 2016).

The neurotoxicity observed in a significant number of patients following treatment with MTAs has suggested modes of action other than just mitotic arrest of dividing cells (Velasco-González and Coffeen, 2022). Indeed, non-dividing chronic lymphocytic leukaemia (CLL) cells have been shown to be highly sensitive to vinca-alkaloids in

culture in comparison with normal dividing lymphocytes (Vilpo et al., 2000), and both Vincristine (Oncovin, the 'O' in R-CHOP) and vinblastine are commonly used to treat CLL, as well as other B-cell malignancies and solid tumours. The consequent effects of tubulin disruption on microtubule associated proteins, cell morphology (Gertsch et al., 2009), kinase activation (Teicher, 2008) and gene transcription (Pan et al., 2018) are likely contributors to the mode of action (Bates and Eastman, 2017).

In line with other established treatments for B-cell malignancies, unfortunately, patients can develop resistance to anti-mitotic drugs through expression of microtubule-associated proteins (MAPs) which stabilise microtubules against depolymerisation (Kavallaris, 2010), which further evidences the need for alternative treatment modalities.

It is clear that MTAs continue to be effective in first-line treatment regimes in a wide range of cancer types, including B-cell malignancies. While neurotoxicity and neuropathy are key treatment limiting and debilitating symptoms for patients treated with MTAs, newer generations of treatments (e.g., Ixabepilone, eribulin, epothilones) have demonstrated reduced severity and swifter reduction in neuropathic symptoms in response to dose reduction in animal models and early phase clinical trials (Carlson and Ocean, 2011; Staff et al., 2017; Cook et al., 2018). Identification and refinement of new compounds with microtubule destabilisation activity may allow for enhanced tumour specificity, reduced neurotoxicity, and insensitivity to chemoresistance mechanisms, by differing effects on microtubule associated proteins (Bates and Eastman, 2017).

1.7.1.2 Anthracyclines

Anthracycline antibiotic drugs, including doxorubicin (Adriamycin) and daunorubicin, are from the drug class known as intercalating agents, due to their disruption of DNA replication, and the enzymes topoisomerase I and II associated with it, which leads to cell death via apoptosis (Tacar et al., 2012). The addition of doxorubicin, in the form of hydroxydoxorubicin (the 'h' in CHOP), helped to establish the CHOP chemotherapy regimen as the first choice for NHLs (Jones et al., 1979) and it has been

in clinical use for over 30 years (Tacar et al., 2012). Its mechanism of action includes the disruption to topoisomerase I and II enzymes, which play a key role in the unravelling of DNA, preventing it from uncoiling, combined with intercalating into DNA and RNA which prevents their polymerisation, and leads to programmed cell death when cellular DNA repair mechanisms fail and commit the cell to apoptosis (Tacar et al., 2012). Doxorubicin can also increase the cellular production of free radicals, contributing to further DNA damage but also to the toxicity associated with their clinical use, which limits the dosage that can be administered safely (Tacar et al., 2012).

1.7.1.3 DNA Targeting Agents

Cyclophosphamide, chlorambucil and bendamustine are all examples of alkylating agents, drugs which act via damage to DNA to prevent the expansion of tumour cells (Tacar et al., 2012). They are the oldest class of anti-neoplastic drugs, having been first licensed for use in the 1940s (Puyo et al., 2014). Alkylating agents, as their name suggests, have a mechanism of action by which they add alkyl groups via covalent bonding to proteins and DNA, which interferes with essential tasks such as transcription, leading to accumulation of crosslinking between DNA strands and cell death (Emadi et al., 2009; Puyo et al., 2014). However, DNA repair mechanisms can lessen the effects of alkylating agents, meaning they are often used in conjunction with other anti-neoplastic drugs (Sampath and Plunkett, 2007). Fludarabine is an example of a purine analogue, frequently used in the treatment of CLL. Purine analogues are anti-metabolites that interfere with DNA synthesis and trigger cytotoxicity and cell death via their incorporation into DNA and RNA, inducing apoptosis in the S-phase of the cell cycle (Galmarini et al., 2002). Despite being first introduced in to CLL treatment regimes in 1985, Fludarabine continues to form part of frontline therapy for these patients (as part of the FCR regime) (Walewska et al., 2022), since in younger fitter patients long-term data shows impressive results in terms of overall survival and safety profile. However, older CLL patients' risk for adverse events and toxicities from Fludarabine are much higher, and toxicity is also

considered to be an issue in those patients with renal dysfunction. Hence alternatives are needed for these patient groups.

1.7.1.4 Glucocorticoids

Glucocorticoids (GCs), including the drugs prednisolone and dexamethasone, are well established treatments for B-cell and T-cell malignancies and are able to trigger lymphoid cell death via apoptosis (Schmidt et al., 2004). The effects of GCs are mediated by the glucocorticoid receptor (GR), a ligand-activated transcription factor found in the cytoplasm, the activation of which upregulates gene expression (Schmidt et al., 2004). The mechanism of action includes interaction with the pro-apoptotic members of the Bcl-2 family of proteins, specifically the indirect upregulation of pro-apoptotic Bim protein, together with suppression of the anti-apoptotic members of the same family leading to caspase mediated apoptosis (Schmidt et al., 2004; Smith and Cidlowski, 2010). GCs have historically been an exciting treatment modality in CLL given that Dexamethasone-induced apoptosis appears to be unaffected by p53 dysfunction, and hence can be used in TP53-mutated cases, and seems to be more pronounced in cases with unmutated *IGHV* genes, again providing a useful treatment approach in this poor prognostic patient group (Melarangi et al., 2012). Prednisolone forms the 'P' in CHOP therapy which continues to be used in the treatment of NHL, but in some cases prednisolone is used in isolation to manage the autoimmune complications such as Autoimmune Haemolytic Anaemia (AIHA) that can develop in patients with mature B-cell malignancies (Autore et al., 2021). However, patients can begin to develop resistance to glucocorticoid treatment, through mechanisms that have yet to be fully elucidated, but that seem to involve an acquired inability to activate the pro-apoptotic proteins Bax and Bak (Melarangi et al., 2012). Resistance to GCs contributes to poor prognosis in B-cell malignancies (Schmidt et al., 2004; Smith and Cidlowski, 2010).

1.7.2 Anti-CD20 Antibodies

First licenced for treatment in the USA in 1998, the introduction of rituximab has had a huge impact in the treatment of B-cell malignancies, with benefits to both progression free survival and overall survival (Salles et al., 2017). It is a monoclonal antibody (mAB) of chimeric origin (human/murine) specified to the ubiquitous B-cell transmembrane protein CD20, to which rituximab binds with high affinity (Salles et al., 2017). Rituximab is thought to trigger cell death via at least four different pathways: through activating the complement component of the humoral immune system leading to complement-dependent cytotoxicity (CDC); through recognition of the rituximab antibody by natural killer (NK) cells leading to antibody-dependent cellular cytotoxicity (ADCC); through the cross-linking of several molecules of CD20 and rituximab and the formation of lipid rafts which leads to Src kinase-mediated apoptosis; and through the recognition of complement-bound rituximab and the rituximab Fc region by Fc-receptors on macrophages, leading the phagocytosis (Salles et al., 2017). Rituximab has formed part of the treatment regimens for DLCBL, FL, MCL and CLL, both as upfront treatment, (frequently as part of the R-CHOP regimen), as maintenance and as part of salvage chemotherapy regimens (McNamara et al., 2012; Dreyling et al., 2016; Dreyling et al., 2017), and continues to be used in current treatment guidelines. However as outlined above, disease progression and relapse are still prevalent, leading to the search for alternative treatments.

More recently (in 2019), Obinutuzumab was recommended by National Institute for Health & Care Excellence (NICE) as a newer anti-CD20 monoclonal antibody for treatment of CLL. Its efficacy was tested in the CLL11 trial, a multicentre, open-label, 3-arm trial, comparing obinutuzumab plus chlorambucil (OC), rituximab plus chlorambucil (CR) and chlorambucil (Clb) alone in patients with untreated CLL, for whom full-dose fludarabine-based therapy was not appropriate (Seiter and Mamorska-Dyga, 2015). Significant superiority of OC when compared with either Clb alone or CR was demonstrated, with regards to progression-free survival (PFS). Significant superiority of OC over Clb alone was also shown when overall survival was considered. In a follow-up study, patients treated with OC were shown to remain

without new anti-leukemic treatment for over 50 months on average, demonstrating a superior "time-to-next-treatment" for this new CIT regime (Goede et al., 2015). Given these very positive data, Obinutuzumab is currently a front line therapy for several CLL patient groups, particularly those with *TP53* mutations who are otherwise extremely difficult to treat (Walewska et al., 2022).

1.7.3 Targeted therapies

A significant amount of progress has been made with regards to treatments which target cell signalling pathways in B-cell malignancies. Many of these now form part of well-established treatment protocols (Figure 1.2) and many more are still under development.

1.7.3.1 Bruton Tyrosine Kinase inhibitors

Ibrutinib is a first in class BTK inhibitor, which became a routine part of treatment schedules, particularly in CLL, used upfront for patients with poor prognostic markers such as *TP53* mutation, as well as in maintenance following chemotherapy treatment and following disease relapse (Routledge and Bloor, 2016). Ibrutinib has also shown selective activity for the DLBCL ABC subgroup, and is now a main choice for second-line therapy in CLL. Ibrutinib covalently binds to the BTK enzyme in the BCR activation pathway see Figure 1-1, inhibiting numerous downstream cell signalling pathways including MAP kinase and extracellular signal-regulated kinase (ERK) signalling, NF-κB DNA binding as well as reducing CLL cell proliferation (Byrd et al., 2013; Routledge and Bloor, 2016). In a phase 1b-2 trial in relapsed CLL, single agent use of ibrutinib resulted in an overall response rate of 71 %, and progression free survival of 75 % and overall survival of 83 % at 26 months, which demonstrated its efficacy in this setting (Byrd et al., 2013). However, due to off-target effects of ibrutinib (including bleeding in some patients), the search of alternative targeted treatments has expanded. Acalabrutinib, a second generation BTK inhibitor, was approved in 2017 following promising results in clinical trials focusing on relapsed CLL, with an overall response rate of 95 % demonstrated at 14.3 months follow up (Byrd et al., 2016). Again, acalabrutinib is now a main choice for second-line therapy in CLL (Figure 1-2)

and has an improved adverse event profile in comparison with ibrutinib. However, the search for improved BTK inhibitors continues, with Zanubrutinib showing greater BTK selectivity than ibrutinib and acalabrutinib, with minimal off-target *in vitro* inhibition, in early trials (Y. Guo et al., 2019).

1.7.3.2 Phosphatidylinositol-3 kinase inhibitors

Idelalisib is a selective, reversible, PI3Kδ inhibitor, with its target PI3Kδ upstream of BTK and other essential signalling pathways responsible for proliferation and resistance to apoptosis including Akt, mTOR, ERK (Fruman and Rommel, 2014; Jain and O'Brien, 2016). Idelalisib is now offered as third line therapy for CLL patients in CLL in combination with rituximab and in the relapsed setting (Routledge and Bloor, 2016), as well as in FL (Dreyling et al., 2016) and in relapsed MCL (Dreyling et al., 2017). A phase 3 clinical trial of placebo plus rituximab vs idelalisib in combination with rituximab, showed and overall response for the idealisib treatment arm of 81 % and overall survival at 12 months of 92 % (Furman et al., 2014) leading to its licensing in this setting (Routledge and Bloor, 2016).

More recently attention has focused on the efficacy of buparlisib, an orally available pan-Class I PI3K inhibitor, that is reported to be more potent than idelalisib. A phase I clinical trial has investigated dual targeting of the BCR via BTK inhibition (ibrutinib) and PI3K inhibition (buparlisib) in FL, MCL and DLBCL (Stewart et al., 2022), hypothesising that dual targeting would potentially increase the duration of response to therapy and prevent the development of resistant subclones. Results have shown high overall response and complete response rates, particularly in MCL.

1.7.3.3 B-cell lymphoma-2 inhibitors

The anti-apoptotic protein Bcl-2, naturally located in the membranes of the endoplasmic reticulum (ER), nuclear envelope, and in the outer membranes of mitochondria, is highly expressed in many mature B-cell malignancies and so represents an interesting therapeutic target. Mature B-cell malignancies are very

different from conventional cancers in that the level of proliferation of these malignant cells is very low. However, the cells fail to undergo apoptosis and so accumulate within the lymph nodes and peripheral blood (Rozman and Montserrat, 1995). Bcl-2 overexpression, regulated by the proto-oncogene BCL-2, is essential to this continued survival. Bcl-2 inhibits the pro-apoptotic molecules Bax and Bak from disrupting the mitochondrial membrane and releasing Cytochrome C into the cytoplasm. Caspase activity is then initiated leading to intrinsic pathway-mediated apoptosis. Venetoclax, a small molecule, mimics BH3. Normally, BH3 binds to bcl-2 at the outer wall of mitochondria inhibiting its activity. But in cells over-expressing Bcl-2, far more BH3 would be required to exert the same effects.

Venetoclax has shown an excellent safety profile and high efficacy in CLL, including relapsed/refractory cases with TP53 disruption (Roberts et al., 2016; Seymour et al., 2018; Fischer et al., 2019). It is now offered as a first line therapy for TP53 disrupted cases and as a second and third line therapy in relapsed cases either alone or in combination with rituximab (Walewska et al., 2022). Indeed, trials involving combination treatments with venetoclax have reported that venetoclax dose is not compromised when combined with other drugs and continues to demonstrate an excellent safety profile (Mato et al., 2018). The availability of venetoclax represents a major advance in CLL treatment. It is also able to overcome a dysfunctional *TP53* that is a major hallmark of chemorefractoriness to conventional antineoplastic agents, thereby representing a step-change in management of this sub-group of patients.

However, despite the reported successes with venetoclax, there are concerns that resistance can occur, and in fact, drug disease progression has been reported in 35–37% of CLL patients undergoing venetoclax treatment (Anderson et al., 2017). This drug resistance is thought to be mediated by microenvironmental signals, particularly T-cell signals. It has been shown that CLL cells that recently migrate from lymph nodes, where they receive supportive signals from the tumour microenvironment, show higher levels of the anti-apoptotic proteins BCL-XL and

MCL-1 compared to those returning back to these areas (Haselager et al., 2020). Although both BCL-XL and MCL are members of the Bcl-2 family of proteins, they are not targeted by venetoclax. Hence, it is hypothesised that tissue-resident leukemic cells with microenvironmental support might not be properly targeted by venetoclax alone. Further, a combination of very recent research has shown that resting CLL cells, but not the dividing subpopulation of the leukemic clone, preferentially respond to venetoclax (Lu et al., 2021), and that those cells that survive to a first venetoclax-exposure are capable to resist a second treatment, suggesting that venetoclax select the most activated leukemic cells with the highest proliferative capacity (Elias et al., 2022). These resistant cells show an aggressive phenotype, characterized by increased expression of BCL-XL and/or MCL-1 expression (Elias et al. 2022). As work continues on the refinement of Bcl-2 inhibitors, it will be critical to fully elucidating the mechanisms involved in the development of Bcl-2-inhibitor resistance and to determine the optimal approaches to preventing or overcoming such resistance.

1.8 Novel thienopyridine compounds

1.8.1 Thieno[*2,3-b*]pyridine containing compounds in drug discovery

The search for compounds that can effectively eliminate the apoptotic-resistant B-cells present in mature B-cell malignancies, while minimising the emergence of resistant, more aggressive sub-clones continues. It would appear, based on relative successes of the BTK inhibitors and PI3K inhibitors (Byrd et al., 2013; Flinn et al., 2014; Byrd et al., 2016) that targeting components of the BCR signalling pathway or protein kinases downstream of this is a solid approach.

Molecules containing a thieno[*2,3-b*]pyridine moiety (T[*2,3-b*]P) have been synthesised by organic chemists since the 1960s (Klemm and Zell, 1968) with an increased interest over the past 15 years in their incorporation into the structures of compounds for use in a wide range of conditions (Dotsenko et al., 2020) often based on preliminary *in silico* screening and structural activity relationship (SAR) studies. Thieno[*2,3-b*]pyridine scaffolds are also commonly used in drug discovery for the

synthesis of other targeted compounds, particularly in the search for new anti-microbial and anti-cancer agents (Mohi El-Deen et al., 2022).

Thienopyridines have been identified as a potential class of molecule/drug with anti-cancer properties (Reynisson et al., 2009), with a model of action that targets the phosphoinositide specific-phospholipase C (PLC) family of enzymes, specifically PLCγ (Arabshahi et al., 2014; Leung et al., 2014). The PLC enzyme is a membrane bound protein which has six subfamilies, PLCβ, PLCγ, PLCδ, PLCε, PLCζ, PLCη (Arabshahi et al., 2014). PLCγ in particular has been shown to regulate a range of cancer cell behaviours including tumourigenesis, metastasis and invasion, making it an attractive therapeutic target (Arabshahi et al., 2014).

Initial studies of commercially available known-inhibitors of PLCγ2, including compounds containing a thieno[*2,3-b*]pyridine structure, found GI_{50} values comparable to the mean in an NCI60 panel against leukaemia cell lines at low micromolar concentrations, with GI_{50} in the nanomolar range for melanoma (MDA-MB-435), breast (MDA-MB-468), non-small cell lung cancer (NCI-H522) and CNS (SF-295) cell lines (Feng et al., 2012).

Further *in silico* and cell line studies of synthetic thienopyridines found good specificity for PLC enzyme class inhibition, with GI_{50} in the nanomolar range for melanoma, breast, lung, CNS and leukaemia cell lines (Arabshahi et al., 2014; Hung et al., 2014). A virtual screen using PLC found increased specificity against leukaemia cell lines, possibly indicating thienopyridine specificity against PLCγ2 which is exclusively expressed in haematopoietic cells (Arabshahi et al., 2014).

In breast cancer cell line studies, cell cycle arrest was found to occur at M phase of cell cycle when treated with thienopyridines. M phase is known to be regulated by PLCγ-Akt interaction, while the PLCβ1 isoform is also implicated in the G_2/M cell cycle progression (Leung et al., 2014). The cell cycle arrest was found not to be induced as a result of DNA damage by thienopyridine compounds, a finding confirmed by comparing with the known DNA topoisomerase inhibiting agent Camptothecin and

assessing DNA damage via phosphorylated γH2AX (histone H2A family) level (Reynisson et al., 2016).

PLCγ and other PLC isoforms (except PLCζ) have been found to be inhibited in breast cancer cell lines suggesting a potential synergistic effect between the main PLCγ isoform and other PLC isoforms in tumour cell lines (Leung et al., 2014).

Work by the New Zealand group[1] identified that side chain modifications to the phenyl ring of the molecule (Figure 1-8) had effects on antiproliferative activity, with Ortho- and Meta- substitutions favouring increased antiproliferative effects while Para- substitutions were shown to decrease these effects (103.0 % cell viability at NCI60 panel for compound with this substitution vs 100 % untreated control) (Arabshahi et al., 2014; Hung et al., 2014; Eurtivong et al., 2016). Further modifications to the size of the cycloaliphatic ring moiety, was found to increase cytotoxicity; Eight-membered rings show higher cytotoxicity when compared to seven-membered rings, and cyclohexanone moieties have more of a cytostatic effect on cells (Arabshahi et al., 2015; Leung et al., 2016).

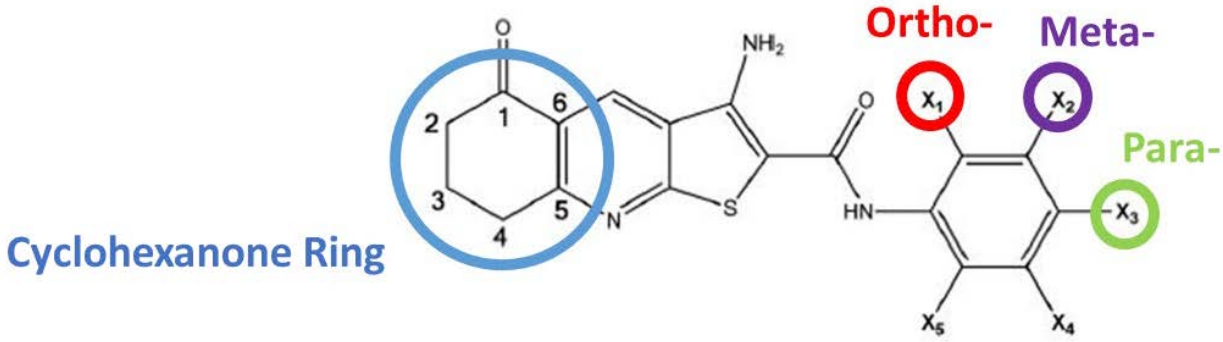

Figure 1-8 Aryl side chain modifications as well as changes to the size of the cyclohexanone moiety impact both the cytotoxicity and antiproliferative effects of novel thienopyridine compounds. Adapted from (Arabshahi et al., 2015)

[1] The New Zealand/Auckland Group refers to all works produced by Professor David Barker's lab in the School of Chemical Sciences, University Of Auckland, New Zealand

A kinase screen using KINOMEscan excluded off target inhibition, with molecular modelling of docking against Chk1 and Aurora B, which are key cell cycle regulators, showing potential direct binding of thienopyridine compounds to these specific kinases, which could explain their effects on cell cycle progression (Arabshahi et al., 2015). Fluorescent micrographs using MDA-MB-231 breast cancer cell lines stained for β-tubulin showed effects on microtubule formation (Reynisson et al., 2016) while further studies using a sea urchin embryo model demonstrated microtubule destabilisation and molecular modelling suggesting thienopyridine inhibition of the tubulin colchicine binding site (Eurtivong et al., 2017) which is a mode of action suggested in previous studies of thienopyridine containing compounds (Romagnoli et al., 2013).

Further side chain modification have been made by the Auckland group[2] to produce novel thienopyridine compounds that act against the glycophenotype and glucose metabolism of breast and prostate cancer cells (Mastelic et al., 2017; Marijan et al., 2020; Pervan et al., 2022). They have also investigated the possibility of modifying thienopyridines to act as inhibitors of the DNA repair enzyme tyrosyl-DNA phosphodiesterase (TDP1), to increase cell sensitivity to the chemotherapy drug, Camptothecin (Leung et al., 2021). These works demonstrate a broad range of potential thienopyridine targets and their promise as antiproliferative agents, with effects directly linked to the molecular structure of the compound.

Although the work mentioned thus far is all pre-clinical, some members of the thienopyridine family are currently used clinically. The thienopyridine Clopidogrel is prescribed for the treatment of acute coronary syndromes (ACS) and atherothrombosis, with activity as a platelet $P2Y_{12}$ receptor inhibitor central to its action (Thomas et al., 2015). Previous research from the present research group at Manchester Metropolitan University has shown that novel thienopyridine compounds have potent anti-platelet effects and demonstrate synergy with antithrombotic drugs such as aspirin. Interestingly, the novel thienopyridines were

[2] The New Zealand/Auckland Group refers to all works produced by Professor David Barker's lab in the School of Chemical Sciences, University Of Auckland, New Zealand

found to result in greater reductions in maximum platelet aggregation when compared with those following clopidogrel treatment (Binsaleh et al., 2018). Platelets express $P2Y_{12}$ receptors in large numbers, and ligation of this receptor with its ligand, ADP, results in a cascade of signalling events that ultimately results in platelet activation and aggregation (Gachet, 2012). This signalling cascade includes PLC, PI3K, Akt and BTK. In addition to their anti-platelet activity, Thomas et al. (2015) have found $P2Y_{12}$ inhibitors to have significant anti-inflammatory properties, reducing levels of cytokines interleukin-6 (IL-6), tumour necrosis factor alpha (TNFα) and C-C Motif Chemokine Ligand 2 (CCL2, also known as monocyte chemoattractant protein-1 (MCP-1)) in patients taking these drugs. In a disease such as CLL with a pro-inflammatory microenvironment thought to be essential to progression of the disease, thienopyridines would seem ideal candidates as new therapies.

Thienopyridines in clinical use, including clopidogrel, ticlopidine and prasugrel have also been in tested in a range of animal models for potential direct anti-cancer effects (reviewed in Ballerini et al. (2018), see Figure 1-9 for their structures), and in studies versus a range of immortalised cancer cell lines (AlKhalil et al., 2020), with their activity linked to the expression of $P2Y_{12}$ receptors on a wide range of cells other than platelets (Mansour et al., 2020). Metabolites generated by the breakdown of clopidogrel by Cytochromes P450 family (CYP450s) of enzymes has also suggested as a model of action (Kuszynski and Lauver, 2022). The antiproliferative activities of existing thienopyridines suggests that novel compounds sharing analogous chemical structures may also offer similar effects.

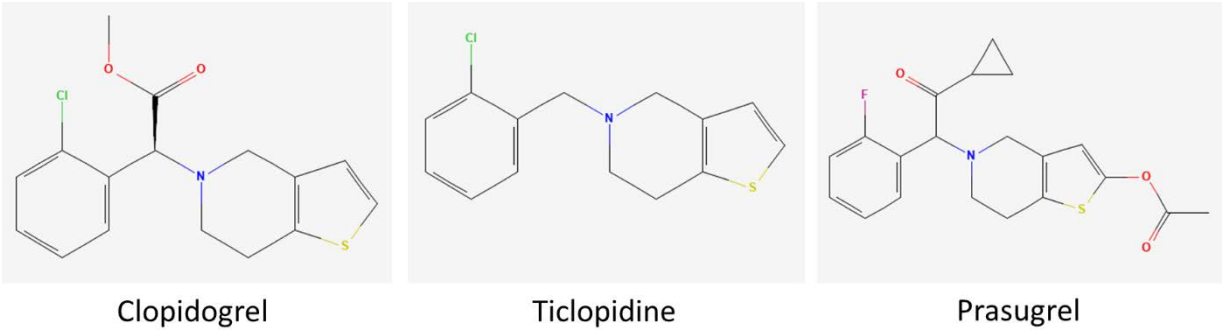

Figure 1-9 Chemical structures of thienopyridine drugs Clopidogrel, Ticlopidine and Prasugrel which are in clinical use as $P2Y_{12}$ inhibitors but have been trialled as anti-cancer agents. Structures taken from NCBI PubChem Database (Kim et al., 2023).

1.9 Thieno[*2,3-b*]pyridines as anti-cancer agents

Preliminary studies have shown Thieno[*2,3-b*]pyridine containing compounds to have cytotoxicity in the nanomolar range against gastric (NUGC cells), colon (DLDI cells), liver (HA22t cells) and breast (MCF) cancer cells by MTT/MTS assay in the absence of toxicity against normal fibroblast (W138) cells (Mohareb and Ibrahim, 2017) and against liver (HepG2) and breast (MCF7) cell lines (Abuelhassan et al., 2022). A common feature of novel thieno[*2,3-b*]pyridine class compounds is their effects on cancer cell proliferation, with effects against copper trafficking via inhibition of cytosolic copper chaperones (CCS and Atox1) and reduced cellular ATP generation (via inhibition of AMP-activated protein kinase (AMPK)) demonstrated in lung (H1229), leukaemia (K562) and breast (MDA-MD-231) cell lines with corresponding reductions in cell viability (Wang et al., 2015). Previous studies had demonstrated thieno[*2,3-b*]pyridine moiety containing compounds which were investigated as potential Adenosine A_{2A} Receptor GPCR antagonists, showed inhibition of cyclic adenosine monophosphate (cAMP) production at 10 nM concentration in a non-Adenosine A_{2A} Receptor antagonist manner (Katritch et al., 2010).

A series of novel thieno[*2,3-b*]pyridine containing compounds were found to show antiproliferative activity, including an increase in apoptosis (HeLa cells), G_2/M cell cycle arrest (Jurkat, HT-29 colorectal and HeLa cells), more potent inhibition of tubulin polymerisation compared to known Colchicine inhibitor Combrestatin A-4 (CA-4) and competition for colchicine binding sites with reduction of tumour burden shown *in vivo* in Balb/c mice, in the absence of effects against lymphocytes taken from healthy donors (Romagnoli et al., 2013). This study also demonstrated efficacy against multi-drug resistant cells lines (lymphoblastic leukaemia $CEM^{VBL-100}$ and colon carcinoma $Lovo^{Doxo}$) which express elevated levels of the adenosine triphosphate (ATP)-binding cassette (ABC) transporters and further work on a different class of thieno[*2,3-b*]pyridines showed similar inhibitory effects against P-glycoprotein (P-gp), multidrug resistance-associated protein 1 (MRP1) and breast cancer resistance protein (BCRP1) (Krauze et al., 2014).

Recent studies have shown inhibition of the oncoprotein Forkhead box M1 (FOXM1), which regulates genes involved in cell cycle progression and cell proliferation, including their dysregulation in oncogenesis, with thieno[*2,3-b*]pyridine compounds demonstrating G_2/M cell cycle arrest and apoptosis in breast cancer cell lines (G. Luo et al., 2021; Huerta-Garcia et al., 2022). Novel thieno[*2,3-b*]pyridine containing compounds have also been investigated as potential chemotherapy drugs which can be incorporated into nanoparticles for drug delivery directly to tumours (Lopes et al., 2022; Ribeiro et al., 2022).

An additional class of thieno[*2,3-b*]pyridine compounds were designed and modified to target PIM-1 again with cytotoxicity against cancer cell lines and direct PIM-1 inhibition demonstrated and side chain modifications to the chemical structures shown to both increase or decrease efficacy (Naguib and El-Nassan, 2016; Abdelaziz et al., 2018) and work done to combine VEGF and PIM-1 inhibition in the same chemical structure (Rizk et al., 2019).

1.10 Thieno[*2,3-b*]pyridine use in other conditions

Novel thieno[*2,3-b*]pyridine containing compounds have been synthesised and tested for a wide range of conditions other than neoplasms and malignancies, however there is only limited, or speculative, laboratory data to support many of these claims. The results of these papers are summarised in Table 1-2.

Table 1-2 Summary of novel thienopyridine literature

Target	Cell Lines / Conditions	Results	References
Anti-cancer	Gastric (NUGC cells) Colon (DLDI cells) Liver (HA22t cells) Breast (MCF)	Cytotoxicity in the nanomolar range by MTT/MTS assay in the absence of toxicity against normal fibroblast (W138) cells	(Mohareb and Ibrahim, 2017)
	Liver (HepG2) Breast (MCF7)		(Abuelhassan et al., 2022)
	Lung (H1229) Leukaemia (K562) Breast (MDA-MD-231)	Inhibition of cell proliferation with reduced cellular ATP generation (via inhibition of AMP-activated protein kinase (AMPK)) and effects against copper trafficking via inhibition of cytosolic copper chaperones (CCS and Atox1)	(Wang et al., 2015)
	Human embryonic kidney (HEK293)	Inhibition of cyclic adenosine monophosphate (cAMP) production at 10 nM concentration in a non-Adenosine A_{2A} Receptor antagonist manner	(Katritch et al., 2010)
	HeLa cells T-lymphocyte (Jurkat) Colorectal (HT-29)	increase in apoptosis (HeLa), G_2/M cell cycle arrest (Jurkat, HT-29 colorectal and HeLa cells), more potent inhibition of tubulin polymerisation compared to known Colchicine inhibitor Combrestatin A-4 (CA-4) and competition for colchicine binding sites with reduction of tumour burden shown *in vivo* in Balb/c mice	(Romagnoli et al., 2013)
	Lymphoblastic leukaemia ($CEM^{VBL-100}$) Colon carcinoma ($Lovo^{Doxo}$)	Efficacy against multi-drug resistant (MDR) cells lines	
	Normal mouse fibroblast (NIH3T3) Human uterine sarcoma (MES-SA) Doxorubicin resistant human uterine sarcoma (MES-SA/Dx5) Human lung cancer (H69)	Inhibition of multidrug resistance proteins: P-glycoprotein (P-gp), multidrug resistance-associated protein 1 (MRP1) and breast cancer resistance protein (BCRP1) at micromolar concentrations.	(Krauze et al., 2014)

	Doxorubicin resistant human lung cancer (H69/Dx5) Rat aorta smooth muscle (A7R5)		
	Prostate cancer endothelial cell (PC3)	Inhibition of dimethylarginine dimethylaminohydrolase 1 (DDAH1) which regulates nitric oxide production and tumour angiogenesis in prostate cancer	(Kami Reddy et al., 2019)
	Breast (MDA-MD-231)	Inhibition of the oncoprotein Forkhead box M1 (FOXM1) (involved in cell cycle progression and cell proliferation) demonstrating G_2/M cell cycle arrest, growth inhibition and apoptosis in breast cancer cell lines	(G. Luo et al., 2021; Huerta-Garcia et al., 2022)
	NCI60 Panel Hepatocellular carcinoma (HepG2) Colon adenocarcinoma (HCT116) Colorectal adenocarcinoma (Caco-2) Breast (MCF7) Prostate cancer endothelial cell (PC3) Non-small lung cancer (A549)	Cytotoxicity against cancer cell lines and direct PIM-1 inhibition demonstrated	(Naguib and El-Nassan, 2016; Abdelaziz et al., 2018)
Anti-bacterial	*Escherichia coli* *Pseudomonas aeruginosa* *Staphylococcus aureus* *Bacillus subtilis*	Moderate antibacterial effects in comparison to tetracycline by zone of inhibition assay	(Elsherif, 2020; Zaki et al., 2022)
Anti-viral	Human Immunodeficiency Virus (HIV)	Inhibition of cellular replication of HIV in Human PBSC model of infection, possibly due to anti-Rev-RRE complex inhibition.	(Nakamura et al., 2017)
	Mayaro arbovirus (MAYV)	Inhibited virus replication and morphogenesis in Vero cell model (African Green Monkey cells)	(Amorim et al., 2017)
Anti-malarial	*Plasmodium falciparum*	Specificity and activity against *P. falciparum* GSK-3 (*Pf*GSK-3) enzyme	(Masch and Kunick, 2015; Masch et al., 2019)

Anti-neurological	Alzheimer's Disease	Anti-acetylcholinesterase (anti-AChE) and anti-butyrylcholinesterase (anti-BChE) activity alongside inhibitory activity against amyloid-beta (βA) aggregation	(Saeedi et al., 2020)
		Anti-acetylcholinesterase (anti-AChE) activity	(Ahmed et al., 2022a; 2022b)
	Epilepsy	Highly selective adenosine A_1 receptor agonists in radioligand binding assays using Male Sprague-Dawley rat brain striatal membrane model.	(Nkomba et al., 2022)
	Anti-convulsant therapy	Interaction with the γ-Aminobutyric acid A ($GABA_A$) receptor demonstrated in mice and rat studies	(Dabaeva et al., 2022)
Other	Bone	Demonstrated to be bone anabolic agents which increased bone mineral density *in vivo* in ovariectomised rat model	(Saito et al., 2021)
	Cardiac	Inhibitor of the Epac1 (Exchange Protein Directly Activated by cAMP 1) a guanine-nucleotide exchange factor (GEF) which is implicated in cardiac hypertrophy	(Laudette et al., 2019)
	Diuretics	Inhibition against transmembrane urea transporters in renal vasa recta micro vessels shown *in vivo* in adult SD rat model	(Zhao et al., 2019)

1.11 Aims, Objectives and Ethical Considerations

1.11.1 Academic Aims

This project aims to explore the potential anti-cancer properties of novel thienopyridine derivatives synthesised by our collaborators at the School of Chemical Sciences, University of Auckland, NZ. There are ten derivatives in total with slight side chain modifications which are predicted to affect efficacy.

1.11.2 Objectives

1: To determine the cytotoxic/cytostatic effects of compounds on DAUDI B-cell Burkitt Lymphoma cell lines.

2. To determine the effects on the cell cycle.

3. To determine any direct effects on tubulin polymerisation

4. To investigate any pathways for cell cycle arrest using genomic and proteomic techniques.

5: To elucidate the signalling pathways affected by the compounds.

1.11.3 Ethical Considerations

This study has been submitted for MMU Ethos approval.

2. MATERIALS AND METHODS

2 MATERIALS AND METHODS

2.1 Materials

2.1.1 Consumables

0.5ml Microcentrifuge Reaction Tubes with cap Product Number 667201

Greiner Bio-One

Gloucestershire, UK

1.5ml Microcentrifuge Reaction Tube with cap Product Number 616201

Greiner Bio-One

Gloucestershire, UK

12-Well CytoOne® Plate, Non-treated Product Number CC7672-7512

Star Lab

Milton Keynes, UK

15ml Falcon Tube Product Number 62.554.502

Sarstedt

Nümbrecht, Germany

50ml Falcon Tube Product Number 62.547.254

Sarstedt

Nümbrecht, Germany

2.0ml Microcentrifuge Reaction Tube with cap Product Number 623201

Greiner Bio-One

Gloucestershire, UK

Corning® 96 Half Area Well Clear Flat Bottom TC-treated Microplate, Individually Wrapped, with Lid, Sterile Product Number 3696

Corning Life Sciences

Loughborough, UK

Falcon® 5mL Round Bottom Polystyrene Test Tube, with Snap Cap Product Number 352058

Corning Life Sciences

Loughborough, UK

Grade 3MM Chr Blotting Paper, sheet, 31.5 × 33.5 cm Product Number 3030-335

GE Healthcare Life Sciences

Buckinghamshire, UK

Immobilon-FL PVDF Membrane, 0.45 µm, 8.5 cm x 10 m roll Product Number IPFL85R

Merck/Millipore

Hertfordshire, UK

Menzel™ Microscope Coverslips Product Number 11708701

Fisher Scientific

Loughborough, UK

Nunc Non-treated T25 EasYFlask, Filter Cap Product Number 169900

Fisher Scientific

Loughborough, UK

Nunc™ Cell Culture Treated EasYFlasks™ 25cm2 Product Number 156367

Fisher Scientific

Loughborough, UK

Nunc™ MicroWell™ 96-Well Microplates Product Number 167008

Fisher Scientific

Loughborough, UK

Sterilin™ 100mm Square Petri Dishes Product Number 109-17

Thermo Scientific™

Loughborough, UK

Super PAP Pen Product Number 008899

Fisher Scientific

Loughborough, UK

Superfrost Plus™ Adhesion Microscope Slides Product Number J1800AMNT

Fisher Scientific

Loughborough, UK

Type f Immersion Oil Product Number 11513859

Leica Microsystems

Mannheim, Germany

2.1.1.1 Cell Lines

DAUDI (ECACC 85011437) Product Number 85011437

European Collection of Authenticated Cell Cultures

(ECACC)

Salisbury, UK

HK-2 (ATCC® CRL-2190™) Product Number CRL-2190

American Type Culture Collection

Manassas, Virginia, USA

Jurkat E6.1 (ECACC 88042803) Product Number 88042803

European Collection of Authenticated Cell Cultures

(ECACC)

Salisbury, UK

U937 (ECACC 85011440) Product Number 85011440

European Collection of Authenticated Cell Cultures

(ECACC)

Salisbury, UK

2.1.1.2 Cell Culture, Cell Stimulation and Treatments

Dimethyl Sulfoxide Product Number BP231-100

Fisher BioReagents

Loughborough, UK

Dulbecco's Phosphate Buffered Saline (DPBS) Product Number BE17-512F

without Ca++ and Mg++

Lonza

Verviers, Belgium

Ethanol 99+% (GLC) Absolute Product Number E/0600/17

Fisher Chemical

Loughborough, UK

Fetal Bovine Serum, qualified, E.U.-approved, South America origin Product Number 10270-106

Gibco (Fisher Scientific)

Loughborough, UK

Goat F(ab')2 Anti-Human IgM-UNLB Product Number 2022-01

Cambridge Bioscience

Cambridge, UK

RPMI 1640 with 25mM HEPES and L-Glutamine Product Number BE12-115F

Lonza

Verviers, Belgium

Trypan Blue solution, 0.4%, liquid, sterile-filtered Product Number T8154-100ML

Sigma-Aldrich

Dorset, UK

Paclitaxel, from Taxus brevifolia, >=95% (HPLC), powder Product Number T7402-5MG

Scientific Laboratory Supplies (SLS)

Nottingham, UK

Nocodazole ≥99% (TLC), powder Product Number M1404-10MG

Scientific Laboratory Supplies (SLS)

Nottingham, UK

2.1.1.3 Cell Viability and Flow Cytometry

Annexin V Binding Buffer, 10X concentrate, 0.2 µm sterile filtered 0.1M Hepes (pH 7.4), 1.4M NaCl, and 25 mM CaCl2 solution Product Number 556454

BD Pharmingen™

Oxford, UK

BD FACSFlow™ Sheath Fluid Product Number 342003

BD Biosciences

Oxford, UK

CellTiter 96® AQueous One Solution Cell Proliferation Assay (MTS) Product Number G3582

Promega UK

Southampton, UK

FITC Annexin V Aqueous buffered solution containing BSA and ≤0.09% sodium azide. Product Number 556419

BD Pharmingen™

Oxford, UK

Propidium iodide powder for reconstitution (25mg) Product Number P4170-25MG

Sigma

Dorset, UK

Propidium Iodide Staining Solution 50 µg/ml in PBS (pH 7.4) Product Number 556463

BD Pharmingen™

Oxford, UK

2.1.1.4 Tubulin Polymerisation

General Tubulin Buffer (80 mM PIPES pH 6.9, 2 mM MgCl2, 0.5mM EGTA) Product Number BST01-001

Cytoskeleton, Inc.

Denver, USA

GTP Stock (100 mM GTP) Product Number BST06

Cytoskeleton, Inc.

Denver, USA

HTS Porcine Tubulin Protein, >97% pure Product Number: HTS03-A

Cytoskeleton, Inc.

Denver, USA

HTS-Tubulin Polymerization Assay Biochem Kit™ Product Number BK004P

(>97% pure tubulin, Porcine Tubulin)

Cytoskeleton, Inc.

Denver, USA

Paclitaxel Stock Product Number TXD01

Cytoskeleton, Inc.

Denver, USA

2.1.1.5 Western Blotting

2-Propanol ≥99.0%, GPR RECTAPUR® Product Number 296942D

VWR Chemicals

Lutterworth, Leicestershire, UK

4X Protein Sample Loading Buffer for Western Blots Product Number 928-40004

LI-COR Biosciences UK Ltd

Cambridge, UK

Ammonium persulfate for molecular biology, for electrophoresis, ≥98% Product Number A3678-25G

Sigma

Dorset, UK

Blocking Buffer Optimization Kit Product Number 927-40040

LI-COR Biosciences UK Ltd

Cambridge, UK

Bovine Serum Albumin lyophilized powder, ≥96% (agarose gel electrophoresis) Product Number A2153

Sigma

Dorset, UK

Chameleon Duo Pre-stained Protein Ladder Product Number 928-60000

LI-COR Biosciences UK Ltd

Cambridge, UK

Dried Skimmed Milk Powder Product Number 11992

ASDA

Leeds, UK

Ethylenediaminetetraacetic Acid (EDTA), Extra Pure, SLR, Fisher Chemical Product Number 10080060

Fisher Scientific

Loughborough, UK

Glycerol Product Number G7893

Honeywell

Loughborough, UK

Glycine, Certified AR for Analysis Product Number 10070150

Fisher Scientific

Loughborough, UK

Intercept® (TBS) Blocking Buffer Product Number 927-60001

LI-COR Biosciences UK Ltd

Cambridge, UK

Methanol, Certified AR for Analysis Product Number 11976961

Fisher Scientific

Loughborough, UK

NP-40 Surfact-Amps™ Detergent Solution Product Number 85124

Thermo Scientific

Loughborough, UK

Odyssey® Blocking Buffer (TBS) Product Number 927-40040

LI-COR Biosciences UK Ltd

Cambridge, UK

Phosphatase Inhibitor Cocktail 2 Product Number P5726

Sigma

Dorset, UK

Pierce™ BCA Protein Assay Kit Product Number 23227

Fisher Scientific

Loughborough, UK

Protease Inhibitor Cocktail Product Number P8340

Sigma

Dorset, UK

REVERT™ Total Protein Stain Kit Product Number 926-11016

LI-COR Biosciences UK Ltd

Cambridge, UK

RIPA Lysis and Extraction Buffer Product Number 89900

Fisher Scientific

Loughborough, UK

Sodium Chloride, Extra Pure, SLR Product Number 10112640

Fisher Scientific

Loughborough, UK

Sodium Dodecyl Sulfate Product Number 10090490

Fisher Scientific

Loughborough, UK

TEMED (tetramethylethylenediamine) Product Number #1610800

Bio-Rad

Hertfordshire, UK

TGX Stain-Free™ FastCast™ Acrylamide Starter Kit, 10% Product Number #1610182

Bio-Rad

Hertfordshire, UK

Tris Base (White Crystals or Crystalline Powder/Molecular Biology) Product Number 10376743

Fisher Scientific

Loughborough, UK

Triton X-100 Product Number: T9284

Sigma Aldrich

Dorset, UK

TWEEN 20, viscous liquid Product Number: P1379-500ML

Sigma Aldrich

Dorset, UK

β-Mercaptoethanol Product Number M3148

Sigma

Dorset, UK

PARAFILM® M Product Number P7793

Sigma-Aldrich

Dorset, UK

2.1.1.6 Western Blot Buffer Recipes

Table 2-1 Western Blot Buffer Recipes

Buffer	Recipe	Volume/Mass of Reagents
Modified RIPA buffer	100 mL Solution	
	50 mM Tris Base (Fisher Scientific, Loughborough, UK) pH 7.5	5 mL of 1M Tris
	150 mM NaCl (Fisher Scientific, Loughborough, UK)	0.88 g NaCL
	1 % NP-40 (Thermo Scientific, Loughborough, UK)	10 mL of 10 % v/v
	10 % Glycerol (Honeywell, Loughborough, UK)	10 mL of 100 %
	5 mM EDTA (Fisher Scientific, Loughborough, UK)	1 mL of 0.5 M EDTA pH 8.0
	Ultrapure(18.2 MΩ) H_2O (Model: Milli-Q® Integral 3 Water Purification System, Merck/Millipore, Hertfordshire, UK)	
	Make up to 100 mL with ultrapure dH_2O	
SDS Running Buffer	1 L 10X Stock Soution	
	25 mM Tris Base (Fisher Scientific, Loughborough, UK)	30.3 g Tris
	192 mM Glycine (Fisher Scientific, Loughborough, UK)	144.2 g Glycine
	0.1 % w/v Sodium Dodecyl Sulfate (SDS) (Fisher Scientific, Loughborough, UK)	10 g SDS
	100 mL 10X stock diluted with 900 mL ultrapure dH_2O to give 1X Running buffer	
Transfer buffer	1 L 1X Stock Solution	
	25 mM Tris Base (Fisher Scientific, Loughborough, UK)	3.03 g Tris
	192 mM Glycine (Fisher Scientific, Loughborough, UK)	14.42 g Glycine
	10 % Methanol (Fisher Scientific, Loughborough, UK)	100 mL Methanol
	Made up to 1 L with ultrapure dH_2O fresh before each transfer	
Tris Buffered Saline (TBS)	1 L 10X Stock Solution	
	20 mM Tris Base (Fisher Scientific, Loughborough, UK) pH 7.5	24.23 g Tris
	100 mM NaCl (Fisher Scientific, Loughborough, UK)	87.6 g NaCl
	ultrapure H_2O to 900 mL, pH to 7.5 with concentrated HCl, Make up to 1 L with ultrapure H_2O	
	Dilute 100 mL 10X stock with 900 mL ultrapure dH_2O to give 1X TBS	
TBS-Tween (TBS-T)	0.1% TWEEN 20 (Sigma Aldrich, Dorset, UK)	1 ml of TWEEN 20 in 1 litre TBS

10 % Ammonium Persulfate	Ammonium persulfate (Sigma Aldrich, Dorset, UK)	10 % w/v in ultrapure H_2O

Table 2-2 Pierce BCA Protein Quantification Assay Working Reagent Recipe

Buffer	Recipe	Volume/Mass of Reagents
Bicinchoninic acid (BCA) working reagent	Make volume as required for number of replicates	
	Reagent A, sodium carbonate, sodium bicarbonate, bicinchoninic acid and sodium tartrate in 0.1 M sodium hydroxide	50 parts
	Reagent B, 4 % cupric sulfate	1 part

Table 2-3 Bio-Rad Fastcast Western Blot Gel Recipes. Adapted from Bio-Rad TGX™ and TGX Stain-Free™ FastCast™ Acrylamide Kit and Starter Kit Instruction Manual

Buffer	Recipe	Volume/Mass of Reagents
Resolving Gel	Solutions to cast one 1 mm gel using Bio-Rad Glass Plates	
	Resolver A (10 % acrylamide/bis-acrylamide)	3 mL
	Resolver B (Tris-Glycine eXtended solution)	3 mL
	TEMED	3 µL
	10 % Ammonium Persulfate	30 µL
Stacking Gel	Stacker A (acrylamide/bis-acrylamide)	1 mL
	Stacker B (Tris-Glycine eXtended solution)	1 mL
	TEMED	2 µL
	10 % Ammonium Persulfate	10 µL

2.1.1.7 Primary Antibodies

Table 2-4 List of Primary Antibodies and Dilutions used for Western Blots

Name	Supplier	Location	Product Number	Dilution
Mouse monoclonal Anti-PLCG 2 antibody [MM087134S3]	Abcam	Cambridge, UK	ab201645	1:2000
Akt (pan) (40D4) Mouse mAb	Cell Signalling Technology	London, UK	#2920	1:1000
Btk (D6T2C) Mouse mAb	Cell Signalling Technology	London, UK	#56044	1:1000
Chk1 (2G1D5) Mouse mAb	Cell Signalling Technology	London, UK	#2360	1:1000
Cyclin B1 Rabbit Antibody	Cell Signalling Technology	London, UK	#4138	1:1000
Pan-cdc2 Mouse mAb Antibody	Cell Signalling Technology	London, UK	#9116	1:1000
GAPDH (14C10) Rabbit IgG mAb	Cell Signalling Technology	London, UK	#2118	1:1000
Phospho-Akt (Ser473) Rabbit Antibody	Cell Signalling Technology	London, UK	#9271	1:1000

Phospho-Btk (Tyr223) Rabbit Antibody	Cell Signalling Technology	London, UK	#5082	1:1000
Phospho-cdc2 (Tyr15) (10A11) Rabbit mAb	Cell Signalling Technology	London, UK	#4539	1:1000
Phospho-Chk1 (Ser296) Rabbit Antibody	Cell Signalling Technology	London, UK	#2349	1:1000
Phospho-Chk1 (Ser345) Rabbit Antibody	Cell Signalling Technology	London, UK	#2341	1:1000
Phospho-PLCγ2 (Tyr759) Rabbit Antibody	Cell Signalling Technology	London, UK	#3874	1:1000

2.1.1.8 Secondary Antibodies

Table 2-5 List of Secondary Antibodies and Dilutions used for Western Blots

Name	**Supplier**	**Location**	**Product Number**	**Dilution**
IRDye® 680RD Goat anti-Mouse IgG (H + L)	LI-COR Biosciences UK Ltd	Cambridge, UK	925-68070	1:15000
IRDye® 680RD Goat anti-Rabbit IgG (H + L)	LI-COR Biosciences UK Ltd	Cambridge, UK	925-68071	1:15000
IRDye® 800CW Goat anti-Mouse IgG (H + L)	LI-COR Biosciences UK Ltd	Cambridge, UK	925-32210	1:15000

IRDye® 800CW Goat anti-Rabbit IgG (H + L)	LI-COR Biosciences UK Ltd	Cambridge, UK	925-32211	1:15000

2.1.1.9 RTq-PCR

Ambion™ RNAlater™ Stabilization Solution Product Number AM7021

Invitrogen (Fisher Scientific)

Loughborough, UK

Ambion™ RT-PCR Grade Water Product Number AM9935

Invitrogen (Fisher Scientific)

Loughborough, UK

RNeasy® Mini Kit (50) Product Number 74104

Qiagen

Manchester, UK

QuantiNova® SYBR® Green PCR Kit (500) Product Number 208054

Qiagen

Manchester, UK

Bioline Tetro™ cDNA Synthesis Kit (100 Reactions) Product Number BIO-65043

Meridian Bioscience

Nottingham, UK

96-Well PCR Plate, Semi-Skirted, Raised Rim, Low Profile (for FAST® Systems), natural (Case Size) Product Number E1403-7700-C

Star Lab

Milton Keynes, UK

Adhesive PCR Plate Seals Product Number AB0558

Thermo Scientific

Loughborough, UK

MicroAmp™ Adhesive Film Applicator Product Number 4333183

Applied Biosystems™

Loughborough, UK

2.1.1.10 RT-qPCR Gel Electrophoresis

Bioline Molecular Grade Agarose Product Number BIO-41025

Meridian Bioscience

Nottingham, UK

Bioline HyperLadder™ 50bp Product Number BIO-33054

Meridian Bioscience

Nottingham, UK

Bioline 5X Loading Dye Product Number BIO-33054

Meridian Bioscience

Nottingham, UK

MIDORI^{Green} Advance Product Number MG04

Nippon Genetics Europe

Düren, Germany

Ethylenediaminetetraacetic Acid, Disodium Salt Dihydrate (Crystalline/Certified ACS), Fisher Chemical™ Product Number S311500

Fisher Scientific

Loughborough, UK

Acetic Acid Glacial, Extra Pure, SLR, meets analytical specification of Ph.Eur., BP, USP, Fisher Chemical™ Product Number 10384970

Fisher Scientific

Loughborough, UK

2.1.1.11 RT-qPCR Gel Electrophoresis Buffers and Gel Recipe

Table 2-6 Tris-Acetate-EDTA (TAE) Buffer Recipe

Buffer	Recipe	Volume/Mass of Reagents
	1 L 1X Stock Solution	
50X Tris-Acetate-EDTA (TAE) Buffer	2 M Tris	242.2 g
	50 mM EDTA-Na_2	372.24 g
	1 M Acetic Acid	57.1 mL
	Make up to 1 L with ultrapure dH_2O, pH to 8.5	
1X TAE	Add 1 mL 50X TAE buffer to 49 mL ultrapure dH_2O	

Table 2-7 DNA Agarose Gel Recipes

Buffer	Recipe	Volume/Mass of Reagents
2.5 % Agarose Gel	For 1X 7 cm by 7cm Agarose Gel	
	Molecular Grade Agarose	1.25 g
	Midori Green	3 µL
	1X TAE Buffer	50 mL
2.5 % Agarose Gel	For 1X 15 cm by 15 cm Agarose Gel	
	Molecular Grade Agarose	5.5 g
	Midori Green	13.2 µL
	1X TAE Buffer	220 mL

2.1.2 Equipment

BD Accuri™ C6 Flow Cytometer

Becton Dickinson

Oxford, UK

BD FACSCalibur™ Flow Cytometer

Becton Dickinson

Oxford, UK

BD FACSVerse™ Flow Cytometer

Becton Dickinson

Oxford, UK

BioTek Synergy™ HT microplate reader Product Number 7091000

BioTek® Instruments, Inc.

Vermont, USA

Blue Cooling Unit Product Number 1703919

Bio-Rad

Hertfordshire, UK

Buffer Tank and Lid Product Number 1658040

Bio-Rad

Hertfordshire, UK

Centrifuge angle rotor, 24 x 1.5/2.2 ml, incl lid Product Number 12154

Sigma

Harz, Germany

Centrifuge rotor buckets Product Number 13190

Sigma

Harz, Germany

Cytology Insert Product Number 15224

Sigma Laborzentrifugen GmbH

Osterode am Harz, Germany

Cytology Support Container Product Number 115223

Sigma Laborzentrifugen GmbH

Osterode am Harz, Germany

Cytospin Swing-out Cytology Buckets Product Number 13224

Sigma Laborzentrifugen GmbH

Osterode am Harz, Germany

Cytospin Swing-out Cytology Rotor Product Number 11224

Sigma Laborzentrifugen GmbH

Osterode am Harz, Germany

Foam Pads for Mini Trans-Blot® Cell Product Number 1703933

Bio-Rad

Hertfordshire, UK

Gel Releasers Product Number 1653320

Bio-Rad

Hertfordshire, UK

GXM-XDS-5 40X-400X Research, Inverted Biological, Product Number 0456

Phase Contrast, Microscope

GT Vision

Suffolk, UK

Hirschmann Laborgerate Neubauer-Improved Product Number 8100104

Counting chamber Haemocytometer

Hirschmann Laborgeräte GmbH & Co. KG

Eberstadt, Germany

Leica TSC SPE 1000 Confocal Microscope

Leica Microsystems

Mannheim, Germany

Milli-Q® Integral 3 Water Purification System Product Number ZRXQ003WW

Merck/Millipore

Hertfordshire, UK

Mini Cell Buffer Dams Product Number 1653130

Bio-Rad

Hertfordshire, UK

Mini Gel Holder Cassette Product Number 1703931

Bio-Rad

Hertfordshire, UK

Mini Trans-Blot Central Core Product Number 1703812

Bio-Rad

Hertfordshire, UK

Mini Trans-Blot® Electrophoretic Transfer Cell Product Number 1703930

Bio-Rad

Hertfordshire, UK

Mini-PROTEAN Comb, 15-well, 1.0 mm, 26 µl Product Number 1653360

Bio-Rad

Hertfordshire, UK

Mini-PROTEAN® Comb, 10-well, 1.0 mm, 44 µl Product Number 1653359

Bio-Rad

Hertfordshire, UK

Mini-PROTEAN® Short Plates Product Number 1653308

Bio-Rad

Hertfordshire, UK

Mini-PROTEAN® Tetra Vertical Electrophoresis Cell, 4-gel, for 1.0 mm thick handcast gels Product Number 1658001FC

Bio-Rad

Hertfordshire, UK

Mini-PROTEAN® Tetra Cell Casting Module Product Number 1658013

Bio-Rad

Hertfordshire, UK

Mini-PROTEAN® Tetra Companion Running Module Product Number 1658038

Bio-Rad

Hertfordshire, UK

Mini-PROTEAN® Tetra Electrode Assembly Product Number 1658037

Bio-Rad

Hertfordshire, UK

Mr. Frosty™ Freezing Container Product Number 5100-0001

ThermoScientific

Loughborough, UK

NanoDrop™ One Microvolume UV-Vis Spectrophotometer Product Number ND-ONE-W

Thermo Fisher

Loughborough, UK

Odyssey® Fc Imaging System LI-COR Product Number 2801-00SPCM

Biosciences UK Ltd

Cambridge, UK

PowerPRO 300 Power Supply, 300V, 700mA, 150W Product Number 5055323269479

Cleaver Scientific

Warwickshire, UK

Refrigerated SIGMA 3-16KL Centrifuge Product Number 146119

Sigma

Harz, Germany

Spacer Plates with 1.0 mm Integrated Spacers Product Number 1653311

Bio-Rad

Hertfordshire, UK

Swing out rotor for 4 buckets, basic rotor Product Number 11180

Sigma

Harz, Germany

Thermo Scientific Multiskan GO Plate Reader Product Number N10588

Thermo Fisher

Loughborough, UK

Bio-Rad CFX96 Touch Real-Time PCR Detection System Product Number 1855196

Bio-Rad

Hertfordshire, UK

Mini-Sub Cell GT Cell Electrophoresis Tank Product Number 1704487EDU

Bio-Rad

Hertfordshire, UK

Mini-Gel Caster Product Number 1704422EDU

Bio-Rad

Hertfordshire, UK

15-well Fixed Height Comb Product Number 1704465EDU

Bio-Rad

Hertfordshire, UK

Sub-Cell GT Horizontal Electrophoresis System Product Number 1704401

Bio-Rad

Hertfordshire, UK

Sub-Cell GT Casting Gates Product Number 1704415

Bio-Rad

Hertfordshire, UK

30-Well Comb, Fixed Height, 1.5 mm Thickness Product Number 1704449

Bio-Rad

Hertfordshire, UK

ChemiDoc™ Touch Gel Imaging System Product Number 1708370

Bio-Rad

Hertfordshire, UK

Stuart SSL4 See-Saw Rocker Product Number MIX2066

Bibby Scientific Ltd

Staffordshire, UK

2.1.3 Software

BD CellQuest™ Pro software

Becton Dickinson

Oxford, UK

BD FACSuite™ software

Becton Dickinson

Oxford, UK

Empiria Studio Analysis Software Product Number 9141-500

LI-COR Biosciences UK Ltd

Cambridge, UK

Gen5 Microplate Reader and Imager Software

BioTek® Instruments, Inc.

Vermont, USA

Image Studio 5.x CLx Product Number 3600-500

LI-COR Biosciences UK Ltd

Cambridge, UK

Image Studio Lite Version Number 5.2.5

LI-COR Biosciences UK Ltd

Cambridge, UK

LAS X Software

Leica Microsystems

Mannheim, Germany

ModFit LT Version Number 5.0.9

Verity Software House

Topsham, Maine, USA

Odyssey Fc Image Studio Analysis Software Product Number 2800-500

LI-COR Biosciences UK Ltd

Cambridge, UK

SkanIt Software Product Number 5187139

Thermo Fisher

Loughborough, UK

Bio-Rad CFX Maestro 1.1 software version Product Number 12013758

4.1.2433.1219

Bio-Rad

Hertfordshire, UK

2.2 Methods

2.2.1 Cell Culture

DAUDI Burkitt's Lymphoma (ECACC 85011437) and Jurkat E6.1 T cell leukaemia (ECACC 88042803) cell lines were maintained according to the instructions issued by the European Collection of Authenticated Cell Cultures (ECACC). Cells were cultured in 25 cm^2 vented cell culture flasks in RPMI 1640 medium (supplemented with 25mM HEPES and L-Glutamine) (Lonza, Verviers, Belgium) with 10 % Foetal Bovine Serum (FBS) (% v/v) (subsequently referred to as complete media). Cell culture flasks were maintained at 37 °C in 5 % CO_2 atmosphere in humidified incubators. Cells were passaged when flasks reached approximately 80 % confluence and maintained at a cell density of approximately $4x10^5$ cells/mL.

2.2.2 Cell Counting

In preparation of each assay, DAUDI and Jurkat cells were counted using the trypan blue exclusion method. Two 100 µL aliquots of cell culture were removed from the relevant flasks and placed into 0.5 mL Eppendorf tubes. A 100 µL volume of trypan blue (0.4 %) solution was then added to each Eppendorf tube and mixed thoroughly using a pipette. A 10 µL volume from each Eppendorf tube was loaded to each chamber of a Hirschmann haemocytometer with cover slip and viewed using a bright-field microscope. Cells were counted in the 0.04 mm centre square and in four 0.04 mm corner squares, this was repeated twice and an average was taken (n=4). Cells that had taken up the trypan blue and hence were non-viable were excluded from the counts. The total number of cells per 1 mL was then calculated using the following formula:

1

Total number of cells per mL = cell count x 5 x dilution factor x 10,000

2.2.3 Seeding cells in preparation for treatment

The seeding density of the cells used was dependent on the specific assay being performed and ranged from 5 x 10^4 to 1 x 10^6 cells/well. Cells were re-suspended in fresh complete media prior to seeding into culture plates.

An equal volume of cells and test compound was loaded into each well, with each concentration of compound repeated in triplicate (n=3). Each assay plate also contained untreated control samples, which contained cell culture and an equal volume of fresh complete media to allow for comparison between treated and untreated cell populations. For assays that required it, positive (pos) or negative (neg) controls, including dead cell control samples or apoptotic/necrotic controls were included. Preparation of these controls are specified in the relevant sections.

2.2.4 Preparation of Thienopyridine Compounds

Stock solutions of novel thienopyridine compounds were reconstituted from powdered solute supplied by our collaborators at the University of Auckland using DMSO (Fisher BioReagents, Loughborough, UK) to give a final concentration of 15 mM (Table 2-8 to Table 2-10) prepared using aseptic conditions in a class 2 biosafety cabinet. Thienopyridines have been loosely grouped by the shared features of the chemical structures into three working groups, the cyclooctane-ring containing compounds (Table 2-8), the cycloheptane-ring containing compounds (Table 2-9) and the cyclohexanone-ring containing compounds (Table 2-10).

From these stock solutions, working solutions were made via serial dilution, with a log concentration scale (100 µM to 0.001 µM). These concentrations were selected for the preliminary investigations based on research that had been conducted using these compounds against the National Cancer Institute NCI60 panel of cells (Shoemaker, 2006).

Table 2-8 Molecular weights and chemical structures of the Cyclooctane-ring containing thienopyridine compounds.

Compound Name	Molecular weight	Molecular structure
DJ0014	431.48	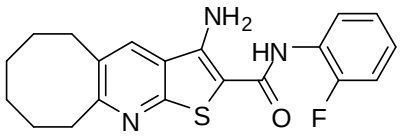
DJ0021	381.49	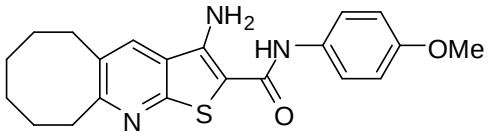
DJ0199	351.47	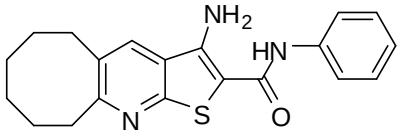
DJ0206	444.39	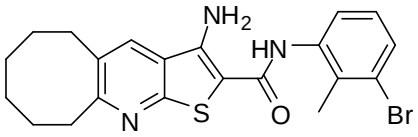
DJ0209	447.94	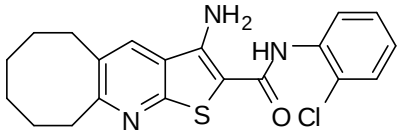

Table 2-9 Molecular weights and chemical structures of the Cycloheptane-ring containing thienopyridine compounds.

Compound Name	Molecular weight	Molecular structure
DJ0081	385.91	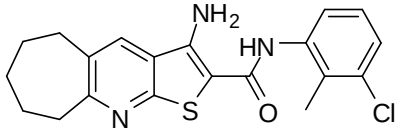
DJ0041	349.46	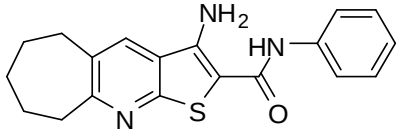

Table 2-10 Molecular weights and chemical structures of the Cyclohexanone-ring containing thienopyridine compounds.

Compound Name	Molecular weight	Molecular structure
DJ0097	371.84	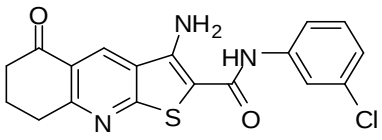
DJ0109	367.39	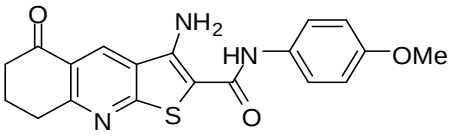
DJ0171	371.84	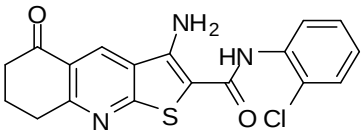

2.2.5 Preparation of Paclitaxel and Nocodazole controls

Control drugs with known effects on tubulin destabilisation were used as controls, with nocodazole selected as a known tubulin destabiliser and paclitaxel selected as a known tubulin stabiliser. DAUDI cells were cultured, counted and seeded as per 2.2.1, 2.2.2, and 2.2.3. Both paclitaxel (SLS, Nottingham, UK) and nocodazole (SLS, Nottingham, UK) were reconstituted to 2 mM stock concentrations in DMSO. Both treatments were then diluted to working concentrations as required by each relevant assay.

2.2.6 Plate treatment of DAUDI Cells

DAUDI cells were maintained as per Section 2.2.1, counted as per Section 2.2.2 and seeded as per Section 2.2.3. Thienopyridine treatments were prepared as per Section 2.2.4 with an equal volume of working solution added to each well containing cells and complete media.

Cells were incubated in the presence of thienopyridine compounds for up to 72 h at 37 °C in 5 % CO_2 atmosphere, in humidified conditions.

2.2.7 Flask treatment of DAUDI Cells

DAUDI cells were maintained as per Section 2.2.1 and counted as per Section 2.2.2. The seeding density of the cells for flask treatment was 1 x 10^7 cells in 10 mL of complete media containing Thienopyridine treatments or complete media alone for untreated controls.

Thienopyridine treatments were prepared as per Section 2.2.4 with the following modifications:

For 1 µM concentration: A 1 µL volume of 15 mM stock solution was diluted into 14 µL fresh complete media in a 0.5 mL Eppendorf Tube to make a 1 mM stock solution. A 10 µL volume of 1 mM stock solution was then diluted in 10 mL of fresh complete media.

For 10 µM concentration: A 6.67 µL volume of 15 mM stock solution was added to 10 mL of fresh complete media.

Cells were incubated in the presence of thienopyridine compounds for up to 72 h at 37 °C in 5 % CO_2 atmosphere, in humidified conditions.

2.2.8 MTS Assay

MTS or 5-[3-(carboxymethoxy)phenyl]-3-(4,5-dimethyl-2-thiazolyl)-2-(4-sulfophenyl)-2H-tetrazolium inner salt, is a solubilised tetrazolium salt-based colorimetric cell proliferation assay for the measurement of cell activity in response to potential cytotoxic compounds (Berridge et al., 2005). Similar to other tetrazolium salt-based assays (e.g., MTT, XTT, WST-1), MTS is reduced by NAD(P)H and at the cell surface to a coloured formazan product, the absorbance of which can be detected spectrophotometrically at 490 nm. Production of the formazan product indicates that cells are metabolically active and can be used as an indicator of cell proliferation or cell viability, but does not offer any information on the mechanism of how viability has been affected (Berridge et al., 2005). Unlike MTT, MTS does not form a crystalised product on reduction and therefore does not require additional processing steps,

which makes it more suitable for use with suspension cell lines such as DAUDI which have been used in this thesis (Mossman, 1983; Berridge et al., 2005).

Cells were counted and adjusted to the required cell count/mL as per section 2.2.2 and 2.2.3. Cells were adjusted to $5x10^4$ to $5x10^5$ cells/well, as per manufacturer's instructions, in 50 µL of fresh complete medium and were loaded in to a 96-well plate. An equal volume (50 µL) of compound was added to the plate. When preparing the working solutions of the compounds, they were prepared at double concentration to account for the 1:1 dilution upon adding drug to the cell culture. Untreated control samples were treated with an equal volume of complete media. A "dead cell control" was also set up with cells treated with 100 % ethanol (50 % ethanol following dilution with cells). Treatments were incubated for up to 72 h at 37 °C in 5 % CO_2 atmosphere, in humidified conditions. Post-incubation, the contents of each well were removed from the 96-well plate and transferred in to 0.5 mL Eppendorf tubes and centrifuged at 500 *g* for 5 min to remove supernatant and treatment compounds. The cell pellet was then re-suspended in an equal volume of fresh complete and placed back into the 96-well plate in the corresponding well. A 20 µL volume of CellTiter 96® AQueous One Solution Cell Proliferation Assay (MTS) (Promega, Southampton, UK) was added to each well containing cells and incubated for 2.5 h. Following incubation, the absorbance of each well was read at 490 nm using a BioTek Synergy™ HT microplate reader (GT Vision, Suffolk, UK).

2.2.9 Annexin V / Propidium Iodide Assay

Flow cytometric techniques utilising Annexin V-FITC conjugated antibodies, which bind to phospholipid proteins in the cell membrane, in conjunction with propidium iodide staining of DNA, are well established for the investigation of novel compounds and their potential effects on cell death (Menyhart et al., 2016). Phosphatidylserine is a phospholipid which is expressed on the inner cell membrane in healthy cells, but a characteristic of apoptosis is its exposure on the cell surface, which aids phagocytosis of cells or cell debris by neighbouring or immune cells in programmed cell death (Crowley et al., 2016). The 36 kDa protein Annexin V binds to

phosphatidylserine with high affinity in a calcium dependent manner, meaning that FITC and other fluorophores can be bound to Annexin V to provide an indication of the number of apoptotic cells present in a sample (Vermes et al., 1995; van Engeland et al., 1996; Crowley et al., 2016). The DNA dye propidium iodide is impermeable to cell membranes in health cells, but will readily bind to DNA released during cell rupture in necrosis and in permeabilised membranes in apoptosis (Crowley et al., 2016). These properties allow cells to be categorised relative to their fluorescence using flow cytometry, by plotting Annexin V-FITC against propidium iodide and using quadrants to identify single or dual stained cells, with cells negative for both Annexin V-FITC/propidium iodide deemed healthy, positive for AV-FITC alone indicating early apoptosis, positive for both AV-FITC and PI deemed to be in late apoptosis and positive for PI alone indicating necrosis (Vermes et al., 1995; van Engeland et al., 1996; Rasola and Geuna, 2001).

Cells were counted and adjusted to the required cell count/mL as per section 2.2.2 and 2.2.3. Cells were adjusted to $1x10^5$ cells/well in 50-100 µL of fresh complete medium (dependent on duration of incubation) and were loaded in to a 96-well plate. When preparing the working solutions of the compounds, they were prepared at double concentration to account for the 1:1 dilution upon adding drug to the cell culture.

Up to three compounds were analysed per plate. Untreated control and "no stain control" samples were treated with an equal volume of complete media. A positive necrosis control (dead cell) was set up with cells treated with 100 % ethanol (50 % ethanol following dilution with cells) for 24 h. On the day of analysis, a positive apoptosis control was set up by removing untreated controls into 0.5 mL Eppendorf tubes and heating for 2 h at 43 °C in a water bath. Treatments were incubated for up to 72 h at 37 °C in 5 % CO_2 atmosphere, in humidified conditions.

Post-incubation, the contents of each well were removed from the 96-well plate and transferred in to 2 mL Eppendorf tubes and centrifuged at 500 *g* for 5 min to remove supernatant and treatment compounds. The supernatant was removed by careful pouring to minimise cell loss, and the cell pellet was washed in 300 µL of ice-cold

Dulbecco's Phosphate Buffered Saline (DPBS) (LONZA, Belgium) and centrifuged for a further 5 min at 500 *g*. The supernatant was removed by careful pouring and the cell pellet was re-suspended in 100 µL 1X Annexin V binding buffer (BD Pharmingen™, Oxford, UK) and the sample transferred to a flow cytometry tube (Corning, Tamaulipas, Mexico).

All treated samples and untreated controls were then double stained with 5 µL FITC-Annexin V (BD Pharmingen™, Oxford, UK) and 10 µL of 50 µg/mL Propidium Iodide solution (BD Pharmingen™, Oxford, UK) and incubated in the dark, at room temperature, for 15 minutes. The positive necrosis control was single stained with 10 µL of 50 µg/mL Propidium Iodide solution (BD Pharmingen™). The positive apoptosis control was single stained with 5 µL of FITC-Annexin V (BD Pharmingen™). For single stained controls, the volume of the missing stain was replaced with an equal volume of 1X binding buffer, to ensure all samples had an equal total volume. No stain controls received no staining. Following staining, 400 µL 1X Annexin V binding buffer (BD Pharmingen™) was added to each sample and analysed using the BD FACSVerse™ Flow Cytometer (BD Bioscience, UK) and BD FACSuite™ software (BD Bioscience, UK) or the BD Accuri C6 Flow Cytometer C6 software (BD Bioscience, UK).

2.2.10 Cell Cycle Assay

DAUDI Cells were counted and adjusted to the required cell count/mL as per sections 2.2.2 and 2.2.3. Cells were adjusted to 1 x 10^6 cells/well in 100 µL of fresh complete medium and were loaded in to a 96-well plate. An equal volume (100 µL) of compound was added to the plate. When preparing the working solutions of the compounds, they were prepared at double concentration to account for the 1:1 dilution upon adding drug to the cell culture.

The compounds were tested at concentrations of 100 µM, 10 µM and 1 µM in triplicate. Untreated and “no stain controls” were treated with an equal volume of complete media. Treatments were incubated for up to 72 h at 37 °C in 5 % CO_2 atmosphere, in humidified conditions.

Post-incubation, the contents of each well were removed from the 96-well plate and transferred in to 2 mL Eppendorf tubes and centrifuged at 500 *g* for 5 min to remove supernatant and treatment compounds. The supernatant was removed by careful pouring to minimise cell loss, and the cell pellet was washed in 500 µL of ice-cold Dulbecco's Phosphate Buffered Saline (DPBS) (LONZA) and centrifuged for a further 5 min at 500 *g*. The supernatant was removed by careful pouring and the cell pellet was then fixed and permeabilised by the dropwise addition of 500 µL ice cold 70 % ethanol (Fisher Chemical, UK) while vortexing the sample, to minimise cell clumping. Cells were then fixed for a minimum of 30 minutes at 4 °C.

The cells were then centrifuged at 850 *g* for 5 min and the ethanol removed by gentle pouring. Cells were washed in 500 µL DPBS (Lonza) and centrifuged for a further 5 min at 850 *g.* The cell pellet was re-suspended in 50 µL of 100 µg/mL RNAse A (Fisher Scientific, UK) to prevent staining of RNA by Propidium Iodide. Cells were then stained with 200 µL of 50 µg/mL Propidium Iodide, transferred to flow cytometer tubes and incubated in the dark at 4°C for a minimum of 30 min.

Following staining, 500 µL of FACS Flow solution (BD Bioscience, UK) was added to each sample and cell cycle analysis was analysed using the BD FACSCalibur™ Flow Cytometer (BD Bioscience, UK) and BD CellQuest™ Pro software (BD Bioscience, UK). Data was analysed using ModFit LT 5.0 software (Verity Software House, USA).

2.2.11 Tubulin Polymerisation Assay

This assay was performed as per the manufacturer's instructions included in the HTS-Tubulin Polymerization Assay Biochem Kit™ (>97% pure tubulin, Porcine Tubulin) (Cytoskeleton, Inc., Denver, USA). It is a turbidometric-based assay which allows for the investigation of any direct effects of novel compounds on isolated tubulin *in vitro* (Davis et al., 2010). Based upon the method first identified by Shelanski et al. (1973) and refined by Lee and Timasheff (1977), the assay utilises tubulin isolated and purified from porcine brain in combination with microtubule associated proteins (MAPs) to measure the spontaneous dynamic polymerisation of tubulin in a 96-well

plate format, whereby the absorbance of each well (e.g., the amount of light scattered in the well) is proportional to the polymerisation of tubulin into microtubules.

2.2.11.1 Preparation of Buffers

General Tubulin Buffer (PEM buffer) (80 mM PIPES pH 6.9, 2 mM $MgCl_2$, 0.5mM EGTA) (Cytoskeleton, Inc) was reconstituted in 10 mL dH_2O and stored at room temperature until use. Guanosine triphosphate (GTP) stock solution (Cytoskeleton, Inc) was reconstituted to 100 mM concentration in ice cold (4 °C) dH_2O and stored on ice until use. G-PEM Buffer (PEM buffer plus GTP) (80 mM PIPES pH 6.9, 2 mM $MgCl_2$, 0.5mM EGTA, 1 mM GTP) (Cytoskeleton, Inc.) was prepared by the dilution of GTP stock solution to 1 mM concentration in General Tubulin Buffer and stored on ice until use.

2.2.11.2 Preparation of Thienopyridines and Controls

Thienopyridine compounds were diluted from 15 mM stock solutions as per section 2.2.4 to 2 mM in DMSO (Fisher BioReagents) and final volume of 15 µL. A 2 mM stock solution of paclitaxel (Cytoskeleton, Inc.) was reconstituted in 100 µL DMSO (Fisher BioReagents). Both thienopyridines and paclitaxel were then diluted to a working concentration of 100 µM in G-PEM Buffer (Cytoskeleton, Inc.), as per manufacturer's specifications, which was 10x concentrated to account for 1:10 dilution in the wells of 96-well plate for the assay.

2.2.11.3 Preparation of Porcine Tubulin Protein

Porcine Tubulin Protein (Cytoskeleton, Inc.) was reconstituted in ice cold (4 °C) dH_2O in G-PEM Buffer (Cytoskeleton, Inc.) to a working concentration of 4 mg/mL and stored on ice until use. The Porcine Tubulin stock solution used in this assay is 97 % pure tubulin and also contains microtubule associated proteins (MAPs) which enhance the rate of tubulin polymerisation during the nucleation phase of the assay.

2.2.11.4 Plate Reader Set Up and Kinetic Assay

A protocol for the kinetic assay was set up using SkanIt Software (Thermo Fisher, Loughborough, UK) on a microplate reader (Multiskan Go, Thermo Fisher, Loughborough, UK). A half area 96-well plate (Corning Life Sciences, Loughborough, UK) was pre-heated to 37 °C for 30 minutes followed by ejection of plate for loading of 10 µL of thienopyridine compounds plus paclitaxel tubulin stabiliser control (Cytoskeleton, Inc.) and G-PEM buffer untreated controls (Cytoskeleton, Inc.) in duplicate. The plate was then heated for a further 2 minutes at 37 °C before loading of 100 µL ice cold 4 mg/mL tubulin in G-PEM buffer (Cytoskeleton, Inc.) to each well containing thienopyridines or controls using a multichannel pipette. The plate was immediately placed back into the microplate reader (Multiskan Go, Thermo Fisher, Loughborough, UK) at 37 °C to initiate tubulin polymerisation and the kinetic assay started. The 96-well plate was shaken on medium setting for 5 seconds and was recorded at absorbance at 340 nm every 30 seconds for 61 minutes in total, with the temperature maintained at 37 °C throughout the assay. Data was recorded using SkanIt Software (Thermo Fisher, Loughborough, UK) and exported as an Excel file for analysis.

2.2.11.5 Data Analysis

Average rate of reaction (in section 4.4) for the kinetic assay was calculated by the least linear squares method in SkanIt Software and statistics were exported to Microsoft Excel for analysis.

Calculated rates of reaction for G-PEM, Paclitaxel and each thienopyridine were then calculated as the fold change of the G-PEM control and visualised in GraphPad Prism (version 8.1.1).

2.2.12 Western Blotting

2.2.12.1 Preparation of cells

DAUDI cells were maintained as per Section 2.2.1, counted as per Section 2.2.2 and seeded in flasks as per Section 2.2.7.

2.2.12.2 Protein Extraction

Post-incubation, the contents of each flask was transferred in to 15 mL falcon tubes and centrifuged at 500 *g* for 5 min to remove supernatant and treatment compounds. The cell pellet was then re-suspended in 300 µL DPBS and the cells transferred to a 2 mL Eppendorf tube on ice. Cells were then centrifuged at 500 *g* for 5 min to remove supernatant. The cell pellet was then re-suspended in 300 µL of RIPA lysis buffer (Table 2-1) containing 1:1000 Protease Inhibitor Cocktail (SIGMA, Dorset, UK) and 1:1000 Phosphatase Inhibitor Cocktail 2 (SIGMA, Dorset, UK). Cells were incubated on ice throughout lysis for 30 minutes with samples vortexed for 20 seconds at 5 minute intervals throughout. Cells were then centrifuged at 13500 *g* in a pre-chilled centrifuge at 4 °C for 10 minutes to remove cell debris/lysis products. Protein lysates were then transferred to new 2 mL Eppendorf tubes on ice and the cell pellet discarded. A 50 µL aliquot of each protein lysate for theinopyridine treated and untreated controls was then transferred to a 0.5 mL Eppendorf tube to complete protein quantification. Protein lysates were transferred from ice to a -20 °C freezer for storage.

2.2.12.3 Protein Quantification

Protein concentration was calculated using the Pierce BCA Protein Assay Kit (Thermo Scientific, Loughborough, UK) using the microplate procedure, with theinopyridine and untreated control protein lysates compared to a concentration gradient of known concentrations of bovine serum albumin (BSA).

Protein lysate replicates (n=2) of 25 µL were pipetted into a 96 well plate, together with separate BSA standards (n=2) in a concentration range of 2000 µg/mL to 25

µg/mL (with a 0 µg/mL blank). To each well containing protein lysate/BSA standards, 200 µL of bicinchoninic acid (BCA) working reagent (Table 2-2) was added and then the plate was incubated at 37°C for 30 minutes. Following incubation, the absorbance of each well was read at 562 nm using a BioTek Synergy™ HT microplate reader (GT Vision, Suffolk, UK).

A standard curve was plotted to show BSA standards versus protein concentration, with a trendline and straight-line equation (2) added to the graph using Microsoft Excel.

Treated and untreated protein lysate concentrations were calculated using the straight-line equation:

2

$$y = mx + c$$

Where y equals absorbance, x equals protein lysate concentration, m equals the gradient of the line and c equals where the straight line intercepts the y-axis.

By rearranging equation [2], the concentrations of the protein lysates (x) were calculated using the absorbance values recorded in the BCA assay:

3

$$x = (y - c) / m$$

2.2.12.4 Protein Dilution

With the protein lysate sample concentrations calculated, the lysate samples were then diluted to the desired concentrations for each western blot using RIPA lysis buffer (Table 2-1) with a final volume of 12-15 µL as required for individual western blot analysis.

2.2.12.5 Gel Casting

Bis-Acrylamide gels were hand cast using Bio-Rad casting stands and glass plates supplied with the Mini-PROTEAN Tetra system (Bio-Rad, Hertfordshire, UK).

Glass casting spacer and short plates (Bio-Rad, Hertfordshire, UK) were secured using clamps frames and loaded onto Mini-PROTEAN® Tetra Cell Casting Stand (Bio-Rad, Hertfordshire, UK), with base of glass plates in contact with gasket (Bio-Rad, Hertfordshire, UK).

2.2.12.6 Resolving and stacking gels

Resolving gel was made following the recipe supplied with the Bio-Rad TGX Stain-Free™ FastCast™ Acrylamide Kit, 10 % (Table 2-3). For each gel cast, 2.5 mL Resolver A (acrylamide/bis acrylamide) and 2.5 mL of Resolver B (Tris-HCL buffer) were mixed in a Universal Container. To this, 25 µL of fresh 10 % w/v Ammonium Persulfate (Table 2-1) and 2.5 µL of TEMED (tetramethylethylenediamine – Bio-Rad, Hertfordshire, UK) were added, with the solution pulse vortex mixed for 5 seconds and then loaded to the casting plates.

Stacking gel was made following the recipe supplied with the Bio-Rad TGX Stain-Free™ FastCast™ Acrylamide Kit, 10 % (Table 2-3). For each gel cast, 750 µL of Stacker A (acrylamide/bis acrylamide) and 750 µL of Stacker B (Tris-HCL buffer) were mixed in a Universal Container. To this, 7.5 µL of fresh 10 % Ammonium Persulfate and 1.5 µL of TEMED were added, with the solution pulse vortex mixed for 5 seconds and then loaded on top of the resolving gel to the casting plates. A well comb was then inserted to the top of the gel and gels were allowed to polymerise for up to 45 minutes until fully set.

2.2.12.7 Protein Lysate Denature and Boiling

DAUDI cell lysates for each blot were defrosted on ice, then pulse centrifuged for 5 seconds to ensure all of lysate located at the bottom of the Eppendorf tubes. A 4X concentration of Protein Sample Loading Buffer for Western Blots (LI-COR

Biosciences UK Ltd, Cambridge, UK) was prepared by the addition of 1:10 dilution of β-mercaptoethanol (SIGMA, Dorset, UK). A volume of 3 µL 4X Loading Buffer was added to each 12 µL protein lysate sample, with samples kept on ice throughout.

Samples were then transferred to a heat block and boiled at 95 °C for 10 minutes to denature and add a negative charge to the proteins in preparation for separation during gel electrophoresis. Following boiling, protein lysates were pulse centrifuged for 5 seconds and then kept on ice until they were ready to be loaded on the acrylamide gels.

2.2.12.8 Gel tank preparation

Gels were loaded into the Mini-PROTEAN® Tetra Electrode Assembly (Bio-Rad, Hertfordshire, UK) with gel combs facing inwards. The Electrode Assembly was then loaded into the Mini-PROTEAN Vertical Electrophoresis tank (Bio-Rad, Hertfordshire, UK) and the tank was filled with SDS Running Buffer (Table 2-1) to level indicated on the tank casing, and to the height of the gel plates in the Electrode Assembly. Where four gels were to be run, additional gels were loaded into the Mini-PROTEAN® Tetra Companion Running Module (Bio-Rad, Hertfordshire, UK) with this also loaded into the Mini-PROTEAN Electrophoresis tank. When one gel was to be run, a Mini Cell Buffer Dam (Bio-Rad, Hertfordshire, UK) was used to seal the Electrode Assembly in place of a second gel. Gel combs were removed from each gel carefully to prevent bubbles entering the wells.

2.2.12.9 Loading Protein Lysates and Molecular Weight Ladder

Each gel was loaded with a minimum of one well containing Chameleon Duo Pre-stained Protein Ladder (LI-COR Biosciences UK Ltd, Cambridge, UK), to allow for quantification of bands of interest by comparison to protein markers of a known molecular weight. DAUDI cell lysates were then loaded to the remaining empty wells in each gel, with care taken to avoid lysates spilling over into neighbouring wells. A

blot plan was then recorded to identify the location of each lysate in all the gels being run.

2.2.12.10 Gel Electrophoresis and Membrane Transfer

The Mini-PROTEAN Electrophoresis tank (Bio-Rad, Hertfordshire, UK) was connected to PowerPRO 300 Power Supply (Cleaver Scientific, Warwickshire, UK) and proteins were resolved at a constant voltage of 100 volts for 90 minutes. During electrophoresis, fresh transfer buffer was prepared (Table 2-1) and six sheets of Whatman 3MM Chr filter paper (GE Healthcare Life Sciences, Buckinghamshire, UK) per gel were cut to fit the transfer cassette.

Following electrophoresis, gels were removed from the glass plates using gel releasers (Bio-Rad, Hertfordshire, UK) and transferred to a container filled with transfer buffer (Table 2-1) to equilibrate for 15 minutes. Immobilon-FL PVDF membrane (Merck/Millipore, Hertfordshire, UK) was 'wetted' in 100 % methanol (Fisher Scientific, Loughborough, UK) for up to 1 minute and then equilibrated in transfer buffer for 15 minutes, together with filter papers and Foam Pads for Mini Trans-Blot® Cell (Bio-Rad, Hertfordshire, UK), all in separate containers.

Post equilibration, the transfer stack cassette was built as shown in Figure 2-1. Transfer cassettes (Bio-Rad, Hertfordshire, UK) were loaded into the Mini Trans-Blot Central Core (Bio-Rad, Hertfordshire, UK) with care taken to ensure black side of cassette faced the black electrode (cathode), and clear plastic side faced the red electrode (anode). The Central Core was then loaded to Mini Trans-Blot® Electrophoretic Transfer Cell, together with the Blue Cooling Unit (Bio-Rad, Hertfordshire, UK) to prevent the transfer system from overheating during transfer. A magnetic flea was placed in the gel tank, and the tank placed on a magnetic stirrer, to ensure circulation of buffer during transfer. Proteins were transferred from the gel to the membrane at constant voltage of 100 volts and constant current of 350 mA for 60 minutes.

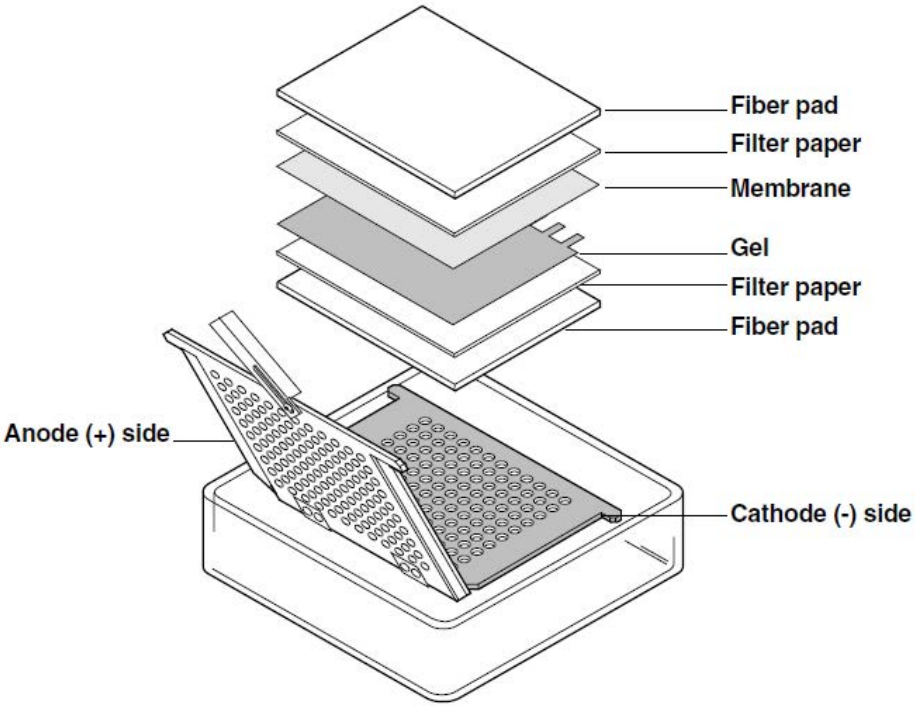

Figure 2-1 Western Blot 'Wet Transfer' Cassette Stack. The transfer stack was built by placing a fiber pad on the cathode (black) side of the transfer cassette. On top of this, filter paper was placed and rolled to eliminate any air bubbles followed by careful placement of the acrylamide gel. A PVDF membrane was then placed on top of the gel, followed by filter paper and again this was rolled to eliminate air bubbles. A second fiber pad was positioned at the top of the stack, rolled again to eliminate air bubbles, and then the cassette was closed. All pads, filter paper, gel and membrane had been equilibrated in transfer buffer for 20 minutes prior to building the transfer cassette stack. Adapted from Bio-Rad.(Unknown) *'Trans-Blot Electrophoretic Transfer Cell Instruction Manual'. [Online][Accessed 9th July 2020] https://www.bio-rad.com/webroot/web/pdf/lsr/literature/M1703910D.pdf*

2.2.12.11 Total Protein Stain

To check the quality of the protein transfer from the acrylamide gel to the PVDF membrane, membranes were stained for using the Li-Cor REVERT Total Protein staining kit (LI-COR Biosciences UK Ltd, Cambridge, UK) as per the manufacturer's instructions. Briefly, membranes were rinsed with dH_2O, transferred to a clean square Petri Dish (Thermo Scientific, Loughborough, UK) and then had 5 mL REVERT Total Protein Stain (LI-COR Biosciences UK Ltd, Cambridge, UK) pipetted over the membrane. Membranes were then incubated at room temperature on a Stuart SSL4 rocker (Bibby Scientific LTD, Staffordshire, UK) for 5 minutes, followed by REVERT Stain removal and two 30 second washes with REVERT Wash Solution (LI-COR

Biosciences UK Ltd, Cambridge, UK). Membraned were then rinsed in dH_2O and imaged immediately on the 700 nm channel of the Odyssey® Fc Imaging System (LI-COR Biosciences UK Ltd, Cambridge, UK) for a 2 minute exposure.

Membranes were then treated with REVERT Reversal Solution (LI-COR Biosciences UK Ltd, Cambridge, UK) for 10 minutes on a rocker at room temperature, followed by washing in dH_2O and proceeding to blocking and immunoblotting.

2.2.12.12 Blocking

Membranes were blocked using 5 mL Odyssey® Blocking Buffer in Tris Buffer Saline (TBS) (LI-COR Biosciences UK Ltd, Cambridge, UK) for 1 hour at room temperature on a rocker to block any non-specific binding sites.

2.2.12.13 Immunoblotting

Primary antibodies were prepared according to manufacturer's suggested dilutions (Table 2-4) in 2 mL Odyssey® Blocking Buffer in TBS (LI-COR Biosciences UK Ltd, Cambridge, UK). A bench top autoclave bag was cut to fit the membrane, and the membrane was placed inside it, with 2 sides heat sealed. Primary antibody solution was then added to the autoclave bag, any air bubbles were removed and then the remaining side heat sealed. Or blots were incubated in a clean square petri dish in 10 mL of Odyssey® Blocking Buffer in TBS, with the edges of the petri dish lid sealed with Parafilm M (Sigma-Aldrich, Dorset, UK) to prevent evaporation. Blots were then incubated over night at 4 °C on a rocker.

Following incubation with primary antibodies, membranes were washed 4 times in Tris Buffered Saline (Table 2-1) on a rocker at room temperature for 5 minutes per wash. TBS was discarded after each wash step.

Secondary antibodies were prepared to manufacturer's instruction (Table 2-5) in Odyssey® Blocking Buffer in TBS (LI-COR Biosciences UK Ltd, Cambridge, UK) with 0.01 % w/v Sodium Dodecyl Sulfate (SDS) (Fisher Scientific, Loughborough, UK).

For Mouse anti-Human primary antibodies, either IRDye® 680RD Goat anti-Mouse IgG (H + L) fluorescent secondary antibodies (LI-COR Biosciences UK Ltd, Cambridge, UK) or IRDye® 800CW Goat anti-Mouse IgG (H + L) fluorescent secondary antibodies (LI-COR Biosciences UK Ltd, Cambridge, UK) were used.

For Rabbit anti-Human primary antibodies, either IRDye® 680RD Goat anti-Rabbit IgG (H + L) fluorescent secondary antibodies (LI-COR Biosciences UK Ltd, Cambridge, UK) or IRDye® 800CW Goat anti-Rabbit IgG (H + L) fluorescent secondary antibodies (LI-COR Biosciences UK Ltd, Cambridge, UK) were used.

The IRDye® 680RD antibody fluorescence was detected on the 700 nm channel of the Odyssey® Fc Imaging System (LI-COR Biosciences UK Ltd, Cambridge, UK), while the IRDye® 800CW antibody fluorescence was detected on the 800 nm channel.

For multiplex western blots, the most abundant protein (e.g., pan-proteins or housekeeper proteins) was detected using the IRDye® 680RD antibodies while less abundant proteins (e.g., phospho-proteins) were detected using the IRDye® 800CW antibodies in accordance with the manufacturer's instructions.

Following washing in TBS, membranes were incubated with secondary antibodies in a clean square Petri Dish (Thermo Scientific, Loughborough, UK) protected from light on a rocker at room temperature for 1 hour.

Membranes were then washed 4 times in TBS-T (Table 2-1) on a rocker at room temperature for 5 minutes per wash. TBS-T was discarded after each wash step. Membranes were then placed between two pieces of Whatman 3MM Chr filter paper (GE Healthcare Life Sciences, Buckinghamshire, UK) and dried for 20 minutes at 60 °C in a drying cabinet prior to imaging.

2.2.12.14 Imaging

Membranes were imaged using the Odyssey® Fc Imaging System (LI-COR Biosciences UK Ltd, Cambridge, UK). Membranes were imaged on the 700 nm and 800 nm

channels for 2–10-minute exposure on each channel to reduce background fluorescence. Membranes were protected from light throughout.

2.2.12.15 Image Analysis

Blot images were analysed using Image Studio 5.x CLx (LI-COR Biosciences UK Ltd, Cambridge, UK), Image Studio Lite (LI-COR Biosciences UK Ltd, Cambridge, UK) and Empiria Studio Analysis Software (LI-COR Biosciences UK Ltd, Cambridge, UK).

2.2.13 Reverse Transcription Quantitative Polymerase Chain Reaction (RT-qPCR)

2.2.13.1 Preparation of DAUDI cells

DAUDI cells (ECACC 85011437) were counted and adjusted to $1x10^6$ cells/1 mL complete media (Fisher Scientific, Loughborough, UK) as per sections 2.2.2 and 2.2.3. Thienopyridine compounds at 10 µM concentration were prepared as per section 2.2.4, Paclitaxel and Nocodazole positive controls at 10 µM concentration were prepared as per section 2.2.5, with untreated controls prepared with an equal volume of cells and complete media. Each Thienopyridine compound was loaded to cells in triplicate in a 6-well plate and plates were incubated for 48 hours as per section 2.2.5.

2.2.13.2 *Anti-IgM stimulation and storage of cells in RNAlater*

Post-incubation, cells were transferred to 2 mL Eppendorf tubes and centrifuged at 500 *g* for 5 minutes at room temperature, cell media containing Thienopyridine treatments was discarded, the cell pellet was resuspended in 1 mL of serum free RPMI 1640 media and cells were transferred back to a 6-well plate and incubated at 37 °C in 5 % CO_2 atmosphere, in humidified conditions for 15 minutes.

Following this incubation step, cells were transferred to a 1.5 mL Eppendorf tube, centrifuged at 500 *g* for 5 minutes at room temperature and were then washed in 300 µL of DPBS that had been pre-warmed to 37 °C. Cells were centrifuged again at

500 *g* for 5 minutes at room temperature and the cell pellet was resuspended in 144 µL of 37 °C DPBS and then stimulated with 6 µL of Goat F(ab')2 Anti-Human IgM-UNLB (Cambridge Bioscience Cambridge, UK) (concentration 20 µg/µL) for 1 minute with the stimulation halted by the addition of 150 µL of ice cold DPBS.

To prevent the loss of mRNA in the samples, DAUDI cells were then centrifuged at 500 *g* for 5 minutes followed by addition of 200 µL of Ambion RNA*later* Stabilization Solution (Invitrogen (Thermo Scientific), Loughborough, UK) to the cell pellet and then stored overnight at 4 °C. Samples were transferred to a -20 °C Freezer the following day as per RNA*later* instructions, and then stored at -20 °C until extraction and reverse transcription of mRNA to cDNA.

2.2.13.3 RNA extraction, quantification, and reverse-transcription of mRNA to cDNA

All DAUDI cells were defrosted on ice, with RNA*later* solution carefully removed from the cell pellet via pipetting. Total RNA for each sample was then extracted on ice via spin column purification using a Qiagen RNeasy® Mini Kit (Qiagen, Manchester, UK) as per the manufacturer's instructions.

Total RNA concentration was quantified using a NanoDrop™ One Microvolume UV-Vis Spectrophotometer (Thermo Fisher, Loughborough, UK), with 1.5 µL of RNA added to the pedestal of the NanoDrop.

A Bioline Tetro™ cDNA Synthesis Kit (Meridian Bioscience, Nottingham, UK) was used as per manufacturer's instructions for the generation of cDNA from mature mRNA, using Oligo(dT) primers. The cDNA was then stored at -20 °C until use in RT-qPCR.

2.2.13.4 Pooling of cDNA to create cDNA standards

A pooled sample of cDNA, representative of all sample conditions (10 x Thienopyridines, Nocodazole, Paclitaxel and untreated controls), was created as a stock to perform a standard curve dilution series to test primer pair efficiency for

each gene of interest, and to generate a percentage efficiency value for use in normalisation of data relative to reference genes.

2.2.13.5 Dilution of cDNA

Working stocks of cDNA for use in RT-qPCR reactions were made at a 1:10 dilution (18 µL cDNA + 162 µL RT-PCR-grade water (Ambion, Loughborough, UK) containing QuantiNova Yellow Template Dilution Buffer (1:100 dilution) (Qiagen, Manchester, UK)). Samples were stored at -20 °C until use in RT-qPCR.

A 1:10 serial dilution of pooled cDNA, with a range from undiluted pooled cDNA to 1:10000 dilution was created. Stock pooled cDNA was diluted 1:10 with RT-PCR-grade water (10 µL cDNA + 90 µL RT-PCR grade water) to created 1:10 cDNA. This was then serially diluted 1:10 to create 1:100 cDNA, 1:1000 cDNA and 1:10000 cDNA stocks.

A 1:5 (range 1:1 to 1:3125) and a 1:2 (range 1:1 to 1:128) serial dilution series of pooled cDNA, were also created and used to establish primer efficiencies over a narrower range when 1:10 standards was not suitable for the gene of interest due to expression levels.

2.2.13.6 Design of RT-qPCR primers

Primer sequences were designed using the publicly available information available on the United States National Institutes for Health (NIH) National Center for Biotechnology Information (NCBI) 'Gene' and 'Nucleotide' databases, with gene mRNA coding sequences (cds) used in conjunction with the NCBI Primer-BLAST webtool. Where possible, primers were designed to have a product size between 70-200 base pairs (bp), an optimal melt temperature (T_m) of 60 °C and to span and exon-exon junction to exclude annealing to genomic DNA. In cases where these setting did not return suitable primers, product size between 70-300 bp, inclusion of separation of primers by at least one intron on genomic DNA and amendments to T_m were included.

2.2.13.7 Preparation of primer stocks

All primer pairs were reconstituted to a stock concentration of 100 µM by addition of 10 µL of RT-PCR grade water for every 1 nanomolar of primer supplied. Working stocks of each primer were diluted to 14 µM in RT-PCR grade water for use in RT-qPCR reactions.

2.2.13.8 Quality control of primers

2.2.13.8.1 Temperature gradient plates (Tm)

A temperature gradient RT-qPCR reaction was conducted for each primer pair, to confirm optimum primer annealing temperature and to check for the presence of primer dimer formation during PCR cycling conditions. All primers were designed to anneal at 60 °C unless otherwise stated, and a temperature gradient between 55-65 °C (55-70 °C for non-60 °C primers) was used to assess the annealing temperature. Identical cDNA samples taken from pooled untreated control DAUDI samples that had been diluted 1:10 with RT-PCR grade water were loaded to a 96-well Semi-Skirted PCR plate (Star Lab, Milton Keynes, UK) containing RT-qPCR SYBR Green Master Mix (Qiagen, Manchester, UK), forward and reverse primers and RT-PCR grade water as per Table 2-11. A No Template Control (NTC) was also prepared for each primer pair, which contained RT-PCR grade water rather than cDNA in the reaction mix. The NTC sample was loaded in the well corresponding to the 55 °C temperature. The 96-well plates were sealed using Adhesive PCR Plate Seals (Thermo Scientific, Loughborough, UK), with pressure applied to the edges and inter-well gaps using MicroAmp™ Adhesive Film Applicator (Applied Biosystems, Loughborough, UK), to prevent loss of samples through evaporation during heating in the thermocycler.

Table 2-11 RT-qPCR master mix reagent volumes use per reaction. Master mix volumes were scaled up for the total number of reaction (n) required per plate.

Reagent	1 x reaction	n x reactions
SYBR 2x Master Mix	5 µL	n x 5 µL
Primer A (Forward [14 µM])	0.5 µL	n x 0.5 µL
Primer B (Reverse [14 µM])	0.5 µL	n x 0.5 µL
RT-PCR grade water	3 µL	n x 3 µL
cDNA	1 µL	n x 1 µL
Total volume	10 µL	n x 10 µL

2.2.13.8.2 Thermocycling conditions (Tm plates)

Temperate gradient plates were run for 40 cycles with the thermocycling conditions listed in Figure 2-2 and Table 2-12 using the Bio-Rad CFX96 Touch Real-Time PCR Detection System thermocycler (Bio-Rad, Hertfordshire, UK) and Bio-Rad CFX Maestro 1.1 software (Bio-Rad, Hertfordshire, UK) with a temperature gradient from 55 °C to 65 °C (or 55-70 °C for non-60 °C primers) followed by melt curve analysis.

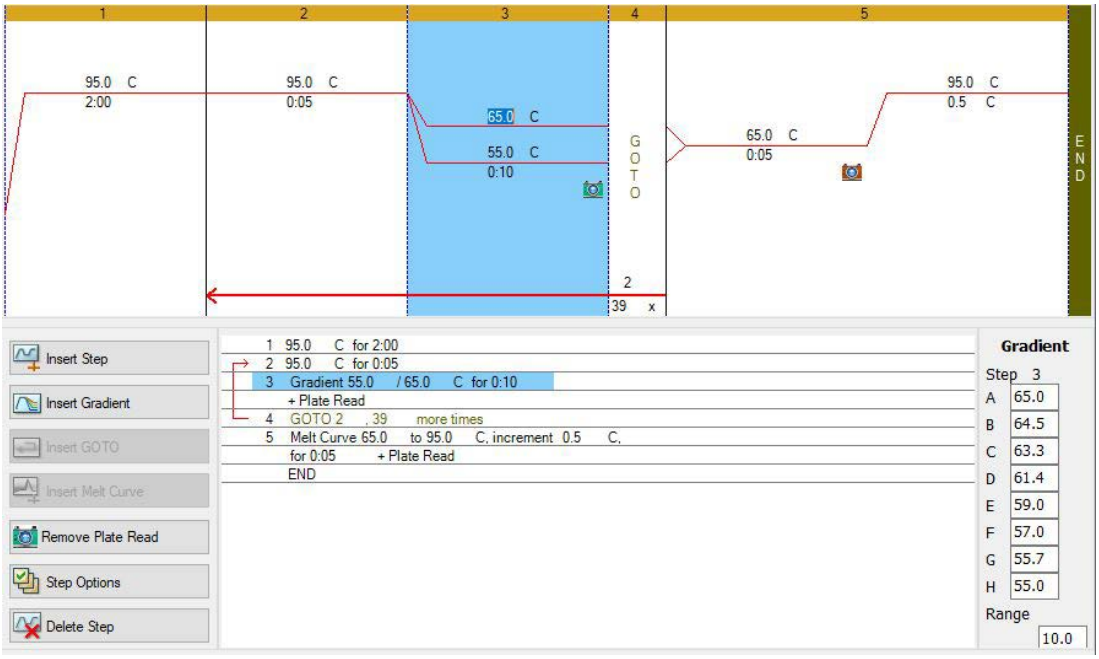

Figure 2-2 Temperature gradient RT-qPCR thermocycling conditions used on Bio-Rad CFX Maestro 1.1 software version 4.1.2433.1219

Table 2-12 RT-qPCR temperature gradient plate thermocycler settings.

Step	**Time**	**Temperature**	**Ramp rate**
PCR Initial activation step	2 min	95 °C	Maximal/fast mode
Denaturation	5 s	95 °C	Maximal/fast mode
Combined annealing/extension	10 s	55-65 °C	Maximal/fast mode
Number of cycles	40		

2.2.13.8.3 Analysis of Tm plate melt curves peaks

Melt curve peaks for each set of primers, each temperature gradient tested and corresponding NTCs were visualised using CFX Maestro Software to check for any unexpected PCR products, genomic DNA contamination, or the presence of primer dimers. Melt peaks were compared between each temperature gradient and those with the lowest Ct value were considered optimal for each primer pair.

2.2.13.8.4 Agarose gel electrophoresis of Tm plate PCR products

The PCR products with the lowest Ct value from the temperature gradient closest to the designed annealing temperature, and the corresponding NTC, for each primer pair prepared in Section 2.2.13.8.3 was added to 2.4 µL Bioline 5X Loading Dye (Meridian Bioscience, Nottingham, UK) and then loaded to a 2.5 % agarose gel (Table 2-7) in 1X Tris-Acetate-EDTA (TAE) buffer (Table 2-6) in either Mini-Sub Cell GT Cell or Sub Cell GT Electrophoresis Tanks (both: Bio-Rad, Hertfordshire, UK). Each gel was loaded with a minimum of one well containing 5 µL of Bioline HyperLadder™ 50bp (Meridian Bioscience, Nottingham, UK) to allow for quantification of PCR amplicon bands of interest by comparison to DNA molecular weight markers of a known fragment size. PCR products were then separated by electrophoresis at 100 volts for 45 minutes (7 cm^2 gels)/1 h 45 minutes (15cm^2) and gels were imaged using Gel Green Optimal Auto-exposure settings on the ChemiDoc™ Touch Gel Imaging System (Bio-Rad, Hertfordshire, UK). The analysis of melt curve peak and agarose gel

electrophoresis was used to screen primer specificity, to confirm that the PCR product was the expected size (in base pairs) and to eliminate any primer pairs that showed evidence of primer dimers or unexpected bands at fragment sizes which did not correspond to the size of the expected primer product.

2.2.13.9 Thermocycling conditions for Reference Gene and Gene of Interest (GOI) Plates

RT-qPCR plates for all candidate reference genes and gene of interest were run at an annealing/extension temperature or either 58 °C, 60 °C, 61 °C or 63 °C using the thermocycler setting in Table 2-12 in accordance on the Tm temperature identified in section 2.2.13.8.2 and 2.2.13.8.3, followed by melt curve analysis.

2.2.13.10 Selection of stable reference genes

2.2.13.10.1 Panel of candidate reference genes

A panel of candidate reference genes were identified via systematic review of literature as detailed in 5.3.1 Systematic review of literature.

2.2.13.11 Data collection

Data for each GOI or candidate/stable reference gene was collected by running a single gene per 96-well per plate in a 'sample maximisation strategy' as recommended in the MIQE guidelines (Bustin et al., 2009; Bustin et al., 2010). This strategy was selected as it would allow statistical comparison of results between treated and control samples for each gene due to the number of thienopyridine treated samples, controls, and technical replicates to be included in each gene study. Conducting multiple genes per plate ('gene maximisation strategy' (Bustin et al., 2009; Bustin et al., 2010) would not have allowed for this comparison. A minimum of two technical replicates per sample were also run on each plate.

2.2.13.12 Data analysis

2.2.13.12.1 Data quality control strategy

The Ct values for technical replicates for each sample were compared against each other and those with a Ct value greater that 0.5 Ct apart were excluded from analysis in Bio-Rad CFX Maestro software as obvious outliers, as instructed in Nolan et al. (2006). Bio-Rad CFX Maestro software also calculated mean Ct values between technical replicate groups and post-quality control, data was exported to Microsoft Excel for further analysis and normalisation.

2.2.13.12.2 Calculation percentage efficiency of RT-qPCR reactions

Dilution of standards prepared in section 2.2.13.4 was plotted against Ct value by Bio-Rad CFX Maestro Software to provide a percentage efficiency (%E) value and R^2 value. As listed in the Taylor et al. (2019) a %E value between 90-110 % and an R^2 value < 0.980 was required for each GOI or reference gene to include in data analysis. Where any initial 1:10 dilution standard curves failed %E and R^2 thresholds, or where any outliers occurred within standard replicates, standards were repeated at 1:10, 1:5 or 1:2 dilution, with the top and bottom standard Ct values used as the range of detection for each gene.

2.2.13.12.3 Calculation of relative gene expression using Vandesompele method and multiple reference genes

The average of technical replicate Ct values of each sample for each GOI and reference gene were used for data normalisation using the 'Vandesompele Method' (Vandesompele et al., 2002; Hellemans et al., 2007) of normalisation using multiple reference genes. In Microsoft Excel, the following calculations were performed:

A 'calibrator sample' was calculated for each GOI and reference gene by taking the mean of Ct of all untreated control values (Equation 4):

4

Calibrator Ct = Mean of untreated control Ct values

The relative change in Ct value (ΔCt) for each sample was calculated by subtraction of the calibrator Ct value from the sample Ct for each GOI and reference gene (Equation 5):

5

ΔCt = Average sample Ct value – Calibrator Ct value

The 'Relative Quantity' of GOI and stable reference genes was then calculated by multiplying the percentage efficiency value (%E) from the standard curve for each gene to the power of ΔCt (Equation 6):

6

$$RQ = \%E^{\Delta Ct}$$

A 'normalisation factor' (NF) was then calculated for each sample by taking the geometric mean of each reference gene RQ (Equation 7):

7

$$NF = \text{Geometric Mean } (RQ_{REF1}, RQ_{REF2}, RQ_{REF3}, RQ_{REF4})$$

The gene expression ratio for each sample was then calculated by dividing the RQ of the GOI by the normalisation factor for each sample (Equation 8):

8

$$RQ_{GOI}/NF$$

Finally, the mean, standard deviation (SD) and standard error of mean (SEM) were calculated for each grouping of thienopyridines, untreated control and positive controls (paclitaxel and nocodazole treated samples).

2.2.13.12.4 Statistics

Data was analysed using GraphPad PRISM Version 9.2.0 (332). Data was grouped by thienopyridine chemical structure, log_2 transformed and analysed using One-Way ANOVA by comparison to untreated control samples with Dunnett's post hoc test.

3. Effect of Novel Thienopyridine Compounds on Cell Viability, Cell Death and Cell Cycle of DAUDI Cells

3 CHAPTER 3: EFFECT OF NOVEL THIENOPYRIDINE COMPOUNDS ON CELL VIABILITY, CELL DEATH AND CELL CYCLE OF DAUDI CELLS

3.1 Introduction

3.1.1 Hallmarks of cancer and drug discovery

The classic hallmarks of cancer: resisting cell death, sustained proliferative signalling, evasion of growth suppression, gaining replicative immortality, avoiding immune regulation and destruction, genomic instability, metastasis, deregulated cell energy metabolism, maintenance of tumour inflammatory conditions, and generation of blood vessels (Hanahan and Weinberg, 2000; 2011) are well established, with a recent update adding further physiological conditions to this list of pathways for cancer survival (Hanahan, 2022). Each of these elements provides a useful starting point when considering how novel compounds may reduce or modify the behaviour of cancer cells in drug discovery. Key to any potential anti-cancer therapy is its ability to overcome these cancer hallmarks, and indeed there a range of assay types that allow the precise mechanisms of action to be determined (Menyhart et al., 2016). Fundamental to any potential treatment for patients is the induction of a favourable mode of cell death via apoptosis, with limited damage to healthy tissues, or rather a necrotic pathway (Bailon-Moscoso et al., 2014)

3.1.2 Cell death pathways

3.1.2.1 Apoptosis

Apoptosis, or programmed cell death, is the preferred pathway for any potential chemotherapeutic intended to be administered to human patients. It is achieved via two cellular routes, the intrinsic (BCL-2 or Cytochrome C mediated) and extrinsic (or death ligand, caspase cascade) pathways (Singh and Lim, 2022). Either the restoration of usual pathways for apoptosis that a cancer cell has overcome, or the extracellular triggering of apoptosis are the two mechanisms by which anti-cancer agents can induce cell death (Fesik, 2005). In brief, the various pathways for apoptotic cell death can be tracked using assays which measure activity such as

caspase activity, death ligand activation (Anania and Lill, 2015) or features of programmed cell death such as membrane flipping with fluorescent conjugated dyes such as FITC-Annexin V flow cytometry (Vermes et al., 1995).

3.1.2.2 Necrosis

Necrotic cell death is characterised by disordered cell death, usually accompanied by cellular rupture and damage to surrounding tissues as intracellular enzymes are spilled into the extracellular matrix (Golstein and Kroemer, 2007) adding to the NF-κB (nuclear factor kappa B)-induced pro-inflammatory conditions which often precede necrosis (D'Arcy, 2019). Flow cytometry can be used to differentiate this type of cell death from apoptosis, via staining of released DNA by the intercalating dye propidium iodide, which when used in combination with Annexin V-FITC allows the differential between intact cell membranes present in apoptosis (Annexin V-FITC positive) vs the lysed cell in necrotic cell death (propidium iodide positive) (Vermes et al., 1995).

3.1.2.3 Autophagy

Autophagy and cell stress responses are intermediate points between the impact of a treatment on a cell and the triggering of cell death pathways. Sub-optimal treatment doses may give cancer cells a stay of execution, during which time they can partially cannibalise cellular organelles either for energy use or repurposing (Mizushima et al., 2008; Nakatogawa et al., 2009; D'Arcy, 2019). Indeed, autophagy may be triggered by many of the same cellular stress response routes as those in apoptosis (Marino et al., 2014), including reactive oxygen species (ROS) and DNA damage responses which are key to halting progression through the mitotic cell cycle.

3.1.2.4 Cell stress, ROS and DNA damage

Cells have a number of pathways to prevent damage or respond to damage before progression through the various stages of the cell cycle. ROS can induce DNA damage but conversely may also be utilised by cancer cells during proliferation (Moloney and Cotter, 2018). Multiple DNA damage responses that may trigger apoptosis or autophagy are also linked to this pathway, with the ‘guardian of the genome’ p53

and its ability to halt mitosis at the G_2/M phase also linked to this response (Roos and Kaina, 2013).

NADPH (reduced Nicotinamide adenine dinucleotide phosphate), part of the normal cellular response to ROS may be upregulated in response to cell stress (Jeon et al., 2012). This feature is exploited MTT/MTS cytotoxicity assays to investigate the basic metabolic response of a cell to potential cytotoxic agents (Berridge and Tan, 1993).

3.1.3 Cell cycle analysis

Investigation of the cell cycle, via flow cytometry, can provide further clues as to the mechanism of action of novel compounds on cancer cell models. There are four classical phases of the cell cycle: Growth phase 1 (G_1/G_0), synthesis phase (S), growth phase 2 (G_2) and mitosis (M), with regulator checkpoints within these phases which halt cell cycle progression if conditions in a cell become unfavourable (Stewart et al., 2003; Ovejero et al., 2020). Arrest during G_1/S checkpoint is indicative of DNA damage and inhibition of further replication (Sancar et al., 2004), while arrest at the intra-S phase checkpoint can indicate replicative stress and an impact on DNA synthesis (Grallert and Boye, 2008; Errico and Costanzo, 2012; Ovejero et al., 2020). The G_2/M checkpoint is also linked to DNA damage that has occurred post-S phase, and mediated by p53, it allows for a pausing of cell division until repair to cellular damage has been initiated. Alternatively, apoptotic cell death or senescence are triggered during prolonged perturbation of the cell resulting from an inability to repair the cellular damage (Giono and Manfredi, 2006; Poehlmann et al., 2011; Lara-Gonzalez et al., 2019). Finally, the spindle assembly checkpoint (SAC) prevents entry into mitosis until the correct alignment of chromosomes on the mitotic spindle is met (Musacchio and Salmon, 2007; Musacchio, 2015), with failure at this phase linked to the action of microtubule poisons or the inhibition of the various kinases and regulators of spindle assembly. If a novel cancer treatment elicits cell cycle arrest, the phase at which arrest occurs can give an indication of the type of effects the treatment is having on the cell (Pozarowski and Darzynkiewicz, 2004).

3.2 Aims and Objectives

3.2.1 Aim

The aim of this chapter was to establish the effects of the ten novel thienopyridine compounds on cell viability and the cell cycle in DAUDI B cells.

3.2.2 Objectives

- To assess the basic biochemical changes in response to a range of thienopyridine concentrations using the MTS assay.
- To assess the type of cell death caused by thienopyridines at a reduced range of concentrations using the Annexin V / Propidium Iodide flow cytometry.
- To assess the effects of the thienopyridine compounds on the cell cycle in DAUDI B cells.

3.3 Methods

3.3.1 Cell culture, cell seeding and thienopyridine treatments

All cell culture, cell seeding and treatment preparations and incubations were as described in section 2.2.1 to 2.2.10.

3.3.2 Apoptosis Assay Flow Cytometry gating and settings

As described in section 2.2.9, no stain (i.e., viable control), positive apoptosis (single stain Annexin V-FITC) and positive necrosis (single stain propidium iodide) DAUDI cell controls were prepared for each assay and were used to allow gating of populations in the Flow Cytometry Standard (FCS) files generated by the Flow Cytometers use in this chapter.

3.3.2.1 BD FACSVerse set up and gating

All Flow Cytometry Standard (FCS) files generated by the BD FACSVerse flow cytometer were analysed using BD FACSuite™ software (BD Bioscience, UK). Prior to recording data on thienopyridine-treated DAUDI cells, FACSuite software was used to identify viable, apoptotic and necrotic cell populations, through selective gating of cell populations relative to the fluorescence (Figure 3-1).

The FACSVerse was equipped with photomultipler tubes (PMT) for detection of fluorescence in samples stained with specific fluorophores, with adjustable voltage settings which allowed set up of the apoptosis assay to be tailored for DAUDI cells. The flow cytometer was set up using excitation (blue laser at 488nm) with Annexin V-FITC detected with bandpass filter at 527/32 and propidium iodide detected with bandpass filter at 586/42.

No stain controls were used to identify healthy (i.e., viable, non-apoptotic or necrotic, cell populations), with the Forward Scatter Height (FSC-H) vs Side Scatter Height (SSC-H) plot used to gate for cells and exclude debris from analysis (Figure 3-1A), Positive apoptosis (i.e., FITC control) and positive necrosis (i.e., PI control) were then used sequentially in combination with the FACSuite software to confirm ‘true’ positive results (Figure 3-1B-C).

Figure 3-1D shows an example untreated DAUDI control sample used to confirm setting were correct, after which the voltage settings were retained for use across the remaining assays using the FACSverse.

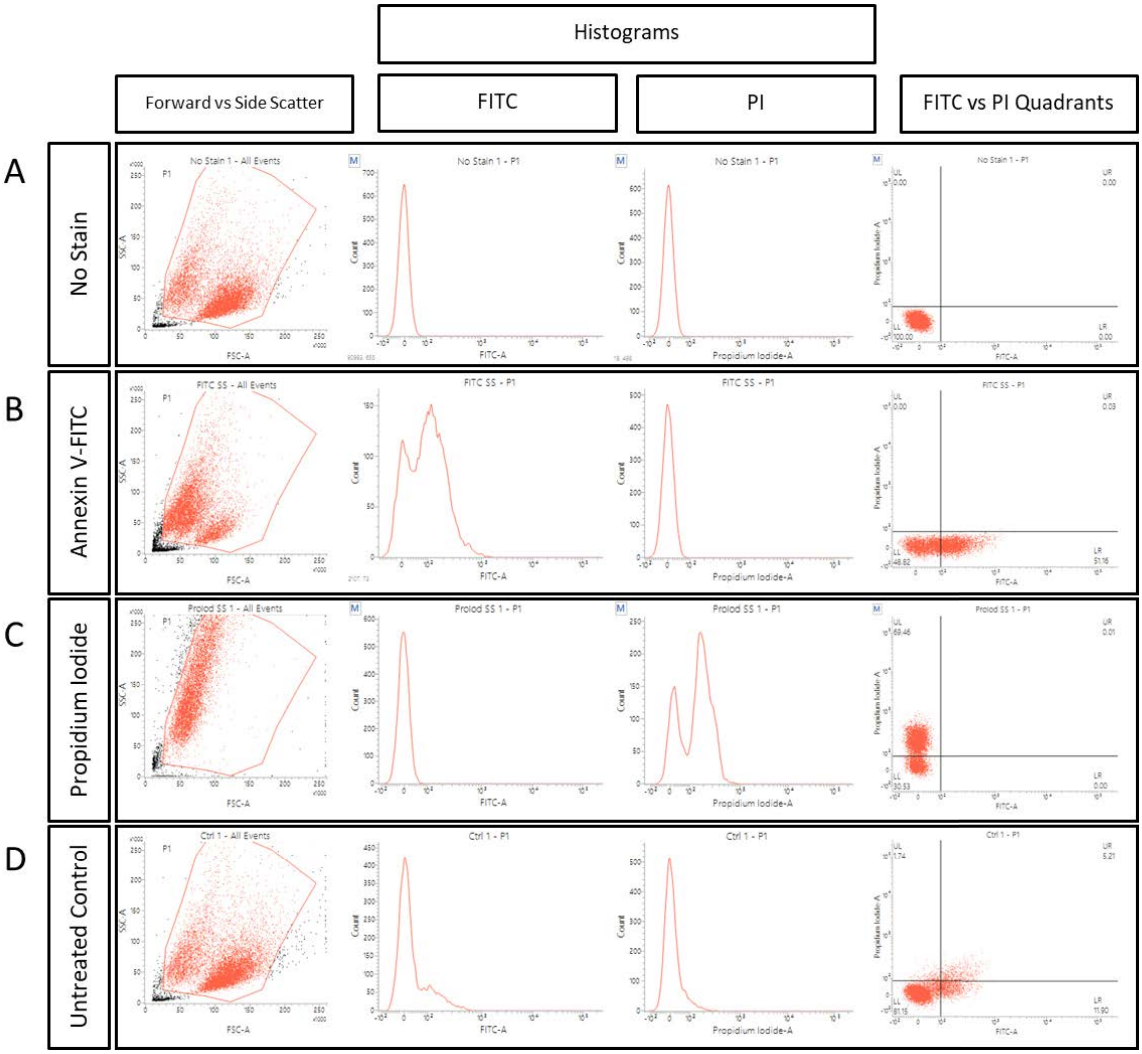

Figure 3-1 FACSVerse and FACSuite Apoptosis assay set up and gating. (A) No stain (viable) DAUDI cells were gated on Forward Scatter Area (FSC-A) versus Side Scatter Area (SSC-A) cell area to include viable cells for analysis. Analysis channels for FITC and PI were adjusted to display a peak over zero signal (FITC and PI Histograms) and a quadrant was added to the FITC versus PI plot to allow identification of cells that were viable (lower left quadrant LL), early apoptotic (lower right quadrant LR), late apoptotic (upper right quadrant UR) and necrotic (upper left quadrant UL). (B) Set up process was repeated with single Annexin V-FITC stain positive (apoptosis) control DAUDI cells to correct for spectral overlap between FITC and PI fluorescence. With the same FSC vs SSC cell gating as in (A), the FITC histogram was adjusted to display signal in the LR quadrant while PI histogram was adjusted to display zero signal. (C) Set up process was repeated again with single propidium iodide positive (necrosis) control DAUDI cells to further correct for spectral overlap between FITC and PI fluorescence. With same FSC vs SSC cell gating as (A), the PI histogram was adjusted to display signal in the UL quadrant while the PI histogram was adjusted to display zero signal. This process was repeated with at least one additional Annexin V-FITC and PI control, then voltage setting were recorded for use in future assays with DAUDI cells. (D) Data from a dual stained (Annexin V-FITC and PI) untreated DAUDI cell control sample, which displays signal for both FITC and PI on the histogram plots and corresponding positive cell populations on the FITC vs PI quadrants.

3.3.2.2 BD Accuri C6 set up and gating

The BD Accuri C6 flow cytometer and associated software (BD Bioscience, UK) has fixed voltage settings for each PMT detector however the same set up process utilising no stain, positive apoptosis and positive necrosis controls was used to set up the apoptosis assay (see Figure 3-2), with 'Compensation Settings' used to correct for fluorescent spillover before analysis of treated samples as described in the software user guide (see Table 3-1).

Table 3-1 BD Accuri C6 compensation settings for spectral overlap between fluorophores used in the Annexin V apoptosis assay. FL1 was used to detect FITC while FL3 was used to detect propidium iodide while other detectors (FL2 and FL4) were not used to generate date for this assay. The percentages below were subtracted from each detector channel after comparison of median fluorescence values for single stain (positive apoptosis and necrosis) controls as listed in the Accuri C6 Software User Guide and settings were applied to all assay datasets to ensure consistency.

Detector	FL1	FL2	FL3	FL4
FL1		0.00 %	0.46 %	0.00 %
FL2	13.16 %		0.00 %	0.00 %
FL3	3.11 %	0.00 %		0.00 %
FL4	0.00 %	3.53 %	0.00 %	

The flow cytometer was set up using excitation (blue laser at 488nm) with Annexin V-FITC detected with bandpass filter at 533/30 and propidium iodide detected with bandpass filter at 670 LP. As with the BD FACSVerse setup in section 3.3.2.1, no stain (Figure 3-2A), positive apoptosis control (Figure 3-2B) and positive necrosis control (Figure 3-2C) were used to add gates for viable cells for analysis (Forward vs Side Scatter plot), and add quadrants to identify healthy, early apoptosis, late apoptosis and necrosis cell populations.

Compensation settings were then applied to all data sets for the apoptosis assay using the BC Accuri C6 and all FCS data files were analysed and exported to MS Excel via batch analysis in the C6 software.

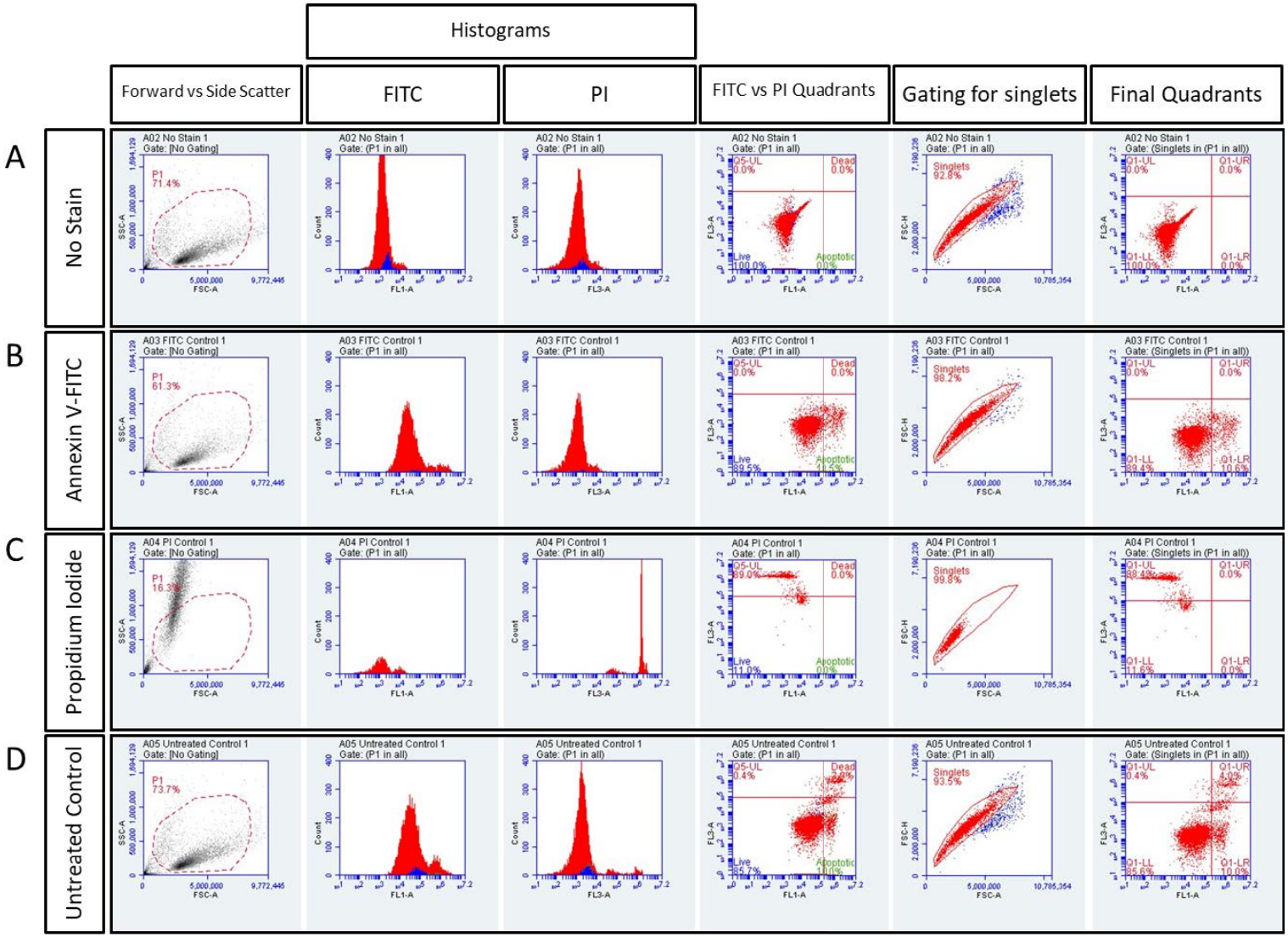
Histograms
Forward vs Side Scatter
FITC
PI
FITC vs PI Quadrants
Gating for singlets
Final Quadrants
A
No Stain
B
Annexin V-FITC
C
Propidium Iodide
D
Untreated Control

Figure 3-2 BD Accuri C6 Apoptosis assay set up and gating. (A) No stain (viable) DAUDI cells were gated on Forward Scatter Area (FSC-A) versus Side Scatter Area (SSC-A) cell area to include viable cells for analysis. FITC was assigned to FL1-A channel and PI was assigned to FL3-A channel with no stain histogram plots for each fluorophore allowing for identification of true signal for each channel in treated samples by observation of the shift in signal from these baseline values. A quadrant was added to the FITC versus PI plot to allow identification of cells that were viable (lower left quadrant LL), early apoptotic (lower right quadrant LR), late apoptotic (upper right quadrant UR) and necrotic (upper left quadrant UL) and Forward Scatter Area (FSC-A) versus Forward Scatter Height (FSC-H) plot was further gates to include singlet cells only in analysis.

Single Annexin V-FITC stain positive (apoptosis) control DAUDI cells (B) and single propidium iodide stain positive (necrosis) control DAUDI cells (C) were used to correct for spectral overlap between the two fluorophores and identify true signal for each population via comparison of the shift in signal in each histogram plot compared to no stain controls.

(D) Data from a dual stained (Annexin V-FITC and PI) untreated DAUDI cell control sample, which displays signal for both FITC and PI on the histogram plots and corresponding positive cell populations on the FITC vs PI quadrants.

3.3.3 Cell Cycle Flow Cytometry gating and settings

3.3.4 ModFit LT 5.0 Analysis

3.3.4.1 Gating

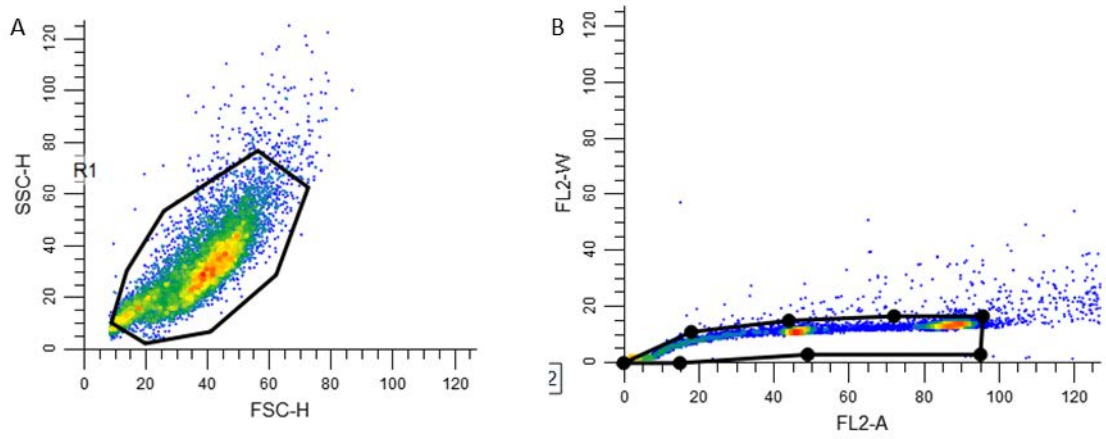

Figure 3-3 ModFit LT 5.0 Manual Model strategy for gating cells on FSC-H vs SSC-H plot (A), and FL2-A vs FL2-W plot (B) for cell cycle analysis.

All Flow Cytometry Standard (FCS) files generated by the BD FACS Calibur were gated on Forward Scatter Height (FSC-H) vs Side Scatter Height (SSC-H) plot, with all individual data sets checked to ensure their cell populations were included within the gates for analysis (Figure 3-3A), to account for any inter-assay variability in cell populations or staining between assays, and to ensure that the same analysis template was applied to all data sets. An additional gate was added to FL2 channel (e.g., channel which detected Propidium Iodide) for the FL2-Area (FL2-A) vs FL2-Width (FL2-W) plot (Figure 3-3B) to ensure only singlet populations were included in the analysis, to exclude cell doublets/clumps which could be misconstrued as cells with DNA-Tetraploid populations.

3.3.4.2 ModFit Setting Analysis Model

Data was analysed using a manual model, with the settings shown in Figure 3-4. A Manual Model was selected, due to the limitations of the ModFit LT 5.0 software on producing replicable data analysis when using its Auto Analysis tool. The Auto Analysis tool applied a different mathematical model to each individual dataset, highlighting multiple DNA-ploidy models, and for replicates identified as DNA-

tetraploid, the software is unable to differentiate between true tetraploid populations and those cells that are in G_2/M phase. Review of the data highlighted that thienopyridine treatments had no effect on the DNA index of DAUDI cells (Shankey et al., 1993).

Auto Analysis command options of 'Debris' and 'Aggregates' were included in the model. The Linearity setting of 1.94 was calculated using the mean G_2/G_1 ratio data from the untreated DAUDI + complete controls from each (Figure 3-4). Analysis of Apoptosis was done using the Annexin V/ Propidium Iodide assay see section 2.2.9 and was excluded from this analysis.

No internal standards were used in this set of experiments, as all cells used are of the DAUDI lineage. For Ploidy Determination, one cell cycle, with the 'First cycle is diploid' was selected to be modelled, as examination of the data sets showed no obvious aneuploidy populations across the data set, and this setting allowed for the generation of data showing total percentages for G_0/G_1, S and G_2/M populations. All other settings were left as standard.

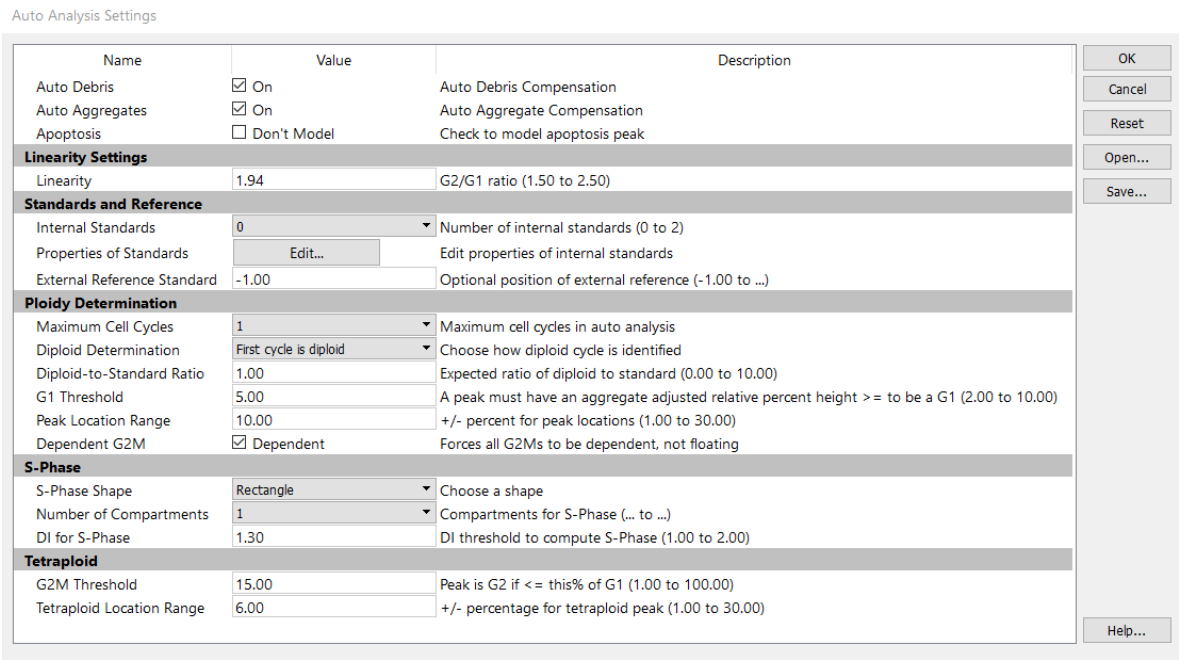

Figure 3-4 ModFit LT 5.0 Auto Analysis Settings for manual model applied to analysis of Cell Cycle FCS files.

3.3.4.3 ModFit Peak Finder Settings

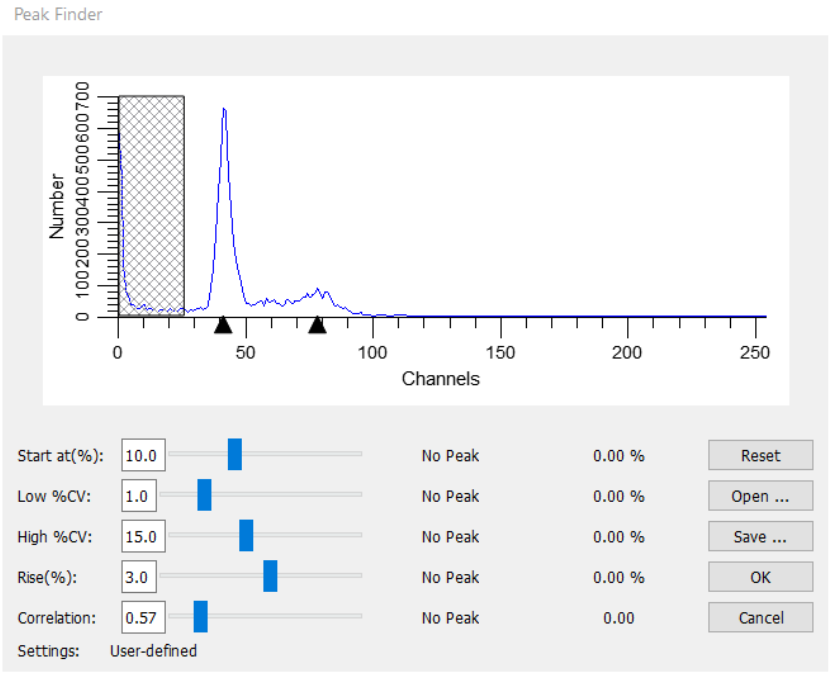

Figure 3-5 ModFit LT 5.0 Peak Finder Settings for Manual Analysis Model

ModFit 'Peak Finder' command settings were adjusted to those shown in Figure 3-5, and the same settings were applied across all datasets.

3.3.4.4 Applying Manual Model to Datasets

With ModFit settings adjusted as shown in Figure 3-3, 2 and 3, all FCS files for each assay were opened in the batch analysis tool within the software, and the 'Fit' of the manual model was checked across all replicates, to ensure that G_0/G_1, S and G_2/M populations were identified correctly. 'Fit' was also checked to ensure that the model generated data with Reduced Chi Squared (RCS) values less than 5.0, with any replicates with an RCS value about 5.0 being excluded from the analysis (for ModFit RCS values of 1.0-3.0 show a 'Good' goodness of fit, values of 3.0-5.0 show a 'Fair' goodness of fit, while any values about 5.0 show 'poor' goodness of fit), and that % coefficient of variance (% CV) were less than 8 % threshold as advised in Sharkey et al (1993) 'Guidelines for Implementation of Clinical DNA Cytometry'. The 'Fit' of the Manual Model was finalised using a Control (complete media treatment only) replicate in each dataset, and the 'Choose Model' command settings were used to

fix the Manual Model to this replicate with the options finalised as shown in Figure 3-6.

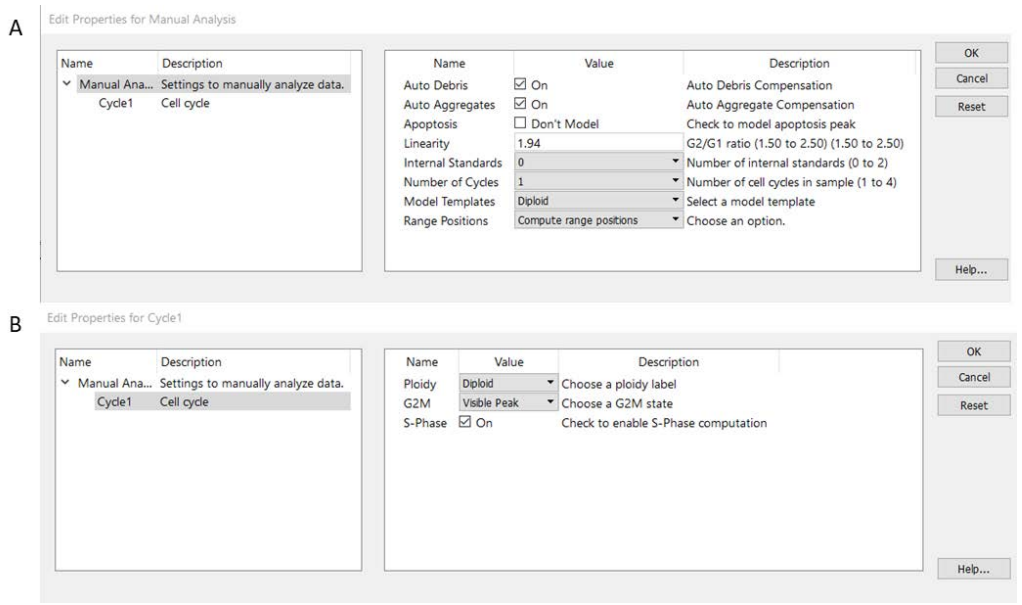

Figure 3-6 ModFit LT 5.0 Manual Analysis Settings for Manual Model applied to analysis of all data sets (A) and the settings applied by the Model during batch analysis (B).

The final option in 'Choose Model' command settings allows for adjusting the range positions, for where ModFit will look for the relevant G_0/G_1, G_2/M and Debris cell populations as shown in Figure 3-7. To keep the Manual Model consistent across all replicates in each dataset, no adjustments were made to the range position, and the displayed range positions based on the 'Fit' of the Model for the Control replicate were accepted, to allow for replication of the data analysis.

The Manual Model Analysis was applied to all replicates using the batch analysis tool, with data exported to a database for further statistical analysis.

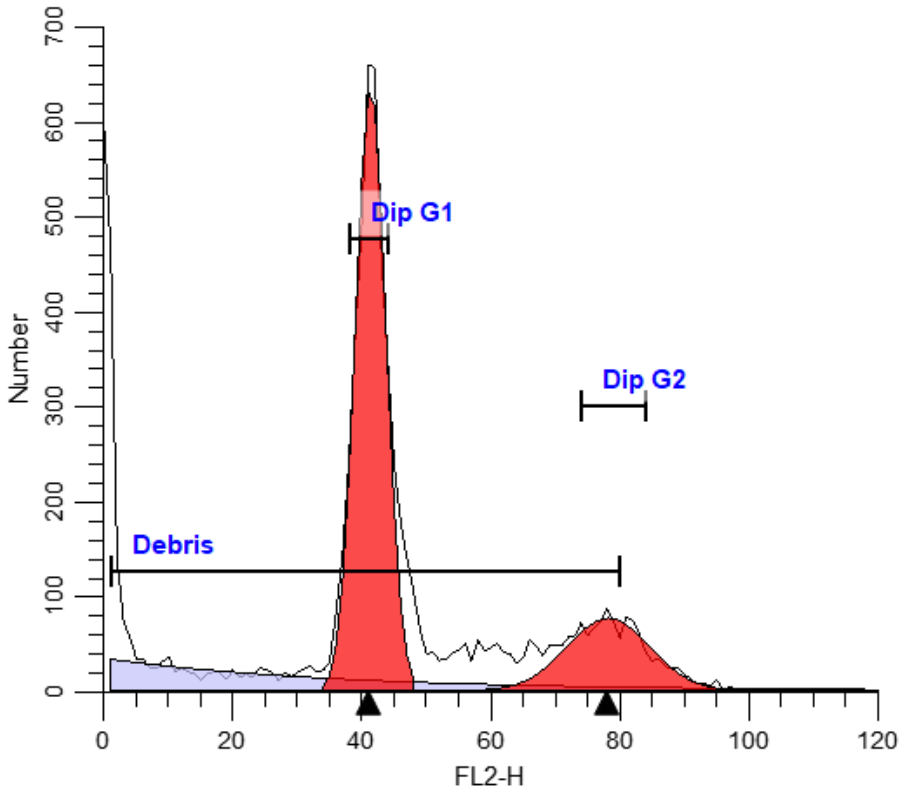

Figure 3-7 ModFit 'Choose Model' command settings options for adjusting range positions. The above settings are the unmodified range positions recommended by the ModFit software. Debris range position corresponds to the 'Auto Debris Compensation' setting shown in Figure 3-6, while the Dip G1 and Dip G2 positions were based on the 'Fit' of the model to an untreated control sample.

Debris – cell population that is sub-Diploid G1, Dip G1 – cell population corresponding to Diploid G1 DNA content, Dip G2 – cell population corresponding to Diploid G2 DNA content.

3.3.5 Data analysis

All data was exported to Microsoft Excel and analysed using One-Way Analysis of Variance (ANOVA) and Dunnett's post hoc test in GraphPad PRISM Version 9.2.0 (332), with thienopyridine treated samples compared to untreated controls.

3.4 Results

3.4.1 Effects of novel thienopyridines on cell viability and apoptosis

The cell viability assay (MTS assay) was used to study the effect of the novel thienopyridines on DAUDI cells. Flow cytometry apoptosis assay (AVPI assay) with dual staining of cells with Annexin V and propidium iodide was used to study the effect of the novel thienopyridines on apoptosis and necrosis.

3.4.1.1 Effects of novel thienopyridines with a cyclooctane moiety on cell viability

Novel thienopyridines DJ0014, DJ0021, DJ0199, DJ0206 and DJ0209 all share a cyclooctane-moiety in their molecular structure, which together with the cycloheptane moiety, has been shown to promote more cytotoxic effects on cells treated with these compounds in previous studies, rather than cytostatic effects seen in the thienopyridine compounds with cyclohexanone rings (Arabshahi et al., 2015).

3.4.1.1.1 DJ0014 effects on DAUDI cell viability

Figure 3-8 to Figure 3-10 show viability (MTS) and apoptosis (AVPI) assay results for DAUDI cells cultured in the presence of novel thienopyridine DJ0014 for 24 hours, 48 hours, and 72 hours respectively. For the viability assay, at 24 hours (Figure 3-8A), there was only slight increases in cell viability across all concentrations investigated , while at both 48 hours (Figure 3-9A) and 72 hours (Figure 3-10A), there was a statistically significant reduction in cell viability at 10 µM and 100 µM concentrations ($P<0.001$), with the most pronounced effects shown at 72 hours (16.9 % cell viability for 10 µM and 29.2 % for 100 µM).

For the apoptosis assay, at 24 hours (Figure 3-8B), there were small but statistically significant increases in both early apoptotic and late apoptotic cell populations at 10 µM and 100 µM concentrations ($P<0.001$), with corresponding decreases in the live cell population ($P<0.001$). There were larger increases in the early and late apoptotic cell populations at both 48 hours (Figure 3-9B) and 72 hours (Figure 3-10B), with a combined 63.4 % of cells apoptotic at 10 µM ($P<0.001$) and 64.1 % at 100 µM ($P<0.001$) at 72 hours versus 15.3 % of cells in the untreated control replicates (DAUDI + complete media only).

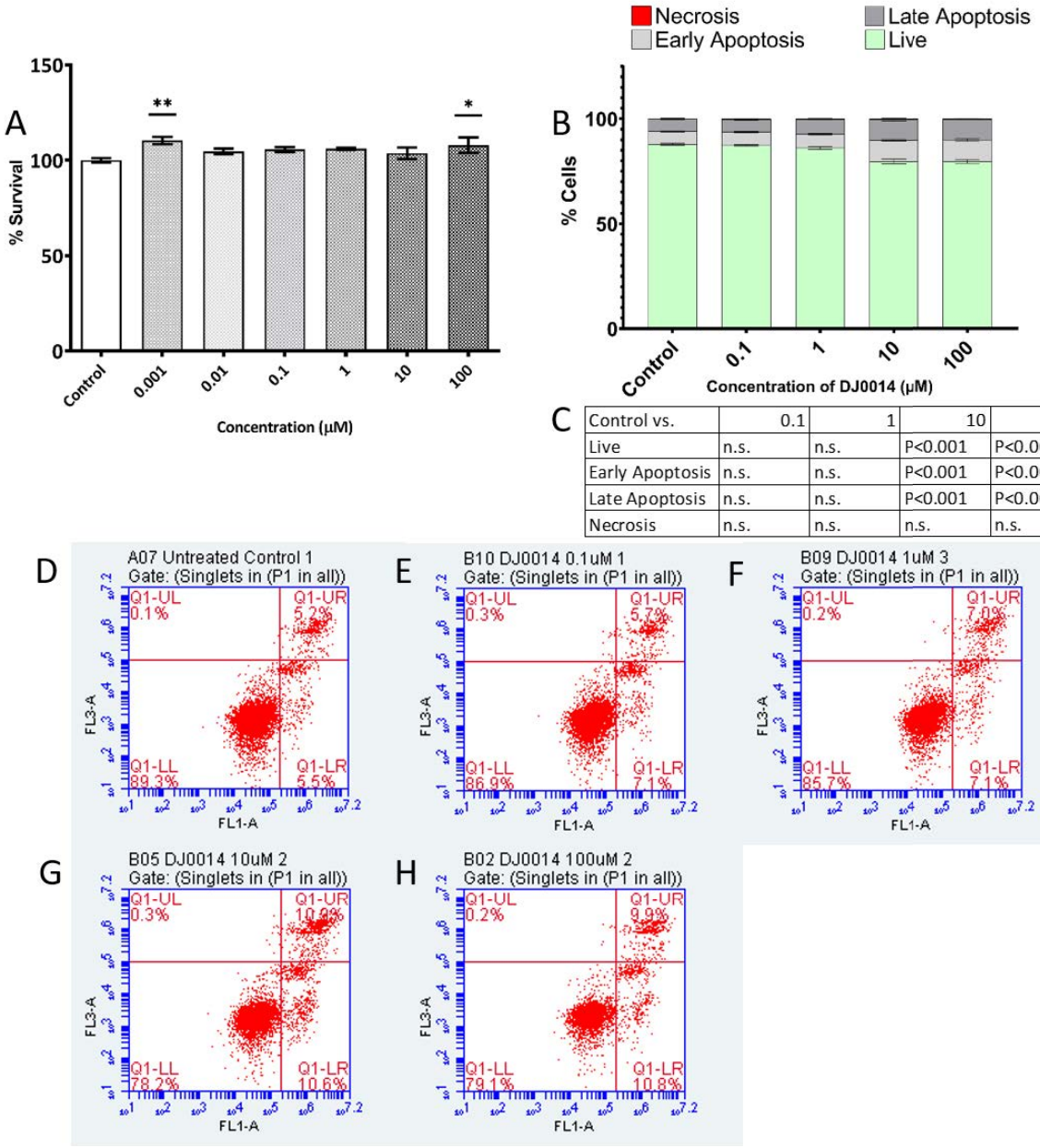

C

Control vs.	0.1	1	10	100
Live	n.s.	n.s.	P<0.001	P<0.001
Early Apoptosis	n.s.	n.s.	P<0.001	P<0.001
Late Apoptosis	n.s.	n.s.	P<0.001	P<0.001
Necrosis	n.s.	n.s.	n.s.	n.s.

Figure 3-8 Cell viability assays for DAUDI cells treated with various concentrations of Thienopyridine DJ0014 for 24 hours as determined by MTS assay (A) and Annexin V/Propidium Iodine Flow Cytometry (B), and Significance values for One-Way ANOVA with Dunnett's post-hoc test of Untreated Control (DAUDI + complete media) vs each concentration of DJ0014 (C). Representative dot plots for Annexin V/PI Flow Cytometry Untreated Control (D), DJ0014 0.1 µM (E), DJ0014 1 µM (F), DJ0014 10 µM (G) and DJ0014 100 µM (H) are presented where Early Apoptosis (Lower Right Quadrant (LR)) = Annexin V+/PI-, Late Apoptosis (Upper Right Quadrant (UR)) = Annexin V+/PI+, Live Cell (Lower Left Quadrant (LL)) = Annexin V-/PI-, Necrosis (Upper Left Quadrant (UR)) = Annexin V-/PI+.

Data are presented as mean ±SEM of n=3 (untreated control n=6). For MTS (A) data have been normalised against 100 % survival for un-treated cells, and 0 % survival for cells treated with 50 % ethanol for 24 h. For Annexin V/Propidium Iodide (B) data are presented as mean ±SEM of n=3, untreated control n=6.

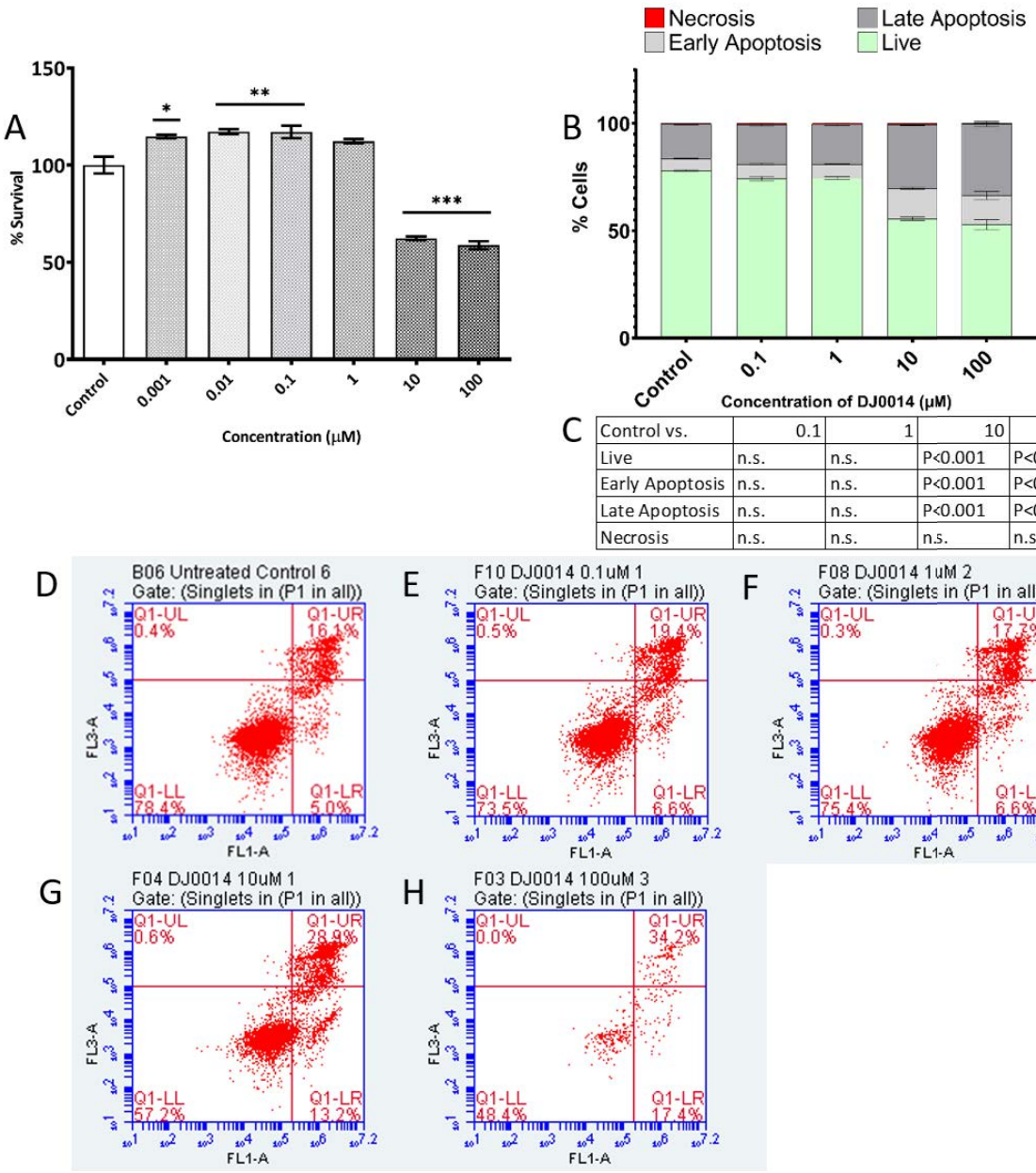

C

Control vs.	0.1	1	10	100
Live	n.s.	n.s.	P<0.001	P<0.001
Early Apoptosis	n.s.	n.s.	P<0.001	P<0.001
Late Apoptosis	n.s.	n.s.	P<0.001	P<0.001
Necrosis	n.s.	n.s.	n.s.	n.s.

Figure 3-9 Cell viability assays for DAUDI cells treated with various concentrations of Thienopyridine DJ0014 for 48 hours as determined by MTS assay (A) and Annexin V/Propidium Iodine Flow Cytometry (B), and Significance values for One-Way ANOVA with Dunnett's post-hoc test of Untreated Control (DAUDI + complete media) vs each concentration of DJ0014 (C). Representative dot plots for Annexin V/PI Flow Cytometry Untreated Control (D), DJ0014 0.1 μM (E), DJ0014 1 μM (F), DJ0014 10 μM (G) and DJ0014 100 μM (H) are presented where Early Apoptosis (Lower Right Quadrant (LR)) = Annexin V+/PI-, Late Apoptosis (Upper Right Quadrant (UR)) = Annexin V+/PI+, Live Cell (Lower Left Quadrant (LL)) = Annexin V-/PI-, Necrosis (Upper Left Quadrant (UR)) = Annexin V-/PI+.

Data are presented as mean ±SEM of n=3 (untreated control n=6). For MTS (A) data have been normalised against 100 % survival for un-treated cells, and 0 % survival for cells treated with 50 % ethanol for 24 h. For Annexin V/Propidium Iodide (B) data are presented as mean ±SEM of n=3, untreated control n=6.

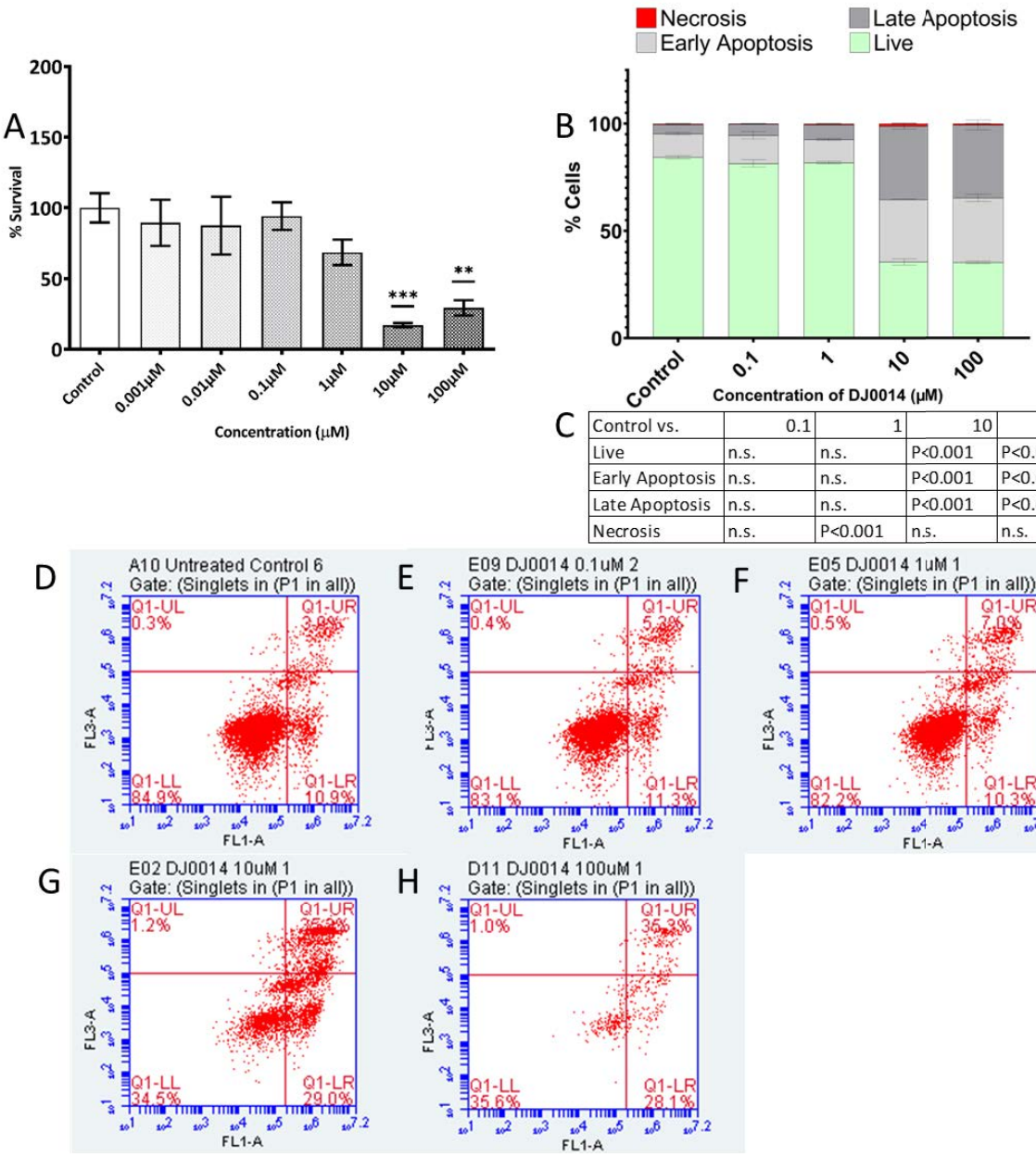

Control vs.	0.1	1	10	100
Live	n.s.	n.s.	P<0.001	P<0.001
Early Apoptosis	n.s.	n.s.	P<0.001	P<0.001
Late Apoptosis	n.s.	n.s.	P<0.001	P<0.001
Necrosis	n.s.	P<0.001	n.s.	n.s.

Figure 3-10 Cell viability assays for DAUDI cells treated with various concentrations of Thienopyridine DJ0014 for 72 hours as determined by MTS assay (A) and Annexin V/Propidium Iodine Flow Cytometry (B), and Significance values for One-Way ANOVA with Dunnett's post-hoc test of Untreated Control (DAUDI + complete media) vs each concentration of DJ0014 (C). Representative dot plots for Annexin V/PI Flow Cytometry Untreated Control (D), DJ0014 0.1 μM (E), DJ0014 1 μM (F), DJ0014 10 μM (G) and DJ0014 100 μM (H) are presented where Early Apoptosis (Lower Right Quadrant (LR)) = Annexin V+/PI-, Late Apoptosis (Upper Right Quadrant (UR)) = Annexin V+/PI+, Live Cell (Lower Left Quadrant (LL)) = Annexin V-/PI-, Necrosis (Upper Left Quadrant (UR)) = Annexin V-/PI+.

Data are presented as mean ±SEM of n=3 (untreated control n=6). For MTS (A) data have been normalised against 100 % survival for un-treated cells, and 0 % survival for cells treated with 50 % ethanol for 24 h. For Annexin V/Propidium Iodide (B) data are presented as mean ±SEM of n=3, untreated control n=6.

3.4.1.1.2 DJ0021 effects on DAUDI cell viability

Figure 3-11 to Figure 3-13 show viability (MTS) and apoptosis (AVPI) assay results for DAUDI cells cultured in the presence of novel thienopyridine DJ0021 for 24 hours, 48 hours, and 72 hours respectively. For the viability assay, at 24 hours (Figure 3-11A), 48 hours (Figure 3-12A) and 72 hours (Figure 3-13B) there is a general trend of increased cell viability versus untreated control, with a statistically significant increase ($P<0.05$) at 0.001 μM at 48 hours of treatment.

For the apoptosis assay, no effects are seen at 24 hours (Figure 3-11B), while at 48 hours (Figure 3-12B) there is a small but statistically significant increase in late apoptotic cells at 10 μM ($P<0.01$) and 100 μM ($P<0.001$) with a corresponding decrease in necrotic cells, rather than a decrease in the live cell population as seen with DJ0014. For the cells treated with 0.1 μM there is a statistically significant decrease in both live cell and necrotic populations ($P<0.05$).

At 72 hours (Figure 3-13B), there is a statistically significant increase in both early and late apoptotic populations, with corresponding decreases in live and necrotic cells at both 10 μM and 100 μM concentrations.

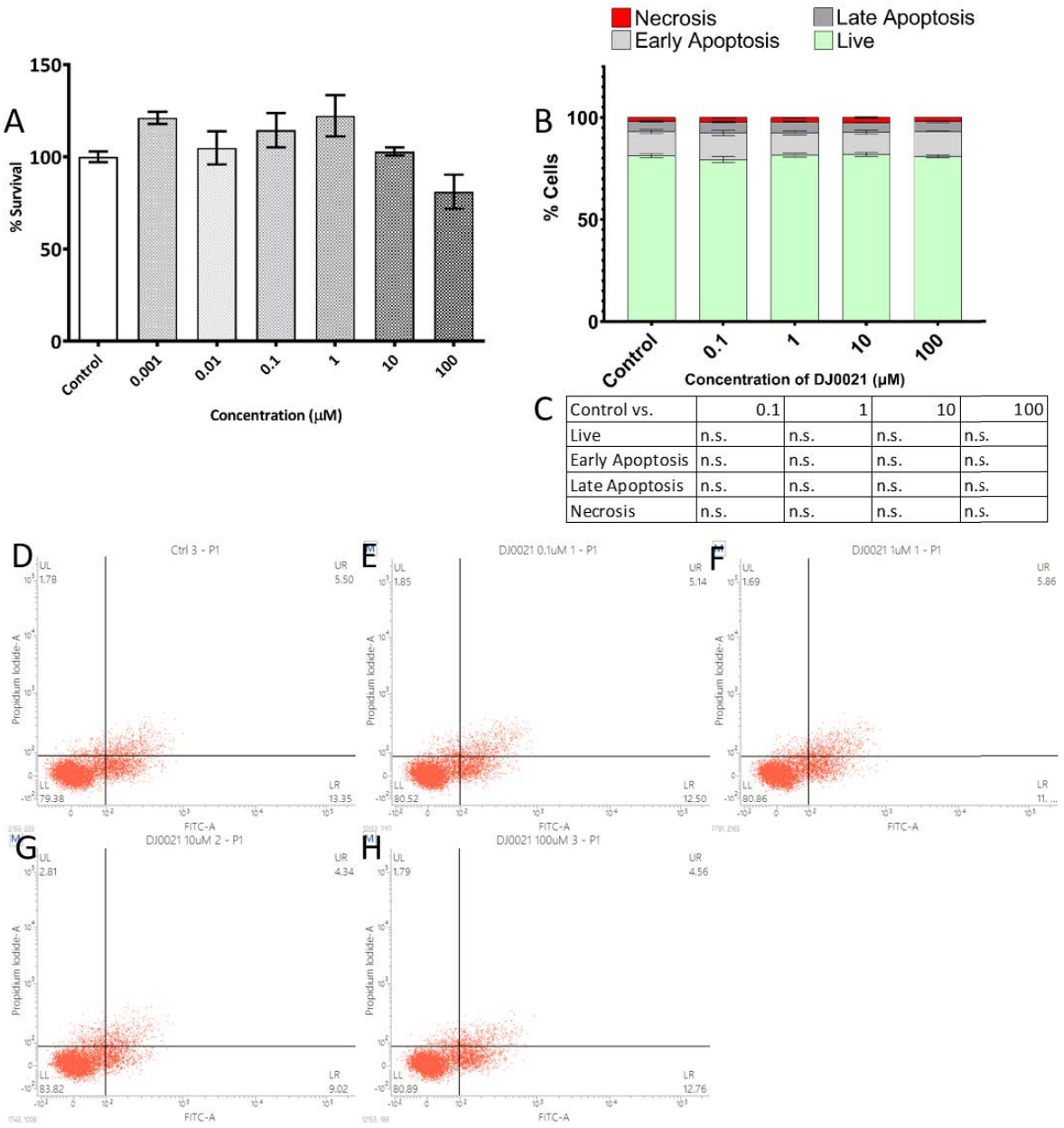

Control vs.	0.1	1	10	100
Live	n.s.	n.s.	n.s.	n.s.
Early Apoptosis	n.s.	n.s.	n.s.	n.s.
Late Apoptosis	n.s.	n.s.	n.s.	n.s.
Necrosis	n.s.	n.s.	n.s.	n.s.

Figure 3-11 Cell viability assays for DAUDI cells treated with various concentrations of Thienopyridine DJ0021 for 24 hours as determined by MTS assay (A) and Annexin V/Propidium Iodine Flow Cytometry (B), and Significance values for One-Way ANOVA with Dunnett's post-hoc test of Untreated Control (DAUDI + complete media) vs each concentration of DJ0021 (C). Representative dot plots for Annexin V/PI Flow Cytometry Untreated Control (D), DJ0021 0.1 µM (E), DJ0021 1 µM (F), DJ0021 10 µM (G) and DJ0021 100 µM (H) are presented where Early Apoptosis (Lower Right Quadrant (LR)) = Annexin V+/PI-, Late Apoptosis (Upper Right Quadrant (UR)) = Annexin V+/PI+, Live Cell (Lower Left Quadrant (LL)) = Annexin V-/PI-, Necrosis (Upper Left Quadrant (UR)) = Annexin V-/PI+.

Data are presented as mean ±SEM of n=3 (untreated control n=3(MTS), n=6 (AVPI)). For MTS (A) data have been normalised against 100 % survival for un-treated cells, and 0 % survival for cells treated with 50 % ethanol for 24 h. For Annexin V/Propidium Iodide (B) data are presented as mean ±SEM of n=3, untreated control n=6.

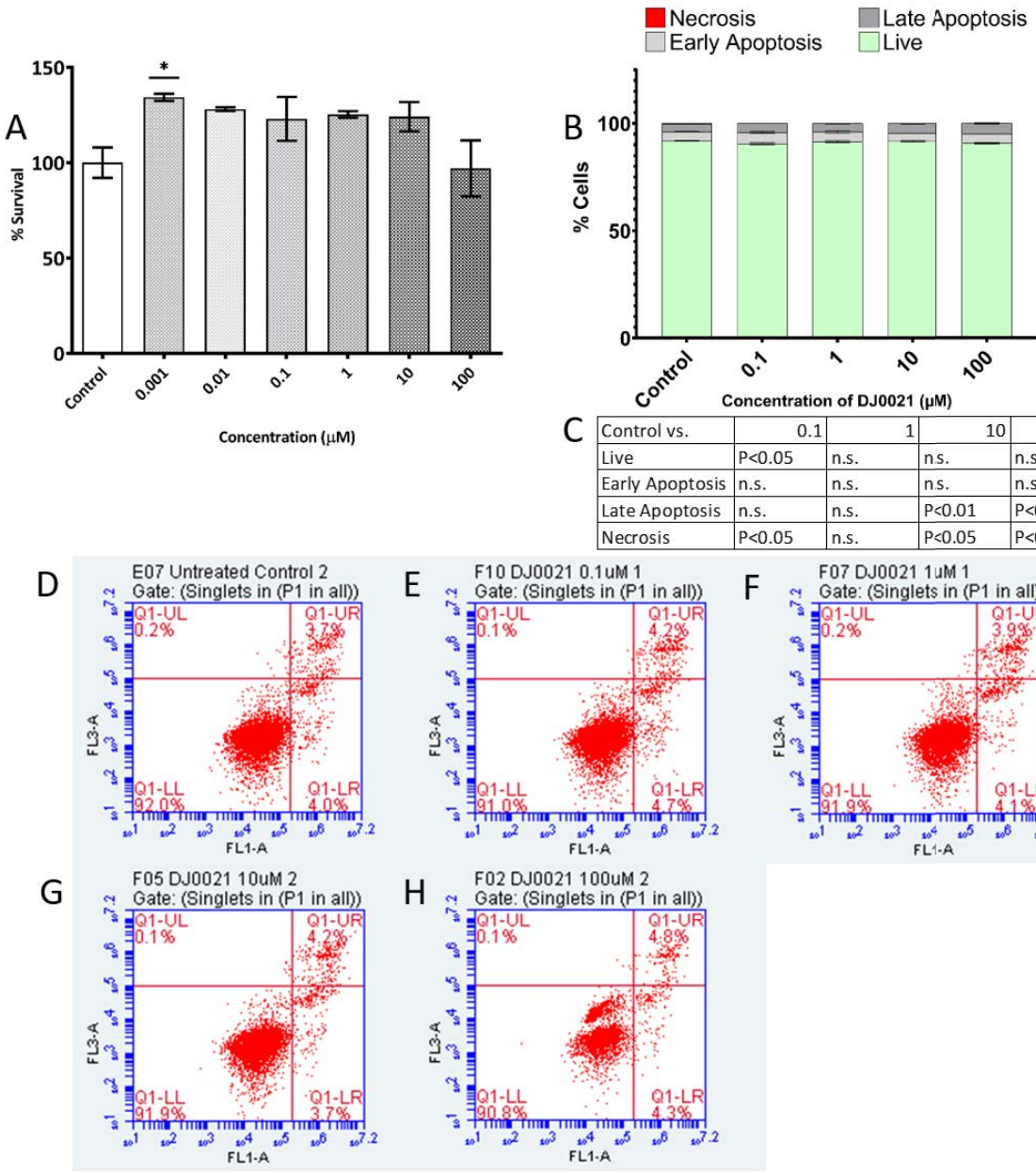

C

Control vs.	0.1	1	10	100
Live	P<0.05	n.s.	n.s.	n.s.
Early Apoptosis	n.s.	n.s.	n.s.	n.s.
Late Apoptosis	n.s.	n.s.	P<0.01	P<0.001
Necrosis	P<0.05	n.s.	P<0.05	P<0.01

Figure 3-12 Cell viability assays for DAUDI cells treated with various concentrations of Thienopyridine DJ0021 for 48 hours as determined by MTS assay (A) and Annexin V/Propidium Iodine Flow Cytometry (B), and Significance values for One-Way ANOVA with Dunnett's post-hoc test of Untreated Control (DAUDI + complete media) vs each concentration of DJ0021 (C). Representative dot plots for Annexin V/PI Flow Cytometry Untreated Control (D), DJ0021 0.1 μM (E), DJ0021 1 μM (F), DJ0021 10 μM (G) and DJ0021 100 μM (H) are presented where Early Apoptosis (Lower Right Quadrant (LR)) = Annexin V+/PI-, Late Apoptosis (Upper Right Quadrant (UR)) = Annexin V+/PI+, Live Cell (Lower Left Quadrant (LL)) = Annexin V-/PI-, Necrosis (Upper Left Quadrant (UR)) = Annexin V-/PI+.

Data are presented as mean ±SEM of n=3 (untreated control n=6). For MTS (A) data have been normalised against 100 % survival for un-treated cells, and 0 % survival for cells treated with 50 % ethanol for 24 h. For Annexin V/Propidium Iodide (B) data are presented as mean ±SEM of n=3, untreated control n=6.

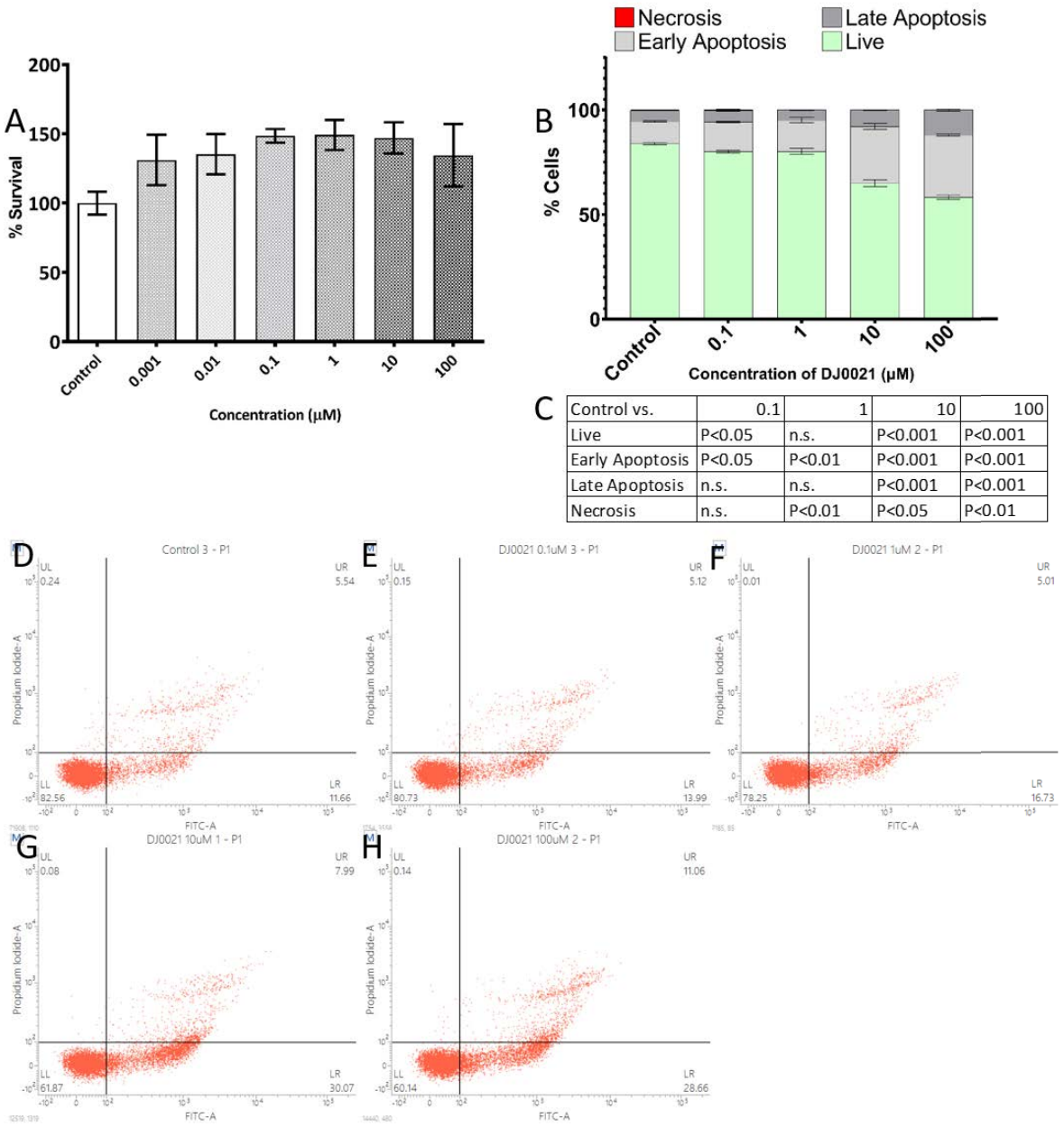

C

Control vs.	0.1	1	10	100
Live	P<0.05	n.s.	P<0.001	P<0.001
Early Apoptosis	P<0.05	P<0.01	P<0.001	P<0.001
Late Apoptosis	n.s.	n.s.	P<0.001	P<0.001
Necrosis	n.s.	P<0.01	P<0.05	P<0.01

Figure 3-13 Cell viability assays for DAUDI cells treated with various concentrations of Thienopyridine DJ0021 for 72 hours as determined by MTS assay (A) and Annexin V/Propidium Iodine Flow Cytometry (B), and Significance values for One-Way ANOVA with Dunnett's post-hoc test of Untreated Control (DAUDI + complete media) vs each concentration of DJ0021 (C). Representative dot plots for Annexin V/PI Flow Cytometry Untreated Control (D), DJ0021 0.1 µM (E), DJ0021 1 µM (F), DJ0021 10 µM (G) and DJ0021 100 µM (H) are presented where Early Apoptosis (Lower Right Quadrant (LR)) = Annexin V+/PI-, Late Apoptosis (Upper Right Quadrant (UR)) = Annexin V+/PI+, Live Cell (Lower Left Quadrant (LL)) = Annexin V-/PI-, Necrosis (Upper Left Quadrant (UR)) = Annexin V-/PI+.

Data are presented as mean ±SEM of n=3 (untreated control n=6 (MTS), N=5 (AVPI)). For MTS (A) data have been normalised against 100 % survival for un-treated cells, and 0 % survival for cells treated with 50 % ethanol for 24 h. For Annexin V/Propidium Iodide (B) data are presented as mean ±SEM of n=3, untreated control n=6.

3.4.1.1.3 DJ0199 effects on DAUDI cell viability

Figure 3-14 to Figure 3-16 show viability (MTS) and apoptosis (AVPI) assay results for DAUDI cells cultured in the presence of novel thienopyridine DJ0199 for 24 hours, 48 hours, and 72 hours respectively.

For the viability assay, DJ0199 shows no statistically significant activity at 24 hours, but showed slight reductions in cell viability for 10 μM and 100 μM concentrations (Figure 3-14A). At both 48 hours (Figure 3-15A) and 72 hours (Figure 3-16A) post-incubation with DJ0199, there is a significant reduction in cell viability at 1 μM ($P<0.01$) , 10 μM ($P<0.001$) and 100 μM ($P<0.001$). Cell viability for 10 μM and 100 μM at 48 hours were 43.5 % and 28.8 %, and at 72 hours were 23.0 % and 25.9 % respectively, showing greater activity at the latter time point.

For the apoptosis assay, there was a slight statistically significant increase in cells at late apoptosis for 10 μM ($P<0.001$) and 100 μM ($P<0.001$) at 24 hours (Figure 3-14B). More pronounced effects were seen at 48 hours (Figure 3-15B) and 72 hours (Figure 3-16B), with significant increases in both early and late apoptotic populations, with corresponding decreases in live cell populations. At 48 hours, the combined early and late apoptotic populations for 10 μM was 51.8 % and for 100 μM was 47.4 % versus 16.3 % for complete media control. At 72 hours, the combined early and late apoptotic cell populations for 1 μM, 10 μM and 100 μM were 33.7 % ($P<0.001$), 67.4 % ($P<0.001$) and 70.5 % ($P<0.001$) versus 17.4 % for complete media control.

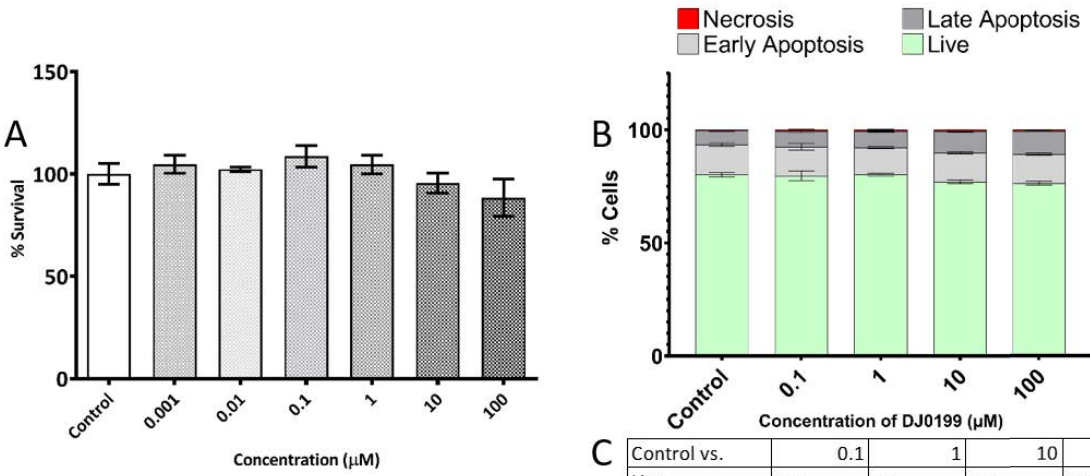

C

Control vs.	0.1	1	10	100
Live	n.s.	n.s.	n.s.	n.s.
Early Apoptosis	n.s.	n.s.	n.s.	n.s.
Late Apoptosis	n.s.	n.s.	P<0.001	P<0.001
Necrosis	n.s.	n.s.	n.s.	n.s.

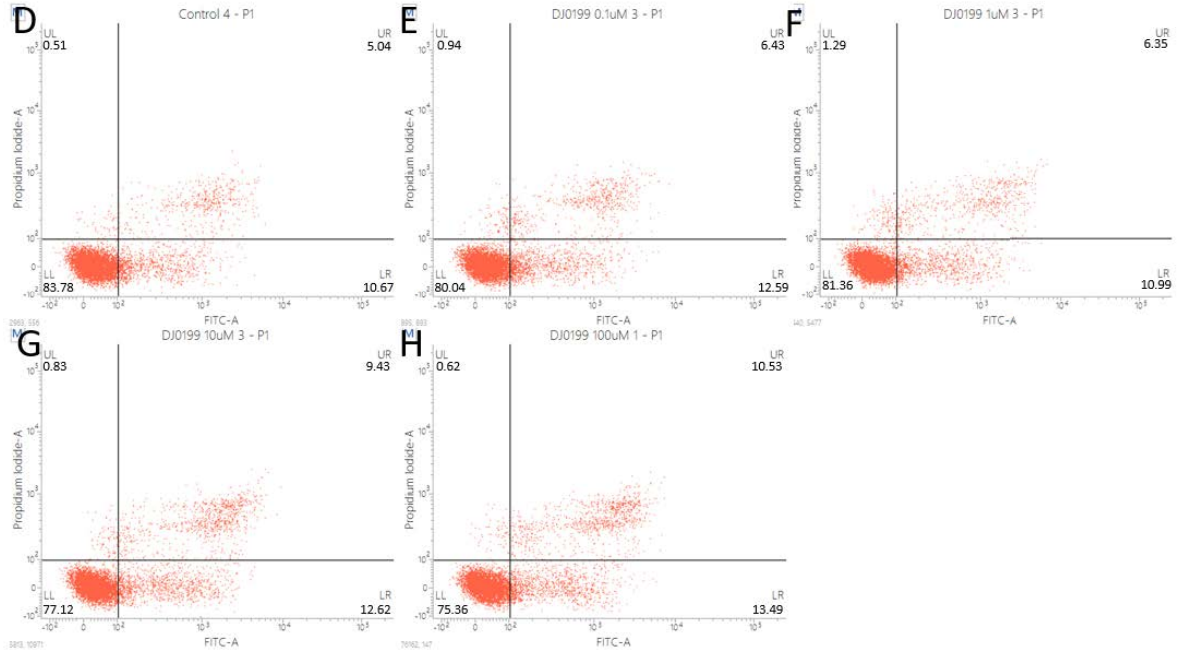

Figure 3-14 Cell viability assays for DAUDI cells treated with various concentrations of Thienopyridine DJ0199 for 24 hours as determined by MTS assay (A) and Annexin V/Propidium Iodine Flow Cytometry (B), and Significance values for One-Way ANOVA with Dunnett's post-hoc test of Untreated Control (DAUDI + complete media) vs each concentration of DJ0199 (C). Representative dot plots for Annexin V/PI Flow Cytometry Untreated Control (D), DJ0199 0.1 μM (E), DJ0199 1 μM (F), DJ0199 10 μM (G) and DJ0199 100 μM (H) are presented where Early Apoptosis (Lower Right Quadrant (LR)) = Annexin V+/PI-, Late Apoptosis (Upper Right Quadrant (UR)) = Annexin V+/PI+, Live Cell (Lower Left Quadrant (LL)) = Annexin V-/PI-, Necrosis (Upper Left Quadrant (UR)) = Annexin V-/PI+.

Data are presented as mean ±SEM of n=3 (untreated control n=6). For MTS (A) data have been normalised against 100 % survival for un-treated cells, and 0 % survival for cells treated with 50 % ethanol for 24 h. For Annexin V/Propidium Iodide (B) data are presented as mean ±SEM of n=3, untreated control n=6.

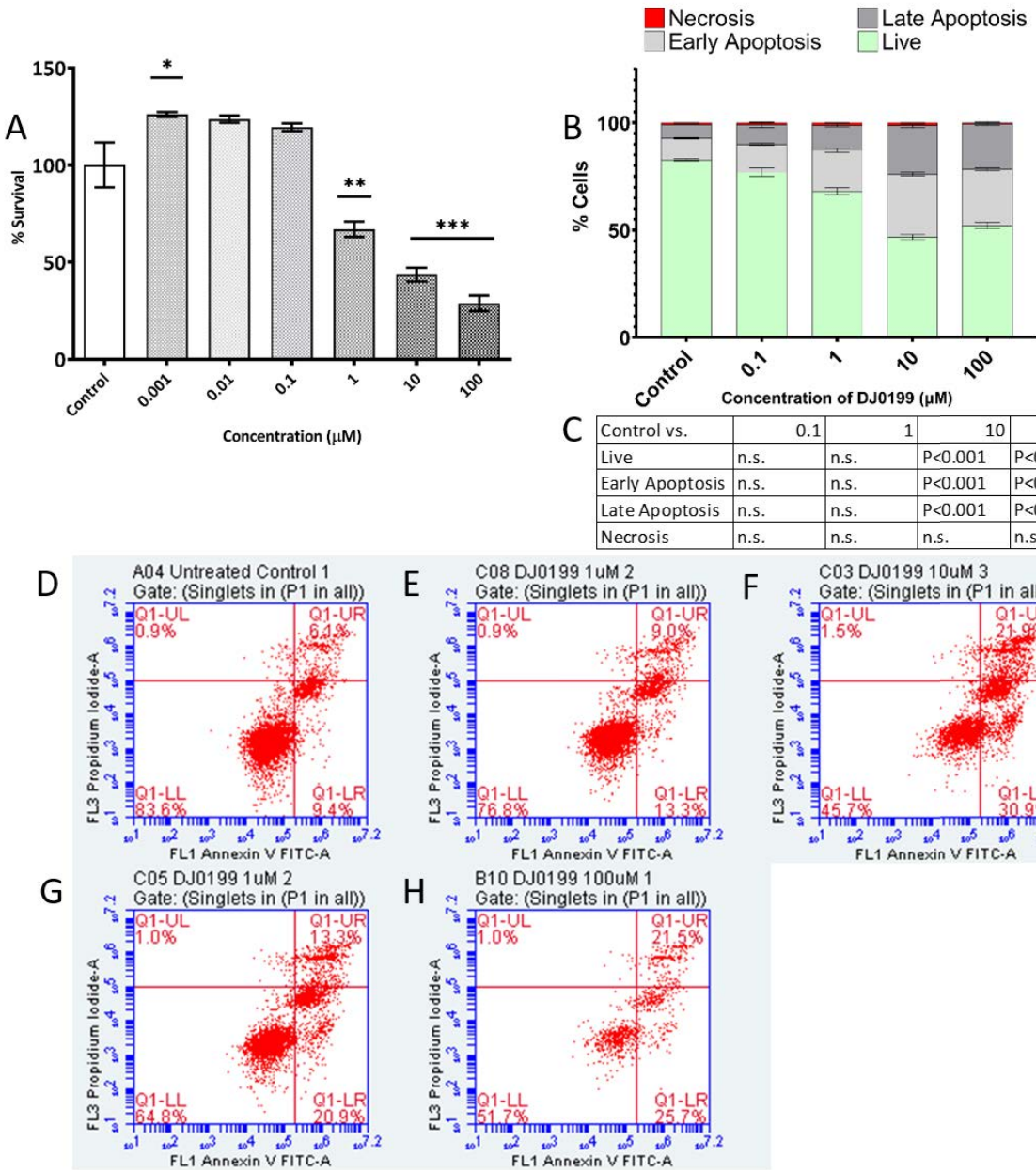

C

Control vs.	0.1	1	10	100
Live	n.s.	n.s.	P<0.001	P<0.001
Early Apoptosis	n.s.	n.s.	P<0.001	P<0.001
Late Apoptosis	n.s.	n.s.	P<0.001	P<0.001
Necrosis	n.s.	n.s.	n.s.	n.s.

Figure 3-15 Cell viability assays for DAUDI cells treated with various concentrations of Thienopyridine DJ0199 for 48 hours as determined by MTS assay (A) and Annexin V/Propidium Iodine Flow Cytometry (B), and Significance values for One-Way ANOVA with Dunnett's post-hoc test of Untreated Control (DAUDI + complete media) vs each concentration of DJ0199 (C). Representative dot plots for Annexin V/PI Flow Cytometry Untreated Control (D), DJ0199 0.1 μM (E), DJ0199 1 μM (F), DJ0199 10 μM (G) and DJ0199 100 μM (H) are presented where Early Apoptosis (Lower Right Quadrant (LR)) = Annexin V+/PI-, Late Apoptosis (Upper Right Quadrant (UR)) = Annexin V+/PI+, Live Cell (Lower Left Quadrant (LL)) = Annexin V-/PI-, Necrosis (Upper Left Quadrant (UR)) = Annexin V-/PI+.

Data are presented as mean ±SEM of n=3 (untreated control n=4 (MTS), n=6 (AVPI). For MTS (A) data have been normalised against 100 % survival for un-treated cells, and 0 % survival for cells treated with 50 % ethanol for 24 h. For Annexin V/Propidium Iodide (B) data are presented as mean ±SEM of n=3, untreated control n=6.

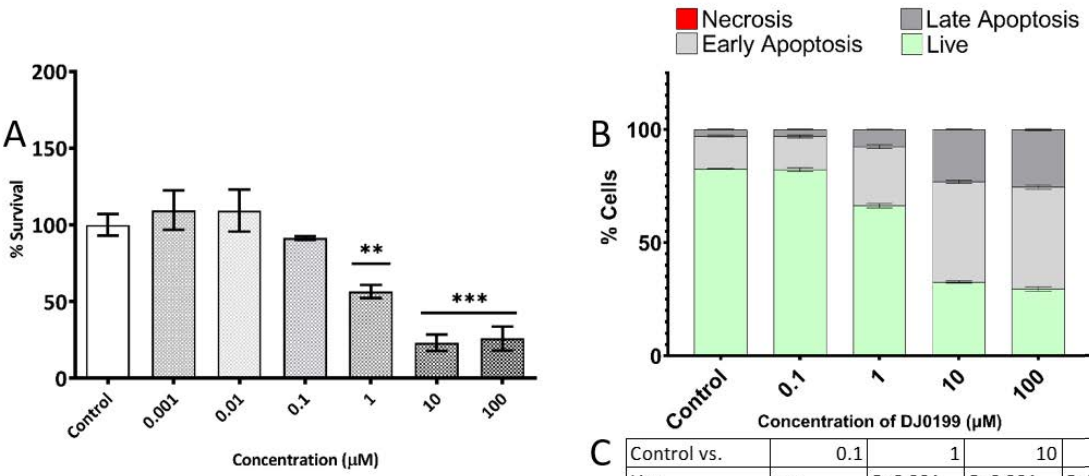

C

Control vs.	0.1	1	10	100
Live	n.s.	P<0.001	P<0.001	P<0.001
Early Apoptosis	n.s.	P<0.001	P<0.001	P<0.001
Late Apoptosis	n.s.	P<0.001	P<0.001	P<0.001
Necrosis	n.s.	n.s.	n.s.	n.s.

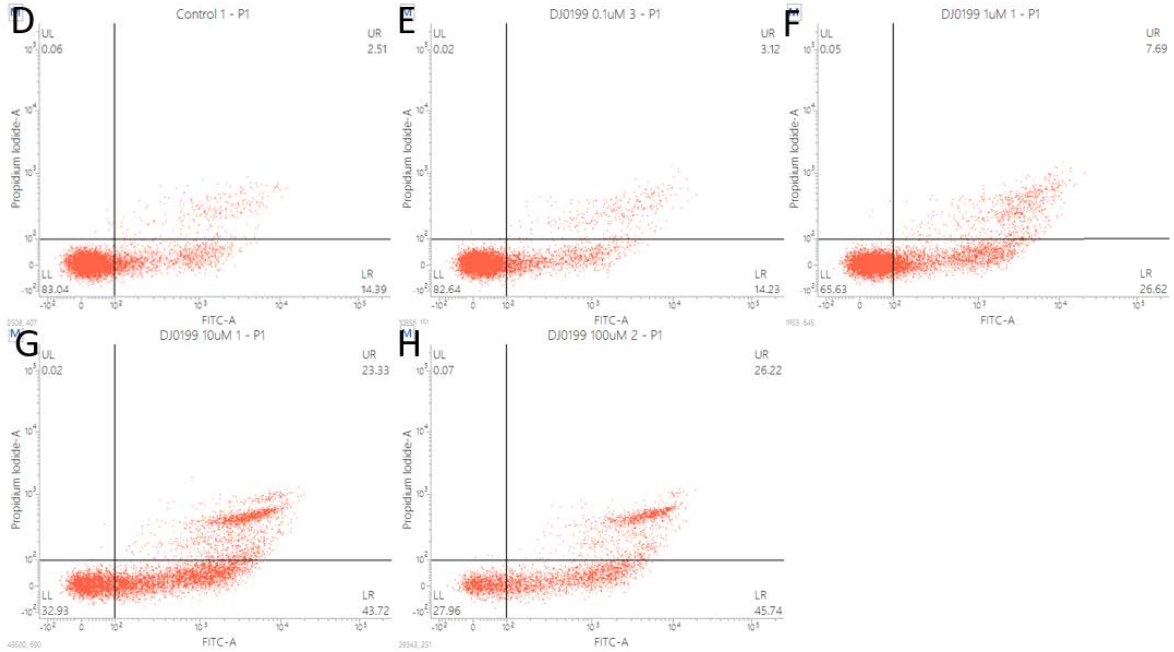

Figure 3-16 Cell viability assays for DAUDI cells treated with various concentrations of Thienopyridine DJ0199 for 72 hours as determined by MTS assay (A) and Annexin V/Propidium Iodine Flow Cytometry (B), and Significance values for One-Way ANOVA with Dunnett's post-hoc test of Untreated Control (DAUDI + complete media) vs each concentration of DJ0199 (C). Representative dot plots for Annexin V/PI Flow Cytometry Untreated Control (D), DJ0199 0.1 μM (E), DJ0199 1 μM (F), DJ0199 10 μM (G) and DJ0199 100 μM (H) are presented where Early Apoptosis (Lower Right Quadrant (LR)) = Annexin V+/PI-, Late Apoptosis (Upper Right Quadrant (UR)) = Annexin V+/PI+, Live Cell (Lower Left Quadrant (LL)) = Annexin V-/PI-, Necrosis (Upper Left Quadrant (UR)) = Annexin V-/PI+.

Data are presented as mean ±SEM of n=3 (untreated control n=6). For MTS (A) data have been normalised against 100 % survival for un-treated cells, and 0 % survival for cells treated with 50 % ethanol for 24 h. For Annexin V/Propidium Iodide (B) data are presented as mean ±SEM of n=3, untreated control n=6.

3.4.1.1.4 DJ0206 effects on DAUDI cell viability

Figure 3-17 to Figure 3-19 show viability (MTS) and apoptosis (AVPI) assay results for DAUDI cells cultured in the presence of novel thienopyridine DJ0206 for 24 hours, 48 hours, and 72 hours respectively.

At 24 hours, DJ0206 shows no significant activity for the viability assay at any concentration (Figure 3-17A). At 48 hours, DAUDI cells treated with 0.1 µM DJ0206 showed a significant ($P<0.01$) increase in cell viability of 184.8 % when normalised to complete media and 50 % EtOH treated DAUDI cells, while there were also non-significant reductions in cell viability to 63.4 % for 10 µM, and 48.5 % for 100 µM treatments (Figure 3-18A). A similar pattern of activity was shown at 72 hours (Figure 3-19A), with significant increases in cell viability at 0.001 µM and 0.01 µM (both $P<0.01$), while cells treated with 1-100- µM (all $P<0.001$) showing reductions in viability to 22.4 %, 18.1 % and -1.2 %, with the 100 µM value the lowest of any of the thienopyridines across all time points and concentrations investigated.

For the apoptosis assay, at 24 hours post-treatment with DJ0206 (Figure 3-17B), the 100 µM showed a small statistically significant increase in late apoptotic and necrotic cells (both $P<0.01$) with a corresponding decrease in live cell population ($P<0.05$). There was also an increase in late apoptosis for 1 µM ($P<0.01$) and necrosis for 10 µM ($P<0.01$). Mirroring the MTS results for DJ0206, at 48 hours (Figure 3-18B) all concentrations showed significantly increased early and late apoptosis (0.1 µM: $P<0.01$, 1-100 µM: $P<0.001$), with reduced live cell populations (all $P<0.001$). The largest effects were seen at 1 µM, 10 µM and 100 µM which showed mean combined apoptotic populations of 49.9 %, 50.9 % and 52.9 % respectively, compared to 16.3 % in the complete media treated cells. Cells treated with 10 µM DJ0206 again showed a small but statistically significant increase in necrosis ($P<0.05$). At 72 hours, there were increased effects at 1 µM to 100 µM (Figure 3-19B), with combined apoptotic populations of 70.3 % ($P<0.001$), 68.7 % ($P<0.001$) and 75.5 % ($P<0.001$) compared to 17.4 % in complete media treated cells. An increase in early apoptosis and decrease in live cell was also seen at 0.1 µM concentration (both $P<0.01$).

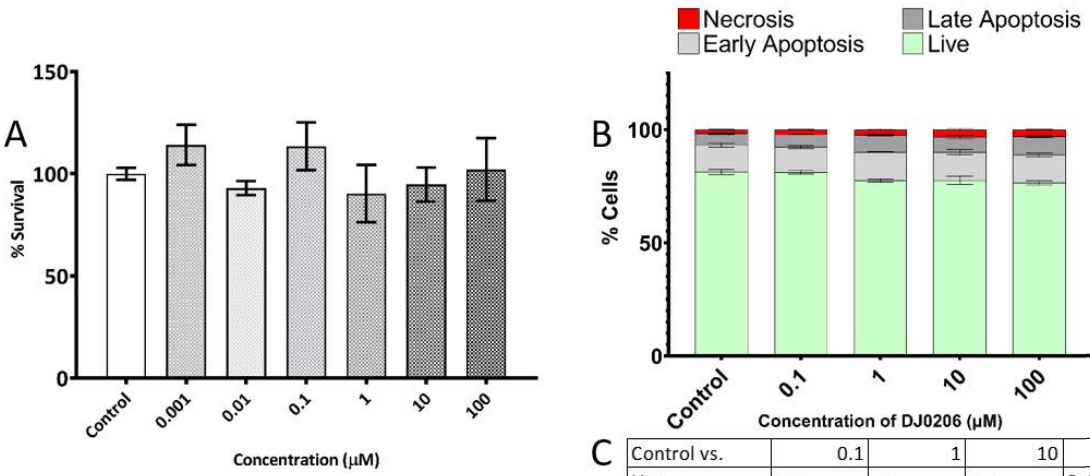

C

Control vs.	0.1	1	10	100
Live	n.s.	n.s.	n.s.	P<0.05
Early Apoptosis	n.s.	n.s.	n.s.	n.s.
Late Apoptosis	n.s.	P<0.01	n.s.	P<0.01
Necrosis	n.s.	n.s.	P<0.01	P<0.01

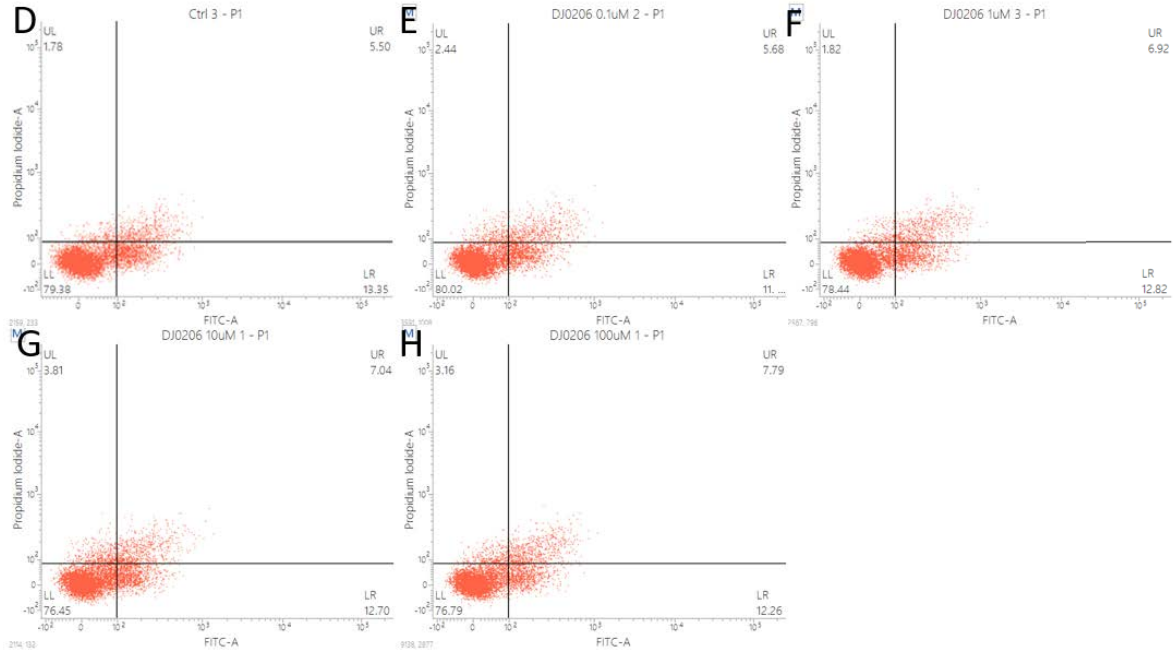

Figure 3-17 Cell viability assays for DAUDI cells treated with various concentrations of Thienopyridine DJ0206 for 24 hours as determined by MTS assay (A) and Annexin V/Propidium Iodine Flow Cytometry (B), and Significance values for One-Way ANOVA with Dunnett's post-hoc test of Untreated Control (DAUDI + complete media) vs each concentration of DJ0206 (C). Representative dot plots for Annexin V/PI Flow Cytometry Untreated Control (D), DJ0206 0.1 μM (E), DJ0206 1 μM (F), DJ0206 10 μM (G) and DJ0206 100 μM (H) are presented where Early Apoptosis (Lower Right Quadrant (LR)) = Annexin V+/PI-, Late Apoptosis (Upper Right Quadrant (UR)) = Annexin V+/PI+, Live Cell (Lower Left Quadrant (LL)) = Annexin V-/PI-, Necrosis (Upper Left Quadrant (UR)) = Annexin V-/PI+.

Data are presented as mean ±SEM of n=3 (untreated control n=6 (MTS, n=3 (AVPI)). For MTS (A) data have been normalised against 100 % survival for un-treated cells, and 0 % survival for cells treated with 50 % ethanol for 24 h. For Annexin V/Propidium Iodide (B) data are presented as mean ±SEM of n=3, untreated control n=6.

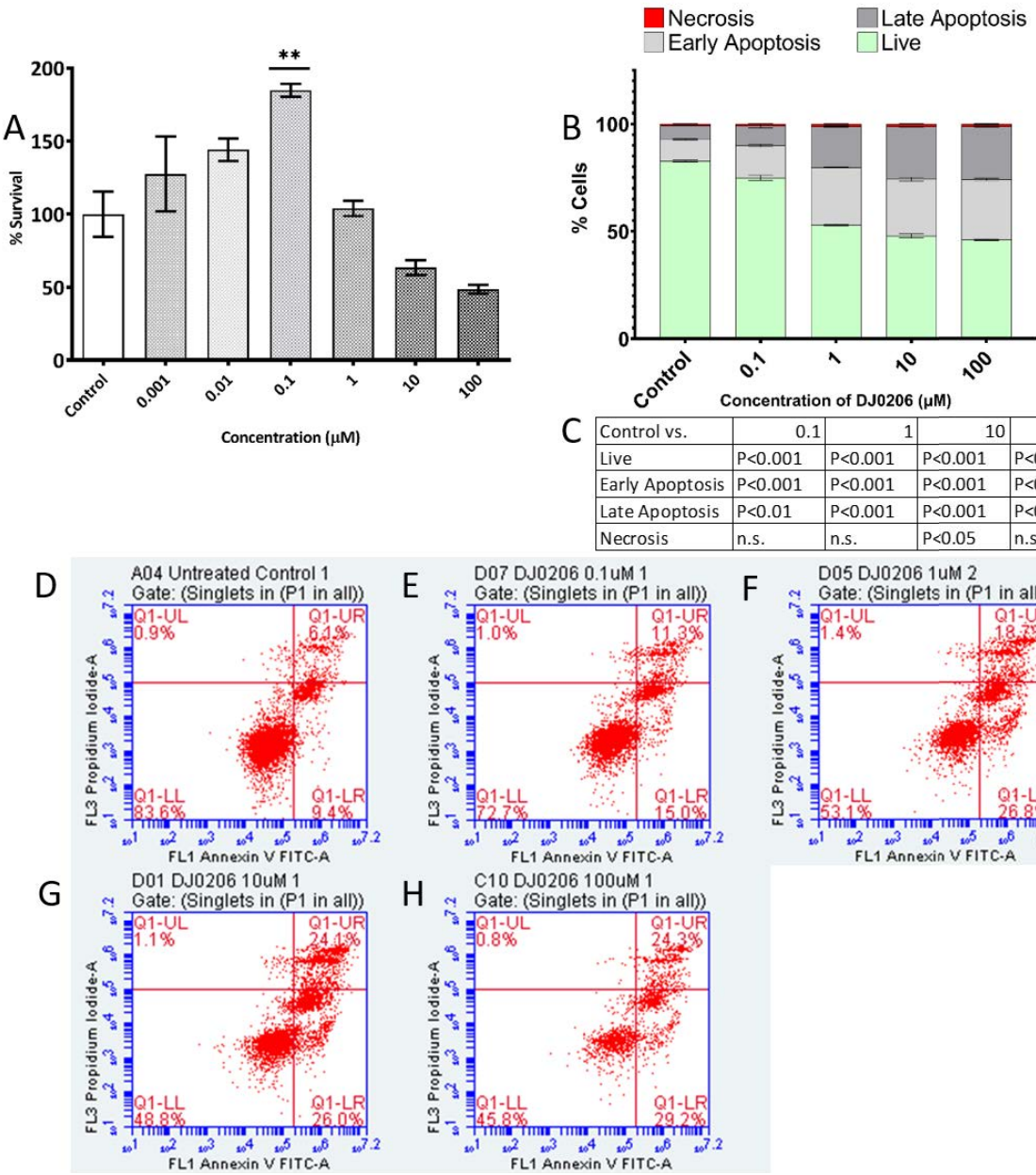

C

Control vs.	0.1	1	10	100
Live	P<0.001	P<0.001	P<0.001	P<0.001
Early Apoptosis	P<0.001	P<0.001	P<0.001	P<0.001
Late Apoptosis	P<0.01	P<0.001	P<0.001	P<0.001
Necrosis	n.s.	n.s.	P<0.05	n.s.

Figure 3-18 Cell viability assays for DAUDI cells treated with various concentrations of Thienopyridine DJ0206 for 48 hours as determined by MTS assay (A) and Annexin V/Propidium Iodine Flow Cytometry (B), and Significance values for One-Way ANOVA with Dunnett's post-hoc test of Untreated Control (DAUDI + complete media) vs each concentration of DJ0206 (C). Representative dot plots for Annexin V/PI Flow Cytometry Untreated Control (D), DJ0206 0.1 µM (E), DJ0206 1 µM (F), DJ0206 10 µM (G) and DJ0206 100 µM (H) are presented where Early Apoptosis (Lower Right Quadrant (LR)) = Annexin V+/PI-, Late Apoptosis (Upper Right Quadrant (UR)) = Annexin V+/PI+, Live Cell (Lower Left Quadrant (LL)) = Annexin V-/PI-, Necrosis (Upper Left Quadrant (UR)) = Annexin V-/PI+.

Data are presented as mean ±SEM of n=3 (untreated control n=6). For MTS (A) data have been normalised against 100 % survival for un-treated cells, and 0 % survival for cells treated with 50 % ethanol for 24 h. For Annexin V/Propidium Iodide (B) data are presented as mean ±SEM of n=3, untreated control n=6.

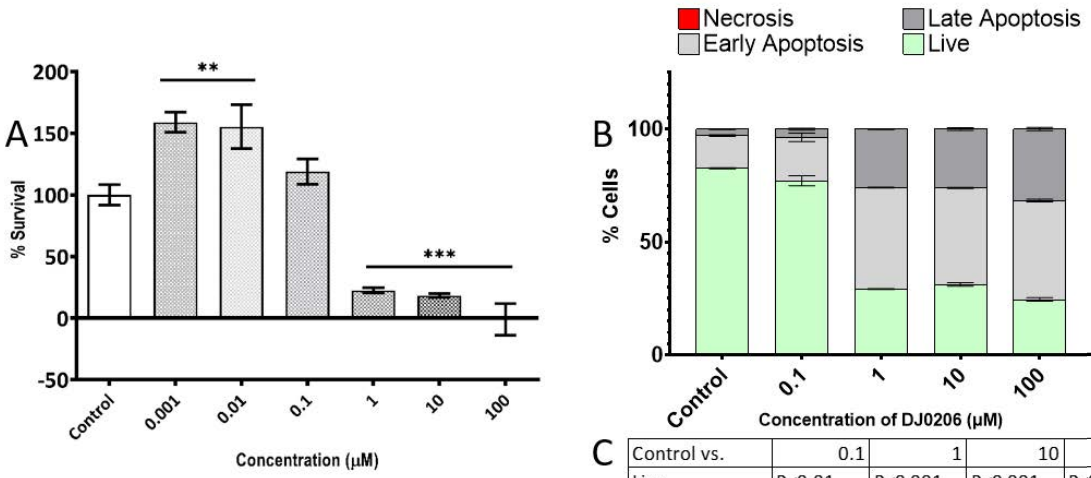

C

Control vs.	0.1	1	10	100
Live	P<0.01	P<0.001	P<0.001	P<0.001
Early Apoptosis	P<0.01	P<0.001	P<0.001	P<0.001
Late Apoptosis	n.s.	P<0.001	P<0.001	P<0.001
Necrosis	n.s.	n.s.	n.s.	n.s.

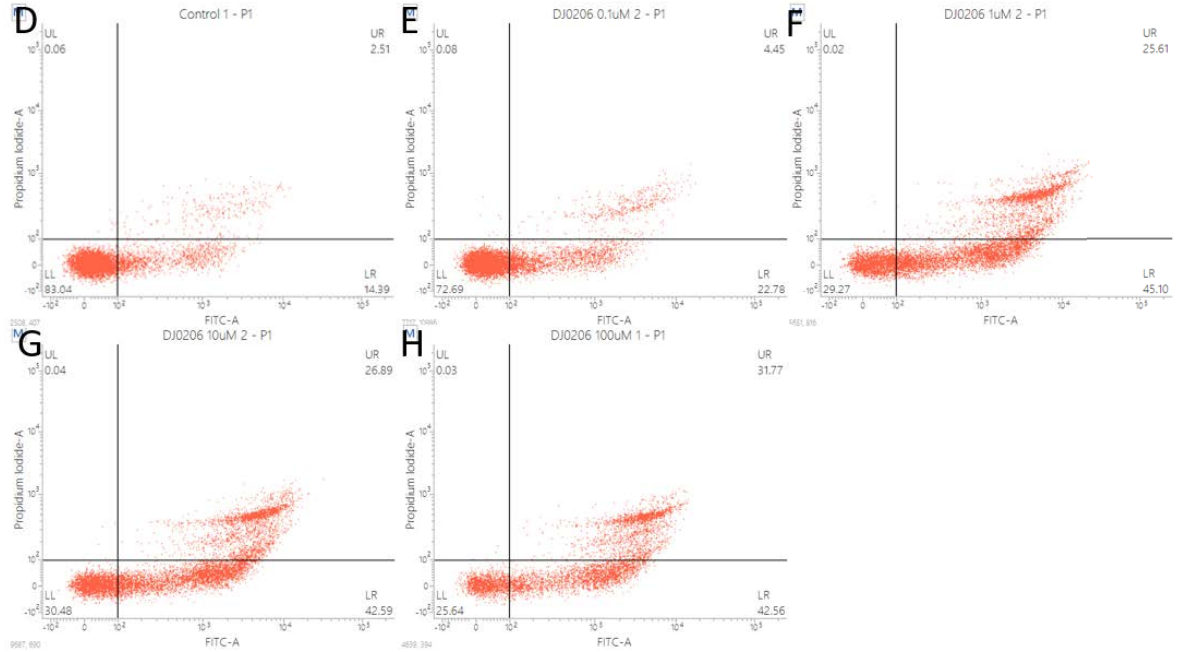

Figure 3-19 Cell viability assays for DAUDI cells treated with various concentrations of Thienopyridine DJ0206 for 72 hours as determined by MTS assay (A) and Annexin V/Propidium Iodine Flow Cytometry (B), and Significance values for One-Way ANOVA with Dunnett's post-hoc test of Untreated Control (DAUDI + complete media) vs each concentration of DJ0206 (C). Representative dot plots for Annexin V/PI Flow Cytometry Untreated Control (D), DJ0206 0.1 μM (E), DJ0206 1 μM (F), DJ0206 10 μM (G) and DJ0206 100 μM (H) are presented where Early Apoptosis (Lower Right Quadrant (LR)) = Annexin V+/PI-, Late Apoptosis (Upper Right Quadrant (UR)) = Annexin V+/PI+, Live Cell (Lower Left Quadrant (LL)) = Annexin V-/PI-, Necrosis (Upper Left Quadrant (UR)) = Annexin V-/PI+.

Data are presented as mean ±SEM of n=3 (untreated control n=6). For MTS (A) data have been normalised against 100 % survival for un-treated cells, and 0 % survival for cells treated with 50 % ethanol for 24 h. For Annexin V/Propidium Iodide (B) data are presented as mean ±SEM of n=3, untreated control n=6.

3.4.1.1.5 DJ0209 effects on DAUDI cell viability

Figure 3-20 to Figure 3-22 show viability (MTS) and apoptosis (AVPI) assay results for DAUDI cells cultured in the presence of novel thienopyridine DJ0209 for 24 hours, 48 hours, and 72 hours respectively.

In keeping with the other cyclooctane ring containing thienopyridines, DJ0209 also showed no effects on cell viability at 24 hours (Figure 3-20A). At 48 hours, there were slight, non-statistically significant increases at 0.001 µM to 1 µM concentrations, while there were reductions in cell viability at both 10 µM ($P<0.01$) and 100 µM ($P<0.001$) (Figure 3-21B). At 72 hours, there were again no statistically significant results, however there was an increase in cell viability at 10 µM and 100 µM compared to complete media control cells (Figure 3-22B).

For the apoptosis assay, no effects were seen at 24 hours (Figure 3-20B), apart from a decrease in necrotic cells at 100 µM ($P<0.05$). After 48 hours of treatment with DJ0209 (Figure 3-21B), there was an increase in early apoptosis at 0.1 µM ($P<0.01$), in late apoptosis at 1 µM ($P<0.05$) and in both early and late apoptosis at 10 µM and 100 µM concentrations (all $P<0.001$), with corresponding decreases in live cell populations (0.1 µM / 1 µM $P<0.05$; 10 µM / 100 µM $P<0.001$). The combined mean early and late apoptotic cell populations for 10 µM and 100 µM were 33.1 % and 41.8 %, compared to 21.6 % in complete media control cell replicates. At 72 hours (Figure 3-22B), there was an increase in early apoptosis at 1 µM ($P<0.05$), and early and late apoptosis at 10 µM and 100 µM (both $P<0.001$) with corresponding decreases in live cell populations. There was also a slight increase in necrotic cells at 10 µM ($P<0.01$). The combined early and late apoptotic populations for 10 µM was 45.3 % while at 100 µM it was 34.2 %, compared to 15.3 % for complete media treated cells, which is similar level to that seen at 48 hours.

Across all datasets, there were increases in cell viability at lower concentrations of thienopyridine treatment, possible due to cell stress effects (D'Arcy, 2019).

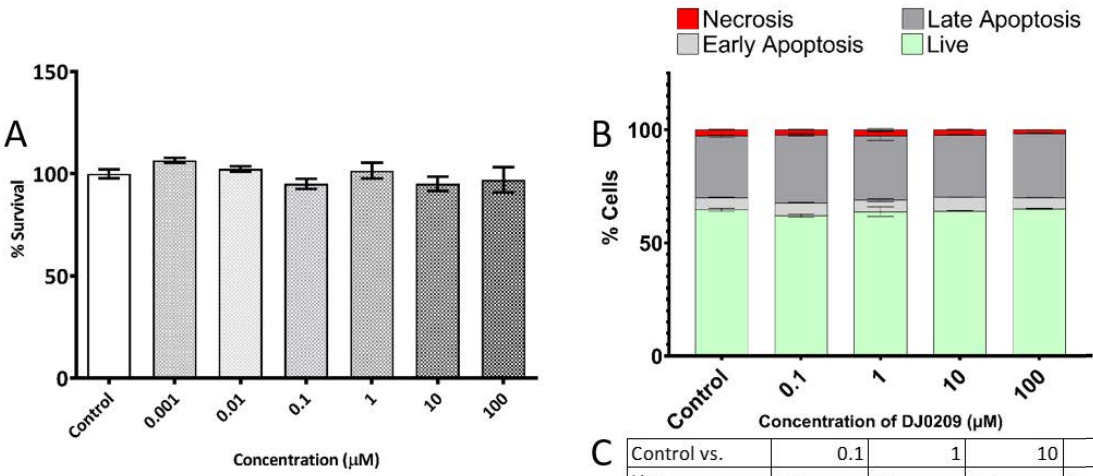

C

Control vs.	0.1	1	10	100
Live	n.s.	n.s.	n.s.	n.s.
Early Apoptosis	n.s.	n.s.	n.s.	n.s.
Late Apoptosis	n.s.	n.s.	n.s.	n.s.
Necrosis	n.s.	n.s.	n.s.	P<0.05

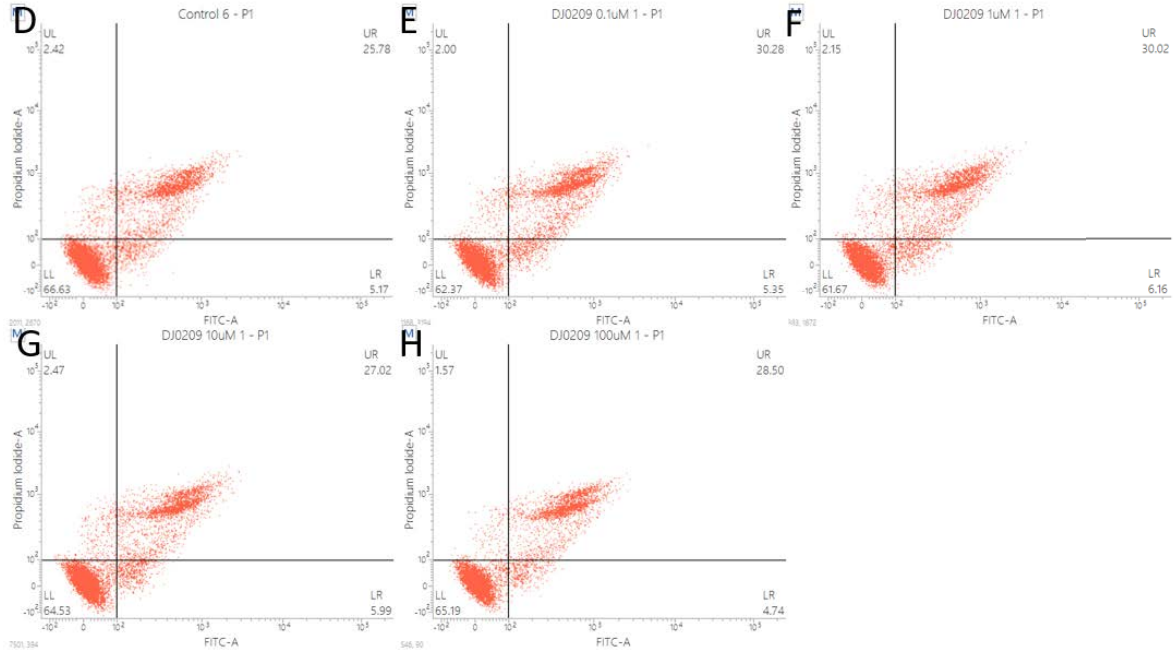

Figure 3-20 Cell viability assays for DAUDI cells treated with various concentrations of Thienopyridine DJ0209 for 24 hours as determined by MTS assay (A) and Annexin V/Propidium Iodine Flow Cytometry (B), and Significance values for One-Way ANOVA with Dunnett's post-hoc test of Untreated Control (DAUDI + complete media) vs each concentration of DJ0209 (C). Representative dot plots for Annexin V/PI Flow Cytometry Untreated Control (D), DJ0209 0.1 μM (E), DJ0209 1 μM (F), DJ0209 10 μM (G) and DJ0209 100 μM (H) are presented where Early Apoptosis (Lower Right Quadrant (LR)) = Annexin V+/PI-, Late Apoptosis (Upper Right Quadrant (UR)) = Annexin V+/PI+, Live Cell (Lower Left Quadrant (LL)) = Annexin V-/PI-, Necrosis (Upper Left Quadrant (UR)) = Annexin V-/PI+.

Data are presented as mean ±SEM of n=3 (untreated control n=6). For MTS (A) data have been normalised against 100 % survival for un-treated cells, and 0 % survival for cells treated with 50 % ethanol for 24 h. For Annexin V/Propidium Iodide (B) data are presented as mean ±SEM of n=3, untreated control n=6.

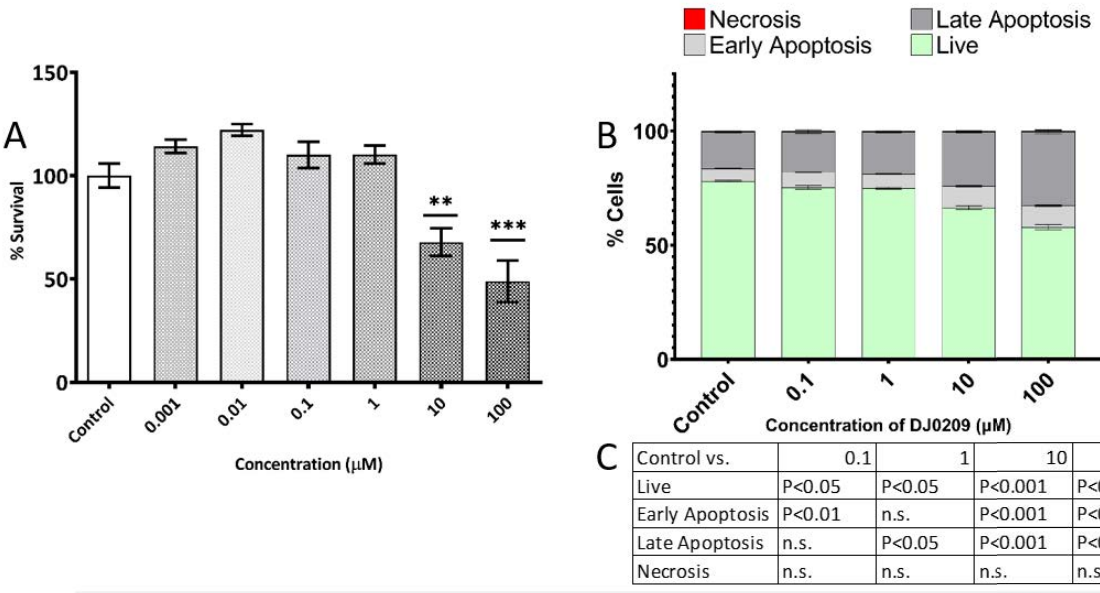

C

Control vs.	0.1	1	10	100
Live	P<0.05	P<0.05	P<0.001	P<0.001
Early Apoptosis	P<0.01	n.s.	P<0.001	P<0.001
Late Apoptosis	n.s.	P<0.05	P<0.001	P<0.001
Necrosis	n.s.	n.s.	n.s.	n.s.

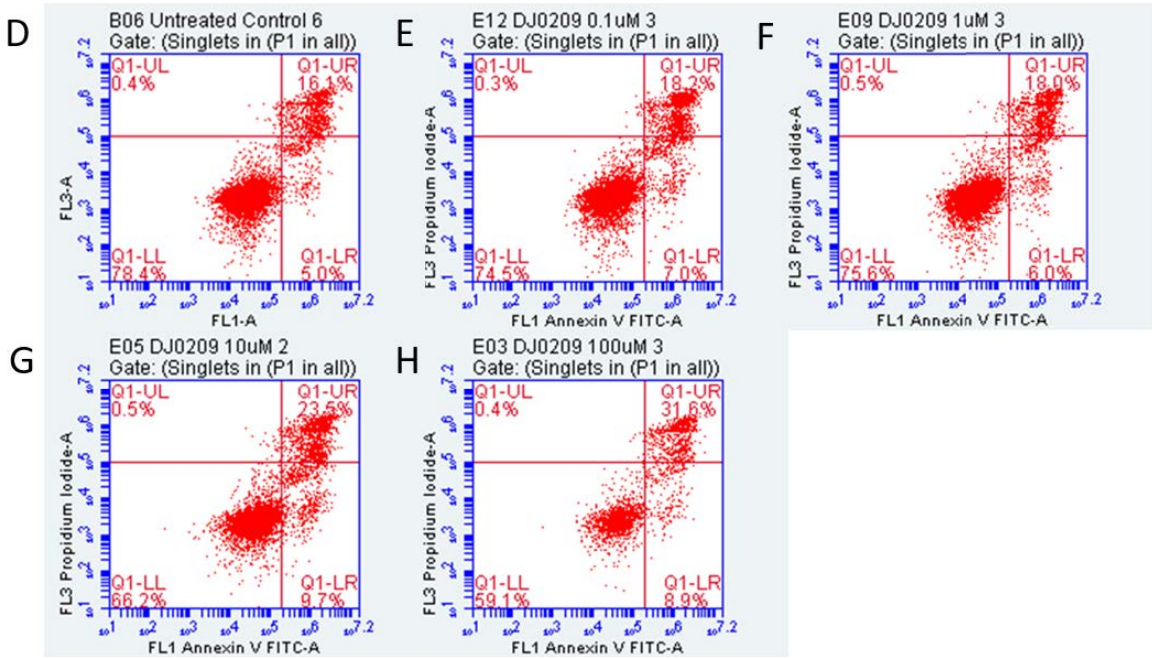

Figure 3-21 Cell viability assays for DAUDI cells treated with various concentrations of Thienopyridine DJ0209 for 48 hours as determined by MTS assay (A) and Annexin V/Propidium Iodine Flow Cytometry (B), and Significance values for One-Way ANOVA with Dunnett's post-hoc test of Untreated Control (DAUDI + complete media) vs each concentration of DJ0209 (C). Representative dot plots for Annexin V/PI Flow Cytometry Untreated Control (D), DJ0209 0.1 μM (E), DJ0209 1 μM (F), DJ0209 10 μM (G) and DJ0209 100 μM (H) are presented where Early Apoptosis (Lower Right Quadrant (LR)) = Annexin V+/PI-, Late Apoptosis (Upper Right Quadrant (UR)) = Annexin V+/PI+, Live Cell (Lower Left Quadrant (LL)) = Annexin V-/PI-, Necrosis (Upper Left Quadrant (UR)) = Annexin V-/PI+.

Data are presented as mean ±SEM of n=3 (untreated control n=6). For MTS (A) data have been normalised against 100 % survival for un-treated cells, and 0 % survival for cells treated with 50 % ethanol for 24 h. For Annexin V/Propidium Iodide (B) data are presented as mean ±SEM of n=3, untreated control n=6.

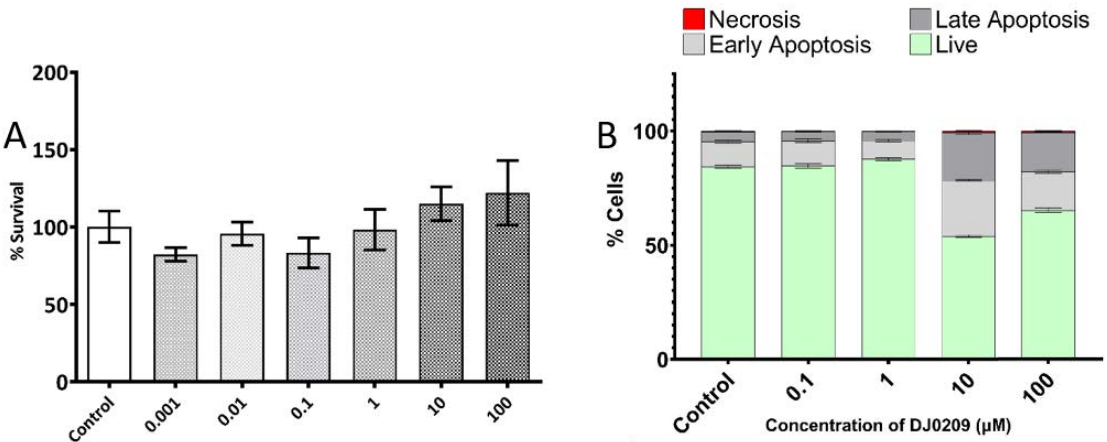

C

Control vs.	0.1	1	10	100
Live	n.s.	P<0.05	P<0.001	P<0.001
Early Apoptosis	n.s.	P<0.05	P<0.001	P<0.001
Late Apoptosis	n.s.	n.s.	P<0.001	P<0.001
Necrosis	n.s.	n.s.	P<0.01	n.s.

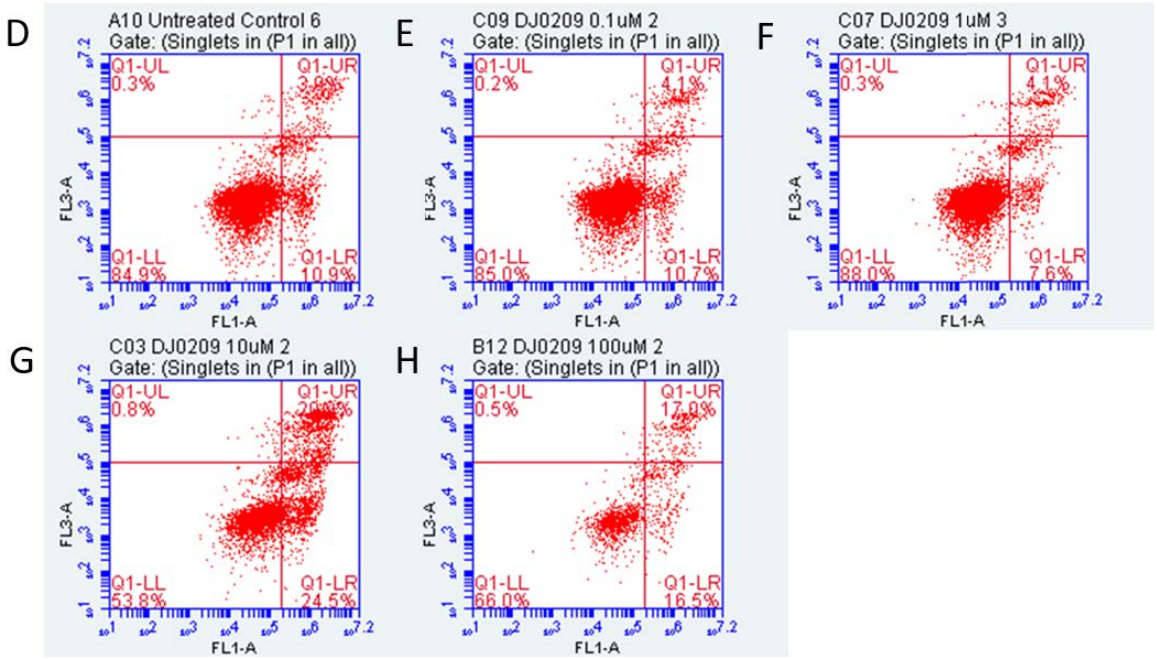

Figure 3-22 Cell viability assays for DAUDI cells treated with various concentrations of Thienopyridine DJ0209 for 72 hours as determined by MTS assay (A) and Annexin V/Propidium Iodine Flow Cytometry (B), and Significance values for One-Way ANOVA with Dunnett's post-hoc test of Untreated Control (DAUDI + complete media) vs each concentration of DJ0209 (C). Representative dot plots for Annexin V/PI Flow Cytometry Untreated Control (D), DJ0209 0.1 μM (E), DJ0209 1 μM (F), DJ0209 10 μM (G) and DJ0209 100 μM (H) are presented where Early Apoptosis (Lower Right Quadrant (LR)) = Annexin V+/PI-, Late Apoptosis (Upper Right Quadrant (UR)) = Annexin V+/PI+, Live Cell (Lower Left Quadrant (LL)) = Annexin V-/PI-, Necrosis (Upper Left Quadrant (UR)) = Annexin V-/PI+.

Data are presented as mean ±SEM of n=3 (untreated control n=6). For MTS (A) data have been normalised against 100 % survival for un-treated cells, and 0 % survival for cells treated with 50 % ethanol for 24 h. For Annexin V/Propidium Iodide (B) data are presented as mean ±SEM of n=3, untreated control n=6.

3.4.1.2 Effects of novel thienopyridines with a cycloheptane moiety on cell viability

Novel thienopyridine compounds DJ0041 and DJ0081 both share a cycloheptane moiety in their chemical structure, which as described in section 3.4.1.1, has been shown to induce more cytotoxic effects on cells cultured in the presence of these compounds.

3.4.1.2.1 DJ0041 effects on DAUDI cell viability

Figure 3-23 to Figure 3-25 show viability (MTS) and apoptosis (AVPI) assay results for DAUDI cells cultured in the presence of novel thienopyridine DJ0041 for 24 hours, 48 hours, and 72 hours respectively.

For viability assay, cells treated with 10 µM of DJ0041 showed a statistically significant reduction in cell viability at 24 hours (Figure 3-23A: mean cell viability 87.9 %, $P<0.05$), 48 hours (Figure 3-24A: mean cell viability 71.3 %, $P<0.001$), and at 72 hours (Figure 3-25A: mean cell viability 40.7 %, $P<0.01$).

Non-significant decreases in cell viability were seen at 48 hours at 100 µM (mean cell viability 89.6 %) and at 72 hours at 1 µM (84.5 %) and 100 µM (67.9 %), while at concentrations of 0.001-0.1 µM there was a general increase in cell viability compared to complete media control cell replicates across all three time points investigated.

For the apoptosis assay, across all three time points, cells treated with DJ0041 at 10 µM and 100 µM showed significant increases in early and late apoptotic cells, with a corresponding decrease in live cell populations: (all $P<0.001$). The combined early and late apoptosis at 48 hours (Figure 3-24B) for 10 µM and 100 µM treated cells was 37.8 % and 41.1 % respectively, while at 72 hours (Figure 3-25B) this increased to 55.8 % and 53.5 %.

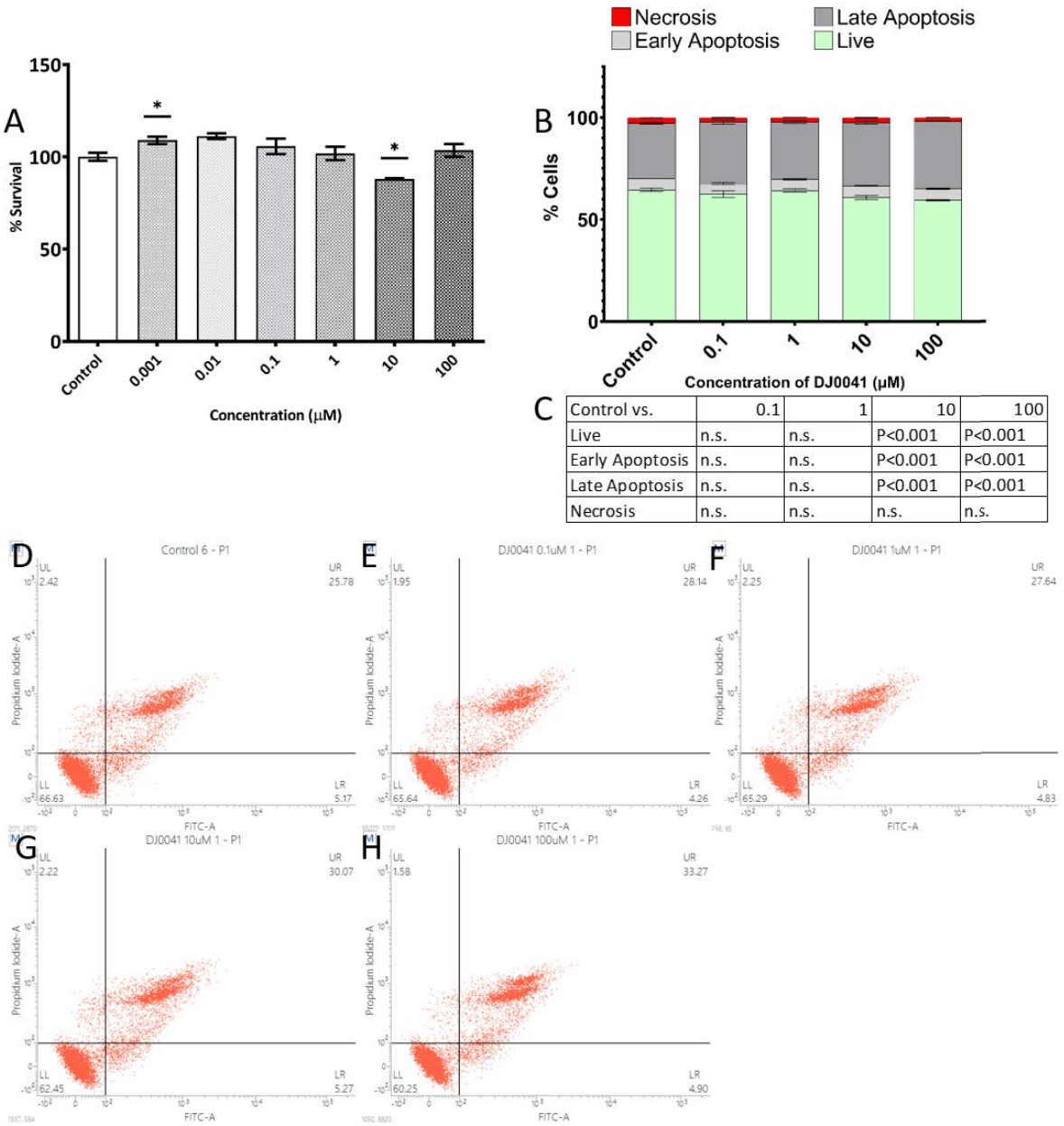

C

Control vs.	0.1	1	10	100
Live	n.s.	n.s.	P<0.001	P<0.001
Early Apoptosis	n.s.	n.s.	P<0.001	P<0.001
Late Apoptosis	n.s.	n.s.	P<0.001	P<0.001
Necrosis	n.s.	n.s.	n.s.	n.s.

Figure 3-23 Cell viability assays for DAUDI cells treated with various concentrations of Thienopyridine DJ0041 for 24 hours as determined by MTS assay (A) and Annexin V/Propidium Iodine Flow Cytometry (B), and Significance values for One-Way ANOVA with Dunnett's post-hoc test of Untreated Control (DAUDI + complete media) vs each concentration of DJ0041 (C). Representative dot plots for Annexin V/PI Flow Cytometry Untreated Control (D), DJ0041 0.1 μM (E), DJ0041 1 μM (F), DJ0041 10 μM (G) and DJ0041 100 μM (H) are presented where Early Apoptosis (Lower Right Quadrant (LR)) = Annexin V+/PI-, Late Apoptosis (Upper Right Quadrant (UR)) = Annexin V+/PI+, Live Cell (Lower Left Quadrant (LL)) = Annexin V-/PI-, Necrosis (Upper Left Quadrant (UR)) = Annexin V-/PI+.

Data are presented as mean ±SEM of n=3 (untreated control n=6). For MTS (A) data have been normalised against 100 % survival for un-treated cells, and 0 % survival for cells treated with 50 % ethanol for 24 h. For Annexin V/Propidium Iodide (B) data are presented as mean ±SEM of n=3, untreated control n=6.

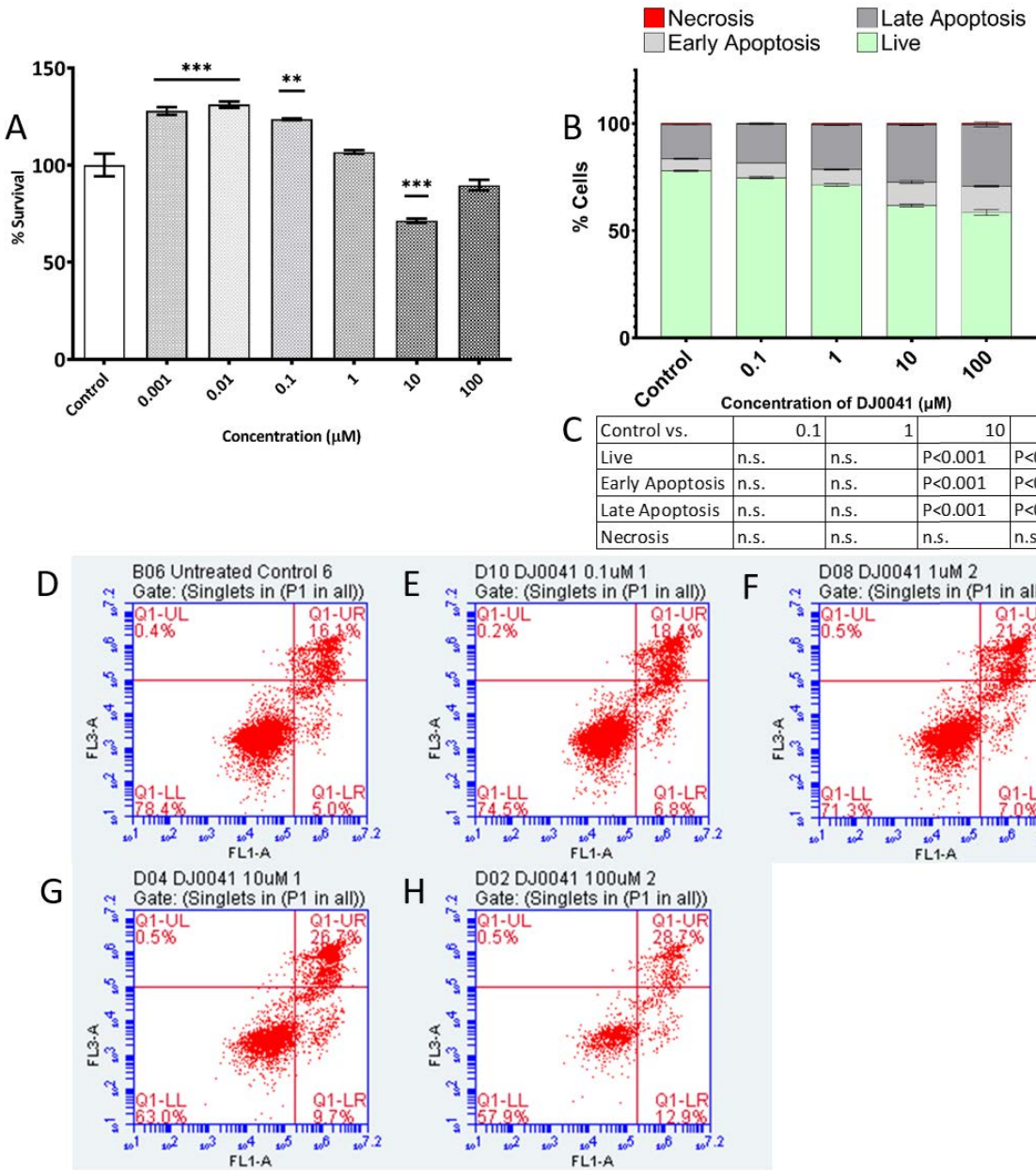

Control vs.	0.1	1	10	100
Live	n.s.	n.s.	P<0.001	P<0.001
Early Apoptosis	n.s.	n.s.	P<0.001	P<0.001
Late Apoptosis	n.s.	n.s.	P<0.001	P<0.001
Necrosis	n.s.	n.s.	n.s.	n.s.

Figure 3-24 Cell viability assays for DAUDI cells treated with various concentrations of Thienopyridine DJ0041 for 48 hours as determined by MTS assay (A) and Annexin V/Propidium Iodine Flow Cytometry (B), and Significance values for One-Way ANOVA with Dunnett's post-hoc test of Untreated Control (DAUDI + complete media) vs each concentration of DJ0041 (C). Representative dot plots for Annexin V/PI Flow Cytometry Untreated Control (D), DJ0041 0.1 μM (E), DJ0041 1 μM (F), DJ0041 10 μM (G) and DJ0041 100 μM (H) are presented where Early Apoptosis (Lower Right Quadrant (LR)) = Annexin V+/PI-, Late Apoptosis (Upper Right Quadrant (UR)) = Annexin V+/PI+, Live Cell (Lower Left Quadrant (LL)) = Annexin V-/PI-, Necrosis (Upper Left Quadrant (UR)) = Annexin V-/PI+.

Data are presented as mean ±SEM of n=3 (untreated control n=6). For MTS (A) data have been normalised against 100 % survival for un-treated cells, and 0 % survival for cells treated with 50 % ethanol for 24 h. For Annexin V/Propidium Iodide (B) data are presented as mean ±SEM of n=3, untreated control n=6.

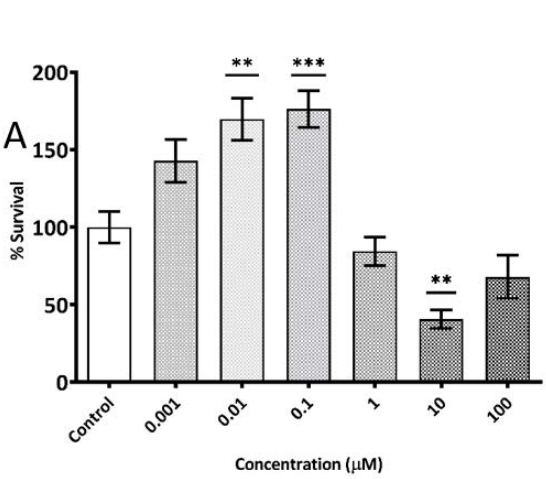

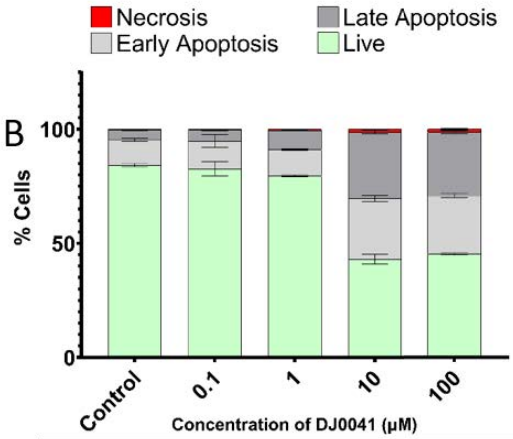

C

Control vs.	0.1	1	10	100
Live	n.s.	n.s.	P<0.001	P<0.001
Early Apoptosis	n.s.	n.s.	P<0.001	P<0.001
Late Apoptosis	n.s.	n.s.	P<0.001	P<0.001
Necrosis	n.s.	n.s.	n.s.	n.s.

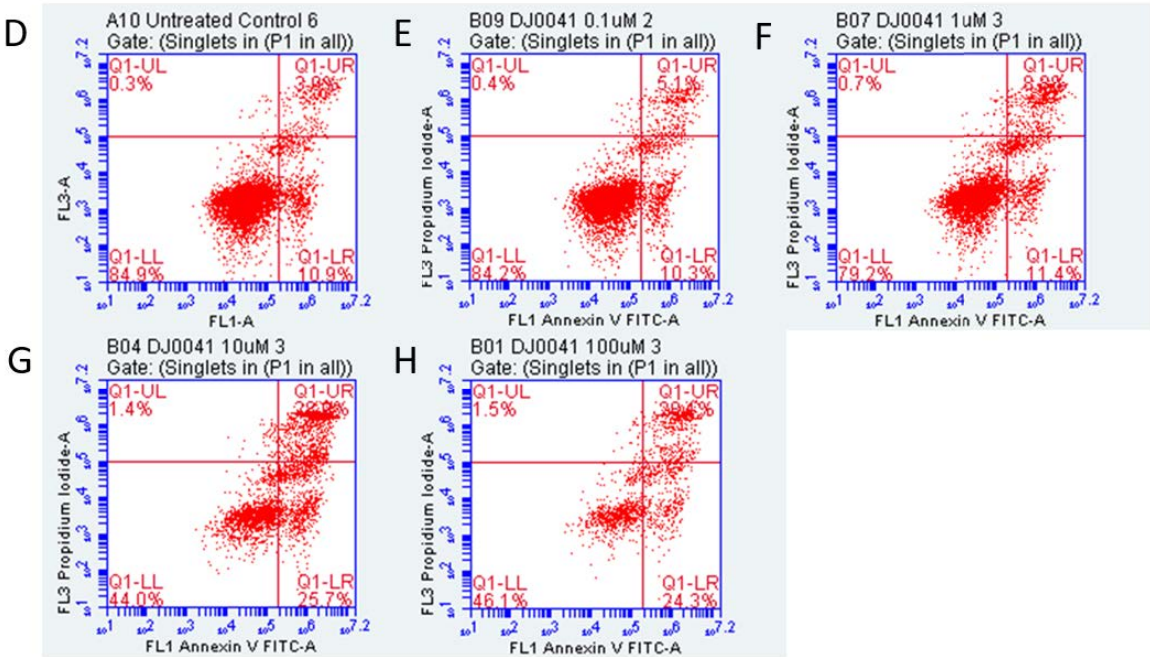

Figure 3-25 Cell viability assays for DAUDI cells treated with various concentrations of Thienopyridine DJ0041 for 72 hours as determined by MTS assay (A) and Annexin V/Propidium Iodine Flow Cytometry (B), and Significance values for One-Way ANOVA with Dunnett's post-hoc test of Untreated Control (DAUDI + complete media) vs each concentration of DJ0041 (C). Representative dot plots for Annexin V/PI Flow Cytometry Untreated Control (D), DJ0041 0.1 μM (E), DJ0041 1 μM (F), DJ0041 10 μM (G) and DJ0041 100 μM (H) are presented where Early Apoptosis (Lower Right Quadrant (LR)) = Annexin V+/PI-, Late Apoptosis (Upper Right Quadrant (UR)) = Annexin V+/PI+, Live Cell (Lower Left Quadrant (LL)) = Annexin V-/PI-, Necrosis (Upper Left Quadrant (UR)) = Annexin V-/PI+.

Data are presented as mean ±SEM of n=3 (untreated control n=6). For MTS (A) data have been normalised against 100 % survival for un-treated cells, and 0 % survival for cells treated with 50 % ethanol for 24 h. For Annexin V/Propidium Iodide (B) data are presented as mean ±SEM of n=3, untreated control n=6.

3.4.1.2.2 DJ0081 effects on DAUDI cell viability

Figure 3-26 to Figure 3-28 show viability (MTS) and apoptosis (AVPI) assay results for DAUDI cells cultured in the presence of novel thienopyridine DJ0081 for 24 hours, 48 hours, and 72 hours respectively.

Similarly to DJ0041, at 24 hours on the viability assay, no effects were seen apart from a slight increase in cell viability compared to complete media control for all concentrations of DJ0081 (Figure 3-26A). At both 48 hours (Figure 3-27A) and 72 hours (Figure 3-28A) similar effects were seen, with significant reduction in cell viability at 1 µM (mean cell viability:–48 h - 50.3 %/ 72 h -49.4 %; both $P<0.01$), 10 µM (mean cell viability:–48 h - 51.3 %/ 72 h -37.7 %; both $P<0.01$) and 100 µM (mean cell viability: 48 h – 33.4 %/ 72 h -32.8 %; both <0.001).

For the apoptosis assay, at 24 hours of treatment there was a small, statistically significant increase in cells at late apoptosis across all concentrations investigated, while 100 µM also showed an increase in early apoptotic cells as well as a corresponding decrease in live cell population (Figure 3-26B). Figure 3-27B shows that a larger increase in early and late apoptotic cells was seen at 48 hours both at 10 µM (combined early and late apoptosis 31.9 %, both $P<0.001$) and at 100 µM (combined early and late apoptosis 48.3 %, both $P<0.001$) compared to 16.3 % total apoptosis in complete media controls. More pronounced effects were seen at 72 hours (Figure 3-28B), with combined early and late apoptosis at 1 µM of 60.5 % (both $P<0.001$); 63.3 % at 10 µM (both $P<0.001$); and 69.6 % at 100 µM, with corresponding decrease in live cell populations (all $P<0.001$), compared to combined early and late apoptosis of 17.4 % in complete media control replicates.

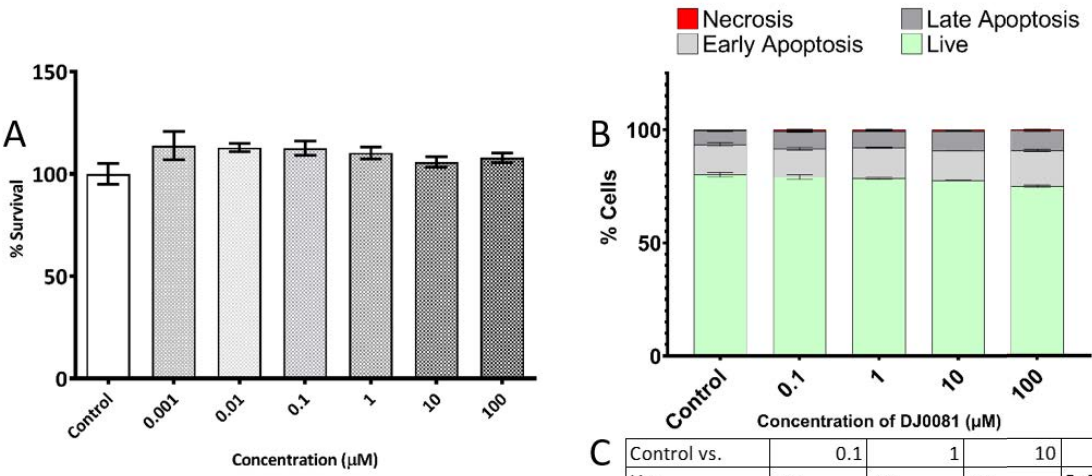

C

Control vs.	0.1	1	10	100
Live	n.s.	n.s.	n.s.	P<0.01
Early Apoptosis	n.s.	n.s.	n.s.	P<0.05
Late Apoptosis	P<0.01	P<0.05	P<0.001	P<0.001
Necrosis	n.s.	n.s.	n.s.	n.s.

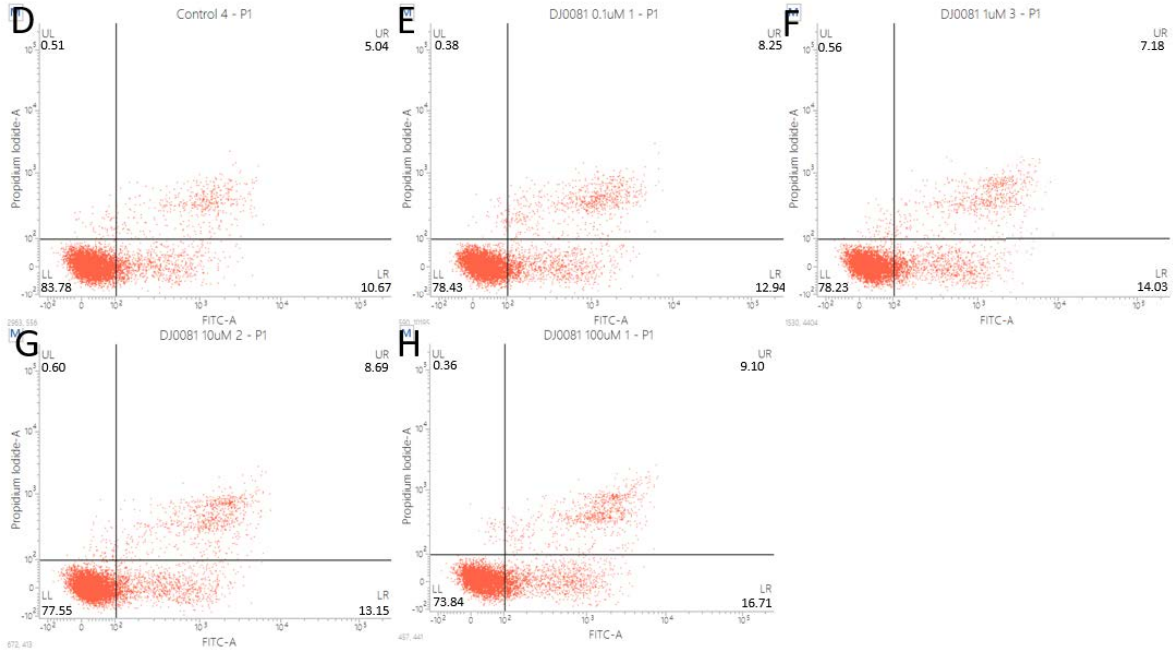

Figure 3-26 Cell viability assays for DAUDI cells treated with various concentrations of Thienopyridine DJ0081 for 24 hours as determined by MTS assay (A) and Annexin V/Propidium Iodine Flow Cytometry (B), and Significance values for One-Way ANOVA with Dunnett's post-hoc test of Untreated Control (DAUDI + complete media) vs each concentration of DJ0081 (C). Representative dot plots for Annexin V/PI Flow Cytometry Untreated Control (D), DJ0081 0.1 μM (E), DJ0081 1 μM (F), DJ0081 10 μM (G) and DJ0081 100 μM (H) are presented where Early Apoptosis (Lower Right Quadrant (LR)) = Annexin V+/PI-, Late Apoptosis (Upper Right Quadrant (UR)) = Annexin V+/PI+, Live Cell (Lower Left Quadrant (LL)) = Annexin V-/PI-, Necrosis (Upper Left Quadrant (UR)) = Annexin V-/PI+.

Data are presented as mean ±SEM of n=3 (untreated control n=6). For MTS (A) data have been normalised against 100 % survival for un-treated cells, and 0 % survival for cells treated with 50 % ethanol for 24 h. For Annexin V/Propidium Iodide (B) data are presented as mean ±SEM of n=3, untreated control n=6.

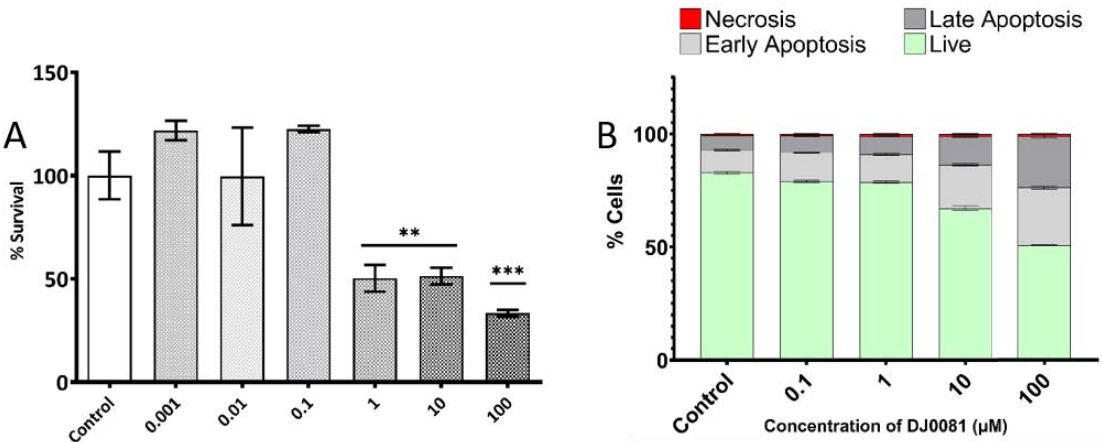

C

Control vs.	0.1	1	10	100
Live	n.s.	n.s.	P<0.001	P<0.001
Early Apoptosis	n.s.	n.s.	P<0.001	P<0.001
Late Apoptosis	n.s.	n.s.	P<0.001	P<0.001
Necrosis	n.s.	n.s.	n.s.	n.s.

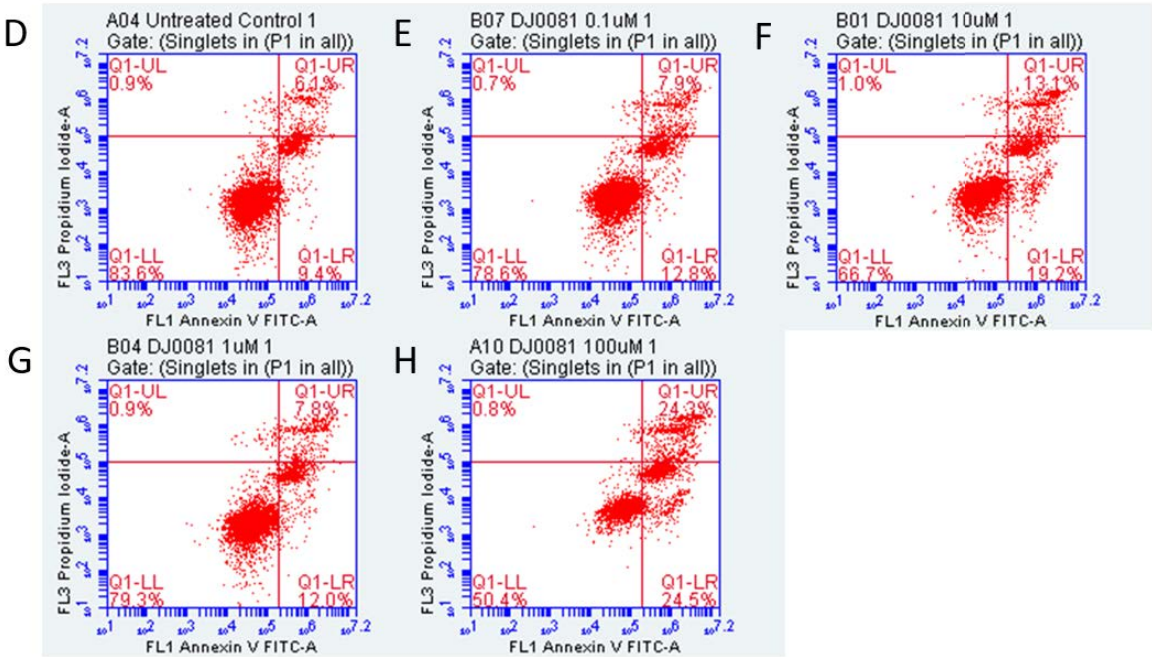

Figure 3-27 Cell viability assays for DAUDI cells treated with various concentrations of Thienopyridine DJ0081 for 48 hours as determined by MTS assay (A) and Annexin V/Propidium Iodine Flow Cytometry (B), and Significance values for One-Way ANOVA with Dunnett's post-hoc test of Untreated Control (DAUDI + complete media) vs each concentration of DJ0081 (C). Representative dot plots for Annexin V/PI Flow Cytometry Untreated Control (D), DJ0081 0.1 μM (E), DJ0081 1 μM (F), DJ0081 10 μM (G) and DJ0081 100 μM (H) are presented where Early Apoptosis (Lower Right Quadrant (LR)) = Annexin V+/PI-, Late Apoptosis (Upper Right Quadrant (UR)) = Annexin V+/PI+, Live Cell (Lower Left Quadrant (LL)) = Annexin V-/PI-, Necrosis (Upper Left Quadrant (UR)) = Annexin V-/PI+.

Data are presented as mean ±SEM of n=3 (0.001 μM n=2 (MTS), untreated control n=4 (MTS), n=6 (AVPI). For MTS (A) data have been normalised against 100 % survival for un-treated cells, and 0 % survival for cells treated with 50 % ethanol for 24 h. For Annexin V/Propidium Iodide (B) data are presented as mean ±SEM of n=3, untreated control n=6.

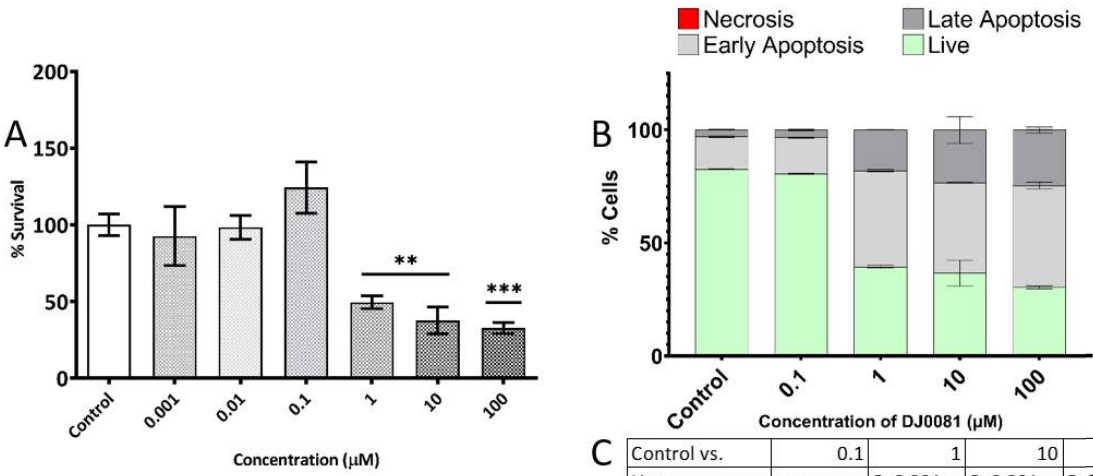

C

Control vs.	0.1	1	10	100
Live	n.s.	P<0.001	P<0.001	P<0.001
Early Apoptosis	n.s.	P<0.001	P<0.001	P<0.001
Late Apoptosis	n.s.	P<0.001	P<0.001	P<0.001
Necrosis	n.s.	n.s.	n.s.	n.s.

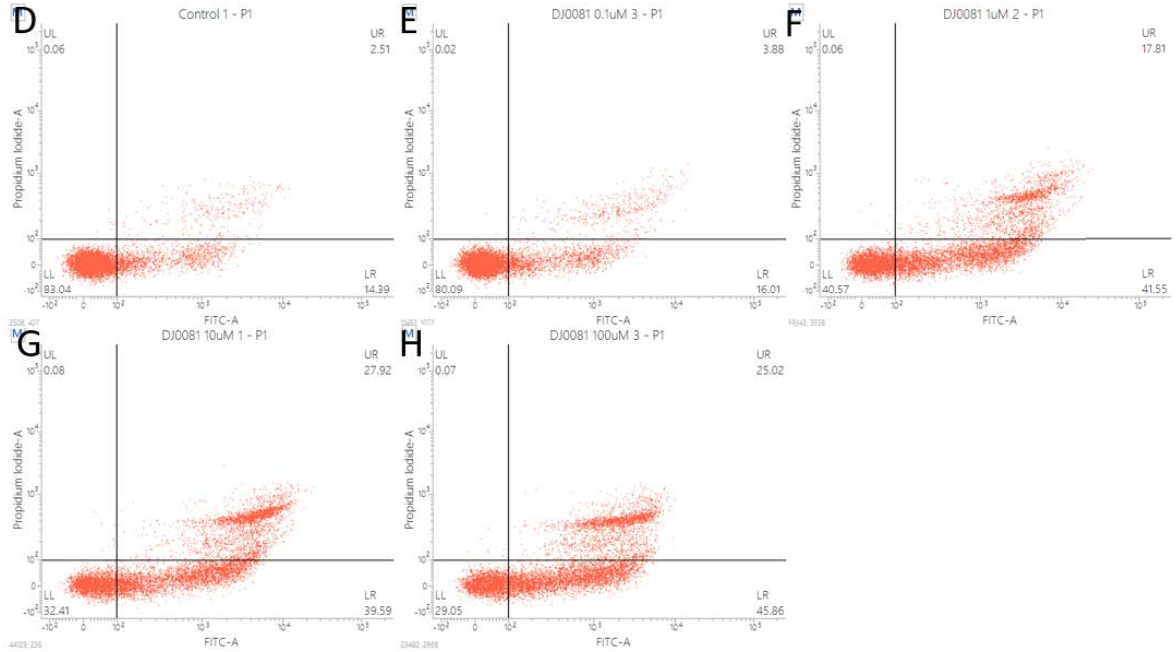

Figure 3-28 Cell viability assays for DAUDI cells treated with various concentrations of Thienopyridine DJ0081 for 72 hours as determined by MTS assay (A) and Annexin V/Propidium Iodine Flow Cytometry (B), and Significance values for One-Way ANOVA with Dunnett's post-hoc test of Untreated Control (DAUDI + complete media) vs each concentration of DJ0081 (C). Representative dot plots for Annexin V/PI Flow Cytometry Untreated Control (D), DJ0081 0.1 μM (E), DJ0081 1 μM (F), DJ0081 10 μM (G) and DJ0081 100 μM (H) are presented where Early Apoptosis (Lower Right Quadrant (LR)) = Annexin V+/PI-, Late Apoptosis (Upper Right Quadrant (UR)) = Annexin V+/PI+, Live Cell (Lower Left Quadrant (LL)) = Annexin V-/PI-, Necrosis (Upper Left Quadrant (UR)) = Annexin V-/PI+.

Data are presented as mean ±SEM of n=3 (untreated control n=6). For MTS (A) data have been normalised against 100 % survival for un-treated cells, and 0 % survival for cells treated with 50 % ethanol for 24 h. For Annexin V/Propidium Iodide (B) data are presented as mean ±SEM of n=3, untreated control n=6.

3.4.1.3 Effects of novel thienopyridines with a cyclohexanone moiety on cell viability

The final three novel thienopyridine compounds DJ0097, DJ0109 and DJ0171 all share a cyclohexanone moiety in their chemical structure (see Table 2-8), which as described in sections 3.4.2.1 and 0 have been shown in previous research to induce more cytostatic effects on cells cultured in the presence of these compounds, in comparison to the more cytotoxic effects in cyclooctane and cycloheptane moiety containing thienopyridine.

3.4.1.3.1 DJ0097 effects on DAUDI cell viability

Figure 3-29 to Figure 3-31 show the results for DAUDI cells cultured in the presence of novel thienopyridine DJ0097 for 24 hours, 48 hours, and 72 hours respectively. Figure 3-29A shows the viability assay results at 24 hours of treatment with DJ0097, where only slight, non-statistically significant reductions in cell viability are seen at 0.01 to 100 µM concentrations. Figure 3-30A showed a mixed picture at 48 hours of treatment, with 0.001 µM, 0.1 µM ($P<0.05$) and 1 µM concentrations showed an increase in cell viability compared to complete media control, while the other concentrations showed a slight decrease. At 72 hours of treatment (Figure 3-31A), 0.001 µM and 0.01 µM show large but non-statistically significant increases in cell viability (165.1 % and 137.6 % respectively), while 0.1 µM (59.4 % cell viability), 1 µM (28.7% cell viability, $P<0.05$), 10 µM (20.6 % cell viability, $P<0.05$) and 100 µM (cell viability 75.9%) all showed decreases.

For the apoptosis assay, at both 24 hours (Figure 3-29B) and 48 hours (Figure 3-30B), there was a modest but statistically significant increase in early and late apoptosis, with a corresponding decrease in live cell populations (apart from 24 hour, 100 µM late apoptosis which was non-significant). However, the largest effects were seen at 72 hours of incubation with DJ0097 (Figure 3-31B), where the combined early and late apoptotic populations for 1 µM was 50.8 % (early and late both $P<0.001$), at 10 µM was 58.2 % (early and late; both $P<0.001$), and at 100 µM it was 51.7 % (early and late; both $P<0.001$), compared to 15.9 % for complete media treated cells, all with corresponding reductions in live cell populations.

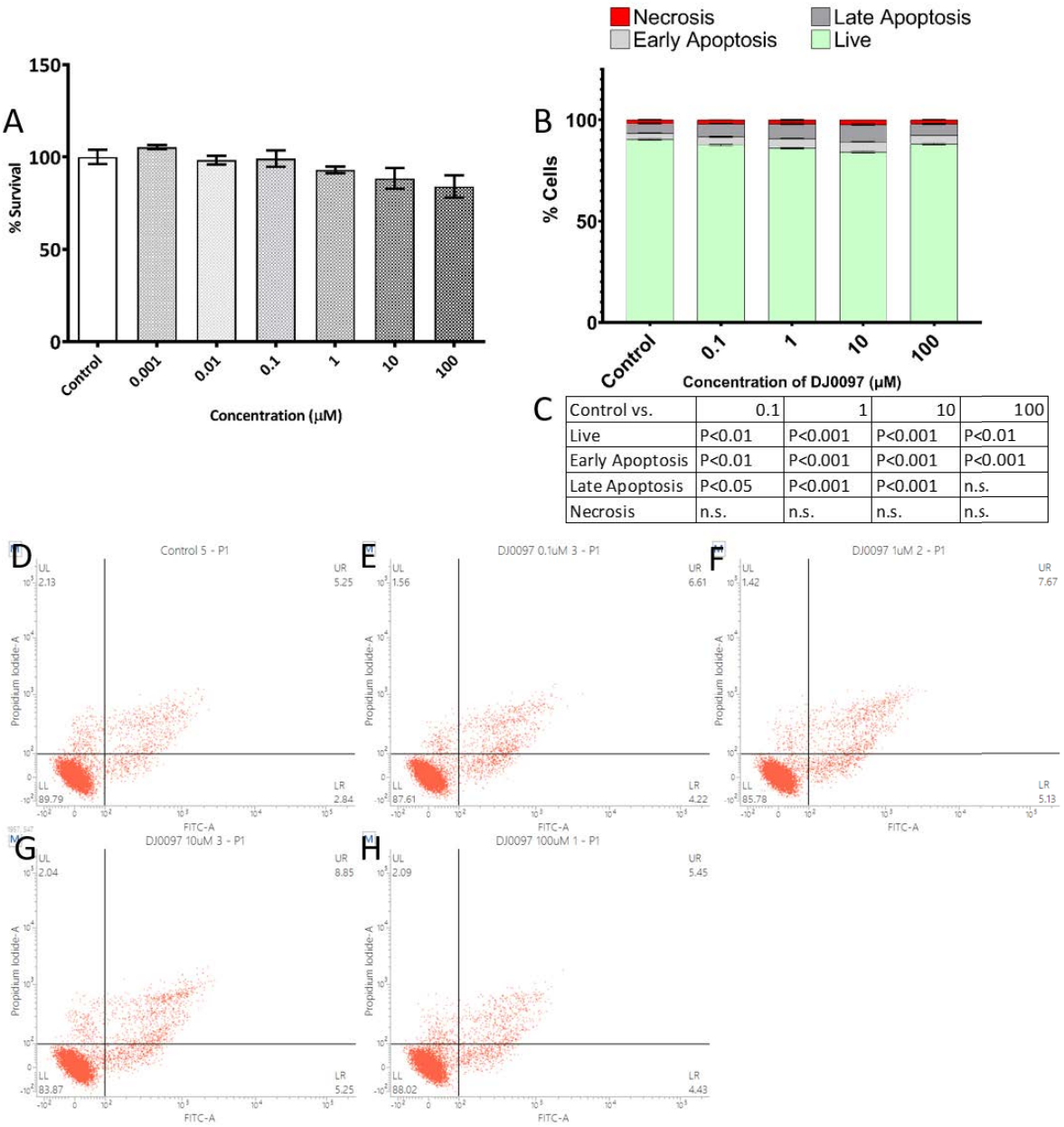

C

Control vs.	0.1	1	10	100
Live	P<0.01	P<0.001	P<0.001	P<0.01
Early Apoptosis	P<0.01	P<0.001	P<0.001	P<0.001
Late Apoptosis	P<0.05	P<0.001	P<0.001	n.s.
Necrosis	n.s.	n.s.	n.s.	n.s.

Figure 3-29 Cell viability assays for DAUDI cells treated with various concentrations of Thienopyridine DJ0097 for 24 hours as determined by MTS assay (A) and Annexin V/Propidium Iodine Flow Cytometry (B), and Significance values for One-Way ANOVA with Dunnett's post-hoc test of Untreated Control (DAUDI + complete media) vs each concentration of DJ0097 (C). Representative dot plots for Annexin V/PI Flow Cytometry Untreated Control (D), DJ0097 0.1 μM (E), DJ0097 1 μM (F), DJ0097 10 μM (G) and DJ0097 100 μM (H) are presented where Early Apoptosis (Lower Right Quadrant (LR)) = Annexin V+/PI-, Late Apoptosis (Upper Right Quadrant (UR)) = Annexin V+/PI+, Live Cell (Lower Left Quadrant (LL)) = Annexin V-/PI-, Necrosis (Upper Left Quadrant (UR)) = Annexin V-/PI+.

Data are presented as mean ±SEM of n=3 (untreated control n=6). For MTS (A) data have been normalised against 100 % survival for un-treated cells, and 0 % survival for cells treated with 50 % ethanol for 24 h. For Annexin V/Propidium Iodide (B) data are presented as mean ±SEM of n=3, untreated control n=6.

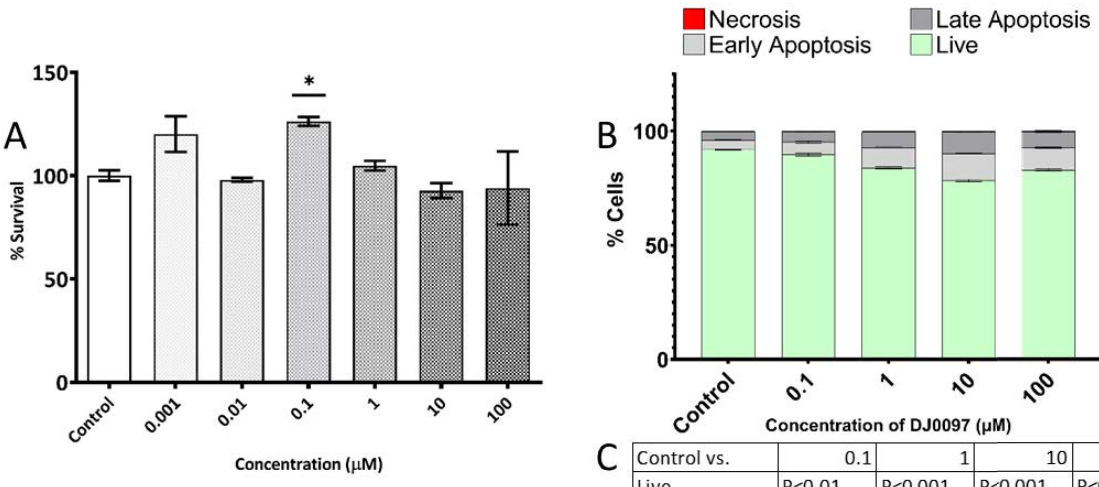

C

Control vs.	0.1	1	10	100
Live	P<0.01	P<0.001	P<0.001	P<0.001
Early Apoptosis	P<0.05	P<0.001	P<0.001	P<0.001
Late Apoptosis	P<0.01	P<0.001	P<0.001	P<0.001
Necrosis	n.s.	n.s.	n.s.	n.s.

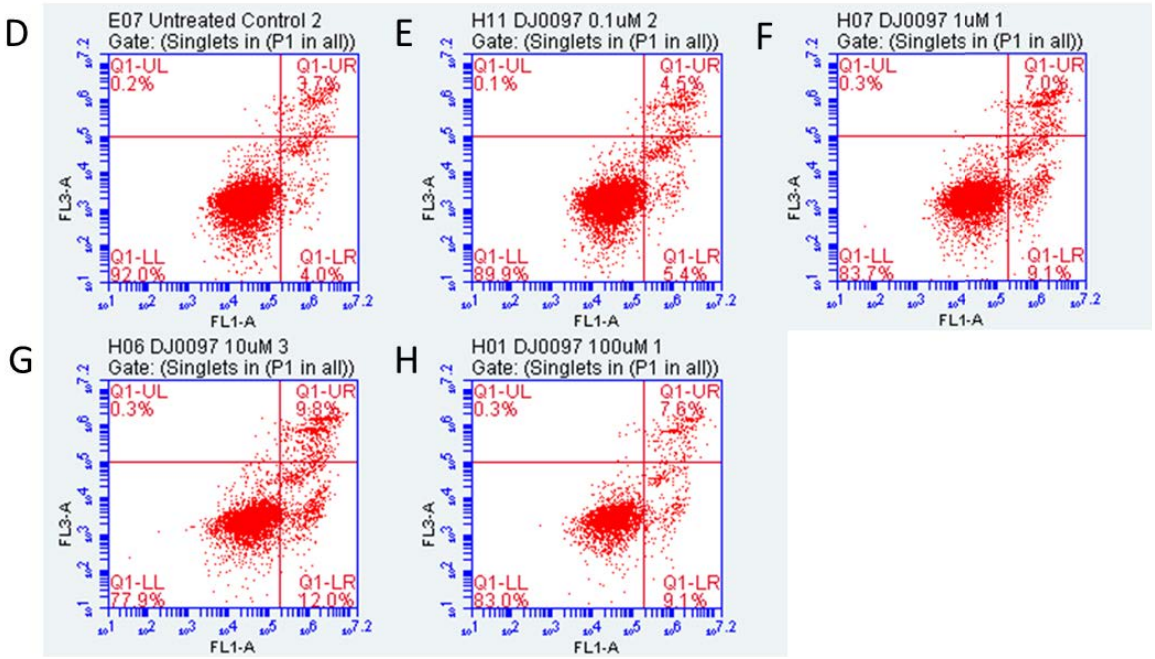

Figure 3-30 Cell viability assays for DAUDI cells treated with various concentrations of Thienopyridine DJ0097 for 48 hours as determined by MTS assay (A) and Annexin V/Propidium Iodine Flow Cytometry (B), and Significance values for One-Way ANOVA with Dunnett's post-hoc test of Untreated Control (DAUDI + complete media) vs each concentration of DJ0097 (C). Representative dot plots for Annexin V/PI Flow Cytometry Untreated Control (D), DJ0097 0.1 μM (E), DJ0097 1 μM (F), DJ0097 10 μM (G) and DJ0097 100 μM (H) are presented where Early Apoptosis (Lower Right Quadrant (LR)) = Annexin V+/PI-, Late Apoptosis (Upper Right Quadrant (UR)) = Annexin V+/PI+, Live Cell (Lower Left Quadrant (LL)) = Annexin V-/PI-, Necrosis (Upper Left Quadrant (UR)) = Annexin V-/PI+.

Data are presented as mean ±SEM of n=3 (untreated control n=6 (MTS), n=5(AVPI)). For MTS (A) data have been normalised against 100 % survival for un-treated cells, and 0 % survival for cells treated with 50 % ethanol for 24 h. For Annexin V/Propidium Iodide (B) data are presented as mean ±SEM of n=3, untreated control n=6.

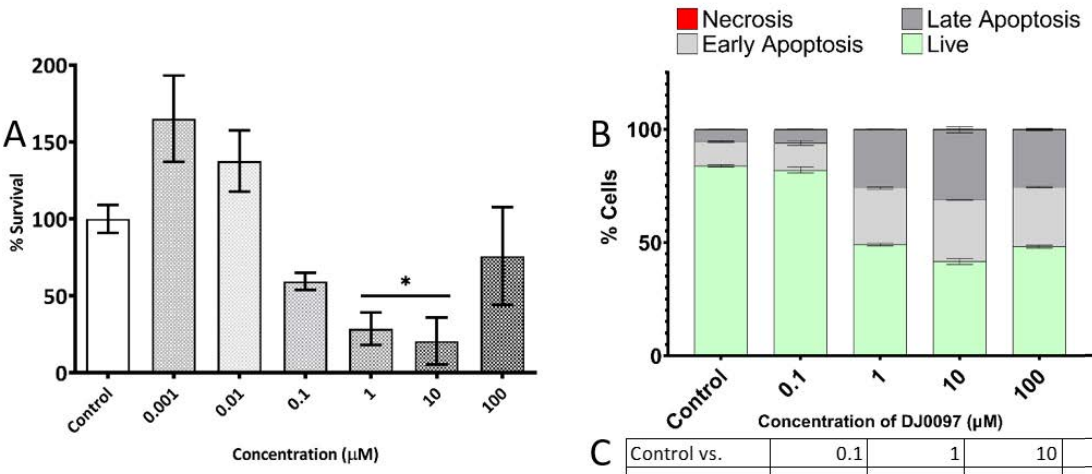

C

Control vs.	0.1	1	10	100
Live	n.s.	P<0.001	P<0.001	P<0.001
Early Apoptosis	n.s.	P<0.001	P<0.001	P<0.001
Late Apoptosis	n.s.	P<0.001	P<0.001	P<0.001
Necrosis	n.s.	n.s.	n.s.	n.s.

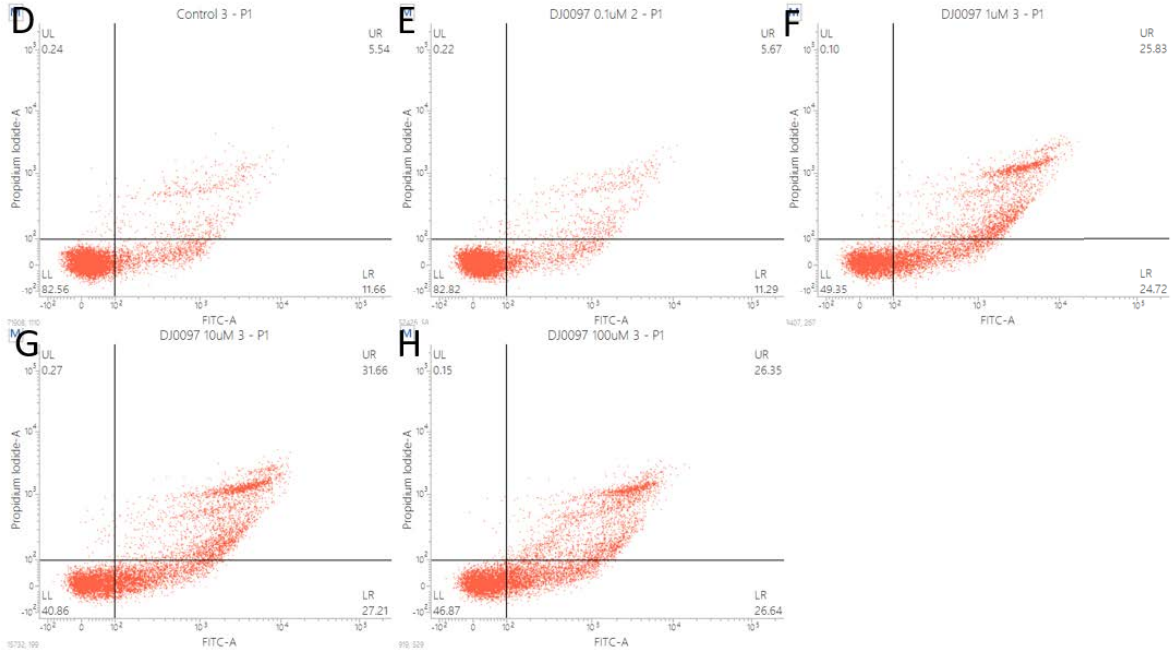

Figure 3-31 Cell viability assays for DAUDI cells treated with various concentrations of Thienopyridine DJ0097 for 72 hours as determined by MTS assay (A) and Annexin V/Propidium Iodine Flow Cytometry (B), and Significance values for One-Way ANOVA with D'nnett's post-hoc test of Untreated Control (DAUDI + complete media) vs each concentration of DJ0097 (C). Representative dot plots for Annexin V/PI Flow Cytometry Untreated Control (D), DJ0097 0.1 μM (E), DJ0097 1 μM (F), DJ0097 10 μM (G) and DJ0097 100 μM (H) are presented where Early Apoptosis (Lower Right Quadrant (LR)) = Annexin V+/PI-, Late Apoptosis (Upper Right Quadrant (UR)) = Annexin V+/PI+, Live Cell (Lower Left Quadrant (LL)) = Annexin V-/PI-, Necrosis (Upper Left Quadrant (UR)) = Annexin V-/PI+.

Data are presented as mean ±SEM of n=3 (untreated control n=6). For MTS (A) data have been normalised against 100 % survival for un-treated cells, and 0 % survival for cells treated with 50 % ethanol for 24 h. For Annexin V/Propidium Iodide (B) data are presented as mean ±SEM of n=3, untreated control n=6.

3.4.1.3.2 DJ0109 effects on DAUDI cell viability

Figure 3-32 to Figure 3-34 show the results for DAUDI cells cultured in the presence of novel thienopyridine DJ00109 for 24 hours, 48 hours, and 72 hours respectively. Figure 3-32A and Figure 3-33A show viability assay results for 24 hour and 48 hour incubations, where the only significant result was a reduction in cell viability at 100 µM at 24 hours (mean cell viability 83.5 %), while there was also a non-significant reduction at the same concentration at 48 hours (mean cell viability 83.5 %). In line with DJ0097 there was a general picture of slight non-significant increase at 0.001 µM and 0.01 µM at 24 hours with slight increases at higher concentrations, and all concentrations apart from 100 µM showing slight increases at 48 hours. At 72 hours (Figure 3-34A), both 0.001 µM (mean cell viability 148.1 %, $P<0.05$) and 0.01 µM (mean cell viability 146.3 %, P0.05) showed increases, while 0.1 µM (mean cell viability 65.6 %), 1 µM (63.7 %), 10 µM (74.7 %) and 100 µM (85.9 %) showed non-significant decreases.

For the apoptosis assay, at 24 hours no significant effects are seen for DJ0109 (Figure 3-32B), while at 48 hours there is a slight but statistically significant decrease in the live cell populations at all concentrations, with increases in early apoptosis at 0.1 µM and 1 µM, while 100 µM shows an increase in both early and late apoptosis (Figure 3-33B). At 72 hours post-incubation with DJ0109, there are no effects at any concentration seen (Figure 3-34B).

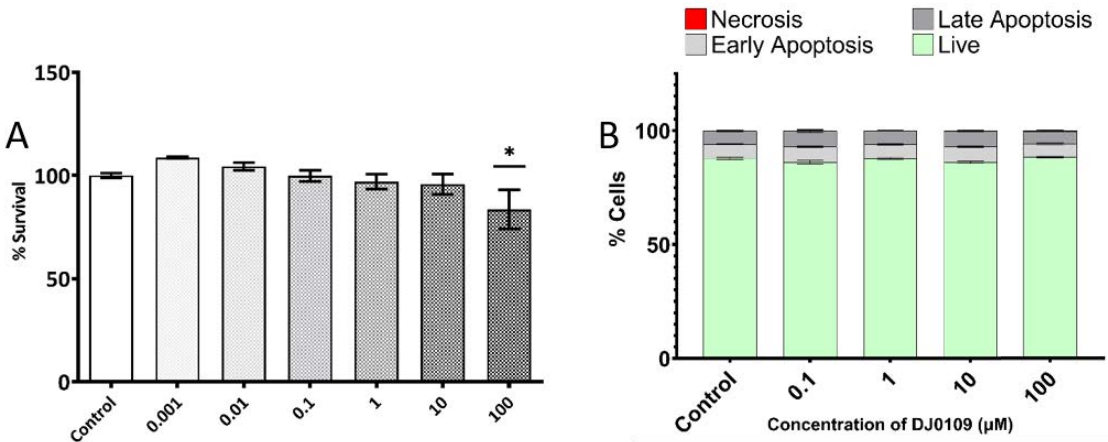

C

Control vs.	0.1	1	10	100
Live	n.s.	n.s.	n.s.	n.s.
Early Apoptosis	n.s.	n.s.	n.s.	n.s.
Late Apoptosis	n.s.	n.s.	n.s.	n.s.
Necrosis	n.s.	n.s.	n.s.	n.s.

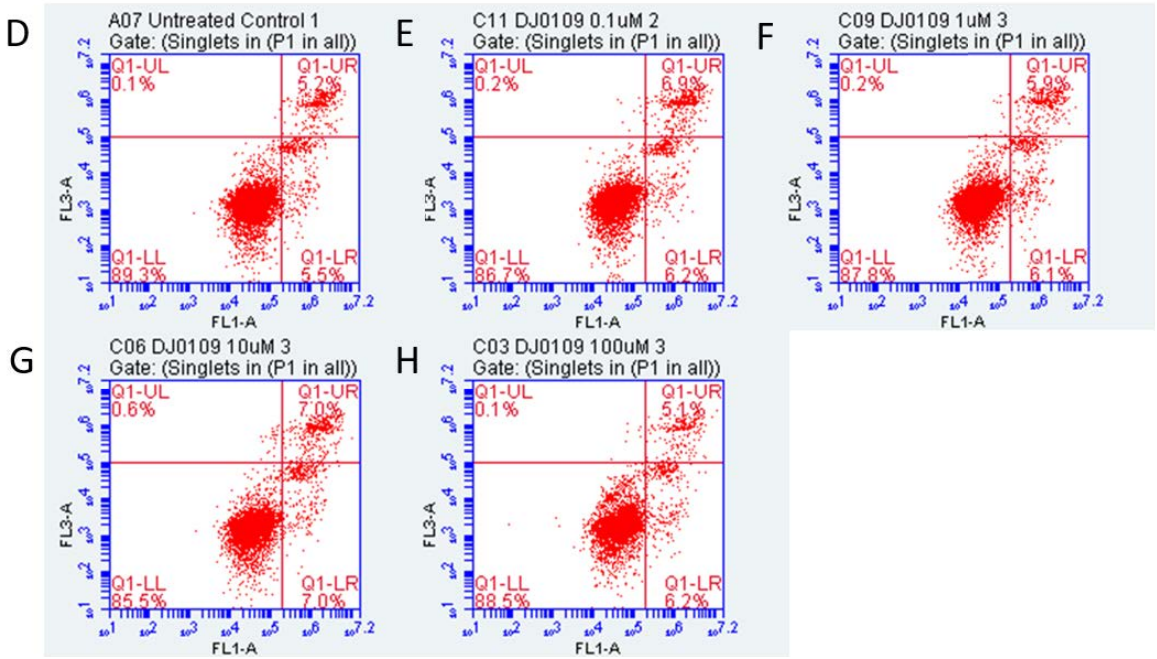

Figure 3-32 Cell viability assays for DAUDI cells treated with various concentrations of Thienopyridine DJ0109 for 24 hours as determined by MTS assay (A) and Annexin V/Propidium Iodine Flow Cytometry (B), and Significance values for One-Way ANOVA with Dunnett's post-hoc test of Untreated Control (DAUDI + complete media) vs each concentration of DJ0109 (C). Representative dot plots for Annexin V/PI Flow Cytometry Untreated Control (D), DJ0109 0.1 μM (E), DJ0109 1 μM (F), DJ0109 10 μM (G) and DJ0109 100 μM (H) are presented where Early Apoptosis (Lower Right Quadrant (LR)) = Annexin V+/PI-, Late Apoptosis (Upper Right Quadrant (UR)) = Annexin V+/PI+, Live Cell (Lower Left Quadrant (LL)) = Annexin V-/PI-, Necrosis (Upper Left Quadrant (UR)) = Annexin V-/PI+.

Data are presented as mean ±SEM of n=3 (untreated control n=6). For MTS (A) data have been normalised against 100 % survival for un-treated cells, and 0 % survival for cells treated with 50 % ethanol for 24 h. For Annexin V/Propidium Iodide (B) data are presented as mean ±SEM of n=3, untreated control n=6.

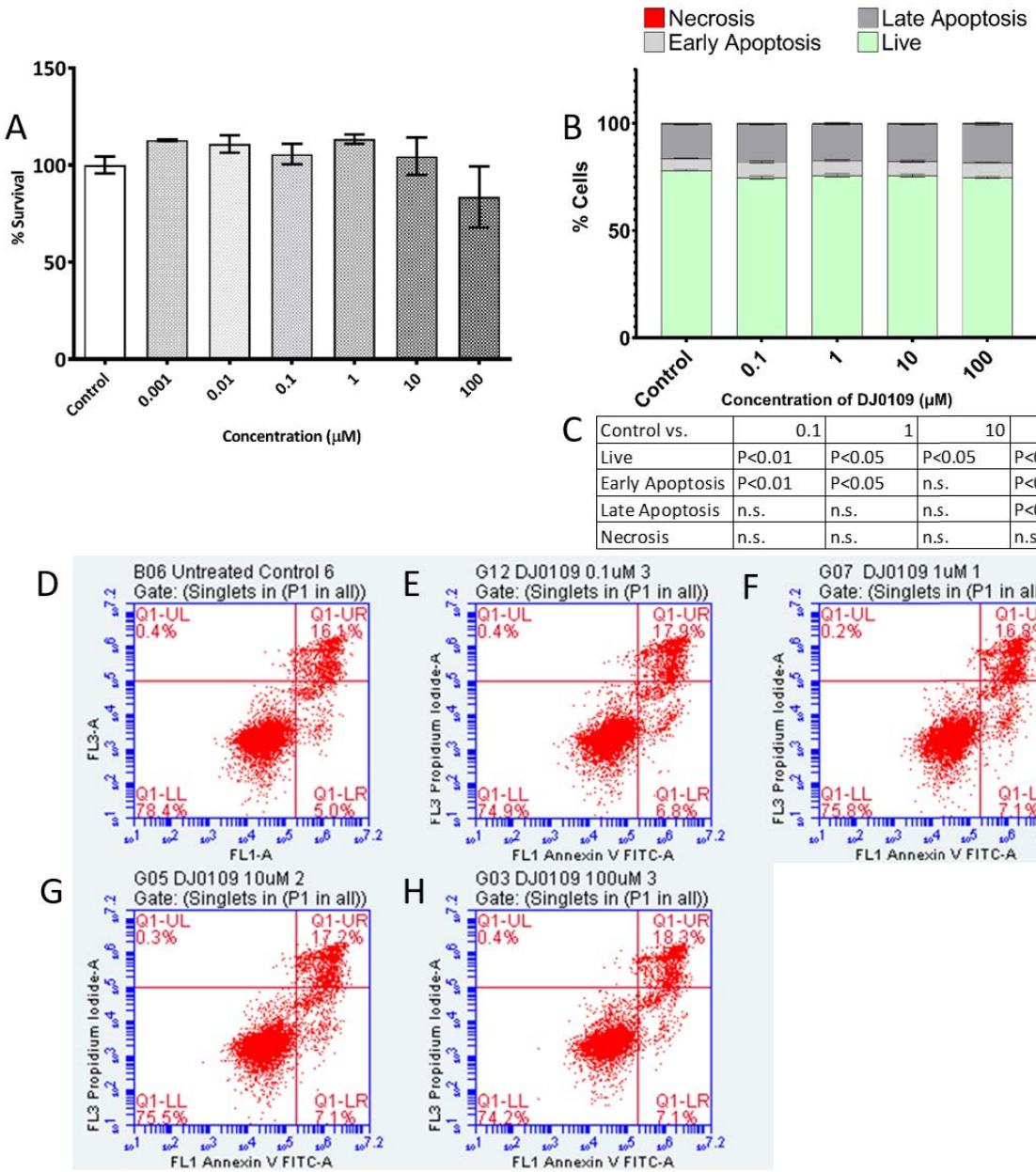

C

Control vs.	0.1	1	10	100
Live	P<0.01	P<0.05	P<0.05	P<0.01
Early Apoptosis	P<0.01	P<0.05	n.s.	P<0.05
Late Apoptosis	n.s.	n.s.	n.s.	P<0.05
Necrosis	n.s.	n.s.	n.s.	n.s.

Figure 3-33 Cell viability assays for DAUDI cells treated with various concentrations of Thienopyridine DJ0109 for 48 hours as determined by MTS assay (A) and Annexin V/Propidium Iodine Flow Cytometry (B), and Significance values for One-Way ANOVA with Dunnett's post-hoc test of Untreated Control (DAUDI + complete media) vs each concentration of DJ0109 (C). Representative dot plots for Annexin V/PI Flow Cytometry Untreated Control (D), DJ0109 0.1 μM (E), DJ0109 1 μM (F), DJ0109 10 μM (G) and DJ0109 100 μM (H) are presented where Early Apoptosis (Lower Right Quadrant (LR)) = Annexin V+/PI-, Late Apoptosis (Upper Right Quadrant (UR)) = Annexin V+/PI+, Live Cell (Lower Left Quadrant (LL)) = Annexin V-/PI-, Necrosis (Upper Left Quadrant (UR)) = Annexin V-/PI+.

Data are presented as mean ±SEM of n=3 (untreated control n=6). For MTS (A) data have been normalised against 100 % survival for un-treated cells, and 0 % survival for cells treated with 50 % ethanol for 24 h. For Annexin V/Propidium Iodide (B) data are presented as mean ±SEM of n=3, untreated control n=6.

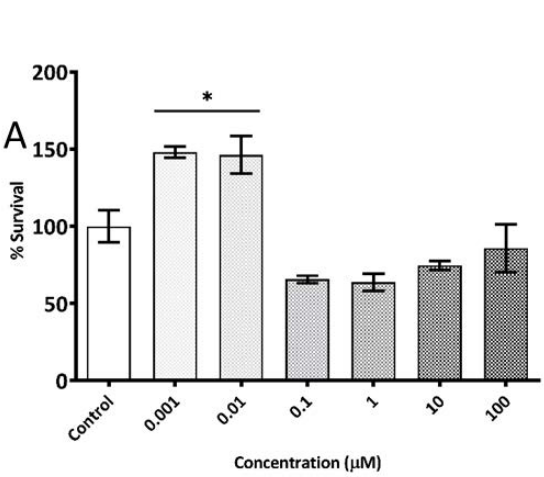

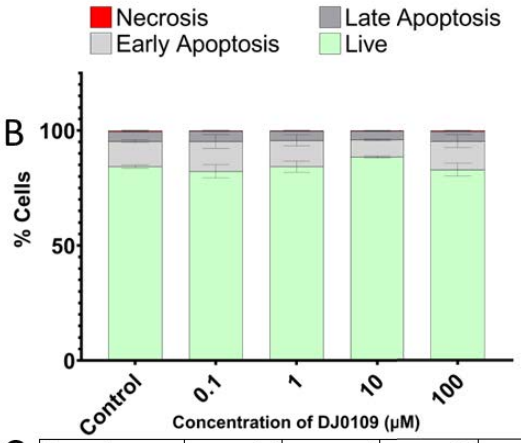

C

Control vs.	0.1	1	10	100
Live	n.s.	n.s.	n.s.	n.s.
Early Apoptosis	n.s.	n.s.	n.s.	n.s.
Late Apoptosis	n.s.	n.s.	n.s.	n.s.
Necrosis	n.s.	n.s.	n.s.	n.s.

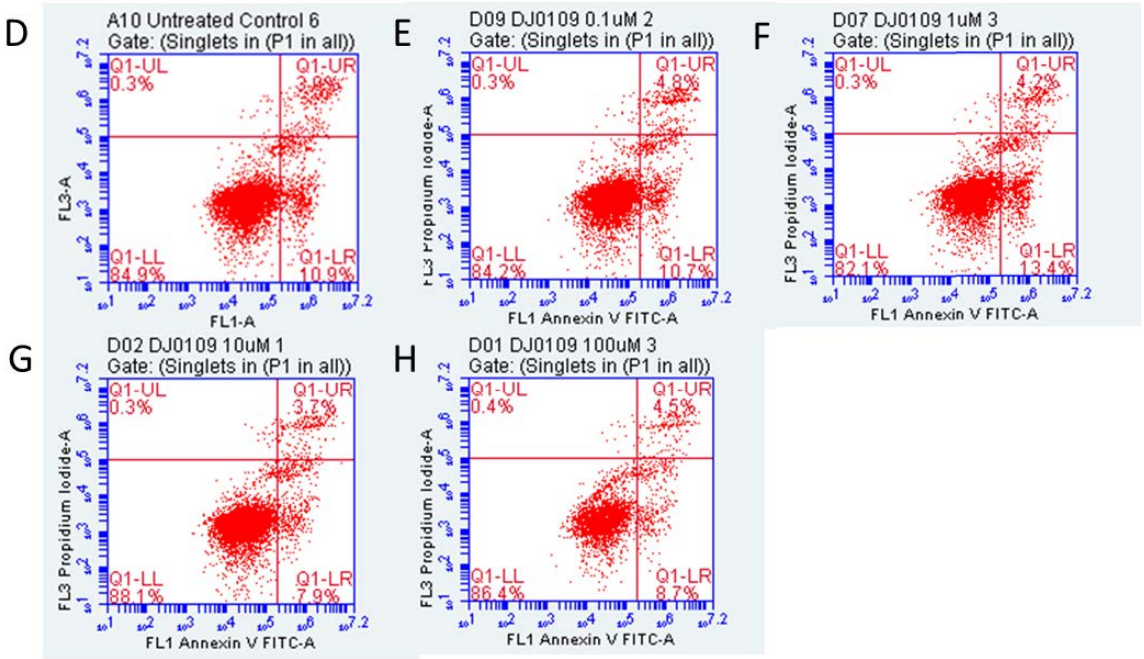

Figure 3-34 Cell viability assays for DAUDI cells treated with various concentrations of Thienopyridine DJ0109 for 72 hours as determined by MTS assay (A) and Annexin V/Propidium Iodine Flow Cytometry (B), and Significance values for One-Way ANOVA with Dunnett's post-hoc test of Untreated Control (DAUDI + complete media) vs each concentration of DJ0109 (C). Representative dot plots for Annexin V/PI Flow Cytometry Untreated Control (D), DJ0109 0.1 µM (E), DJ0109 1 µM (F), DJ0109 10 µM (G) and DJ0109 100 µM (H) are presented where Early Apoptosis (Lower Right Quadrant (LR)) = Annexin V+/PI-, Late Apoptosis (Upper Right Quadrant (UR)) = Annexin V+/PI+, Live Cell (Lower Left Quadrant (LL)) = Annexin V-/PI-, Necrosis (Upper Left Quadrant (UR)) = Annexin V-/PI+.

Data are presented as mean ±SEM of n=3 (untreated control n=6). For MTS (A) data have been normalised against 100 % survival for un-treated cells, and 0 % survival for cells treated with 50 % ethanol for 24 h. For Annexin V/Propidium Iodide (B) data are presented as mean ±SEM of n=3, untreated control n=6.

3.4.1.3.3 DJ0171 effects on DAUDI cell viability

Figure 3-35 to Figure 3-37 show the viability (MTS) and apoptosis (AVPI) results for DAUDI cells treated with various concentrations of novel thienopyridine DJ0171 for 24 hours, 48 hours and 72 hours respectively.

The results for the viability assay are broadly in keeping with those seen in DJ0097 and DJ0109, at 24 hours with Figure 3-35A showing increases in cell viability at 0.01 µM ($P<0.01$) and 0.1 µM ($P<0.05$), while all other concentrations showed non-significant increases with only concentration 10 µM showing a non-significant decrease. At 48 hours, all concentrations tested showed a significant increase in cell viability (Figure 3-36A), while there were no significant results at 72 hours (Figure 3-37A) and only DAUDI cells treated at 10 µM showed a non-significant reduction in cell viability to 58.3 % (SEM ±16.6%), with large SEM values likely contributing to the lack of statistical significance at this time point.

For the apoptosis assay, at 24 hours of treatment with DJ0171 (Figure 3-35B), all concentrations tested showed a small but statistically significant increase in early apoptosis, while 0.1 µM, 10 µM and 100 µM showed a decrease in live cell populations and the lowest two concentrations also showed an increase in late apoptosis. At 48 hours, concentrations 1 µM to 100 µM showed a small but significant increase in both early and late apoptosis, with a decrease in live cell (Figure 3-36B). Only at the 72 hour time point (Figure 3-37B) were larger increases in early and late apoptosis seen at 10 µM (combined early and late apoptosis 34.5 %) and 100 µM (combined early and late apoptosis 53.2 %), compared to 15.9 % in the complete media control replicates, results that are broadly similar to DJ0097 although at higher concentrations.

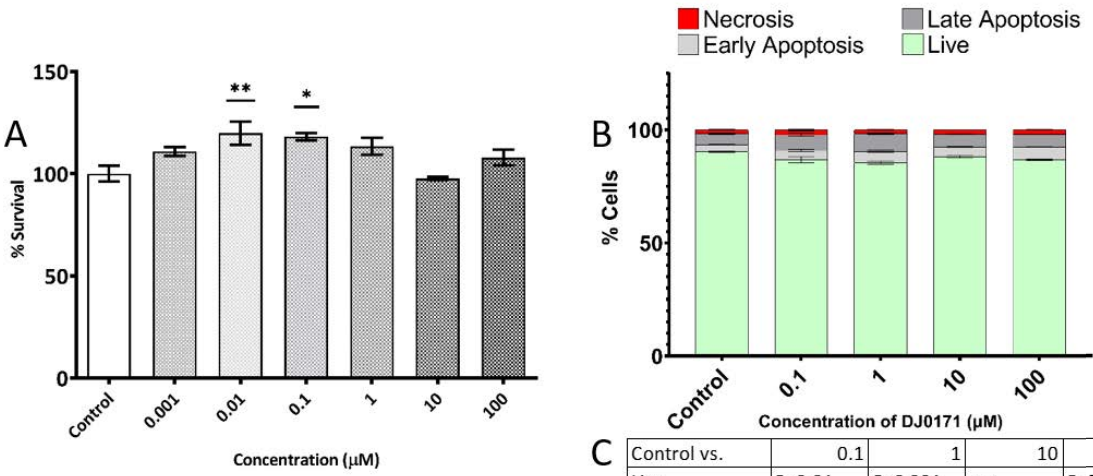

C

Control vs.	0.1	1	10	100
Live	P<0.01	P<0.001	n.s.	P<0.01
Early Apoptosis	P<0.05	P<0.001	P<0.01	P<0.001
Late Apoptosis	P<0.01	P<0.001	n.s.	n.s.
Necrosis	n.s.	n.s.	n.s.	n.s.

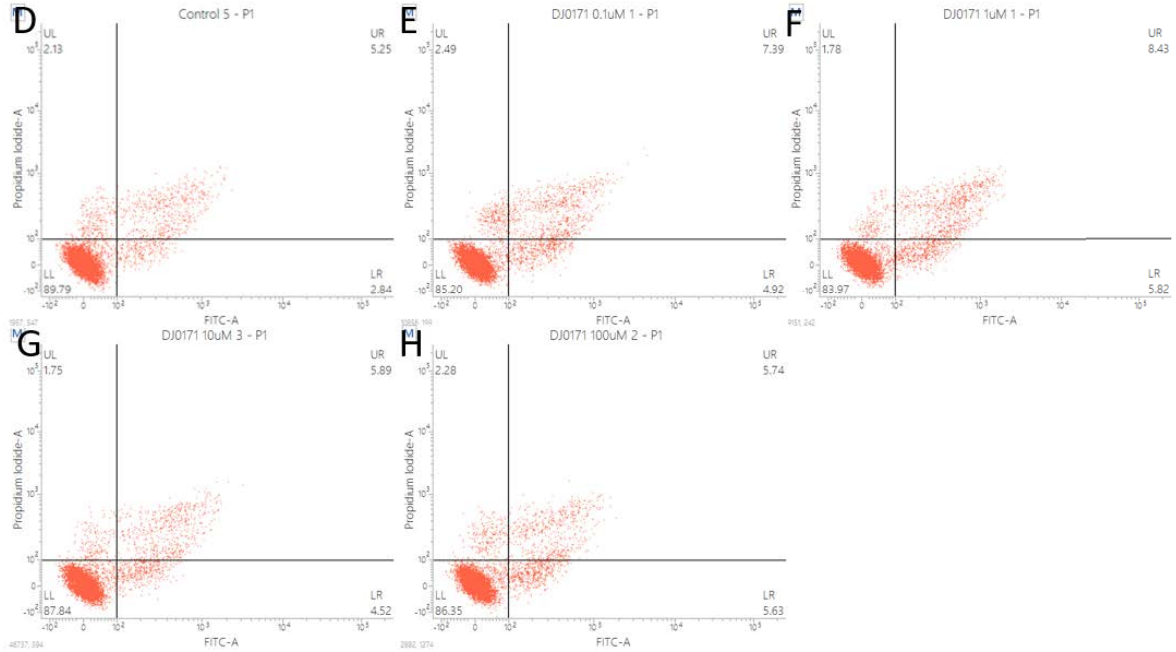

Figure 3-35 Cell viability assays for DAUDI cells treated with various concentrations of Thienopyridine DJ0171 for 24 hours as determined by MTS assay (A) and Annexin V/Propidium Iodine Flow Cytometry (B), and Significance values for One-Way ANOVA with Dunnett's post-hoc test of Untreated Control (DAUDI + complete media) vs each concentration of DJ0171 (C). Representative dot plots for Annexin V/PI Flow Cytometry Untreated Control (D), DJ0171 0.1 μM (E), DJ0171 1 μM (F), DJ0171 10 μM (G) and DJ0171 100 μM (H) are presented where Early Apoptosis (Lower Right Quadrant (LR)) = Annexin V+/PI-, Late Apoptosis (Upper Right Quadrant (UR)) = Annexin V+/PI+, Live Cell (Lower Left Quadrant (LL)) = Annexin V-/PI-, Necrosis (Upper Left Quadrant (UR)) = Annexin V-/PI+.

Data are presented as mean ±SEM of n=3 (untreated control n=6). For MTS (A) data have been normalised against 100 % survival for un-treated cells, and 0 % survival for cells treated with 50 % ethanol for 24 h. For Annexin V/Propidium Iodide (B) data are presented as mean ±SEM of n=3, untreated control n=6.

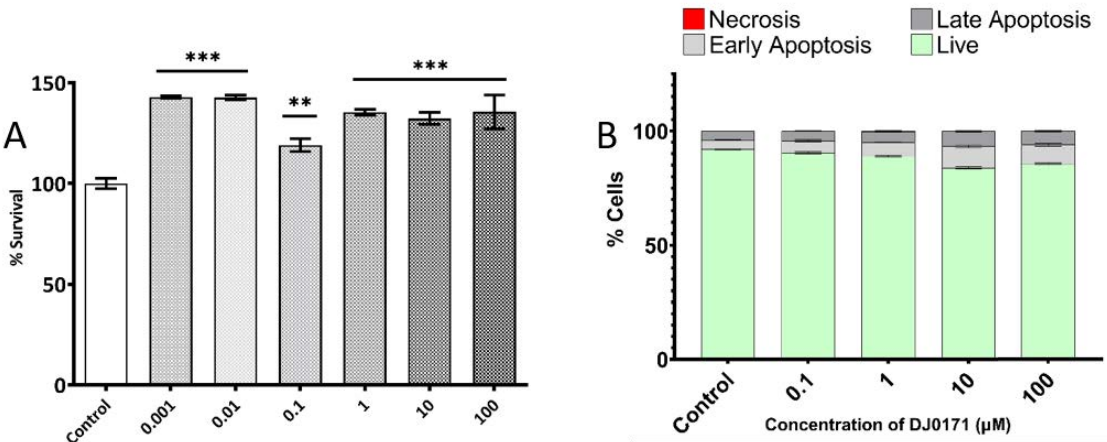

C

Control vs.	0.1	1	10	100
Live	P<0.05	P<0.001	P<0.001	P<0.001
Early Apoptosis	n.s.	P<0.05	P<0.001	P<0.001
Late Apoptosis	n.s.	P<0.01	P<0.001	P<0.001
Necrosis	n.s.	n.s.	n.s.	n.s.

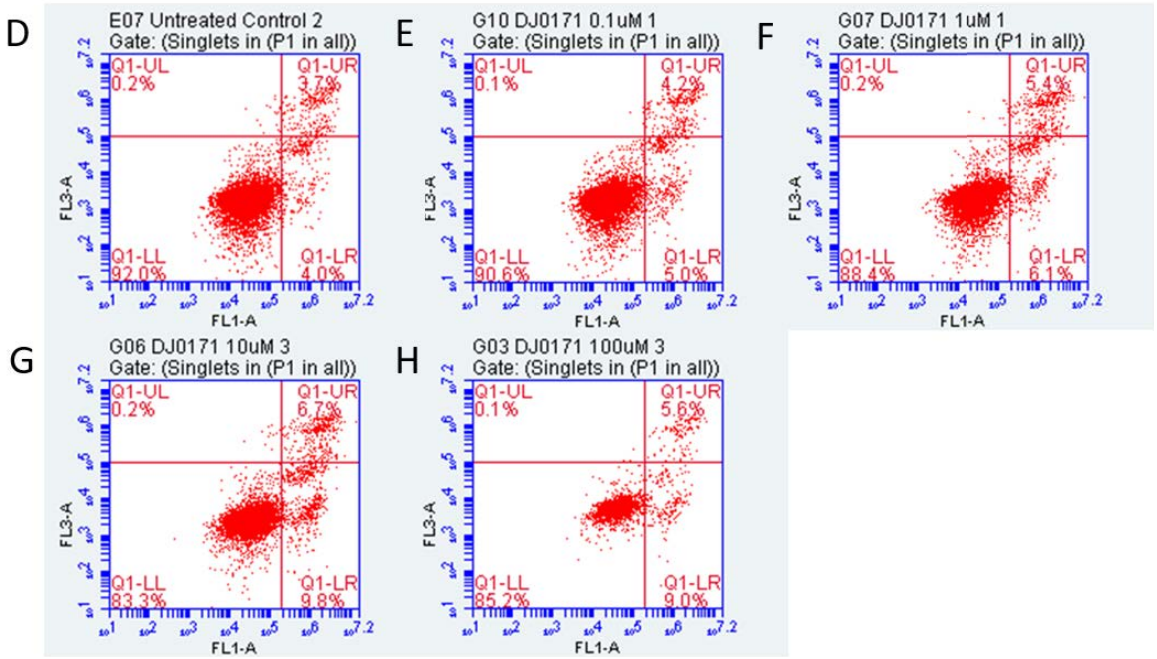

Figure 3-36 Cell viability assays for DAUDI cells treated with various concentrations of Thienopyridine DJ0171 for 48 hours as determined by MTS assay (A) and Annexin V/Propidium Iodine Flow Cytometry (B), and Significance values for One-Way ANOVA with Dunnett's post-hoc test of Untreated Control (DAUDI + complete media) vs each concentration of DJ0171 (C). Representative dot plots for Annexin V/PI Flow Cytometry Untreated Control (D), DJ0171 0.1 μM (E), DJ0171 1 μM (F), DJ0171 10 μM (G) and DJ0171 100 μM (H) are presented where Early Apoptosis (Lower Right Quadrant (LR)) = Annexin V+/PI-, Late Apoptosis (Upper Right Quadrant (UR)) = Annexin V+/PI+, Live Cell (Lower Left Quadrant (LL)) = Annexin V-/PI-, Necrosis (Upper Left Quadrant (UR)) = Annexin V-/PI+.

Data are presented as mean ±SEM of n=3 (untreated control n=6 (MTS), n=5 (AVPI)). For MTS (A) data have been normalised against 100 % survival for un-treated cells, and 0 % survival for cells treated with 50 % ethanol for 24 h. For Annexin V/Propidium Iodide (B) data are presented as mean ±SEM of n=3, untreated control n=6.

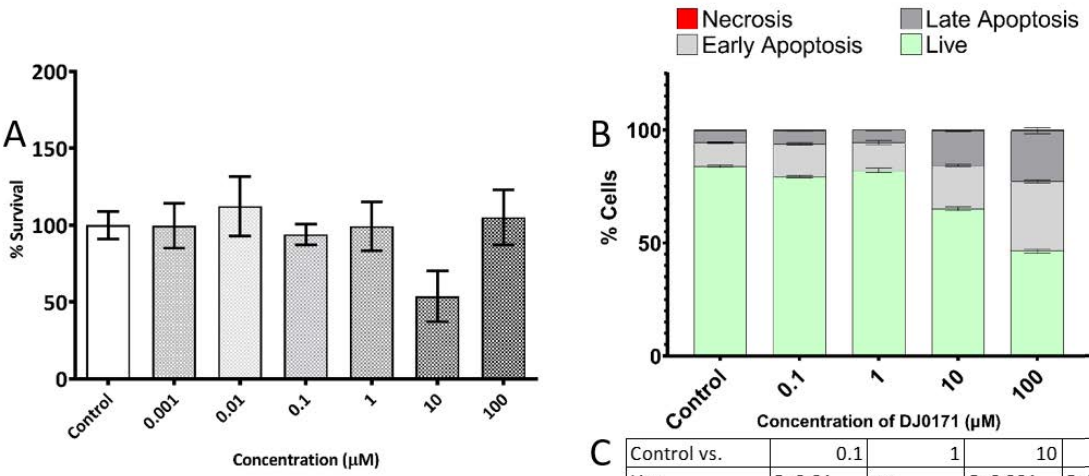

C

Control vs.	0.1	1	10	100
Live	P<0.01	n.s.	P<0.001	P<0.001
Early Apoptosis	P<0.001	n.s.	P<0.001	P<0.001
Late Apoptosis	n.s.	n.s.	P<0.001	P<0.001
Necrosis	n.s.	n.s.	n.s.	n.s.

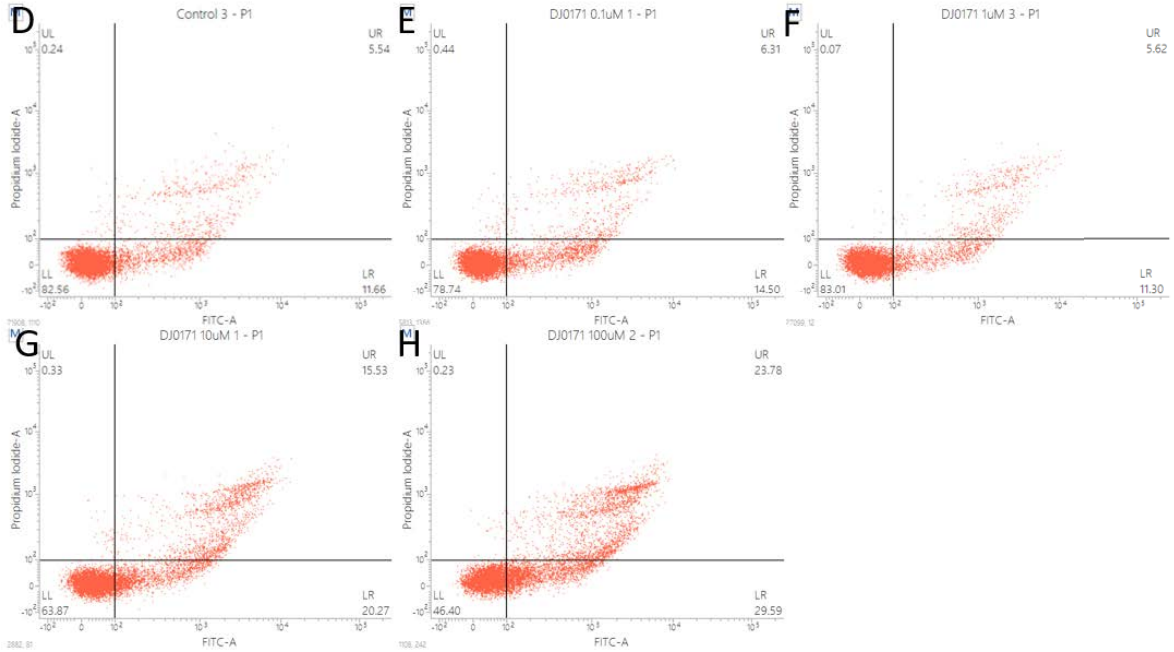

Figure 3-37 Cell viability assays for DAUDI cells treated with various concentrations of Thienopyridine DJ0171 for 72 hours as determined by MTS assay (A) and Annexin V/Propidium Iodine Flow Cytometry (B), and Significance values for One-Way ANOVA with Dunnett's post-hoc test of Untreated Control (DAUDI + complete media) vs each concentration of DJ0171 (C). Representative dot plots for Annexin V/PI Flow Cytometry Untreated Control (D), DJ0171 0.1 µM (E), DJ0171 1 µM (F), DJ0171 10 µM (G) and DJ0171 100 µM (H) are presented where Early Apoptosis (Lower Right Quadrant (LR)) = Annexin V+/PI-, Late Apoptosis (Upper Right Quadrant (UR)) = Annexin V+/PI+, Live Cell (Lower Left Quadrant (LL)) = Annexin V-/PI-, Necrosis (Upper Left Quadrant (UR)) = Annexin V-/PI+.

Data are presented as mean ±SEM of n=3 (untreated control n=6). For MTS (A) data have been normalised against 100 % survival for un-treated cells, and 0 % survival for cells treated with 50 % ethanol for 24 h. For Annexin V/Propidium Iodide (B) data are presented as mean ±SEM of n=3, untreated control n=6.

3.4.2 Effects of novel thienopyridines on cell cycle

Flow cytometry with single staining of cells using propidium iodide was used to study the effects of novel thienopyrines on the cell cycle progression of DAUDI cells.

3.4.2.1 Effects of novel thienopyridines with a cyclooctane moiety on cell cycle

3.4.2.1.1 DJ0014 effects on DAUDI cell cycle

Figure 3-38 to Figure 3-40 show the results for DAUDI cells cultured in the presence of novel thienopyridine DJ0014 for 24 hours, 48 hours, and 72 hours respectively.

At 24 hours (Figure 3-38), DJ0014 showed small but statistically significant increases in G_2/M populations at 1 µM (5.85 % cells), 10 µM (14.99 % cells) and 100 µM (14.76 % cells) vs 3.56 % of cells in G_2/M in the untreated controls (1 µM: $P < 0.05$; 10 µM and 100 µM: both $P < 0.001$), with corresponding significant decreases in G1 and S phase cells.

At 48 (Figure 3-39) and 72 hours (Figure 3-40), there were pronounced, significant increases in G_2/M cells at 10 µM and 100 µM concentrations (All: $P < 0.001$), while no effects were seen at 1 µM.

Untreated control cells at 48 hours showed 9.12 % G_2/M phase cells compared to 67.01 % at 10 µM and 64.91 % at 100 µM of compound DJ0014, with similar results seen at 72 hours (11.82 % Control G_2/M vs 67.98 % for 10 µM and 67.25 % for 100 µM).

A

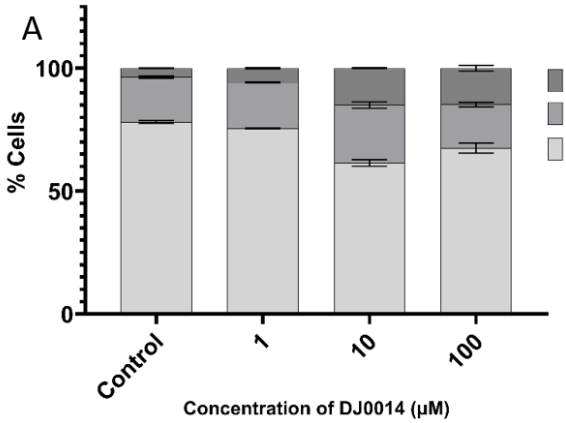

B

Control vs.	1	10	100
G0/G1	n.s.	P<0.001	P<0.001
S	n.s.	P<0.01	n.s.
G2/M	P<0.05	P<0.001	P<0.001

C

	DJ0014 (µM)			
	0	**1**	**10**	**100**
G2/G1, mean (SEM)	1.938 (0.003)	1.94 (0.000)	1.930 (0.000)	1.923(0.003)
% CV, mean (SEM)	3.148 (0.097)	2.743 (0.088)	2.830 (0.220)	2.953 (0.088)
RCS, mean (SEM)	3.243 (0.160)	3.078 (0.122)	3.124 (0.130)	2.920 (0.180)
n	5	3	3	3

D E F G

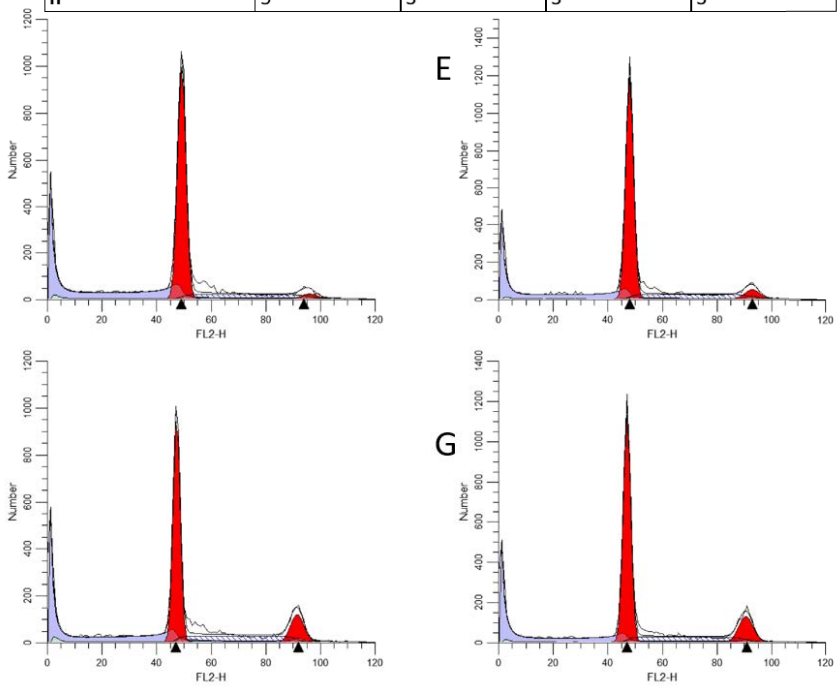

Figure 3-38 Cell cycle analysis for DAUDI cells treated with various concentrations of Thienopyridine DJ0014 for 24 hours as determined by propidium Iodide flow cytometry. Cell cycle flow cytometry RCS files were analysed using a fixed manual model in ModFit LT 5.0 and data were analysed using the one-way ANOVA with Dunnett's post hoc test.

***(A)** Comparison of cell cycle phases (G0/G1, S and G2/M phase) of DAUDI cells treated with complete media (control) versus 1-100 µM of DJ0014. **(B)** Results from One-way ANOVA with Dunnett's post hoc test comparing cell cycle phases of the DJ0014 treated cells vs complete media (Control). **(C)** Descriptive statistics for cell cycle analysis, showing mean ratio of G2/M channel over G0/G1 channel (G2/G1), mean % coefficient of variance (% CV), mean reduced chi squared (RCS) and number of replicates for each data set (n). **(D-G)** Representative histogram for Cell Cycle analysis for Control (complete media) (D); DJ0014 1 µM (E); DJ0014 10 µM (F); and DJ0014 100 µM (G).*

A

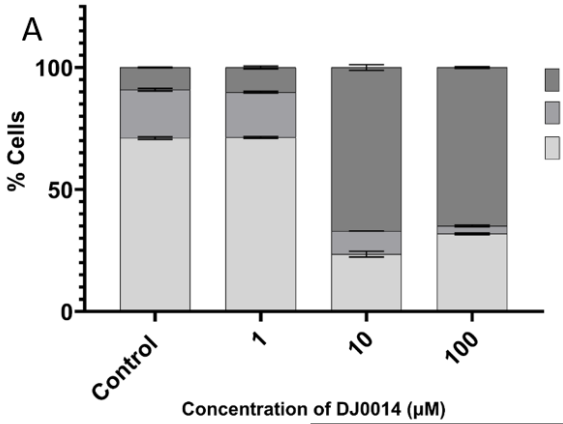

B

Control vs.	1	10	100
G0/G1	n.s.	P<0.001	P<0.001
S	n.s.	P<0.001	P<0.001
G2/M	n.s.	P<0.001	P<0.001

C

	DJ0014 (µM)			
	0	**1**	**10**	**100**
G2/G1, mean (SEM)	1.940 (0.000)	1.940 (0.000)	1.920 (0.000)	1.910 (0.000)
% CV, mean (SEM)	2.495 (0.066)	2.943 (0.069)	2.983 (0.105)	2.870 (0.286)
RCS, mean (SEM)	2.192 (0.225)	2.369 (0.105)	2.362 (0.121)	2.445 (0.071)
n	6	3	3	3

D E F G

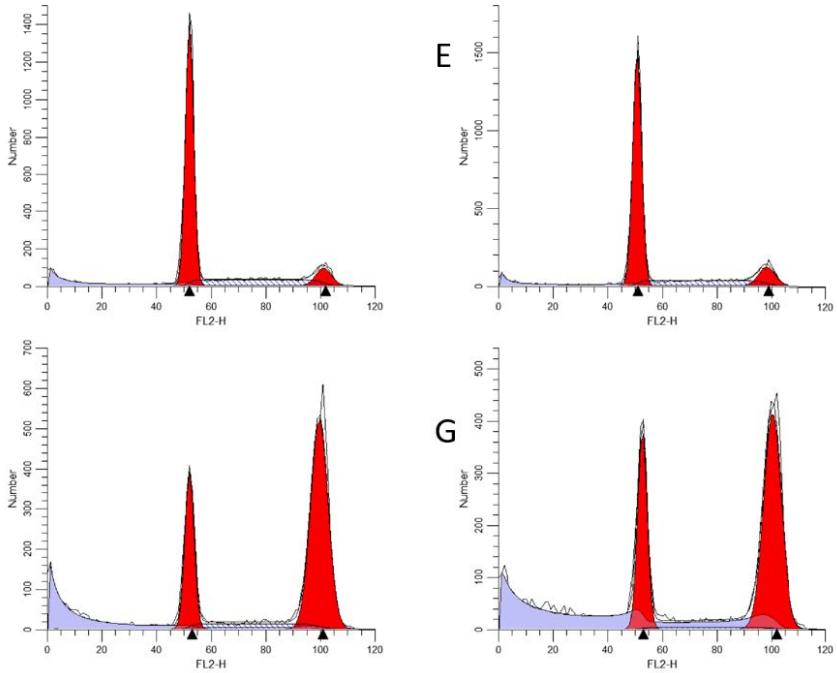

Figure 3-39 Cell cycle analysis for DAUDI cells treated with various concentrations of Thienopyridine DJ0014 for 48 hours as determined by propidium Iodide flow cytometry. Cell cycle flow cytometry RCS files were analysed using a fixed manual model in ModFit LT 5.0 and data were analysed using the one-way ANOVA with Dunnett's post hoc test.

***(A)** Comparison of cell cycle phases (G0/G1, S and G2/M phase) of DAUDI cells treated with complete media (control) versus 1-100 µM of DJ0014. **(B)** Results from One-way ANOVA with Dunnett's post hoc test comparing cell cycle phases of the DJ0014 treated cells vs complete media (Control). **(C)** Descriptive statistics for cell cycle analysis, showing mean ratio of G2/M channel over G0/G1 channel (G2/G1), mean % coefficient of variance (% CV), mean reduced chi squared (RCS) and number of replicates for each data set (n). **(D-G)** Representative histogram for Cell Cycle analysis for Control (complete media) (D); DJ0014 1 µM (E); DJ0014 10 µM (F); and DJ0014 100 µM (G).*

A

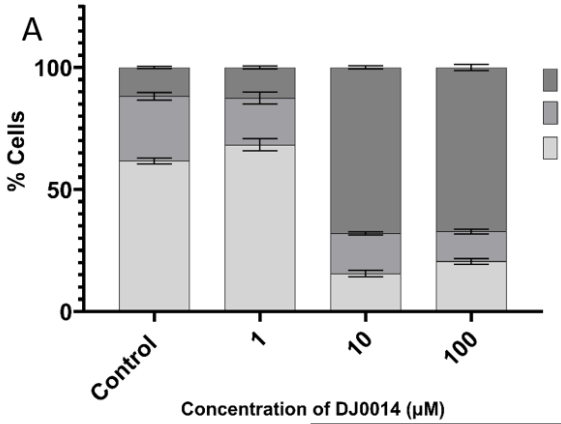

B

Control vs.	1	10	100
G0/G1	P<0.05	P<0.001	P<0.001
S	P<0.05	P<0.01	P<0.001
G2/M	n.s.	P<0.001	P<0.001

C

	DJ0014 (µM)			
	0	**1**	**10**	**100**
G2/G1, mean (SEM)	1.943 (0.003)	1.947 (0.003)	1.940 (0.000)	1.943 (0.003)
% CV, mean (SEM)	4.982 (0.128)	4.577 (0.085)	4.107 (0.026)	4.103 (0.112)
RCS, mean (SEM)	1.649 (0.089)	1.889 (0.198)	2.426 (0.122)	2.862 (0.265)
n	6	3	3	3

D E F G

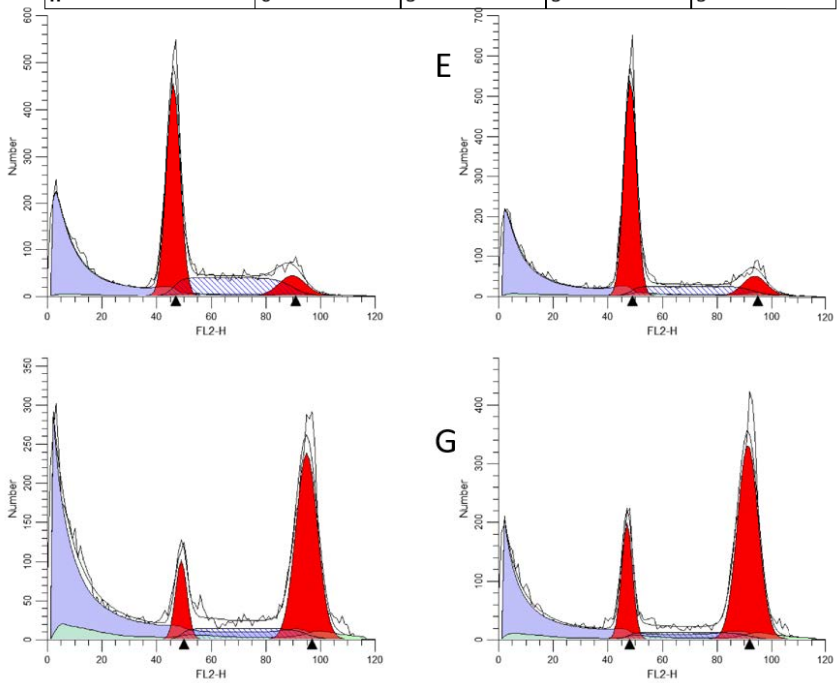

Figure 3-40 Cell cycle analysis for DAUDI cells treated with various concentrations of Thienopyridine DJ0014 for 72 hours as determined by propidium Iodide flow cytometry. Cell cycle flow cytometry RCS files were analysed using a fixed manual model in ModFit LT 5.0 and data were analysed using the one-way ANOVA with Dunnett's post hoc test.

***(A)** Comparison of cell cycle phases (G0/G1, S and G2/M phase) of DAUDI cells treated with complete media (control) versus 1-100 µM of DJ0014. **(B)** Results from One-way ANOVA with Dunnett's post hoc test comparing cell cycle phases of the DJ0014 treated cells vs complete media (Control). **(C)** Descriptive statistics for cell cycle analysis, showing mean ratio of G2/M channel over G0/G1 channel (G2/G1), mean % coefficient of variance (% CV), mean reduced chi squared (RCS) and number of replicates for each data set (n). **(D-G)** Representative histogram for Cell Cycle analysis for Control (complete media) (D); DJ0014 1 µM (E); DJ0014 10 µM (F); and DJ0014 100 µM (G).*

3.4.2.1.2 DJ0021 effects on DAUDI cell cycle

Figure 3-41 to Figure 3-43 show the results for DAUDI cells cultured in the presence of novel thienopyridine DJ0021 for 24 hours, 48 hours, and 72 hours respectively.

Unlike DJ0014, DJ0021 showed no effects across 24 hour (Figure 3-41), 48 hour (Figure 3-42), or 72 hour incubations (Figure 3-43) apart from at 100 µM concentration at 72 hours which showed a small, significant reduction in G_2/M population vs untreated control DAUDI cell (8.47 % vs untreated control 11.71 %; $P < 0.01$).

A

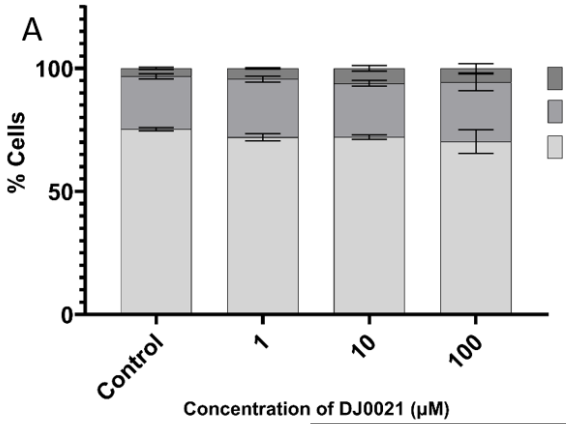

B

Control vs.	1	10	100
G0/G1	n.s.	n.s.	n.s.
S	n.s.	n.s.	n.s.
G2/M	n.s.	n.s.	n.s.

C

	DJ0021 (µM)			
	0	**1**	**10**	**100**
G2/G1, mean (SEM)	1.950 (0.006)	1.950 (0.010)	1.943 (0.003)	1.947 (0.012)
% CV, mean (SEM)	3.173 (0.057)	2.823 (0.228)	4.997 (1.907)	3.093 (0.162)
RCS, mean (SEM)	3.076 (0.323)	3.247 (0.498)	3.380 (0.253)	5.015 (1.683)
n	3	3	3	3

D E F G

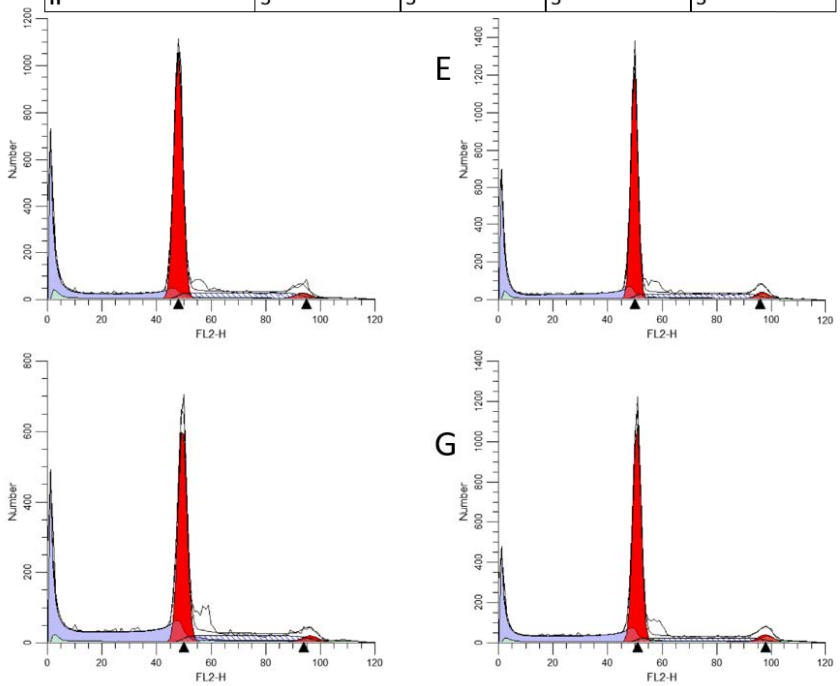

Figure 3-41 Cell cycle analysis for DAUDI cells treated with various concentrations of Thienopyridine DJ0021 for 24 hours as determined by propidium Iodide flow cytometry. Cell cycle flow cytometry RCS files were analysed using a fixed manual model in ModFit LT 5.0 and data were analysed using the one-way ANOVA with Dunnett's post hoc test.

***(A)** Comparison of cell cycle phases (G0/G1, S and G2/M phase) of DAUDI cells treated with complete media (control) versus 1-100 µM of DJ0021. **(B)** Results from One-way ANOVA with Dunnett's post hoc test comparing cell cycle phases of the DJ0021 treated cells vs complete media (Control). **(C)** Descriptive statistics for cell cycle analysis, showing mean ratio of G2/M channel over G0/G1 channel (G2/G1), mean % coefficient of variance (% CV), mean reduced chi squared (RCS) and number of replicates for each data set (n). **(D-G)** Representative histogram for Cell Cycle analysis for Control (complete media) (D); DJ0021 1 µM (E); DJ0021 10 µM (F); and DJ0021 100 µM (G).*

A

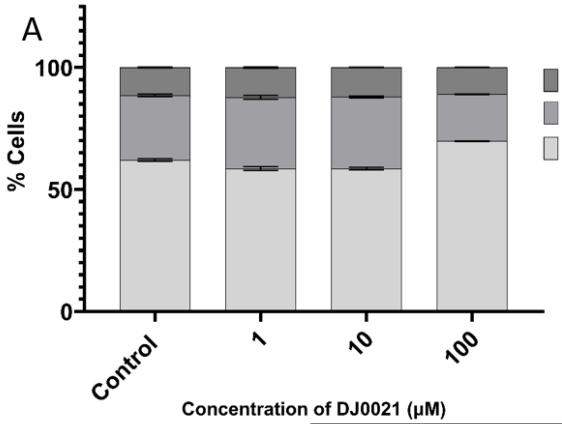

B

Control vs.	1	10	100
G0/G1	P<0.01	P<0.01	P<0.001
S	P<0.05	P<0.01	P<0.001
G2/M	n.s.	n.s.	n.s.

C

	DJ0021 (µM)			
	0	**1**	**10**	**100**
G2/G1, mean (SEM)	1.940 (0.000)	1.950 (0.000)	1.950 (0.000)	1.947 (0.003)
% CV, mean (SEM)	2.598 (0.047)	2.420 (0.057)	2.603 (0.047)	2.843 (0.034)
RCS, mean (SEM)	2.203 (0.203)	1.731 (0.072)	2.155 (0.059)	2.128 (0.182)
n	6	3	3	3

D E F G

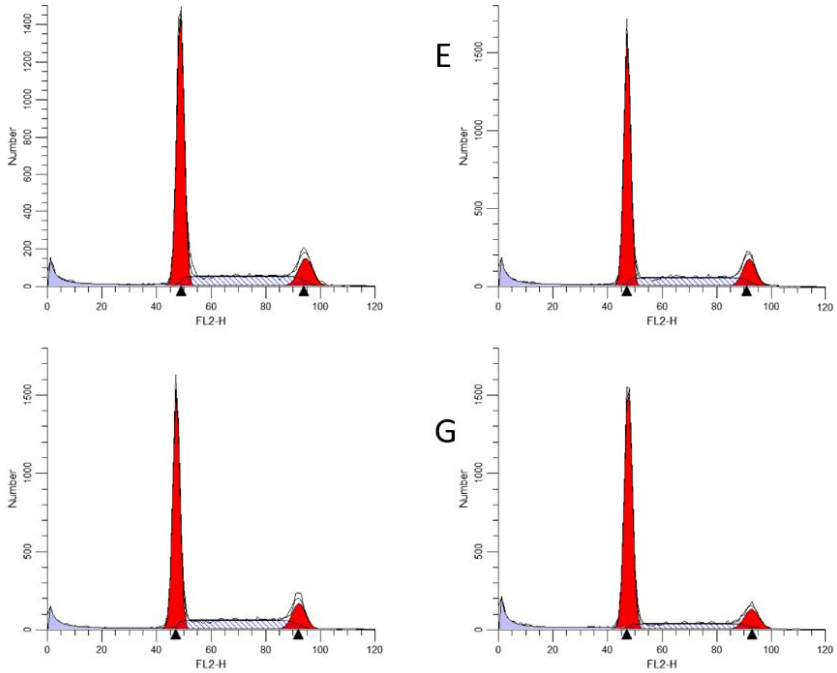

Figure 3-42 Cell cycle analysis for DAUDI cells treated with various concentrations of Thienopyridine DJ0021 for 48 hours as determined by propidium Iodide flow cytometry. Cell cycle flow cytometry RCS files were analysed using a fixed manual model in ModFit LT 5.0 and data were analysed using the one-way ANOVA with Dunnett's post hoc test.

***(A)** Comparison of cell cycle phases (G0/G1, S and G2/M phase) of DAUDI cells treated with complete media (control) versus 1-100 µM of DJ0021. **(B)** Results from One-way ANOVA with Dunnett's post hoc test comparing cell cycle phases of the DJ0021 treated cells vs complete media (Control). **(C)** Descriptive statistics for cell cycle analysis, showing mean ratio of G2/M channel over G0/G1 channel (G2/G1), mean % coefficient of variance (% CV), mean reduced chi squared (RCS) and number of replicates for each data set (n). **(D-G)** Representative histogram for Cell Cycle analysis for Control (complete media) (D); DJ0021 1 µM (E); DJ0021 10 µM (F); and DJ0021 100 µM (G).*

A

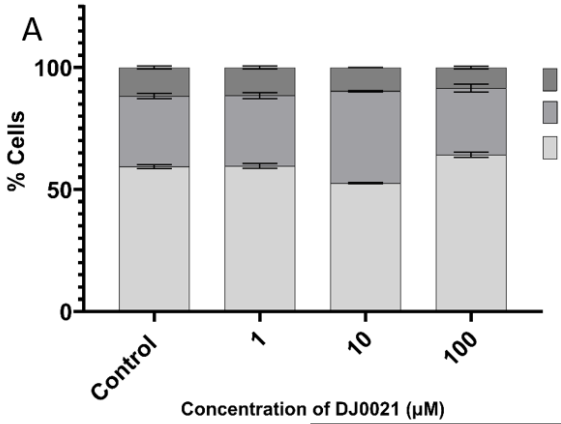

B

Control vs.	1	10	100
G0/G1	n.s.	P<0.001	P<0.01
S	n.s.	P<0.001	n.s.
G2/M	n.s.	n.s.	P<0.01

C

	DJ0021 (µM)			
	0	**1**	**10**	**100**
G2/G1, mean (SEM)	1.928 (0.003)	1.933 (0.003)	1.953 (0.003)	1.940 (0.006)
% CV, mean (SEM)	4.885 (0.126)	4.717 (0.083)	4.847 (0.099)	4.777 (0.174)
RCS, mean (SEM)	1.325 (0.094)	1.543 (0.148)	1.925 (0.257)	1.665 (0.184)
n	6	3	3	3

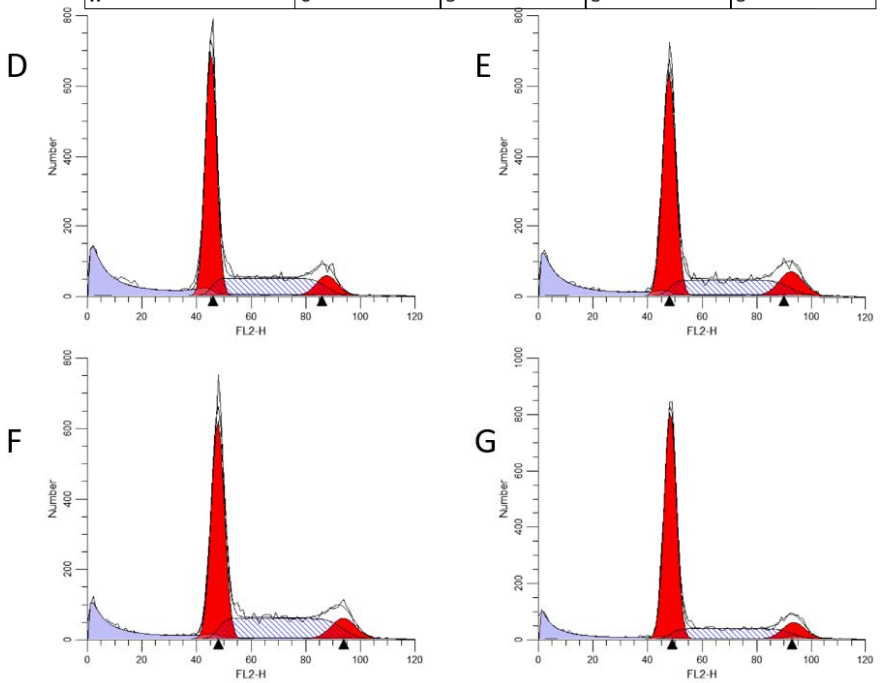

Figure 3-43 Cell cycle analysis for DAUDI cells treated with various concentrations of Thienopyridine DJ0021 for 72 hours as determined by propidium Iodide flow cytometry. Cell cycle flow cytometry RCS files were analysed using a fixed manual model in ModFit LT 5.0 and data were analysed using the one-way ANOVA with Dunnett's post hoc test.

***(A)** Comparison of cell cycle phases (G0/G1, S and G2/M phase) of DAUDI cells treated with complete media (control) versus 1-100 µM of DJ0021. **(B)** Results from One-way ANOVA with Dunnett's post hoc test comparing cell cycle phases of the DJ0021 treated cells vs complete media (Control). **(C)** Descriptive statistics for cell cycle analysis, showing mean ratio of G2/M channel over G0/G1 channel (G2/G1), mean % coefficient of variance (% CV), mean reduced chi squared (RCS) and number of replicates for each data set (n). **(D-G)** Representative histogram for Cell Cycle analysis for Control (complete media) (D); DJ0021 1 µM (E); DJ0021 10 µM (F); and DJ0021 100 µM (G).*

3.4.2.1.3 DJ0199 effects on DAUDI cell cycle

Figure 3-44 to Figure 3-46 show the results for DAUDI cells cultured in the presence of novel thienopyridine DJ00199 for 24 hours, 48 hours, and 72 hours respectively.

No effects were seen following a 24 hour incubation with DJ0199 (Figure 3-44), however akin to DJ0014, significant increases in G_2/M populations were seen at all concentrations at 48 hour (Figure 3-45) and 72 hour (Figure 3-46) timepoints (all $P < 0.001$). Where untreated DAUDI cells at 48 hours of incubation showed 11.48 % of cells in G_2/M, this increased to 17.11 % at 1 µM, 66.17 % at 10 µM and 66.26 % at 100 µM concentrations of DJ0199, whereas at 72 hours of incubation a larger increase in G_2/M cells was seen at 1 µM concentration (27.45 % vs untreated control 11.71 %) while 10 µM (65.53 %) and 100 µM (63.82 %) showed similar levels to the 48 hour incubation, suggesting that the effects are relative to both concentration and duration of exposure to the thienopyridines.

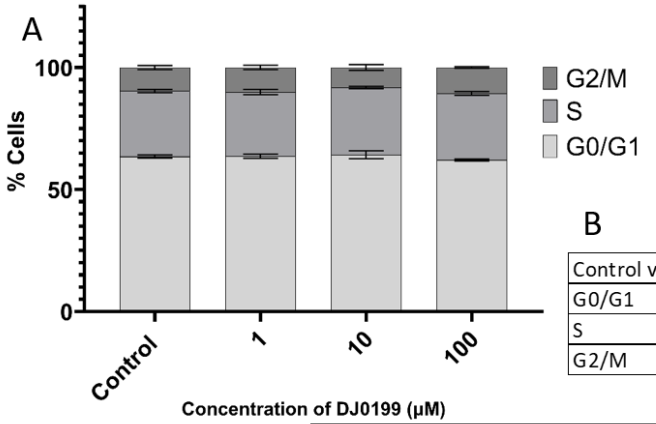

B

Control vs.	1	10	100
G0/G1	n.s.	n.s.	n.s.
S	n.s.	n.s.	n.s.
G2/M	n.s.	n.s.	n.s.

C

	DJ0199 (µM)			
	0	**1**	**10**	**100**
G2/G1, mean (SEM)	1.957 (0.006)	1.947 (0.009)	1.967 (0.007)	1.957 (0.003)
% CV, mean (SEM)	6.138 (0.359)	7.220 (0.469)	6.873 (0.250)	7.243 (0.380)
RCS, mean (SEM)	1.628 (0.102)	1.815 (0.131)	2.005 (0.206)	2.121 (0.229)
n	9	3	3	3

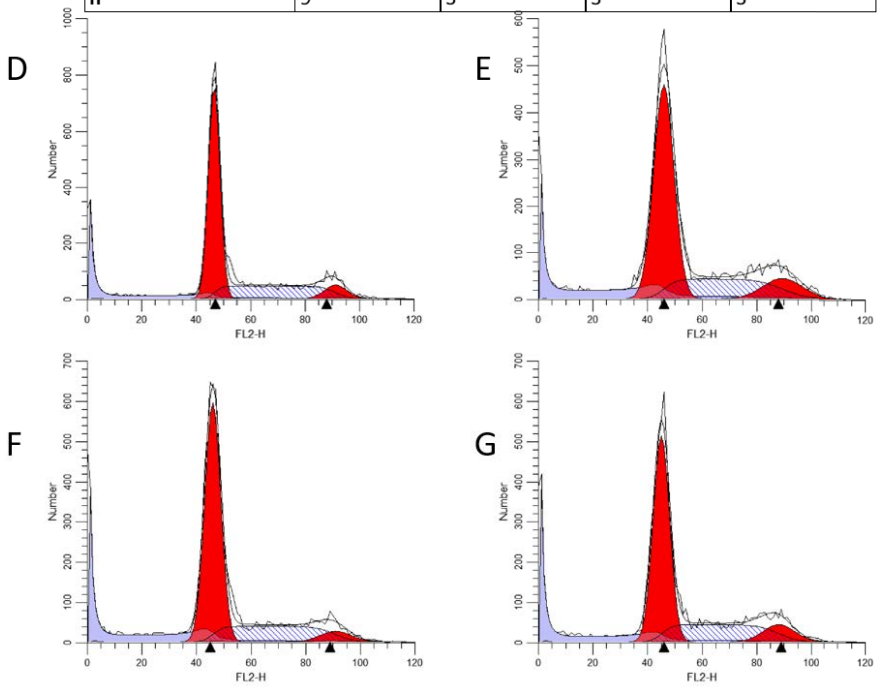

Figure 3-44 Cell cycle analysis for DAUDI cells treated with various concentrations of Thienopyridine DJ0199 for 24 hours as determined by propidium Iodide flow cytometry. Cell cycle flow cytometry RCS files were analysed using a fixed manual model in ModFit LT 5.0 and data were analysed using the one-way ANOVA with Dunnett's post hoc test.

(A) *Comparison of cell cycle phases (G0/G1, S and G2/M phase) of DAUDI cells treated with complete media (control) versus 1-100 µM of DJ0199.* ***(B)*** *Results from One-way ANOVA with Dunnett's post hoc test comparing cell cycle phases of the DJ0199 treated cells vs complete media (Control).* ***(C)*** *Descriptive statistics for cell cycle analysis, showing mean ratio of G2/M channel over G0/G1 channel (G2/G1), mean % coefficient of variance (% CV), mean reduced chi squared (RCS) and number of replicates for each data set (n).* ***(D-G)*** *Representative histogram for Cell Cycle analysis for Control (complete media) (D); DJ0199 1 µM (E); DJ0199 10 µM (F); and DJ0199 100 µM (G).*

A

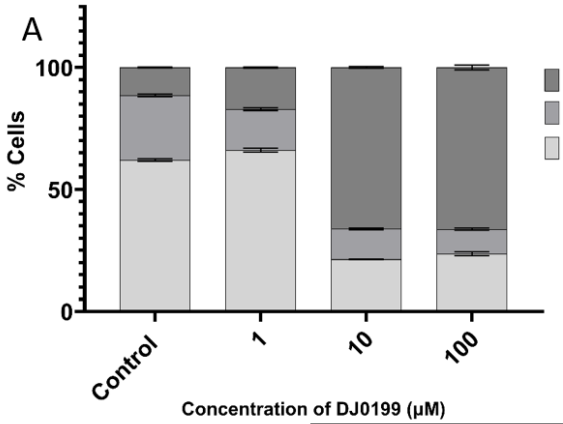

B

Control vs.	1	10	100
G0/G1	P<0.01	P<0.001	P<0.001
S	P<0.001	P<0.001	P<0.001
G2/M	P<0.001	P<0.001	P<0.001

C

	DJ0199 (µM)			
	0	**1**	**10**	**100**
G2/G1, mean (SEM)	1.940 (0.000)	1.930 (0.000)	1.900 (0.006)	1.890 (0.006)
% CV, mean (SEM)	2.598 (0.047)	2.827 (0.034)	2.590 (0.057)	2.657 (0.092)
RCS, mean (SEM)	2.203 (0.203)	1.952 (0.181)	1.974 (0.122)	2.252 (0.105)
n	6	3	3	3

D E F G

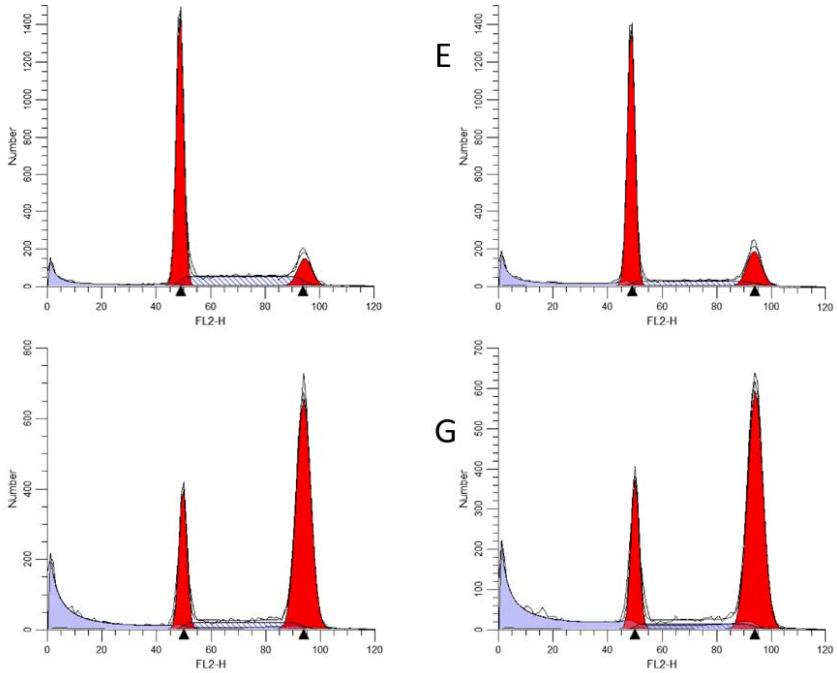

Figure 3-45 Cell cycle analysis for DAUDI cells treated with various concentrations of Thienopyridine DJ0199 for 48 hours as determined by propidium Iodide flow cytometry. Cell cycle flow cytometry RCS files were analysed using a fixed manual model in ModFit LT 5.0 and data were analysed using the one-way ANOVA with Dunnett's post hoc test.

***(A)** Comparison of cell cycle phases (G0/G1, S and G2/M phase) of DAUDI cells treated with complete media (control) versus 1-100 µM of DJ0199. **(B)** Results from One-way ANOVA with Dunnett's post hoc test comparing cell cycle phases of the DJ0199 treated cells vs complete media (Control). **(C)** Descriptive statistics for cell cycle analysis, showing mean ratio of G2/M channel over G0/G1 channel (G2/G1), mean % coefficient of variance (% CV), mean reduced chi squared (RCS) and number of replicates for each data set (n). **(D-G)** Representative histogram for Cell Cycle analysis for Control (complete media) (D); DJ0199 1 µM (E); DJ0199 10 µM (F); and DJ0199 100 µM (G).*

A

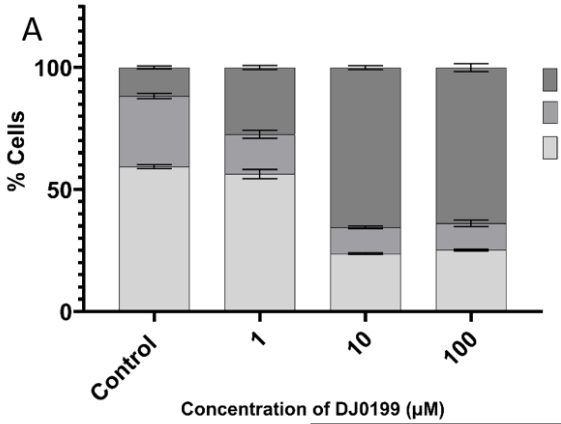

B

Control vs.	1	10	100
G0/G1	n.s.	P<0.001	P<0.001
S	P<0.001	P<0.001	P<0.001
G2/M	P<0.001	P<0.001	P<0.001

C

	DJ0199 (µM)			
	0	**1**	**10**	**100**
G2/G1, mean (SEM)	1.928 (0.003)	1.927 (0.003)	1.903 (0.009)	1.903 (0.003)
% CV, mean (SEM)	4.885 (0.126)	4.483 (0.194)	4.210 (0.036)	4.193 (0.166)
RCS, mean (SEM)	1.325 (0.094)	1.835 (0.065)	2.077 (0.110)	2.188 (0.108)
n	6	3	3	3

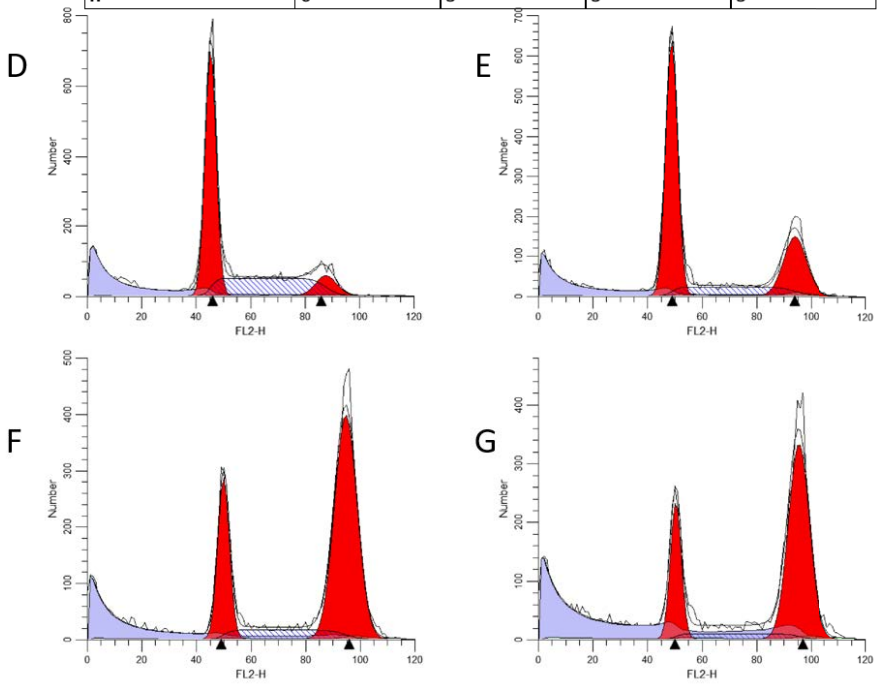

Figure 3-46 Cell cycle analysis for DAUDI cells treated with various concentrations of Thienopyridine DJ0199 for 72 hours as determined by propidium Iodide flow cytometry. Cell cycle flow cytometry RCS files were analysed using a fixed manual model in ModFit LT 5.0 and data were analysed using the one-way ANOVA with Dunnett's post hoc test.

***(A)** Comparison of cell cycle phases (G0/G1, S and G2/M phase) of DAUDI cells treated with complete media (control) versus 1-100 µM of DJ0199. **(B)** Results from One-way ANOVA with Dunnett's post hoc test comparing cell cycle phases of the DJ0199 treated cells vs complete media (Control). **(C)** Descriptive statistics for cell cycle analysis, showing mean ratio of G2/M channel over G0/G1 channel (G2/G1), mean % coefficient of variance (% CV), mean reduced chi squared (RCS) and number of replicates for each data set (n). **(D-G)** Representative histogram for Cell Cycle analysis for Control (complete media) (D); DJ0199 1 µM (E); DJ0199 10 µM (F); and DJ0199 100 µM (G).*

3.4.2.1.4 DJ0206 effects on DAUDI cell cycle

Figure 3-47 to Figure 3-49 show the results for DAUDI cells cultured in the presence of novel thienopyridine DJ00206 for 24 hours, 48 hours, and 72 hours respectively.

From the thienopyridine compounds with a cyclooctane moiety, DJ0206 is the most active across all three incubation timepoints and concentrations tested. At 24 hours (Figure 3-47), DJ0206 showed a significant (all $P < 0.001$) increased G_2/M population at 1 µM (42.98 %), 10 µM (32.65 %) and 100 µM (32.17 %) compared to untreated control DAUDI cells (3.31 %). At 48 hours (Figure 3-48) these effects increased further, with 70.46 % DAUDI cells in G_2/M at 1 µM, 66.72 % at 10 µM and 71.37 % at 100 µM concentrations, compared to 11.48 % in untreated controls. Similar statistically significant ($P < 0.001$) shifts to G_2/M were see following 72 hour incubation (Figure 3-49) with 1 µM (67.81 %), 10 µM (67.53 %) and 100 µM (58.97 %) showing increases compared to untreated controls (11.71 %). The lower percentage of cells treated with 100 µM DJ0206 may possibly be accounted for by the number of apoptotic cells seen in Figure 3-19B following 72 hours of incubation.

A

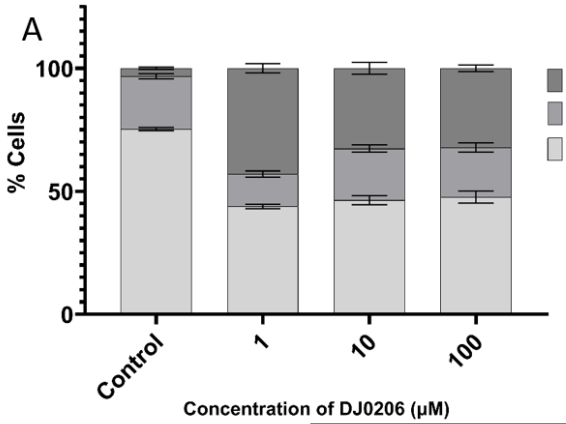

B

Control vs.	1	10	100
G0/G1	P<0.001	P<0.001	P<0.001
S	P<0.01	n.s.	n.s.
G2/M	P<0.001	P<0.001	P<0.001

C

	DJ0206 (µM)			
	0	**1**	**10**	**100**
G2/G1, mean (SEM)	1.950 (0.006)	1.913 (0.003)	1.923 (0.003)	1.917 (0.003)
% CV, mean (SEM)	3.173 (0.057)	3.320 (0.157)	3.320 (0.195)	3.877 (0.400)
RCS, mean (SEM)	3.076 (0.323)	2.491 (0.264)	2.144 (0.316)	2.393 (0.319)
n	3	3	3	3

D E F G

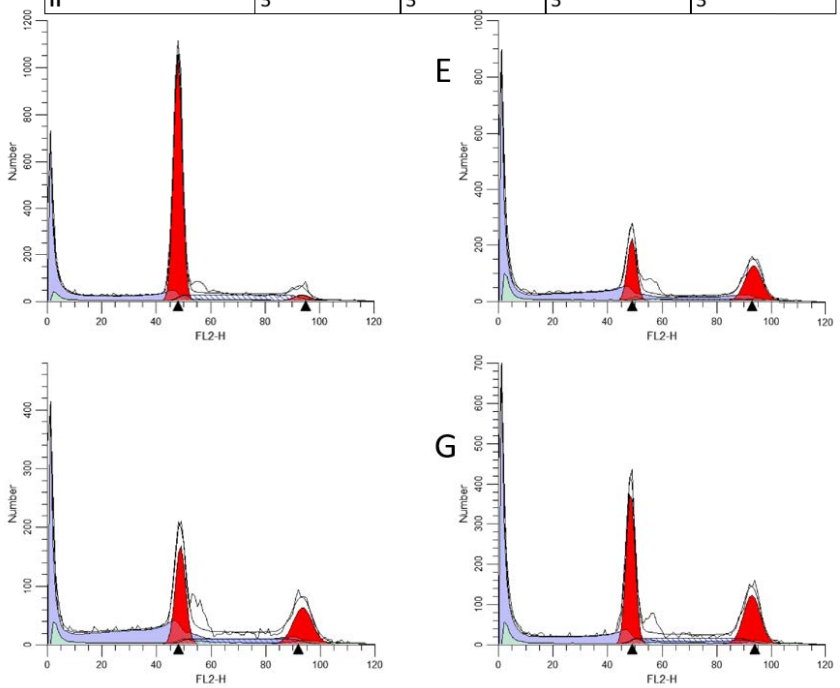

Figure 3-47 Cell cycle analysis for DAUDI cells treated with various concentrations of Thienopyridine DJ0206 for 24 hours as determined by propidium Iodide flow cytometry. Cell cycle flow cytometry RCS files were analysed using a fixed manual model in ModFit LT 5.0 and data were analysed using the one-way ANOVA with Dunnett's post hoc test.

(A) *Comparison of cell cycle phases (G0/G1, S and G2/M phase) of DAUDI cells treated with complete media (control) versus 1-100 µM of DJ0206.* ***(B)*** *Results from One-way ANOVA with Dunnett's post hoc test comparing cell cycle phases of the DJ0206 treated cells vs complete media (Control).* ***(C)*** *Descriptive statistics for cell cycle analysis, showing mean ratio of G2/M channel over G0/G1 channel (G2/G1), mean % coefficient of variance (% CV), mean reduced chi squared (RCS) and number of replicates for each data set (n).* ***(D-G)*** *Representative histogram for Cell Cycle analysis for Control (complete media) (D); DJ0206 1 µM (E); DJ0206 10 µM (F); and DJ0206 100 µM (G).*

A

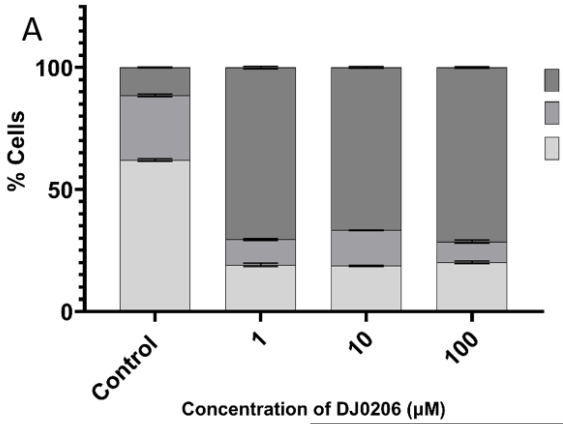

B

Control vs.	1	10	100
G0/G1	P<0.001	P<0.001	P<0.001
S	P<0.001	P<0.001	P<0.001
G2/M	P<0.001	P<0.001	P<0.001

C

	DJ0206 (µM)			
	0	**1**	**10**	**100**
G2/G1, mean (SEM)	1.940 (0.000)	1.907 (0.003)	1.910 (0.006)	1.907 (0.003)
% CV, mean (SEM)	2.598 (0.047)	2.723 (0.067)	2.893 (0.125)	2.857 (0.086)
RCS, mean (SEM)	2.203 (0.203)	2.073 (0.231)	2.453 (0.065)	2.401 (0.035)
n	6	3	3	3

D

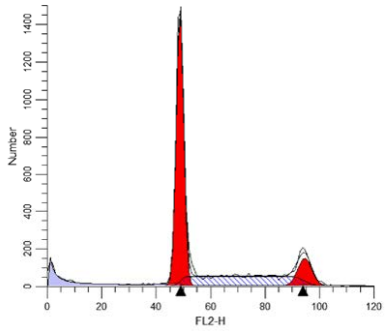

E

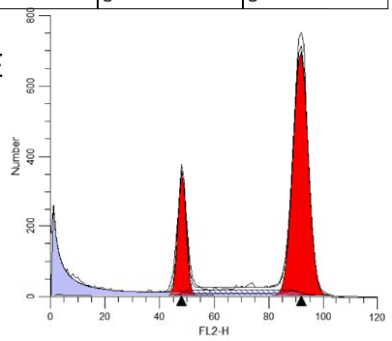

F

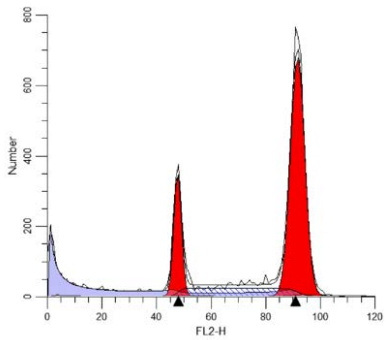

G

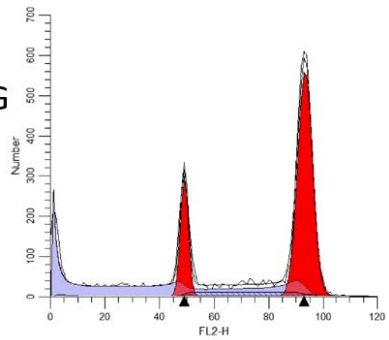

Figure 3-48 Cell cycle analysis for DAUDI cells treated with various concentrations of Thienopyridine DJ0206 for 48 hours as determined by propidium Iodide flow cytometry. Cell cycle flow cytometry RCS files were analysed using a fixed manual model in ModFit LT 5.0 and data were analysed using the one-way ANOVA with Dunnett's post hoc test.

***(A)** Comparison of cell cycle phases (G0/G1, S and G2/M phase) of DAUDI cells treated with complete media (control) versus 1-100 µM of DJ0206. **(B)** Results from One-way ANOVA with Dunnett's post hoc test comparing cell cycle phases of the DJ0206 treated cells vs complete media (Control). **(C)** Descriptive statistics for cell cycle analysis, showing mean ratio of G2/M channel over G0/G1 channel (G2/G1), mean % coefficient of variance (% CV), mean reduced chi squared (RCS) and number of replicates for each data set (n). **(D-G)** Representative histogram for Cell Cycle analysis for Control (complete media) (D); DJ0206 1 µM (E); DJ0206 10 µM (F); and DJ0206 100 µM (G).*

A

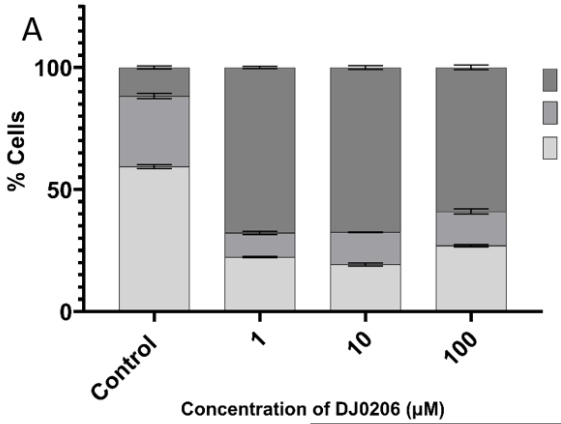

B

Control vs.	1	10	100
G0/G1	P<0.001	P<0.001	P<0.001
S	P<0.001	P<0.001	P<0.001
G2/M	P<0.001	P<0.001	P<0.001

C

	DJ0206 (µM)			
	0	**1**	**10**	**100**
G2/G1, mean (SEM)	1.928 (0.003)	1.910 (0.000)	1.913 (0.003)	1.913 (0.003)
% CV, mean (SEM)	4.885 (0.126)	4.173 (0.087)	3.997 (0.047)	4.163 (0.139)
RCS, mean (SEM)	1.325 (0.094)	2.526 (0.073)	2.176 (0.209)	1.653 (0.2912)
n	6	3	3	3

D E F G

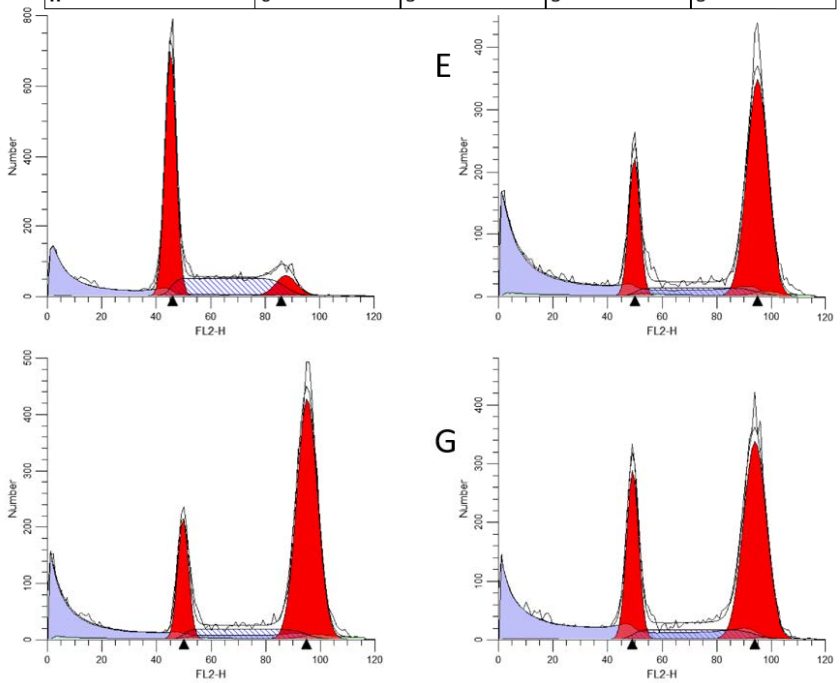

Figure 3-49 Cell cycle analysis for DAUDI cells treated with various concentrations of Thienopyridine DJ0206 for 72 hours as determined by propidium Iodide flow cytometry. Cell cycle flow cytometry RCS files were analysed using a fixed manual model in ModFit LT 5.0 and data were analysed using the one-way ANOVA with Dunnett's post hoc test.

***(A)** Comparison of cell cycle phases (G0/G1, S and G2/M phase) of DAUDI cells treated with complete media (control) versus 1-100 µM of DJ0206. **(B)** Results from One-way ANOVA with Dunnett's post hoc test comparing cell cycle phases of the DJ0206 treated cells vs complete media (Control). **(C)** Descriptive statistics for cell cycle analysis, showing mean ratio of G2/M channel over G0/G1 channel (G2/G1), mean % coefficient of variance (% CV), mean reduced chi squared (RCS) and number of replicates for each data set (n). **(D-G)** Representative histogram for Cell Cycle analysis for Control (complete media) (D); DJ0206 1 µM (E); DJ0206 10 µM (F); and DJ0206 100 µM (G).*

3.4.2.1.5 DJ0209 effects on DAUDI cell cycle

Figure 3-50 to Figure 3-52 show the results for DAUDI cells cultured in the presence of novel thienopyridine DJ0209 for 24 hours, 48 hours, and 72 hours respectively.

Following 24 hours of incubation with DJ0209 (Figure 3-50), the only effect seen was a small, statistically significant ($P < 0.001$) increase in G_2/M population at 100 µM. At 48 hours, a mixed set of results was shown (Figure 3-51), with a small significant ($p < 0.05$) decrease in G_2/M population at 1 µM (12.13 %), while there were significant ($P < 0.001$) increased at both 10 µM (33.70 %) and 100 µM (19.96 %) compared to 14.33 % in untreated controls.

At 72 hours (Figure 3-52), there was a small, statistically significant decrease in G_2/M at 1 µM (9.22 %, $P < 0.05$), 10 µM (8.73 %, $P < 0.01$) and 100 µM (8.54 %, $P < 0.01$). Like with DJ0206, this reduction in G_2/M cell populations at 72 hours may be accounted for by apoptotic cell death seen in the annexin V/propidium iodine assay in Figure 3-22B.

A

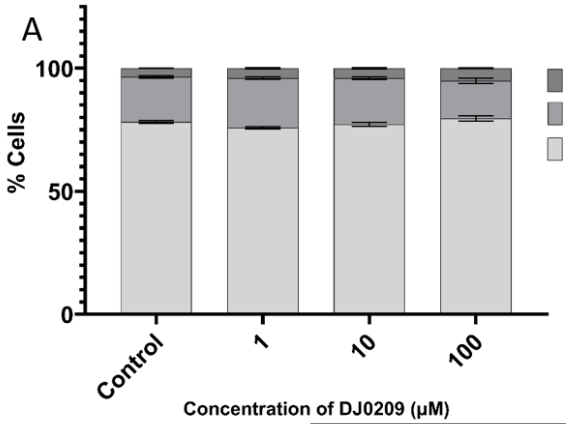

B

Control vs.	1	10	100
G0/G1	n.s.	n.s.	n.s.
S	n.s.	n.s.	P<0.05
G2/M	n.s.	n.s.	P<0.001

C

	DJ0209 (µM)			
	0	**1**	**10**	**100**
G2/G1, mean (SEM)	1.938 (0.003)	1.950 (0.006)	1.947 (0.003)	1.937 (0.003)
% CV, mean (SEM)	3.148 (0.097)	2.720 (0.116)	2.967 (0.271)	2.837 (0.123)
RCS, mean (SEM)	3.243 (0.160)	2.460 (0.431)	2.535 (0.056)	3.221 (0.178)
n	5	3	3	3

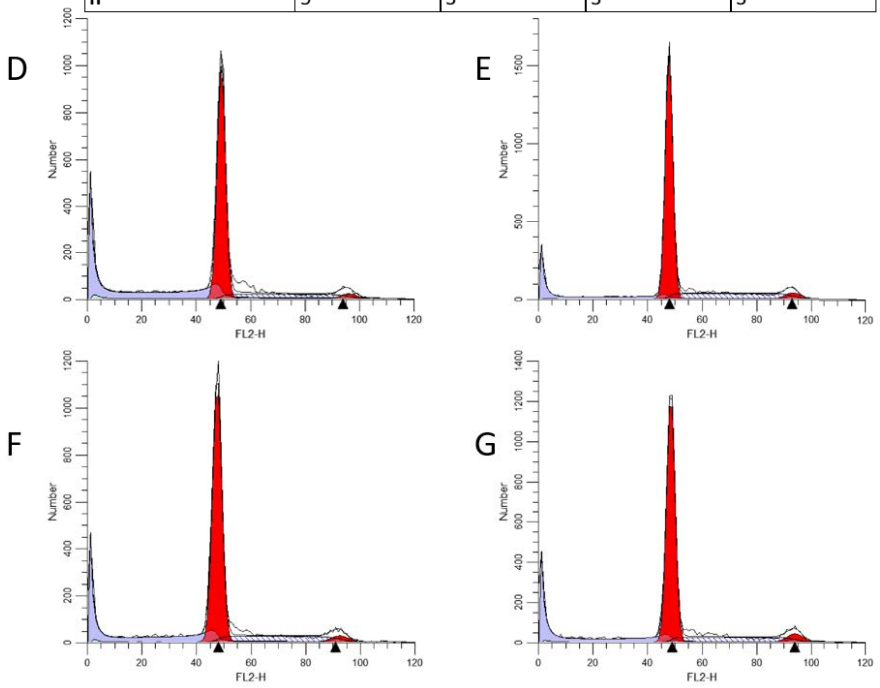

Figure 3-50 Cell cycle analysis for DAUDI cells treated with various concentrations of Thienopyridine DJ0209 for 24 hours as determined by propidium Iodide flow cytometry. Cell cycle flow cytometry RCS files were analysed using a fixed manual model in ModFit LT 5.0 and data were analysed using the one-way ANOVA with Dunnett's post hoc test.

***(A)** Comparison of cell cycle phases (G0/G1, S and G2/M phase) of DAUDI cells treated with complete media (control) versus 1-100 µM of DJ0209. **(B)** Results from One-way ANOVA with Dunnett's post hoc test comparing cell cycle phases of the DJ0209 treated cells vs complete media (Control). **(C)** Descriptive statistics for cell cycle analysis, showing mean ratio of G2/M channel over G0/G1 channel (G2/G1), mean % coefficient of variance (% CV), mean reduced chi squared (RCS) and number of replicates for each data set (n). **(D-G)** Representative histogram for Cell Cycle analysis for Control (complete media) (D); DJ0209 1 µM (E); DJ0209 10 µM (F); and DJ0209 100 µM (G).*

A

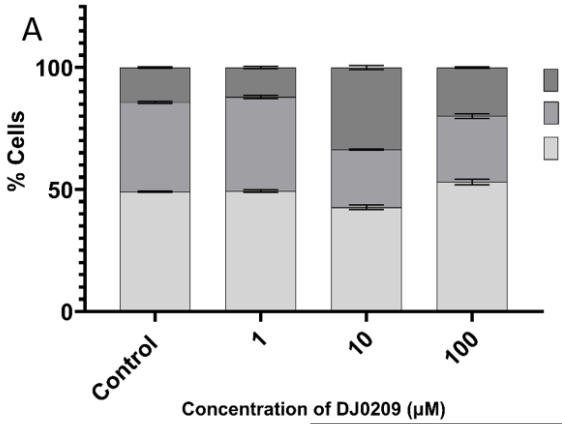

B

Control vs.	1	10	100
G0/G1	n.s.	P<0.001	P<0.01
S	n.s.	P<0.001	P<0.001
G2/M	P<0.05	P<0.001	P<0.001

C

	DJ0209 (µM)			
	0	**1**	**10**	**100**
G2/G1, mean (SEM)	1.900 (0.006)	1.930 (0.000)	1.907 (0.003)	1.907 (0.003)
% CV, mean (SEM)	6.380 (0.340)	3.147 (0.048)	3.520 (0.065)	3.463 (0.107)
RCS, mean (SEM)	2.703 (0.426)	2.332 (0.090)	2.434 (0.094)	2.023 (0.076)
n	6	3	3	3

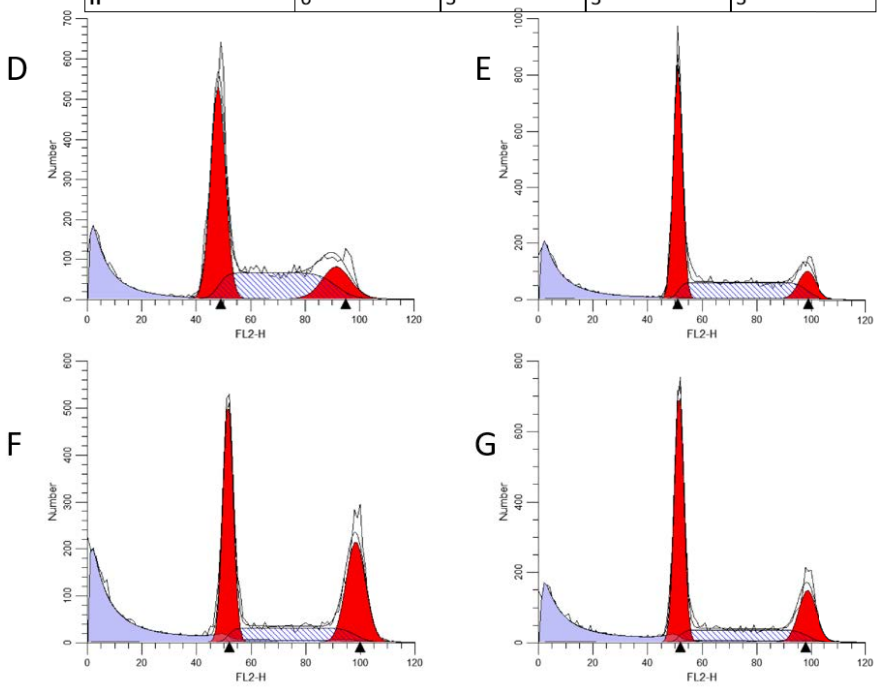

Figure 3-51 Cell cycle analysis for DAUDI cells treated with various concentrations of Thienopyridine DJ0209 for 48 hours as determined by propidium Iodide flow cytometry. Cell cycle flow cytometry RCS files were analysed using a fixed manual model in ModFit LT 5.0 and data were analysed using the one-way ANOVA with Dunnett's post hoc test.

***(A)** Comparison of cell cycle phases (G0/G1, S and G2/M phase) of DAUDI cells treated with complete media (control) versus 1-100 µM of DJ0209. **(B)** Results from One-way ANOVA with Dunnett's post hoc test comparing cell cycle phases of the DJ0209 treated cells vs complete media (Control). **(C)** Descriptive statistics for cell cycle analysis, showing mean ratio of G2/M channel over G0/G1 channel (G2/G1), mean % coefficient of variance (% CV), mean reduced chi squared (RCS) and number of replicates for each data set (n). **(D-G)** Representative histogram for Cell Cycle analysis for Control (complete media) (D); DJ0209 1 µM (E); DJ0209 10 µM (F); and DJ0209 100 µM (G).*

A

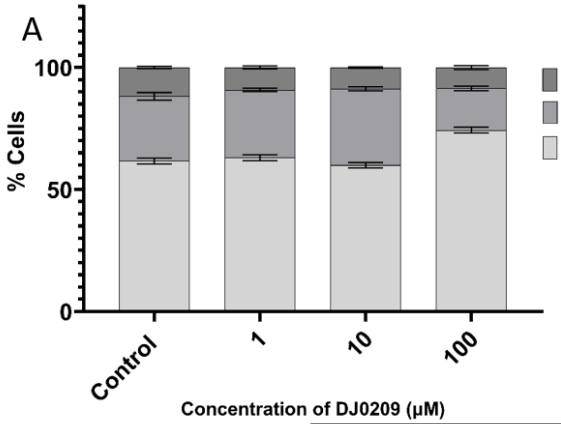

B

Control vs.	1	10	100
G0/G1	n.s.	n.s.	P<0.001
S	n.s.	n.s.	P<0.01
G2/M	P<0.05	P<0.01	P<0.01

C

	DJ0209 (µM)			
	0	**1**	**10**	**100**
G2/G1, mean (SEM)	1.943 (0.003)	1.950 (0.000)	1.953 (0.007)	1.947 (0.007)
% CV, mean (SEM)	4.982 (0.128)	4.643 (0.128)	4.6733 (0.121)	4.680 (0.115)
RCS, mean (SEM)	1.649 (0.089)	1.842 (0.141)	1.623 (0.117)	2.133 (0.052)
n	6	3	3	3

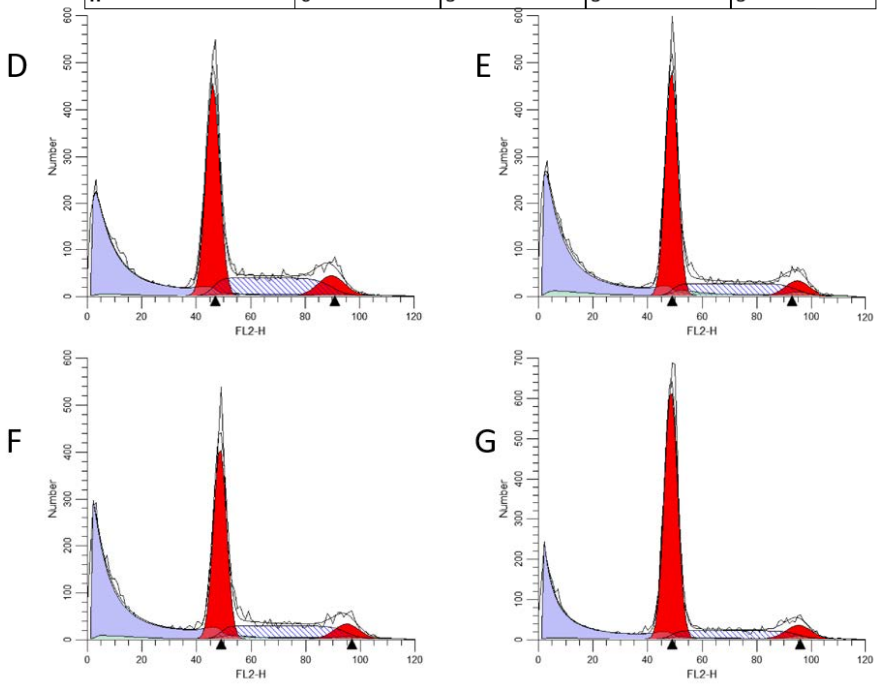

Figure 3-52 Cell cycle analysis for DAUDI cells treated with various concentrations of Thienopyridine DJ0209 for 72 hours as determined by propidium Iodide flow cytometry. Cell cycle flow cytometry RCS files were analysed using a fixed manual model in ModFit LT 5.0 and data were analysed using the one-way ANOVA with Dunnett's post hoc test.

***(A)** Comparison of cell cycle phases (G0/G1, S and G2/M phase) of DAUDI cells treated with complete media (control) versus 1-100 µM of DJ0209. **(B)** Results from One-way ANOVA with Dunnett's post hoc test comparing cell cycle phases of the DJ0209 treated cells vs complete media (Control). **(C)** Descriptive statistics for cell cycle analysis, showing mean ratio of G2/M channel over G0/G1 channel (G2/G1), mean % coefficient of variance (% CV), mean reduced chi squared (RCS) and number of replicates for each data set (n). **(D-G)** Representative histogram for Cell Cycle analysis for Control (complete media) (D); DJ0209 1 µM (E); DJ0209 10 µM (F); and DJ0209 100 µM (G).*

3.4.2.2 Effects of novel thienopyridines with a cycloheptane moiety on cell cycle

Figure 3-53 to Figure 3-55 show the results for DAUDI cells cultured in the presence of novel thienopyridine DJ0041 for 24 hours, 48 hours, and 72 hours respectively.

3.4.2.2.1 DJ0041 effects on DAUDI cell cycle

Compound DJ0041 showed statistically significant increases in G_2/M populations across all concentrations and timepoints tested. Smaller statistically significant increases (all P <0.001) were seen at 24 hours (Figure 3-53) with 1 µM (12.06 %), 10 µM (12.41 %) and 100 µM (12.50 %) broadly showing similar effects when compared to untreated control DAUDI cells (3.56 %). Larger increases in G_2/M populations were seen at 48 hours (Figure 3-54) where 1 µM, 10 µM and 100 µM showed increases to 26.01 %, 70.94 % and 68.23 % respectively (all P < 0.001) compared to untreated controls (14.33 %), while similar increases were seen post 72 hours of incubation (Figure 3-55) with 1 µM (29.13 %), 10 µM (68.87 %) and 100 µM (63.09 %) (all P < 0.001).

A

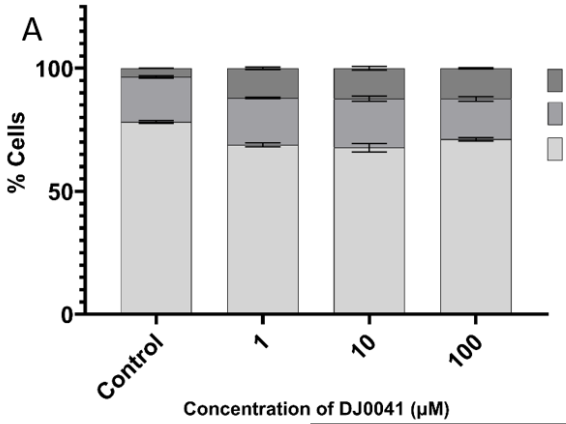

B

Control vs.	1	10	100
G0/G1	P<0.001	P<0.001	P<0.001
S	n.s.	n.s.	n.s.
G2/M	P<0.001	P<0.001	P<0.001

C

	DJ0041 (µM)			
	0	**1**	**10**	**100**
G2/G1, mean (SEM)	1.938 (0.004)	1.927 (0.003)	1.937 (0.007)	1.923 (0.003)
% CV, mean (SEM)	3.148 (0.097)	3.007 (0.171)	3.053 (0.084)	2.830 (0.021)
RCS, mean (SEM)	3.243 (0.160)	2.734 (0.047)	3.134 (0.831)	2.393 (0.112)
n	5	3	3	3

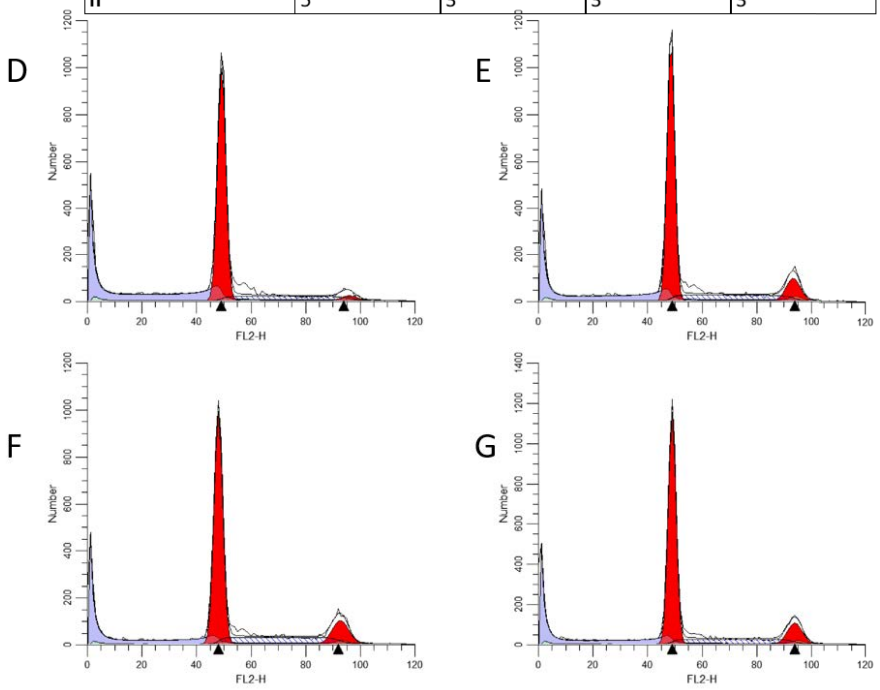

Figure 3-53 Cell cycle analysis for DAUDI cells treated with various concentrations of Thienopyridine DJ0041 for 24 hours as determined by propidium Iodide flow cytometry. Cell cycle flow cytometry RCS files were analysed using a fixed manual model in ModFit LT 5.0 and data were analysed using the one-way ANOVA with Dunnett's post hoc test.

(A) *Comparison of cell cycle phases (G0/G1, S and G2/M phase) of DAUDI cells treated with complete media (control) versus 1-100 µM of DJ0041.* ***(B)*** *Results from One-way ANOVA with Dunnett's post hoc test comparing cell cycle phases of the DJ0041 treated cells vs complete media (Control).* ***(C)*** *Descriptive statistics for cell cycle analysis, showing mean ratio of G2/M channel over G0/G1 channel (G2/G1), mean % coefficient of variance (% CV), mean reduced chi squared (RCS) and number of replicates for each data set (n).* ***(D-G)*** *Representative histogram for Cell Cycle analysis for Control (complete media) (D); DJ0041 1 µM (E); DJ0041 10 µM (F); and DJ0041 100 µM (G).*

A

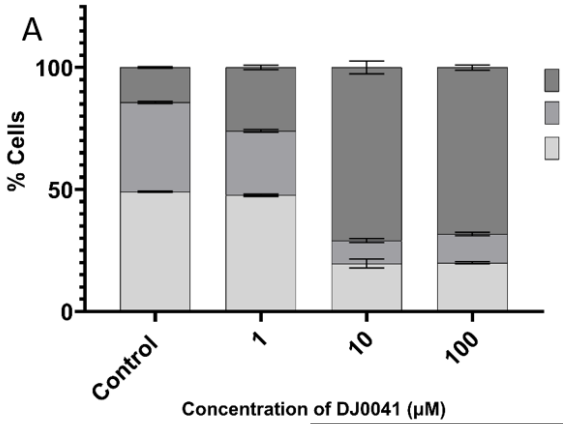

B

Control vs.	1	10	100
G0/G1	n.s.	P<0.001	P<0.001
S	P<0.001	P<0.001	P<0.001
G2/M	P<0.001	P<0.001	P<0.001

C

	DJ0041 (µM)			
	0	**1**	**10**	**100**
G2/G1, mean (SEM)	1.900 (0.006)	1.910 (0.000)	1.887 (0.003)	1.893 (0.003)
% CV, mean (SEM)	6.380 (0.340)	3.560 (0.040)	3.530 (0.290)	3.310 (0.104)
RCS, mean (SEM)	2.703 (0.426)	1.912 (0.216)	3.221 (0.214)	3.368 (0.404)
n	6	3	3	3

D E F G

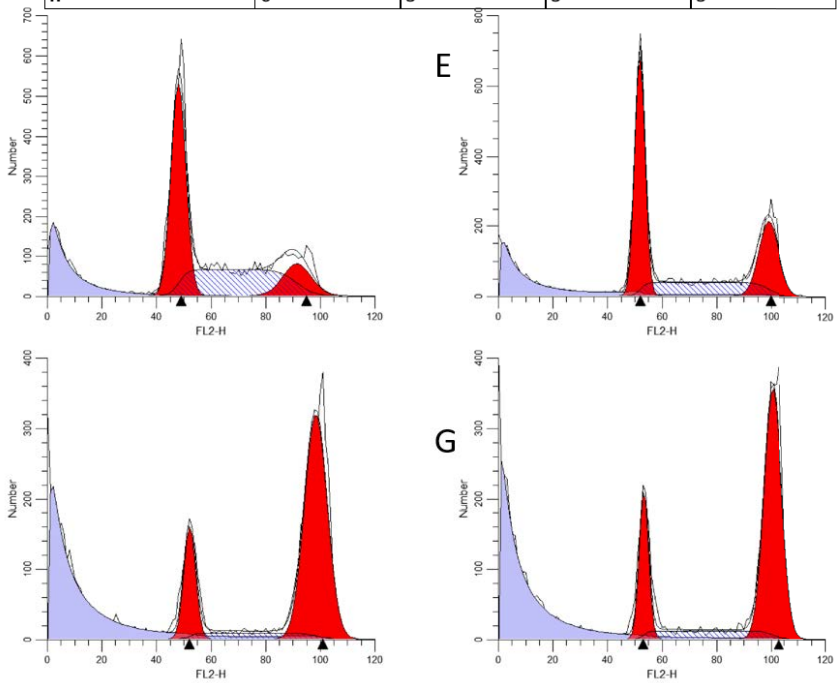

Figure 3-54 Cell cycle analysis for DAUDI cells treated with various concentrations of Thienopyridine DJ0041 for 48 hours as determined by propidium Iodide flow cytometry. Cell cycle flow cytometry RCS files were analysed using a fixed manual model in ModFit LT 5.0 and data were analysed using the one-way ANOVA with Dunnett's post hoc test.

***(A)** Comparison of cell cycle phases (G0/G1, S and G2/M phase) of DAUDI cells treated with complete media (control) versus 1-100 µM of DJ0041. **(B)** Results from One-way ANOVA with Dunnett's post hoc test comparing cell cycle phases of the DJ0041 treated cells vs complete media (Control). **(C)** Descriptive statistics for cell cycle analysis, showing mean ratio of G2/M channel over G0/G1 channel (G2/G1), mean % coefficient of variance (% CV), mean reduced chi squared (RCS) and number of replicates for each data set (n). **(D-G)** Representative histogram for Cell Cycle analysis for Control (complete media) (D); DJ0041 1 µM (E); DJ0041 10 µM (F); and DJ0041 100 µM (G).*

A

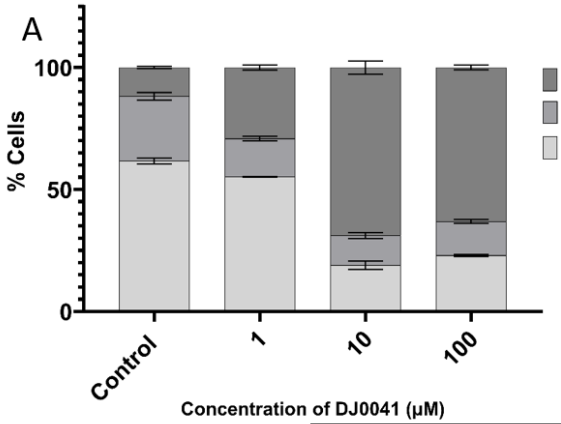

B

Control vs.	1	10	100
G0/G1	p<0.01	P<0.001	P<0.001
S	P<0.001	P<0.001	P<0.001
G2/M	P<0.001	P<0.001	P<0.001

C

	DJ0041 (µM)			
	0	**1**	**10**	**100**
G2/G1, mean (SEM)	1.943 (0.003)	1.943 (0.003)	1.923 (0.003)	1.937 (0.003)
% CV, mean (SEM)	4.982 (0.128)	4.813 (0.082)	4.213 (0.110)	4.340 (0.093)
RCS, mean (SEM)	1.649 (0.089)	1.712 (0.149)	1.893 (0.032)	2.323 (0.194)
n	6	3	3	3

D E F G

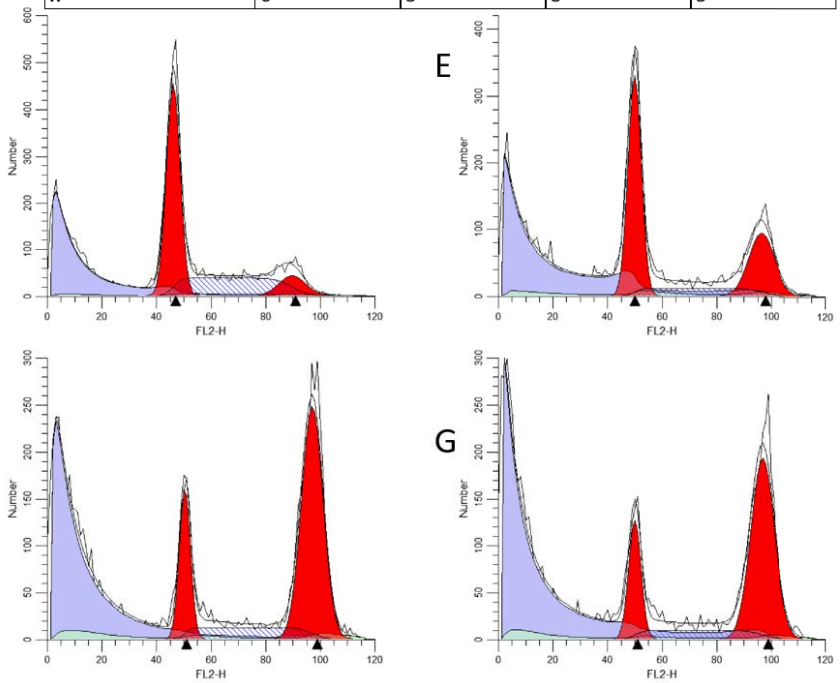

Figure 3-55 Cell cycle analysis for DAUDI cells treated with various concentrations of Thienopyridine DJ0041 for 72 hours as determined by propidium Iodide flow cytometry. Cell cycle flow cytometry RCS files were analysed using a fixed manual model in ModFit LT 5.0 and data were analysed using the one-way ANOVA with Dunnett's post hoc test.

***(A)** Comparison of cell cycle phases (G0/G1, S and G2/M phase) of DAUDI cells treated with complete media (control) versus 1-100 µM of DJ0041. **(B)** Results from One-way ANOVA with Dunnett's post hoc test comparing cell cycle phases of the DJ0041 treated cells vs complete media (Control). **(C)** Descriptive statistics for cell cycle analysis, showing mean ratio of G2/M channel over G0/G1 channel (G2/G1), mean % coefficient of variance (% CV), mean reduced chi squared (RCS) and number of replicates for each data set (n). **(D-G)** Representative histogram for Cell Cycle analysis for Control (complete media) (D); DJ0041 1 µM (E); DJ0041 10 µM (F); and DJ0041 100 µM (G).*

3.4.2.2.2 DJ0081 effects on DAUDI cell cycle

Figure 3-56 to Figure 3-58 show the results for DAUDI cells cultured in the presence of novel thienopyridine DJ0081 for 24 hours, 48 hours, and 72 hours respectively.

Unlike DJ0041, DJ0081 did not show any effects, at any of the concentrations tested at 24 hours (Figure 3-56). However, at 48 hours post incubation (Figure 3-57), a comparatively larger, statistically significant effect was seen at 1 µM concentration (54.52 %, P <0.001) for DJ0081 that for DJ0041 at the same timepoint, while similar sized increases in G_2/M cells were seen at 10 µM (62.84 %, P <0.001) and 100 µM (54.53 %, P <0.001) compared to 11.48 % of cells in untreated controls. This pattern of results was continued post the 72 hour incubation (Figure 3-58) with increases to 59.20 % (1 µM, P <0.001), 67.97 % (10 µM, P < 0.001) and 58.65 % (100 µM, P < 0.001) against 11.71 % of cells in untreated controls.

From the two cycloheptane moiety containing thienopyridine compounds, DJ0041 appears to show greater effect sizes on the cell cycle than DJ0081, apart from at 1 µM concentration at 48 and 72 hours.

A

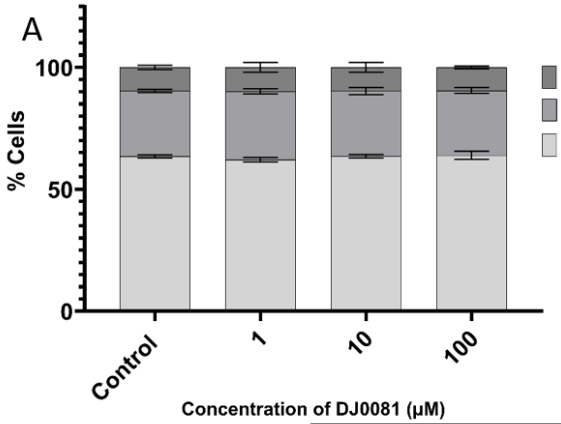

B

Control vs.	1	10	100
G0/G1	n.s.	n.s.	n.s.
S	n.s.	n.s.	n.s.
G2/M	n.s.	n.s.	n.s.

C

	DJ0081 (µM)			
	0	**1**	**10**	**100**
G2/G1, mean (SEM)	1.957 (0.006)	1.957 (0.009)	1.950 (0.021)	1.957 (0.003)
% CV, mean (SEM)	6.138 (0.359)	6.593 (0.697)	7.110 (0.538)	6.037 (0.273)
RCS, mean (SEM)	1.628 (0.102)	2.695 (0.850)	1.722 (0.281)	2.098 (0.296)
n	9	3	3	3

D E F G

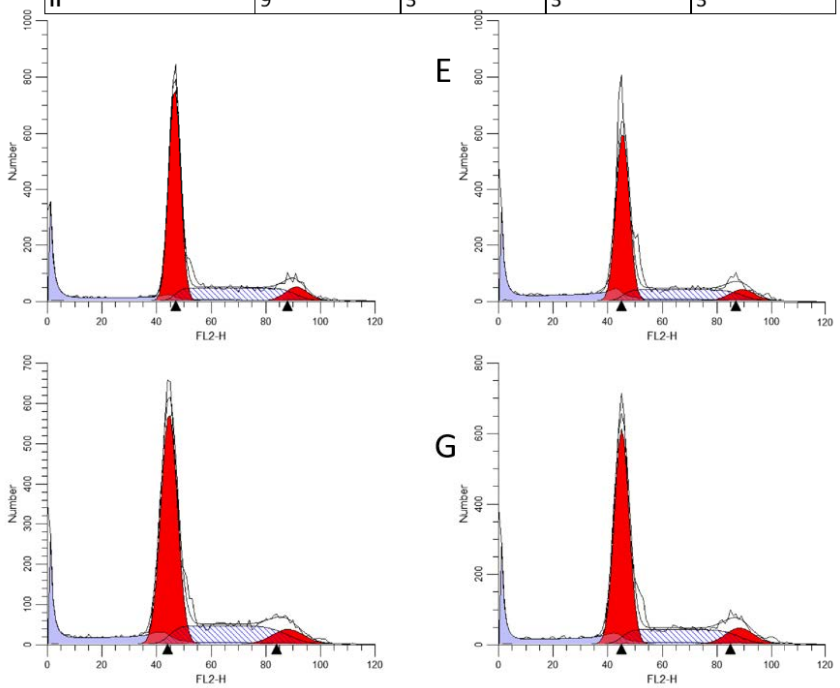

Figure 3-56 Cell cycle analysis for DAUDI cells treated with various concentrations of Thienopyridine DJ0081 for 24 hours as determined by propidium Iodide flow cytometry. Cell cycle flow cytometry RCS files were analysed using a fixed manual model in ModFit LT 5.0 and data were analysed using the one-way ANOVA with Dunnett's post hoc test.

(A) *Comparison of cell cycle phases (G0/G1, S and G2/M phase) of DAUDI cells treated with complete media (control) versus 1-100 µM of DJ0081.* ***(B)*** *Results from One-way ANOVA with Dunnett's post hoc test comparing cell cycle phases of the DJ0081 treated cells vs complete media (Control).* ***(C)*** *Descriptive statistics for cell cycle analysis, showing mean ratio of G2/M channel over G0/G1 channel (G2/G1), mean % coefficient of variance (% CV), mean reduced chi squared (RCS) and number of replicates for each data set (n).* ***(D-G)*** *Representative histogram for Cell Cycle analysis for Control (complete media) (D); DJ0081 1 µM (E); DJ0081 10 µM (F); and DJ0081 100 µM (G).*

A

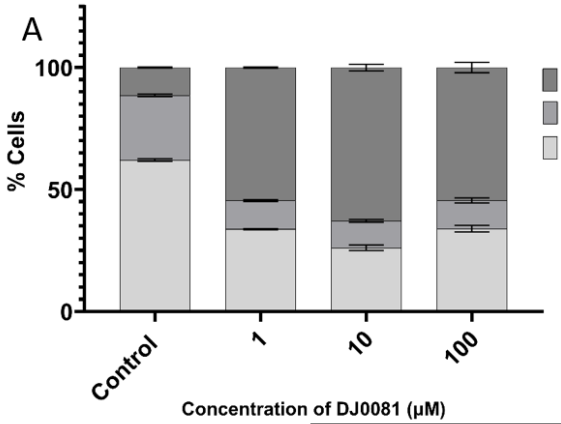

B

Control vs.	1	10	100
G0/G1	P<0.001	P<0.001	P<0.001
S	P<0.001	P<0.001	P<0.001
G2/M	P<0.001	P<0.001	P<0.001

C

	DJ0081 (µM)			
	0	**1**	**10**	**100**
G2/G1, mean (SEM)	1.940 (0.000)	1.910 (0.000)	1.897 (0.007)	1.903 (0.013)
% CV, mean (SEM)	2.598 (0.047)	2.650 (0.038)	2.740 (0.142)	2.587 (0.170)
RCS, mean (SEM)	2.203 (0.203)	3.098 (0.109)	2.198 (0.135)	2.690 (0.159)
n	6	3	3	3

D E F G

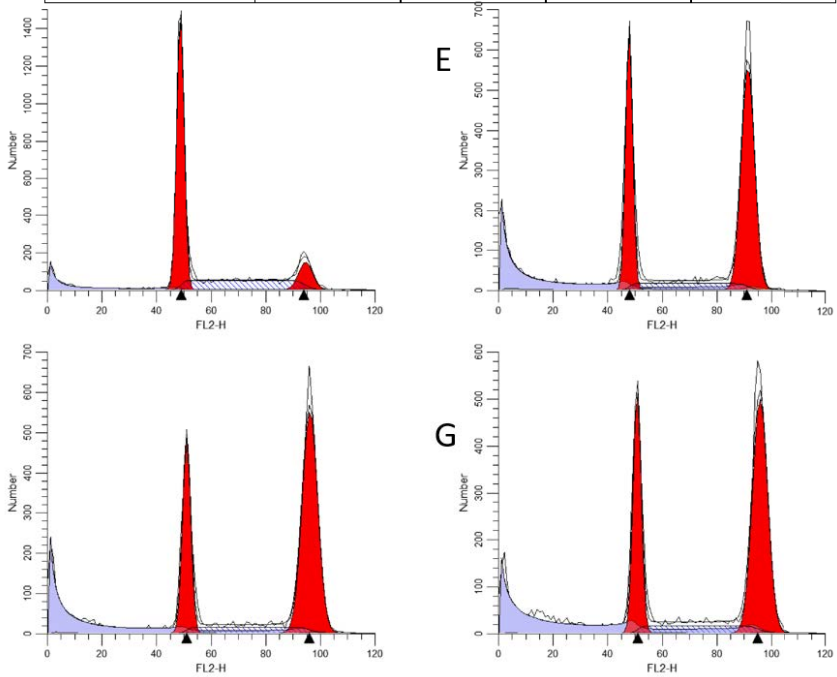

Figure 3-57 Cell cycle analysis for DAUDI cells treated with various concentrations of Thienopyridine DJ0081 for 48 hours as determined by propidium Iodide flow cytometry. Cell cycle flow cytometry RCS files were analysed using a fixed manual model in ModFit LT 5.0 and data were analysed using the one-way ANOVA with Dunnett's post hoc test.

***(A)** Comparison of cell cycle phases (G0/G1, S and G2/M phase) of DAUDI cells treated with complete media (control) versus 1-100 µM of DJ0081. **(B)** Results from One-way ANOVA with Dunnett's post hoc test comparing cell cycle phases of the DJ0081 treated cells vs complete media (Control). **(C)** Descriptive statistics for cell cycle analysis, showing mean ratio of G2/M channel over G0/G1 channel (G2/G1), mean % coefficient of variance (% CV), mean reduced chi squared (RCS) and number of replicates for each data set (n). **(D-G)** Representative histogram for Cell Cycle analysis for Control (complete media) (D); DJ0081 1 (E); DJ0081 10 µM (F); and DJ0081 100 µM (G).*

A

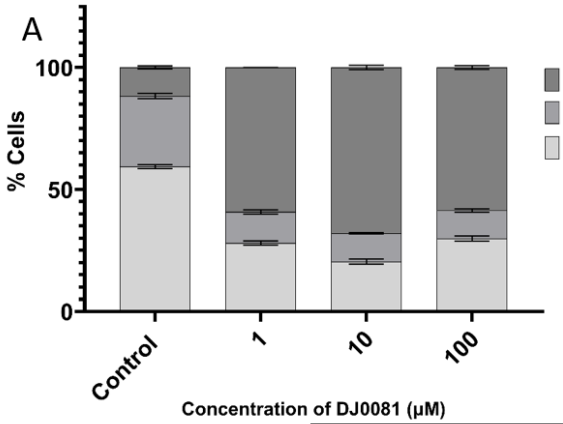

B

Control vs.	1	10	100
G0/G1	P<0.001	P<0.001	P<0.001
S	P<0.001	P<0.001	P<0.001
G2/M	P<0.001	P<0.001	P<0.001

C

	DJ0081 (µM)			
	0	**1**	**10**	**100**
G2/G1, mean (SEM)	1.928 (0.003)	1.907 (0.003)	1.893 (0.003)	1.890 (0.000)
% CV, mean (SEM)	4.885 (0.126)	4.760 (0.092)	4.497 (0.048)	4.550 (0.114)
RCS, mean (SEM)	1.325 (0.094)	2.040 (0.123)	1.737 (0.244)	1.458 (0.031)
n	6	3	3	3

D E F G

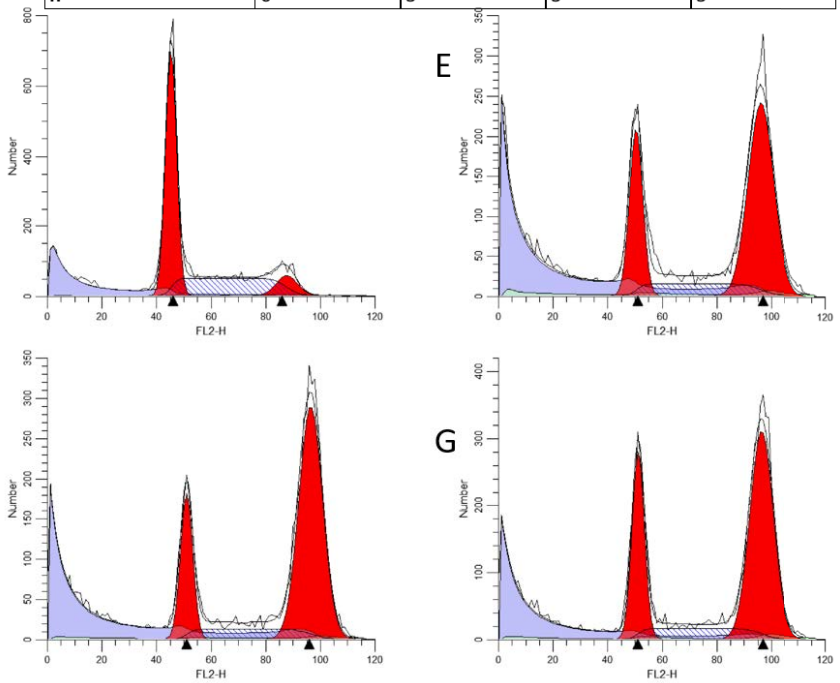

Figure 3-58 Cell cycle analysis for DAUDI cells treated with various concentrations of Thienopyridine DJ0081 for 72 hours as determined by propidium Iodide flow cytometry. Cell cycle flow cytometry RCS files were analysed using a fixed manual model in ModFit LT 5.0 and data were analysed using the one-way ANOVA with Dunnett's post hoc test.

***(A)** Comparison of cell cycle phases (G0/G1, S and G2/M phase) of DAUDI cells treated with complete media (control) versus 1-100 µM of DJ0081. **(B)** Results from One-way ANOVA with Dunnett's post hoc test comparing cell cycle phases of the DJ0081 treated cells vs complete media (Control). **(C)** Descriptive statistics for cell cycle analysis, showing mean ratio of G2/M channel over G0/G1 channel (G2/G1), mean % coefficient of variance (% CV), mean reduced chi squared (RCS) and number of replicates for each data set (n). **(D-G)** Representative histogram for Cell Cycle analysis for Control (complete media) (D); DJ0081 1 µM (E); DJ0081 10 µM (F); and DJ0081 100 µM (G).*

3.4.2.3 Effects of novel thienopyridines with a cyclohexanone moiety on cell cycle

3.4.2.3.1 DJ0097 effects on DAUDI cell cycle

Figure 3-59 to Figure 3-61 show the results for DAUDI cells cultured in the presence of novel thienopyridine DJ0097 for 24 hours, 48 hours, and 72 hours respectively.

Post 24 hours of incubation in the presence of DJ0097 (Figure 3-59), all three concentrations tested showed a statistically significant shift towards G_2/M cell populations (all $P < 0.001$), with 1 µM (17.28 %), 10 µM (36.23 %) and 100 µM (28.85 %) showing increases when compared to untreated controls (3.31 %).

These effects increased in line with the duration of incubation, with 1 µM (48.85 %), 10 µM (67.13 %) and 100 µM (48.22 %) versus 14.33 % in untreated controls at 48 hours (Figure 3-60) and 1 µM (58.61 %), 10 µM (66.68 %) and 100 µM (64.31 %) versus 11.82 % in untreated controls at 72 hours (Figure 3-61) (all $P < 0.001$).

A

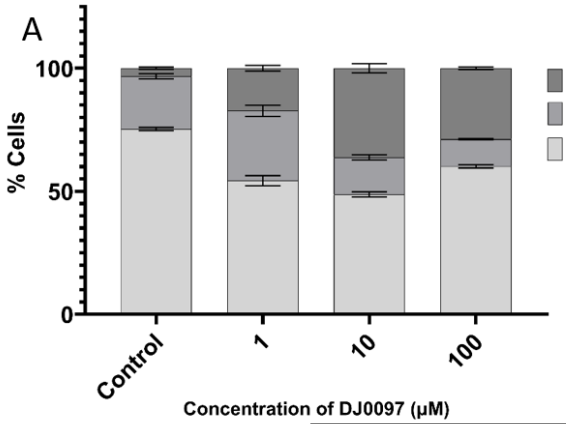

B

Control vs.	1	10	100
G0/G1	P<0.001	P<0.001	P<0.001
S	P<0.05	P<0.05	P<0.01
G2/M	P<0.001	P<0.001	P<0.001

C

	DJ0097 (µM)			
	0	**1**	**10**	**100**
G2/G1, mean (SEM)	1.950 (0.006)	1.920 (0.006)	1.920 (0.000)	1.927 (0.003)
% CV, mean (SEM)	3.173 (0.057)	3.207 (0.1745)	3.043 (0.299)	2.957 (0.075)
RCS, mean (SEM)	3.076 (0.323)	2.411 (0.214)	2.008 (0.218)	2.121 (0.0574)
n	3	3	3	3

D E F G

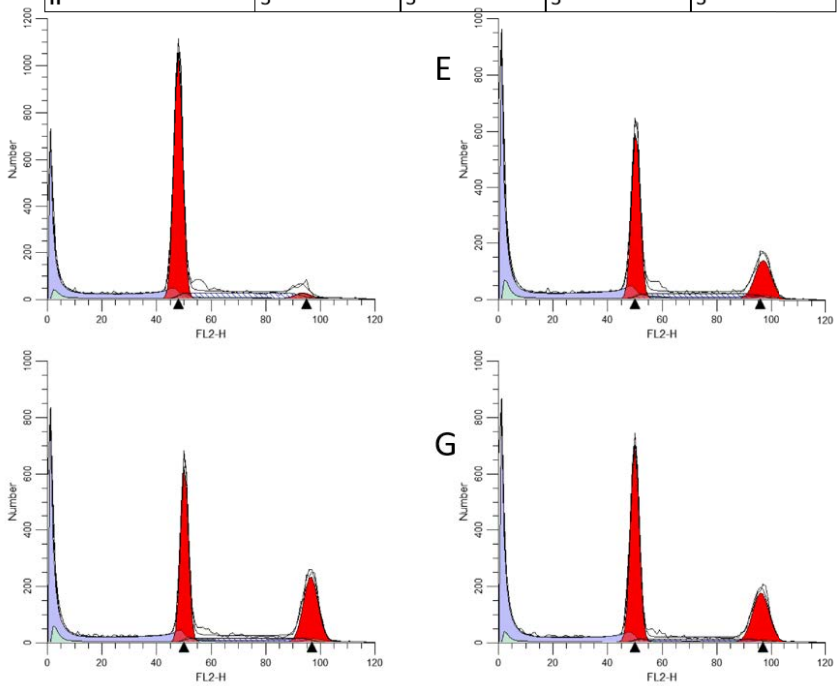

Figure 3-59 Cell cycle analysis for DAUDI cells treated with various concentrations of Thienopyridine DJ0097 for 24 hours as determined by propidium Iodide flow cytometry. Cell cycle flow cytometry RCS files were analysed using a fixed manual model in ModFit LT 5.0 and data were analysed using the one-way ANOVA with Dunnett's post hoc test.

***(A)** Comparison of cell cycle phases (G0/G1, S and G2/M phase) of DAUDI cells treated with complete media (control) versus 1-100 µM of DJ0097. **(B)** Results from One-way ANOVA with Dunnett's post hoc test comparing cell cycle phases of the DJ0097 treated cells vs complete media (Control). **(C)** Descriptive statistics for cell cycle analysis, showing mean ratio of G2/M channel over G0/G1 channel (G2/G1), mean % coefficient of variance (% CV), mean reduced chi squared (RCS) and number of replicates for each data set (n). **(D-G)** Representative histogram for Cell Cycle analysis for Control (complete media) (D); DJ0097 1 µM (E); DJ0097 10 µM (F); and DJ0097 100 µM (G).*

A

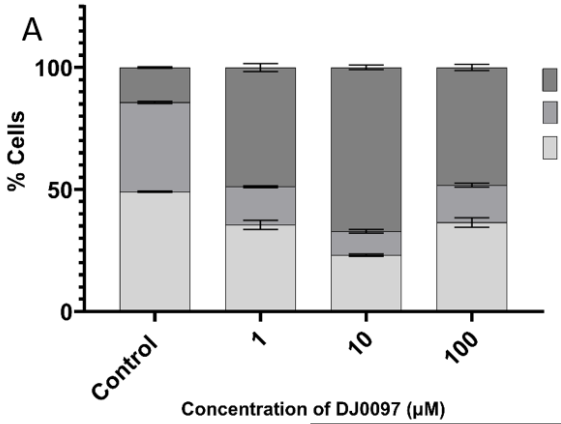

B

Control vs.	1	10	100
G0/G1	P<0.001	P<0.001	P<0.001
S	P<0.001	P<0.001	P<0.001
G2/M	P<0.001	P<0.001	P<0.001

C

	DJ0097 (µM)			
	0	**1**	**10**	**100**
G2/G1, mean (SEM)	1.900 (0.006)	1.910 (0.000)	1.900 (0.000)	1.900 (0.000)
% CV, mean (SEM)	6.380 (0.340)	3.047 (0.094)	2.883 (0.080)	3.553 (0.134)
RCS, mean (SEM)	2.703 (0.426)	2.886 (0.327)	2.204 (0.331)	2.037 (0.014)
n	6	3	3	3

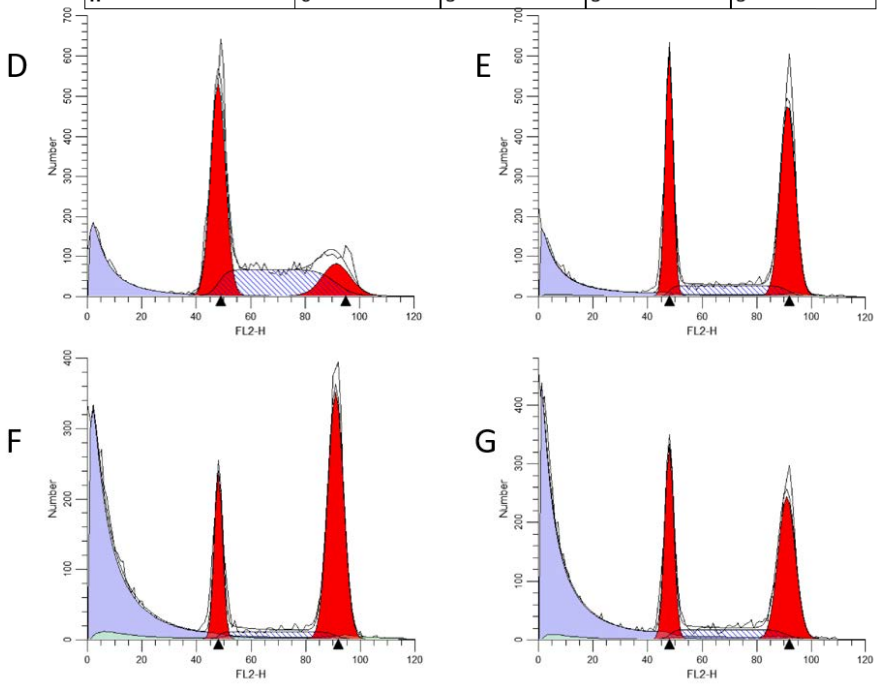

Figure 3-60 Cell cycle analysis for DAUDI cells treated with various concentrations of Thienopyridine DJ0097 for 48 hours as determined by propidium Iodide flow cytometry. Cell cycle flow cytometry RCS files were analysed using a fixed manual model in ModFit LT 5.0 and data were analysed using the one-way ANOVA with Dunnett's post hoc test.

***(A)** Comparison of cell cycle phases (G0/G1, S and G2/M phase) of DAUDI cells treated with complete media (control) versus 1-100 µM of DJ0097. **(B)** Results from One-way ANOVA with Dunnett's post hoc test comparing cell cycle phases of the DJ0097 treated cells vs complete media (Control). **(C)** Descriptive statistics for cell cycle analysis, showing mean ratio of G2/M channel over G0/G1 channel (G2/G1), mean % coefficient of variance (% CV), mean reduced chi squared (RCS) and number of replicates for each data set (n). **(D-G)** Representative histogram for Cell Cycle analysis for Control (complete media) (D); DJ0097 1 (E); DJ0097 10 µM (F); and DJ0097 100 µM (G).*

A

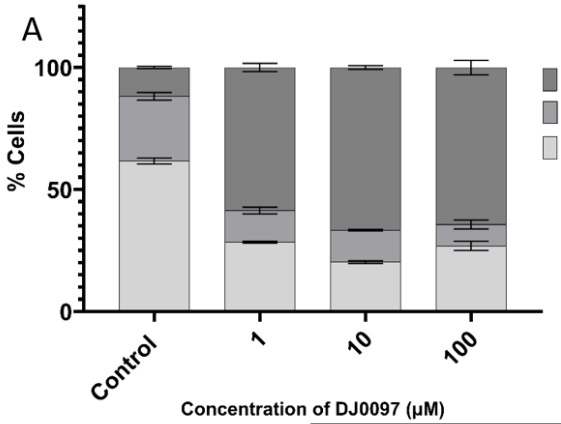

B

Control vs.	1	10	100
G0/G1	P<0.001	P<0.001	P<0.001
S	P<0.001	P<0.001	P<0.001
G2/M	P<0.001	P<0.001	P<0.001

C

	DJ0097 (µM)			
	0	**1**	**10**	**100**
G2/G1, mean (SEM)	1.943 (0.003)	1.930 (0.000)	1.927 (0.003)	1.927 (0.003)
% CV, mean (SEM)	4.982 (0.128)	4.807 (0.033)	4.803 (0.302)	4.330 (0.012)
RCS, mean (SEM)	1.649 (0.089)	2.293 (0.253)	2.149 (0.260)	2.250 (0.103)
n	6	3	3	3

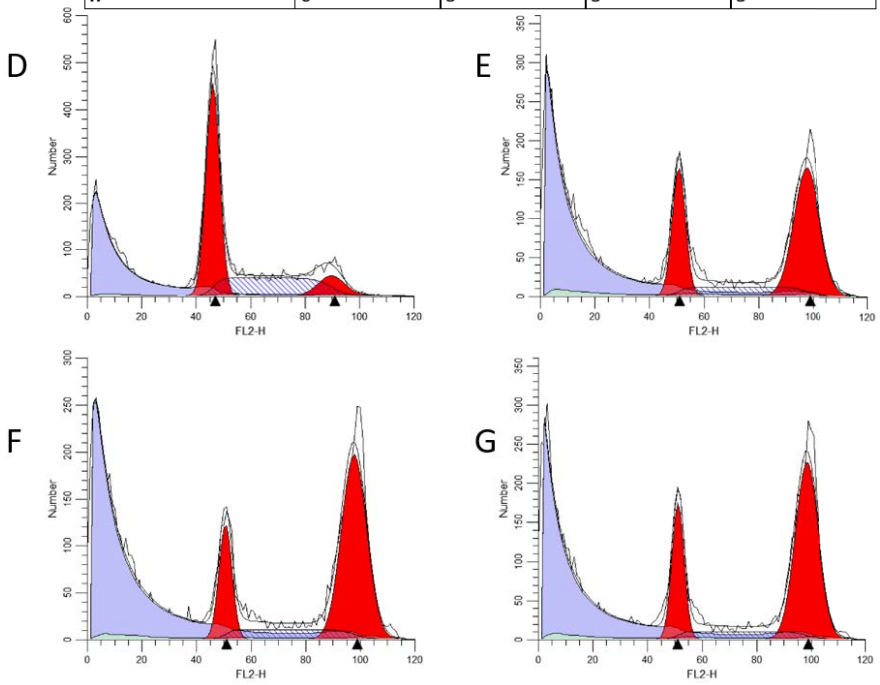

Figure 3-61 Cell cycle analysis for DAUDI cells treated with various concentrations of Thienopyridine DJ0097 for 72 hours as determined by propidium Iodide flow cytometry. Cell cycle flow cytometry RCS files were analysed using a fixed manual model in ModFit LT 5.0 and data were analysed using the one-way ANOVA with Dunnett's post hoc test.

***(A)** Comparison of cell cycle phases (G0/G1, S and G2/M phase) of DAUDI cells treated with complete media (control) versus 1-100 µM of DJ0097. **(B)** Results from One-way ANOVA with Dunnett's post hoc test comparing cell cycle phases of the DJ0097 treated cells vs complete media (Control). **(C)** Descriptive statistics for cell cycle analysis, showing mean ratio of G2/M channel over G0/G1 channel (G2/G1), mean % coefficient of variance (% CV), mean reduced chi squared (RCS) and number of replicates for each data set (n). **(D-G)** Representative histogram for Cell Cycle analysis for Control (complete media) (D); DJ0097 1 µM (E); DJ0097 10 µM (F); and DJ0097 100 µM (G).*

3.4.2.3.2 DJ0109 effects on DAUDI cell cycle

Figure 3-62 to Figure 3-64 show the results for DAUDI cells cultured in the presence of novel thienopyridine DJ0109 for 24 hours, 48 hours, and 72 hours respectively.

Across all timepoints, DJ0109 showed no significant differences in G_2/M phase of the cell cycle when compared to the respective untreated controls at 24 hours (Figure 3-62), 48 hours (Figure 3-63) apart from a decrease in G_2/M at 72 hours (Figure 3-64) at 100 µM (9.15 % vs 11.82 % untreated control; $P < 0.05$), with a corresponding increase in G1 phase cells.

A

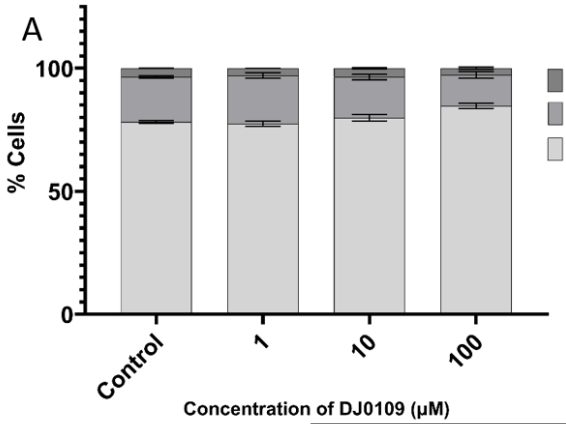

B

Control vs.	1	10	100
G0/G1	n.s.	n.s.	P<0.01
S	n.s.	n.s.	P<0.01
G2/M	n.s.	n.s.	n.s.

C

	DJ0109 (µM)			
	0	**1**	**10**	**100**
G2/G1, mean (SEM)	1.938 (0.003)	1.970 (0.010)	1.943 (0.007)	1.950 (0.006)
% CV, mean (SEM)	3.148 (0.097)	4.380 (0.563)	2.717 (0.038)	2.767 (0.097)
RCS, mean (SEM)	3.243 (0.160)	2.331 (0.223)	2.958 (0.047)	2.869 (0.160)
n	5	3	3	3

D

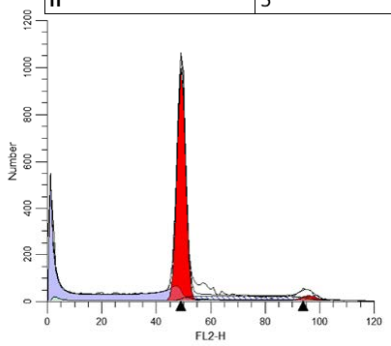

E

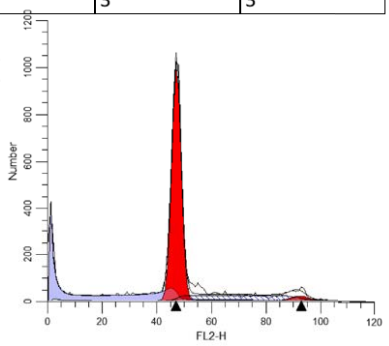

F

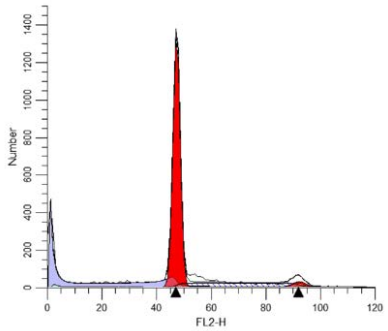

G

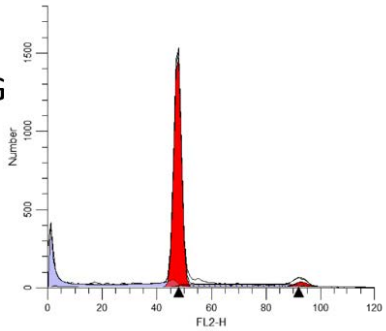

Figure 3-62 Cell cycle analysis for DAUDI cells treated with various concentrations of Thienopyridine DJ0109 for 24 hours as determined by propidium Iodide flow cytometry. Cell cycle flow cytometry RCS files were analysed using a fixed manual model in ModFit LT 5.0 and data were analysed using the one-way ANOVA with Dunnett's post hoc test.

***(A)** Comparison of cell cycle phases (G0/G1, S and G2/M phase) of DAUDI cells treated with complete media (control) versus 1-100 µM of DJ0109. **(B)** Results from One-way ANOVA with Dunnett's post hoc test comparing cell cycle phases of the DJ0109 treated cells vs complete media (Control). **(C)** Descriptive statistics for cell cycle analysis, showing mean ratio of G2/M channel over G0/G1 channel (G2/G1), mean % coefficient of variance (% CV), mean reduced chi squared (RCS) and number of replicates for each data set (n). **(D-G)** Representative histogram for Cell Cycle analysis for Control (complete media) (D); DJ0109 1 µM (E); DJ0109 10 µM (F); and DJ0109 100 µM (G).*

A

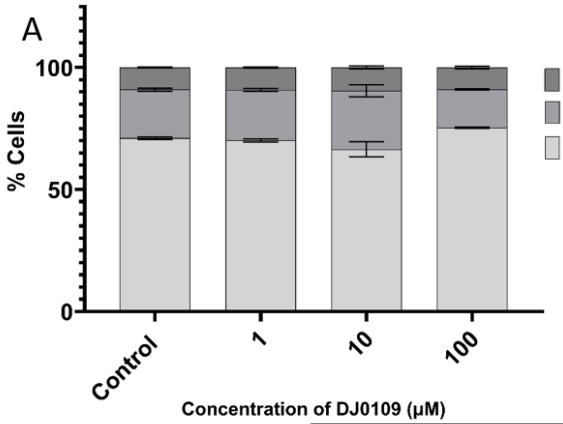

B

Control vs.	1	10	100
G0/G1	n.s.	n.s.	n.s.
S	n.s.	n.s.	n.s.
G2/M	n.s.	n.s.	n.s.

C

	DJ0109 (µM)			
	0	**1**	**10**	**100**
G2/G1, mean (SEM)	1.940 (0.000)	1.943 (0.003)	1.950 (0.000)	1.940 (0.000)
% CV, mean (SEM)	2.495 (0.066)	2.470 (0.010)	2.440 (0.151)	2.910 (0.150)
RCS, mean (SEM)	2.192 (0.225)	1.657 (0.178)	1.736 (0.226)	2.234 (0.453)
n	6	3	3	2

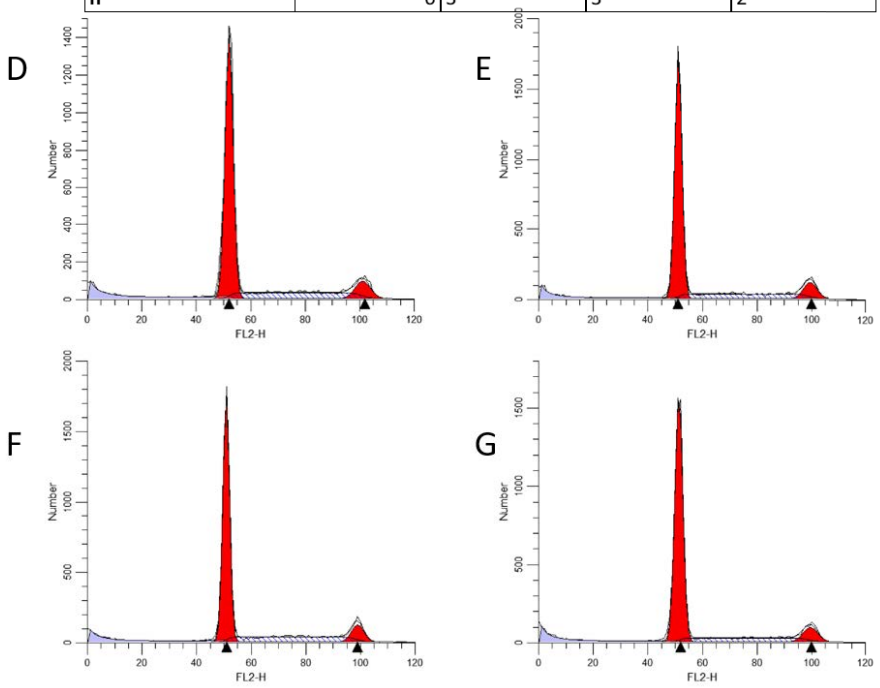

Figure 3-63 Cell cycle analysis for DAUDI cells treated with various concentrations of Thienopyridine DJ0109 for 48 hours as determined by propidium Iodide flow cytometry. Cell cycle flow cytometry RCS files were analysed using a fixed manual model in ModFit LT 5.0 and data were analysed using the one-way ANOVA with Dunnett's post hoc test.

***(A)** Comparison of cell cycle phases (G0/G1, S and G2/M phase) of DAUDI cells treated with complete media (Control) versus 1-100 µM of DJ0109. **(B)** Results from One-way ANOVA with Dunnett's post hoc test comparing cell cycle phases of the DJ0109 treated cells vs complete media (Control). **(C)** Descriptive statistics for cell cycle analysis, showing mean ratio of G2/M channel over G0/G1 channel (G2/G1), mean % coefficient of variance (% CV), mean reduced chi squared (RCS) and number of replicates for each data set (n). **(D-G)** Representative histogram for Cell Cycle analysis for Control (complete media) (D); DJ0109 1 (E); DJ0109 10 µM (F); and DJ0109 100 µM (G).*

A

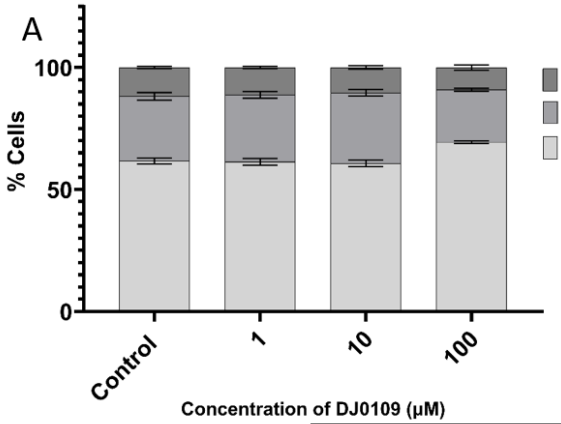

B

Control vs.	1	10	100
G0/G1	n.s.	n.s.	P<0.01
S	n.s.	n.s.	n.s.
G2/M	n.s.	n.s.	P<0.05

C

	DJ0109 (µM)			
	0	**1**	**10**	**100**
G2/G1, mean (SEM)	1.943 (0.003)	1.943 (0.003)	1.957 (0.003)	1.957 (0.003)
% CV, mean (SEM)	4.982(0.128)	4.647 (0.274)	4.590 (0.065)	4.607 (0.086)
RCS, mean (SEM)	1.649 (0.089)	1.640 (0.097)	1.895 (0.279)	1.709 (0.021)
n	6	3	3	3

D E F G

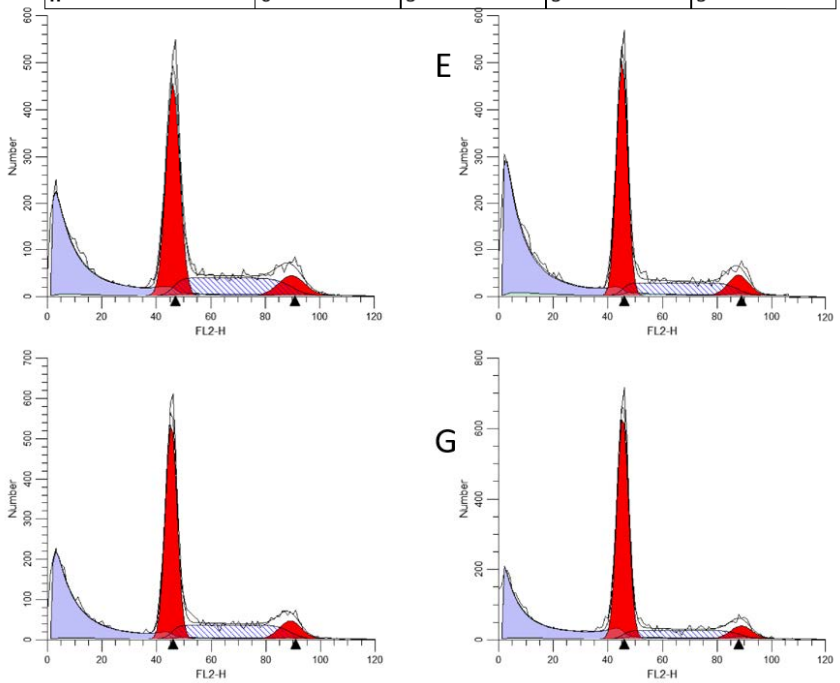

Figure 3-64 Cell cycle analysis for DAUDI cells treated with various concentrations of Thienopyridine DJ0109 for 72 hours as determined by propidium Iodide flow cytometry. Cell cycle flow cytometry RCS files were analysed using a fixed manual model in ModFit LT 5.0 and data were analysed using the one-way ANOVA with Dunnett's post hoc test.

***(A)** Comparison of cell cycle phases (G0/G1, S and G2/M phase) of DAUDI cells treated with complete media (Control) versus 1-100 µM of DJ0109. **(B)** Results from One-way ANOVA with Dunnett's post hoc test comparing cell cycle phases of the DJ0109 treated cells vs complete media (Control). **(C)** Descriptive statistics for cell cycle analysis, showing mean ratio of G2/M channel over G0/G1 channel (G2/G1), mean % coefficient of variance (% CV), mean reduced chi squared (RCS) and number of replicates for each data set (n). **(D-G)** Representative histogram for Cell Cycle analysis for Control (complete media) (D); DJ0109 1 µM (E); DJ0109 10 µM (F); and DJ0109 100 µM (G).*

3.4.2.3.3 DJ0171 effects on DAUDI cell cycle

Figure 3-65 to Figure 3-67 show the results for DAUDI cells cultured in the presence of novel thienopyridine DJ0171 for 24 hours, 48 hours, and 72 hours respectively.

At all three timepoints tested, DJ0171 showed a statistically significant (all $P < 0.001$) increase in G_2/M phase cells at 10 µM and 100 µM concentrations when compared to untreated controls. Following 24 hours of incubation, 18.52 % cells at 10 µM and 25.75 % cells at 100 µM were in G_2/M phase compared to 3.31 % in untreated controls (Figure 3-65). At 48 hours, this increased to 38.92 % for 10 µM and 27.32 % for 100 µM versus 14.33 % in untreated controls (Figure 3-66), with similar effects also seen post 72 hours of treatment (10 µM 26.72 % / 100 µM 50.23 % compared to 11.71 % untreated G_2/M phase DAUDI cells) (Figure 3-67).

A

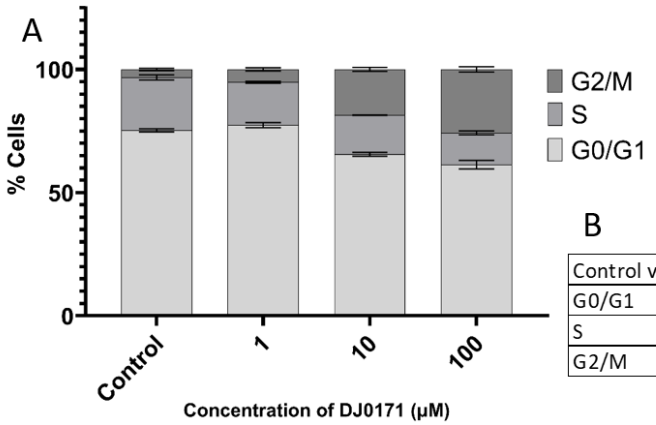

B

Control vs.	1	10	100
G0/G1	n.s.	P<0.001	P<0.001
S	P<0.01	P<0.01	P<0.001
G2/M	n.s.	P<0.001	P<0.001

C

	DJ0171 (µM)			
	0	**1**	**10**	**100**
G2/G1, mean (SEM)	1.950 (0.006)	1.943 (0.003)	1.927 (0.003)	1.923 (0.003)
% CV, mean (SEM)	3.173 (0.057)	2.930 (0.070)	2.873 (0.038)	3.097 (0.061)
RCS, mean (SEM)	3.076 (0.323)	2.834 (0.068)	2.288 (0.372)	2.467 (0.251)
n	3	3	3	3

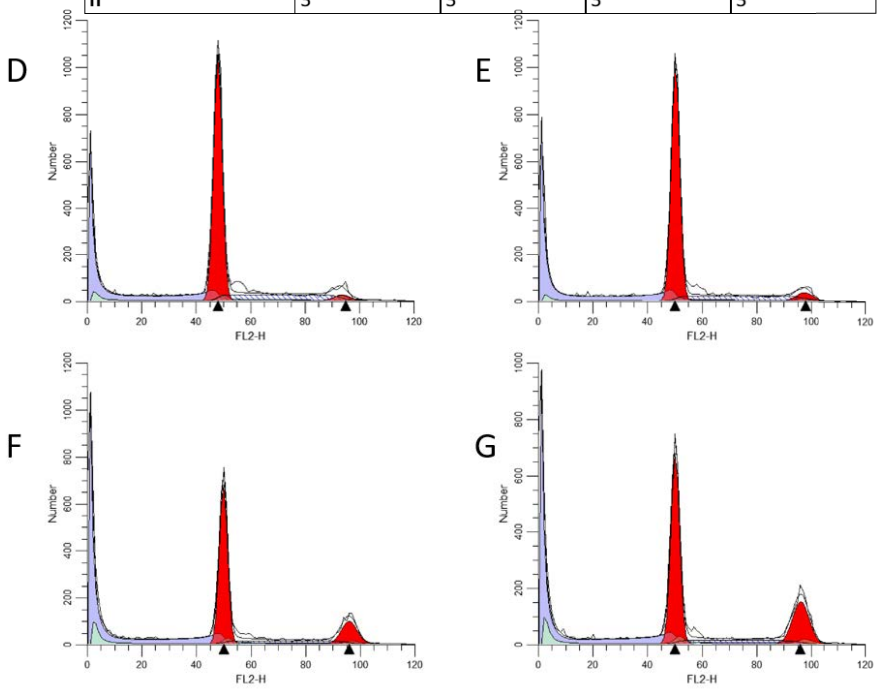

Figure 3-65 Cell cycle analysis for DAUDI cells treated with various concentrations of Thienopyridine DJ0171 for 24 hours as determined by propidium Iodide flow cytometry. Cell cycle flow cytometry RCS files were analysed using a fixed manual model in ModFit LT 5.0 and data were analysed using the one-way ANOVA with Dunnett's post hoc test.

***(A)** Comparison of cell cycle phases (G0/G1, S and G2/M phase) of DAUDI cells treated with complete media (Control) versus 1-100 µM of DJ0171. **(B)** Results from One-way ANOVA with Dunnett's post hoc test comparing cell cycle phases of the DJ0171 treated cells vs complete media (Control). **(C)** Descriptive statistics for cell cycle analysis, showing mean ratio of G2/M channel over G0/G1 channel (G2/G1), mean % coefficient of variance (% CV), mean reduced chi squared (RCS) and number of replicates for each data set (n). **(D-G)** Representative histogram for Cell Cycle analysis for Control (complete media) (D); DJ0171 1 µM (E); DJ0171 10 µM (F); and DJ0171 100 µM (G).*

A

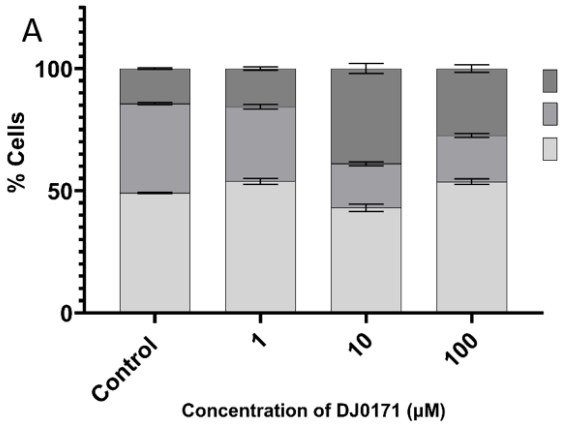

B

Control vs.	1	10	100
G0/G1	P<0.01	P<0.01	P<0.01
S	P<0.001	P<0.001	P<0.001
G2/M	n.s.	P<0.001	P<0.001

C

	DJ0171 (µM)			
	0	**1**	**10**	**100**
G2/G1, mean (SEM)	1.900 (0.006)	1.933 (0.003)	1.903 (0.007)	1.887 (0.007)
% CV, mean (SEM)	6.380 (0.340)	3.227 (0.159)	3.927 (0.068)	6.443 (1.572)
RCS, mean (SEM)	2.703 (0.426)	1.603 (0.097)	1.416 (0.383)	2.527 (0.338)
n	6	3	3	3

D E F G

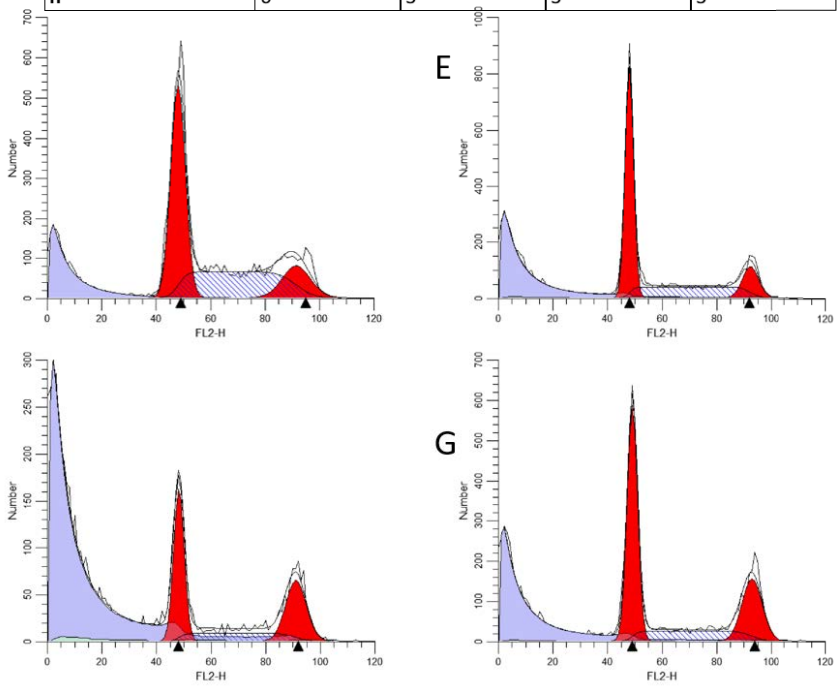

Figure 3-66 Cell cycle analysis for DAUDI cells treated with various concentrations of Thienopyridine DJ0171 for 48 hours as determined by propidium Iodide flow cytometry. Cell cycle flow cytometry RCS files were analysed using a fixed manual model in ModFit LT 5.0 and data were analysed using the one-way ANOVA with Dunnett's post hoc test.

***(A)** Comparison of cell cycle phases (G0/G1, S and G2/M phase) of DAUDI cells treated with complete media (Control) versus 1-100 µM of DJ0171. **(B)** Results from One-way ANOVA with Dunnett's post hoc test comparing cell cycle phases of the DJ0171 treated cells vs complete media (Control). **(C)** Descriptive statistics for cell cycle analysis, showing mean ratio of G2/M channel over G0/G1 channel (G2/G1), mean % coefficient of variance (% CV), mean reduced chi squared (RCS) and number of replicates for each data set (n). **(D-G)** Representative histogram for Cell Cycle analysis for Control (complete media) (D); DJ0171 1 µM (E); DJ0171 10 µM (F); and DJ0171 100 µM (G).*

A

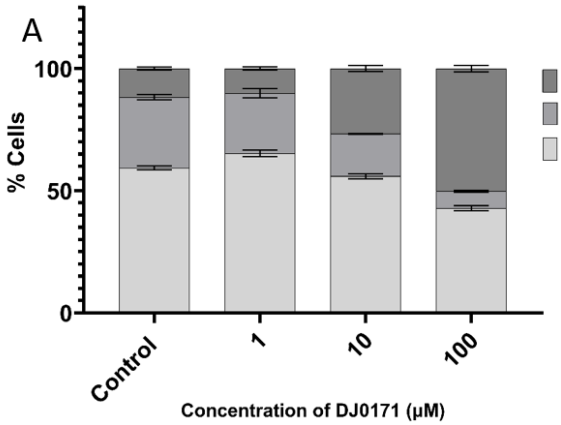

B

Control vs.	1	10	100
G0/G1	P<0.01	n.s.	P<0.001
S	n.s.	P<0.001	P<0.001
G2/M	n.s.	P<0.001	P<0.001

C

	DJ0171 (µM)			
	0	**1**	**10**	**100**
G2/G1, mean (SEM)	1.928 (0.003)	1.937 (0.003)	1.930 (0.000)	1.913 (0.003)
% CV, mean (SEM)	4.885 (0.126)	4.893 (0.190)	4.577 (0.074)	4.470 (0.091)
RCS, mean (SEM)	1.325 (0.094)	1.687 (0.033)	1.679 (0.161)	2.006 (0.273)
n	6	3	3	3

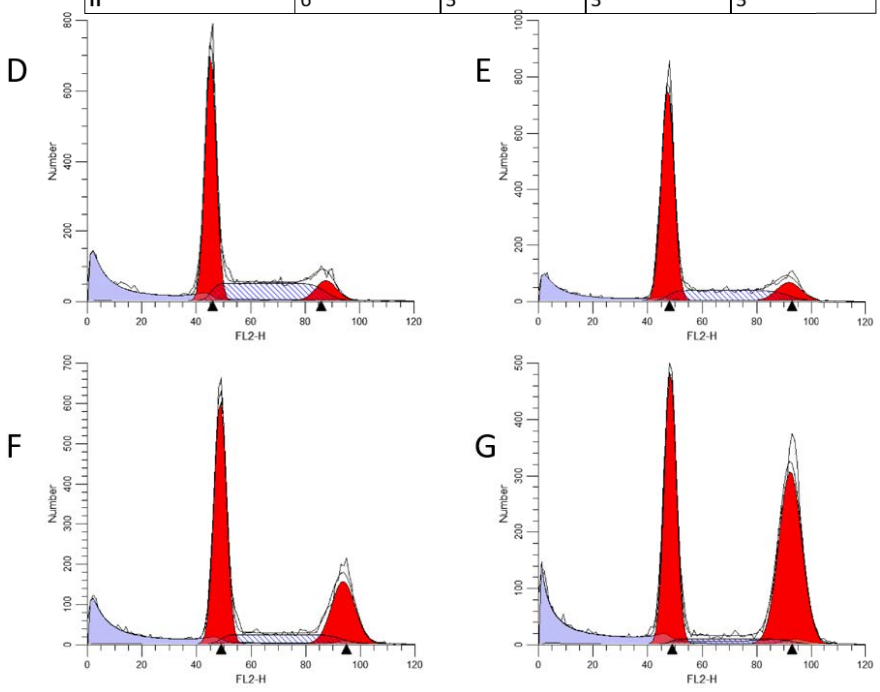

Figure 3-67 Cell cycle analysis for DAUDI cells treated with various concentrations of Thienopyridine DJ0171 for 72 hours as determined by propidium Iodide flow cytometry. Cell cycle flow cytometry RCS files were analysed using a fixed manual model in ModFit LT 5.0 and data were analysed using the one-way ANOVA with Dunnett's post hoc test.

***(A)** Comparison of cell cycle phases (G0/G1, S and G2/M phase) of DAUDI cells treated with complete media (control) versus 1-100 µM of DJ0171. **(B)** Results from One-way ANOVA with Dunnett's post hoc test comparing cell cycle phases of the DJ0171 treated cells vs complete media (Control). **(C)** Descriptive statistics for cell cycle analysis, showing mean ratio of G2/M channel over G0/G1 channel (G2/G1), mean % coefficient of variance (% CV), mean reduced chi squared (RCS) and number of replicates for each data set (n). **(D-G)** Representative histogram for Cell Cycle analysis for Control (complete media) (D); DJ0171 1 µM (E); DJ0171 10 µM (F); and DJ0171 100 µM (G).*

3.4.3 Summary of the effects of thienopyridines with a cyclooctane moiety on cell viability and cell cycle

Table 3-2 summarises the results for the cell viability (MTS), cell death (Annexin V-Propidium Iodide flow cytometry and cell cycle (G_2/M cell population identified via single stain propidium iodide flow cytometry) for novel thienopyridines DJ0014, DJ0021, DJ0199, DJ0206 and DJ0209.

Table 3-2 Summary of cyclooctane-ring containing Thienopyridines on cell viability, cell death and cell cycle.

**For cell viability results that showed an increase above 100 % viability, this is reflective of increased mitochondrial metabolism, presumably a cell stress or autophagy response.*

Compound Name	Time Point (Hours)	MTS (Cell Viability)	AVPI (Cell Death)	Cell Cycle (G_2/M population)
DJ0014	**24**	Significant increase (0.001 - 100 µM)	Small significant increase in early/late apoptosis (10 - 100 µM)	Small significant G_2/M increase (1 – 100 µM)
	48	Significant decrease (10 - 100 µM)	Large significant increase in early/late apoptosis (10 - 100 µM)	Large significant G_2/M increase (10 – 100 µM)
	72	Significant decrease (10 - 100 µM)	Large significant increase in early/late apoptosis (10 - 100 µM)	Large significant G_2/M increase (10 – 100 µM)
DJ0021	**24**	Non-significant increase	No effects	No effects
	48	Non-significant increase	Small significant increase late apoptosis (10 µM)	No effects
	72	Non-significant increase	Significant increase late apoptosis (10 - 100 µM)	No effects apart from significant decrease in G_2/M (100 µM)
DJ0199	**24**	Non-significant decrease (10 - 100 µM)	Small significant increase late apoptosis (10 - 100 µM)	No effects
	48	Significant decrease (1 - 100 µM)	Large significant increase in early/late apoptosis (10 - 100 µM)	Large significant G_2/M increase (1 – 100 µM)
	72	Significant decrease (1 - 100 µM)	Large significant increase in early/late apoptosis (1 - 100 µM)	Large significant G_2/M increase (1 – 100 µM)
DJ0206	**24**	No effects	Significant increase late apoptosis and necrosis (100 µM)	Large significant G_2/M increase (1 – 100 µM)
	48	Significant increase (0.1 µM)	Large significant increase in early/late apoptosis (0.1 - 100 µM)	Large significant G_2/M increase (1 – 100 µM)
	72	Significant increase (0.001 – 0.01 µM). Significant decrease (1 -100 µM)	Large significant increase in early/late apoptosis (1 - 100 µM)	Large significant G_2/M increase (1 – 100 µM)
DJ0209	**24**	No effects	No effects	Small significant G_2/M increase (100 µM)
	48	Significant decrease (10 - 100 µM)	Significant increase in early/late apoptosis (1 - 100 µM)	Small significant G_2/M decrease (1 µM) Significant G_2/M increase (10 - 100 µM)
	72	No effects	Significant increase in early/late apoptosis (1 - 100 µM)	Small significant G_2/M decrease (1 - 100 µM)

3.4.4 Summary of the effects of thienopyridines with a cycloheptane moiety on cell viability and cell cycle

Table 3-3 summarises the results for the cell viability (MTS), cell death (Annexin V-Propidium Iodide flow cytometry and cell cycle (G_2/M cell population identified via single stain propidium iodide flow cytometry) for novel thienopyridines DJ0041 and DJ0081.

Table 3-3 Summary of cycloheptane-ring containing Thienopyridines on cell viability, cell death and cell cycle.

**For cell viability results that showed an increase above 100 % viability, this is reflective of increased mitochondrial, presumably a cell stress or autophagy response.*

Compound Name	Time Point (Hours)	MTS (Cell Viability)	AVPI (Cell Death)	Cell Cycle (G_2/M population)
DJ0041	24	Small significant decrease (10 µM)	Small significant increase in early/late apoptosis (10 - 100 µM)	Small significant G_2/M increase (1 - 100 µM)
	48	Significant increase (0.001 – 1 µM) Significant decrease (10 µM)	Significant increase in early/late apoptosis (10 - 100 µM)	Large significant G_2/M increase (1 - 100 µM)
	72	Significant increase (0.01 – 1 µM) Significant decrease (10 µM)	Significant increase in early/late apoptosis (10 - 100 µM)	Large significant G_2/M increase (1 - 100 µM)
DJ0081	24	Non-significant increase (all concentrations)	Small significant increase in late apoptosis (0.1 – 10 µM), early/late apoptosis (100 µM)	No effects
	48	Significant decrease (1 - 100 µM)	Significant increase in early/late apoptosis (10 - 100 µM)	Large significant G_2/M increase (1 - 100 µM)
	72	Significant decrease (1 - 100 µM)	Significant increase in early/late apoptosis (1 - 100 µM)	Large significant G_2/M increase (1 - 100 µM)

3.4.5 Summary of the effects of thienopyridines with a cyclohexanone moiety on cell viability and cell cycle

Table 3-4 summarises the results for the cell viability (MTS), cell death (Annexin V-Propidium Iodide flow cytometry and cell cycle (G_2/M cell population identified via single stain propidium iodide flow cytometry) for novel thienopyridines DJ0097, DJ0109 and DJ0171.

Table 3-4 Summary of cyclohexanone-ring containing Thienopyridines on cell viability, cell death and cell cycle.

**For cell viability results that showed an increase above 100 % viability, this is reflective of increased mitochondrial, presumably a cell stress or autophagy response.*

Compound Name	Time Point (Hours)	MTS (Cell Viability)	AVPI (Cell Death)	Cell Cycle (G_2/M population)
DJ0097	**24**	Slight non-significant decrease (1 – 100 µM)	Small significant increase early/late apoptosis (0.1 - 100 µM)	Moderate significant G_2/M increase (1 – 100 µM)
	48	Significant increase (0.1 µM)	Small significant increase early/late apoptosis (0.1 - 100 µM)	Large significant G_2/M increase (1 – 100 µM)
	72	Slight non-significant decrease (1 – 10 µM)	Large significant increase early/late apoptosis (1 - 100 µM)	Large significant G_2/M increase (1 – 100 µM)
DJ0109	**24**	Small significant decrease (100 µM)	No effects	No effects
	48	Non-significant decrease (100 µM)	Small significant increase early apoptosis (0.1 – 1 µM), increase early/late apoptosis (100 µM)	No effects
	72	Non-significant decrease (0.1 - 100 µM)	Significant increase early/late apoptosis (10 - 100 µM)	Small significant G_2/M decrease (100 µM)
DJ0171	**24**	Significant increase (0.01 - 0.1 µM), non-significant decrease (10 µM)	Small significant increase early apoptosis (all concentrations)	Moderate significant G_2/M increase (10 – 100 µM)
	48	Significant increase (all concentrations	Small Significant increase early/late apoptosis (1 – 100 µM)	Large significant G_2/M increase (10 – 100 µM)
	72	Non-significant reduction (10 µM)	Moderate significant increase early/late apoptosis (10 – 100 µM)	Large significant G_2/M increase (10 – 100 µM)

3.5 Discussion

Across MTS and AVPI assays, there was a general trend of reduced cell viability at 10 µM and 100 µM at 48 hour and 72 hour time points, in similar effects demonstrated in this compound family by NCI 60 cell panel testing (Shoemaker, 2006; Feng et al., 2012) and in further testing in breast cancer cell lines (Leung et al., 2014).

The most potent inducers of apoptosis from each thienopyridine compound grouping were DJ0206 from the cyclooctane-ring family (see section 3.4.1.1), DJ0041 from the cycloheptane thienopyridines (3.4.1.2), and DJ0097 from the cyclohexanone-ring compounds (see section 3.4.1.3). The pattern of effects for these three compounds also confirms data on the size of the cyclic carbon ring moiety modifying the cytotoxicity of the novel thienopyridine (Leung et al., 2016), with DJ0206 showing activity at 48 hours and lower concentrations, with DJ0041 the next most effective followed by DJ0097 in this DAUDI cell model. Based on the DJ0097 AVPI and MTS results taken in isolation, this compound seemed to have limited effects, however at cell cycle, it demonstrated a clear shift to tetraploidy and presumed G_2/M arrest (see 3.4.2.3). which is supportive of using multiple strategies to investigate novel compounds (Ediriweera et al., 2019).

Treatments at 10 µM and 100 µM at 48 hours seem most effective at causing apoptotic cell death and a shift to G_2/M phase of cell cycle, however effects at 72 hours could be masked by the increase in cell death at that timepoint, with apoptosis an established pathway for cell fate in unresolved cell stress (Fesik, 2005).

DJ00206, DJ0041 and DJ0097 all showed the most pronounced effects on the cell cycle out of the thienopyridines tested, but there is no apparent pattern related to the aryl-ring substitutions in these compounds (see Table 2-8), other than the *meta*-substitution chlorine/bromine-groups present on DJ0206 and DJ0097 (Arabshahi et al., 2014; Hung et al., 2014). DJ0041 has no aryl-substitutions, so this does not seem a hindrance to the effect of this compound *in vitro*.

These assays also highlight some of the limitations in the use of MTS as a basic cell function assay, with almost all compounds displaying percentage survival values in excess of 100 % at lower concentrations of thienopyridines. This is a presumed cell stress, or autophagy response (Mizushima et al., 2008; Jeon et al., 2012; D'Arcy, 2019) but the inclusion of lower concentrations in these assays may have masked statistical significance at the higher concentrations. G_2/M arrest induced by paclitaxel has also been shown to increase ROS production (Hao et al., 2022), so important to elucidate the mechanism for G_2/M arrest, whether this is microtubule destabilisation or DNA damage response related.

3.6 Conclusions

- Novel thienopyridines demonstrate cytotoxicity and cell cycle arrest in a DAUDI B cell model of leukaemia.
- The most potent thienopyridines from each chemical grouping were DJ0206, DJ0041 and DJ0097 respectively.
- MTS assay is limited in its findings, however both AVPI and Cell Cycle flow cytometry can be used successfully to investigate the activity of novel compounds.

4. Novel Thienopyridines Induce Tubulin Destabilisation And Mitotic Dysfunction

4 CHAPTER 4: NOVEL THIENOPYRIDINES INDUCE TUBULIN DESTABILISATION AND MITOTIC DYSFUNCTION

4.1 Introduction

In the field of novel compound identification and testing, discovery of compounds which show anti-tubulin or G_2/M arrest is a frequent finding (Miao et al., 2018; Wang et al., 2020; Wang et al., 2021), and there are likely thousands of synthesised of compounds in existence with these properties (Ebenezer et al., 2022), however few journal articles go beyond the establishment of these effects without identifying potential underlying mechanisms for how the compounds effect cells and model organisms *in vitro* and *in vivo* (Romagnoli et al., 2013).

4.1.1 Tubulin in normal physiological conditions

Tubulin is a key cytoskeletal protein, with intracellular microtubules formed from repeated heterodimers of α- and β-tubulin monomer subunits (Naaz et al., 2019). Microtubule formation is characterised by dynamic instability (Pasquier and Kavallaris, 2008), with polymerisation and depolymerisation occurring in a GTP dependent manner (Dumontet and Jordan, 2010). Microtubules play a role in the maintenance of cell structure, vesicle trafficking and cell migration (H. Guo et al., 2019), but they are of particular significance during cellular mitosis (Jordan et al., 1992). Spindle assembly is coordinated by microtubule organising centres (MTOCs), pairs of centrosomes from which the spindle polymerises via interaction with the microtubule associated protein γ-tubulin (Petry, 2016; Kapoor, 2017; Sanchez and Feldman, 2017). Correct orientation and chromosome attachment to the mitotic spindle is a key regulatory step in cell cycle progression, as is correct polarity of the spindle (Fukuyama et al., 2022) with failure of the spindle leading to mitotic arrest or to potential mitotic slippage, whereby cells proceed with mitosis despite cell cycle checkpoint activation (London and Biggins, 2014; Hayward et al., 2019; Lara-Gonzalez et al., 2019).

4.1.2 Tubulin binding domains

The α- and β-tubulin monomers both feature a number of domains which existing anti-tubulin treatments have been shown to bind to and inhibit polymerisation (Steinmetz and Prota, 2018). Binding domains on α- and β-tubulin which targets tubulin stabilisation include:

- Taxol binding site (Weaver, 2014)

While tubulin destabilisation occurs with drugs binding to the following targets:

- Vinca-binding site (Gigant et al., 2005)
- Colchicine-binding site (Ravelli et al., 2004)
- Maytansine-binding site (Lopus et al., 2010)

4.1.3 Existing anti-tubulin drugs and their effects at mitosis

There are a number of established compounds in both clinical (Jordan, 2002; Jordan and Wilson, 2004; Dumontet and Jordan, 2010; Kavallaris, 2010) and laboratory use with known anti-tubulin activity.

4.1.3.1 Paclitaxel

Paclitaxel has been demonstrated to stabilise microtubule polymerisation *in vitro* via binding to the taxol binding site on β-tubulin (Weaver, 2014; Steinmetz and Prota, 2018) leading to the arrest of mitosis at prometaphase via the activation of the spindle assembly checkpoint (Silva et al., 2017). This is observable microscopically as a pattern of astral microtubule fibre projections at the mitotic spindle with loss of cell polarity and leads to reduced cell proliferation at higher concentrations of paclitaxel (Jordan et al., 1993).

4.1.3.2 Nocodazole

Nocodazole is a potent tubulin destabiliser which binds to the colchicine-binding site on β-tubulin (Jordan et al., 1998; Steinmetz and Prota, 2018), reduces the dynamic polymerisation of microtubules (Vasquez et al., 1997) and induces star-shaped pattern of tubulin bundles at mitosis (Jordan et al., 1992). Indeed, it can be utilised in *in vitro* experiments to synchronise the cell cycle (Zieve et al., 1980; Matsui et al.,

2012) with a speedy recovery with the removal of the microtubule block (Kuo et al., 2021).

4.1.3.3 Colchicine

Colchicine is in clinical use as a remedy for gout and is one of the most established tubulin binding agents (Jordan et al., 1998; Ravelli et al., 2004). Nocodazole completes with colchicine for binding to microtubules, indicating both bind via the colchicine site.

4.1.3.4 Novel thienopyridines and anti-tubulin effects

Several of the thienopyridines synthesised by the New Zealand group[3][4] have demonstrated G_2/M arrest and anti-tubulin effects in both breast cancer cell lines (Reynisson et al., 2016) and sea urchin embryo models (Eurtivong et al., 2017), while thienopyridine compounds synthesised by other groups have also demonstrated effects via the colchicine binding site (Romagnoli et al., 2013), so there is potential for similar effects to be demonstrated in B lymphocytes in this study.

[4] The New Zealand Group refers to all works produced by Professor David Barker's lab in the School of Chemical Sciences, University Of Auckland, New Zealand

4.2 Aims and objectives

4.2.1 Aims

The aim of this chapter was to investigate whether the arrest demonstrated by the ten novel thienopyridine compounds in Chapter 3 was at G_2/M, or at prometaphase by SAC activation as a result of spindle microtubule perturbation.

4.2.2 Objectives

- to observe if novel thienopyridine compounds show direct effects on isolated tubulin via tubulin polymerisation assay.

4.3 Methods

4.3.1 Tubulin Polymerisation

All methods were performed as per section 2.2.11 of main methods chapter.

4.4 Results

4.4.1 Effects of novel thienopyridines on α-tubulin at mitosis and polymerisation in vitro

4.4.1.1 The arrangement of α-tubulin at mitosis and polymerisation in vitro of untreated DAUDI cells

Unperturbed tubulin polymerisation is shown as the G-PEM control in Figure 4-1A, Figure 4-2A and Figure 4-3A. Percentage fold change of the average rate of polymerisation reaction (absorbance/second) for all the novel thienopyridine, nocodazole and paclitaxel treatments, expressed as a ratio of G-PEM activity, is shown in (Figure 4-1, 10 and 14B), with the known tubulin destabiliser nocodazole exhibiting a -43.5 % reduction in rate of reaction, while know tubulin stabiliser paclitaxel showed +84.4 % increase rate of polymerisation.

4.4.1.2 Effects of novel thienopyridines with a cyclooctane moiety on α-Tubulin and tubulin polymerisation in vitro

Direct treatment of tubulin with DJ0014 showed a 28.8 % decreased average rate of polymerisation when compared to G-PEM controls Figure 4-1, which while was approaching the 43.5 % reduction shown by the tubulin destabiliser nocodazole. DJ0014 compound features a cyclooctane ring, thought to promote more potent cytotoxicity rather than cytostatic effects on the cell (Arabshahi et al., 2015).

DJ0021 showed negligible direct effects on tubulin polymerisation, with a fold reduction of -0.3 % compared to G-PEM controls, furthering the evidence of the inhibitory effect of the methoxy-side chain (see Figure 4-1A-B).

Similarly, to DJ0014, DJ0199 also showed reduced average rate of tubulin polymerisation (see Figure 4-1A-B), with a fold reduction of -21.9 % compared to the G-PEM control, again displaying a trend towards reduced polymerisation like DJ0014 and nocodazole control.

DJ0206 induced significant G_2/M arrest at 1 µM concentration during cell cycle analysis via flow cytometry (Chapter 3), while other thienopyridines featuring a cyclooctane ring induced effects from 10 µM concentration. This could be due to the

presence of both ortho (methyl) and meta (Bromine) substitutions on the benzene ring of the compound, both of which have been shown to be advantageous for growth inhibition (Arabshahi et al., 2014). DJ0206 demonstrated the biggest decrease in the average rate of tubulin polymerisation of any of the thienopyridines tested, with a reduction of 42.9 % comparable to the 43.5 % fold decreased shown by nocodazole inhibition of tubulin (see Figure 4-1A-B).

DJ0209 also only showed a slightly increased average rate of tubulin polymerisation compared to G-PEM control, showing +7.7 % fold increase (see Figure 4-1A-B), which shows similar effects to the *para*-substituted DJ0021 compound than *ortho*-substituted DJ0014. DJ0209 would be expected to share the same cytotoxic properties as the other cyclooctane thienopyridines, as it features a chloride substitution at the *ortho*-position of the benzene ring (Arabshahi et al., 2014; Arabshahi et al., 2015; Leung et al., 2016).

4.4.1.2.1 Cyclooctane Thienopyridines Tubulin Polymerisation

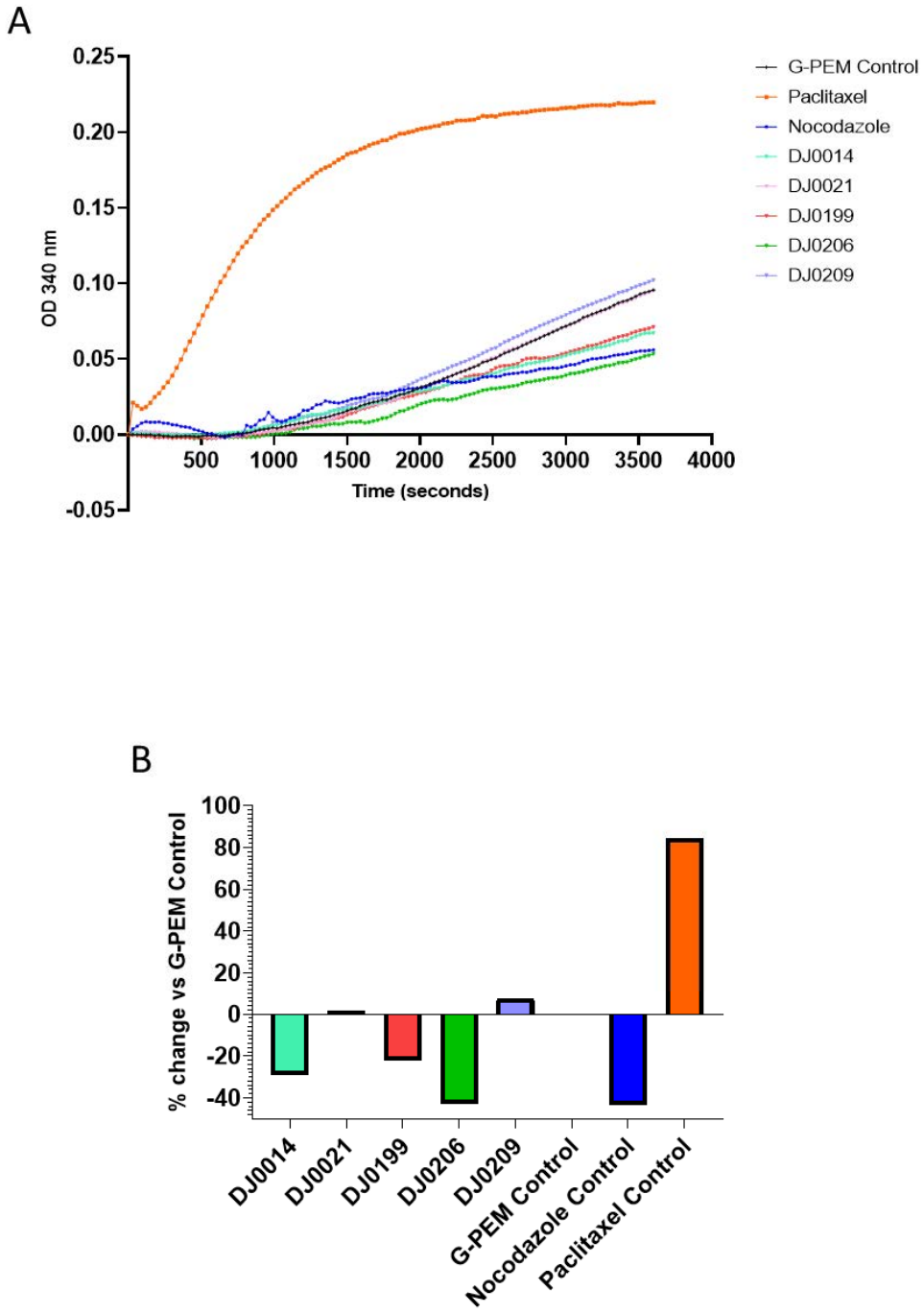

Figure 4-1 Effects of novel cyclooctane-ring thienopyridines on tubulin polymerisation in vitro. Tubulin was exposed to 10 µM thienopyridine compounds, nocodazole, paclitaxel controls with G-PEM buffer acting as an untreated control. Increasing absorbance at 340 nm is used as a marker for tubulin polymerisation (A) Time vs absorbance at 340 nm plot for tubulin polymerisation kinetic assay, with plotted line mean of n=2 replicates. The average rate of tubulin polymerisation was calculated using the SkanIt software from this data. (B) Percentage change relative to the G-PEM untreated control of the average rate of tubulin polymerisation (calculated from data presented in (A)) for each treatment.

4.4.1.3 Effects of novel thienopyridines with a cycloheptane moiety on α-Tubulin and tubulin polymerisation in vitro

Both cycloheptane compounds showed slightly different direct effects on tubulin polymerisation, with DJ0081 showing -11.5 % change, and DJ0041 showing +2.5 % increased polymerisation (see Figure 4-2A-B). Indeed, this may be due to the presence of the methyl- and chloro- groups in the ortho and para positions of benzene ring of compound DJ0081 compared to the unsubstituted benzene ring present in DJ0041 (see Table 2-9).

4.4.1.3.1 Cycloheptane Thienopyridines Tubulin Polymerisation

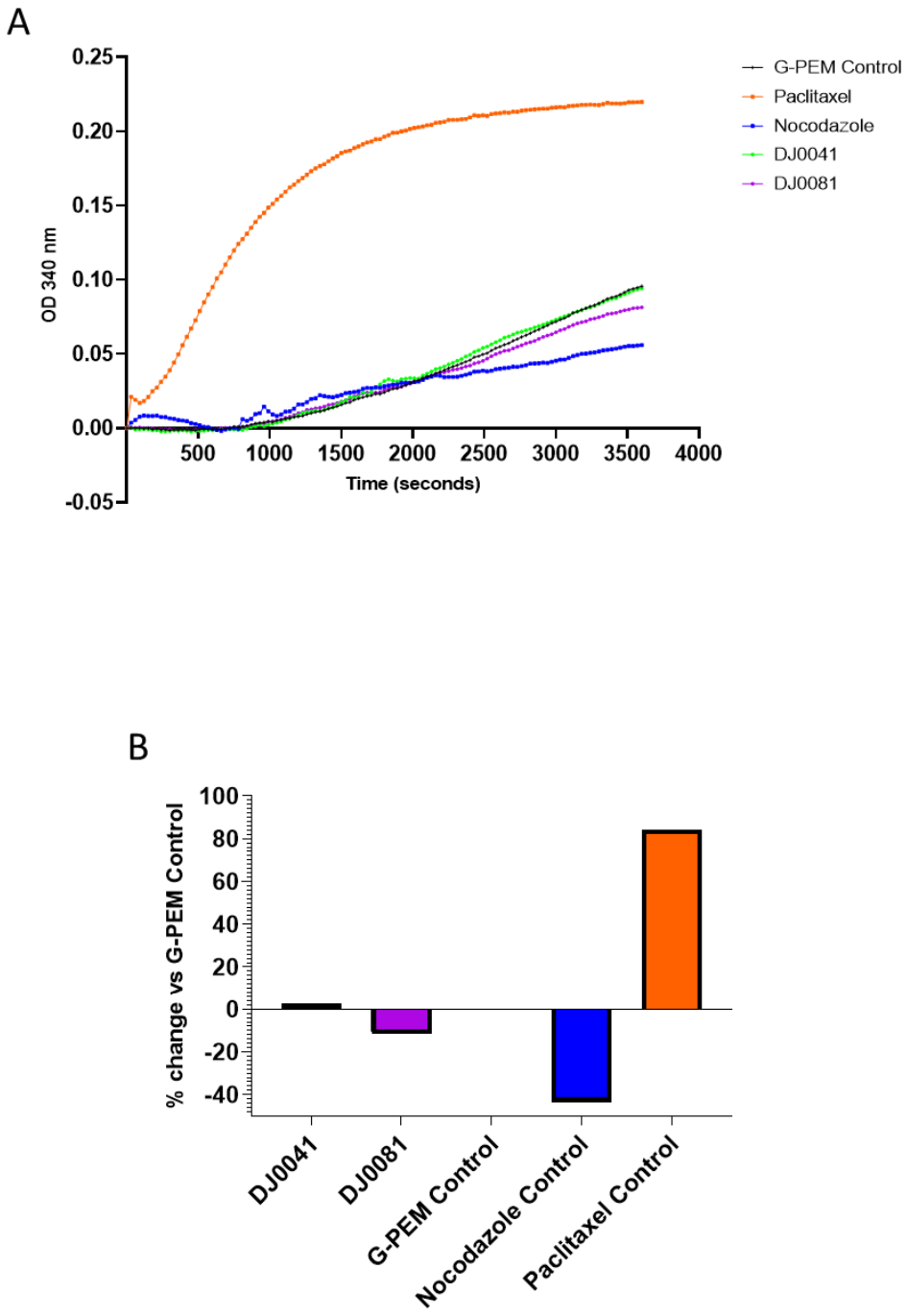

Figure 4-2 Effects of novel cycloheptane-ring thienopyridines on tubulin polymerisation in vitro. Tubulin was exposed to 10 µM thienopyridine compounds, nocodazole, paclitaxel controls with G-PEM buffer acting as an untreated control Increasing absorbance at 340 nm is used as a marker for tubulin polymerisation (A) Time vs absorbance at 340 nm plot for tubulin polymerisation kinetic assay, with plotted line mean of n=2 replicates. The average rate of tubulin polymerisation was calculated using the SkanIt software from this data. (B) Percentage change relative to the G-PEM untreated control of the average rate of tubulin polymerisation (calculated from data presented in (A)) for each treatment.

4.4.1.4 Effects of novel thienopyridines with a cyclohexanone moiety on α-Tubulin and tubulin polymerisation in vitro

The effects of the cyclohexanone-ring thienopyridines on average rate of reaction of tubulin polymerisation was broadly similar across all three compounds, with DJ0109 surprisingly showing the most activity *in vitro* with increased polymerisation followed by DJ0097 and DJ0171 (fold change +35.2 %, +29.5 % and +25.1 % respectively) (Figure 4-3A-B). These were the biggest increases of any thienopyridine compounds tested, albeit not at the magnitude displayed in the paclitaxel control, +84.4 % fold change (see Figure 4-3B), and a somewhat surprising result for DJ0109, which showed no cytotoxicity or G_2/M arrest in Chapter 3.

Compound DJ0171 appears to have a similar effect on the tubulin polymerisation as compound DJ0097 (Figure 4-3A-B), while DJ0097 had more potent effects on the cell cycle (see section 3.4.2.3) and at inducing apoptosis (section 3.4.1.3) shown in Chapter 3, which may be due to the position of the chloride ion in the para position of the benzene ring of DJ0097 compared to its presence in the ortho position of DJ0171 (see Table 2-10).

4.4.1.4.1 Cyclohexanone Thienopyridines Tubulin Polymerisation

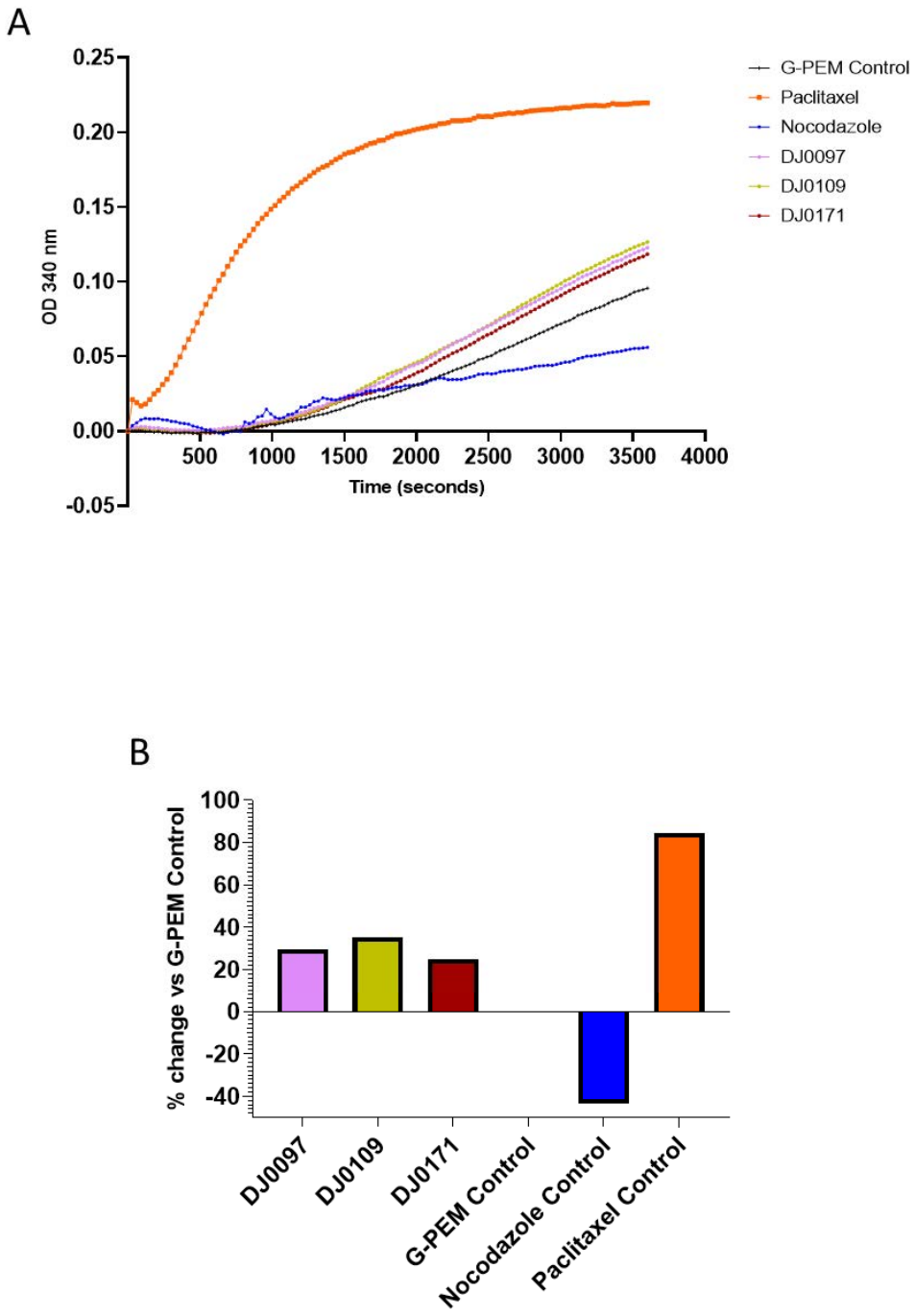

Figure 4-3 Effects of novel cyclohexanone-ring thienopyridines on tubulin polymerisation in vitro. Tubulin was exposed to 10 µM thienopyridine compounds, nocodazole, paclitaxel controls with G-PEM buffer acting as an untreated control. Increasing absorbance at 340 nm is used as a marker for tubulin polymerisation (A) Time vs absorbance at 340 nm plot for tubulin polymerisation kinetic assay, with plotted line mean of n=2 replicates. The average rate of tubulin polymerisation was calculated using the SkanIt software from this data. (B) Percentage change relative to the G-PEM untreated control of the average rate of tubulin polymerisation (calculated from data presented in (A)) for each treatment.

4.4.2 Summary of the effects of thienopyridines with a cyclooctane moiety on tubulin polymerisation

Table 4-1 summarises the results of the cyclooctane moiety containing novel thienopyridines on tubulin polymerisation.

Table 4-1 Summary of results for cyclooctane thienopyridines on tubulin polymerisation

Compound Name	Effect on tubulin polymerisation (vs untreated GPEM control)	
DJ0014	↓	28.8 % decrease
DJ0021	↓	0.3 % decrease
DJ0199	↓	21.9 % decrease
DJ0206	↓	42.9 % decrease
DJ0209	↑	7.7 % increase

4.4.3 Summary of the effects of thienopyridines with a cycloheptane moiety on tubulin polymerisation

Table 4-2 summarises the results of the cycloheptane moiety containing novel thienopyridines on tubulin polymerisation.

Table 4-2 Summary of results for cycloheptane thienopyridines on tubulin polymerisation

Compound Name	Effect on tubulin polymerisation (vs untreated GPEM control)	
DJ0041	↓	11.5 % decrease
DJ0081	↑	2.5 % increase

4.4.4 Summary of the effects of thienopyridines with a cyclohexanone moiety on tubulin polymerisation

Table 4-3 summarises the results of the cyclohexanone moiety containing novel thienopyridines on tubulin polymerisation.

Table 4-3 Summary of results for cyclohexanone thienopyridines on tubulin polymerisation

Compound Name	Effect on tubulin polymerisation (vs untreated GPEM control)	
DJ0097		35.2 % increase
DJ0109		29.5 % increase
DJ0171		25.1 % increase

4.5 Discussion

DJ0021 and DJ0109 both feature the methoxy para-substitution which was predicted to limit their cellular activity, and this was borne out in the data in Chapter 3 as well as both the confocal microscopy and tubulin polymerisation in this chapter (see section 4.4.1.2 and 4.4.1.4), showing that the aryl-side chain modifications limit presumed increased cytotoxicity of the cyclooctane-ring in DJ0021 over the cytostatic cyclohexanone-ring in DJ0109 (Arabshahi et al., 2014; Arabshahi et al., 2015; Leung et al., 2016). DJ0109 showed an increase in the average rate of tubulin polymerisation (Figure 4-3B) but this was not reflected in the Chapter 3 results, with no effects observed on G_2/M arrest.

DJ0209 also showed limited activity against tubulin, and while it shares a very similar chemical structure to compounds DJ0014 (which showed decreased polymerisation and disruption of α-tubulin), it appears that the fluoro-substitution at the *ortho*-position increases cell activity (DJ0014) relative to a chloro-substitution (DJ0209) (Arabshahi et al., 2014; Arabshahi et al., 2015; Leung et al., 2016). DJ0209 did show small effects on G_2/M arrest in Chapter 3 at 10 µM concentration at 48 hours of treatment with DAUDI cells, but this was a comparatively smaller effect that the other active cyclooctane-ring thienopyridines.

DJ0014 reduced tubulin polymerisation to a greater extent a than DJ0199 (Figure 4-1, percentage fold change -28.9 % vs -21.9 % respectively), while DJ0199, with no aryl-ring substitutions in its chemical structure, demonstrated G_2/M arrest at 1 µM concentration at the 48 hour time points (section 3.4.2.1), so the fluoro-substitution may influence any direct effects on α-tubulin while showing comparable cytotoxic and anti-tubulin effects.

Of the cyclooctane ring containing thienopyridines DJ0206, in line with the cytotoxicity and cell cycle results highlighted in Chapter 3, was also the most active compound, inducing an average rate of polymerisation reduction comparable with

nocodazole (see Figure 4-1). DJ0206 features a dual substitution of its aryl-ring with CH_3 group in the *ortho*-position and a bromo-group in the *meta*-position (see Figure 1-8). DJ0081 has a similar chemical structure to DJ0206, albeit with a cycloheptane-ring and a chloro-group in place of the bromine ion in the *meta*-position, but demonstrated lower reduction in the average rate of tubulin polymerisation than DJ0206, -11.5 % vs -42.9 % reductions respectively (See Figure 4-1B and Figure 4-2B). This suggests a Br > Cl > F order of halide substitutions in terms of the magnitude of their cellular effects, and that, as predicted, cyclooctane-ring containing thienopyridines are more cytotoxic than its cycloheptane counterparts (Arabshahi et al., 2014; Arabshahi et al., 2015; Leung et al., 2016)).

Of the cyclohexanone compounds which showed activity in Chapter 3, DJ0097 and DJ0171 both showed an increase in rate of tubulin polymerisation while displaying similar effects on α-tubulin by confocal microscopy (see section 4.4.1.4).

4.5.1 Conclusions

Compounds DJ0014, DJ0041, DJ0081, DJ0199 and DJ0206 appear to be successful destabilisers of microtubule dynamics, while DJ0097 and DJ0171 show stabilising effects (Jordan and Wilson, 2004). Compounds with a thienopyridine structure have previously been identified as causing G_2/M arrest via the colchicine-binding site, which could be a possibility with these compounds (Romagnoli et al., 2013) as was demonstrated in alternate cell models (Reynisson et al., 2016; Eurtivong et al., 2017).

5. Chapter 5 Identification of RT-qPCR stable reference genes

5 CHAPTER 5: IDENTIFICATION OF RT-QPCR STABLE REFERENCE GENES

5.1 Introduction

5.1.1 Stable reference genes in RT-qPCR

Quantitative reverse transcription polymerase chain reaction (RT-qPCR) is a commonly used, robust technique in molecular biology to establish the regulation of genes in response to disease states (Pede et al., 2013), changes in physiological condition (Engelstoft et al., 2013) or in response to treatment with drugs (Patel et al., 2017). The quantitative aspect of RT-qPCR relies on normalisation of genes of interest to stable reference genes, that is genes that are stably expressed and not effected by the experimental conditions being investigated in a research study (De Spiegelaere et al., 2015). There are several well-established methods for RT-qPCR normalisation, including the ΔCt (relative quantification method); $2^{-\Delta\Delta CT}$ (Livak and Schmittgen, 2001); Pfaffl method (incorporating primer efficiencies) (Pfaffl, 2001); Vandesompele Method (normalisation to multiple reference genes) (Vandesompele et al., 2002); as well as numerous iterative modifications to these methods since their publication (Rao et al., 2013; Riedel et al., 2014). The identification of stable reference genes requires that the candidate reference genes have been tested for stability in relation to experimental conditions being investigated and there are multiple robust algorithms to establish reference gene stability including GeNorm (Vandesompele et al., 2002), BestKeeper (Pfaffl et al., 2004) and NormFinder (Andersen et al., 2004). Following the publication of 'The MIQE guidelines: Minimum Information for Publication of Quantitative Real-Time PCR Experiments' by Bustin *et al* (2009), normalisation to a single reference gene is not recommended (with validation against 3 or more reference genes suggested (Derveaux et al., 2010)) and a specified stability algorithm should be used to identify the optimal number of reference genes (Bustin et al., 2009). However, research articles regularly report the use of single 'housekeeper' genes (e.g., GAPDH, β-Actin) without reference to how they were selected for normalisation (X. Liu et al., 2020; Alsubaie et al., 2021) or consideration of how poor selection of reference gene could severely skew results (Ma et al., 2018).

5.1.2 Rationale

DAUDI (ECACC 85011437) cells are an immortalised, mature B lymphocyte cancer cell line derived from a 16-year-old patient with Burkitt's Lymphoma (ECACC General Cell Collection: DAUDI, Catalogue No.: 85011437) and for this study are being used as a model for the mature B cell malignancy of Chronic Lymphocytic Leukaemia. A basic literature search returned a limited number of candidate reference genes, with frequent use of single reference genes or use of 'housekeeper' genes reported (M. Ma et al., 2016; Li et al., 2017; Koike et al., 2020; Pastuszak-Lewandoska et al., 2020), necessitating a wider search for relevant literature.

5.2 Aims and objectives

5.2.1 Aims

The primary aim of this chapter was to screen the available literature to identify a panel of candidate reference genes to use in normalisation of experimental data generated from the treatment of DAUDI cells with ten novel thienopyridine compounds, as well as paclitaxel and nocodazole controls.

5.2.2 Objectives

The objectives were;

- to design primers for each identified candidate reference gene from the literature search.
- to generate data on Ct values in RT-qPCR assays using the designed primers.
- To analyse the generated data, using GeNorm, to identify stable reference genes that could be used to normalise all experimental data from thienopyridine-treated DAUDI cells in subsequent RT-qPCR experiments performed in Chapter 6.

5.3 Methods

All methods described in section 5.3.1 to section 5.3.2.7 were drafted as per the guidance in the 'Preferred reporting items for systematic review and meta-analysis protocols (PRISMA-P) 2015' guidelines (Moher et al., 2015; Shamseer et al., 2015), and acted as the protocol followed while conducting the database searches and systematic review of the literature in this chapter. Planning of the systematic review, search strategies, data collection and analysis was done in accordance with the PRISMA (2020) guidelines (Page et al., 2021b; Page et al., 2021a).

5.3.1 Systematic review of literature

5.3.1.1 Eligibility Criteria

Literature was selected based on the following inclusion/exclusion criteria:

Inclusion criteria:

Study title, abstract or keywords mention:

- PCR, qPCR or RT-qPCR
- DAUDI cells
- B lymphocytes
- Plasma cells
- Reference genes
- Human research subjects or human derived cell lines
- Published post-2000
- Published in English
- Able to access full text article

Exclusion criteria:

Study title, abstract or keywords mention:

- The study used reference genes for non-mRNA targets (e.g., miRNA, rRNA, sRNA, tRNA)
- The study used reference genes for other cell lines

- The study focuses on other haematopoietic cell lines (e.g., monocytes, neutrophils, dendritic cells, basophils, eosinophils, T lymphocytes)
- Non-human cell lines or organisms
- Published pre-2000
- Not published in English
- Full text article not available
- No details of RT-qPCR in full text

5.3.1.2 and Information Sources

MEDLINE (OVID interface, 1946 onwards) and EMBASE (OVID interface, 1980 onwards) databases were searched for two combinations of key words. Additionally, a Google Scholar search for key words was used to identify additional literature that may be held outside of OVID.

5.3.1.3 Literature Search Strategy

5.3.1.4 Search 1 for 'PCR and DAUDI Cells'

	Database(s)	Search Term	
	Saved Results		Viewing (203)
1	Medline	"POLYMERASE CHAIN REACTION"/ OR "REAL-TIME POLYMERASE CHAIN REACTION"/	View Results (305,730)
2	Medline	(pcr*).ti,ab	View Results (547,101)
3	Medline	(qpcr*).ti,ab	View Results (51,000)
4	Medline	("polymerase chain reaction*").ti,ab	View Results (258,021)
5	Medline	*(1 OR 2 OR 3 OR 4)*	View Results (827,153)
6	Medline	(daudi).ti,ab	View Results (2,107)
7	Medline	*(5 AND 6)*	View Results (127)
8	Medline	*7 [Languages English]*	View Results (110)
9	EMBASE	"POLYMERASE CHAIN REACTION"/	View Results (435,556)
10	EMBASE	"REAL TIME REVERSE TRANSCRIPTION POLYMERASE CHAIN REACTION"/	View Results (15,146)
11	EMBASE	"QUANTITATIVE METHYLATION SPECIFIC POLYMERASE CHAIN REACTION"/	View Results (178)
12	EMBASE	"MULTIPLEX REAL TIME POLYMERASE CHAIN REACTION"/	View Results (595)
13	EMBASE	"FLUORESCENCE QUANTITATIVE POLYMERASE CHAIN REACTION"/	View Results (851)
14	EMBASE	"ALLELE SPECIFIC REAL TIME POLYMERASE CHAIN REACTION"/	View Results (127)
15	EMBASE	"REAL TIME POLYMERASE CHAIN REACTION"/	View Results (298,525)
16	EMBASE	(pcr*).ti,ab	View Results (783,691)
17	EMBASE	(qpcr*).ti,ab	View Results (89,875)
18	EMBASE	("polymerase chain reaction*").ti,ab	View Results (291,270)
19	EMBASE	*(9 OR 10 OR 11 OR 12 OR 13 OR 14 OR 15 OR 16 OR 17 OR 18)*	View Results (1,218,778)
20	EMBASE	"DAUDI CELL LINE"/	View Results (264)
21	EMBASE	(daudi).ti,ab	View Results (2,578)
22	EMBASE	*(20 OR 21)*	View Results (2,693)
23	EMBASE	*(19 AND 22)*	View Results (198)
24	EMBASE	*23 [English language]*	View Results (179)

Figure 5-1 OVID database search terms using the Medline and EMBASE databases for PCR and DAUDI

5.3.1.5 Search 2 for 'B-cells and reference genes'

	Database(s)	Search Term	
	Saved Results		Viewing (143)
1	Medline	"B-LYMPHOCYTES"/ OR "B-LYMPHOCYTE SUBSETS"/ OR "PLASMA CELLS"/ OR "PRECURSOR CELLS, B-LYMPHOID"/	View Results (99,059)
2	Medline	("b-cell*" OR "b-lymphocyte*").ti,ab	View Results (183,547)
3	Medline	*(1 OR 2)*	View Results (216,571)
4	Medline	"GENES, ESSENTIAL"/	View Results (2,619)
5	Medline	("housekeeping gene*" OR "house-keeping gene*" OR "housekeeper gene*" OR "house-keeper gene*").ti,ab	View Results (6,028)
6	Medline	("reference gene*").ti,ab	View Results (3,654)
7	Medline	("essential gene*").ti,ab	View Results (5,136)
8	Medline	*(4 OR 5 OR 6 OR 7)*	View Results (12,634)
9	Medline	*(3 AND 8)*	View Results (94)
10	Medline	"POLYMERASE CHAIN REACTION"/ OR "AMPLIFIED FRAGMENT LENGTH POLYMORPHISM ANALYSIS"/ OR "MULTIPLEX POLYMERASE CHAIN REACTION"/ OR "REVERSE TRANSCRIPTASE POLYMERASE CHAIN REACTION"/ OR "REAL-TIME POLYMERASE CHAIN REACTION"/ OR "RANDOM AMPLIFIED POLYMORPHIC DNA TECHNIQUE"/ OR "PRIMED IN SITU LABELING"/	View Results (456,527)
11	Medline	(pcr* OR qpcr*).ti,ab	View Results (582,730)
12	Medline	*(10 OR 11)*	View Results (819,937)
13	Medline	*(9 AND 12)*	View Results (37)
14	Medline	*13 [Languages English] [Humans]*	View Results (24)
15	EMBASE	"B LYMPHOCYTE"/ OR "B LYMPHOCYTE SUBPOPULATION"/ OR "IMMUNOGLOBULIN PRODUCING CELL"/ OR "MEMORY CELL"/ OR "PLASMA CELL"/ OR "SPLENIC B CELL"/ OR "REGULATORY B LYMPHOCYTE"/ OR "PRE B LYMPHOCYTE"/ OR PLASMABLAST/	View Results (195,394)
16	EMBASE	("b-cell*" OR "b-lymphocyte*").ti,ab	View Results (259,721)
17	EMBASE	*(15 OR 16)*	View Results (326,966)
18	EMBASE	"HOUSEKEEPING GENE"/	View Results (8,972)
19	EMBASE	("housekeeping gene*" OR "house-keeping gene*" OR "housekeeper gene*" OR "house-keeper gene*").ti,ab	View Results (8,633)
20	EMBASE	("reference gene*").ti,ab	View Results (5,138)
21	EMBASE	("essential gene*").ti,ab	View Results (5,798)
22	EMBASE	*(18 OR 19 OR 20 OR 21)*	View Results (22,187)
23	EMBASE	*(17 AND 22)*	View Results (367)
24	EMBASE	"POLYMERASE CHAIN REACTION"/ OR "REAL TIME POLYMERASE CHAIN REACTION"/ OR "ALLELE SPECIFIC REAL TIME POLYMERASE CHAIN REACTION"/ OR "FLUORESCENCE QUANTITATIVE POLYMERASE CHAIN REACTION"/ OR "MULTIPLEX REAL TIME POLYMERASE CHAIN REACTION"/ OR "QUANTITATIVE METHYLATION SPECIFIC POLYMERASE CHAIN REACTION"/ OR "REAL TIME REVERSE TRANSCRIPTION POLYMERASE CHAIN REACTION"/	View Results (742,014)
25	EMBASE	(pcr* OR qpcr*).ti,ab	View Results (850,510)
26	EMBASE	*(24 OR 25)*	View Results (1,159,641)
27	EMBASE	*(23 AND 26)*	View Results (189)
28	EMBASE	*27 [English language] [Humans]*	View Results (142)

Figure 5-2 OVID database search terms using the Medline and EMBASE databases for B Lymphocytes and reference genes

5.3.1.6 Search 3 in Google Scholar for additional sources of information

In addition to the two searches conducted in MEDLINE and EMBASE, the Google Scholar advance search function was populated with the following information:

Find articles:

with all of the words: **lymphocyte qPCR**

with at least one of the words: **genorm normfinder bestkeeper**

without the words: **porcine bovine mouse rat equine ovine plant canine chicken**

5.3.2 Study Records

5.3.2.1 Data Management

All records returned in Medline/EMBASE search 1 (Section 5.3.1.4), search 2 (Section 5.3.1.5) and the records additional records identified in search 3 (Section 5.3.1.6) of the literature search were screened against the inclusion/exclusion criteria in Section 5.3.1.1 with full articles sought for all records deemed eligible.

5.3.2.2 Selection Process

Eligible literature search results were collated in Microsoft Excel and duplicate entries were identified in ENDNOTE referencing software (Bramer et al., 2017). Full articles (where available) were then reviewed to confirm that studies met the inclusion/exclusion criteria.

5.3.2.3 Data Collection Process

Full reports for all titles, abstracts and keywords were then screened for mention of named genes used as stable reference genes in data normalisation by any normalisation method. A list of candidate reference genes was then collated in a Microsoft Excel table to enable cross-reference of publications with candidate reference genes.

5.3.2.4 Data Items

The names of all potential candidate genes listed in Section 5.3.2.3 were collated, and had duplicates removed, until a final list of candidate reference genes was produced as a narrative synthesis (See section 5.4.2). This list of candidate reference genes were then taken forward to primer design and evaluation in RT-qPCR Tm plates, via gel electrophoresis to check product size and finally RT-qPCR reactions with DAUDI cDNA samples generated in section 2.2.13.

5.3.2.5 Outcomes and prioritization

The primary outcome of this systematic review was the creation of a list of candidate reference genes for investigation for use as stable reference genes in normalisation and analysis of RT-qPCR data generated to assess the regulation of genes of interest in relation to treatment of DAUDI cells with novel thienopyridine compounds.

5.3.2.6 Risk of Bias

Not assessed as narrative synthesis of primary research data.

5.3.2.7 Data Synthesis

Candidate reference genes were collated in Microsoft Excel, tabulated (see Table 5-1) and described by narrative synthesis in section 5.4.2.

5.3.3 Identification of candidate reference genes

Completion of the systematic review resulted in 499 total records for screening (see Figure 5-3). Screening of abstracts against the inclusion/exclusion criteria (see section 5.3.1.1) and full text searches brought this down to 123 journal articles/abstracts for in depth review. A total of 90 full text documents were included in the review (see Table 5-1), with 33 excluded (see Table 5-2). One candidate reference gene (PABPC4) was identified locally outside of any literature search.

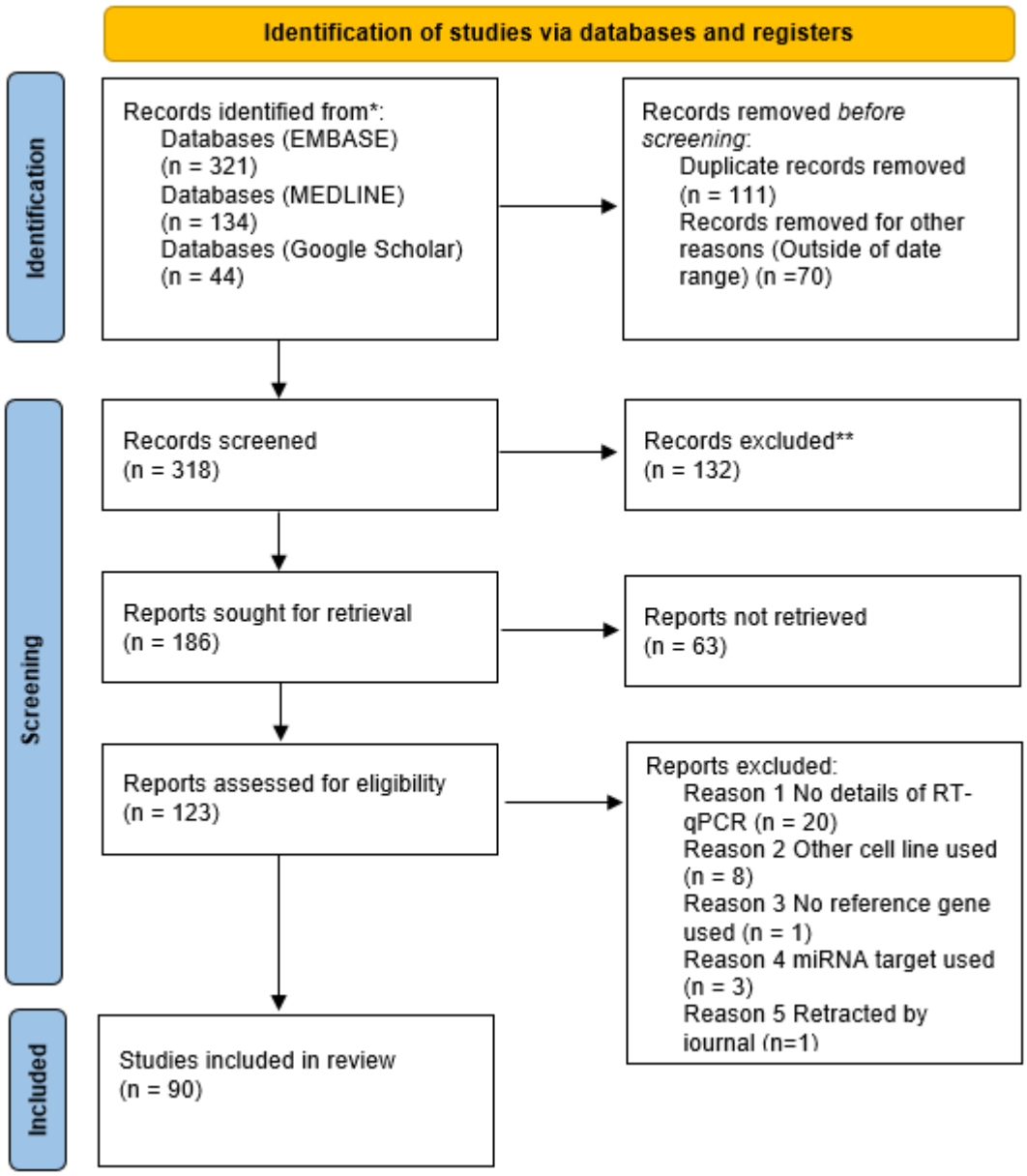

Figure 5-3 PRISMA Flow Diagram listing the stages of systematic review of literature identified by the EMBASE, MEDLINE and Google Scholar database searches.

Table 5-1 Results of systematic review of literature. All candidate references genes listed were included in the GeNorm stability assessment in CFX Maestro following completion of RT-qPCR assays.

Candidate Reference Gene	Full Gene Name	Referenced by	Number of references
ABL1	Homo sapiens ABL proto-oncogene 1, non-receptor tyrosine kinase (ABL1)	(Tajeddine et al., 2006; Green et al., 2009; Diamantopoulos et al., 2011; Sevinc et al., 2011; Pira et al., 2012; Wolach et al., 2012; Papakonstantinou et al., 2013; Pede et al., 2013; Hansen et al., 2020)	9
ACTB	Homo sapiens actin beta (ACTB)	(Naves et al., 2006; Hu et al., 2009; Yan et al., 2010; Kristensen et al., 2011b; 2011a; Huang et al., 2012; Arababadi, 2014; Kristensen et al., 2015; Potashnikova et al., 2015; M. Ma et al., 2016; Jahid et al., 2018; Ge et al., 2019; Jha et al., 2019; Yousefi et al., 2019; Wu et al., 2020; Caballero-Palacios et al., 2021)	16
B2M	Homo sapiens beta-2-microglobulin (B2M)	(Valceckiene et al., 2010; Shlapatska et al., 2014; Appe et al., 2015; Azoulay et al., 2016; Istasi et al., 2017; Zavridou et al., 2018)	7
CD19	Homo sapiens CD19 molecule (CD19)	(Azoulay et al., 2016)	1
EIF2B1	Homo sapiens eukaryotic translation initiation factor 2B subunit alpha (EIF2B1)	(Przybyl et al., 2014)	1
GAPDH	Homo sapiens glyceraldehyde-3-phosphate dehydrogenase (GAPDH)	(Congmin et al., 2006; Krumbholz et al., 2008; Drolet et al., 2010; Han et al., 2010; Ichinohasama et al., 2010; Murphy et al., 2010; Schmeisser et al., 2010; Yan et al., 2010; Yang et al., 2010; De Cassia Carvalho Melo et al., 2011; Ebi et al., 2011; Feng et al., 2011; Nishimura et al., 2011; Adamski et al., 2012; Okumura et al., 2012; Brugnoletti et al., 2013; Pop et al., 2014; Bosl et al., 2015; Kozmus and Potočnik, 2015; Lou et al., 2015; Rene et al., 2015; Di Nisio et al., 2016; Liu et al., 2016; Murphy et al., 2016; Desjardins et al., 2017; Li et al., 2017; Matou-Nasri et al., 2017; Makino et al., 2018; Zhang et al., 2018; Himi et al.,	35

		2020; Koike et al., 2020; Zhang et al., 2020; Alsubaie et al., 2021; Caballero-Palacios et al., 2021; Mao et al., 2021)	
GUSB	Homo sapiens glucuronidase beta (GUSB	(Green et al., 2009; Rocci et al., 2010a; Rocci et al., 2010b; Valceckiene et al., 2010; Gambella et al., 2013; Appe et al., 2015; Roisman et al., 2015; Hansen et al., 2020)	9
HMBS	Homo sapiens hydroxymethylbilane synthase (HMBS)	(Bernasconi et al., 2006; Sánchez-Espiridión et al., 2009)	2
HPRT1	Homo sapiens hypoxanthine phosphoribosyltransferase 1 (HPRT1)	(Gladkikh et al., 2010; Valceckiene et al., 2010; De Cassia Carvalho Melo et al., 2011; Potashnikova et al., 2012; Oturai et al., 2016; Urrutia et al., 2016; Torun et al., 2021)	7
MRPL19	Homo sapiens mitochondrial ribosomal protein L19 (MRPL19)	(Valceckiene et al., 2010)	1
PABPC4	Homo sapiens poly(A) binding protein cytoplasmic 4 (PABPC4)	Identified locally	1
POLR2A	Homo sapiens RNA polymerase II subunit A (POLR2A)	(Urrutia et al., 2016)	1
PPIA	Homo sapiens peptidylprolyl isomerase A (PPIA)	(Krumbholz et al., 2008; Ferraresso et al., 2015)	2
PSMC4	Homo sapiens proteasome 26S subunit, ATPase 4 (PSMC4)	(Przybyl et al., 2014)	1
RPL4	Homo sapiens ribosomal protein L4 (RPL4)	(Ferraresso et al., 2015)	1

RPL13A	Homo sapiens ribosomal protein L13a (RPL13A)	(Ritz et al., 2013)	1
RPL19	Homo sapiens ribosomal protein L19 (RPL19)	(Urrutia et al., 2016)	1
RPLP0	Homo sapiens ribosomal protein lateral stalk subunit P0 (RPLP0)	(Kim et al., 2010; Vukić et al., 2015; Magne et al., 2018)	3
RPS17	Homo sapiens ribosomal protein S17 (RPS17)	(Usarek et al., 2017)	1
TBP	Homo sapiens TATA-box binding protein (TBP)	(Nikitin et al., 2007; Green et al., 2009; Cozen et al., 2013; Rene et al., 2015; Gordiienko et al., 2016; Urrutia et al., 2016; Kovalevska and Kashuba, 2020)	7
UBC	Homo sapiens ubiquitin C (UBC)	(Gladkikh et al., 2010; Potashnikova et al., 2012; Potashnikova et al., 2015; Oturai et al., 2016)	4
UBE2D2	Homo sapiens ubiquitin conjugating enzyme E2 D2 (UBE2D2)	(Oturai et al., 2016)	1
YWHAZ	Homo sapiens tyrosine 3-monooxygenase/tryptophan 5-monooxygenase activation protein zeta (YWHAZ)	(Gladkikh et al., 2010; Potashnikova et al., 2012; Potashnikova et al., 2015)	3
18S	Homo sapiens RNA, 18S ribosomal N1 (RNA18SN1)	(Green et al., 2009; Perez-Chacon et al., 2014; Jahid et al., 2018)	2

Table 5-2 List of full text exclusions from systematic review and with reason for omission from study

Reason for full text exclusion	Reference	Number of references
No details of Rt-qPCR	(Goff et al., 2000; Ma et al., 2000; Wu et al., 2000; Yu et al., 2000; De Bont et al., 2001; Gamper et al., 2001; Hattori et al., 2001; Morelon et al., 2001; Oshima et al., 2001; Efferth et al., 2002; Jiang et al., 2002; Huang et al., 2003; Garcia-Vallejo et al., 2004; Hansen et al., 2005; Horiguchi-Yamada et al., 2005; Quer et al., 2005; Alisi et al., 2007; Jasinski-Bergner et al., 2018; Yan et al., 2020; Zhong et al., 2020)	20
Excluded cell line used	(Carvalheiro et al., 2012b; Carvalheiro et al., 2012a; Blengio et al., 2013; Pierobon et al., 2013; Ryynänen et al., 2013; Azzaoui et al., 2016; Torrance et al., 2018; Dwivedi et al., 2020)	8
No reference gene used	(X. Liu et al., 2020)	1
miRNA target	(Watanabe et al., 2014; de Siqueira Figueredo et al., 2015; Pastuszak-Lewandoska et al., 2020)	3
Retracted	(Zhang and Li, 2015)	1

5.3.4 Primer design

5.3.4.1 Primer sequences and expected product sizes

Based on the list of identified candidate reference genes in Table 5-1, primers were designed using NCBI Primer-BLAST webtool as described in section 2.2.13.6 (Ye et al., 2012). NCBI Primer-BLAST was selected so all primers could be designed consistently. All forward and reverse primer sequences for candidate reference genes are shown in Table 5-3, together with the expected primer product size, the NCBI accession number (that the primers were designed against), and the short and full names of the genes used to identify each target.

5.3.5 Primer reconstitution

See section 2.2.13.7.

5.3.6 Temperature gradient (Tm) Plates

See section 2.2.13.8.1.

5.3.7 Screening of Tm plate primer products

Data from Tm plates was reviewed in CFX Maestro to compare melt peak data between all temperature points tested (see section 5.3.6) for each primer pair. Melt peak charts were used to visually check primer products, and in conjunction with the Ct values for each temperature point, were used to identify the optimum annealing temperature for use in RT-qPCR reactions with thienopyridine-treated cDNA samples for each set of primers. Tm plate primer products were then assessed via agarose gel electrophoresis to confirm digital screening of primers.

Table 5-3 Forward and reverse primers sequences and expected primer product sizes of all candidate reference genes investigated as potential stable reference genes for use in RT-qPCR data normalisation.

Primer sequence (5' to 3')	Primer Short Name	NCBI Accession Number	NCBI Input PCR template	Primer Product Size	% Efficiency	Standard Dilutions?
GCTGTTATCTGGAAGAAGCCCT	ABL1 Forward	NM_005157.6	Homo sapiens ABL proto-oncogene 1, non-receptor tyrosine kinase (ABL1), transcript variant a	139	104.30%	1:10 (3 logs)
GCAACGAAAAGGTTGGGGTC	ABL1 Reverse					
CTCACCATGGATGATGATATCGC	ACTB forward	NM_001101.5	Homo sapiens actin beta (ACTB)	163	92.40%	1:10 (4 logs)
AGGAATCCTTCTGACCCATGC	ACTB reverse					
TGGAGGCTATCCAGCGTACT	B2M Forward	NM_004048.4	Homo sapiens beta-2-microglobulin (B2M)	108	93.10%	1:10 (5 logs)
CGGATGGATGAAACCCAGACA	B2M Reverse					
GTCGCCAGGACAATGGACTT	CD19 FWD	NM_001770.6	Homo sapiens CD19 molecule (CD19), transcript variant 2, mRNA	298	102.20%	1:10 (4 logs)
TGGGGACTTGAGGAGATCCA	CD19 RVS					
AGATGCTGCTGTCGGCTAC	EIF2B1 Forward	NM_001414.4	Homo sapiens eukaryotic translation initiation factor 2B subunit alpha (EIF2B1)	184	101.00%	1:10 (4 logs)
TGGAAAGAGCCGGACAAACT	EIF2B1 Reverse					
CGGATTTGGTCGTATTGGGCG	GAPDH forward	NM_002046.7	Homo sapiens glyceraldehyde-3-phosphate dehydrogenase (GAPDH), transcript variant 1	297	92.00%	1:10 (5 logs)
GCCTTCTCCATGGTGGTGAAGAC	GAPDH reverse					
TGCAGCGGTCTGTACTTCTG	GUSB Forward	NM_000181.4	Homo sapiens glucuronidase beta (GUSB), transcript variant 1	100	Failed primers	Redesigned Primers
TGGTAATTCACCAGCCCACT	GUSB Reverse					
ACTGACACCTCCAAGTATCCCA	GUSB FWD 2	NM_000181.4	Homo sapiens glucuronidase beta (GUSB), transcript variant 1, mRNA	198	99.60%	1:10 (4 logs)
CAGGTTACTGCCCTTGACAGA	GUSB RVS 2					
GCTGCAACGGCGGAAGA	HMBS Forward	NM_000190.4	Homo sapiens hydroxymethylbilane synthase (HMBS), transcript variant 1	159	101.90%	1:10 (5 logs)
CCCTGTGGTGGACATAGCAA	HMBS Reverse					
CCCTGGCGTCGTGATTAGTG	HPRT1 Forward	NM_000194.3	Homo sapiens hypoxanthine phosphoribosyltransferase 1 (HPRT1)	139	95.20%	1:10 (5 logs)
TCGAGCAAGACGTTCAGTCC	HPRT1 Reverse					
AACCGGAACGCAGGTTCTT	MRPL19 Forward	NM_014763.4	Homo sapiens mitochondrial ribosomal protein L19 (MRPL19)	187	102.40%	1:10 (4 logs)
TGGCTGATTTTTCCACTGGC	MRPL19 Reverse					
AAGCCAATCCGCATCATGTG	PABPC4 forward	NM_001135653.2	Homo sapiens poly(A) binding protein cytoplasmic 4 (PABPC4), transcript variant 1	210	101.60%	1:10 (5 logs)
CTCTTGGGTCTCGAAGTGG	PABPC4 reverse					
CGGCCTGTCATGGGTATTGT	POLR2A Forward	NM_000937.5	Homo sapiens RNA polymerase II subunit A (POLR2A)	92	Failed Primers	Redesigned Primers
TTCATCACTTCACCCCGCTC	POLR2A Reverse					
TCCTCGCATGATTGTCACCC	POLR2A FWD 2	NM_000937.5	Homo sapiens RNA polymerase II subunit A (POLR2A), mRNA	124	108.10%	1:10 (4 logs)
GTTCATCACTTCACCCCGCT	POLR2A RVS 2					
CCACCGTGTTCTTCGACATTG	PPIA Forward	NM_021130.5	Homo sapiens peptidylprolyl isomerase A (PPIA), transcript variant 1	71	101.40%	1:10 (4 logs)
GTCTGCAAACAGCTCAAAGG	PPIA Reverse					
GGAGGTGCAGGAGGAATACAT	PSMC4 Forward	NM_006503.4	Homo sapiens proteasome 26S subunit, ATPase 4 (PSMC4), transcript variant 1	180	97.80%	1:10 (4 logs)
CGCACATAATAGTTGGAGCCTGT	PSMC4 Reverse					
GCCGCTTCCCTCAAGAGTAA	RPL4 Forward	NM_000968.4	Homo sapiens ribosomal protein L4 (RPL4)	126	94.70%	1:10 (5 logs)
GCGATGGATCTTCTTGCGTG	RPL4 Reverse					
TAAACAGGTACTGCTGGGCCG	RPL13A Forward	NM_012423.4	Homo sapiens ribosomal protein L13a (RPL13A), transcript variant 1	134	92.80%	1:10 (5 logs)
CTCGGGAAGGGTTGGTGTTC	RPL13A Reverse					
CAATGCCAACTCCCGTCAGC	RPL19 Forward	NM_000981.4	Homo sapiens ribosomal protein L19 (RPL19), transcript variant 1	181	Failed Primers	Redesigned Primers
GACCTTCTCTGGCATTCGGG	RPL19 Reverse					
GAGCGAGCTCTTTCCTTTCGC	RPL19 FWD 2	NM_000981.4	Homo sapiens ribosomal protein L19 (RPL19), transcript variant 1, mRNA	286	98.30%	1:10 (5 logs)
ACCCTTCCGCTTACCTATGCC	RPL19 RVS 2					
GCAGCAGATCCGCATGTCCC	RPLP0 forward	NM_001002.4	Homo sapiens ribosomal protein lateral stalk subunit P0 (RPLP0), transcript variant 1	134	98.10%	1:10 (5 logs)
TCCCCCGGATATGAGGCAGCA	RPLP0 reverse					
ACCAAAACCGTGAAGAAGGC	RPS17 Forward	NM_001021.6	Homo sapiens ribosomal protein S17 (RPS17), transcript variant 1	153	92.50%	1:10 (5 logs)
ATGCGTGACATAACCTGCTA	RPS17 Reverse					
CCACGCCAGCTTCGGAGAGT	TBP forward	NM_003194.5	Homo sapiens TATA-box binding protein (TBP), transcript variant 1	183	98.90%	1:10 (4 logs)
TCAGTGCCGTGGTTCGTGGC	TBP reverse					
CGTCGCAGCCGGGATTTG	UBC Forward	NM_021009.7	Homo sapiens ubiquitin C (UBC), mRNA	77	94.30%	1:10 (5 logs)
CACGAAGATCTGCATTGTCAAGT	UBC Reverse					
GAGAATCCACAAGGAATTGAATGA	UBE2D2 FWD	NM_003339.3	Homo sapiens ubiquitin conjugating enzyme E2 D2 (UBE2D2), transcript variant 1, mRNA	133	91.30%	1:10 (5 logs)
TCCACCCTGATAGGGACTGT	UBE2D2 RVS					
CTGGGTCTGGCCCTTAACTT	YWHAZ Forward	NM_003406.4	Homo sapiens tyrosine 3-monooxygenase/tryptophan 5-monooxygenase	97	99.70%	1:10 (5 logs)
TGGCTTCATCAAAAGCTGTCT	YWHAZ Reverse					
GGGCGACGACCCATTCGAAC	18S FWD	NR_145820.1	Homo sapiens RNA, 18S ribosomal N1 (RNA18SN1), ribosomal RNA	99	100.40%	1:10 (5 logs)
GAATCGAACCCTGATTCCCCGTC	18S RVS					

5.3.7.1 Data quality control and melt peak analysis

Following data collection from Tm plates, melt peak data (see Figure 5-4) for each set of primers was screened in CFX Maestro software to check for the presence of any unexpected peaks that indicated contamination with genomic DNA or peaks that indicated the presence of primer dimer formation, and for confirmation of negative no template controls (an additional check for primer dimer formation as well as contamination of RT-qPCR reagents). Melt peaks that showed a single PCR product (as shown in Figure 5-4A) and a negative NTC (blue line in Figure 5-4A) were considered suitable for further investigation with thienopyridine-treated DAUDI cDNA. Any primer pair melt peaks that showed multiple PCR products (as shown by red arrow in Figure 5-4B) or that displayed evidence of positive NTCs (as shown by red line in Figure 5-4B) were considered unsuitable for further investigation, and primers were then re-designed as per section 5.3.4 and repeat Tm plates and screening was conducted.

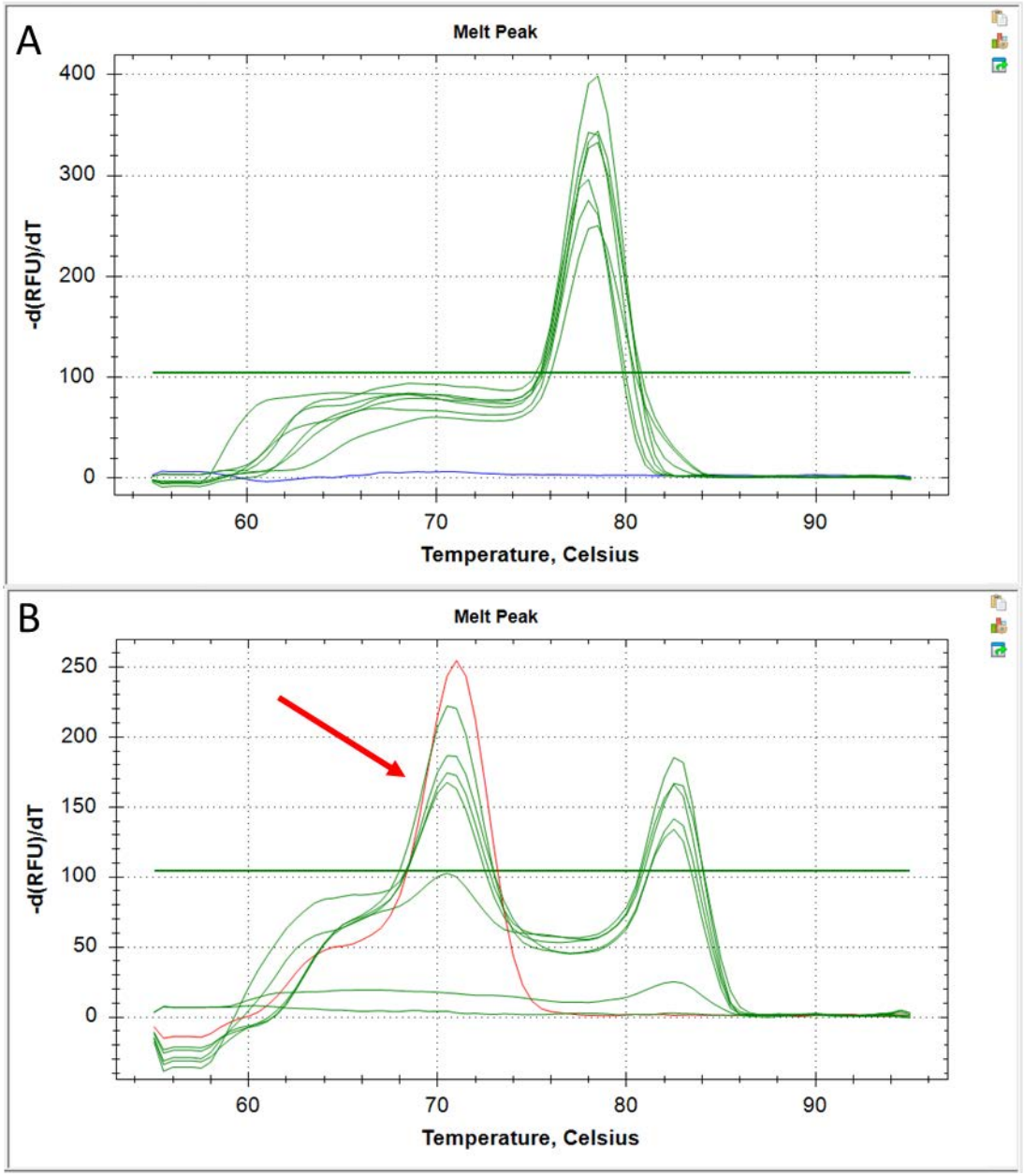

Figure 5-4 Comparison of SYBR Green RT-qPCR melt peak data showing formation of a single PCR product across multiple cDNA samples and a negative no template control (NTC – indicated by melt peak highlighted in blue) (A) and RT-qPCR melt peak data showing evidence of primer dimer formation (peaks indicated by the red arrow) as well as a positive no template control (indicated by melt peak highlighted in red) (B).

5.3.7.2 Agarose gel electrophoresis and analysis

The primer products from the temperature gradient point with the lowest Ct value, as identified in Section 5.3.7.1, was then run on a 2.5 % agarose gel in TAE buffer as described in section 2.2.13.8.4 and the size of the electrophoresis separated PCR products were compared to the predicted product sizes listed in Table 5-3. Any

product size that deviated from its predicted size, any lanes that showed multiple bands, or any NTCs that showed the presence of a primer product were used to further screen primer pairs, was used to indicate any primers that may require redesign prior to their inclusion in the data collection part of this chapter.

5.3.7.3 Primer redesign

Any primer pairs which failed the quality control steps in Sections 5.3.7.1 and 5.3.7.2 were redesigned with

- changes made to target product size (from 70 – 200 bp to 70 – 300 bp),
- different combinations of inclusion of an exon-exon junction or exclusion of an intron,
- adjustments made to predicted Tm values,
- were designed to target an alternate splice variant of reference gene mRNA (where available)

Primer design was repeated in NCBI Primer-BLAST as per section 2.2.13.6.

5.3.8 RT-qPCR of candidate reference genes and Thienopyridine treated DAUDI samples

5.3.8.1 RT-qPCR data quality control

Was conducted as described in section 2.2.13.12.1. Details of DNA gel electrophoresis, running conditions and imaging can be found in section 2.2.13.8.4.

5.3.9 Assessment of candidate reference gene stability

5.3.9.1 GeNorm reference gene stability assessment

Establishing the stability of expression of candidate reference genes across all conditions tested in these experiments (i.e. stability of gene expression across thienopyridine-treated, untreated and paclitaxel and nocodazole positive controls) was essential prior to the use of reference genes in data normalisation. This was determined using the 'Reference Gene Selection Tool' as part of the Gene Study

functionality in Bio-Rad CFX Maestro Software, which utilised the GeNorm algorithm established by Vandesomplele *et al* (2002), whereby all candidate reference genes are compared to produce an M value, and genes with the lowest M values are the most stability expressed. The stability of candidate reference genes is displayed graphically by the CFX software with 'ideal' reference genes having the lowest M value, 'Acceptable' reference genes having an intermediate M value, while 'Unstable' reference genes have the lowest M values. In the absence of 'Ideal' candidate reference genes, 'Acceptable' candidates could be selected, however any 'unstable' genes should not be used in normalisation.

5.4 Results

5.4.1 Primer products gel electrophoresis

As shown in Figure 5-5 to Figure 5-11, only three candidate reference genes showed positive NTCs with evidence of primer dimer formation in the primer pairs for GUSB (see Figure 5-6), POLR2A (see Figure 5-7) and RPL19 (see Figure 5-8), which necessitated primer redesign as per section 5.3.7.3. All other primer pairs investigated showed no evidence of primer dimers or other contamination either in primer products or NTCs.

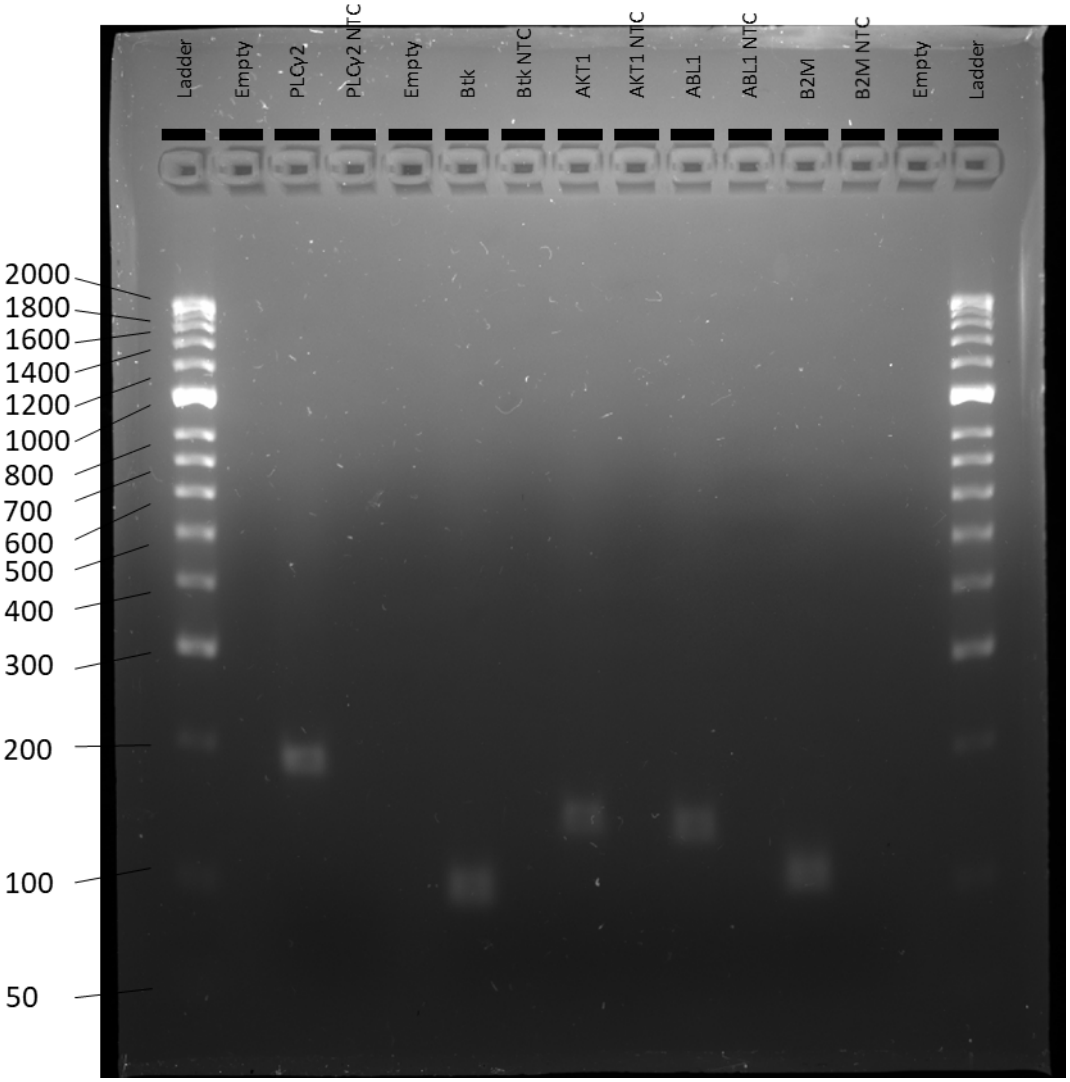

Figure 5-5 The PCR product and corresponding No Template Control (NTC) for each primer pair assessed on RT-qPCR Temperature Gradient (Tm) plates were added to 2.4 µL Bioline 5X Loading Dye and then loaded to a 2.5 % agarose gel in 1X TAE buffer. PCR products were separated via electrophoresis at 80 volts for 25 minutes, followed by 100 volts for 35 minutes. Gel was imaged using ChemiDoc™ Touch Gel Imaging System using Gel Green Optimal Auto-exposure settings. The predicted PCR product sizes in base pairs (bp) for each set of primers featured on the gel were as follows:

PLCγ2 - 182 bp; BTK – 98 bp; AKT1 – 142 bp; ABL1 – 139 bp; B2M – 108 bp. PCR product size was compared to Bioline HyperLadder™ 50bp molecular weight markers for confirmation of expected band size and presence/absence of any bands in NTC samples was used to confirm suitability of primers for use in RT-qPCR gene of interest/reference gene studies.

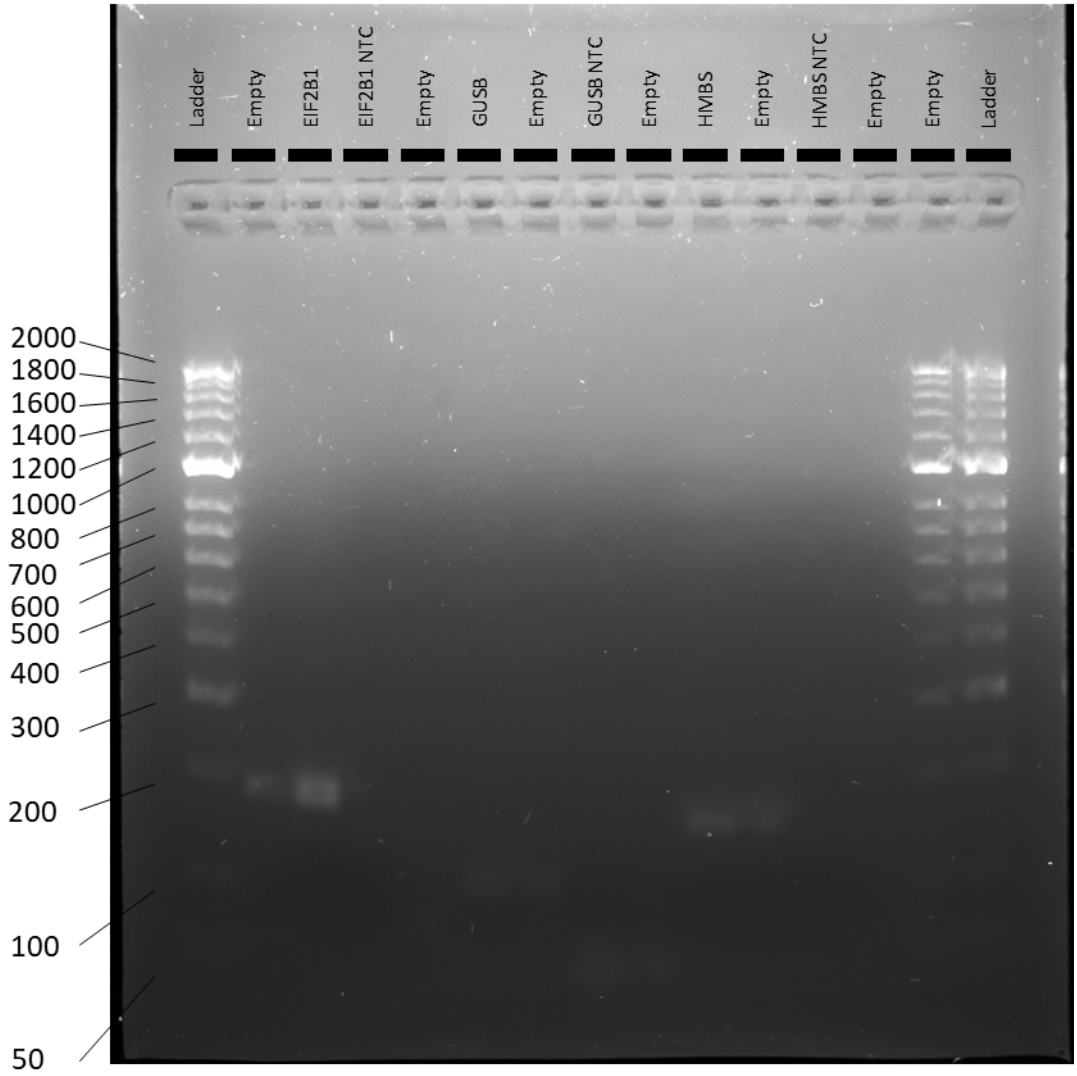

Figure 5-6 The PCR product and corresponding No Template Control (NTC) for each primer pair assessed on RT-qPCR Temperature Gradient (Tm) plates were added to 2.4 µL Bioline 5X Loading Dye and then loaded to a 2.5 % agarose gel in 1X TAE buffer. PCR products were separated via electrophoresis at 100 volts for 45 minutes. The loading wells of the gel were torn during comb removal and PCR products were leached into adjacent wells for EIF2B1, GUSB, GUSB NTC and HMBS. Gel was imaged using ChemiDoc™ Touch Gel Imaging System using Gel Green Optimal Auto-exposure settings. The predicted PCR product sizes in base pairs (bp) for each set of primers featured on the gel were as follows:

EIF2B1 - 184 bp; GUSB – 100 bp; HMBS – 159 bp. PCR product size was compared to Bioline HyperLadder™ 50bp molecular weight markers for confirmation of expected band size and presence/absence of any bands in NTC samples was used to confirm suitability of primers for use in RT-qPCR gene of interest/reference gene studies.

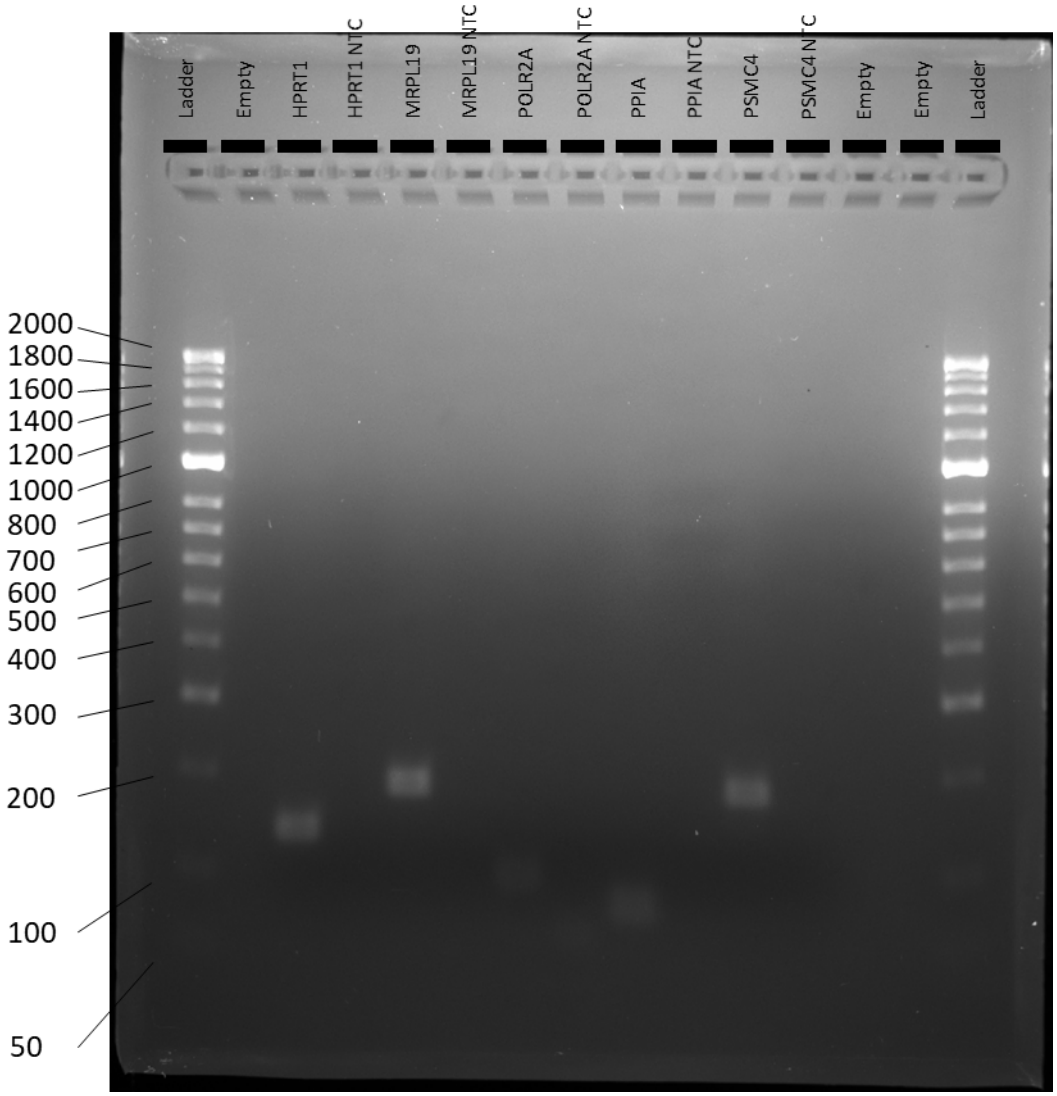

Figure 5-7 The PCR product and corresponding No Template Control (NTC) for each primer pair assessed on RT-qPCR Temperature Gradient (Tm) plates were added to 2.4 µL Bioline 5X Loading Dye and then loaded to a 2.5 % agarose gel in 1X TAE buffer. PCR products were separated via electrophoresis at 100 volts for 57 minutes. Gel was imaged using ChemiDoc™ Touch Gel Imaging System using Gel Green Optimal Auto-exposure settings. The predicted PCR product sizes in base pairs (bp) for each set of primers featured on the gel were as follows:

HPRT1 - 139 bp; MRPL19 – 187 bp; POLR2A – 92 bp; PPIA – 71 bp; PSMC4 – 180 bp. PCR product size was compared to Bioline HyperLadder™ 50bp molecular weight markers for confirmation of expected band size and presence/absence of any bands in NTC samples was used to confirm suitability of primers for use in RT-qPCR gene of interest/reference gene studies.

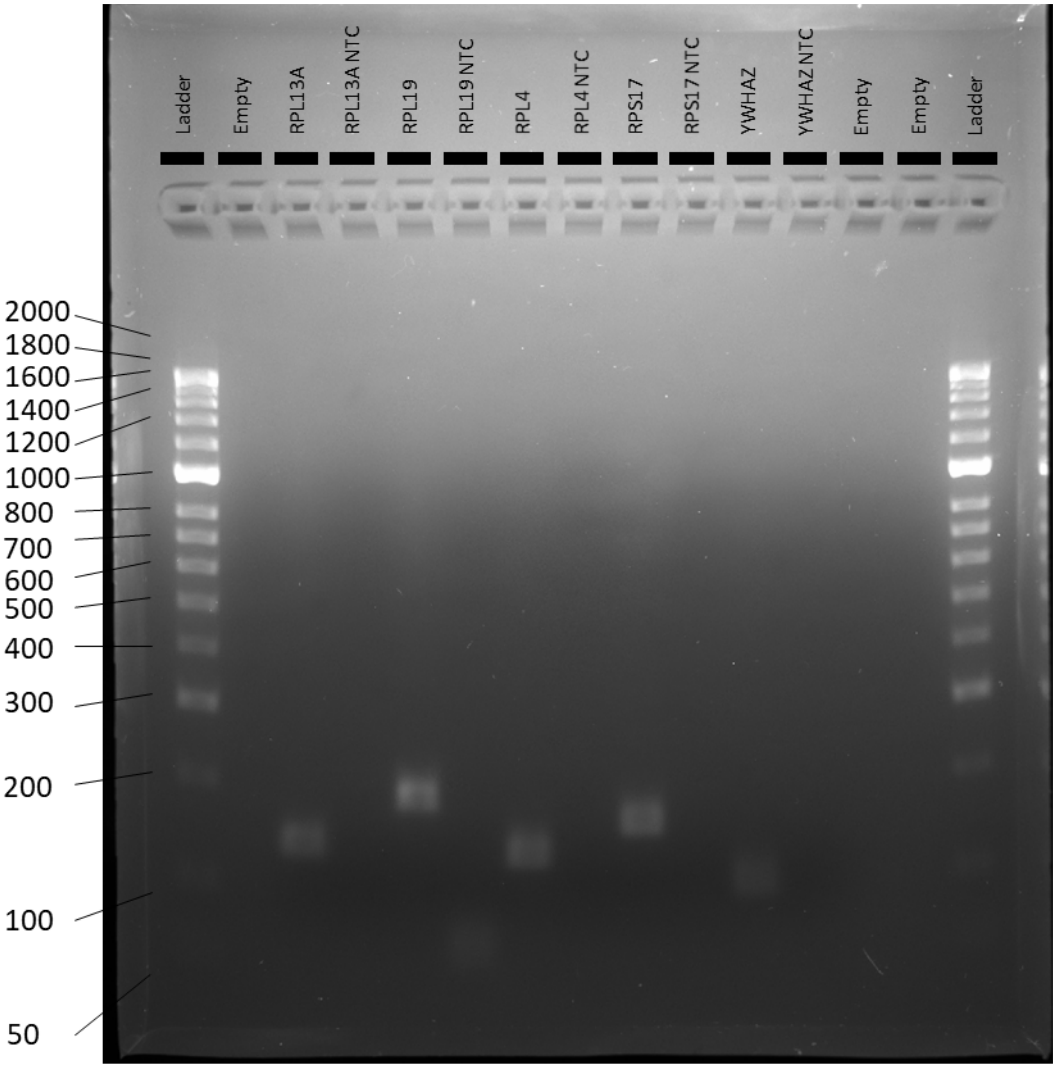

Figure 5-8 The PCR product and corresponding No Template Control (NTC) for each primer pair assessed on RT-qPCR Temperature Gradient (Tm) plates were added to 2.4 µL Bioline 5X Loading Dye and then loaded to a 2.5 % agarose gel in 1X TAE buffer. PCR products were separated via electrophoresis at 100 volts for 50 minutes. Gel was imaged using ChemiDoc™ Touch Gel Imaging System using Gel Green Optimal Auto-exposure settings. The predicted PCR product sizes in base pairs (bp) for each set of primers featured on the gel were as follows:

RPL13A - 134 bp; RPL19 – 181 bp; RPL4 – 126 bp; RPS17 – 153 bp; YWHAZ – 97 bp. PCR product size was compared to Bioline HyperLadder™ 50bp molecular weight markers for confirmation of expected band size and presence/absence of any bands in NTC samples was used to confirm suitability of primers for use in RT-qPCR gene of interest/reference gene studies.

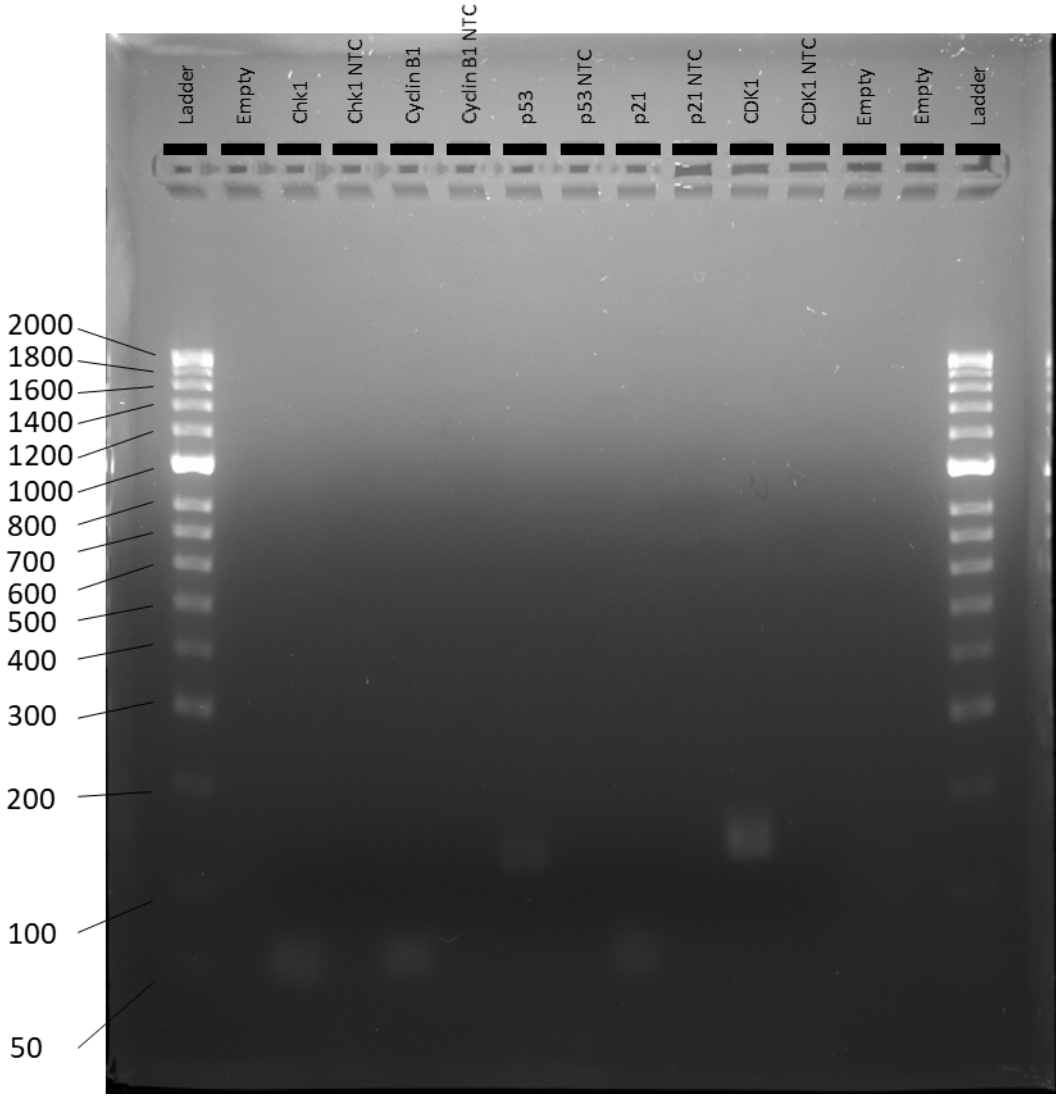

Figure 5-9 The PCR product and corresponding No Template Control (NTC) for each primer pair assessed on RT-qPCR Temperature Gradient (Tm) plates were added to 2.4 µL Bioline 5X Loading Dye and then loaded to a 2.5 % agarose gel in 1X TAE buffer. PCR products were separated via electrophoresis at 100 volts for 50 minutes. Gel was imaged using ChemiDoc™ Touch Gel Imaging System using Gel Green Optimal Auto-exposure settings. The predicted PCR product sizes in base pairs (bp) for each set of primers featured on the gel were as follows:

Chk1 - 51 bp; Cyclin B1 – 52 bp; p53 – 132 bp; p21 – 55 bp; CDK1 – 148 bp. PCR product size was compared to Bioline HyperLadder™ 50bp molecular weight markers for confirmation of expected band size and presence/absence of any bands in NTC samples was used to confirm suitability of primers for use in RT-qPCR gene of interest/reference gene studies.

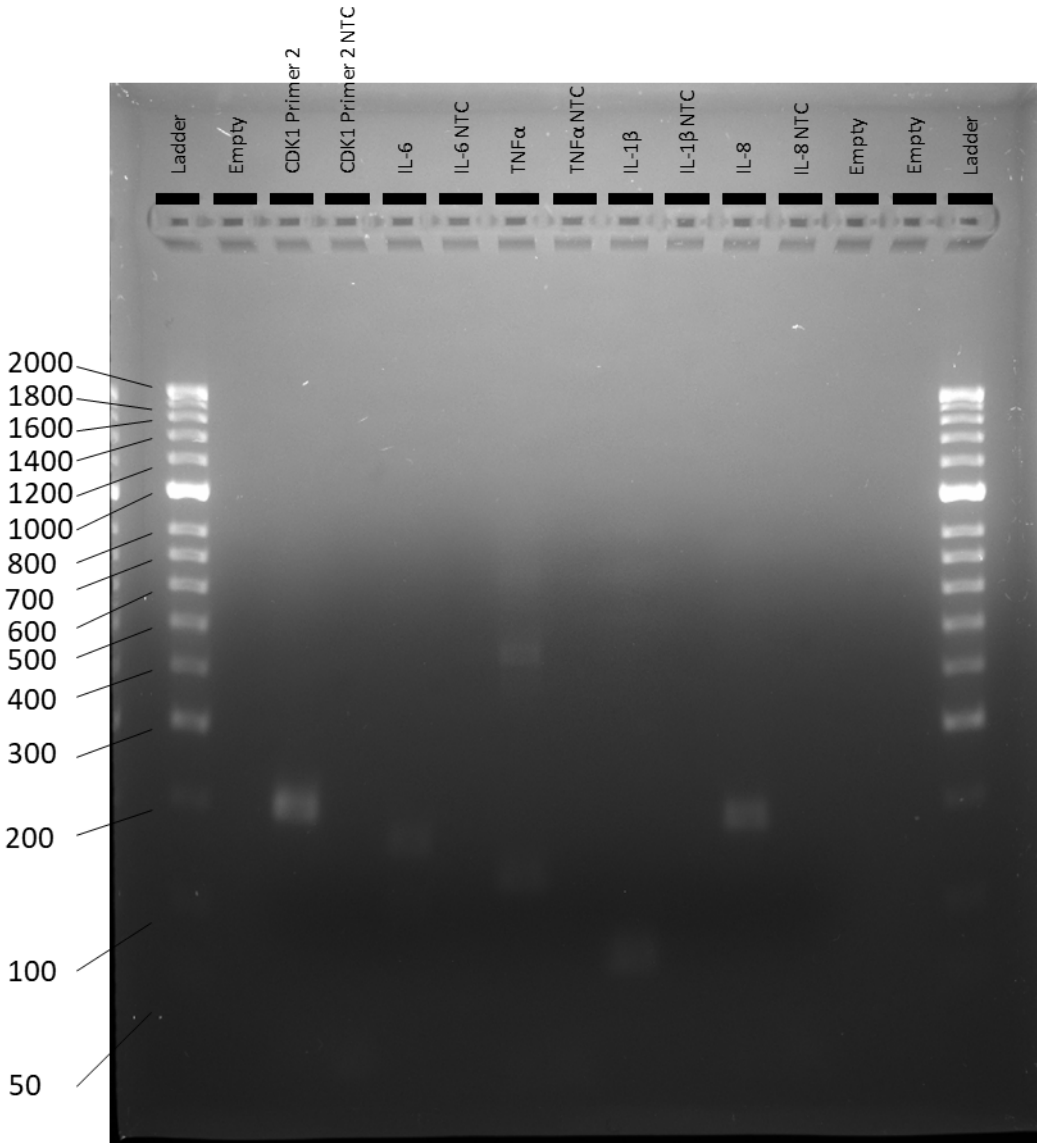

Figure 5-10 The PCR product and corresponding No Template Control (NTC) for each primer pair assessed on RT-qPCR Temperature Gradient (Tm) plates were added to 2.4 µL Bioline 5X Loading Dye and then loaded to a 2.5 % agarose gel in 1X TAE buffer. PCR products were separated via electrophoresis at 100 volts for 50 minutes. Gel was imaged using ChemiDoc™ Touch Gel Imaging System using Gel Green Optimal Auto-exposure settings. The predicted PCR product sizes in base pairs (bp) for each set of primers featured on the gel were as follows:

CDK1 Primer 2 - 203 bp; IL-6– 164 bp; TNFα – 132 bp; IL-1ϐ – 65 bp; IL-8 – 192 bp. PCR product size was compared to Bioline HyperLadder™ 50bp molecular weight markers for confirmation of expected band size and presence/absence of any bands in NTC samples was used to confirm suitability of primers for use in RT-qPCR gene of interest/reference gene studies.

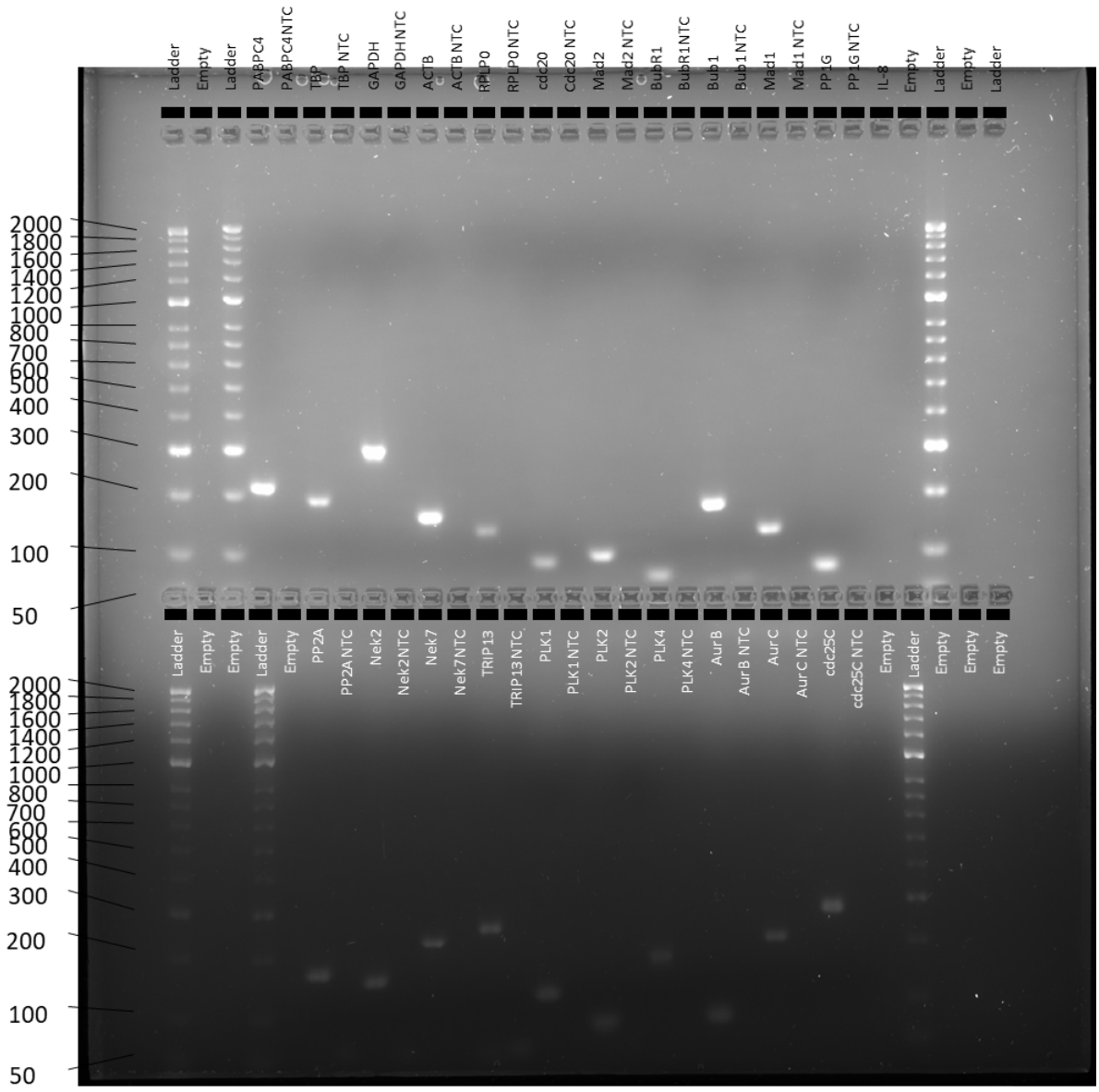

Figure 5-11 The PCR product and corresponding No Template Control (NTC) for each primer pair assessed on RT-qPCR Temperature Gradient (Tm) plates were added to 2.4 µL Bioline 5X Loading Dye and then loaded to a 2.5 % agarose gel in 1X TAE buffer. PCR products were separated via electrophoresis at 100 volts for 105 minutes. Gel was imaged using ChemiDoc™ Touch Gel Imaging System using Gel Green Optimal Auto-exposure settings. The predicted PCR product sizes in base pairs (bp) for each set of primers featured on the gel were as follows:

PABPC4 - 210 bp; TBP– 183 bp; GAPDH – 297 bp ; ACTB – 163 bp ; RPLP0 – 134 bp; cdc20 - 92 bp; Mad2– 103 bp; BubR1 – 70 bp ; Bub1 – 187 bp ; Mad1 – 103 bp; PP1G - 76 bp; (PP2A)-B56 – 167 bp; Nek2 – 151 bp ; Nek7 – 215 bp ; TRIP13 – 245 bp; PLK1 - 118 bp; PLK2– 73 bp; PLK4 – 168 bp; Aurora B – 76 bp; Aurora C – 199 bp ; cdc25C – 270 bp. PCR product size was compared to Bioline HyperLadder™ 50bp molecular weight markers for confirmation of expected band size and presence/absence of any bands in NTC samples was used to confirm suitability of primers for use in RT-qPCR gene of interest/reference gene studies.

5.4.2 Identification of stable reference genes using GeNorm

Following quality control of primers, establishment of thermocycling temperatures for RT-qPCR reactions and confirmation of primer product size in the absence of positive NTCs or primer dimers, a 'gene study' was created containing all of the RT-qPCR raw data Ct values in CFX Maestro software. The 'reference gene selection tool was used to produce a 'reference gene stability plot' (see Figure 5-12) and data table of 'M' stability values for all candidate reference genes listed in Table 5-1.

As shown in , the four candidate genes with the highest stability values out of the 24 candidate genes were TBP, PPIA, RPLP0 and EIF2B1. These genes were taken forward as stable reference genes for all further RT-qPCR assays described in this thesis.

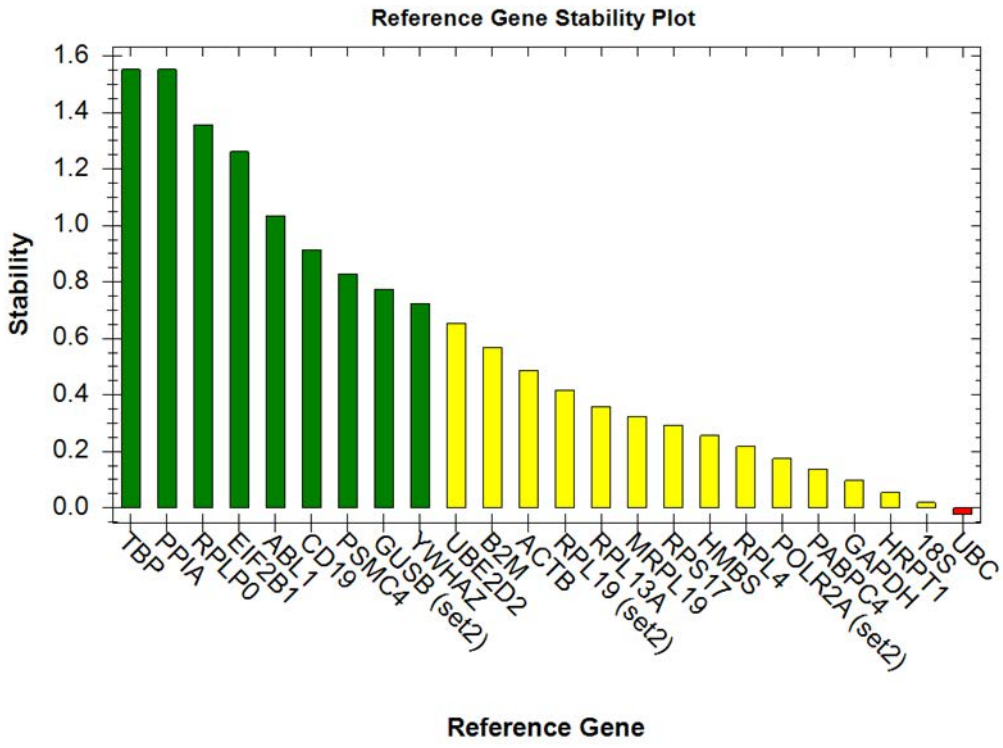

Figure 5-12 CFX Maestro 'Reference Gene Stability Plot' of Stability value 'M' for each candidate reference gene. Green represents 'ideal' stability, yellow represents 'acceptable' stability, while red represents 'unstable' genes according to the GeNorm algorithm.

Table 5-4 GeNorm stability values for CFX Maestro 'Reference Gene Stability Plot'

Order	Gene Name	Evaluation	Avg M Value	Stability (Ln(1/AvgM))	# Samples
1	TBP	Ideal	0.211733505	1.552426848	13
2	PPIA	Ideal	0.211733505	1.552426848	13
3	RPLP0	Ideal	0.257237699	1.357754722	13
4	EIF2B1	Ideal	0.283222715	1.261521714	13
5	ABL1	Ideal	0.355374343	1.034583558	13
6	CD19	Ideal	0.400898632	0.914046671	13
7	PSMC4	Ideal	0.436147012	0.829775908	13
8	GUSB (set2)	Ideal	0.460648231	0.775120584	13
9	YWHAZ	Ideal	0.484915662	0.723780295	13
10	UBE2D2	Acceptable	0.520019687	0.653888608	13
11	B2M	Acceptable	0.566169677	0.568861462	13
12	ACTB	Acceptable	0.613803158	0.488080991	13
13	RPL19 (set2)	Acceptable	0.658484556	0.417814211	13
14	RPL13A	Acceptable	0.697762531	0.359876447	13
15	MRPL19	Acceptable	0.724197265	0.322691459	13
16	RPS17	Acceptable	0.745945598	0.293102606	13
17	HMBS	Acceptable	0.774070985	0.256091698	13
18	RPL4	Acceptable	0.804868537	0.217076323	13
19	POLR2A (set2)	Acceptable	0.83978305	0.174611695	13
20	PABPC4	Acceptable	0.872126733	0.13682053	13
21	GAPDH	Acceptable	0.907143344	0.097454799	13
22	HRPT1	Acceptable	0.946572322	0.054907902	13
23	18S	Acceptable	0.98165761	0.018512697	13
24	UBC	Unstable	1.022668958	-0.022415835	13

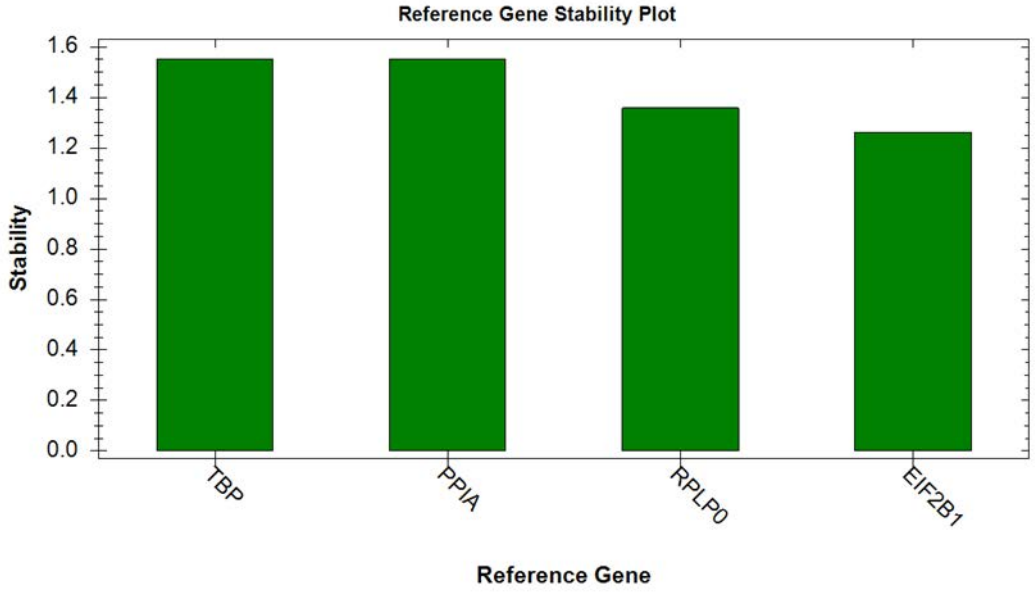

Figure 5-13 The four candidate reference genes with the highest stability values for RT-qPCR of Thienopyridine-treated DAUDI cells

5.5 Discussion

5.5.1 Stable reference genes and comparison to 'housekeeper' genes

The purpose of this chapter was to use a systematic search of available literature to identify reference genes that are stably expressed in DAUDI cells during treatment with novel thienopyridine compounds, nocodazole and paclitaxel controls. The review, RT-qPCR and GeNorm analysis identified TBP, PPIA, RPLP0 and EIF2B1 as the most stable genes out of the selection of 24 genes, which included the traditional 'housekeeper' genes GAPDH and β-Actin (ACTB gene). Indeed, of the literature searched, GAPDH was used in 29.9 % of the studies included in this review and β-Actin was used in 13.7 % of studies, TBP (6.0 %), RPLP0 (2.6 %), PPIA (1.7 %) and EIF2B1 (0.85 %) were less frequently recommend. This suggesting there continues to be a disparity in selection of 'housekeeper' genes despite there being significant evidence that they are not stably expressed (Andersen et al., 2004; Jacob et al., 2013; Odeya et al., 2018) or only acceptable after screening other candidate reference gene options and comparing their stability (Brkljačić et al., 2010). GAPDH placed 21st and β-Actin 12th in the ranking of stability of the genes tested, with both deemed as 'acceptable' (see Figure 5-12), with UBC (Ubiquitin C) ranked as the most unstable candidate reference gene, which may give an indication of the effects on ubiquitination in DAUDI cells in response to Thienopyridine treatments.

As listed in Table 5-1, seventeen authors of the ninety full text documents screened (18.8 % of the journals screened) suggested multiple reference genes with nine of those listing the use of GeNorm (Gladkikh et al., 2010; Rene et al., 2015; Vukić et al., 2015; Urrutia et al., 2016), or GeNorm + NormFinder (Green et al., 2009; Przybyl et al., 2014; Oturai et al., 2016) as the method of reference gene selection. Two sets of authors compared all three gene stability assessment methods (GeNorm, NormFinder and BestKeeper) (Valceckiene et al., 2010; Potashnikova et al., 2015). One additional author listed 'DNA gels' as their method of normalisation (Caballero-Palacios et al., 2021). All of the stable reference genes identified in the systematic review, apart from PPIA were included in papers that used one of more of the stability assessments, although there is a possibility that the inclusion of abstracts in

the search as long as they contained a listed reference gene may have concealed the methods of reference gene selection.

5.5.2 Cellular roles of the stable reference genes

TATA-box binding protein, encoded by the gene TBP, has functions in the initiation of gene transcription, and is a part of key transcription complexes in association with RNA polymerases I, II and III (Johnson et al., 2003; Mishal and Luna-Arias, 2022).

Peptidylprolyl Isomerase A (encoded by the gene PPIA), also known as Peptidyl-Prolyl Cis-Trans Isomerase A or Cyclophilin A, is an enzyme responsible for the conversion of proline amino acids from a *cis* to a *trans* isomer structural arrangement to allow post-translational folding of proteins (Wang and Heitman, 2005; Agarwal, 2006) as well as being the target of immunosuppressive drug Cyclosporin A, cellular responses to viral infection and in a range of diseases (Nigro et al., 2013; Liao et al., 2021).

Ribosomal Protein Lateral Stalk Subunit P0 (encoded by the gene RPLP0) is a ribosomal protein implicated in recruitment to corrections of double strand breaks in the DNA repair response (Wang et al., 2022) with a role in both protein synthesis and triggering of autophagy responses in its gene knockout (Artero-Castro et al., 2015).

Eukaryotic Translation Initiation Factor 2B Subunit Alpha (encoded by the gene EIF2B1), is another protein involved in cellular protein synthesis, with gene deletions leading to neonatal diabetes (De Franco et al., 2020) and mutations leading to leukoencephalopathy (Rudenskaya and Zakharova, 2017).

It would seem unlikely that any of the effects of the novel thienopyridines would be linked to any of the identified stable reference genes, and it is essential for reference genes to be selected based on the cell lines and conditions being investigated (Roy et al., 2020).

5.5.3 Conclusions

The four most stable reference genes found via systematic review and confirmed via GeNorm analysis were TBP, PPIA, RPLP0 and EIF2B1 These finding support the requirements of the MIQE guidelines (Bustin et al., 2009; Bustin et al., 2010) as well as the more than 20 years of publications advising against the use of 'housekeeper' genes in RT-qPCR normalisation, without checking their stability in the conditions being investigated (Vandesompele et al., 2002; Pfaffl et al., 2004; Huggett et al., 2005; Valceckiene et al., 2010; Jacob et al., 2013; Odeya et al., 2018). In a study such as this one, where the cellular activity of novel compounds is unknown in this cell model, it is an essential step in providing confidence in any findings from the RT-qPCR data in the next chapter.

6. EFFECT OF NOVEL THIENOPYRIDINES ON TRANSCRIPTION AND PROTEIN ABUNDANCE

6 CHAPTER 6: EFFECT OF NOVEL THIENOPYRIDINES ON TRANSCRIPTION AND PROTEIN ABUNDANCE

6.1 Introduction

6.1.1 Identifying potential targets of novel thienopyridine effects on apoptosis

As detailed in the previous experimental chapters, the ten novel thienopyridine compounds investigated have demonstrated varied and oftentimes significant effects on DAUDI B cells, inducing apoptosis in a dose and time dependent manner (Chapter 3), causing a shift to tetraploidy (Chapter 3) and effects on tubulin polymerisation and the mitotic spindle at cell division (Chapter 4).

These compounds were originally synthesised and modified to target the B cell receptor signalling enzyme phospholipase C gamma 2 (PLCγ2/PLCG2) based on in silico screening (Reynisson et al., 2009; Arabshahi et al., 2014; Arabshahi et al., 2015), therefore investigation of the B cell receptor signalling cascade and related cell signalling pathways which converge on PLCG2 is a potential facilitator of the activity of the novel thienopyridines.

6.1.1.1 The B cell receptor initiation of signalling cascade

As shown in Figure 1-1 the B cell receptor is a specialised immunoglobulin antigen receptor which spans the cell membrane of B lymphocytes. The BCR binds to extracellular antigens (often mediated by antigen presenting cells (APCs), leading to BCR clustering and the phosphorylation of membrane bound CD79a and CD79b immunoreceptor tyrosine-based activation motifs (ITAMs) (Bhanja et al., 2022). The phosphorylation of ITAMs creates SH2 interaction domains and allows the kinases Lyn and Syk (spleen tyrosine kinase) to further phosphorylate the ITAMs and triggers signal propagation to other downstream targets, including initiation of the actin cytoskeleton remodelling and phosphorylation of Bruton's tyrosine kinase (Btk) (Pierce and Liu, 2010; Burger and Wiestner, 2018).

6.1.1.2 BCR and secondary messengers

The TEC family tyrosine kinase Btk is a key activator of enzyme PLCG2, via phosphorylation of tyrosine 759, following which PLCG2 generates key secondary messengers diacylglycerol (DAG) and inositol 1,4,5-triphosphate (IP_3) via hydrolysis of membrane-bound phosphoinositol (4,5) biphosphate (PIP_2) (Lowe et al., 2022).

DAG is an upstream activator of the MAPK signalling pathway, and therefore a mediator of cell proliferation and survival (Wheeler et al., 2013), as well as an activator of Protein Kinase C (PKC)-Nuclear factor kappa B (NF-κB) signalling (Yu et al., 2017). Indeed DAG, via Diacylyglycerol Kinase (DGK) has been implicated in cytoskeleton reorganisation via microtubule organisation centres (MTOCs) in both T cells and B cells (Chauveau et al., 2014; Merino-Cortés et al., 2020).

PLCG2 generation of IP_3 stimulates release of cellular stores of additional secondary messenger Calcium (Ca^{2+}), via binding of IP_3 to its receptors present on the surface of the endoplasmic reticulum (Neumann et al., 2023). Calcium then acts on further cytoplasmic targets, including PKC, and NFAT (nuclear factor of activated T cells) transcription factor (via Calmodulin-Calcineurin signalling) (Muller and Rao, 2010; Nadeem and Ahmad, 2023), which provide further cell development, survival and anti-apoptosis protection for B cells.

6.1.1.3 BCR and PI3k-Akt signalling

BCR clustering and activation also leads to phosphorylation of BCR co-factor CD19 by LYN and recruitment of phosphoinositide 3-kinase (PI3K), which in turn phosphorylates membrane bound phosphoinositides to trigger the activation of the AKT1 signalling cascade, with AKT1-mTOR pathway a key regulator of anti-apoptotic, cell proliferation and growth (Vivanco and Sawyers, 2002), multidrug resistance (R. Liu et al., 2020) and in tonic BCR signalling in the absence of antigen binding (Srinivasan et al., 2009; Borbet et al., 2021). The anti-apoptotic effects of AKT1 are a result of inhibition of the BCL-2 family of apoptosis regulators, with the PI3K pathway

identified as a druggable target (Courtney et al., 2010), with PI3K inhibitor drugs (e.g., Idelalisib) in use for breast cancer (Yang et al., 2019) and lymphoma (Flinn et al., 2014). Akt1 also facilitates cell cycle progression (Chang et al., 2003) and cross talks to various related signalling pathways involved with cell growth proliferation, including the Ras-Ref-MEK-ERF (Mitogen-activated protein kinase (MAPK)) and Nuclear factor kappa B (NF-κB) (He et al., 2021).

6.1.1.4 BCR and Ras-MAPK signalling

The MAP kinase cascade, which terminates on the effector ERK1/2 transcription regulator, is another important cell signalling pathway which results in cell growth and proliferation effects. In B cells, Ras is activated downstream of PLCG2 and in parallel via DAG activation of RasGRP (RAS guanyl nucleotide-releasing protein) (Cantrell, 2015). The chain of activating phosphorylation from Ras, Raf, Mek and ERK1/2 leads to gene transcription promoting cell growth, and Raf links to control of the cell cycle via activation of the cdc25 phosphatase which in turn activates cyclin dependent kinases (CDKs) (McCubrey et al., 2007), providing an interesting link between BCR activation and cell cycle progression.

Activation of the BCR leads to multiple cellular responses which increase cell growth, proliferation, resistance to apoptosis, with PLCG2 a key relay in the signalling cascade, meaning that if thienopyridine targeting of PLCG2 was successful, it could explain the apoptotic effects observed in Chapter 3.

6.1.2 Identifying potential targets of novel thienopyridine effects on cell cycle progression

6.1.2.1 The cell cycle in B cells

As shown in Figure 6-1, there are four classical stages of cell cycle control: G_1/G_0-phase (growth phase 1), S-phase (synthesis phase), G_2-phase (growth phase 2) and M-phase (mitosis). Upstream signalling cascades are implicated in the cell decision to proliferate, with ERK implicated in several stages of cell cycle progression including G_1/S phase and the G_2/M transition (Chambard et al., 2007). Movement through each phase of the cell cycle is regulated by interactions between Cyclin dependent kinases (CDKs), which bind to and are activated by specific Cyclins (See Figure 1-3). A cell's decision to progress from the resting G1/G0-phase through to duplication of DNA and cell organelles in S-phase is controlled by the interaction between CDK4/6 and Cyclin D isoforms at the restriction point (See Figure 1-4) (Deshpande et al., 2005; A. Singh et al., 2022). Targets of these kinase complexes including upregulation of Cyclin E and A, which are necessary for progression through to S-phase, via the inhibitory phosphorylation of retinoblastoma protein (RB), which releases the E2F transcription factor and commits the cell to S-phase (see Figure 1-3 and Figure 1-4) (Kastan and Bartek, 2004; Murray, 2004; Deshpande et al., 2005). Progression through to S-phase is coordinated by CDK2-Cyclin E (responsible for DNA replication), CDK2-Cyclin A and CDK1-Cyclin A complexes (responsible for DNA replication and chromosome segregation) (Kastan and Bartek, 2004), with CDK1-Cyclin B becoming the dominant complex which oversees the cell's commitment to mitosis and cell division (Malumbres and Barbacid, 2009; Martinez-Alonso and Malumbres, 2020).

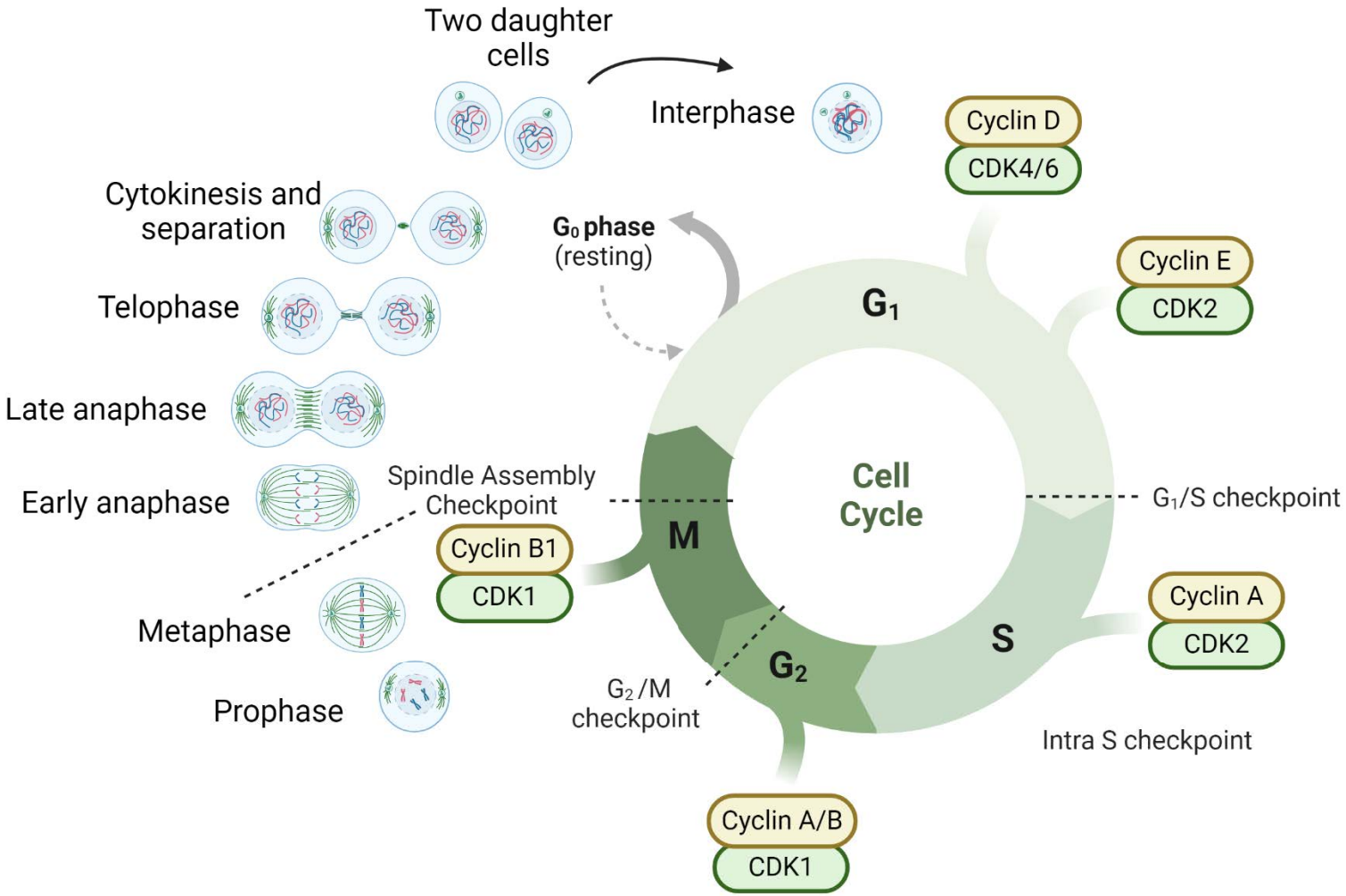

Figure 6-1 The phases of the cell cycle, associated checkpoints and Cyclin/cyclin dependent kinase regulators of each phase. The stages of mitosis are depicted from chromosome condensation at Prophose, chromosme alignment at metaphase, division of sister chromatids at anaphase and seperation into two daughter cells at telophase and cytokinesis. Created with BioRender.com

6.1.2.2 The G_2/M Checkpoint

Throughout cell cycle phases, there are several checkpoints at which the cell ensures conditions are favourable for division (see section 1.6). Based on the results shown in Chapter 3 and 4, and the evidence that DAUDI cells are showing a tetraploid phenotype, containing two copies of all chromosomes at mitosis, the G_2/M and Spindle Assembly checkpoints are most relevant to this study. G_2 arrest can be triggered by DNA damage either single or double strand breaks (Bartek and Lukas, 2007), with response elements such as ATM/ATR Ataxia-telangiectasia-mutated (ATM)/ ataxia telangiectasia and Rad3-related (ATR), p53 and Chk1 (Checkpoint Kinase 1) (Roos and Kaina, 2013; Ovejero et al., 2020) which pause the cell cycle until the underlying fault has been corrected (see Figure 6-2).

One of the limitations of analysing the cell cycle via flow cytometry (see Chapter 3 results in section 3.4) is that the cell analysis does not identify the cause of cell cycle arrest or any post-translational modifications applied to key cell cycle kinases, merely how much DNA is present in the cells, therefore further investigation in required to elucidate the mechanism of action of the novel thienopyridines.

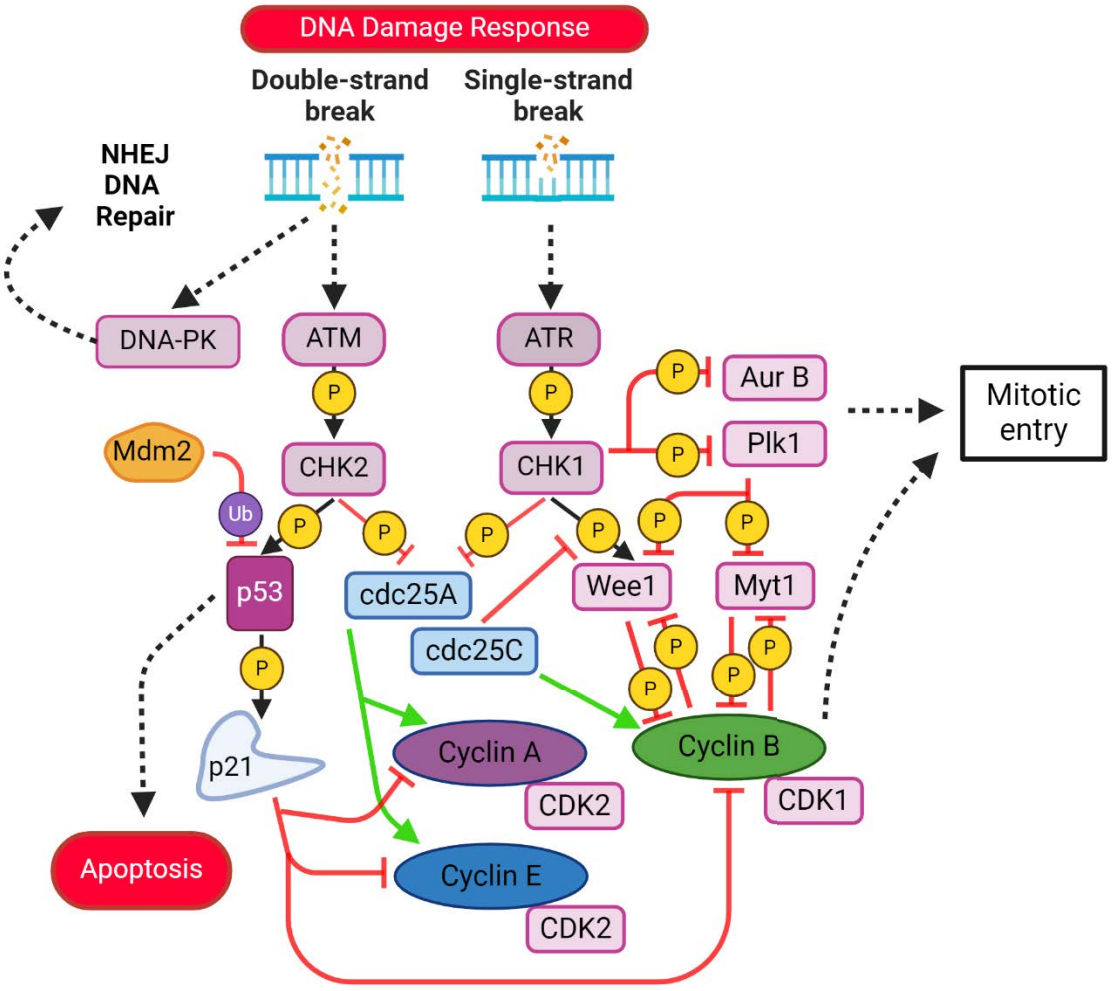

Figure 6-2 The DNA Damage Response Checkpoint in response to double- and single-strand breaks is mediated by the kinases ATM and ATR throughout G_1, S, and G_2 phases of the cycle.

ATM signals via checkpoint kinase 2 (CHK2) to inhibit CDK2 in complex with both Cyclin A and E at the restriction point and throughout S-phase. This is achieved indirectly via phosphorylation of p53 at the recognition site of its mediator Mdm2 (Mouse double minute 2 homolog) which prevents p53 degradation via ubiquitination. In turn p53 upregulates p21 production which directly sequesters both CDK2-Cyclin A and CDK2-Cyclin E complexes. CHK2 also inhibits cdc25A preventing its ability to strip CDK2 of inhibitory phosphorylation by Wee1 (not shown on diagram for clarity). Double strand breaks also activate the DNA-PK kinase which can orchestrate non-homologous end joining repair of the DNA.

The mitotic cyclin dependent kinase CDK1 is activated by its cofactor Cyclin B in late G_2 where progression through to M phase can be restricted by ATR kinase and is downstream effector checkpoint kinase 1 (CHK1) via a variety of phosphorylation events. Targets of CHK1 include Myt1 and Wee1 kinases which in turn add inhibitory phosphorylation to CDK1/CDK2 at threonine-14 and tyrosine-15. CHK1 also inhibits cdc25C at G_2 to prevent CDK1 dephosphorylation, as well as inhibiting Aurora B kinase and Polo-like kinase 1(Plk1) which help to prime the cell for mitosis. Inhibition of Plk1 has the dual effect of inhibiting an inhibitor of Wee1 and Myt1 with the global effect of stall entry to mitosis until DNA damage has been repaired, or triggering p53 directed apoptosis. Created with BioRender.com and based on information in (Kastan and Bartek, 2004; Reinhardt and Yaffe, 2009; Pennycook and Barr, 2020; Rubin et al., 2020; Neizer-Ashun and Bhattacharya, 2021; Matthews et al., 2022)

6.1.2.3 The Spindle Assembly Checkpoint

The Spindle Assembly Checkpoint (SAC), timed at chromosome alignment on the mitotic spindle at the metaphase to anaphase transition is also key to maintaining fidelity of DNA before cytokinesis (see Figure 6-3). At the kinetochores, the site for chromosome attachment to the microtubule spindle poles, any unattached chromosomes are detected by tension sensing kinases such as Aurora B (Musacchio, 2015), as well as parts of the outer kinetochore KNL complex (Lara-Gonzalez et al., 2019; Lara-Gonzalez et al., 2021) triggering the building of a regulator complex of proteins known as the Mitotic Checkpoint Complex (MCC) which inhibits progression of the cell cycle until all kinetochores are correctly connected (Musacchio and Salmon, 2007) (see section 1.6.1.4 and figure Figure 1-7). As soon as the MCC is inactivated, it triggers ubiquitination of the Cyclin B1 in the Mitosis Promoting Factor (MPF, CDK1-Cyclin B1) complex, via upregulation of the Anaphase Promoting Complex/Cyclosome (APC/C) (Kapanidou et al., 2017), with cdc20 key to both the activation of the MCC and APC/C (Kernan et al., 2018).

APC/C_{cdc20} and APC/C_{Cdh1} targets and rapidly degrades key mediators of the SAC and G_2/M DNA damage response, with both targeted at limiting the activity of CDK1 bound to Cyclin B either to halt cell cycle progression but with only the completion of SAC resulting in reduction of the Cyclin B protein itself, allowing for a key distinction in post-translation modification between the two checkpoints.

Elicitation of how cells with tetraploid chromosome content have been generated following treatment with the novel thienopyridine compounds, whether this is via the DNA damage response or the SAC, will provide further understanding of the mechanism of action of these compounds *in vitro*.

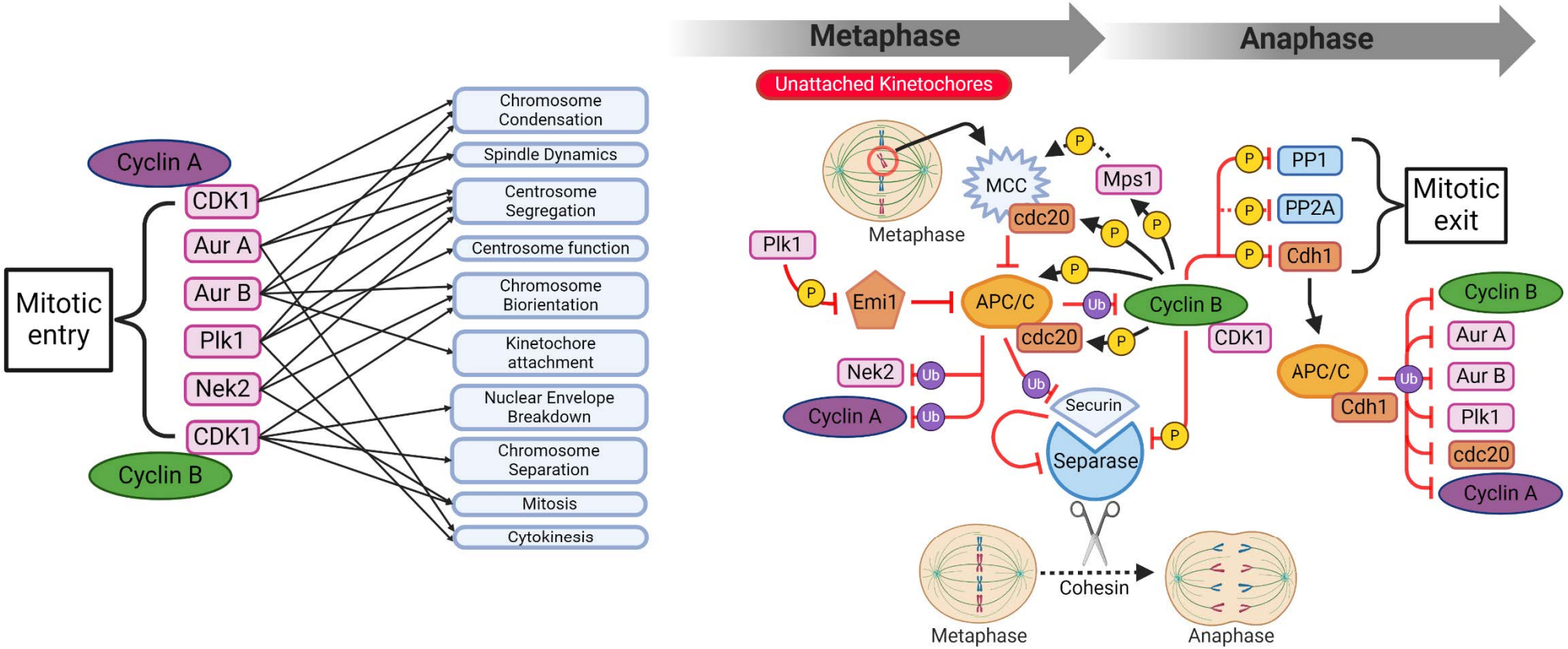
Mitotic entry
Cyclin A
CDK1
Aur A
Aur B
Plk1
Nek2
CDK1
Cyclin B
Chromosome Condensation
Spindle Dynamics
Centrosome Segregation
Centrosome function
Chromosome Biorientation
Kinetochore attachment
Nuclear Envelope Breakdown
Chromosome Separation
Mitosis
Cytokinesis
Metaphase
Anaphase
Unattached Kinetochores
Metaphase
MCC
Mps1
cdc20
Plk1
Emi1
APC/C
Ub
Cyclin B
cdc20
CDK1
Nek2
Cyclin A
Securin
Separase
PP1
PP2A
Cdh1
Mitotic exit
APC/C
Cdh1
Cyclin B
Aur A
Aur B
Plk1
cdc20
Cyclin A
Cohesin
Metaphase
Anaphase

Figure 6-3 Kinase, phosphatase and Ubiquitin E3 ligase control of entry and exit from mitosis, via the Spindle Assembly Checkpoint (SAC).

A wave of phosphorylation events, driving by CDK1, the Aurora, Polo-like kinase and Nek families primes the cell for mitosis, including all of the physical changes in cell architecture required for chromosome condensation, nuclear envelop breakdown, chromosome alignment, spindle formation, spindle attachment, chromatid segregation and cytokinesis. Final commitment to cell division is achieved when all chromosomes are connected to the mitotic spindle at their kinetochores at the Spindle Assembly Checkpoint at the metaphase to anaphase transition. Unattached kinetochores generate the Mitotic Checkpoint Complex (MCC) which sequesters the cofactor protein cdc20 away from the Anaphase Promoting Complex/Cyclosome E3 Ubiquitin ligase. APC/C_{cdc20} ubiquitination and proteosome degradation of securin (and the subsequent enzymatic cleavage of cohesin at the chromosome-connecting centromeres) is the event which triggers chromosome separation and progression to anaphase, telophase and finally cytokinesis.

CDK1-Cyclin B1 phosphorylates thousands of targets to prepare the cell for mitosis, as well as priming APC/C for activation as soon as the SAC is fulfilled. CDK1 also helps to activate the MCC via phosphorylation of Mps1 (monopolar spindle 1 kinase) and inhibition of PP1 and PP2A family phosphatases, and inhibitory phosphorylation of separase. When all kinetochores are successfully attached, the MMC is rapidly inactivated, freeing APC/C from competitive inhibition and allowing cdc20 targeted ubiquitination of Cyclin A, Nek2, Cyclin B and securing to promote chromosome separation. The balance of phosphorylation events by CDK1 inactivation then tips towards the PP1 and PP2A phosphatases, with PP1 reversing many of CDK1 phosphorylation targets to allow the cell to exit mitosis back into $G_{1/0}$. APC/C_{Cdh1} maintains the inhibition of CDK1 via continued ubiquitination of Cyclin A and B, as well as destroying cdc20, Aurora A and B and Plk1, further removing key mitotic kinases from the G_1 cell.

Created with BioRender.com and based on information in (Kops et al., 2005; Malumbres and Barbacid, 2007; Musacchio and Salmon, 2007; Malumbres and Barbacid, 2009; Malumbres, 2014; Musacchio, 2015; Hayward et al., 2019; Holder et al., 2019; Lara-Gonzalez et al., 2019; Martinez-Alonso and Malumbres, 2020; Lara-Gonzalez et al., 2021; Greil et al., 2022)

6.2 Aims and objectives

6.2.1 Aims

The main aim of this chapter was to investigate key genes and proteins regulating the BCR and regulators of cell cycle control in DAUDI B lymphocytes, to try to identify potential mechanisms for thienopyridine effects on cells.

6.2.2 Objectives

- To investigate gene expression relating to cell cycle checkpoints and B cell receptor signalling using RT-qPCR.
- To assess the expression of key proteins regulating these pathways and their post-translational modifications via Western blotting.

6.3 Methods

6.3.1 Reverse Transcription Quantitative Polymerase Chain Reaction (RT-qPCR) assay

Preparation of DAUDI cells, treatment with thienopyridines, paclitaxel and nocodazole controls, IgM stimulation, extraction of RNA, reverse transcription of RNA to cDNA and dilution of cDNA to working stock for these assays were as described in Chapter 2 (see section 2.2.13) and for the establishment of stable reference genes in Chapter 5.

6.3.1.1 RT-qPCR cDNA standards and calculation of primer efficiencies

Pooled cDNA standards were prepared as per section 2.2.13.4, and a five-point dilution of standards was run alongside experimental samples in duplicate on each gene of interest qPCR plate. Primer efficiencies were calculated using the standard curve calculated by CFX Maestro software. Any failed standard curves were repeated, either at 1:10 dilution, 1:5 dilution or 1:2 dilution depending on the expression of the gene in the experimental samples. All primer efficiencies are listed in Table 6-1. Only primers with an efficiency between 90-100 % were included in this Chapter. Two set of primers, for Nek2 and Nek4, fell outside of this range and their results have been included in Appendix Section 8.2.

6.3.1.2 Gene of interest primer design

All primers for genes of interest were designed using NCBI Primer Blast as described in section 2.2.13.6. Full forward and reverse primer sequences are listed in Table 6-1, together with details of any primers which failed (either due to low gene expression or primer dimer formation).

6.3.1.3 Thermocycling conditions, digital assessment of RT-qPCR products and confirmation of estimated product size via DNA gel electrophoresis

All thermocycling conditions were determined via use of pooled cDNA using Tm gradient RT-qPCR assay as described in section 2.2.13.9. Digital assessment of melt curves and confirmation of product size via DNA gel electrophoresis was as listed in section 2.2.13.8.3

6.3.1.4 Data collection and analysis

All data was collected and screened using CFX Maestro software as described in section 2.2.13.12. Data was exported to Microsoft Excel as averaged Ct of technical replicates, outliers were removed using the strategy listed in section 2.2.13.12.1, normalised using the 'Vandesompele method' to the stable reference genes identified in Chapter 5 (TBP, PPIA, RPLP0 and EIF2B1 genes respectively), Log_2 transformed and transferred to GraphPad Prism software for statistical analysis. All data was analysed by thienopyridine chemical group using one-way ANOVA with Dunnett's post hoc test, with all experimental treatments compared to the IgM stimulated DAUDI untreated controls. All experimental figures were also produced in GraphPad Prism software.

Table 6-1 List of primer sequences, expected primer product sizes, calculated primer efficiencies and standard curve dilution range for all genes of interests

Oligo sequence (5' to 3')	Oligo name	NCBI Accession Number	NCBI Input PCR template	Primer Product Size	% Efficiency	Standard Dilutions?
CAATCCGTCCATGCCTCAGA	PLCG2 Forward	NM_002661.5	Homo sapiens phospholipase C gamma 2 (PLCG2)	182	94%	1:10 (4 logs)
CCTCGACGTAGTTGGATGGG	PLCG2 Reverse					
AGCACAACTCTGCAGGACTC	BTK Forward	NM_000061.3	Homo sapiens Bruton tyrosine kinase (BTK), transcript variant 1	98	106.10%	1:10 (4 logs)
CCATGATCCGTATCCCAGGC	BTK Reverse					
CTGCACAAACGAGGGGAGTA	AKT1 Forward	NM_005163.2	Homo sapiens AKT serine/threonine kinase 1 (AKT1), transcript variant 1	142	99.40%	1:10 (4 logs)
GCGCCACAGAGAAGTTGTTG	AKT1 Reverse					
GCCTGAACCAGATGCTCAGAG	Chk1 forward	NM_001114122.3	Homo sapiens checkpoint kinase 1 (CHEK1), transcript variant 1	51	102.20%	1:10 (4 logs)
ACCACCCCTGCCATGAGTT	Chk1 reverse					
CAGGATAATTGTGTGCCCAAGA	Cyclin B forward	NM_001354844.2	Homo sapiens cyclin B1 (CCNB1), transcript variant 2	52	105.70%	1:10 (5 logs)
TGGCAGTGACACCAACCAGT	Cyclin B reverse					
ACACGCTTCCCTGGATTGG	p53 forward	NM_001276761.3	Homo sapiens tumor protein p53 (TP53), transcript variant 2	132	94.00%	1:10 (5 logs)
TTTCAGGAAGTAGTTTCCATAGGT	p53 reverse					
TGTGATGCGCTAATGGCG	p21 forward	NM_001374511.1	Homo sapiens cyclin dependent kinase inhibitor 1A (CDKN1A), transcript variant 8	55	101.00%	1:10 (4 logs)
CGAAGTTCCATCGCTCACG	p21 reverse					
AAACTACAGGTCAAGTGGTAGCC	cdc2 forward	NM_001786.5	Homo sapiens cyclin dependent kinase 1 (CDK1), transcript variant 1	148	101.00%	1:10 (5 logs)
TCCTGCATAAGCACATCCTGA	cdc2 reverse					
AATGTGTGGCCTAGTGCTCC	Cdc20 Forward	NM_001255.3	Homo sapiens cell division cycle 20 (CDC20)	92	90.40%	1:10 (5 logs)
CACCATGCTACGGCCTTGA	Cdc20 Reverse					
CCGAGTTCTTCTCATTCGGC	MAD2L1 (Mad2) FWD	NM_002358.4	Homo sapiens mitotic arrest defi cient 2 like 1 (MAD2L1)	103	102.00%	1:10 (5 logs)
ACAAGCAAGGTGAGTCCGTA	MAD2L1 (Mad2) RVS					
CAGGTCTTCTGGGATGGGTC	BubR1 Forward	NM_001211.6	Homo sapiens BUB1 mitotic checkpoint serine/threonine kinase B (BUB1B)	70	93.60%	1:10 (5 logs)
ACAATTCACCATCTTTTAGCTCAG	BubR1 Reverse					
GGCAATGACCCTCTTGGTGA	Bub1 Forward	NM_004336.5	Homo sapiens BUB1 mitotic checkpoint serine/threonine kinase (BUB1), transcript variant 1	187	100.20%	1:10 (4 logs)
GGTCACTGTTGTACTCAGCAAAT	Bub1 Reverse					
AGCAGATCCGTTCGAAGTCC	MAD1L1 (Mad1) FWD	NM_003550.3	Homo sapiens mitotic arrest defi cient 1 like 1 (MAD1L1), transcript variant 1	137	93.50%	1:5 (5 logs)
GTCGACCTCACGCTCGTAGT	MAD1L1 (Mad1) RVS					
GAAGGCGATGGCGGATTTAG	PPP1CC (PP1G) FWD	NM_002710.4	Homo sapiens protein phosphatase 1 catalytic subunit gamma (PPP1CC), transcript variant 1	76	100.20%	1:10 (5 logs)
CTTGGACCCTCTCACTTCCAG	PPP1CC (PP1G) RVS					
ATGGAGGCTGGTTTCTTGCC	(PP2A)-B56 FWD	NM_002719.4	Homo sapiens protein phosphatase 2 regulatory subunit B'gamma (PPP2R5C), transcript variant 1	167	Primer Dimers	Redesigned Primers
GATCAGCAGGAGGAACATCTCG	(PP2A)-B56 RVS					
GCCTTTCCCGCTGAAGTCTA	(PP2A)-B56 FWD 2	NM_002719.4	Homo sapiens protein phosphatase 2 regulatory subunit B'gamma (PPP2R5C), transcript variant 1,	175	92.80%	1:10 (4 logs)
GGACGCAACACTGACGTAAC	(PP2A)-B56 RVS 2					
CCAGGCTTGAGCTAGGTTT	Cdc25C FWD	NM_001790.5	Homo sapiens cell division cycle 25C (CDC25C), transcript variant 1	270	109.60%	1:5 (5 logs)
AGATCGAGGCAACGTTTTGG	Cdc25C RVS					
GTCTCTGGCAAGTAATCCAGAACT	Nek2 Forward	NM_002497.4	Homo sapiens NIMA related kinase 2 (NEK2), transcript variant 1	151	84.30%	1:10 (5 logs)
CTTCAGGTCCTTGCACTTGG	Nek2 Reverse					
AGGAGTGGACTAGGGTCGCC	Nek3 Forward	NM_002498.3	Homo sapiens NIMA related kinase 3 (NEK3), transcript variant 1	94	Low expression	N/A
CATCCATGCTGGGGCATCCA	Nek3 Reverse					
CGGGACGGCAAGCAGTATGT	Nek4 Forward	NM_003157.6	Homo sapiens NIMA related kinase 4 (NEK4), transcript variant 1,	124	Low expression	N/A
AGGTGACAATGTTGGGATGCT	Nek4 Reverse					
ATGCCCAGGAGAGAAGTTTGC	Nek6 Forward	NM_001145001.3	Homo sapiens NIMA related kinase 6 (NEK6), transcript variant 1	271	Low expression	N/A
TGAACTGTCCTCGGCCTATC	Nek6 Reverse					
CTCCCAACTTCCTGAGTTCTAA	Nek7 Forward	NM_133494.3	Homo sapiens NIMA related kinase 7 (NEK7)	215	126.00%	1:10 (3 logs)
ACTCCATCCAAGAGACAGGC	Nek7 Reverse					
ATCAACTCGGACTTTGGGAGC	Nek9 Forward	NM_001329237.2	Homo sapiens NIMA related kinase 9 (NEK9), transcript variant 1	196	Low expression	N/A
CAACCAGTGAGTCATCCTCG	Nek9 Reverse					
AGCGCGGATCCTAGACAAC	p31 Forward	NM_001003690.2	Homo sapiens MAD2L1 binding protein (MAD2L1BP), transcript variant 1	288	Low expression	N/A
GGGAGGCGTGAGTTTCTTCG	p31 Reverse					
CTTCCCTGTGTGGCCGAGT	TRIP13 Forward	NM_004237.4	Homo sapiens thyroid hormone receptor interactor 13 (TRIP13), transcript variant 1	245	105.80%	1:10 (5 logs)
CATGCACTCAAATCGATGGGC	TRIP13 Reverse					
CGGAAAGGAGTTTGGGTTCC	MPS1 Forward	NM_003318.5	Homo sapiens TTK protein kinase (TTK), transcript variant 1	300	Primer Dimers	N/A
GCATCACTTAGCGGAACACTG	MPS1 Reverse					
AGTACGGCCTTGGGTATCAG	PLK1 Forward	NM_005030.6	Homo sapiens polo like kinase 1 (PLK1)	118	99.70%	1:10 (5 logs)
GTGCCGTCACGCTCTATGTA	PLK1 Reverse					
CATCACCACCATTCGCACTCG	PLK2 Forward	NM_006622.4	Homo sapiens polo like kinase 2 (PLK2), transcript variant 1	73	97.70%	1:10 (4 logs)
AGTAGCGCTTCCCAGTCGT	PLK2 Reverse					
AGCGGCGGTTTAGAGAGC	PLK4 Forward	NM_014264.5	Homo sapiens polo like kinase 4 (PLK4), transcript variant 1	168	102.20%	1:10 (4 logs)
TTTCCAACTTTAAAATCCTCGATCT	PLK4 Reverse					
GTTACTTATTACAGCTAGAGGGTCT	Aurora A FWD	NM_198433.3	Homo sapiens aurora kinase A (AURKA), transcript variant 1	292	Primer Dimers	N/A
CCAACTGGAGCTGTAGCCTTA	Aurora A RVS					
CACCCGACATCTTAACGCGG	Aurora B FWD	NM_004217.4	Homo sapiens aurora kinase B (AURKB), transcript variant 1	76	95.50%	1:5 (4 logs)
CCAAACTTGCCTTTGCCCAG	Aurora B RVS					
GCGCACAGCCACGATAATAGA	Aurora C FWD	NM_001015878.2	Homo sapiens aurora kinase C (AURKC), transcript variant 1	199	Low expression	N/A
CGGCAAGTAGTCCAGTGTCC	Aurora C RVS					
ACGAATCTCCGACCACCACT	IL-1β Forward	NM_000576.3	Homo sapiens interleukin 1 beta (IL1B)	65	105.00%	1:10 (4 logs)
CCATGGCCACAACAACTGAC	IL-1β reverse					
GATTTCTGCAGCTCTGTGTGAA	IL-8 forward	NM_000584.4	Homo sapiens C-X-C motif chemokine ligand 8 (CXCL8), transcript variant 1	192	100.90%	1:2 (6 logs)
AGACAGAGCTCTCTTCCATCA	IL-8 reverse					

6.3.2 Western blot assay

6.3.2.1 Western blot cell lysate preparation

DAUDI cell cell lysates were prepared as per section 2.2.12. Working stocks of each biological replicate were diluted to 8 µg concentration in 12 µL RIPA buffer with 1:1000 phosphatase and 1:1000 protease inhibitor cocktail as per section 2.2.12 and stored at -20 °C until use. Each western blot consisted of three technical replicates of each thienopyridine treated lysate and untreated IgM stimulated controls, and one technical replicate of any nocodazole, paclitaxel, UV-treated DAUDI lysate positive control or Jurkat cell lysate controls.

6.3.2.2 Western blot gel electrophoresis and wet transfer to PVDF membranes

All western blot electrophoresis and wet transfer was conducted as per section 2.2.12.10. Proteins were transferred to Immobilon-FL PVDF membrane (Merck/Millipore, Hertfordshire, UK) under the wet transfer conditions listed in section 2.2.12.10

6.3.2.3 Total protein staining

All western blots were total protein stained using Li-Cor REVERT Total Protein staining kit (LI-COR Biosciences UK Ltd, Cambridge, UK) as described in section 2.2.12.11.

Total protein staining was selected as a dual method to check transfer of proteins from acrylamide gels to PVDF membranes and to provide data for normalisation. With blots imaged as per the REVERT manufacturers protocol on the 700 nm channel of the Odyssey® Fc Imaging System (LI-COR Biosciences UK Ltd, Cambridge, UK) as per section 2.2.12.14.

6.3.2.4 Western blot blocking and incubation with primary and secondary antibodies

All western blots were blocked as per section 2.2.12.12 with Intercept® Blocking Buffer in Tris Buffer Saline (TBS) (LI-COR Biosciences UK Ltd, Cambridge, UK). All primary and secondary antibodies were prepared in Intercept® (TBS) Blocking Buffer as per Table 2-1 Western Blot Buffer Recipes. Blots were incubated with primary

antibody overnight, followed by wash steps, secondary antibody incubation and drying as per section 2.2.12.13 prior to imaging on the Odyssey® Fc Imaging System.

6.3.2.5 Western blot imaging

As described in section 2.2.12.14.

6.3.2.6 Western blot image analysis, local background subtraction and generation of densitometry data

Western blot images were analysed and processed using Image Studio 5.x CLx (LI-COR Biosciences UK Ltd, Cambridge, UK) and Image Studio Lite (LI-COR Biosciences UK Ltd, Cambridge, UK).

Densitometry for each individual image from REVERT staining, and the respective 700 nm or 800 nm channel of single or multiplex blots was assessed in Image Studio. For each blot image, rectangle analysis shapes were added to surround all area of signal for each lane on the western blot (Figure 6-4A, D-E) and positioned using pixel intensity vs location plots to ensure all of the relevant signal for each band was included in analysis. Rectangles were maintained as the same pixel area across wells on each blot to ensure consistency in analysis and were sized to the largest band on the blot but may have been rotated to accurately surround the expression band based on blot-to-blot variation in transfer. Image Studio software background measurement was applied to either the area above and below, or left/right side of the analysis shape and subtraction was calculated by the software (Figure 6-4C). All relevant colours used in images are pseudo-colours for illustration purposes and for user identification of position of expression bands only; densitometry data was generated based on pixel density of the image and 'Signal' value (after background subtraction) was used for all further data analysis (Figure 6-4G).

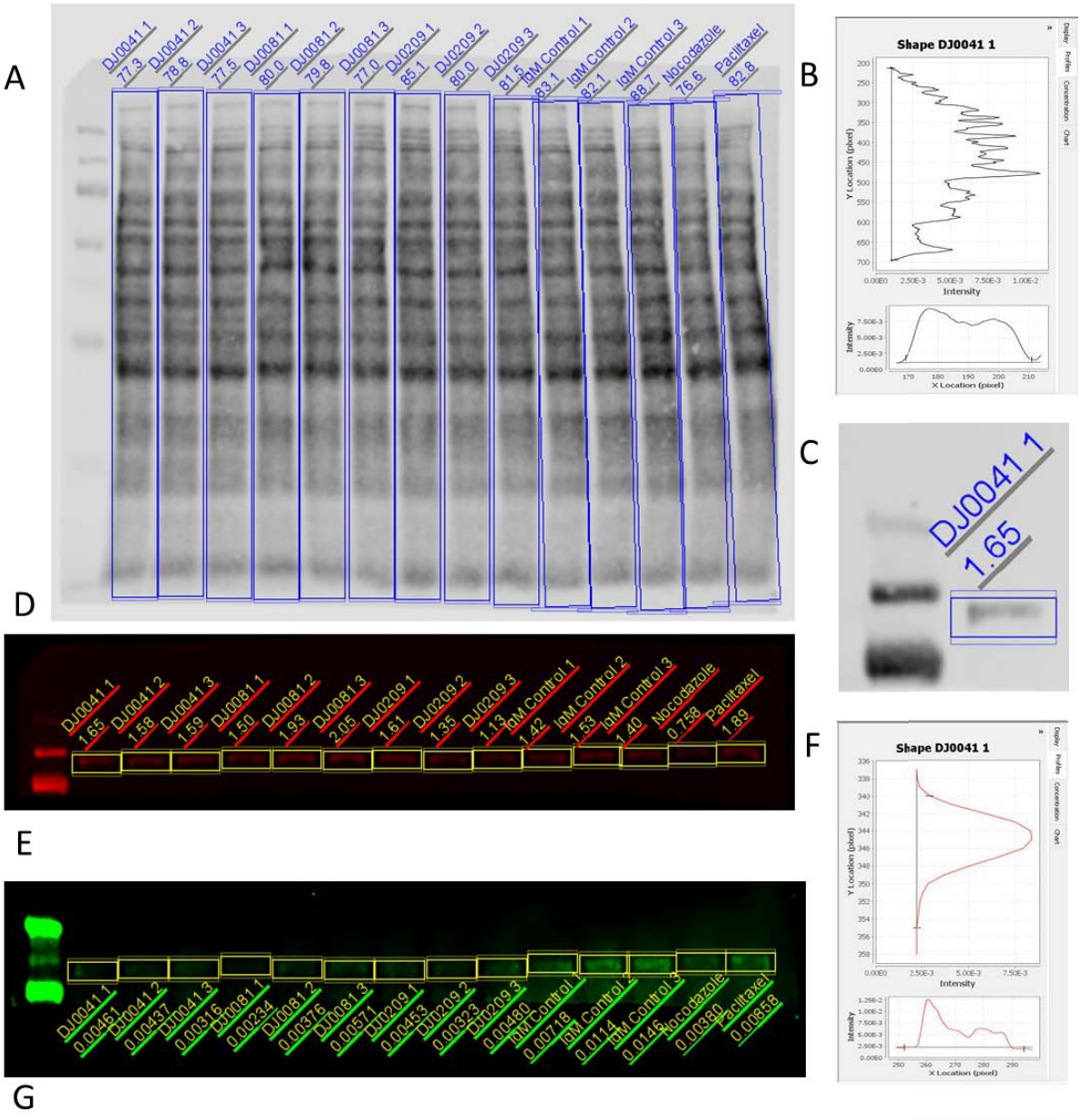

Image Name	Channel	Name	Signal	Total	Area	Bkgnd.	Type
0000021_01	700	DJ0041 1	1.65	3.17	688	0.00221	Signal
0000021_01	700	DJ0041 2	1.58	2.87	688	0.00187	Signal
0000021_01	700	DJ0041 3	1.59	2.84	688	0.00182	Signal

Figure 6-4Example of western blot densitometry analysis strategy in Li-cor Image Studio software. Addition of analysis shapes (rectangles) for total protein stain image (A) and use of pixel intensity vs location plots to accurately position analysis shapes (B). Detail of rectangle fitting to western blot expression band, showing background subtraction above and below rectangle (C). Example of 700 nm channel (pseudo-coloured red) (D) and 800 nm channel (pseudo-coloured green) (E) analysis shape positioning and associated pixel intensity vs location plots for these channels (F). Image Studio data for 'Signal', 'Total Signal', 'Area' of analysis shape, and local 'Background' following positioning of analysis shapes on western blot image (G).

6.3.2.7 Western blot data normalisation strategy

Data for all technical and biological replicates of each western blot target protein was exported from Image Study and collated in Microsoft Excel. A two-step normalisation strategy was used, with pan-proteins normalised to the signal of the total protein stain and phospho-proteins normalised to the pan-protein expression each for the corresponding lane of the blot.

First, a 'lane normalisation factor' (LNF) was calculated where the signal from each individual lane was divided by lane showing the highest signal on the blot:

Lane normalisation factor = lane signal/highest signal

Total protein LNF = Total protein lane signal/highest total protein signal

Pan-protein LNF = Pan-protein lane signal/highest pan-protein lane signal

Next, the signal from each lane was divided by the corresponding lane normalisation factor to give a 'normalised ratio' (NR):

Normalised ratio = target signal/LNF

Pan to total protein NR = pan-protein signal / total protein LNF

Phospho to pan protein NR = phospho-protein signal / pan-protein LNF

Finally, the 'relative normalised ratio' (RNR) was calculated, by dividing the NR by the average of the untreated control NR values:

Relative normalised ratio = Lane NR / (mean NR untreated controls)

By this method, the mean RNR for untreated controls becomes 1, and the expression of all proteins and phospho-targets is an expression of this value, with values <1 showing decreased expression while values >1 show increased expression.

The relative normalised ratio of protein expression was then used for further data and statistical analysis.

Averages, standard deviation, and percentage CV values calculated for all technical replicates of each target RNR and CV values were used to screen outliers prior to data analysis.

6.3.2.8 Western blot data analysis and statistics

Average technical RNR values for each set of thienopyridine-treated DAUDI biological replicates were then used for statistical analysis in GraphPad Prism. Data was analysed for normality using the Shapiro-Wilk normality test and then statistics were generated using one-way ANOVA and Dunnett's post hoc test, where all treated samples were compared to untreated controls. Significance was expressed as * = $p \leq 0.05$, ** = $p \leq 0.01$ and ***= $p \leq 0.001$.

6.4 Results

6.4.1 Effects of novel thienopyridines on regulation of cell cycle progression gene transcription via the Mitotic Checkpoint Complex

RT-qPCR was used to study the effects of novel thienopyridines on the expression of mature RNA (mRNA) for genes regulating the transcription of protein components of the Mitotic Checkpoint Complex (MCC), a key regulator of cell cycle progression in response to incomplete alignment of sister chromosomes on the mitotic spindle (McAinsh and Kops, 2023). Cell division cycle 20 (cdc20), mitotic arrest deficient 2 (Mad2), mitotic arrest deficient 1 (Mad1), Mitotic spindle checkpoint protein BUBR1 (BubR1) and BUB1 Mitotic Checkpoint Serine/Threonine Kinase (Bub1) are all core components of the human MCC, while Aurora kinase B (Aurora B) and Polo-like kinase 1 (PLK1) are known mediators of MCC assembly during failed chromosome alignment (Izawa and Pines, 2015); Aurora B phosphorylates targets to trigger MCC assembly (H. T. Ma and Poon, 2020) a while PLK1 phosphorylates targets to recruit phosphatases (e.g., (PP2A)-B56) which trigger the disassembly of the MCC upon chromosome alignment (Lara-Gonzalez et al., 2019).

6.4.1.1 Effects of cyclooctane thienopyridines on cell cycle progression mediated by the Mitotic Checkpoint Complex

By far the largest changes induced by this set of compounds with regards to genes involved in the MCC was to the expression of cdc20 (Figure 6-5A). There was a general trend of increased expression (found to be statistically significant from non-thienopyridine treated IgM-stimulated control cells) following all treatments with the cyclooctane compounds, mirroring that of the well-established disruptors of spindle formation, paclitaxel and nocodazole. Exceptions to this were the compounds DJ0021 and DJ0209 that did not induce any statistically significant changes to cdc20. As stated in previous chapters, DJ0021 appears an inactive compound as despite its cyclooctane ring, it has the addition of a -OMe group which has previously been described as a “non-favourable substitution” on the para-position (Feng et al., 2012; Arabshahi et al., 2014; Hung et al., 2014). Therefore, the lack of induction of cdc20 by this compound is not surprising. Additionally, DJ0209 has, in previous chapters

shown inactivity at low concentrations, but a small degree of activity at higher concentrations. Again, this has been attributed to the non-favourable -Cl group on its side chain. Of the cyclooctane compounds DJ0014, DJ0199 and DJ0206 were found to be the most potent at inducing cdc20 mRNA levels, inducing +2.774, +2.446 and +2.758-fold changes respectively (all $p \leq 0.001$ from control).

When Mad2 mRNA levels were considered, there was a general trend of increased expression following treatment with the cyclooctane thienopyridines (Figure 6-5B), and again this trend was also seen following paclitaxel and nocodazole treatment. However, generally the increased trends observed were not statistically significant, and only compound DJ0199 was able to significantly increase Mad2 mRNA compared with levels in control cells (+2.111 fold change, P=0.039).

Analysis of Mad2 (Figure 6-5C), BubR1 (Figure 6-5D), Bub1 (Figure 6-5E), Aurora B (Figure 6-5F) and PLK1 (Figure 6-5G) were not significantly affected by treatment with any of the compounds (when tested by one-way ANOVA with Dunnett's post-hoc test). However, there was a general trend of increased BubR1 levels following treatment with the thienopyridines and this change appeared to be greater than that induced by either paclitaxel or nocodazole (Figure 6-5D). In general, in terms of the $\log_2$ fold changes in gene expression, there was very little to note with regards to cyclooctane-induced changes to Mad2, Bub1, Aurora B or PLK1.

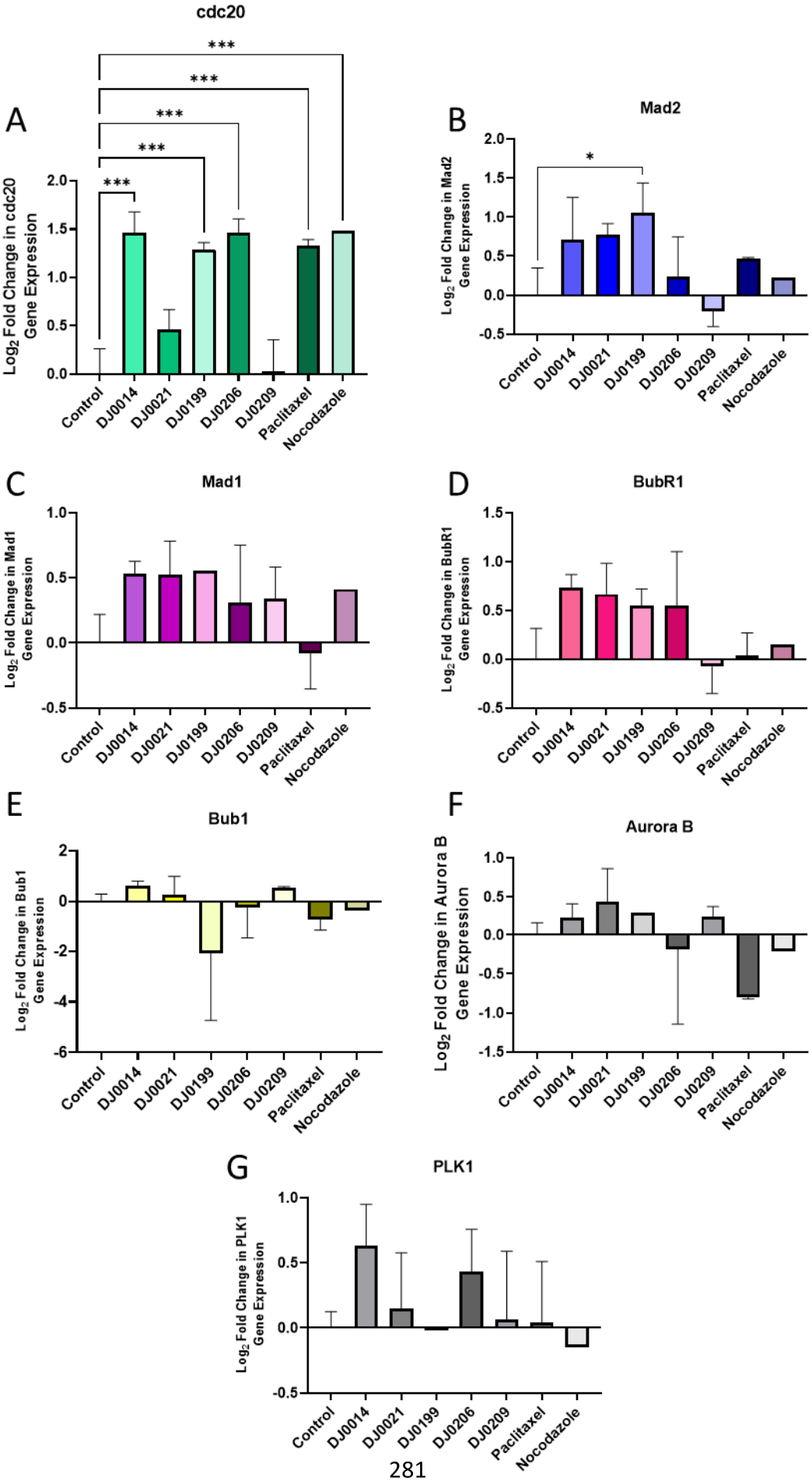
A
cdc20
***
***
***
***
***
Log2 Fold Change in cdc20 Gene Expression
2.0
1.5
1.0
0.5
0.0
Control
DJ0014
DJ0021
DJ0199
DJ0206
DJ0209
Paclitaxel
Nocodazole
B
Mad2
*
Log2 Fold Change in Mad2 Gene Expression
2.0
1.5
1.0
0.5
0.0
-0.5
Control
DJ0014
DJ0021
DJ0199
DJ0206
DJ0209
Paclitaxel
Nocodazole
C
Mad1
Log2 Fold Change in Mad1 Gene Expression
1.0
0.5
0.0
-0.5
Control
DJ0014
DJ0021
DJ0199
DJ0206
DJ0209
Paclitaxel
Nocodazole
D
BubR1
Log2 Fold Change in BubR1 Gene Expression
1.5
1.0
0.5
0.0
-0.5
Control
DJ0014
DJ0021
DJ0199
DJ0206
DJ0209
Paclitaxel
Nocodazole
E
Bub1
Log2 Fold Change in Bub1 Gene Expression
2
0
-2
-4
-6
Control
DJ0014
DJ0021
DJ0199
DJ0206
DJ0209
Paclitaxel
Nocodazole
F
Aurora B
Log2 Fold Change in Aurora B Gene Expression
1.0
0.5
0.0
-0.5
-1.0
-1.5
Control
DJ0014
DJ0021
DJ0199
DJ0206
DJ0209
Paclitaxel
Nocodazole
G
PLK1
Log2 Fold Change in PLK1 Gene Expression
1.0
0.5
0.0
-0.5
Control
DJ0014
DJ0021
DJ0199
DJ0206
DJ0209
Paclitaxel
Nocodazole

Figure 6-5 Multi-normalised relative gene expression in comparison to reference genes (TBP, PPIA, RPLP0 and EIF2B1) and untreated control of mRNA for genes regulating components of the Mitotic Checkpoint Complex in DAUDI cells following 48 hours of treatment with cyclooctane-ring containing thienopyridine compounds (10 µM) and 1 minute stimulation of cells with Goat anti-human f(ab')2 IgM (20 µg/mL). Data represents n=3 biological replicates (unless indicated). Paclitaxel positive control n=2. Nocodazole positive control n=1.

Cdc20 (DJ0199 and DJ0206 n=2) (A); Mad2 (DJ0199 and DJ0206 n=2) (B);Mad1 (DJ0014 and DJ0206 n=2, DJ0199 n=1) (C); BubR1 (DJ0199 and DJ0206 n=2) (D); Bub1 (DJ0014, DJ0199, DJ0206 and DJ0209 n=2) (E); Aurora B (DJ0014 and DJ0206 n=2, DJ0199 n=1) (F); PLK1 (DJ0014 and DJ0206 n=2, DJ0199 n=1) (G).

*Error bars represent SD. * = p-value ≤ 0.5, ** = p-value ≤ 0.1, *** = p-value ≤ 0.01*

6.4.1.2 Effects of cycloheptane thienopyridines on cell cycle progression mediated by the Mitotic Checkpoint Complex

Similar to the results observed for the cyclooctane compounds, the largest changes induced by the cycloheptane compounds with regards to genes involved in the MCC was to the expression of cdc20 (Figure 6-6A); Both DJ0041 and DJ0081 induced statistically significant changes in cdc20 (+2.293 and +3.151-fold changes, $p \leq 0.001$ respectively). Again, this mirrored the changes induced by both paclitaxel and nocodazole. Both cycloheptane compounds were also able to induce a statistically significant increase in Mad2 mRNA (DJ0041 +1.632 fold change, p=0.016; DJ0081 +1.621 fold change, p=0.017), and this was greater than the Mad2 changes induced by either paclitaxel or nocodazole (Figure 6-6B). Changes to Aurora B mRNA levels (Figure 6-6F) were also statistically significant, with DJ0041 and DJ0081 causing +2.348 and (p=0.006) and +1.783 fold changes (p=0.038) respectively, while paclitaxel and nocodazole did not induce any changes to expression of this gene.

Regarding the effect of the cycloheptanes on other genes involved the MCC, there was a general trend of increased mRNA levels of Mad 1 (Figure 6-6C), BubR1 (Figure 6-6D), Bub1 (Figure 6-6E) and PLK1 (Figure 6-6G), however, these were only trends and were not found to be statistically significant upon one-way ANOVA with Dunnett's post hoc test.

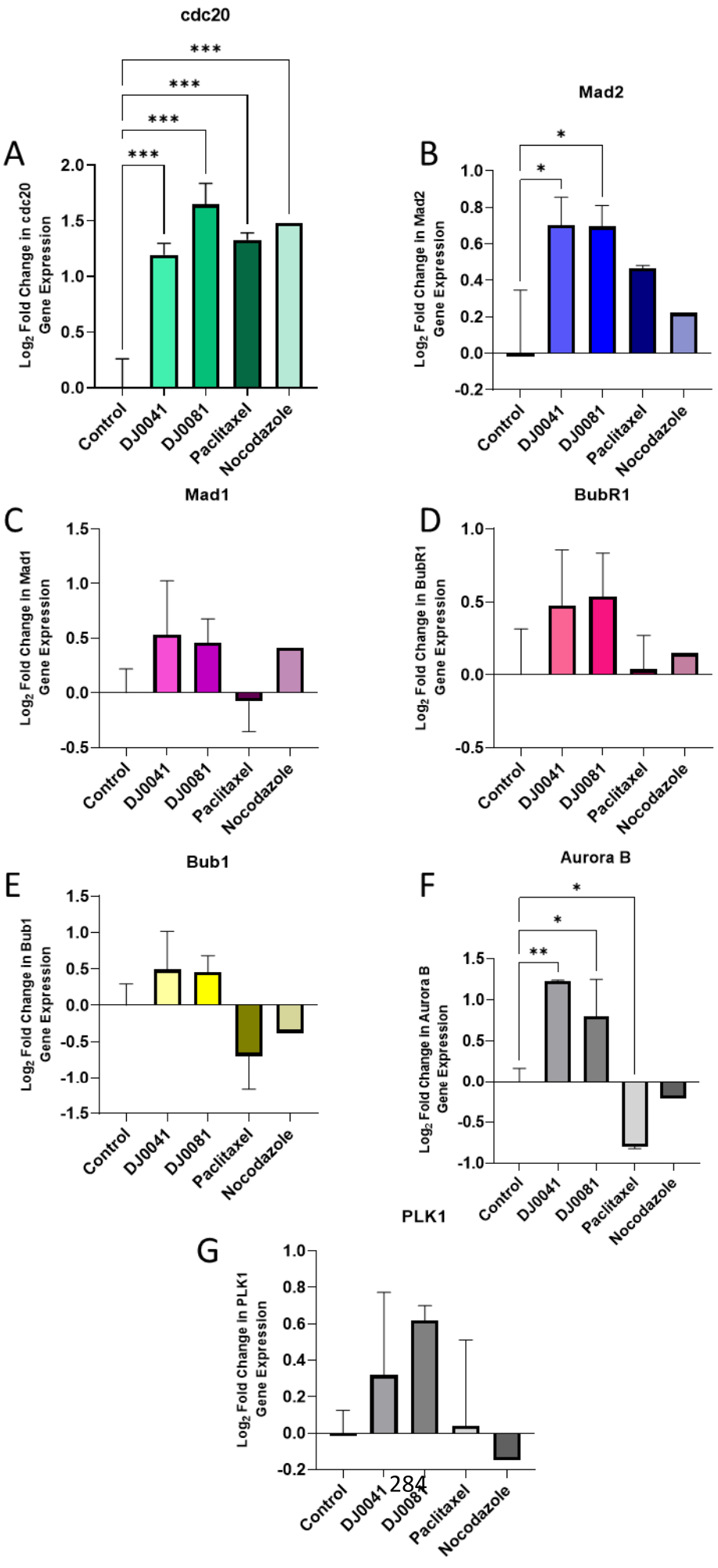
A
cdc20
***
***
***
***
Log2 Fold Change in cdc20 Gene Expression
2.0
1.5
1.0
0.5
0.0
Control
DJ0041
DJ0081
Paclitaxel
Nocodazole
B
Mad2
*
*
Log2 Fold Change in Mad2 Gene Expression
1.0
0.8
0.6
0.4
0.2
0.0
-0.2
Control
DJ0041
DJ0081
Paclitaxel
Nocodazole
C
Mad1
Log2 Fold Change in Mad1 Gene Expression
1.5
1.0
0.5
0.0
-0.5
Control
DJ0041
DJ0081
Paclitaxel
Nocodazole
D
BubR1
Log2 Fold Change in BubR1 Gene Expression
1.0
0.5
0.0
-0.5
Control
DJ0041
DJ0081
Paclitaxel
Nocodazole
E
Bub1
Log2 Fold Change in Bub1 Gene Expression
1.5
1.0
0.5
0.0
-0.5
-1.0
-1.5
Control
DJ0041
DJ0081
Paclitaxel
Nocodazole
F
Aurora B
*
*
**
Log2 Fold Change in Aurora B Gene Expression
1.5
1.0
0.5
0.0
-0.5
-1.0
Control
DJ0041
DJ0081
Paclitaxel
Nocodazole
G
PLK1
Log2 Fold Change in PLK1 Gene Expression
1.0
0.8
0.6
0.4
0.2
0.0
-0.2
Control
DJ0041
DJ0081
Paclitaxel
Nocodazole

Figure 6-6 Multi-normalised relative gene expression in comparison to reference genes (TBP, PPIA, RPLP0 and EIF2B1) and untreated control of mRNA for genes regulating components of the Mitotic Checkpoint Complex in DAUDI cells following 48 hours of treatment with cycloheptane-ring containing thienopyridine compounds (10 µM) and 1 minute stimulation of cells with Goat anti-human f(ab')2 IgM (20 µg/mL). Data represents n=3 biological replicates (unless indicated). Paclitaxel positive control n=2. Nocodazole positive control n=1.

Cdc20 (A); Mad2 (B); Mad1 (C); BubR1 (D); Bub1 (both n=2) (E); Aurora B (both n=2) (F); PLK1 (DJ0081 n=2) (G).

*Error bars represent SD. * = p-value ≤ 0.5, ** = p-value ≤ 0.1, *** = p-value ≤ 0.01*

6.4.1.3 Effects of cyclohexanone thienopyridines on cell cycle progression mediated by the Mitotic Checkpoint Complex

In line with the results seen for the cyclooctane and the cycloheptane compounds, treatment with the cyclohexanone compounds induced significant changes in the mRNA expression levels of cdc20 (Figure 6-7A), with DJ0097 and DJ0171 causing +3.338 and +2.527 fold changes respectively (both $p \leq 0.001$). Again, this mirrored the changes observed following paclitaxel and nocodazole treatment. DJ0109 also appeared to induce cdc20 mRNA levels (+1.484 fold change), however, this change was not statistically significant.

Mad2 expression levels were also generally increased by treatment with the cyclohexanone compounds (Figure 6-7B), reflecting those changes seen following cyclooctane and cycloheptane treatments; All three compounds appeared to show stimulatory effects on this gene, but only the changes following treatment with DJ0097 and DJ0109 (+1.908 fold change, p=0.016 and +1.766 fold change, p=0.03 respectively) were statistically significant.

All three compounds induced significant increases in BubR1 (Figure 6-7D) with +1.685 +1.662 and +2.001 fold changes observed following DJ0097, DJ0109 and DJ0171 treatment (p=0.02, p=0.026 and p=0.008) and these changes were greater than those induced by paclitaxel or nocodazole.

Again, trend of small increases were seen when studying the effects of these compounds on PLK1 (Figure 6-7F), but only compound DJ0171 was able to increase mRNA levels significantly (+2.262 fold change, p=0.049).

There was nothing significant regarding changes to Mad1 (Figure 6-7C), Bub1 (Figure 6-7E or Aurora B (Figure 6-7F). However, of note, DJ0097 showed a trend of inhibiting the mRNA levels of all three of these genes, while the other two cyclohexanones DJ0171 and DJ0109 appeared to stimulate the genes.

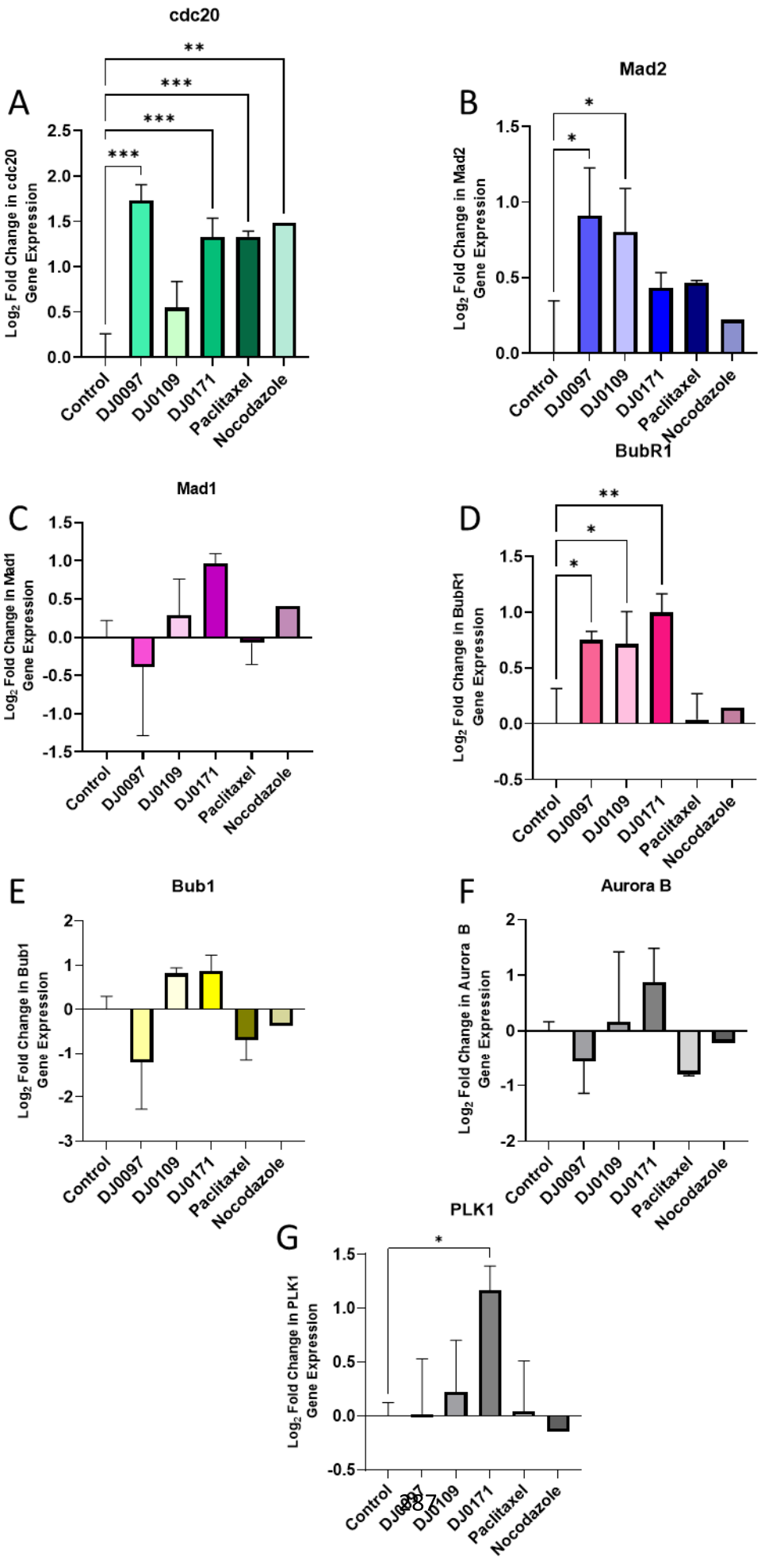
cdc20
A
Log2 Fold Change in cdc20 Gene Expression
Control
DJ0097
DJ0109
DJ0171
Paclitaxel
Nocodazole
Mad2
B
Log2 Fold Change in Mad2 Gene Expression
BubR1
Mad1
C
Log2 Fold Change in Mad1 Gene Expression
D
Log2 Fold Change in BubR1 Gene Expression
Bub1
E
Log2 Fold Change in Bub1 Gene Expression
Aurora B
F
Log2 Fold Change in Aurora B Gene Expression
PLK1
G
Log2 Fold Change in PLK1 Gene Expression

Figure 6-7 Multi-normalised relative gene expression in comparison to reference genes (TBP, PPIA, RPLP0 and EIF2B1) and untreated control of mRNA for genes regulating components of the Mitotic Checkpoint Complex in DAUDI cells following 48 hours of treatment with cyclohexanone-ring containing thienopyridine compounds (10 µM) and 1 minute stimulation of cells with Goat anti-human f(ab')2 IgM (20 µg/mL). Data represents n=3 biological replicates (unless indicated). Paclitaxel positive control n=2. Nocodazole positive control n=1.

Cdc20 (A); Mad2 (DJ0171 n=2) (B); Mad1 (DJ0171 n=2) (C); BubR1 (DJ0171 n=2) (D); Bub1 (DJ0109, and DJ0171 n=2) (E); Aurora B (DJ0171 n=2) (F); PLK1 (DJ0171 n=2) (G).

*Error bars represent SD. * = p-value ≤ 0.5, ** = p-value ≤ 0.1, *** = p-value ≤ 0.01*

6.4.2 Effects of thienopyridine compounds on gene mediators of the G_2/M cell cycle checkpoint

Following progression from S-phase to G_2 phase of the cell cycle, the G_2/M checkpoint is a key waypoint prior to the cell committing to mitosis, during which the various regulators of the cell cycle ensure conditions in the cell are favourable for cell division. Progression of the cell cycle is regulated by fluctuating levels of cyclin proteins and their cofactors the cyclin dependent kinases (CDKs), with cyclins rapidly synthesised and degraded (via ubiquitination) during specific phases of the cell cycle (Greil et al., 2022). The essential mediators of progression through the G_2/M checkpoint are Cyclin B1 and cyclin dependent kinase 1 (CDK1 aka cdc2 'cell division cycle 2' in yeast), also known as the Mitosis Promoting Factor (MPF) (Kishimoto, 2015). When conditions are favourable for cell division (e.g., the conditions of the Spindle Assembly Checkpoint are met, chromosomes are correctly aligned on the cytoskeletal spindle fibres and the Mitotic Checkpoint Complex has been inactivated) the inhibitory effects of the Cyclin B1-CDK1 complex on substrates involved with chromosome alignment is removed to allow separation of sister chromatids (the protease separase is released from its inhibitor securin and acts on cohesion to allow separation of centromeres at anaphase) (Lara-Gonzalez et al., 2019; McAinsh and Kops, 2023) prior to the ubiquitination of Cyclin B1 by the Anaphase Promoting Complex/Cyclosome (APC/C).

Chk1, p53 and its downstream effector p21 are all negative regulators of cell cycle progression, acting as response elements to DNA damage and the Ataxia-telangiectasia-mutated (ATM)/ataxia telangiectasia and Rad3-related (ATR) proteins in cellular DNA damage response (Roos and Kaina, 2013). When DNA damage is detected, ATM/ATR activate Chk1 which in turn phosphorylates and inhibits cdc25C (a key activating phosphatase of CDK1 in the MPF complex); as well as activating p53 and p21 which also directly inhibit MPF (via inhibition of the activating phosphorylation of CDK1 at Thr161) until DNA damage has been corrected (Lemonnier et al., 2020).

PLK1, Aurora B and CDK1 phosphorylation of spindle assembly targets is counteracted by phosphatases, including PP2A and Shugoshin when conditions for cell cycle progression and the SAC are met at anaphase (Konecna et al., 2023).

6.4.2.1 Effects of cyclooctane thienopyridines on cell cycle progression mediated by the G_2/M Checkpoint

Of the supposed 'active' compounds in this group, DJ0014, DJ0199 and DJ0206, all showed a general trend of upregulating Cyclin B1 mRNA levels (Figure 6-8A). This was in line with the effects of paclitaxel and nocodazole. Again, due to the "non-favourable" chemical groups on compounds DJ0021 and DJ0209, no change in Cyclin B1 was observed. The most interesting results when considering genes of the G_2/M checkpoint concern the mirrored results seen when collectively observing Cyclin B1 and CDK1 mRNA levels; As cyclin B1 levels have increased following cyclooctane compound (and paclitaxel/nocodazole treatment), levels of the mRNA for its binding partner CDK1 have decreased (Figure 6-8B); Indeed, statistical analysis revealed significant decreases in CDK1 were following treatment with DJ0014 (-0.600 fold change, p=0.035) and DJ0206 (-0.486 fold change, p=0.008), and also Paclitaxel (-0.411 fold change, p=0.002) and nocodazole (-0.411 fold change, p=0.001). The reduction shown by DJ0206 was comparable to the reduction exhibited by the two known tubulin disrupters and was the most effective, in terms of low CDK1 expression, of any of the thienopyridines tested.

When p21 expression levels were considered, only nocodazole was found to exert any effects, with a significant increase observed following treatment (+2.828 fold change, p=0.037) (Figure 6-8E). Although non-significant, generally the data trend was of increased p21 levels following treatment with the cyclooctanes. No notable changes were observed in mRNA levels of Chk1 (Figure 6-8C), p53 (Figure 6-8D) with any of the treatments tested.

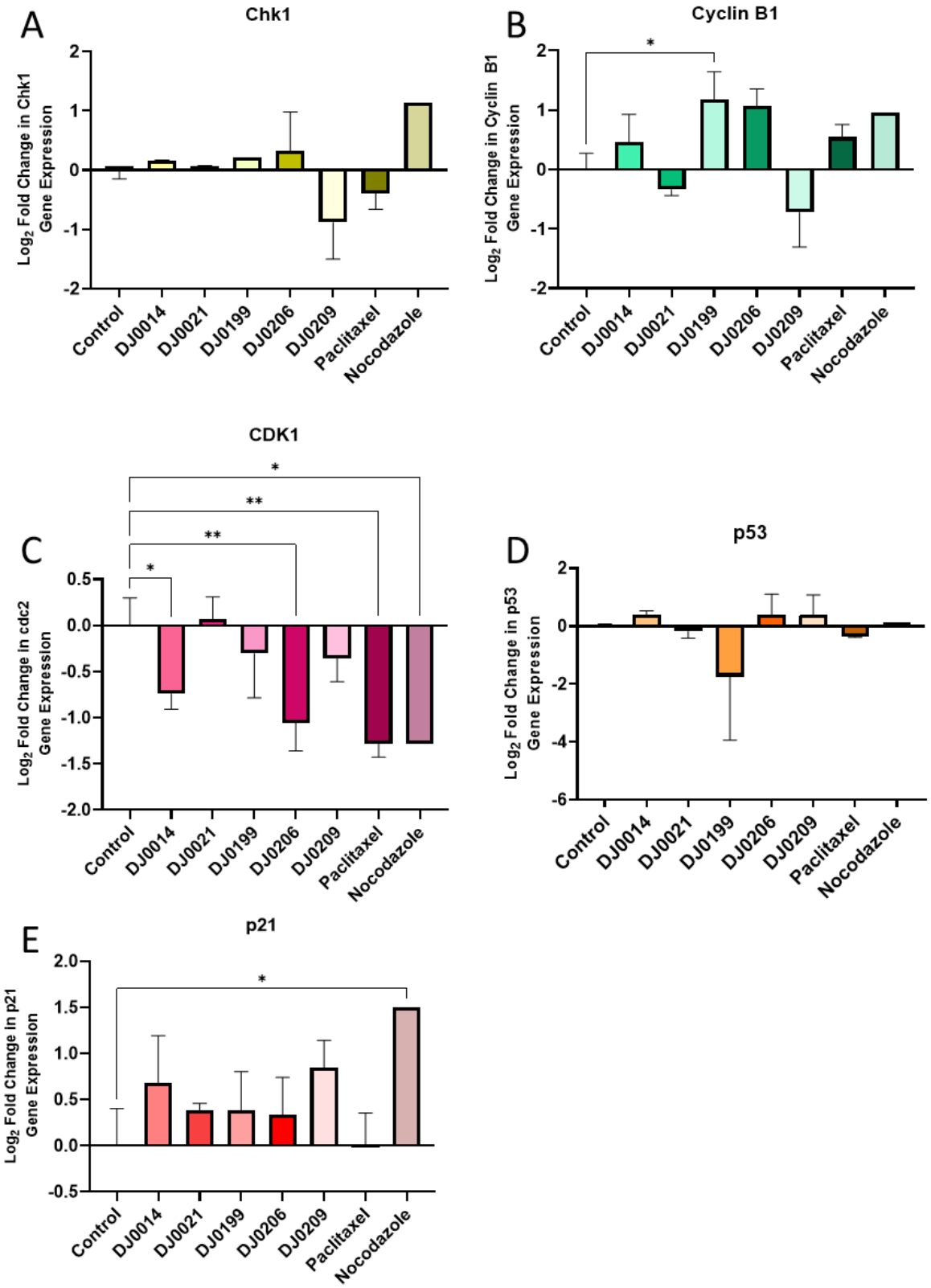
A
Chk1
Log2 Fold Change in Chk1 Gene Expression
2
1
0
-1
-2
Control
DJ0014
DJ0021
DJ0199
DJ0206
DJ0209
Paclitaxel
Nocodazole
B
Cyclin B1
*
Log2 Fold Change in Cyclin B1 Gene Expression
2
1
0
-1
-2
Control
DJ0014
DJ0021
DJ0199
DJ0206
DJ0209
Paclitaxel
Nocodazole
CDK1
*
**
**
*
C
Log2 Fold Change in cdc2 Gene Expression
0.5
0.0
-0.5
-1.0
-1.5
-2.0
Control
DJ0014
DJ0021
DJ0199
DJ0206
DJ0209
Paclitaxel
Nocodazole
p53
D
Log2 Fold Change in p53 Gene Expression
2
0
-2
-4
-6
Control
DJ0014
DJ0021
DJ0199
DJ0206
DJ0209
Paclitaxel
Nocodazole
p21
E
*
Log2 Fold Change in p21 Gene Expression
2.0
1.5
1.0
0.5
0.0
-0.5
Control
DJ0014
DJ0021
DJ0199
DJ0206
DJ0209
Paclitaxel
Nocodazole

Figure 6-8 Multi-normalised relative gene expression in comparison to reference genes (TBP, PPIA, RPLP0 and EIF2B1) and untreated control of mRNA for genes regulating components of the G_2/M Checkpoint in DAUDI cells following 48 hours of treatment with cyclooctane-ring containing thienopyridine compounds (10 µM) and 1 minute stimulation of cells with Goat anti-human f(ab')2 IgM (20 µg/mL). Data represents n=3 biological replicates (unless indicated). Paclitaxel positive control n=2. Nocodazole positive control n=1.

Chk1 (A); Cyclin B1 (DJ0199 and DJ0206 n=2) (B); CDK1 (DJ0021, DJ0199 and DJ0206 n=2) (C); p53 (DJ0014, DJ0021, DJ0199 and DJ0206 n=2) (D); p21 (DJ0021, DJ0199 and DJ0206 n=2) (E).

*Error bars represent SD. * = p-value ≤ 0.5, ** = p-value ≤ 0.1, *** = p-value ≤ 0.01*

6.4.2.2 Effects of cycloheptane thienopyridines on cell cycle progression mediated by the G_2/M Checkpoint

In line with the results observed for the cyclooctane compounds, Cyclin B mRNA levels were shown to be upregulated following treatment with the cycloheptane compounds DJ0041 and DJ0081 (Figure 6-9B), while mRNA levels of Cyclin B1's binding partner CDK1, were reduced; DJ0041 and DJ0081 caused -0.664 (p=0.05) and -0.528 (p=0.006) fold changes in gene expression (Figure 6-9C). Neither of the cycloheptane compounds exerted significant effects on the levels of Chk1 (Figure 6-9A. Neither of the cycloheptanes exerted significant effects on either Chk1 (Figure 6-9A) or p53 (Figure 6-9D), but significant changes in p21 mRNA levels were observed following treatment with DJ0041 (+2.576 fold change, p=0.007) which is the largest increase in p21 expression induced by any of the thienopyridines tested, as well as being comparable to the induction seen following nocodazole treatment (+2.828 fold change) (Figure 6-9E).

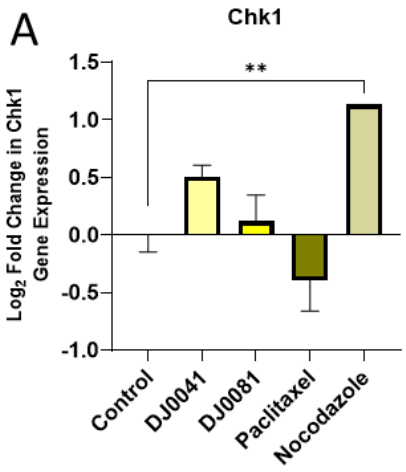
A
Chk1
Log2 Fold Change in Chk1 Gene Expression
1.5
1.0
0.5
0.0
-0.5
-1.0
**
Control
DJ0041
DJ0081
Paclitaxel
Nocodazole

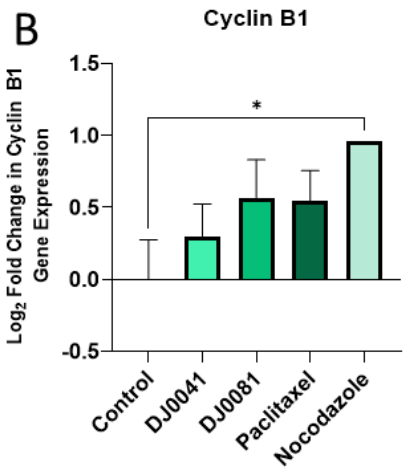
B
Cyclin B1
Log2 Fold Change in Cyclin B1 Gene Expression
1.5
1.0
0.5
0.0
-0.5
*
Control
DJ0041
DJ0081
Paclitaxel
Nocodazole

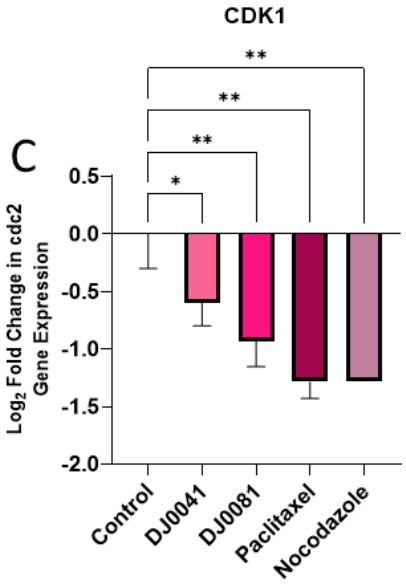
C
CDK1
Log2 Fold Change in cdc2 Gene Expression
0.5
0.0
-0.5
-1.0
-1.5
-2.0
**
**
**
*
Control
DJ0041
DJ0081
Paclitaxel
Nocodazole

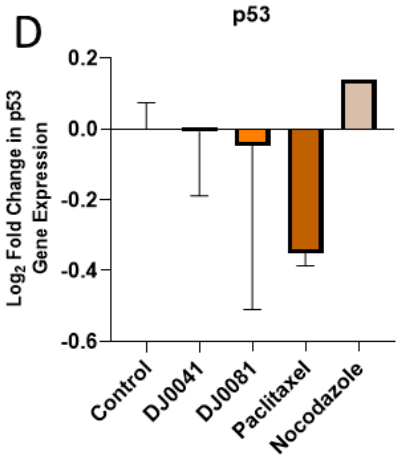
D
p53
Log2 Fold Change in p53 Gene Expression
0.2
0.0
-0.2
-0.4
-0.6
Control
DJ0041
DJ0081
Paclitaxel
Nocodazole

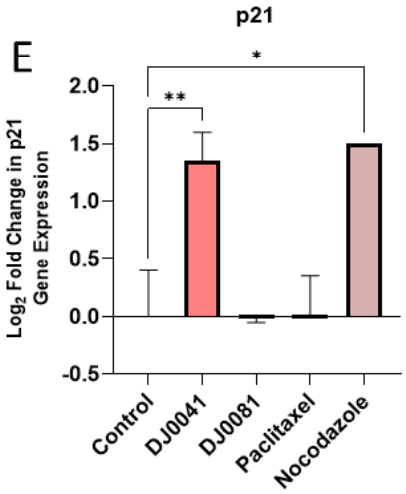
E
p21
Log2 Fold Change in p21 Gene Expression
2.0
1.5
1.0
0.5
0.0
-0.5
**
*
Control
DJ0041
DJ0081
Paclitaxel
Nocodazole

Figure 6-9 Multi-normalised relative gene expression in comparison to reference genes (TBP, PPIA, RPLP0 and EIF2B1) and untreated control of mRNA for genes regulating components of the G_2/M Checkpoint in DAUDI cells following 48 hours of treatment with cycloheptane-ring containing thienopyridine compounds (10 µM) and 1 minute stimulation of cells with Goat anti-human f(ab')2 IgM (20 µg/mL). Data represents n=3 biological replicates (unless indicated). Paclitaxel positive control n=2. Nocodazole positive control n=1.

Chk1 (DJ0041 n=2) (A); Cyclin B1 (B); CDK1 (C); p53 (DJ0041 n=2) (D); p21 (DJ0041 n=2) (E).

*Error bars represent SD. * = p-value ≤ 0.5, ** = p-value ≤ 0.1, *** = p-value ≤ 0.01*

6.4.2.3 Effects of cyclohexanone thienopyridines on cell cycle progression mediated by the G_2/M Checkpoint

The 'active' cyclohexanone compounds tested (DJ0109's unfavourable -oMe substitution rendering it inactive) significantly induced Cyclin B1 mRNA to levels similar to those seen following paclitaxel or nocodazole treatment (Figure 6-10A). Indeed, DJ0097 induced a +1.506 fold change (p=0.024), while DJ0171 induced a +1.700 fold change (p=0.01), compared with fold changes of +1.467 and +1.947 for paclitaxel and nocodazole respectively. Again, mRNA levels of Cyclin B1's binding partner CDK1 were significantly reduced following treatments; DJ0097 caused a -0.577 fold change reduction (p=0.003), while DJ0171 caused a -0.725 fold change reduction (although this was non-significant). Again, these reductions followed the pattern seen following treatment with paclitaxel or nocodazole (Figure 6-10B).

There was nothing noteworthy in terms of effects of these cyclohexanones on the mRNA expression levels of Chk1 (Figure 6-10C), p53 (Figure 6-10D) or p21 (Figure 6-10E). However, despite the statistical insignificance of the data, looking at the general trend, the two active compounds do seem to show opposing effects; As the mRNA of a specific gene is reduced by one of the compounds, it appears to be increased by the other compound, and vice versa (Figure 6-10C-E).

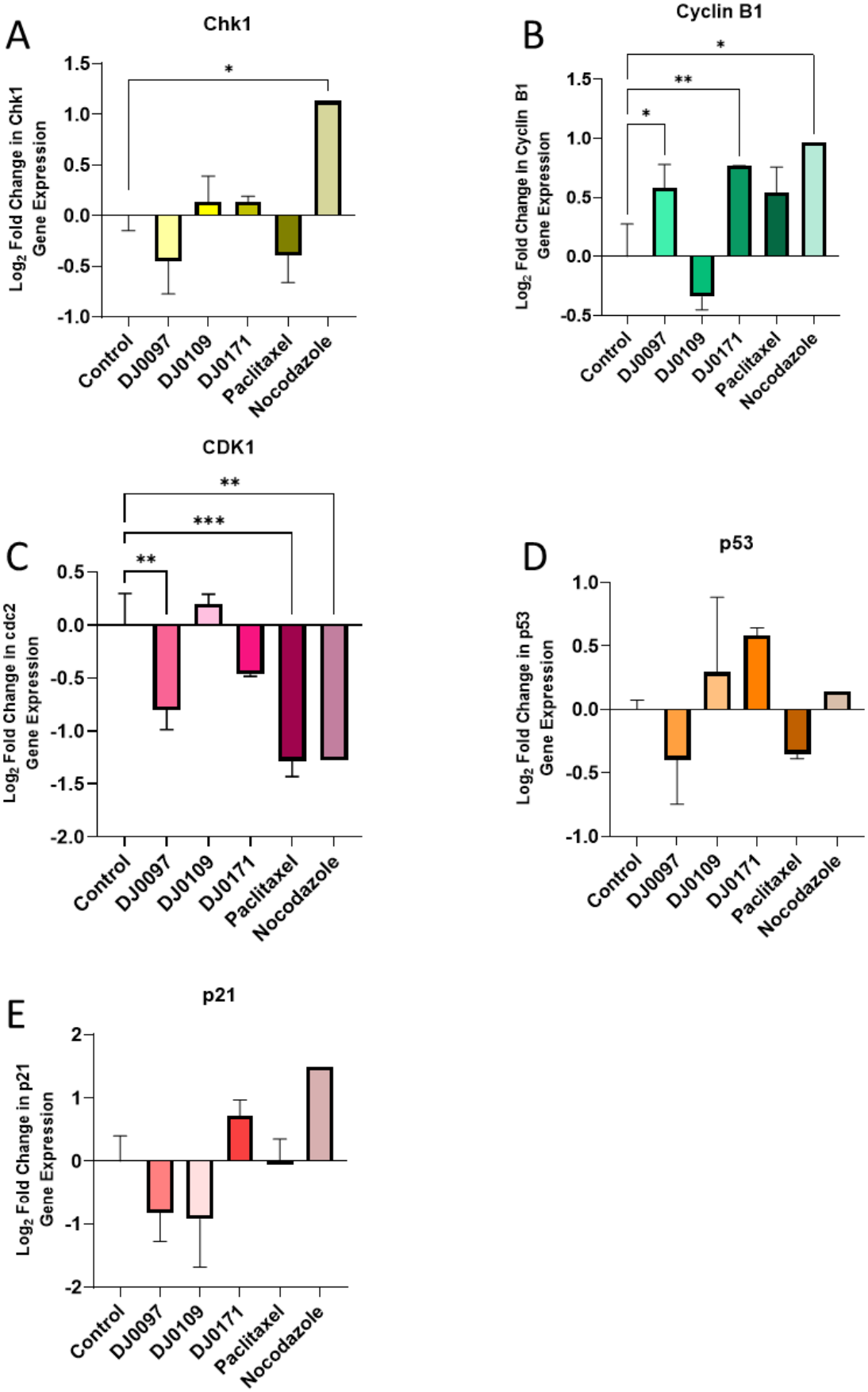
A
Chk1
Log2 Fold Change in Chk1 Gene Expression
1.5
1.0
0.5
0.0
-0.5
-1.0
*
Control
DJ0097
DJ0109
DJ0171
Paclitaxel
Nocodazole
B
Cyclin B1
Log2 Fold Change in Cyclin B1 Gene Expression
1.5
1.0
0.5
0.0
-0.5
*
**
*
Control
DJ0097
DJ0109
DJ0171
Paclitaxel
Nocodazole
C
CDK1
Log2 Fold Change in cdc2 Gene Expression
0.5
0.0
-0.5
-1.0
-1.5
-2.0
**
***
**
Control
DJ0097
DJ0109
DJ0171
Paclitaxel
Nocodazole
D
p53
Log2 Fold Change in p53 Gene Expression
1.0
0.5
0.0
-0.5
-1.0
Control
DJ0097
DJ0109
DJ0171
Paclitaxel
Nocodazole
E
p21
Log2 Fold Change in p21 Gene Expression
2
1
0
-1
-2
Control
DJ0097
DJ0109
DJ0171
Paclitaxel
Nocodazole

Figure 6-10 Multi-normalised relative gene expression in comparison to reference genes (TBP, PPIA, RPLP0 and EIF2B1) and untreated control of mRNA for genes regulating components of the G_2/M Checkpoint in DAUDI cells following 48 hours of treatment with cyclohexanone-ring containing thienopyridine compounds (10 µM) and 1 minute stimulation of cells with Goat anti-human f(ab')2 IgM (20 µg/mL). Data represents n=3 biological replicates (unless indicated). Paclitaxel positive control n=2. Nocodazole positive control n=1.

Chk1 (DJ0171 n=2) (A); Cyclin B1 (DJ0171 n=2) (B); CDK1 (DJ0171 n=2) (C); p53 (DJ0097 and DJ0171 n=2) (D); p21 (DJ0097 n=2) (E).

*Error bars represent SD. * = p-value ≤ 0.5, ** = p-value ≤ 0.1, *** = p-value ≤ 0.01*

6.4.3 Effects of thienopyridines on genes regulating mediators of cell cycle progression at the Spindle Assembly Checkpoint

Just as the Mitotic Checkpoint Complex and the Mitosis Promoting Factor are key regulators of cell cycle progression at the point of spindle assembly and chromosome alignment during metaphase, there are numerous co-factors, kinases and phosphatases, which dynamically respond to and fine tune the signalling complexes of each checkpoint prior to commitment to anaphase and cell division.

Protein Phosphatase 1 (PP1) is a key moderator of the SAC and, in conjunction with completed microtubule attachment to the kinetochores, is essential in silencing the SAC and cell transition to anaphase and sister chromatid separation (Rosenberg et al., 2011), where it effectively acts as a counterbalance to the pro-SAC kinase activity of Aurora B (Meadows et al., 2011).

Protein Phosphatase 2 ((PP2A)-B56) is another essential phosphatase to the chromosome kinetochore attachment and stabilisation and like PP1 it counteracts Aurora B and Plk1 activity, both of which are upregulated at the site of unattached chromosomes (Foley et al., 2011).

The NIMA (Never-in-mitosis *Aspergillus*)-related kinases (NEKs) have a variety of roles in mitotic progress, with Nek2 implicated in the SAC via regulation of the centrosome (and is itself a target of the APC/C for degradation post-anaphase) while Nek7 is also involved in mitotic progression in complex with Nek9 and Nek6 (Malumbres and Barbacid, 2007). The assembly of this complex is regulated by phosphorylation of Nek9 by Plk1, which demonstrates the multifactorial role that the polo-like kinases play throughout mitosis (Fry et al., 2017). Generally, NEKs are associated with microtubule arrangement, with Nek2 functions being essential to centrosome separation at mitosis (Fry et al., 2017).

Polo-like kinases (Plk) have roles in DNA damage checkpoint response (PLK2), with PLK2 being a target of p53 at the G_2 checkpoint while PLK4 appears to have a role in centrosome separation (Malumbres and Barbacid, 2007).

Cell division cycle 25C (cdc25C) is a phosphatase which removes the inhibitory phosphorylation of CDK1, therefore activating the MPF and promoting progression through the G_2/M checkpoint (Lemonnier et al., 2020). Cdc25C is itself a target of Chk1 and downstream of the DNA damage checkpoint, with Chk1 phosphorylating cdc25C at serine 216 residue leading to its sequestering in the cytoplasm and prevents dephosphorylation of CDK1 (Lemonnier et al., 2020).

TRIP13 is a key inactivator of the MCC, which in conjunction with its cofactor $p31^{comet}$, converts Mad2 from a closed (active) to an open (inactive) state, preventing Mad2 binding to cdc20 and the assembly of the MCC at the SAC (Musacchio and Salmon, 2007; H. T. Ma and Poon, 2016).

6.4.3.1 Effects of cyclooctane thienopyridines on cell cycle progression mediated by the Spindle Assembly Checkpoint

None of the cyclooctane compounds tested induced significant changes in the expression levels of PP1G (Figure 6-11A). Neither paclitaxel nor nocodazole effected mRNA levels of this gene. Trend-wise, there appeared to be a slight decrease in expression levels following treatment with DJ0199, DJ0206 and DJ0209, and in comparison mRNA levels were slightly elevated following treatment with DJ0014 and DJ0021, but these changes were negligible.

The gene expression of phosphatase (PP2A)-B56 was significantly increased following treatment with DJ0014 (+1.658 fold change, p=0.02) and DJ0021 (+1.640 fold change, p=0.022) treated cells (Figure 6-11B), while it was also non-significantly increased following treatment with DJ0199 (+1.255 fold change). All increases appeared to be at a greater magnitude than those seen following paclitaxel (+1.132 fold change). This finding was surprising given the non-favourable -OMe group on the DJ0021 molecule. Indeed, the previously mentioned -Cl group on compound DJ0209 appears to have compromised its ability to exert any effects on any of the genes tested in

Figure 6-11. Nocodazole positive control treated DAUDI cells showed a non-significant reduction of approximately 57 % of the mRNA transcript level seen in untreated controls (-0.576 fold change).

No notable changes were observed in the mRNA levels of TRIP13 following treatment with any of the cyclooctanes or the "positive controls" (Figure 6-11C) and this was also the case when considering the expression levels of cdc25C (

Figure 6-11D). However, analysis of PLK2 transcripts following cyclooctane treatments revealed significant differences. The general trend for relative gene expression of PLK2 was for increased expression, with all compounds showing at least a doubling of mRNA transcripts compared to untreated controls (Figure 6-11E). Paclitaxel and Nocodazole also suggested positive effects on the expression of this gene. It should be noted that use of the one-way ANOVA may be masking the significance of each individual thienopyridine compound due to the inclusion of Nocodazole in the comparison.

There were again non-significant changes seen in PLK4 expression, with compounds DJ0014, DJ0021, DJ0199 and DJ0209 all showing increases (Figure 6-11F fold changes, +1.168; +1.393; +1.224; and +1.203 respectively), while DJ0206 showed a decrease (-0.972 fold change) with decreases also seen for Paclitaxel and Nocodazole (-0.564; and -0.850 fold changes respectively).

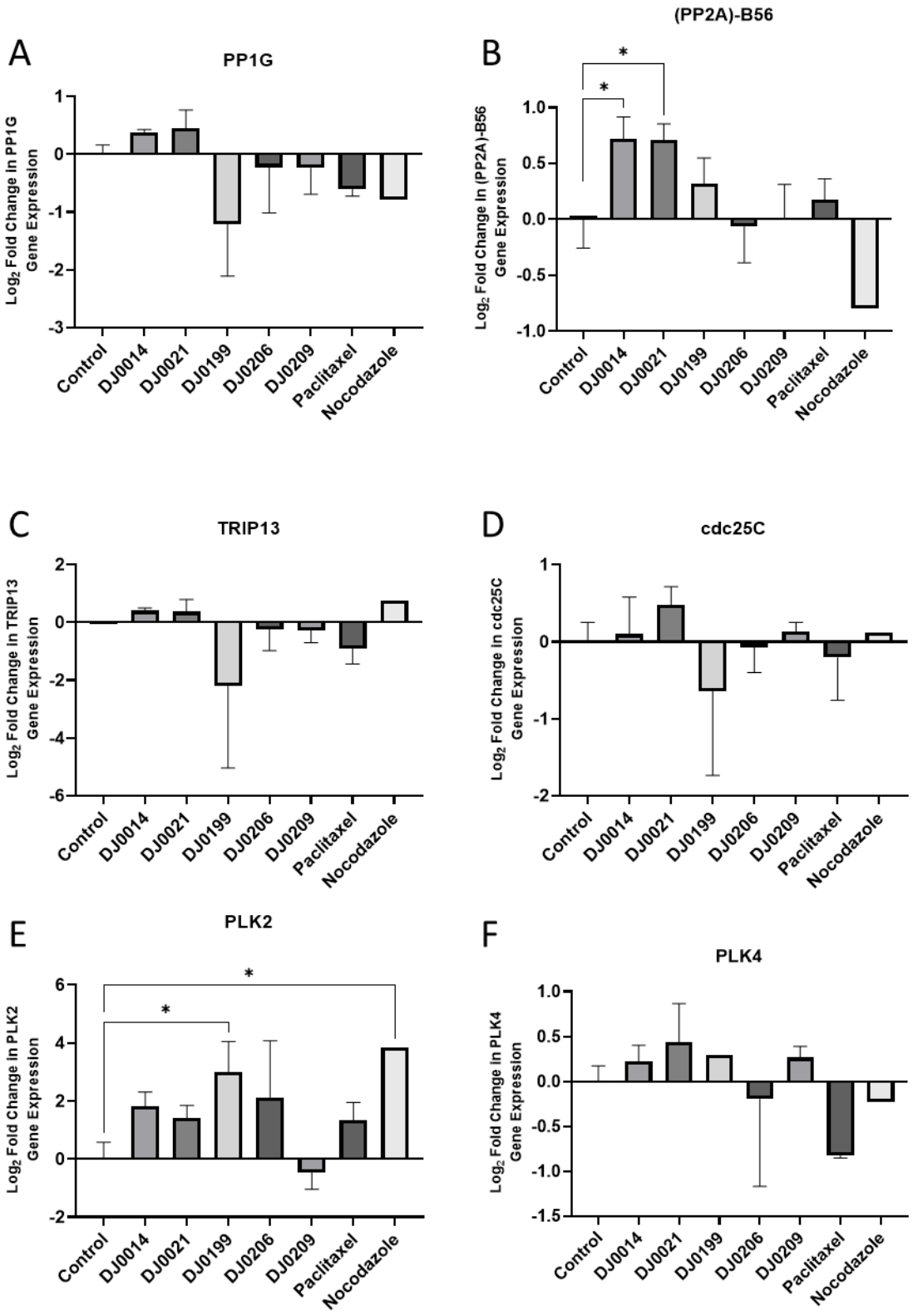
A
PP1G
Log2 Fold Change in PP1G Gene Expression
B
(PP2A)-B56
Log2 Fold Change in (PP2A)-B56 Gene Expression
C
TRIP13
Log2 Fold Change in TRIP13 Gene Expression
D
cdc25C
Log2 Fold Change in cdc25C Gene Expression
E
PLK2
Log2 Fold Change in PLK2 Gene Expression
F
PLK4
Log2 Fold Change in PLK4 Gene Expression
Control
DJ0014
DJ0021
DJ0199
DJ0206
DJ0209
Paclitaxel
Nocodazole

Figure 6-11 Multi-normalised relative gene expression in comparison to reference genes (TBP, PPIA, RPLP0 and EIF2B1) and untreated control of mRNA for genes regulating components of the Spindle Assembly Checkpoint in DAUDI cells following 48 hours of treatment with cyclooctane-ring containing thienopyridine compounds (10 µM) and 1 minute stimulation of cells with Goat anti-human f(ab')2 IgM (20 µg/mL). Data represents n=3 biological replicates (unless indicated). Paclitaxel positive control n=2. Nocodazole positive control n=1.

PP1G (DJ0014, DJ0199 and DJ0206 n=2) (A); (PP2A)-B56 (DJ0199 and DJ0206 n=2) (B); TRIP13 (Control n=1, DJ0014, DJ0199 and DJ0206 n=2) (C); cdc25C (Control, DJ0199 and DJ0206 n=2) (D); PLK2 (DJ0014, DJ0199 and DJ0206 n=2) (E); PLK4 (DJ0014, DJ0206 n=2, DJ0199 n=1) (F).

*Error bars represent SD. * = p-value ≤ 0.5, ** = p-value ≤ 0.1, *** = p-value ≤ 0.01*

6.4.3.2 Effects of cycloheptane thienopyridines on cell cycle progression mediated by the Spindle Assembly Checkpoint

For the cycloheptane-ring containing thienopyridine compounds, neither DJ0041 nor DJ0081 showed any real change compared to untreated controls for any of the SAC-related genes tested (Figure 6-12). However, a significant increase in mRNA transcripts was seen for both polo-like kinase genes; DJ0041 (+4.912 fold change, p=0.008) (Figure 6-12E) and DJ0081 (+3.915 fold change, p=0.011) induced significant increases, with both compounds exceeding the expression seen following paclitaxel treated cells but at a lower induction level than that resulting from nocodazole treatment. Interestingly, although paclitaxel and nocodazole appeared to decrease the levels of PLK4 (Figure 6-12F), both DJ0041 (+2.359 fold change, p=0.007) and DJ0081 (+1.788 fold change, p=0.041) showed statistically significant positive effects on transcript levels.

.

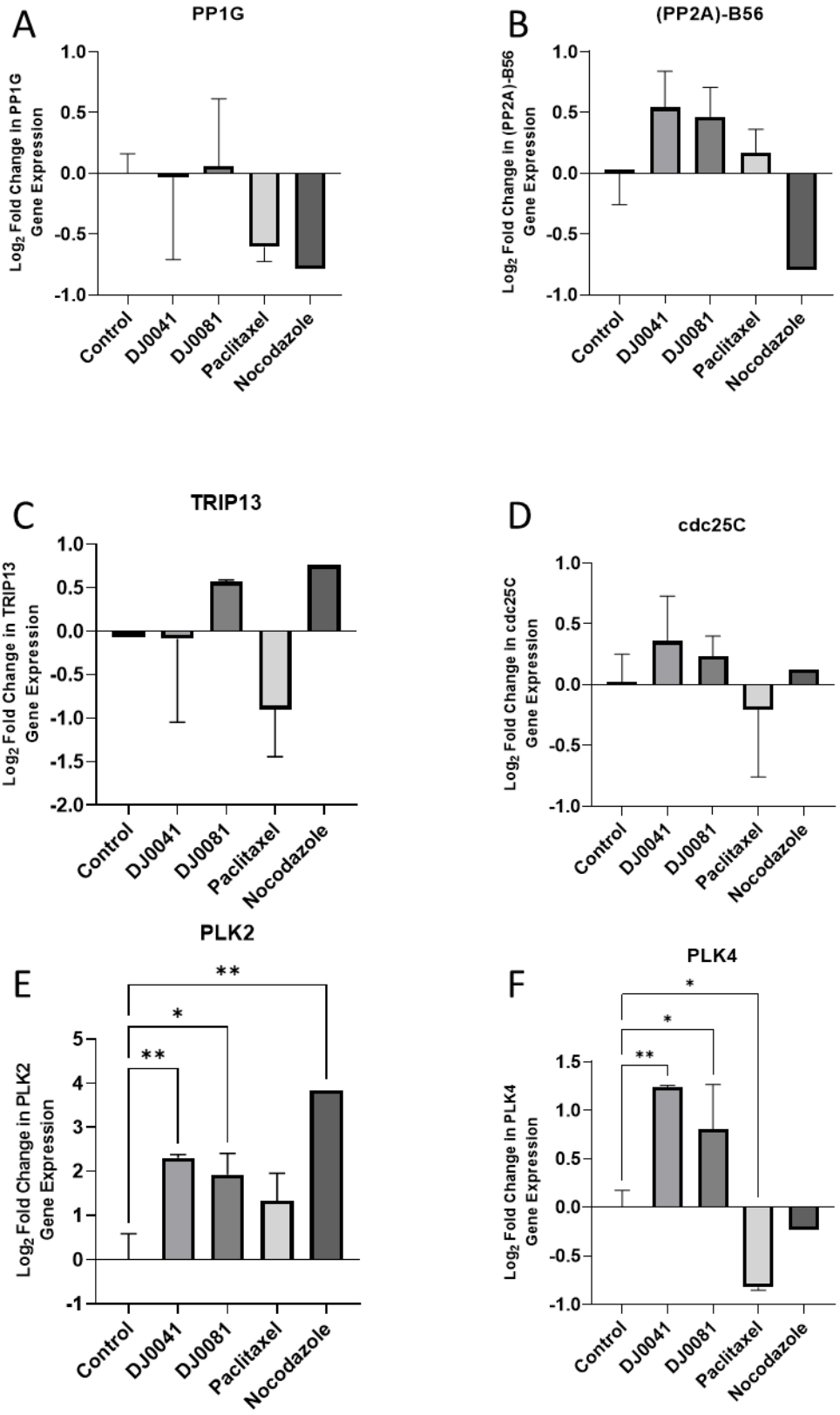
A
PP1G
Log2 Fold Change in PP1G Gene Expression
1.0
0.5
0.0
-0.5
-1.0
Control
DJ0041
DJ0081
Paclitaxel
Nocodazole
B
(PP2A)-B56
Log2 Fold Change in (PP2A)-B56 Gene Expression
C
TRIP13
Log2 Fold Change in TRIP13 Gene Expression
-1.5
-2.0
D
cdc25C
Log2 Fold Change in cdc25C Gene Expression
E
PLK2
Log2 Fold Change in PLK2 Gene Expression
**
*
5
4
3
2
1
0
-1
F
PLK4
Log2 Fold Change in PLK4 Gene Expression
1.5

Figure 6-12 Multi-normalised relative gene expression in comparison to reference genes (TBP, PPIA, RPLP0 and EIF2B1) and untreated control of mRNA for genes regulating components of the Spindle Assembly Checkpoint in DAUDI cells following 48 hours of treatment with cycloheptane-ring containing thienopyridine compounds (10 µM) and 1 minute stimulation of cells with Goat anti-human f(ab')2 IgM (20 µg/mL). Data represents n=3 biological replicates (unless indicated). Paclitaxel positive control n=2. Nocodazole positive control n=1.

PP1G (A); (PP2A)-B56 (B); TRIP13 (Control n=1, DJ0081 n=2) (C); cdc25C (Control n=2) (D); PLK2 (DJ0041 n=2) (E); PLK4 (DJ0041 and DJ0081 n=2) (F).

*Error bars represent SD. * = p-value ≤ 0.5, ** = p-value ≤ 0.1, *** = p-value ≤ 0.01*

6.4.3.3 Effects of cyclohexanone thienopyridines on cell cycle progression mediated by the Spindle Assembly Checkpoint

As with the other thienopyridines, members of the cyclohexanone group did not appear to significantly affect expression levels of the key genes involved in mediating cell cycle progression via the SAC; Levels of Phosphatase PP1G (Figure 6-13A), (PP2A)-B56 (Figure 6-13B), cdc25C (Figure 6-13D) and PLK4 (Figure 6-13E) remained unaffected, and even when considering the general data trend regarding non-significant positive or negative effects, there were mixed results across the cyclohexanone group. Of note, there were some significant changes to TRIP13 ($p=0.038$) (Figure 6-13C) PLK2 ($p=0.029$) (Figure 6-13E) following treatment with DJ0097, with this compound appearing to inhibit TRIP13 mRNA levels below the levels seen in paclitaxel-treated cells, while stimulating PLK2 levels.

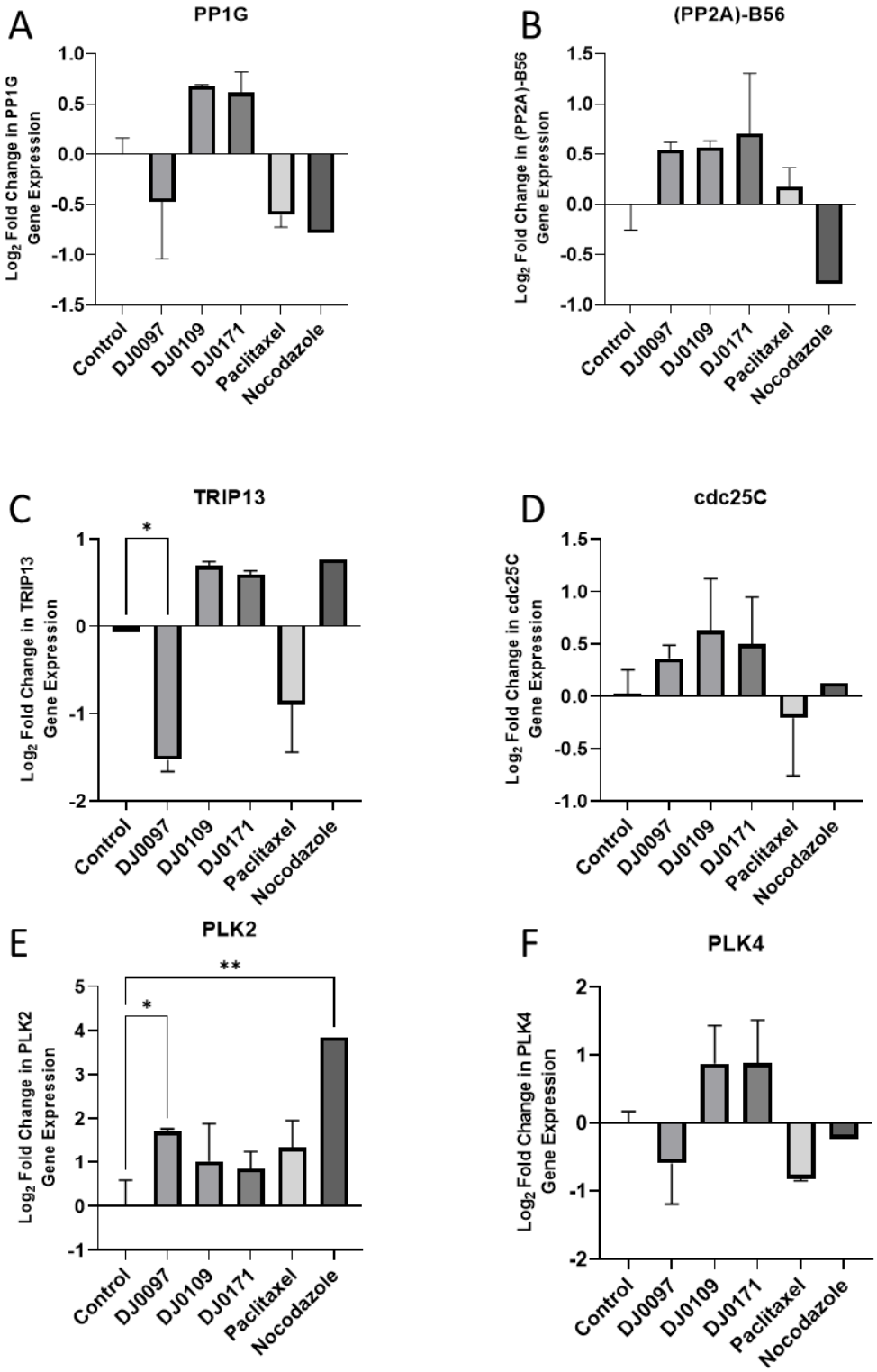
A
PP1G
Log2 Fold Change in PP1G Gene Expression
1.0
0.5
0.0
-0.5
-1.0
-1.5
Control
DJ0097
DJ0109
DJ0171
Paclitaxel
Nocodazole
B
(PP2A)-B56
Log2 Fold Change in (PP2A)-B56 Gene Expression
1.5
1.0
0.5
0.0
-0.5
-1.0
Control
DJ0097
DJ0109
DJ0171
Paclitaxel
Nocodazole
C
TRIP13
*
Log2 Fold Change in TRIP13 Gene Expression
1
0
-1
-2
Control
DJ0097
DJ0109
DJ0171
Paclitaxel
Nocodazole
D
cdc25C
Log2 Fold Change in cdc25C Gene Expression
1.5
1.0
0.5
0.0
-0.5
-1.0
Control
DJ0097
DJ0109
DJ0171
Paclitaxel
Nocodazole
E
PLK2
**
*
Log2 Fold Change in PLK2 Gene Expression
5
4
3
2
1
0
-1
Control
DJ0097
DJ0109
DJ0171
Paclitaxel
Nocodazole
F
PLK4
Log2 Fold Change in PLK4 Gene Expression
2
1
0
-1
-2
Control
DJ0097
DJ0109
DJ0171
Paclitaxel
Nocodazole

Figure 6-13 Multi-normalised relative gene expression in comparison to reference genes (TBP, PPIA, RPLP0 and EIF2B1) and untreated control of mRNA for genes regulating components of the Spindle Assembly Checkpoint in DAUDI cells following 48 hours of treatment with cyclohexanone-ring containing thienopyridine compounds (10 µM) and 1 minute stimulation of cells with Goat anti-human f(ab')2 IgM (20 µg/mL). Data represents n=3 biological replicates (unless indicated). Paclitaxel positive control n=2. Nocodazole positive control n=1.

PP1G (DJ0109 and DJ0171 n=2) (A); (PP2A)-B56 (B); TRIP13 (Control n=1, all n=2) (C); cdc25C (Control n=2) (D); PLK2 (DJ0171 n=2) (E); PLK4 (DJ0109 and DJ0171 n=2) (F).

*Error bars represent SD. * = p-value ≤ 0.5, ** = p-value ≤ 0.1, *** = p-value ≤ 0.01*

6.4.4 Effects of novel thienopyridines on components of the B cell receptor signalling cascade gene transcription

The B cell antigen receptor and its associated intracellular signalling cascade is essential to the role of B cells in the adaptive immune response to pathogens is discussed in section 6.1.1.1 with both Bruton's Kinase (Btk) and Phospholipase C gamma 2 (PLCG2) key mechanisms for signal expansion and cell proliferative signalling.

The PI3K-Akt1 signalling pathway is a key mediator of cell proliferative signals, with the serine/threonine kinase Akt targeting and phosphorylating BCL-2 superfamily members to produce a net anti-apoptotic effect (via sequestering of pro-apoptotic factors which in turn releases anti-apoptotic BCL-2 factors) (Courtney et al., 2010).

6.4.4.1 Effects of cyclooctane thienopyridines on B cell receptor signalling

Similar to the genes tested in the previous section, genes concerning BCR signalling appear unaffected by treatment with cyclooctane thienopyridines, with no significant changes noted across any of the genes tested (BTK, PLCG2 or ATK1) following treatment. Regarding general data trends, there were also inconsistent patterns within this thienopyridine groups; DJ0014, DJ0199 and DJ0206 appeared to exert slight decreases in BTK, comparable to the decrease seen in nocodazole-treated DAUDI cells, while DJ0021 and DJ0209 showed marginal increases in expression. Compounds DJ0014, DJ0199, DJ0206 and DJ0209 all suggested that they might have positive effects on PLCG2 transcripts, which were larger than the magnitude seen for Nocodazole treated cells (Figure 6-14B), while DJ0021 suggested a negative impact on this gene which was smaller than the negative effect seen by Paclitaxel treated cells. Generally, data trends seemed to suggest negative regulation of Akt1 (Figure 6-14C), with only DJ0014 and DJ0021 suggesting positive effects on this gene. In summary though, this class of thienopyridines did not seem to be exerting their effects via modulation of genes involved in immediate BCR signalling.

Akin to Btk and PLCG2, Akt1 only displayed minor variations in gene transcription in comparison to untreated DAUDI controls for thienopyridine treated cells from this

group of compounds (Figure 6-14C). Both DJ0014 and DJ0021 showed non-significant increase expression (+1.194 and +1.445 respective fold change) while DJ0199, DJ0206, DJ0209 and both positive controls all showed a decrease in expression (fold changes: -0.868; -0.883; -0.852; Paclitaxel -0.755; Nocodazole -0.950).

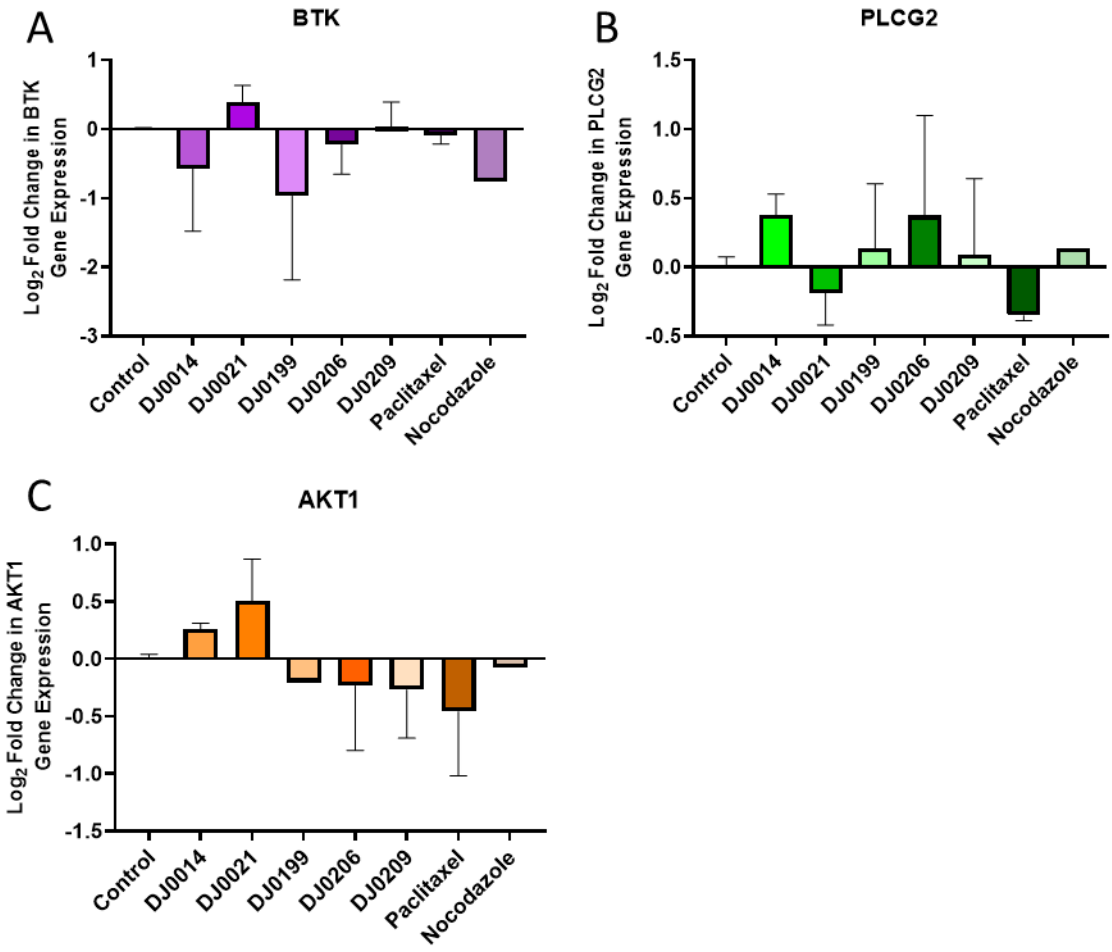

Figure 6-14 Multi-normalised relative gene expression in comparison to reference genes (TBP, PPIA, RPLP0 and EIF2B1) and untreated control of mRNA for genes regulating components of the B cell receptor signalling cascade in DAUDI cells following 48 hours of treatment with cyclooctane-ring containing thienopyridine compounds (10 µM) and 1 minute stimulation of cells with Goat anti-human f(ab')2 IgM (20 µg/mL). Data represents n=3 biological replicates (unless indicated). Paclitaxel positive control n=2. Nocodazole positive control n=1.

Btk (DJ0199 and DJ0206 n=2) (A); PLCG2 (all treated n=2) (B); Akt1 (DJ0014 and DJ0206 n=2, DJ0199 n=1) (C).

*Error bars represent SD. * = p-value ≤ 0.5, ** = p-value ≤ 0.1, *** = p-value ≤ 0.01*

6.4.4.2 Effects of cycloheptane thienopyridines on B cell receptor signalling

Non-significant changes to B cell receptor signalling gene transcripts were also seen for the cycloheptane ring containing thienopyridines.

Compound DJ0041 showed a marginal increase in BTK mRNA transcripts (+1.166 fold change) while DJ0081 showed an equally marginal decrease (-0.939 fold change) (Figure 6-15A).

Both cycloheptane thienopyridines showed almost equivalent PLCG2 gene expression to that shown in IgM stimulated, untreated DAUDI cells (DJ0041 -0.998; DJ0081 +1.002 fold changes) (Figure 6-15B).

Further minor, non-significant changes were seen in the transcription of Akt1, with both DJ0041 and DJ0081 showing slight increase in expression (+1.418 and +1.101 fold changes respectively) (Figure 6-15C).

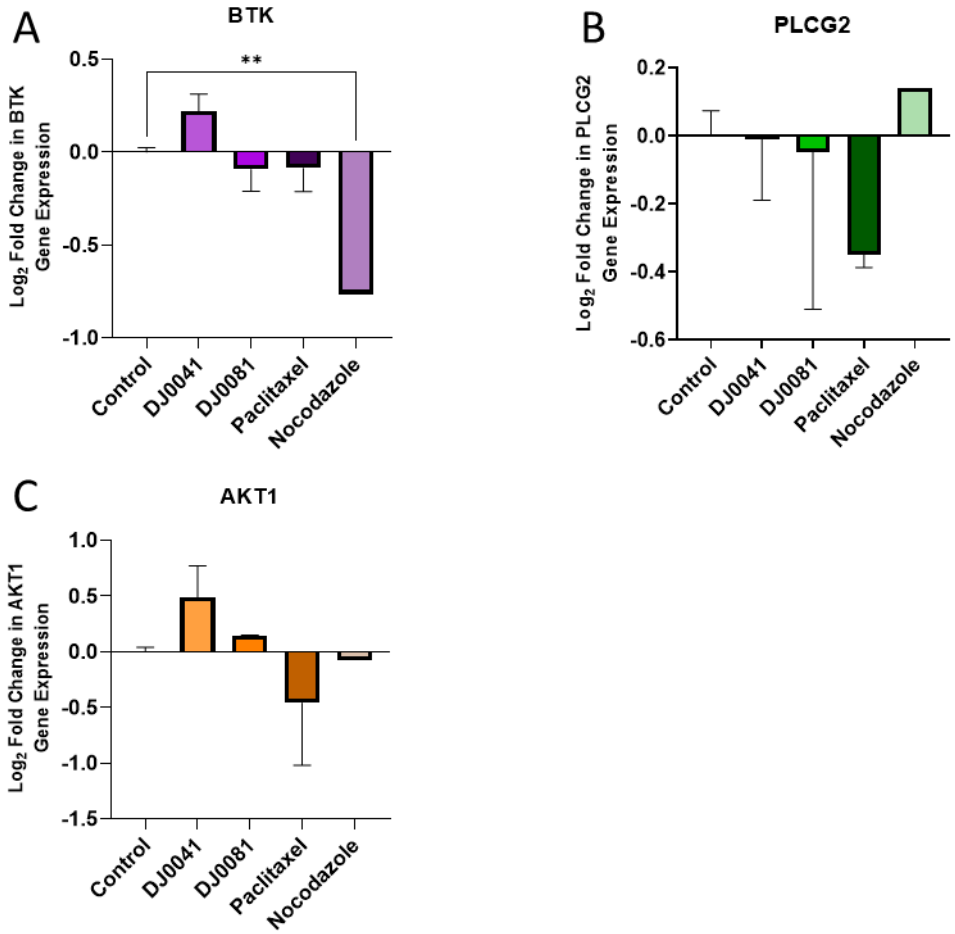

Figure 6-15 Multi-normalised relative gene expression in comparison to reference genes (TBP, PPIA, RPLP0 and EIF2B1) and untreated control of mRNA for genes regulating components of the B cell receptor signalling cascade in DAUDI cells following 48 hours of treatment with cycloheptane-ring containing thienopyridine compounds (10 µM) and 1 minute stimulation of cells with Goat anti-human f(ab')2 IgM (20 µg/mL). Data represents n=3 biological replicates (unless indicated). Paclitaxel positive control n=2. Nocodazole positive control n=1.

Btk (DJ0041 n=2) (A); PLCG2 (DJ0041 n=2) (B); Akt1 (DJ0041 and DJ0081 n=2) (C).

*Error bars represent SD. * = p-value ≤ 0.5, ** = p-value ≤ 0.1, *** = p-value ≤ 0.01*

6.4.4.3 Effects of cyclohexanone thienopyridines on B cell receptor signalling

Of the three cyclohexanone-substituted family of thienopyridine compounds, DJ0097 was shown to decrease the mRNA transcript levels of Btk (-0.847 fold change) while DJ0109 (+1.114 fold change) and DJ0171 (+1.255 fold change, p=0.047) showed an increased expression, with the latter reaching statistical significance (Figure 6-16A).

A similar pattern of effects, albeit non-significant in nature, were observed for PLCG2 gene expression. DJ0097 again showed a non-significant decrease in mRNA transcripts (-0.771 fold change), DJ0109 showed equivalent transcription to the untreated DAUDI controls (+1.024 fold change), and DJ0171 showed a non-significant increase (+1.500 fold change) (Figure 6-16B).

This pattern of gene expression was continued for expression of Akt1, with DJ0097 again showing a non-significant decreased relative gene expression (-0.591 fold change), indeed the lowest of any of the ten thienopyridines included in this study and demonstrating a larger decrease than that seen for Paclitaxel controls (-0.755 fold change) (Figure 6-16C). Both compounds DJ0109 and DJ0171 showed non-significant increased Akt1 expression (+1.226 and +1.206 fold change respectively).

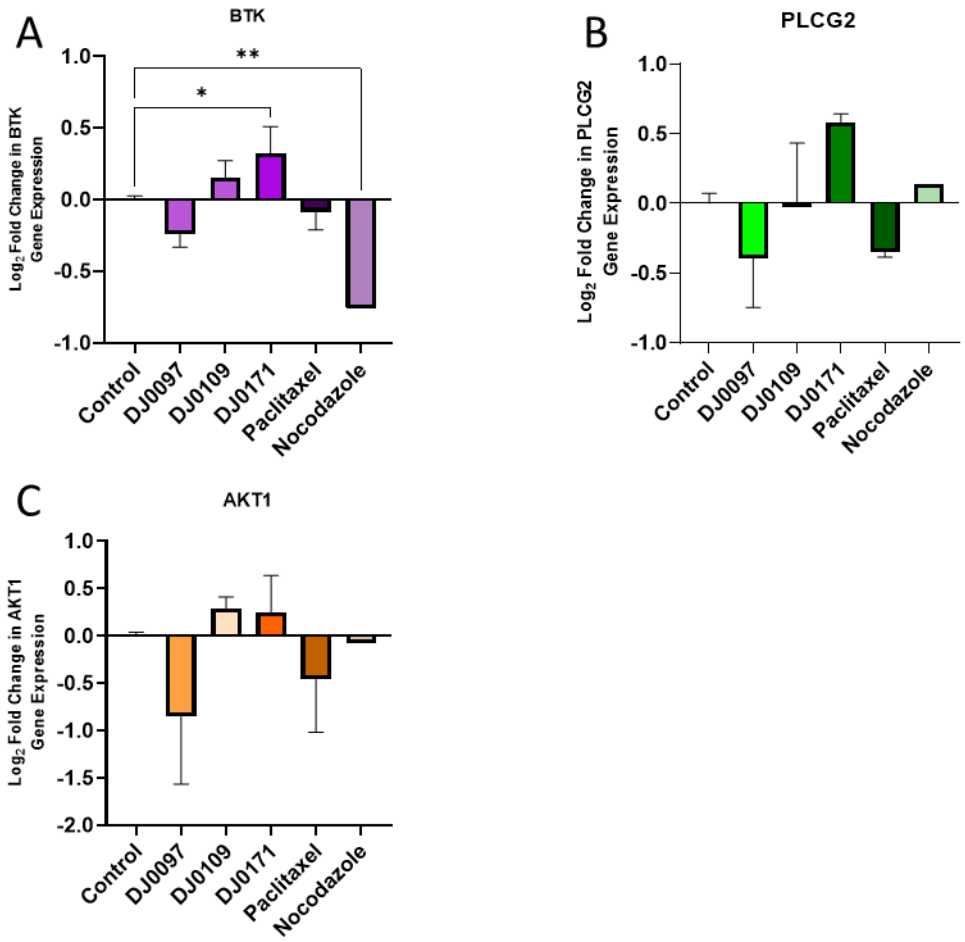

Figure 6-16 Multi-normalised relative gene expression in comparison to reference genes (TBP, PPIA, RPLP0 and EIF2B1) and untreated control of mRNA for genes regulating components of the B cell receptor signalling cascade in DAUDI cells following 48 hours of treatment with cyclohexanone-ring containing thienopyridine compounds (10 µM) and 1 minute stimulation of cells with Goat anti-human f(ab')2 IgM (20 µg/mL). Data represents n=3 biological replicates (unless indicated). Paclitaxel positive control n=2. Nocodazole positive control n=1.

Btk (DJ0171 n=2) (A); PLCG2 (DJ0097, DJ0109 and DJ0171 n=2) (B); Akt1 (DJ0097, DJ0109 and DJ0171 n=2) (C).

*Error bars represent SD. * = p-value ≤ 0.5, ** = p-value ≤ 0.1, *** = p-value ≤ 0.01*

6.4.5 Effects of novel thienopyridines on G_2/M Checkpoint/SAC proteins and their post-translational modifications

The dynamic post-translational modification of the Mitosis Promoting Factor (CDK1-Cyclin B1) at the G_2/M checkpoint during the DNA damage response, particularly Wee1 inhibitory phosphorylation of CDK1 at tyrosine-15, can be used as a key marker for activation of this pathway of cell cycle inhibition (see Figure 6-2). Uninhibited CDK1 would indicate that cell cycle arrest is likely not the result of DDR activation.

As shown in Figure 6-3, the multitude of kinases, phosphatases and targets for degradation by the proteosome (via APC/C in complex with cdc20 or Cdh1) can also provide information on the status of the Spindle Assembly Checkpoint at the point of cell cycle arrest, where elevated levels Cyclin B1 are indicative of active SAC via protection of Cyclin B1 degradation via MCC inhibition of APC/C_{cdc20} formation.

investigating the levels of translated proteins in cells treated with novel thienopyridines is essential to understanding their effects, and whether any changes in gene transcription are representative of changes observed in the proteome.

6.4.5.1 Western blot results for G_2/M checkpoint/SAC proteins in cyclooctane thienopyridine-treated DAUDI cells

The expression of pan-CDK1 protein levels, normalised to total protein of each lane on the western blot, were equivalent across all cyclooctane-ring thienopyridines (Figure 6-17A) with Paclitaxel and Nocodazole controls showing non-significant reductions in CDK1 protein with respective -0.498 and -0.341 fold change compared to untreated IgM stimulated DAUDI cells.

The levels of CDK1 shown to be phosphorylated at the Tyrosine 15 inhibitory regulation site (a marker of G_2/M checkpoint activation) with expression normalised to the levels of pan-CDK1, was non-significantly reduced for compounds DJ0014 (-0.557 fold change), DJ0199 (-0.560 fold change), DJ0206 (-0.592 fold change) and DJ0209 (-0.520 fold change) which showed similar effects to the positive controls

(fold change: Paclitaxel -0.415; Nocodazole -0.267) (Figure 6-17B). Compound DJ0021 is the only thienopyridine from this group to demonstrate an increased phospho-CDK1 (Tyr15) expression (+1.308 fold change)

Cyclin B1, the MPF cofactor and regulatory cyclin partner of CDK1 was demonstrated to have increased expression for all thienopyridine treatments. The biggest increase in expression was seen for DAUDI cells treated with DJ0199 (+7.654 fold change, p=0.0043), followed by DJ0206 which showed a non-significant increased relative expression of +5.282 (Figure 6-17D). Non-significant increases were also seen for DAUDI cells treated with DJ0014 (+1.934 relative expression), DJ0021 (+1.696 fold change), and DJ0209 (+1.856 fold change), while Paclitaxel (-0.353 fold change) and Nocodazole (-0.610 fold change) saw non-significant decreases in Cyclin B1 protein levels (Figure 6-17D).

As Cyclin B1 is rapidly degraded upon a cell progressing through the Spindle Assembly checkpoint at anaphase by APC/C_{cdc20}, elevated levels of protein between double and seven times the expression seen in untreated IgM Control DAUDI cells suggests, as detailed in the preceding chapters, cells are being held at the SAC rather than the preceding G_2/M checkpoint.

The cellular protein levels of the phosphatase cdc25C was also seen to be reduced in all thienopyridine treatments and positive controls, apart from DJ0209 where there was significantly increased relative expression of +1.749 (Figure 6-17F). While DJ0014 showed a non-significant decrease (-0.771 fold change), DJ0021 (-0.439 fold change, p=0.004), DJ0199 (-0.501 fold change, p=0.034) and DJ0206 (-0.566 fold change, p=0.029) all showed significant decreased cdc25C, albeit not to highly significant reductions seen in Paclitaxel (-0.118 fold change, p<0.001) and Nocodazole (-0.086 fold change, p<0.001) (Figure 6-17F).

Reduced levels of cdc25C, a key activator of the MPF via dephosphorylation of CDK1 at Tyrosine 15, would further indicate that conditions in the cells are shifted towards

a phenotype of suspended progression to mitosis, however more replicates of this assay need to be completed to make a firm conclusion based on this data.

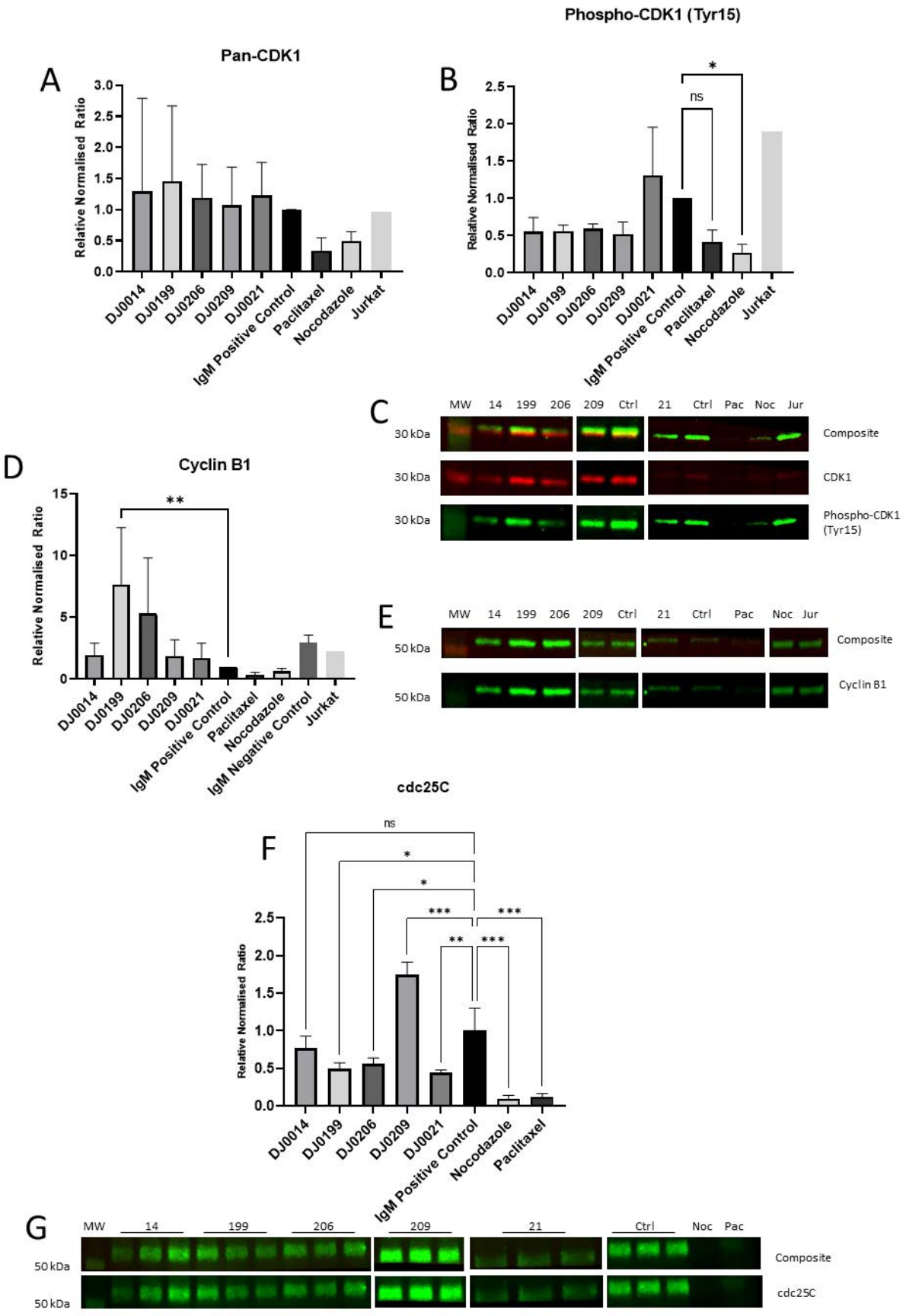
A
Pan-CDK1
Relative Normalised Ratio
DJ0014
DJ0199
DJ0206
DJ0209
DJ0021
IgM Positive Control
Paclitaxel
Nocodazole
Jurkat
B
Phospho-CDK1 (Tyr15)
ns
*
C
MW 14 199 206 209 Ctrl 21 Ctrl Pac Noc Jur
30 kDa
Composite
CDK1
Phospho-CDK1 (Tyr15)
D
Cyclin B1
**
IgM Negative Control
E
MW 14 199 206 209 Ctrl 21 Ctrl Pac Noc Jur
50 kDa
Composite
Cyclin B1
F
cdc25C
ns
*
***
**
G
MW 14 199 206 209 21 Ctrl Noc Pac
50 kDa
Composite
cdc25C

Figure 6-17 Western blotting results for important regulators of the cell cycle following DAUDI cell treatment cyclooctane-ring containing thienopyridines DJ0014, DJ0021, DJ0199, DJ0206 and DJ0209. Pan-CDK1 (A), phospho-CDK1 (Tyr15) (B) and representative blot images (C) show data for n=3 biological replicates with a minimum of n=2 technical replicates on each blot (DJ0199 n=2 biological replicates). Cyclin B1 (D) and representative blot images (E) show data for n=4 biological replicates with a minimum of n=2 technical replicates on each blot. cdc25C (F) and representative blot images(G) show data for n=1 biological replicate and a minimum of n=2 technical replicates. IgM negative, paclitaxel and nocodazole controls show a minimum of n=1 replicates on each blot.

*DAUDI Lysates: Ctrl: IgM positive control; IgM Neg: IgM Negative, unstimulated untreated control; MW: molecular weight ladder; Noc: nocodazole-treated; Pac: Paclitaxel-treated. Error bars represent SD. * = p-value ≤ 0.5, ** = p-value ≤ 0.1, *** = p-value ≤ 0.01*

6.4.5.2 Western blot results for G_2/M checkpoint proteins in cycloheptane thienopyridine-treated DAUDI cells

Pan-CDK1 protein expression levels, normalised to the total protein loaded to each lane of the western blot, were similarly equivalent to the untreated IgM stimulated DAUDI controls for the cycloheptane treated DAUDI cell lysates (Figure 6-18A), while at an mRNA transcription level CDK1 was reduced (Figure 6-9C). The phospho-CDK1 (Tyr15) were shown to be reduced for DJ0041 (-0.812 fold change) and significantly reduced for DJ0081 (-0.469 fold change, p=0.0087), Paclitaxel (-0.431, p=0.0056) and Nocodazole (-0.286, p=0.0011), which is a similar pattern of results as the cyclooctane thienopyridines in the previous section.

Both cycloheptane thienopyridine also showed increased Cyclin B1 protein levels relative to untreated DAUDI controls, with the DJ0041 (+1.573 fold change) and DJ0081 increase (+2.907 fold change, p=0.0255) (Figure 6-18D) also reflective of the mRNA expression levels as assessed by RT-qPCR (Figure 6-9B), and suggestive of cells maintained at pre-anaphase of the cell cycle.

The protein expression of cdc25C was observed to be reduced for both DJ0041 (-0.081 fold change) and DJ0081(-0.332 fold change), as well as for Paclitaxel and Nocodazole(-0.161 and -0.124 fold change respectively) however the low replicate number of this assay restricts making firm conclusions regarding this (Figure 6-18F).

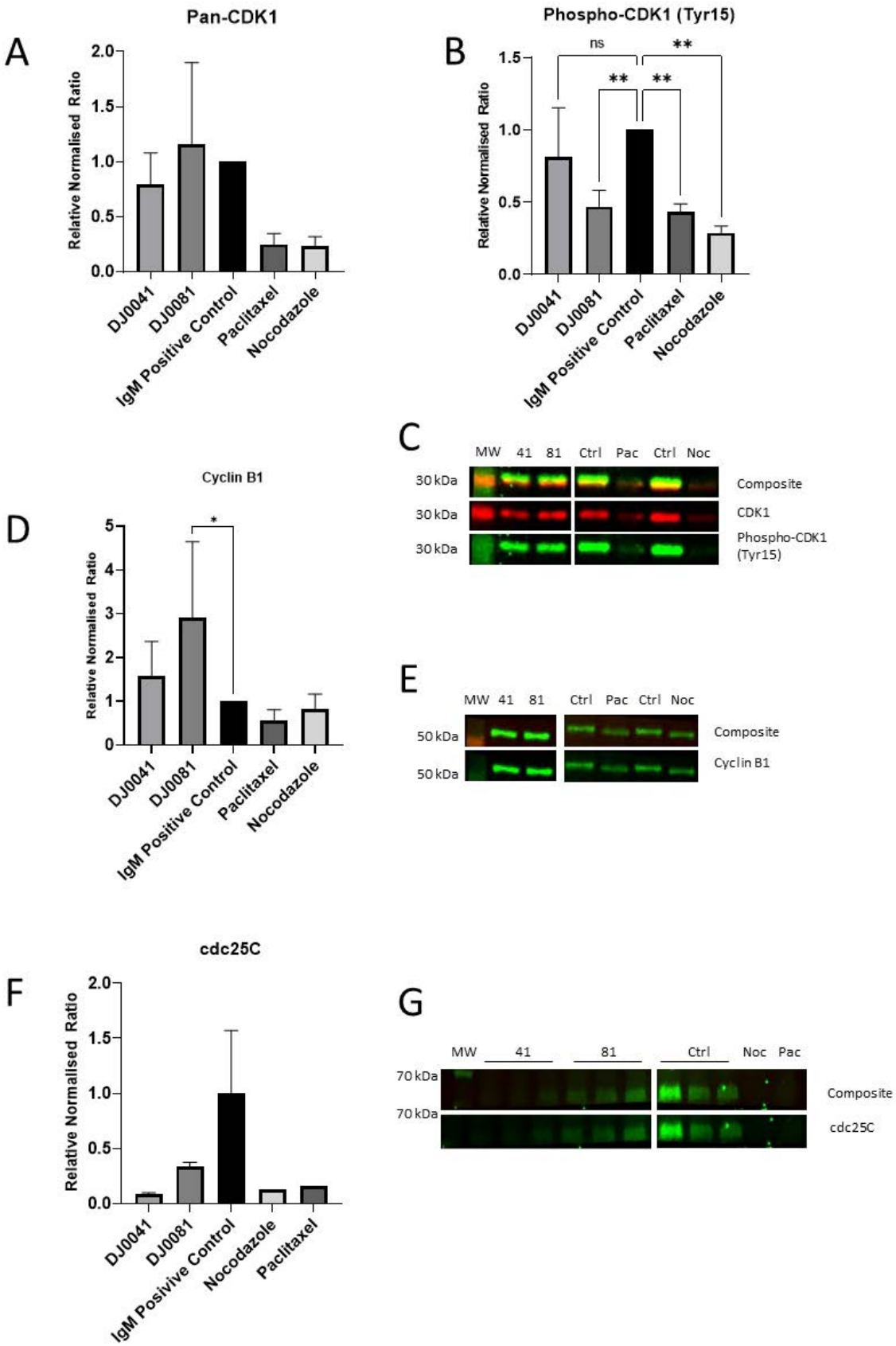
A
Pan-CDK1
Relative Normalised Ratio
2.0
1.5
1.0
0.5
0.0
DJ0041
DJ0081
IgM Positive Control
Paclitaxel
Nocodazole
B
Phospho-CDK1 (Tyr15)
Relative Normalised Ratio
ns
**
**
**
1.5
1.0
0.5
0.0
DJ0041
DJ0081
IgM Positive Control
Paclitaxel
Nocodazole
C
MW 41 81 Ctrl Pac Ctrl Noc
30 kDa
30 kDa
30 kDa
Composite
CDK1
Phospho-CDK1 (Tyr15)
D
Cyclin B1
Relative Normalised Ratio
*
5
4
3
2
1
0
DJ0041
DJ0081
IgM Positive Control
Paclitaxel
Nocodazole
E
MW 41 81 Ctrl Pac Ctrl Noc
50 kDa
50 kDa
Composite
Cyclin B1
F
cdc25C
Relative Normalised Ratio
2.0
1.5
1.0
0.5
0.0
DJ0041
DJ0081
IgM Posivive Control
Nocodazole
Paclitaxel
G
MW 41 81 Ctrl Noc Pac
70 kDa
70 kDa
Composite
cdc25C

Figure 6-18 Western blotting results for important regulators of the cell cycle following DAUDI cell treatment with cycloheptane-ring containing thienopyridines DJ0041 and DJ0081. Pan-CDK1 (A), phospho-CDK1 (Tyr15) (B) and representative blot images (C) show data for n=3 biological replicates with a minimum of n=2 technical replicates on each blot. Cyclin B1 (D) and representative blot images (E) show data for n=4 biological replicates with a minimum of n=2 technical replicates on each blot. cdc25C (F) and representative blot images(G) show data for n=1 biological replicate and a minimum of n=2 technical replicates. IgM negative, paclitaxel and nocodazole controls show a minimum of n=1 replicates on each blot.

*DAUDI Lysates: Ctrl: IgM positive control; IgM Neg: IgM Negative, unstimulated untreated control; MW: molecular weight ladder; Noc: nocodazole-treated; Pac: Paclitaxel-treated. Error bars represent SD. * = p-value ≤ 0.5, ** = p-value ≤ 0.1, *** = p-value ≤ 0.01*

6.4.5.3 Western blot results for G_2/M checkpoint proteins in cyclohexanone thienopyridine-treated DAUDI cells

Levels of pan-CDK1 protein were broadly similar for cyclohexanone treated to the expression seen in untreated DAUDI controls, and the other groupings of thienopyridine-treated cells lysates (Figure 6-19A).

Compound DJ0109 showed almost equivalent levels of phospho-CDK1 (Tyr15) as was seen in untreated controls (+1.025 fold change) (Figure 6-19B), whereas compounds DJ0097 (-0.727 fold change) and DJ0171 (-0.740 fold change) both showed non-significant reductions in phosphorylation. Reduced expression of CDK1 mRNA was seen for both DJ0097 and DJ0171 at RT-qPCR, while DJ0109 showed a slight increase in transcripts (Figure 6-10C) which suggests that CDK1 protein levels are being maintained in response to reduced gene expression.

Cyclin B1 protein levels are also non-significantly increase for all three of the cyclohexanone thienopyridines between two and five times the expression seen in untreated DAUDI controls (Figure 6-19D). The relative normalised ratios of Cyclin B1 were +3.270 for DJ0097, +2.017 for DJ0109 and +5.247 for DJ0171 and while these were non-significant, it again suggests that Cyclin B1 is being maintained following thienopyridine treatment and prevented from degradation, in comparison to untreated DAUDI control cells (Figure 6-19D).

For cdc25C, both DJ0097 (-0.216 fold change, p=0.0083) and DJ0171 (-0.143 fold change, p=0.0051) treated DAUDI cells showed significantly reduced expression compared to untread controls, while expression in DJ0109 only slightly increased compared to untreated controls (+1.134 fold change) (Figure 6-19F).

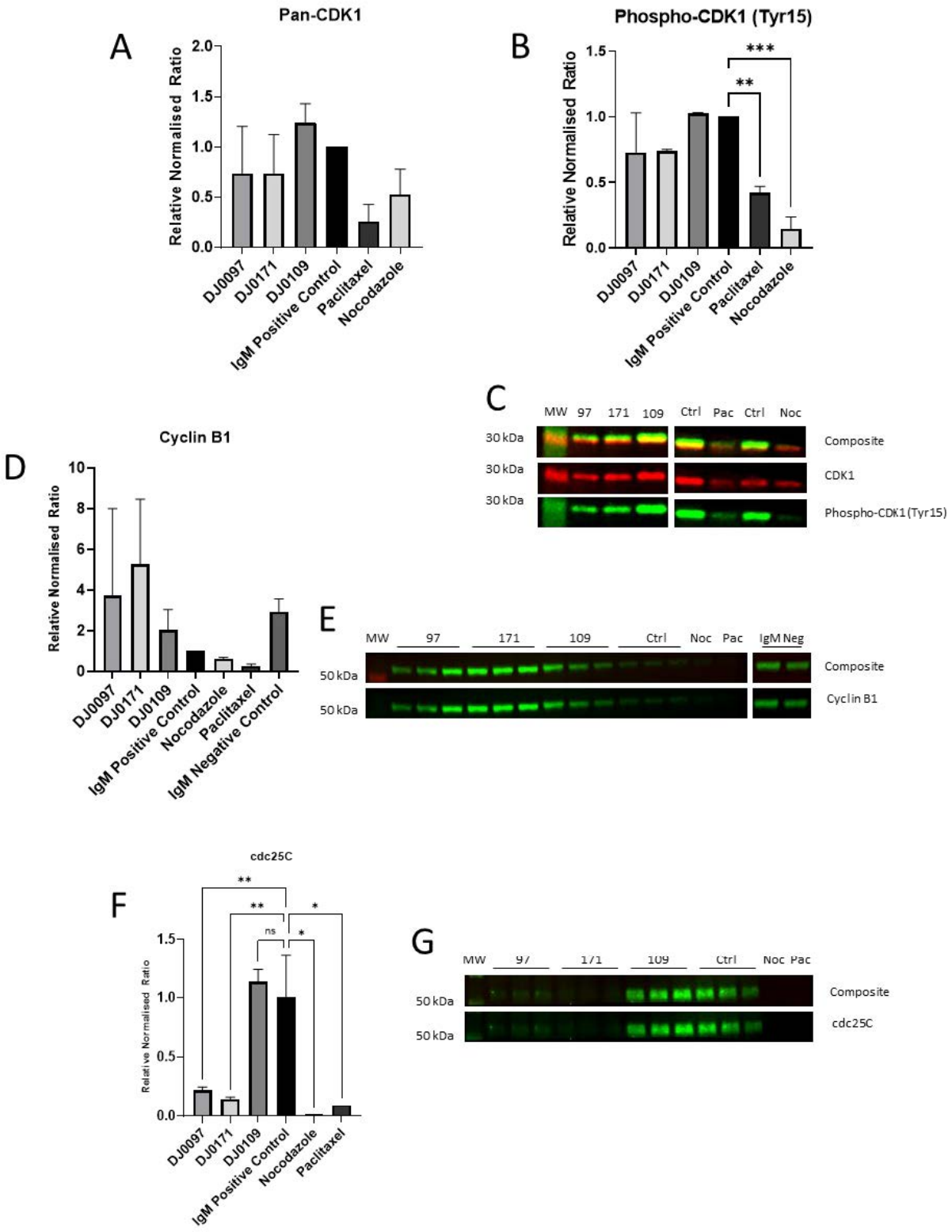
A
Pan-CDK1
Relative Normalised Ratio
2.0
1.5
1.0
0.5
0.0
DJ0097
DJ0171
DJ0109
IgM Positive Control
Paclitaxel
Nocodazole
B
Phospho-CDK1 (Tyr15)
Relative Normalised Ratio
1.5
1.0
0.5
0.0
***
**
DJ0097
DJ0171
DJ0109
IgM Positive Control
Paclitaxel
Nocodazole
C
MW 97 171 109 Ctrl Pac Ctrl Noc
30 kDa
30 kDa
30 kDa
Composite
CDK1
Phospho-CDK1(Tyr15)
D
Cyclin B1
Relative Normalised Ratio
10
8
6
4
2
0
DJ0097
DJ0171
DJ0109
IgM Positive Control
Nocodazole
Paclitaxel
IgM Negative Control
E
MW 97 171 109 Ctrl Noc Pac IgM Neg
50 kDa
50 kDa
Composite
Cyclin B1
F
cdc25C
Relative Normalised Ratio
1.5
1.0
0.5
0.0
**
**
*
ns
*
DJ0097
DJ0171
DJ0109
IgM Positive Control
Nocodazole
Paclitaxel
G
MW 97 171 109 Ctrl Noc Pac
50 kDa
50 kDa
Composite
cdc25C

Figure 6-19 Western blotting results for important regulators of the cell cycle following DAUDI cell treatment with cyclohexanone-ring containing thienopyridines DJ0097, DJ0109, DJ0171. Pan-CDK1 (A), phospho-CDK1 (Tyr15) (B) and representative blot images (C) show data for n=3 biological replicates (DJ0171 and DJ0109 n=2 biological replicates) with a minimum of n=2 technical replicates on each blot. Cyclin B1 (D) and representative blot images (E) show data for n=4 biological replicates with a minimum of n=2 technical replicates on each blot. cdc25C (F) and representative blot images(G) show data for n=1 biological replicate and a minimum of n=2 technical replicates. IgM negative, paclitaxel and nocodazole controls show a minimum of n=1 replicates on each blot.

*DAUDI Lysates: Ctrl: IgM positive control; IgM Neg: IgM Negative, unstimulated untreated control; MW: molecular weight ladder; Noc: nocodazole-treated; Pac: Paclitaxel-treated. Error bars represent SD. * = p-value ≤ 0.5, ** = p-value ≤ 0.1, *** = p-value ≤ 0.01*

6.4.6 Effects of novel thienopyridine on B-cell receptor signalling proteins and their post-translational modifications

Stimulation of the B cell receptor (BCR) should initiate activation of its intracellular signalling cascade. This can be mimicked *in vitro* via stimulation of the BCR with IgM and activation of signalling can be monitored by the phosphorylated state of signalling molecules downstream of the cytoplasmic tail of the receptor. Key propagators of BCR activation include Bruton's kinase (Btk) and Phospholipase C gamma 2 (PLCG2), with two key activating phosphorylation events occurring at Tyrosine 223 in Btk and Tyrosine 759 in PLCG2. Investigation of the activation of these Btk and PLCG2 in thienopyridine-treated cells, when comparison to IgM stimulated untreated DAUDI controls, will help to identify whether the effects of any active thienopyridines are chemically interfering with this signalling cascade at the cell surface, or whether the effects are occurring downstream of the activation of these signalling molecules.

6.4.6.1 Western blot results for cyclooctane thienopyridine-treated DAUDI cells on B-cell receptor signalling

The protein expression of both pan-Btk and pan-PLCG2, normalised to the total protein loaded to each well of the western blots, was broadly similar to that shown in untreated controls (Figure 6-20A and D). The phosphorylation levels of Btk at Tyrosine 233 (Figure 6-20B) and PLCG2 at Tyrosine 759 (Figure 6-20D) were also generally equivalent to those seen in untreated IgM stimulated DAUDI controls. There were slight, non-significant decreases in p-PLCG2 expression observed for DJ0014 (-0.773 fold change), DJ0199 (-0.856 fold change) and DJ0206 (-0.777 fold change) (Figure 6-20D). No effects were seen in the positive control treatments of Paclitaxel and Nocodazole either for phospho-Btk (Tyr223) or phospho-PLCG2 (Tyr759).

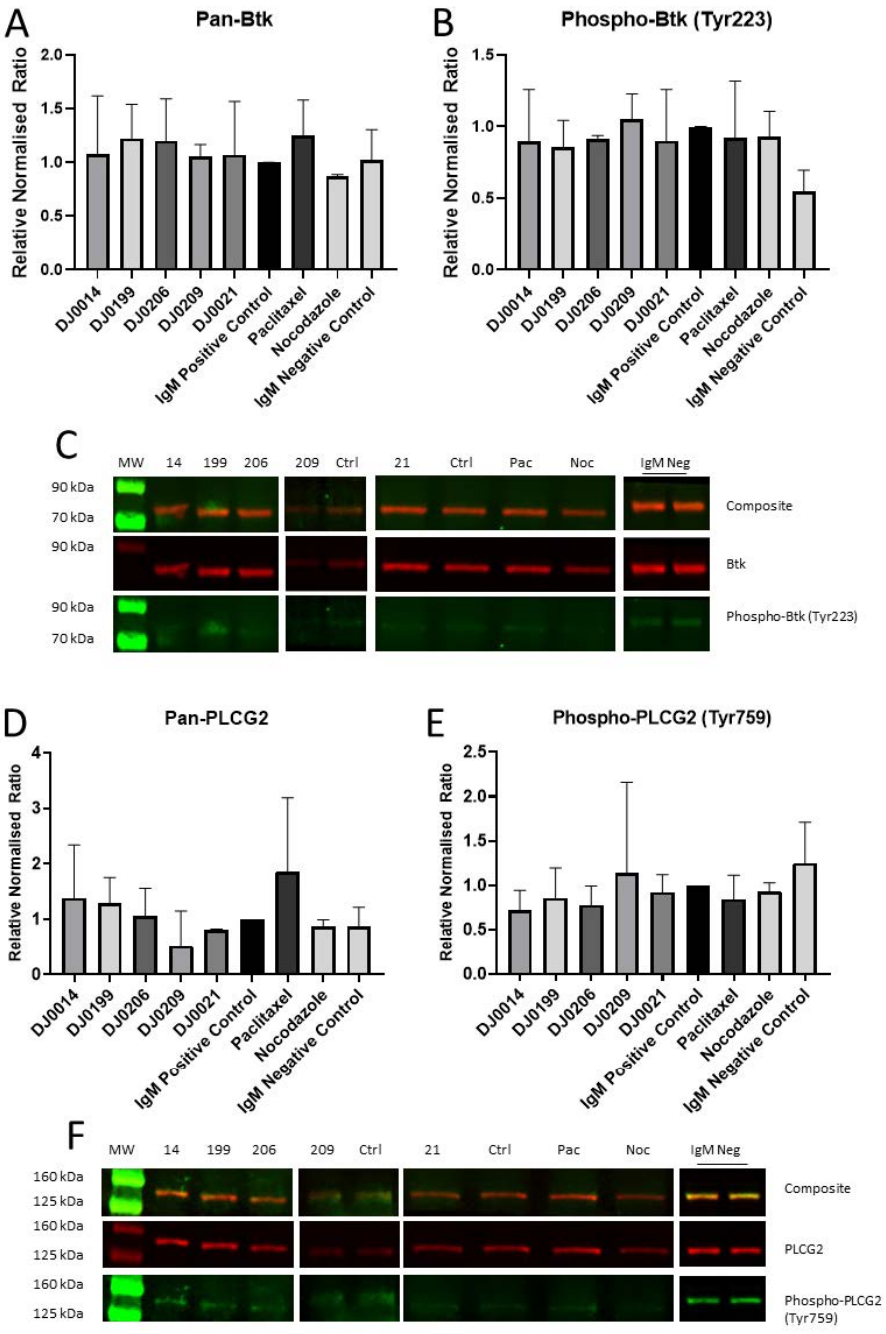

Figure 6-20 Western blotting results for important regulators of B-cell receptor signalling following DAUDI cell treatment with cyclooctane-ring containing thienopyridines DJ0014, DJ0021, DJ0199, DJ0206 and DJ0209. Pan-Btk (A), phospho-Btk (Tyr223) (B) and representative blot images (C) show data for n=4 biological replicates with a minimum of n=2 technical replicates on each blot (DJ0021 n=5, DJ0209 n=3 biological replicates). Pan-PLCG2 (D), phospho-PLCG2 (Tyr759) (E) and representative blot images (F) show data for n=3 biological replicates with a minimum of n=2 technical replicates on each blot (DJ0021 n=3, DJ0209 n=2 biological replicates). IgM Negative, paclitaxel and nocodazole controls show a minimum of n=1 replicates on each blot.

*DAUDI Lysates: Ctrl: IgM positive, untreated control; MW: molecular weight ladder; Noc: nocodazole-treated; Pac: Paclitaxel-treated. Error bars represent SD. * = p-value ≤ 0.5, ** = p-value ≤ 0.1, *** = p-value ≤ 0.01*

6.4.6.2 Western blot results for cycloheptane thienopyridine-treated DAUDI cells on B-cell receptor signalling

For cycloheptane thienopyridine treated DAUDI cells, again the expression levels of pan-Btk (Figure 6-21A) and pan-PLCG2 (Figure 6-21C) were unchanged in comparison to untreated DAUDI controls by one-way ANOVA and with Dunnett's multiple comparisons test. As too were the phosphorylation levels of p-Btk (Figure 6-21B) and p-PLCG2 (Figure 6-21D) with only a slight, non-significant reduction in p-PLCG2 shown by DJ0081 (-0.624 fold change). No effects were seen in the positive control treatments of Paclitaxel and Nocodazole either for phospho-Btk (Tyr223) or phospho-PLCG2 (Tyr759).

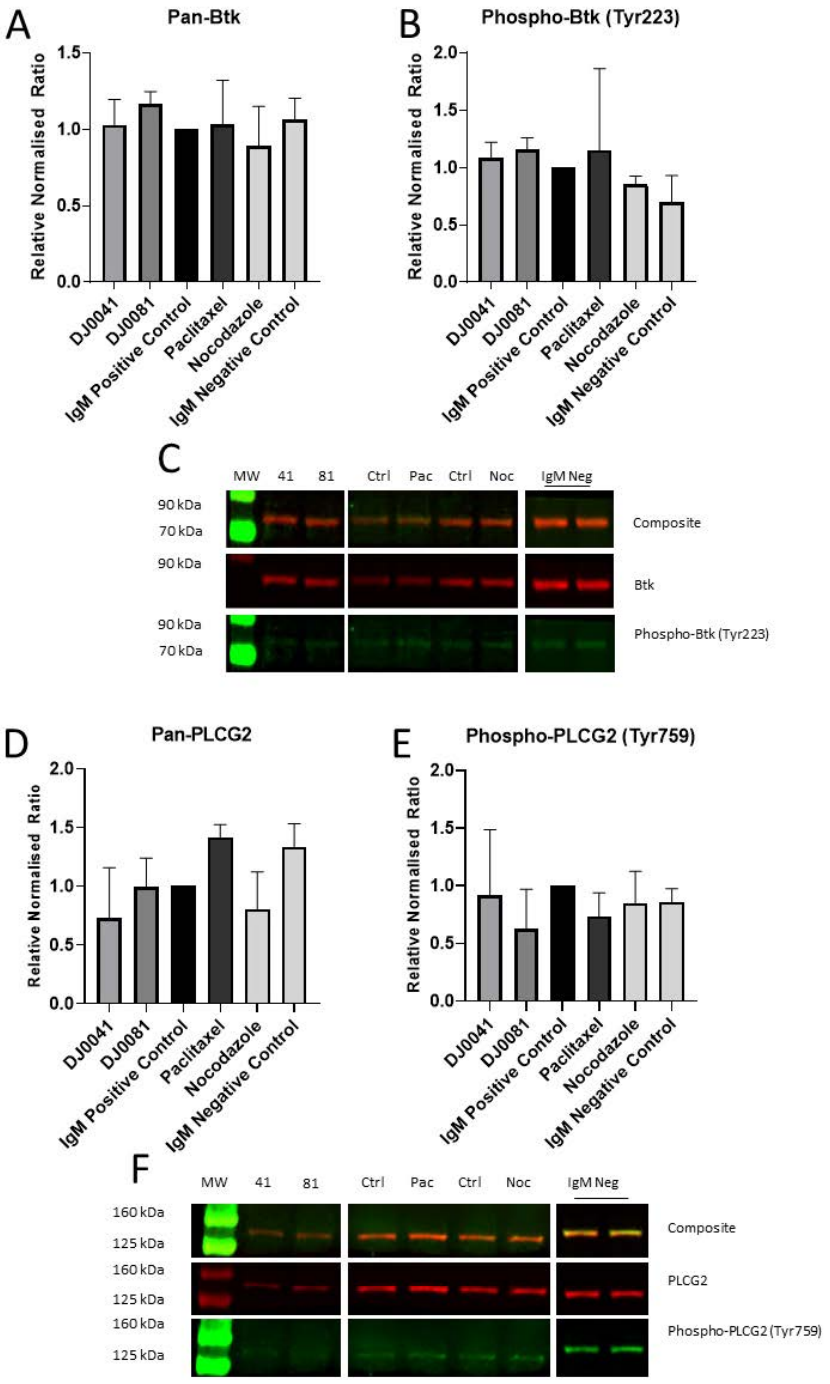

Figure 6-21 Western blotting results for important regulators of B-cell receptor signalling following DAUDI cell treatment with cycloheptane-ring containing thienopyridines DJ0041, DJ0081. Pan-Btk (A), phospho-Btk (Tyr223) (B) and representative blot images (C) show data for n=4 biological replicates with a minimum of n=2 technical replicates on each blot. Pan-PLCG2 (D), phospho-PLCG2 (Tyr759) (E) and representative blot images (F) show data for n=3 biological replicates with a minimum of n=2 technical replicates on each blot. Paclitaxel and nocodazole controls show a minimum of n=1 replicates on each blot.

*DAUDI Lysates: Ctrl: IgM positive, untreated control; MW: molecular weight ladder; Noc: nocodazole-treated; Pac: Paclitaxel-treated. Error bars represent SD. * = p-value ≤ 0.5, ** = p-value ≤ 0.1, *** = p-value ≤ 0.01*

6.4.6.3 Western blot results for cyclohexanone thienopyridine-treated DAUDI cells on B-cell receptor signalling

In a similar pattern of results to the cyclooctane and cycloheptane thienopyridine treatments, no significant changes were seen in pan-Btk (Figure 6-6-22A), phosphor-Btk (Tyr223) (Figure 6-6-22B), pan-PLCG2 (Figure 6-6-22C) or phospho-PLCG2 (Tyr759) (Figure 6-6-22D) although there was a slight non-significant increase shown by DJ0109 (+1.457 fold change). Again, no changes were seen for the Paclitaxel or Nocodazole controls for each data set either.

Generally, phosphorylated activation levels of both Btk and PLCG2 differed no more that 10 % compared to untreated control DAUDI cells.

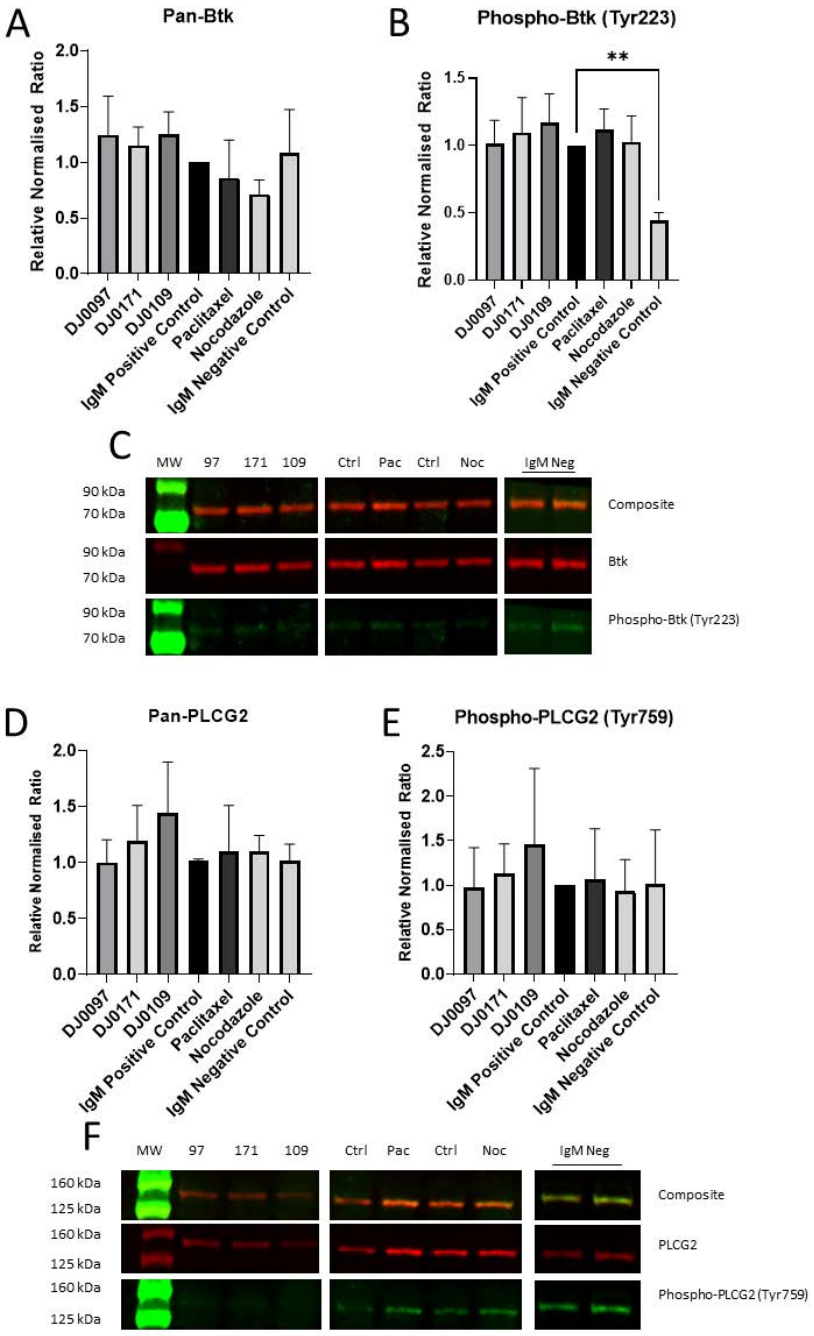

Figure 6-6-22 Western blotting results for important regulators of B-cell receptor signalling following DAUDI cell treatment with cycloheptane-ring containing thienopyridines DJ0097, DJ0109 and DJ0171. Pan-Btk (A), phospho-Btk (Tyr223) (B) and representative blot images (C) show data for n=5 biological replicates with a minimum of n=2 technical replicates on each blot (DJ0109 n=4 biological replicates). Pan-PLCG2 (D), phospho-PLCG2 (Tyr759) (E) and representative blot images (F) show data for n=4 biological replicates with a minimum of n=2 technical replicates on each blot (DJ0109 n=3 biological replicates). Paclitaxel and nocodazole controls show a minimum of n=1 replicates on each blot.

*DAUDI Lysates: Ctrl: IgM positive, untreated control; MW: molecular weight ladder; Noc: nocodazole-treated; Pac: Paclitaxel-treated. Error bars represent SD. * = p-value ≤ 0.5, ** = p-value ≤ 0.1, *** = p-value ≤ 0.01.*

6.5 Summary of the effects of novel thienopyridines on RT-qPCR and Western Blot targets

6.5.1 Summary of the effects of thienopyridines with a cyclooctane moiety on RT-qPCR and Western Blot targets

Table 6-2 summarises the RT-qPCR and Western Blot results for DAUDI cells treated with novel cyclooctane moiety containing thienopyridine compounds.

Table 6-2 Summary of results of the effects of thienopyridines with a cyclooctane moiety on RT-qPCR targets regulating the Mitotic Checkpoint Complex (MCC), DNA Damage Response (DDR) at G_2/M, the Spindle Assembly Checkpoint (SAC) and the B Cell Receptor (BCR) signalling cascade

Compound Name	Effects on MCC mRNA Transcription	Effects on G_2/M mRNA Transcription	Effects on SAC mRNA Transcription	Effects on BCR mRNA Transcription	Effects on G_2/M and SAC protein abundance and post-translational modifications	Effects on BCR protein abundance and post-translational modifications
DJ0014	Significant increase in cdc20 ($P \leq 0.001$). Non-significant increases in Mad2, Mad1, BubR1, Bub1, Aurora B and PLK1	Significant decrease in CDK1. Non-significant increases in Chk1, Cyclin B1, p53 and p21.	Significant increase in (PP2A)-B56 ($P \leq 0.05$). Non-significant increases in PP1G, TRIP13, cdc25C, PLK2 and PLK4.	Non-significant increase in PLCG2 and AKT1. Non-significant decrease in BTK.	Large non-significant increase in Cyclin B1. Non-significant increase in pan-CDK1 and decrease in phospho-CDK1 (Tyr15). Non-significant decrease in cdc25C.	Non-significant increase in pan-BTK and decrease in phospho-BTK (Tyr223). Non-significant increase in pan-PLCG2 and decrease in phospho-PLCG2 (Tyr759).
DJ0021	Non-significant increases in cdc20, Mad2, Mad1, BubR1, Bub1, Aurora B and PLK1.	Non-significant increases in Chk1, CDK1 and p21. Non-significant decreases in Cyclin B1 and p53.	Significant increase in (PP2A)-B56 ($P \leq 0.05$). Non-significant increases in PP1G, TRIP13, cdc25C, PLK2 and PLK4.	Non-significant increase in BTK and AKT1. Non-significant decrease in PLCG2.	Large non-significant increase in Cyclin B1. Significant decrease in cdc25C ($P \leq 0.01$). Non-significant increase in pan-CDK1 and phospho-CDK1 (Tyr15).	Non-significant increase in pan-BTK and decrease in phospho-BTK (Tyr223). Non-significant decrease in pan-PLCG2 and phospho-PLCG2 (Tyr759).
DJ0199	Significant increase in cdc20 ($P \leq 0.001$) and Mad2 ($p = 0.039$). Non-significant increases in Mad1, BubR1 and Aurora B. Non-significant decrease in Bub1 and PLK1.	Significant increase in Cyclin B1 ($P \leq 0.05$). Non-significant increases in Chk1 and p21. Non-significant decreases in CDK1 and p53.	Significant increase in PLK2 ($P \leq 0.05$).. Non-significant increases in (PP2A)-B56 and PLK4. Non-significant decreases in PP1G, TRIP13 and cdc25c.	Non-significant increase in PLCG2. Non-significant decrease in BTK and AKT1.	Large significant increase in Cyclin B1 ($P \leq 0.01$). Significant decrease in cdc25C ($P \leq 0.05$). Non-significant increase in pan-CDK1 and decrease in phospho-CDK1 (Tyr15).	Non-significant increase in pan-BTK and decrease in phospho-BTK (Tyr223). Non-significant increase in pan-PLCG2 and decrease in phospho-PLCG2 (Tyr759).

DJ0206	**Significant increase in cdc20 (P ≤ 0.001). Non-significant increases in Mad2, Mad1, BubR1 and PLK1. Non-significant decreases in Bub1 and Aurora B.**	**Significant decrease in CDK1 (P ≤ 0.01). Non-significant increases in Chk1, Cyclin B1, p53 and p21.**	**Non-significant increase in PLK2. Non-significant decreases in PP1G, (PP2A)-B56, TRIP13, cdc25C.**	**Non-significant increase in PLCG2. Non-significant decrease in BTK and AKT1.**	**Large non-significant increase in Cyclin B1. Significant decrease in cdc25C (P ≤ 0.05). Non-significant increase in pan-CDK1 and decrease in phospho-CDK1 (Tyr15).**	**Non-significant increase in pan-BTK and decrease in phospho-BTK (Tyr223). Non-significant decrease in pan-PLCG2 and phospho-PLCG2 (Tyr759).**
DJ0209	**Non-significant increased cdc20, Mad1, Bub1, Aurora B and PLK1. Non-significant decrease in Mad2 and BubR1.**	**Non-significant increases in p53 and p21. Non-significant decreases in Chk1, Cyclin B1, CDK1**	**Non-significant increases in (PP2A)-B56, cdc25D and PLK4. Non-significant decreases in PP1G, TRIP13 and PLK2.**	**Non-significant increase in BTK and PLCG2. Non-significant decrease in AKT1.**	**Large non-significant increase in Cyclin B1. Significant increase in cdc25C (P ≤ 0.001). Non-significant increase in pan-CDK1 and decrease in phospho-CDK1 (Tyr15).**	**Non-significant increase in pan-BTK and phospho-BTK (Tyr223). Non-significant decrease in pan-PLCG2 and increase in phospho-PLCG2 (Tyr759).**

6.5.2 Summary of the effects of thienopyridines with a cycloheptane moiety on RT-qPCR and Western Blot targets

Table 6-3 summarises the RT-qPCR and Western Blot results for DAUDI cells treated with novel cycloheptane moiety containing thienopyridine compounds.

Table 6-3 Summary of results of the effects of thienopyridines with a cycloheptane moiety on RT-qPCR targets regulating the Mitotic Checkpoint Complex (MCC), DNA Damage Response (DDR) at G_2/M, the Spindle Assembly Checkpoint (SAC) and the B Cell Receptor (BCR) signalling cascade

Compound Name	Effects on MCC mRNA Transcription	Effects on G_2/M mRNA Transcription	Effects on SAC mRNA Transcription	Effects on BCR mRNA Transcription	Effects on G_2/M and SAC protein abundance and post-translational modifications	Effects on BCR protein abundance and post-translational modifications
DJ0041	Significant increases in cdc20 ($P \leq 0.001$), Mad2 ($P \leq 0.05$) and Aurora B ($P \leq 0.01$). Non-significant increases in Mad1, BubR1, Bub1 and PLK1.	Significant decrease in CDK1 ($P \leq 0.05$) and increase in p21 ($P \leq 0.01$). Non-significant increases in Chk1 and Cyclin B1 and decrease in p53.	Significant increase in PLK2 and PLK4 (both ($P \leq 0.01$)). Non-significant increase in (PP2A)-B56 and cdc25C. Non-significant decreases in PP1G and TRIP13.	Non-significant increase in BTK and AKT1. Non-significant decrease in PLCG2.	Non-significant increase in Cyclin B1. Non-significant decrease in pan-CDK1 and phospho-CDK1 (Tyr15). Non-significant decrease in cdc25C.	Non-significant increase in pan-BTK and phospho-BTK (Tyr223). Non-significant decrease in pan-PLCG2 and phospho-PLCG2 (Tyr759).
DJ0081	Significant increases in cdc20 ($P \leq 0.001$), Mad2 ($P \leq 0.05$) and Aurora B ($P \leq 0.05$). Non-significant increases in Mad1, BubR1, Bub1 and PLK1.	Significant decrease in CDK1 ($P \leq 0.01$). Non-significant increases in Chk1, Cyclin B1, and decreases in p53 and p21.	Significant increase in PLK2 and PLK4 (both ($P \leq 0.05$). Non-significant increases in PP1G, (PP2A)-B56, TRIP13 and cdc25C.	Non-significant increase in AKT1. Non-significant decrease in BTK and PLCG2.	Significant increase in Cyclin B1 ($P \leq 0.05$). Non-significant increase in pan-CDK1 and significant decrease in phosphor-CDK1 (Tyr15) ($P \leq 0.01$). Non-significant decrease in cdc25C.	Non-significant increase in pan-BTK and phospho-BTK (Tyr223). Non-significant decrease in pan-PLCG2 and phospho-PLCG2 (Tyr759).

6.5.3 Summary of the effects of thienopyridines with a cyclohexanone moiety on RT-qPCR and Western Blot targets

Table 6-4 summarises the RT-qPCR and Western Blot results for DAUDI cells treated with novel cyclohexanone moiety containing thienopyridine compounds.

Table 6-4 Summary of results of the effects of thienopyridines with a cyclohexanone moiety on RT-qPCR targets regulating the Mitotic Checkpoint Complex (MCC), DNA Damage Response (DDR) at G_2/M, the Spindle Assembly Checkpoint (SAC) and the B Cell Receptor (BCR) signalling cascade

Compound Name	Effects on MCC mRNA Transcription	Effects on G_2/M mRNA Transcription	Effects on SAC mRNA Transcription	Effects on BCR mRNA Transcription	Effects on G_2/M and SAC protein abundance and post-translational modifications	Effects on BCR protein abundance and post-translational modifications
DJ0097	Significant increases in cdc20 ($P \leq 0.001$), Mad2 ($P < 0.05$) and BubR1 ($P < 0.05$). Non-significant increase in PLK1. Non-significant decrease in Mad1, Bub1 and Aurora B.	Significant increase in Cyclin B1 ($P \leq 0.05$) and decrease in CDK1 ($P \leq 0.01$). Non-significant decreases in Chk1, p53 and p21.	Significant increase in PLK2 ($P \leq 0.05$) and decrease in TRIP13 ($P \leq 0.05$). Non-significant increases in (PP2A)-B56 and cdc25C. Non-significant decreases in PP1G and PLK4.	Non-significant decrease in BTK, PLCG2 and AKT1.	Large non-significant increase in Cyclin B1. Non-significant decrease in pan-CDK1 and phospho-CDK1 (Tyr15). Significant decrease in cdc25C ($P \leq 0.01$).	Non-significant increase in pan-BTK and decrease phospho-BTK (Tyr223). Non-significant decrease in pan-PLCG2 and phospho-PLCG2 (Tyr759).
DJ0109	Significant increases in Mad2 ($P < 0.05$) and BubR1 ($P < 0.05$). Non-significant increase in cdc20, Mad1, Bub1, Aurora B and PLK1.	Non-significant increase in Chk1, CDK1 and p53. Non-significant decrease in Cyclin B1 and p21.	Non-significant increases in PP1G, (PP2A)-B56, TRIP13, cdc25C, PLK2 and PLK4.	Non-significant increase in BTK, PLCG2 and AKT1.	Large non-significant increase in Cyclin B1. Non-significant decrease in pan-CDK1 and phospho-CDK1 (Tyr15). Significant decrease in cdc25C ($P \leq 0.01$).	Non-significant increase in pan-BTK and phospho-BTK (Tyr223). Non-significant increase in pan-PLCG2 and phospho-PLCG2 (Tyr759).
DJ0171	Significant increases in cdc20 ($P \leq 0.001$), BubR1 ($P < 0.01$).and PLK1 ($P < 0.05$). Non-significant increases in Mad2, Mad1, Bub1 and Aurora B.	Significant increase in Cyclin B1 ($P \leq 0.01$). Non-significant increases in Chk1, p53 and p21. Non-significant decrease in CDK1.	Non-significant increases in PP1G, (PP2A)-B56, TRIP13, cdc25C, PLK2 and PLK4.	Significant increase in BTK. Non-significant increase in PLCG2 and AKT1.	Large non-significant increase in Cyclin B1. Non-significant increase in pan-CDK1 and phospho-CDK1 (Tyr15). Non-significant increase in cdc25C.	Non-significant increase in pan-BTK and phospho-BTK (Tyr223). Non-significant increase in pan-PLCG2 and phospho-PLCG2 (Tyr759).

6.6 Discussion

6.6.1 Effects of novel thienopyridines on genes regulating the Mitotic Checkpoint Complex

There was a general trend across the genes regulating the Mitotic Checkpoint Complex of increased expression of cdc20, Mad2, Mad1, BubR1 and Bub1 as well as increased expression of both regulators of the MCC assembly, Aurora B Kinase and PLK1 (see section 6.4.1), with the most pronounced increases being seen following treatment with the thienopyridines previously demonstrated to have cytotoxic effects or to induce G_2/M arrest as assessed by flow cytometry (see Chapter 3). Of the three compounds predicted to have limited activity based on their chemical structure, both DJ0021 and DJ0109 showed smaller effects against the regulation of MCC genes, while DJ0209 showed either no change or limited activity compared to mRNA transcripts observed in untreated control DAUDI cells (see sections 6.4.1.1 to 6.4.1.3). In budding yeast models of cell cycle arrest, elevated transcription of cdc20 has been observed in parallel to increased activity levels of CDK1 protein kinase, with cdc2 seen to maintain cdc20 transcription levels until correct orientation of the kinetochores at the spindle assembly checkpoint has been rectified following Nocodazole treatment (Liang et al., 2012), which is similar to the results observed with Nocodazole-treatment of DAUDI cells in this study (See section 6.4.1). Gene expression of cdc20 has been shown to be positively correlated with the expression of Bub1, Cyclin A, Cyclin B1, CDK1, Mad2 and PLK1 in a range of human cancer cell lines (Wu et al., 2021) which supports the findings in this chapter. Care must be taken however due to the possibility that treatment with the active thienopyridine treatments is enriching for cells in mitosis (via SAC activation) where cdc20 is most highly expressed during normal cell cycle progression (Nath et al., 2011).

6.6.2 Effects of novel thienopyridines on genes regulating the G_2/M checkpoint, protein expression and post translational modifications

For genes regulating the G_2/M checkpoint kinases and cyclins, and the effectors of the DNA damage checkpoint, there was a similar trend of 'active' thienopyridine compounds demonstrating increased Cyclin B1, decreased CDK1 with no change in Chk1 expression for the cyclooctane-ring compounds (see section 6.4.2.1), increased Chk1 expression in cycloheptane-ring compounds (see section 6.4.2.2) and varied effects on Chk1 for cyclohexanone-ring thienopyridines (see section 6.4.2.3), while all 'inactive' thienopyridines showed a general trend of decreased Cyclin B1 mRNA transcripts. There was no real consensus in the data on the effects on p53 expression, either within thienopyridine groupings or across the ten tested compounds as a whole. Cyclooctane compounds all appeared to induce p21 expression (see section 6.4.2.1), but there were mixed effects with all other compounds. The cyclical nature of the translation and degradation of cyclins throughout the cell cycle, as opposed to the building up of and maintenance of cyclin-dependant kinase protein stores, is one suggested mechanism for this increase (Lara-Gonzalez et al., 2019), however the role of Cyclin B1 and CDK1 as organisers of the SAC (as well as substrates for the SAC-inhibited APC/C) could also play a role, with protein levels of Cyclin B1 maintained by the SAC until chromosomes have been correctly aligned (Hayward et al., 2019). Western blot protein expression data also support the findings of the RT-qPCR assay (see section 6.4.5), with limited data on Chk1 phosphorylation at the activating Serine 345 residue (See Appendix Figure 8-1) showing similar levels of activation in thienopyridine and untreated DAUDI cell controls. Cyclin B1 protein expression was shown to be elevated following all thienopyridine treatments, while pan-CDK1 was equivalent to expression in untreated IgM stimulated DAUDI controls and inactivating phosphorylation of CDK1 at Tyrosine 15 was shown to be reduced, if not at statistically significant levels in active thienopyridines (see section 6.4.5). Similar effects have been demonstrated in response to vinca alkaloid microtubule poisons in prostate cancer cell lines, whereby mitotic arrest and activation of the SAC/MCC was

accompanied by elevated Cyclin B1 and activated CDK1 (Hsu et al., 2020). Supportive of the RT-qPCR results, despite cells assumed to stop the transcription of genes during mitosis, Cyclin B1 has shown to have sustained mRNA transcription, even at the Spindle Assembly Checkpoint (Mena et al., 2010).

6.6.3 Effects of novel thienopyridines on genes regulating modifiers of the Spindle Assembly Checkpoint

For the key regulators of Spindle Assembly Checkpoint, all thienopyridine compounds were shown to have increased mRNA expression of (PP2A)-B56 phosphatase with the sole exception being compound DJ0206, which showed a slight decrease (see section 6.4.3). Individual thienopyridine compounds generally showed a linked pattern of gene expression for PP1G, TRIP13 and cdc25C, with only DJ0041 and DJ0097 bucking this trend with increased cdc25C expression while showing decreases in the other two genes.

Protein phosphatase 2 ((PP2A)-B56) has been shown to be recruited to the MCC by interaction with BubR1 and where it dephosphorylates cdc20 at sites targeted for inhibition by the MPF at the Spindle Assembly checkpoint (Hein et al., 2021). Interestingly for the RT-qPCR data presented in this chapter, expression of (PP2A)-B56 mRNA also mirrors the expression of BubR1, with all thienopyridines showing an increase in BubR1 transcripts (see section 6.4.1). In *Saccharomyces cerevisiae*, Bub1 and PP2A have been demonstrated to prevent silencing of the Spindle Assembly Checkpoint before chromosomal alignment has been corrected (Jin et al., 2017). Both PP1G and (PP2A)-B56 have been shown to counteract the actions of PLK1 at the SAC in a range of cell lines (Cordeiro et al., 2020), and to co-localise at the kinetochore (Smith et al., 2019). PLK1 expression also mirrors protein phosphatase 2 mRNA levels broadly across active thienopyridine treatments in this study, and while transcription levels do not provide details on protein abundance in the cell, it is possible that

(PP2A)-B56 is the dominate phosphatase active in DAUDI response to treatment in a mechanism that inhibits the activity of Aurora B (Smith et al., 2019).

There was a general trend of increased PLK2 and PLK4 expression across all thienopyridines, with only DJ0209 showing a slight decrease in PLK2, and DJ0097 and DJ0206 showing a decrease in PLK4 (see section 6.4.3). PLK2 mRNA expression, assessed by RT-qPCR, has been demonstrated to be upregulated in B cell chronic lymphocytic leukaemia blood samples in response to established purine analogue chemotherapy drugs in a p53 dependent manner, and that cytotoxicity was correlated with PLK2 gene transcripts (de Viron et al., 2009). PLK2 has been demonstrated to be a pro-apoptotic factor in response to cell stress (Suzuki et al., 2020), and its increased expression in Burkitt Lymphoma cell lines was shown to induce apoptosis (Syed et al., 2006): in this DAUDI cell model, its increased expression is correlated with the apoptotic effects of the thienopyridines described in Chapter 3. PLK4 has a role in centriole production in the cell (Raab et al., 2021) and it was significantly upregulated in DJ0041 and DJ0081 both of which showed a clear absence of centriole organisation at mitosis by confocal microscopy in Chapter 5.

6.6.4 Effects of novel thienopyridines on genes regulating the B cell receptor signalling cascade and their post translational modifications

No significant effects were seen in the gene regulation of Btk or PLCG2, both of which are key transmitters of B cell receptor signalling, or on transcript levels of Akt1, a promoter of apoptotic resistance (see section 6.4.4). Equally, no significant changes were observed in the post-translational modification of Btk or PLCG2 (see section 6.4.6) while limited data on Atk1 phosphorylation at the Serine 473 activation site (See Appendix Figure 8-2) appeared to show that it was unchanged apart from in DJ0081 and DJ0206 treated DAUDI cells, which showed significant reductions in line with the increased levels of apoptosis these compounds induced in Chapter 3. This suggests that any effects induced by the thienopyridines are occurring downstream

of these three signalling molecules. As these thienopyridine compounds were designed to target PLCG2 (Reynisson et al., 2009), effects on Btk would seem unlikely and indeed resistance to Btk-inhibitor drugs has been demonstrated to bypass Btk in propagation of BCR signalling (Woyach et al., 2014; Arthur et al., 2022). Continued activator phosphorylation of PLCG2 at Tyrosine 759 would indicate that signalling is still intact from the BCR, via Lyn, Syk and Btk upstream of PLCG2.

6.7 Conclusion

This chapter demonstrated that the thienopyridine compounds are instigating cell cycle arrest, with activation of the Spindle Assembly Checkpoint and the Mitotic Checkpoint Complex as likely mediators of this activity, rather than activation of the DNA Damage Response. The lack of inhibitory phosphorylation of cyclin dependent kinase 1 at tyrosine-15 as a marker of post-translational regulation following activation of the DNA Damage Response at G_2/M together with sustained Cyclin B1 protein levels suggest that it is the Spindle Assembly Checkpoint which is halting progression of the cell cycle. The thienopyridines also seem to exert no effects on signalling from the B cell receptor to its downstream effectors Btk and PLCG2, suggesting that any direct effects on PLCG2 are occurring downstream of its activation by either Btk or alternate phosphorylation by Syk.

7. DISCUSSION AND FUTURE WORK

7 DISCUSSION AND FUTURE WORK

7.1 Discussion

Much progress has been made in the identification of new treatments for B cell neoplasms over the past two decades, with the introduction of monoclonal antibody treatments such as rituximab (Salles et al., 2017) and subsequent second (ofatumumab (Korycka-Wołowiec et al., 2015)), and third (obintuzumab (Prica and Crump, 2019; C. Luo et al., 2021)) generational refinements to this treatment strategy have provided clinicians with multiple treatment options in haematological cancers which can have a remitting and relapsing disease course (Tilly et al., 2015; Eichhorst et al., 2021; Hallek and Al-Sawaf, 2021). Guided by the success of the first tyrosine kinase inhibitor Imatinib (Druker et al., 2001) in the treatment of Chronic Myeloid Leukaemia, targeted inhibitors have also had a significant impact in lymphoid malignancies, with the Btk inhibitor Ibrutinib (Byrd et al., 2013), the PI3K inhibitor Idelalisib (Flinn et al., 2014; Yang et al., 2019) and the BCL-2 inhibitor venetoclax (Roberts et al., 2016; Stilgenbauer et al., 2016) providing further pathways to remission in these disorders, with patients now able to be offered chemotherapy-free regimes (Eichhorst et al., 2021; Hallek and Al-Sawaf, 2021; Walewska et al., 2022). However, due to the complexity of cell signalling pathways (Chang et al., 2003; McCubrey et al., 2007; Burger and Wiestner, 2018; R. Liu et al., 2020), and the multiple points of crossover between signalling cascades, treatment failure due to clonal progression or kinase phosphorylation of targets downstream of the targets of inhibition, as demonstrated by the bypassing of Btk in progression of CLL (Woyach et al., 2014; Liu et al., 2015), there are continued efforts to identify lead candidates for future treatments.

The thienopyridine compounds investigated in this study were themselves the result of in silico screening of compounds known to target phospholipase C gamma 2, a process which began over 15 years ago (Reynisson et al., 2009; Feng et al., 2012). Those initial studies highlighted potential cytotoxic effects in a range of cell lines via the NCI 60 panel (Shoemaker, 2006), including melanoma, breast, non-small cell lung cancer and CNS tumour cell lines, as well as activity shown against leukaemia cell

lines (Reynisson et al., 2009; Feng et al., 2012; Hung et al., 2014). The main overarching aim of this thesis was to investigate ten novel thienopyridines to establish if they had any effects on a DAUDI mature B cell lymphoma cell model and to hope to gain an understanding of the mechanism of their effects.

For narrative purposes, these compounds were grouped by their shared chemical structure, predominantly the cyclical carbon ring moiety, which was previously demonstrated to bear an influence on cytotoxic or cytostatic effects (Arabshahi et al., 2014; Leung et al., 2016). The results discussed in Chapter 3 soon highlighted seven of these compounds (the 'active' compounds: DJ0014, DJ0014, DJ0081, DJ0097, DJ0171, DJ0199 and DJ0206) as having cytotoxic/cytostatic effects (see Chapter 3), while two thienopyridines consistently showed little effects (the 'inactive' compounds DJ0021 and DJ0109), which was a predicted by their chemical structure and the presence of an unfavourable *para*-position methoxy group side chain on their aryl ring (Arabshahi et al., 2014; Hung et al., 2014; Arabshahi et al., 2015; Leung et al., 2016). The final compound, DJ0209, would have been predicted to show cytotoxic effects, due to its cyclooctane ring, but this has previously been described as 'mildly active' in cancer cell line studies (van Rensburg et al., 2017) and could be described as such based on its activity against DAUDI cells herein.

The results of the three most active thienopyridine compounds from each chemical family, cyclooctane-ring DJ0206, cycloheptane-ring DJ0041 and cyclohexanone-ring DJ0097 from are summarised in Table 7-1, however the other active compounds also showed similar, if slightly reduced, levels of activity across all of these assays too.

Cytotoxicity measured by MTS is a common feature of novel thienopyridine based compounds in drug discovery (Mohareb and Ibrahim, 2017; Abuelhassan et al., 2022) but relatively fewer results exist for the other assays conducted. G_2/M cell cycle arrest has been demonstrated in thienopyridine complex compounds against Jurkat (T cell leukaemia), HeLa (uterine cancer) and colorectal (HT-29) cells has been described (Romagnoli et al., 2013) alongside Forkead box M1 inhibition resulting in G_2/M arrest and apoptosis in breast (MDA-MD-231) cells (G. Luo et al., 2021; Huerta-Garcia et al., 2022). For this study, there was a mixed pattern of effects demonstrated

against tubulin polymerisation, with DJ0206 showing reduced activity comparable with nocodazole controls, DJ0041 showed only slight increases while DJ0097 showed an increased direct polymerisation *in vitro*. Thienopyridine binding to the colchicine binding domain has been suggested as a model of action for similar thienopyridines (Romagnoli et al., 2013), which may suggest the effects of DJ0206 as nocodazole also binds to this site. The stabilising effects of DJ0097 and to a lesser extent DJ0041 are less clear, but G_2/M arrest in conjunction with tubulin stabilisation has been demonstrated in novel, synthesised microtubule binding agents (Zhou et al., 2021; Zhou et al., 2022).

The anti-tubulin effects of the thienopyridines help to add context to the RT-qPCR and western blotting results for these compounds, particularly the upregulation of key spindle assembly checkpoint and mitotic checkpoint complex component cdc20. This cell division regulatory protein has a dual role in halting of mitosis and also downregulation of key cell cycle M phase Cyclin B1 to allow cell cycle progression after mitotic injury has occurred (Kapanidou et al., 2017; Hayward et al., 2019). The combination of cell cycle arrest, tubulin disruption, activation of the SAC and MCC are all characteristics of cdc20 driven checkpoint suspension of the cell cycle (Greil et al., 2022) with cell slippage into aneuploidy and subsequent levels of apoptosis (London and Biggins, 2014; Bonaiuti et al., 2018)

Table 7-1 Summary of results for DJ0206, DJ0041 and DJ0097 across all assays

Thienopyridine	Assay results					
	MTS	**AV/PI**	**Cell Cycle**	**Tubulin**	**RT-qPCR**	**Western Blots**
DJ0206	Non-significant reduction at 10 µM / 100 µM at 48 hours. Significant decreased cell survival at 1 to 100 µM at 72 hours	Significantly increased early/late apoptosis at 0.1 to 100 µM at 48 and 72 hours	Significantly increased G_2/M cell cycle arrest at 1 to 100 µM at all time points	Absence of tubulin spindle at mitosis (confocal) 42.9 % decreased tubulin polymerisation (equivalent to nocodazole control)	Significantly increased cdc20 mRNA expression. Significantly decreased CDK1 mRNA expression	Non-significant but +5.282 increased Cyclin B1. Significant -0.566 decreased fold change of cdc25C
DJ0041	Significantly decreased cell survival at 10 µM at 48 hours and 72 hours	Significantly increased early/late apoptosis at 10 to 100 µM at all time points	Significantly increased G_2/M cell cycle arrest at 1 to 100 µM at all time points	Evidence of spindle failure at mitosis (confocal) 2.5 % increased tubulin polymerisation	Significantly increased cdc20, Mad2, Aurora B, PLK2 and PLK4 mRNA expression. Significantly decreased CDK1 mRNA expression	Non-significant but +1.573 fold increase fold change of Cyclin B1. Non-significant but -0.081 decreased fold change of cdc25C
DJ0097	Significantly decreased cell survival at 1 µM and 10 µM at 72 hours	Small significantly increased early/late apoptosis at 0.1 to 100 µM at 24 and 48 hours. Large significantly increased early/late apoptosis at 1 to 100 µM at 72 hours	Significantly increased G_2/M cell cycle arrest at 1 to 100 µM at all time points	Evidence of spindle failure at mitosis (confocal) 29.5 % increased tubulin polymerisation	Significantly increased cdc20, Mad2, BubR1, Cyclin B1 and PLK2 mRNA expression. Significantly decreased CDK1 and TRIP13 mRNA expression	Non-significant but +3.270 increase fold change of Cyclin B1. Significantly decreased cdc25C

7.2 Limitations and future work

- This study investigated cell signalling via the B cell receptor via Btk and PLCG2, however no further signalling downstream of PLCG2 was elucidated and replication of data on Akt1 signalling via western blot was limited. Future work would investigate whether the effects of the thienopyridines are a result of inhibition of PLCG2 generation of secondary messengers diacylglycerol and Ca^{2+} and their downstream effects via Calcium signalling flowcytometry.
- PLCG2 is a key activator of Protein Kinase C and as shown in Figure 1-1, this signalling cascade links to actin cytoskeleton remodelling in B cells via RAP and Raf, with actin also playing a key role in mitosis alongside microtubules (Rizzelli et al., 2020; Jeruzalska and Mazur, 2023), therefore investigation of the effects of the novel thienopyridines on actin is warranted. Use of transfected cell line or live cell imaging of actin may help to better understand whether the thienopyridines exert direct effects on PLCG2 and its effectors (Kiyomitsu, 2016).
- Limited attempts were made at confocal microscopy for α-tubulin for chapter 4 (data not presented) which highlighted that some of these novel compounds appeared to have direct effects on spindle assembly, with much more rigorous work required to confirm this. Investigation of a wider range of targets which control the spindle assembly would provide mechanistic understanding of the effects seen in the RT-qPCR and western blotting assays. Immunofluorescent or live cell imaging of microtubules (Lukinavicius et al., 2014) or mitotic associated proteins (Dwivedi et al., 2023), combined with cell cycle synchronisation and time lapse microscopy (Pavani et al., 2023; Naso et al., 2024) may allow visualisation of the *in vitro* effects of the thienopyridines on these essential cell cycle regulators.
- This study has investigated the effects of thienopyridines using a DAUDI cell model of mature B cell malignancies, however future work in primary cell from patient donors with B cell lymphomas and leukaemia would see if these effects are translated into the biological variability in these patient groups, or

whether there are any effects of novel thienopyridine in primary lymphocytes in patients who have developed resistance to existing treatments.

7.3 Conclusions

In conclusion, this thesis has demonstrated that the series of novel thienopyridine compounds are significant inducers of apoptosis and cell cycle arrest in a time and concentration dependent manner, with direct disruption of tubulin polymerisation by both destabilising and stabilising mechanisms dependent on the chemical structure of the thienopyridine side chain modifications. Cell cycle arrest is likely caused as a result of interruption to tubulin dynamics, which in turn leads to an absence of mitotic spindle formation and an activation of the Spindle Assembly Checkpoint and Mitotic Checkpoint Complex. Further mechanistic investigation of these compounds is required but shows they show potential as anti-tubulin agents.

I. Appendices

8 APPENDICES

8.1 Chapter 6 – Additional Western Blot Targets

Data for western blot targets for Akt and Chk1 which had n=1 biological replicates are shown in Figure 8-1 and Figure 8-2

8.2 Chapter 6 – Additional RT-qPCR Targets with primer efficiencies outside of the 90-110 % range

Relative expression of the NIMA-related kinase Nek2 was seen to increase in all thienopyridines and positive controls apart from non-significant increases in DJ0014, DJ0021 (fold change 2.682 and 2.022 respectively), and DJ0209 which showed a slight, non-significant decrease in comparison to untreated DAUDI control (Figure 6-8C, fold change 0.925). DJ0199 (fold change 5.831, p=0.002) and DJ0206 (fold change 3.934, p= 0.013) reached statistical significance. While none of the thienopyridines reached the significant increase seen in the positive control Nocodazole (fold change 7.714, p=0.02), all were increased more than the Paclitaxel control (fold change 1.948, non-significant). However, caution needs to be attached to the interpretation of this data, due to the PCR standard curves being outside of the recommended 90-110 % efficiency range.

Expression of Nek7 showed no significant results Figure 8-3.

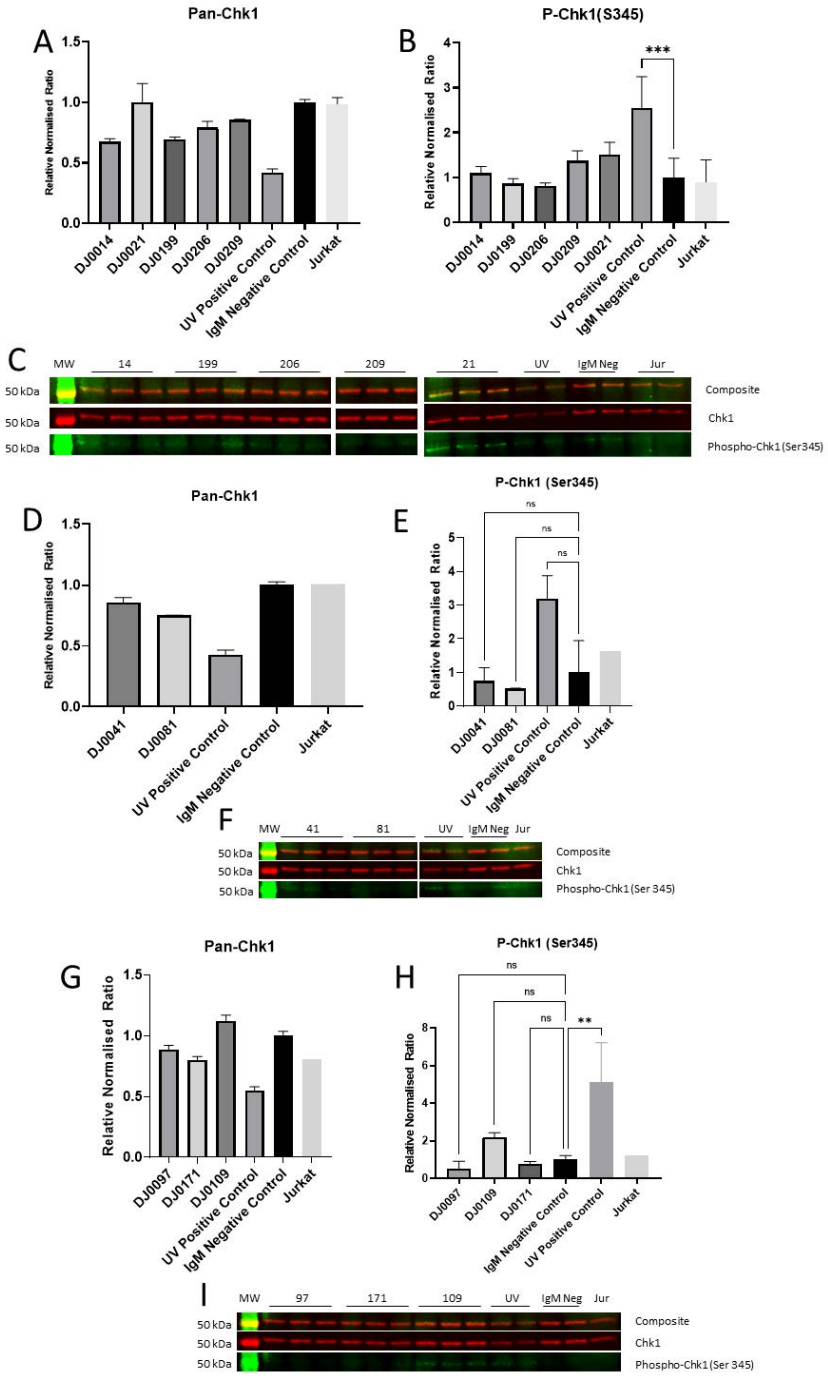

Figure 8-1 Western blotting results for important regulator of the cell cycle Chk1 (Pan- and phospho-Chk1 (Ser345)) following DAUDI cell treatment with: cyclooctane-ring containing thienopyridines DJ0014, DJ0021, DJ0199, DJ0206 and DJ0209, Pan-Chk1(A), phospho-Chk1 (B) and representative blot images (C); with cycloheptane-ring containing thienopyridines DJ0041 and DJ0081, Pan-Chk1(D), phospho-Chk1 (E) and representative blot images (F); and following treatment with cyclohexanone-ring containing thienopyridines DJ0097. DJ0109 and DJ0171, Pan-Chk1(G), phospho-Chk1 (H) and representative blot images (I). All blots show data for n=1 biological replicates with a minimum of n=2 technical replicates on each blot IgM Negative, Jurkat and UV controls show a minimum of n=1 replicates on each blot.

Ctrl: IgM positive control DAUDI lysates; Jur: Jurkat; MW: molecular weight ladder; Noc: nocodazole-treated DAUDI lysates; Pac: Paclitaxel-treated DAUDI lysates, UV-treated DAUDI lysates.

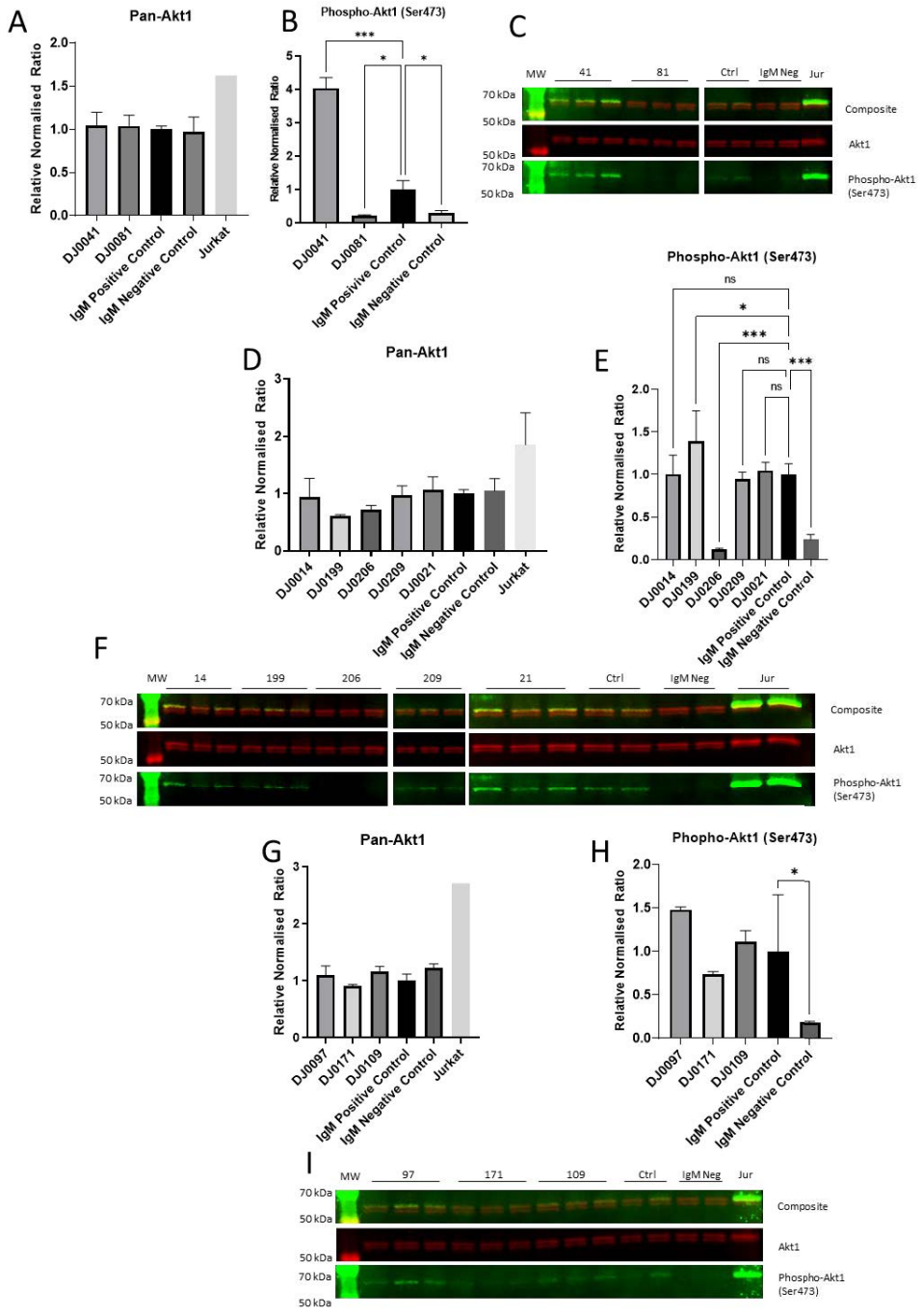

Figure 8-2Western blotting results for important downstream effector of B-cell receptor signalling Akt1 (Pan- and phospho-Akt1 (Ser473)) following DAUDI cell treatment with: cyclooctane-ring containing thienopyridines DJ0014, DJ0021, DJ0199, DJ0206 and DJ0209, Pan-Akt1(A), phospho- Akt1 (B) and representative blot images (C); with cycloheptane-ring containing thienopyridines DJ0041 and DJ0081, Pan- Akt1 (D), phospho- Akt1 (E) and representative blot images (F); and following treatment with cyclohexanone-ring containing thienopyridines DJ0097. DJ0109 and DJ0171, Pan-Akt1 (G), phospho- Akt1 (H) and representative blot images (I) All blots show data for n=1 biological replicates with a minimum of n=2 technical replicates on each blot IgM Negative and Jurkat controls show a minimum of n=1 replicates on each blot.

Ctrl: IgM positive control DAUDI lysates; Jur: Jurkat; MW: molecular weight ladder; Noc: nocodazole-treated DAUDI lysates; Pac: Paclitaxel-treated DAUDI lysates, UV-treated DAUDI lysates

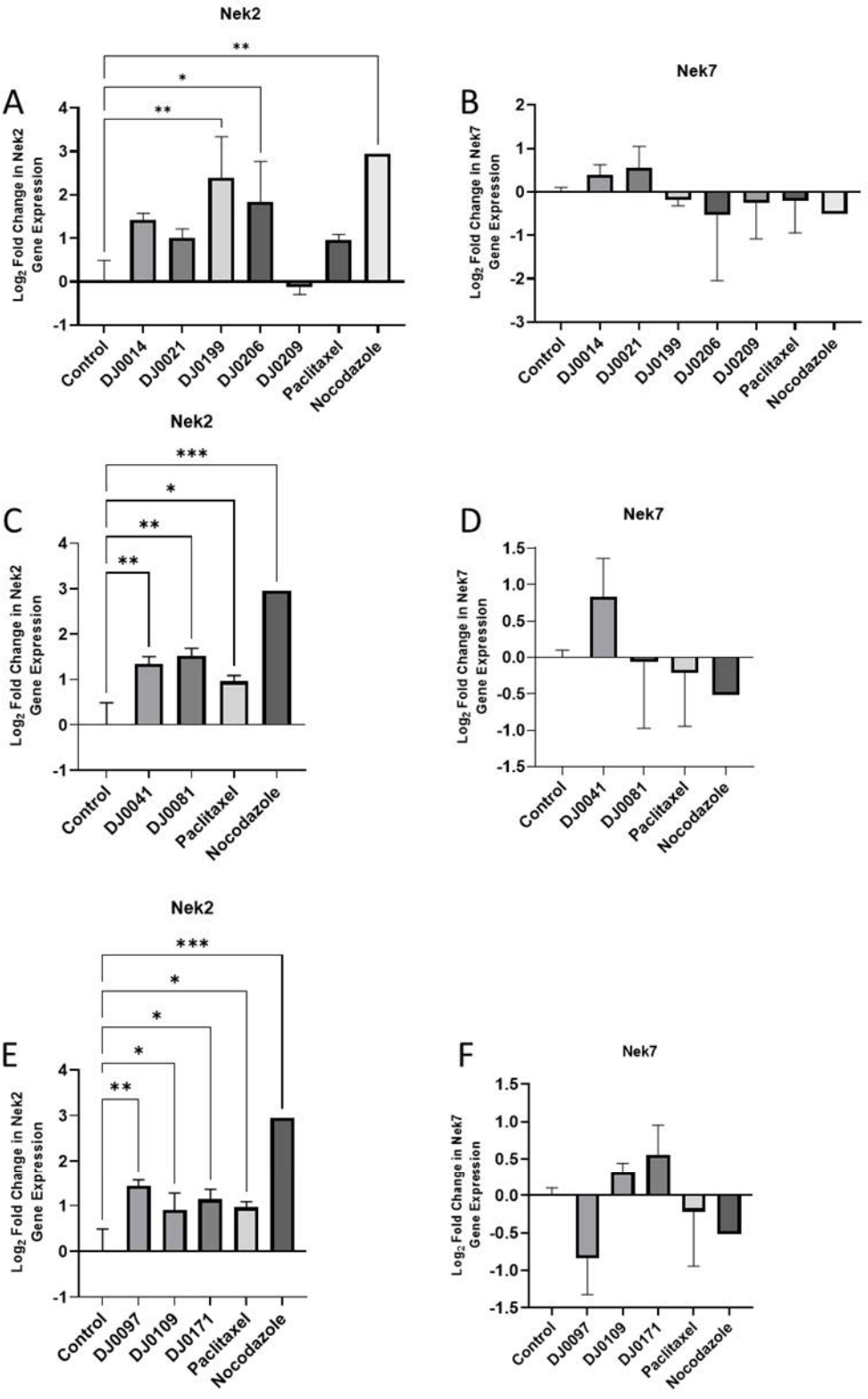
A
Nek2
Log2 Fold Change in Nek2 Gene Expression
Control
DJ0014
DJ0021
DJ0199
DJ0206
DJ0209
Paclitaxel
Nocodazole
B
Nek7
Log2 Fold Change in Nek7 Gene Expression
C
Nek2
DJ0041
DJ0081
D
Nek7
E
Nek2
DJ0097
DJ0109
DJ0171
F
Nek7

Figure 8-3 Figure 8-4 Multi-normalised relative gene expression in comparison to reference genes (TBP, PPIA, RPLP0 and EIF2B1) and untreated control of mRNA for genes regulating components of the Spindle Assembly Checkpoint in DAUDI cells following 48 hours of treatment with cyclohexanone-ring containing thienopyridine compounds (10 µM) and 1 minute stimulation of cells with Goat anti-human f(ab')2 IgM (20 µg/mL). Data represents n=3 biological replicates (unless indicated). Paclitaxel positive control n=2. Nocodazole positive control n=1.

Cyclooctane thienopyridine treated: Nek2 (DJ0014, DJ0199 and DJ0206 n=2) (A); Nek7 (DJ0014, DJ0199 and DJ0206 n=2) (B).

Cycloheptane thienopyridine treated: Nek2 (C); Nek7 (DJ0041 n=2) (D).

Cyclohexanone thienopyridine treated: Nek2 (DJ0171 n=2) (E); Nek7 (DJ0171 n=2) (F).

*Error bars represent SD. * = p-value ≤ 0.5, ** = p-value ≤ 0.1, *** = p-value ≤ 0.01*

REFERENCES

Abdelaziz, M. E., El-Miligy, M. M. M., Fahmy, S. M., Mahran, M. A. and Hazzaa, A. A. (2018) 'Design, synthesis and docking study of pyridine and thieno[2,3-b] pyridine derivatives as anticancer PIM-1 kinase inhibitors.' *Bioorganic Chemistry*, 80 pp. 674-692.

Abuelhassan, S., Bakhite, E. A., Abdel-Rahman, A. E., El-Mahdy, A. F. M., Saddik, A. A., Marae, I. S., Abdel-Hafez, S. H. and Tolba, M. (2022) 'Synthesis, photophysical properties, and biological activities of some new thienylpyridines, thienylthieno[2.3-b]pyridines and related fused heterocyclic compounds.' *Journal of Heterocyclic Chemistry*, pp. 1-13.

Adamski, M. G., Li, Y., Yu, H., Wagner, E., Amarjeet, S., Baird, A. E. and Soper, S. A. (2012) 'Abstract 3259: Leukocyte subset specific gene expression in acute stroke patients.' *Stroke*, 43(2) p. A3259.

Agarwal, P. K. (2006) 'Enzymes: An integrated view of structure, dynamics and function.' *Microbial Cell Factories*, 5(2) pp. 1-12.

Ahmed, A. A. M., Mekky, A. E. M. and Sanad, S. M. H. (2022a) 'New bis(pyrazolo[3,4-b]pyridines) and bis(thieno[2,3-b]pyridines) as potential acetylcholinesterase inhibitors: synthesis, in vitro and SwissADME prediction study.' *Journal of the Iranian Chemical Society*, 19(11) pp. 4457-4471.

Ahmed, A. A. M., Mekky, A. E. M. and Sanad, S. M. H. (2022b) 'New piperazine-based bis(thieno[2,3-b]pyridine) and bis(pyrazolo[3,4-b]pyridine) hybrids linked to benzofuran units: Synthesis and in vitro screening of potential acetylcholinesterase inhibitors.' *Synthetic Communications*, 52(6) pp. 912-925.

Al-Sawaf, O., Zhang, C., Tandon, M., Sinha, A., Fink, A.-M., Robrecht, S., Samoylova, O., Liberati, A. M., et al. (2020) 'Venetoclax plus obinutuzumab versus chlorambucil plus obinutuzumab for previously untreated chronic lymphocytic leukaemia (CLL14): follow-up results from a multicentre, open-label, randomised, phase 3 trial.' *The Lancet Oncology*, 21(9) pp. 1188-1200.

Alisi, A., Giannini, C., Spaziani, A., Anticoli, S., Caini, P., Zignego, A. L. and Balsano, C. (2007) 'Hepatitis C virus core protein enhances B lymphocyte proliferation.' *Digestive and Liver Disease*, 39 pp. S72-S75.

AlKhalil, M., Al-Hiari, Y., Kasabri, V., Arabiyat, S., Al-Zweiri, M., Mamdooh, N. and Telfah, A. (2020) 'Selected pharmacotherapy agents as antiproliferative and anti-inflammatory compounds.' *Drug Development Research*, 81(4) pp. 470-490.

Alsubaie, M., Nasri, S. M., Eidi, H. A., Alsayegh, M., Alabdulkareem, I. B., Aljedai, A., Alaskar, A., Albabtain, S. A., et al. (2021) 'In vitro assessment of the efficiency of the PIM-1 kinase

pharmacological inhibitor as a potential treatment for Burkitt's lymphoma.' *Oncology Letters*, 22(2) pp. 1-8.

Amorim, R., de Meneses, M. D. F., Borges, J. C., da Silva Pinheiro, L. C., Caldas, L. A., Cirne-Santos, C. C., de Mello, M. V. P., de Souza, A. M. T., et al. (2017) 'Thieno[2,3-b]pyridine derivatives: a new class of antiviral drugs against Mayaro virus.' *Archives of Virology*, 162(6) pp. 1577-1587.

Anania, V. G. and Lill, J. R. (2015) 'Proteomic tools for the characterization of cell death mechanisms in drug discovery.' *Proteomics Clinical Applications*, 9(7-8) pp. 671-683.

Andersen, C. L., Jensen, J. L. and Ørntoft, T. F. (2004) 'Normalization of Real-Time Quantitative Reverse Transcription-PCR Data: A Model-Based Variance Estimation Approach to Identify Genes Suited for Normalization, Applied to Bladder and Colon Cancer Data Sets.' *Cancer Research*, 64 pp. 5245–5250.

Anderson, M. A., Tam, C., Lew, T. E., Juneja, S., Juneja, M., Westerman, D., Wall, M., Lade, S., et al. (2017) 'Clinicopathological features and outcomes of progression of CLL on the BCL2 inhibitor venetoclax.' *Blood*, 129(25) pp. 3362-3370.

Appe, A., Hansen, M., Ebbesen, L. H., Aggerholm, A., Bentzen, H. and Nyvold, C. G. (2015) 'Abstract: PB1937 Differential expression of robo1 in mantle cell lymphoma, chronic lymphocytic leukemia and acute myeloid leukemia.' *Haematologica*, 100 pp. 761-762.

Arababadi, M. K. (2014) 'Decreased expressions of TLR9 and its signaling molecules in chronic HBV infected patients.' *Journal of Antivirals and Antiretrovirals*, 2014 p. 204.

Arabshahi, H. J., Leung, E., Barker, D. and Reynisson, J. (2014) 'The development of thieno[2,3-b]pyridine analogues as anticancer agents applying in silico methods.' *Medicinal Chemistry Communications*, 5(2) pp. 186-191.

Arabshahi, H. J., van Rensburg, M., Pilkington, L. I., Jeon, C. Y., Song, M., Gridel, L.-M., Leung, E., Barker, D., et al. (2015) 'A synthesis, in silico, in vitro and in vivo study of thieno[2,3-b]pyridine anticancer analogues.' *Medicinal Chemistry Communications*, 6(11) pp. 1987-1997.

Artero-Castro, A., Perez-Alea, M., Feliciano, A., Leal, J. A., Genestar, M., Castellvi, J., Peg, V., Ramon, Y. C. S., et al. (2015) 'Disruption of the ribosomal P complex leads to stress-induced autophagy.' *Autophagy*, 11(9) pp. 1499-1519.

Arthur, R., Wathen, A., Lemm, E. A., Stevenson, F. K., Forconi, F., Linley, A. J., Steele, A. J., Packham, G., et al. (2022) 'BTK-independent regulation of calcium signalling downstream of the B-cell receptor in malignant B-cells.' *Cellular Signalling*, 96 p. 110358.

Autore, F., Pasquale, R., Innocenti, I., Fresa, A., Sora', F. and Laurenti, L. (2021) 'Autoimmune Hemolytic Anemia in Chronic Lymphocytic Leukemia: A Comprehensive Review.' *Cancers*, 13(22) p. 5804.

Azoulay, D., Herishanu, Y., Shapiro, M., Brenshaft, Y., Suriu, C., Akria, L. and Braester, A. (2016) 'High peripheral blood circulating BDNF levels are associated with good prognosis in CLL patients; A CXCR-4 dependent effect?' *Blood*, 128(22)

Azzaoui, I., Uhel, F., Rossille, D., Pangault, C., Dulong, J., Le Priol, J., Lamy, T., Houot, R., et al. (2016) 'T-cell defect in diffuse large B-cell lymphomas involves expansion of myeloid-derived suppressor cells.' *Blood*, 128(8) pp. 1081-1092.

Bailon-Moscoso, N., Romero-Benavides, J. C. and Ostrosky-Wegman, P. (2014) 'Development of anticancer drugs based on the hallmarks of tumor cells.' *Tumor Biology*, 35(5) pp. 3981-3995.

Ballerini, P., Dovizio, M., Bruno, A., Tacconelli, S. and Patrignani, P. (2018) 'P2Y(12) Receptors in Tumorigenesis and Metastasis.' *Frontiers in Pharmacology*, 9 p. 66.

Bartek, J. and Lukas, J. (2007) 'DNA damage checkpoints: from initiation to recovery or adaptation.' *Current Opinion in Cell Biology*, 19(2) pp. 238-245.

Bates, D. and Eastman, A. (2017) 'Microtubule destabilising agents: far more than just antimitotic anticancer drugs.' *British Journal of Clinical Pharmacology*, 83(2) pp. 255-268.

Bernasconi, M., Berger, C., Sigrist, J. A., Bonanomi, A., Sobek, J., Niggli, F. K. and Nadal, D. (2006) 'Quantitative profiling of housekeeping and Epstein-Barr virus gene transcription in Burkitt lymphoma cell lines using an oligonucleotide microarray.' *Virology Journal*, 3 p. 43.

Berridge, M. V. and Tan, A. S. (1993) 'Characterization of the Cellular Reduction of 3-(4,5-dimethylthiazol-2-yl)-2,5-diphenyltetrazolium bromide (MTT): Subcellular Localization, Substrate Dependence, and Involvement of Mitochondrial Electron Transport in MTT Reduction.' *Archives of Biochemistry and Biophysics*, 303(2) pp. 474-482.

Berridge, M. V., Herst, P. M. and Tan, A. S. (2005) 'Tetrazolium dyes as tools in cell biology: new insights into their cellular reduction.' *In* El-Gewely, M. R. (ed.) El-Gewely, M. R. *Biotechnology Annual Review*. Vol. 11. Elsevier, pp. 127-152. https://www.ncbi.nlm.nih.gov/pubmed/16216776

Bhanja, A., Rey-Suarez, I., Song, W. and Upadhyaya, A. (2022) 'Bidirectional feedback between BCR signaling and actin cytoskeletal dynamics.' *The FEBS Journal*, 289(15) pp. 4430-4446.

Binsaleh, N. K., Wigley, C. A., Whitehead, K. A., van Rensburg, M., Reynisson, J., Pilkington, L. I., Barker, D., Jones, S., et al. (2018) 'Thieno[2,3-b]pyridine derivatives are potent anti-platelet drugs, inhibiting platelet activation, aggregation and showing synergy with aspirin.' *European Journal of Medicinal Chemistry*, 143 pp. 1997-2004.

Blengio, F., Raggi, F., Pierobon, D., Cappello, P., Eva, A., Giovarelli, M., Varesio, L. and Bosco, M. C. (2013) 'The hypoxic environment reprograms the cytokine/chemokine expression profile of human mature dendritic cells.' *Immunobiology*, 218(1) pp. 76-89.

Bonaiuti, P., Chiroli, E., Gross, F., Corno, A., Vernieri, C., Stefl, M., Cosentino Lagomarsino, M., Knop, M., et al. (2018) 'Cells Escape an Operational Mitotic Checkpoint through a Stochastic Process.' *Current Biology*, 28(1) pp. 28-37 e27.

Borbet, T. C., Hines, M. J. and Koralov, S. B. (2021) 'MicroRNA regulation of B cell receptor signaling.' *Immunological Reviews*, 304(1) pp. 111-125.

Bosl, M. W., Osterode, E., Bararia, D., Pastore, A., Hiddemann, W., Weigert, O., Staiger, A. M., Ott, G., et al. (2015) 'STAT6 is recurrently and significantly mutated in follicular lymphoma and enhances the IL-4 induced expression of membrane-bound and soluble CD23.' *Blood*, 126(23) p. 3923.

Bramer, W. M., Milic, J. and Mast, F. (2017) 'Reviewing retrieved references for inclusion in systematic reviews using EndNote.' *Journal of the Medical Library Association*, 105(1) pp. 84-87.

Brkljačić, J., Tanić, N., Milutinović, D. J., Elaković, I., Jovanović, S. M., Perišić, T., Dundjerski, J. and Matić, G. (2010) 'Validation of endogenous controls for gene expression studies in peripheral lymphocytes from war veterans with and without PTSD.' *BMC Molecular Biology*, 11(26) pp. 1-9.

Brugnoletti, F., Chiaretti, S., Elia, L., Negulici, A., Vignetti, M., Vitale, A., Guarini, A., Foa, R., et al. (2013) 'Analysis of CRLF2 expression in a cohort of 91 newly diagnosed adult patients with B-cell precursor acute lymphoblastic leukemia: Correlation with clinico-biological features and outcome.' *Haematologica*, 98 pp. 4-5.

Burger, J. A. and Chiorazzi, N. (2013) 'B cell receptor signaling in chronic lymphocytic leukemia.' *Trends in Immunology*, 34(12) pp. 592-601.

Burger, J. A. and Wiestner, A. (2018) 'Targeting B cell receptor signalling in cancer: Preclinical and clinical advances.' *Nature Reviews Cancer*, 18(3) pp. 148-167.

Bustin, S. A., Beaulieu, J.-F., Huggett, J., Jaggi, R., Kibenge, F. S. B., Olsvik, P. A.,, Penning, L. C. and Toegel, S. (2010) 'MIQE précis Practical implementation of minimum standard

guideliens for fluorescence-based RT-qPCR experiments.' *BMC Molecular Biology*, 11(74) pp. 1-5.

Bustin, S. A., Benes, V., Garson, J. A., Hellemans, J., Huggett, J., Kubista, M., Mueller, R., Nolan, T., et al. (2009) 'The MIQE guidelines: minimum information for publication of quantitative real-time PCR experiments.' *Clinical Chemistry*, 55(4) pp. 611-622.

Byrd, J. C., Furman, R. R., Coutre, S. E., Flinn, I. W., Burger, J. A., Blum, K. A., Grant, B., Sharman, J. P., et al. (2013) 'Targeting BTK with ibrutinib in relapsed chronic lymphocytic leukemia.' *New England Journal of Medicine*, 369(1) pp. 32-42.

Byrd, J. C., Harrington, B., O'Brien, S., Jones, J. A., Schuh, A., Devereux, S., Chaves, J., Wierda, W. G., et al. (2016) 'Acalabrutinib (ACP-196) in relapsed chronic lymphocytic leukemia.' *New England Journal of Medicine*, 374(4) pp. 323-332.

Caballero-Palacios, M. C., Villegas-Ruiz, V., Ramirez-Chiquito, J. C., Juarez-Mendez, S., Medina-Vera, I., Zapata-Tarres, M., Cardenas-Cardos, R., Mojica-Espinosa, R., et al. (2021) 'v-myb avian myeloblastosis viral oncogene homolog expression is a potential molecular diagnostic marker for B-cell acute lymphoblastic leukemia.' *Asia-Pacific Journal of Clinical Oncology*, 17(1) pp. 60-67.

Cantrell, D. (2015) 'Signaling in Lymphocyte Activation.' *Cold Spring Harbor Perspectives in Biology*, 7(6) p. a018788.

Carbone, P. P., Kaplan, H. S., Musshoff, K., Smithers, D. W. and Tubiana, M. (1971) 'Report of the Committee on Hodgkin's Disease Staging Classification.' *Cancer Research*, 31(11) pp. 1860-1861.

Carlson, K. and Ocean, A. J. (2011) 'Peripheral neuropathy with microtubule-targeting agents: occurrence and management approach.' *Clinical Breast Cancer*, 11(2) pp. 73-81.

Carvalheiro, T., Velada, I., Valado, A., Mendes, F., Martinho, A., António, N., Gonçalves, L., Providência, L., et al. (2012a) 'Phenotypic and Functional Alterations on Inflammatory Peripheral Blood Cells After Acute Myocardial Infarction.' *Journal of Cardiovascular Translational Research*, 5(3) pp. 309-320.

Carvalheiro, T., Rodrigues, A., Lopes, A., Inês, L., Velada, I., Ribeiro, A., Martinho, A., Silva, J. A. P., et al. (2012b) 'Tolerogenic versus Inflammatory Activity of Peripheral Blood Monocytes and Dendritic Cells Subpopulations in Systemic Lupus Erythematosus.' *Clinical and Developmental Immunology*, 2012 p. 934161.

Chaganti, S., Illidge, T., Barrington, S., McKay, P., Linton, K., Cwynarski, K., McMillan, A., Davies, A., et al. (2016) 'Guidelines for the management of diffuse large B-cell lymphoma.' *British Journal of Haematology*, 174(1) pp. 43-56.

Chambard, J. C., Lefloch, R., Pouyssegur, J. and Lenormand, P. (2007) 'ERK implication in cell cycle regulation.' *Biochimica et Biophysica Acta*, 1773(8) pp. 1299-1310.

Chang, F., Lee, J. T., Navolanic, P. M., Steelman, L. S., Shelton, J. G., Blalock, W. L., Franklin, R. A. and McCubrey, J. A. (2003) 'Involvement of PI3K/Akt pathway in cell cycle progression, apoptosis, and neoplastic transformation: a target for cancer chemotherapy.' *Leukemia*, 17(3) pp. 590-603.

Chauveau, A., Le Floc'h, A., Bantilan, N. S., Koretzky, G. A. and Huse, M. (2014) 'Diacylglycerol kinase establishes T cell polarity by shaping DAG accumulation at the immunological synapse.' *Science Signaling*, 7(340) p. ra82.

Cheson, B. D., Fisher, R. I., Barrington, S. F., Cavalli, F., Schwartz, L. H., Zucca, E. and Lister, T. A. (2014) 'Recommendations for Initial Evaluation, Staging, and Response Assessment of Hodgkin and Non-Hodgkin Lymphoma: The Lugano Classification.' *Journal of Clinical Oncology*, 32(27) pp. 3059-3067.

Ciccia, A. and Elledge, S. J. (2010) 'The DNA damage response: making it safe to play with knives.' *Molecular Cell*, 40(2) pp. 179-204.

Congmin, G., Mu, Z., Yihui, M. and Hanliang, L. (2006) 'Survivin - An attractive target for RNAi in non-Hodgkin's lymphoma, Daudi cell line as a model.' *Leukemia and Lymphoma*, 47(9) pp. 1941-1948.

Cook, B. M., Wozniak, K. M., Proctor, D. A., Bromberg, R. B., Wu, Y., Slusher, B. S., Littlefield, B. A., Jordan, M. A., et al. (2018) 'Differential Morphological and Biochemical Recovery from Chemotherapy-Induced Peripheral Neuropathy Following Paclitaxel, Ixabepilone, or Eribulin Treatment in Mouse Sciatic Nerves.' *Neurotoxicity Research*, 34(3) pp. 677-692.

Cordeiro, M. H., Smith, R. J. and Saurin, A. T. (2020) 'Kinetochore phosphatases suppress autonomous Polo-like kinase 1 activity to control the mitotic checkpoint.' *Journal of Cell Biology*, 219(12) p. e202002020.

Courtney, K. D., Corcoran, R. B. and Engelman, J. A. (2010) 'The PI3K pathway as drug target in human cancer.' *Journal of Clinical Oncology*, 28(6) pp. 1075-1083.

Cozen, W., Edlund, C. K., Li, D., Timofeeva, M., Byrnes, G., Brennan, P., Conti, D. V., Diepstra, A., et al. (2013) 'A meta-analysis of hodgkin lymphoma reveals 19p13.3 (TCF3) as a novel susceptibility Loc.' *Blood*, 122(21) p. 626.

Crncec, A. and Hochegger, H. (2019) 'Triggering mitosis.' *FEBS Letters*, 593(20) pp. 2868-2888.

Crowley, L. C., Marfell, B. J., Scott, A. P., Boughaba, J. A., Chojnowski, G., Christensen, M. E. and Waterhouse, N. J. (2016) 'Dead Cert: Measuring Cell Death.' *Cold Spring Harbor Protocols*, 2016(12)

D'Arcy, M. S. (2019) 'Cell death: a review of the major forms of apoptosis, necrosis and autophagy.' *Cell Biology International*, 43(6) pp. 582-592.

Dabaeva, V. V., Baghdasaryan, M. R., Paronikyan, R. G., Nazaryan, I. M., Hakobyan, H. G., Hunanyan, L. S., Paronikyan, E. G. and Dashyan, S. S. (2022) 'Synthesis, Neurotropic Activity, and Molecular Docking of New Condensed Thieno[2,3-b]pyridine Derivatives.' *Russian Journal of Bioorganic Chemistry*, 48(1) pp. 125-134.

Davis, A., Martinez, S., Nelson, D. and Middleton, K. (2010) 'A tubulin polymerization microassay used to compare ligand efficacy.' *In* Wilson, L. and Correia, J. J. (eds.) *Microtubules, in vitro*. Vol. 95. Oxford, UK.: Elsevier, pp. 331-351. https://www.ncbi.nlm.nih.gov/pubmed/20466143

De Bont, E. S. J. M., Guikema, J. E. J., Scherpen, F., Meeuwsen, T., Kamps, W. A., Vellenga, E. and Bos, N. A. (2001) 'Mobilized human CD34+ hematopoietic stem cells enhance tumor growth in a nonobese diabetic/severe combined immunodeficient mouse model of human non-Hodgkin's lymphoma.' *Cancer Research*, 61(20) pp. 7654-7659.

De Cassia Carvalho Melo, R., Bigarella, C., Baratti, M. O., Traina, F. and Olalla Saad, S. T. (2011) 'CXCR7 is highly expressed in acute lymphoblastic leukemia and potentiates the chemotactic response to SDF-1.' *Blood*, 118(21) p. 1482.

De Franco, E., Caswell, R., Johnson, M. B., Wakeling, M. N., Zung, A., Dung, V. C., Bich Ngoc, C. T., Goonetilleke, R., et al. (2020) 'De Novo Mutations in EIF2B1 Affecting eIF2 Signaling Cause Neonatal/Early-Onset Diabetes and Transient Hepatic Dysfunction.' *Diabetes*, 69(3) pp. 477-483.

de Siqueira Figueredo, D., Gitaí, D. L. G. and de Andrade, T. G. (2015) 'Daily variations in the expression of miR-16 and miR-181a in human leukocytes.' *Blood Cells, Molecules, and Diseases*, 54(4) pp. 364-368.

De Spiegelaere, W., Dern-Wieloch, J., Weigel, R., Schumacher, V., Schorle, H., Nettersheim, D., Bergmann, M., Brehm, R., et al. (2015) 'Reference gene validation for RT-qPCR, a note on different available software packages.' *PLoS One*, 10(3) p. e0122515.

de Viron, E., Knoops, L., Connerotte, T., Smal, C., Michaux, L., Saussoy, P., Vannuffel, P., Beert, E., et al. (2009) 'Impaired up-regulation of polo-like kinase 2 in B-cell chronic lymphocytic leukaemia lymphocytes resistant to fludarabine and 2-chlorodeoxyadenosine: a potential marker of defective damage response.' *British Journal ofHaematology*, 147(5) pp. 641-652.

Derveaux, S., Vandesompele, J. and Hellemans, J. (2010) 'How to do successful gene expression analysis using real-time PCR.' *Methods*, 50(4) pp. 227-230.

Deshpande, A., Sicinski, P. and Hinds, P. W. (2005) 'Cyclins and cdks in development and cancer: a perspective.' *Oncogene*, 24(17) pp. 2909-2915.

Desjardins, M., Xue, D. and Mazer, B. D. (2017) 'Impaired semaphorin 4C (SEMA4C) induction in patients with common variable immunodeficiency (CVID).' *Journal of Allergy and Clinical Immunology*, 139(2) p. 550.

Di Nisio, C., Sancilio, S., Di Giacomo, V., Rapino, M., Sancillo, L., Genovesi, D., Di Siena, A., Rana, R. A., et al. (2016) 'Involvement of cyclic-nucleotide response element-binding family members in the radiation response of Ramos B lymphoma cells.' *International Journal of Oncology*, 48(1) pp. 28-36.

Diamantopoulos, P. T., Polonyfi, K., Bazanis, E., Saridaki, A. M., Variami, E., Mantzourani, M., Siakantaris, M., Meletis, J., et al. (2011) 'Regulation of apoptosis and oxidative stress by LMP1 oncoprotein of epstein-barr virus in patients with low grade B-cell leukemic lymphomas.' *Blood*, 118(21) p. 5212.

Dotsenko, V. V., Buryi, D. S., Lukina, D. Y. and Krivokolysko, S. G. (2020) 'Recent advances in the chemistry of thieno[2,3-b]pyridines 1. Methods of synthesis of thieno[2,3-b]pyridines.' *Russian Chemical Bulletin*, 69(10) pp. 1829-1858.

Dreyling, M., Ghielmini, M., Rule, S., Salles, G., Vitolo, U. and Ladetto, M. (2016) 'Newly diagnosed and relapsed follicular lymphoma: ESMO Clinical Practice Guidelines for diagnosis, treatment and follow-up.' *Annals of Oncology*, 27(Supplement 5) pp. v83-v90.

Dreyling, M., Campo, E., Hermine, O., Jerkeman, M., Le Gouill, S., Rule, S., Shpilberg, O., Walewski, J., et al. (2017) 'Newly diagnosed and relapsed mantle cell lymphoma: ESMO Clinical Practice Guidelines for diagnosis, treatment and follow-up.' *Annals of Oncology*, 28(Supplement 4) pp. iv62-iv71.

Drolet, J. P., Guay, J., Nouhi, Y. and Mazer, B. (2010) 'Expression of semaphorin 4C by Th2-stimulated B cells.' *Allergy, Asthma and Clinical Immunology*, 6(Supplement 2) p. P23.

Druker, B. J., Talpaz, M., Resta, D. J., Peng, B., Buchdunger, E., Ford, J. M., Lydon, N. B., Kantarjian, H., et al. (2001) 'Efficacy and Safety of a Specific Inhibitor of the BCR-ABL Tyrosine Kinase in Chronic Myeloid Leukemia.' *New England Journal of Medicine*, 344(14) pp. 1031-1037.

Dumontet, C. and Jordan, M. A. (2010) 'Microtubule-binding agents: a dynamic field of cancer therapeutics.' *Nature Reviews Drug Discovery*, 9(10) pp. 790-803.

Dunleavy, K., Erdmann, T. and Lenz, G. (2018) 'Targeting the B-cell receptor pathway in diffuse large B-cell lymphoma.' *Cancer Treatment Reviews*, 65 pp. 41-46.

Dwivedi, D., Harry, D. and Meraldi, P. (2023) 'Mild replication stress causes premature centriole disengagement via a sub-critical Plk1 activity under the control of ATR-Chk1.' *Nature Communications*, 14(1) p. 6088.

Dwivedi, N., Mondal, S., P. K, S., T, S., Sachdeva, K., Bathula, C., K, V., K. S, N., et al. (2020) 'Relative quantification of BCL2 mRNA for diagnostic usage needs stable uncontrolled genes as reference.' *PLOS ONE*, 15(8) p. e0236338.

Ebenezer, O., Shapi, M. and Tuszynski, J. A. (2022) 'A Review of the Recent Developments of Molecular Hybrids Targeting Tubulin Polymerization.' *International Journal of Molecular Sciences*, 23(7) p. 4001.

Ebi, M., Kataoka, H., Shimura, T., Hirata, Y., Mizushima, T., Mizoshita, T., Tanaka, M., Tsukamoto, H., et al. (2011) 'The role of neuregulin4 and HER4 in gastrointestinal malignant lymphoma.' *Molecular Medicine Reports*, 4(6) pp. 1151-1155.

Ediriweera, M. K., Tennekoon, K. H. and Samarakoon, S. R. (2019) 'In vitro assays and techniques utilized in anticancer drug discovery.' *Journal of Applied Toxicology*, 39(1) pp. 38-71.

Efferth, T., Fabry, U. and Osieka, R. (2002) 'Interleukin-6 affects melphalan-induced DNA damage and repair in human multiple myeloma cells.' *Anticancer Research*, 22(1) pp. 231-234.

Eichhorst, B., Robak, T., Montserrat, E., Ghia, P., Hillmen, P., Hallek, M. and Buske, C. (2015) 'Chronic lymphocytic leukaemia: ESMO Clinical Practice Guidelines for diagnosis, treatment and follow-up.' *Annals of Oncology*, 26(Supplement 5) pp. v78-v84.

Eichhorst, B., Robak, T., Montserrat, E., Ghia, P., Niemann, C. U., Kater, A. P., Gregor, M., Cymbalista, F., et al. (2021) 'Chronic lymphocytic leukaemia: ESMO Clinical Practice Guidelines for diagnosis, treatment and follow-up.' *Annals of Oncology*, 32(1) pp. 23-33.

Eichhorst, B., Niemann, C. U., Kater, A. P., Furstenau, M., von Tresckow, J., Zhang, C., Robrecht, S., Gregor, M., et al. (2023) 'First-Line Venetoclax Combinations in Chronic Lymphocytic Leukemia.' *New England Journal of Medicine*, 388(19) pp. 1739-1754.

Elias, E. E., Sarapura Martinez, V. J., Amondarain, M., Colado, A., Cordini, G., Bezares, R. F., Fernandez Grecco, H., Custidiano, M. d. R., et al. (2022) 'Venetoclax-resistant CLL cells show a highly activated and proliferative phenotype.' *Cancer Immunology, Immunotherapy*, 71(4) pp. 979-987.

Elsherif, M. A. (2020) 'Antibacterial evaluation and molecular properties of pyrazolo[3,4-b] pyridines and thieno[2,3-b]pyridines.' *Journal of Applied Pharmaceutical Science*, 11(6) pp. 118-124.

Emadi, A., Jones, R. J. and Brodsky, R. A. (2009) 'Cyclophosphamide and cancer: golden anniversary.' *Nature Reviews Clinical Oncology*, 6 pp. 638–647.

Engelstoft, M. S., Park, W. M., Sakata, I., Kristensen, L. V., Husted, A. S., Osborne-Lawrence, S., Piper, P. K., Walker, A. K., et al. (2013) 'Seven transmembrane G protein-coupled receptor repertoire of gastric ghrelin cells.' *Molecular Metabolism*, 2(4) pp. 376-392.

Errico, A. and Costanzo, V. (2012) 'Mechanisms of replication fork protection: a safeguard for genome stability.' *Critical Reviews in Biochemistry and Molecular Biology*, 47(3) pp. 222-235.

Eurtivong, C., Reynisdottir, I., Kuczma, S., Furkert, D. P., Brimble, M. A. and Reynisson, J. (2016) 'Identification of anticancer agents based on the thieno[2,3-b]pyridine and 1H-pyrazole molecular scaffolds.' *Bioorganic & Medicinal Chemistry*, 24(16) pp. 3521-3526.

Eurtivong, C., Semenov, V., Semenova, M., Konyushkin, L., Atamanenko, O., Reynisson, J. and Kiselyov, A. (2017) '3-Amino-thieno[2,3-b]pyridines as microtubule-destabilising agents: Molecular modelling and biological evaluation in the sea urchin embryo and human cancer cells.' *Bioorganic & Medicinal Chemistry*, 25(2) pp. 658-664.

Fagundes, R. and Teixeira, L. K. (2021) 'Cyclin E/CDK2: DNA Replication, Replication Stress and Genomic Instability.' *Frontiers in Cell Developmental Biology*, 9 p. 774845.

Fanale, D., Bronte, G., Passiglia, F., Calò, V., Castiglia, M., Di Piazza, F., Barraco, N., Cangemi, A., et al. (2015) 'Stabilizing versus Destabilizing the Microtubules: A Double-Edge Sword for an Effective Cancer Treatment Option?' *Analytical Cellular Pathology*, 2015 p. 690916.

Feng, L., Reynisdottir, I. and Reynisson, J. (2012) 'The effect of PLC-gamma2 inhibitors on the growth of human tumour cells.' *European Journal of Medicinal Chemistry*, 54 pp. 463-469.

Feng, M., Huang, B., Xu, X., Chen, Z. and Du, Z. (2011) 'DLC-1 as a modulator of proliferation, apoptosis and migration in Burkitt's lymphoma cells.' *Molecular Biology Reports*, 38(3) pp. 1915-1920.

Ferraresso, M., Turolo, S., Belingheri, M., Tirelli, A. S., Cortinovis, I., Milani, S., Edefonti, A. and Ghio, L. (2015) 'Relationship between mRNA expression levels of CYP3A4, CYP3A5 and SXR in peripheral mononuclear blood cells and aging in young kidney transplant recipients under tacrolimus treatment.' *Pharmacogenomics*, 16(5) pp. 483-491.

Fesik, S. W. (2005) 'Promoting apoptosis as a strategy for cancer drug discovery.' *Nature Reviews Cancer*, 5(11) pp. 876-885.

Fischer, K., Bahlo, J., Fink, A. M., Goede, V., Herling, C. D., Cramer, P., Langerbeins, P., von Tresckow, J., et al. (2016) 'Long-term remissions after FCR chemoimmunotherapy in previously untreated patients with CLL: updated results of the CLL8 trial.' *Blood*, 127(2) pp. 208-215.

Fischer, K., Al-Sawaf, O., Bahlo, J., Fink, A.-M., Tandon, M., Dixon, M., Robrecht, S., Warburton, S., et al. (2019) 'Venetoclax and Obinutuzumab in Patients with CLL and Coexisting Conditions.' *New England Journal of Medicine*, 380(23) pp. 2225-2236.

Flinn, I. W., Kahl, B. S., Leonard, J. P., Furman, R. R., Brown, J. R., Byrd, J. C., Wagner-Johnston, N. D., Coutre, S. E., et al. (2014) 'Idelalisib, a selective inhibitor of phosphatidylinositol 3-kinase-delta, as therapy for previously treated indolent non-Hodgkin lymphoma.' *Blood*, 123(22) pp. 3406-3413.

Foley, E. A., Maldonado, M. and Kapoor, T. M. (2011) 'Formation of stable attachments between kinetochores and microtubules depends on the B56-PP2A phosphatase.' *Nature Cell Biology*, 13(10) pp. 1265-1272.

Fragkos, M., Ganier, O., Coulombe, P. and Mechali, M. (2015) 'DNA replication origin activation in space and time.' *Nature Reviews Molecular Cell Biology*, 16(6) pp. 360-374.

Fruman, D. A. and Rommel, C. (2014) 'PI3K and cancer: Lessons, challenges and opportunities.' *Nature Reviews Drug Discovery*, 13(2) pp. 140-156.

Fry, A. M., Bayliss, R. and Roig, J. (2017) 'Mitotic Regulation by NEK Kinase Networks.' *Frontiers in Cell and Developmental Biology*, 5 p. 102.

Fukuyama, T., Yan, L., Tanaka, M., Yamaoka, M., Saito, K., Ti, S. C., Liao, C. C., Hsia, K. C., et al. (2022) 'Morphological growth dynamics, mechanical stability, and active microtubule mechanics underlying spindle self-organization.' *Proceedings of the National Academy of Sciences of the United States of America*, 119(44) p. e2209053119.

Furman, R. R., Sharman, J. P., Coutre, S. E., Cheson, B. D., Pagel, J. M., Hillmen, P., Barrientos, J. C., Zelenetz, A. D., et al. (2014) 'Idelalisib and rituximab in relapsed chronic lymphocytic leukemia.' *New England Journal of Medicine*, 370(11) pp. 997-1007.

Furstenau, M. and Eichhorst, B. (2021) 'Novel Agents in Chronic Lymphocytic Leukemia: New Combination Therapies and Strategies to Overcome Resistance.' *Cancers (Basel)*, 13(6)

Gachet, C. (2012) 'P2Y12 receptors in platelets and other hematopoietic and non-hematopoietic cells.' *Purinergic Signalling*, 8(3) pp. 609-619.

Gaillard, H., Garcia-Muse, T. and Aguilera, A. (2015) 'Replication stress and cancer.' *Nature Reviews Cancer*, 15(5) pp. 276-289.

Galmarini, C. M., Mackey, J. R. and Dumontet, C. (2002) 'Nucleoside analogues and nucleobases in cancer treatment.' *The Lancet Oncology*, 3(7) pp. 415-424.

Gambella, M., Rocci, A., Gay, F., Omede, P., Boccadoro, M., Palumbo, A., Passera, R., Crippa, C., et al. (2013) 'XBP1 expression as prognostic marker in multiple myeloma patients treated with bortezomib.' *Haematologica*, 98 p. 70.

Gamper, C., Omene, C. O., Van Eyndhoven, W. G., Glassman, G. D. and Lederman, S. (2001) 'Expression and function of TRAF-3 splice-variant isoforms in human lymphoma cell lines.' *Human Immunology*, 62(10) pp. 1167-1177.

Garcia-Vallejo, J. J., Van Het Hof, B., Robben, J., Van Die, I., Van Dijk, W., Van Wijk, J. A. E. and Joziasse, D. H. (2004) 'Approach for defining endogenous reference genes in gene expression experiments.' *Analytical Biochemistry*, 329(2) pp. 293-299.

Ge, X. J., Wang, Y. L., Wu, Y. P., Feng, Z.-X., Liu, L., Li, M. Y. and Jiang, J. Y. (2019) 'Regulatory effect of Act1 on the BAFF pathway in B-cell malignancy.' *Oncology Letters*, 17(4) pp. 3727-3734.

Gertsch, J., Meier, S., Müller, M. and Altmann, K.-H. (2009) 'Differential Effects of Natural Product Microtubule Stabilizers on Microtubule Assembly: Single Agent and Combination Studies with Taxol, Epothilone B, and Discodermolide.' *ChemBioChem*, 10(1) pp. 166-175.

Ghia, P. and Hallek, M. (2014) 'Management of chronic lymphocytic leukemia.' *Haematologica*, 99(6) pp. 965-972.

Gigant, B., Wang, C., Ravelli, R. B., Roussi, F., Steinmetz, M. O., Curmi, P. A., Sobel, A. and Knossow, M. (2005) 'Structural basis for the regulation of tubulin by vinblastine.' *Nature*, 435(7041) pp. 519-522.

Giono, L. E. and Manfredi, J. J. (2006) 'The p53 tumor suppressor participates in multiple cell cycle checkpoints.' *Journal of Cellular Physiology*, 209(1) pp. 13-20.

Gladkikh, A., Potashnikova, D., Korneva, E., Khudoleeva, O. and Vorobjev, I. (2010) 'Cyclin D1 expression in B-cell lymphomas.' *Experimental Hematology*, 38(11) pp. 1047-1057.

Goede, V., Fischer, K., Bosch, F., Follows, G., Frederiksen, H., Cuneo, A., Ludwig, H., Crompton, N., et al. (2015) 'Updated Survival Analysis from the CLL11 Study: Obinutuzumab Versus Rituximab in Chemoimmunotherapy-Treated Patients with Chronic Lymphocytic Leukemia.' *Blood*, 126(23) p. 1733.

Goede, V., Fischer, K., Busch, R., Jaeger, U., Dilhuydy, M. S., Wickham, N., De Guibert, S., Ritgen, M., et al. (2013) 'Chemoimmunotherapy with GA101 plus chlorambucil in patients with chronic lymphocytic leukemia and comorbidity: results of the CLL11 (BO21004) safety run-in.' *Leukemia*, 27(5) pp. 1172-1174.

Goff, L. K., Neat, M. J., Crawley, C. R., Jones, L., Jones, E., Lister, T. A. and Gupta, R. K. (2000) 'The use of real-time quantitative polymerase chain reaction and comparative genomic hybridization to identify amplification of the REL gene in follicular lymphoma.' *British Journal of Haematology*, 111(2) pp. 618-625.

Golstein, P. and Kroemer, G. (2007) 'Cell death by necrosis: towards a molecular definition.' *Trends in Biochemical Sciences*, 32(1) pp. 37-43.

Gordiienko, I. M., Shlapatska, L. M., Kovalevska, L. M. and Sidorenko, S. P. (2016) 'Differential expression of CD150/SLAMF1 in normal and malignant b cells on the different stages of maturation.' *Experimental Oncology*, 38(2) pp. 101-107.

Grallert, B. and Boye, E. (2008) 'The multiple facets of the intra-S checkpoint.' *Cell Cycle*, 7(15) pp. 2315-2320.

Green, T. M., De Stricker, K. and Moller, M. B. (2009) 'Validation of putative reference genes for normalization of Q-RT-PCR data from paraffin-embedded lymphoid tissue.' *Diagnostic Molecular Pathology*, 18(4) pp. 243-249.

Greil, C., Engelhardt, M. and Wasch, R. (2022) 'The Role of the APC/C and Its Coactivators Cdh1 and Cdc20 in Cancer Development and Therapy.' *Frontiers in Genetics*, 13 p. 941565.

Guo, H., Li, X., Guo, Y. and Zhen, L. (2019) 'An overview of tubulin modulators deposited in protein data bank.' *Medicinal Chemistry Research*, 28(7) pp. 927-937.

Guo, Y., Liu, Y., Hu, N., Yu, D., Zhou, C., Shi, G., Zhang, B., Wei, M., et al. (2019) 'Discovery of Zanubrutinib (BGB-3111), a Novel, Potent, and Selective Covalent Inhibitor of Bruton's Tyrosine Kinase.' *Journal of Medicinal Chemistry*, 62(17) pp. 7923-7940.

Hallek, M. and Al-Sawaf, O. (2021) 'Chronic lymphocytic leukemia: 2022 update on diagnostic and therapeutic procedures.' *American Journal of Hematology*, 96(12) pp. 1679-1705.

Hallek, M., Cheson, B. D., Catovsky, D., Caligaris-Cappio, F., Dighiero, G., Döhner, H., Hillmen, P., Keating, M. J., et al. (2008) 'Guidelines for the diagnosis and treatment of chronic lymphocytic leukemia: a report from the International Workshop on Chronic Lymphocytic Leukemia updating the National Cancer Institute–Working Group 1996 guidelines.' *Blood*, 111(12) pp. 5446-5456.

Hallek, M., Cheson, B. D., Catovsky, D., Caligaris-Cappio, F., Dighiero, G., Döhner, H., Hillmen, P., Keating, M., et al. (2018) 'iwCLL guidelines for diagnosis, indications for treatment, response assessment, and supportive management of CLL.' *Blood*, 131(25) pp. 2745-2760.

Han, M. H., Eom, H. S., Park, W. S., Kim, H. J., Kong, S. Y., Yun, T., Park, S. and Jeon, C. H. (2010) 'Detection of circulating lymphoma cells in patients with non-Hodgkin lymphoma using MAGE-A3 gene expression in peripheral blood.' *Leukemia Research*, 34(9) pp. 1127-1131.

Hanahan, D. (2022) 'Hallmarks of Cancer: New Dimensions.' *Cancer Discovery*, 12(1) pp. 31-46.

Hanahan, D. and Weinberg, R. A. (2000) 'Hallmarks of Cancer.' *Cell*, 100(1) pp. 57-70.

Hanahan, D. and Weinberg, R. A. (2011) 'Hallmarks of Cancer: The Next Generation.' *Cell*, 144(5) pp. 646-674.

Hansen, A., Reiter, K., Dorner, T. and Pruss, A. (2005) 'Cryopreserved human B cells as an alternative source for single cell mRNA analysis.' *Cell and Tissue Banking*, 6(4) pp. 299-308.

Hansen, S. V., Blum, M. K., Abildgaard, N. and Nyvold, C. G. (2020) 'Efficient, non-viral and reproducible protocol for stableknockdown of genes in mantle cell lymphoma cell lines.' *Blood*, 136 pp. 1-2.

Hao, X., Bu, W., Lv, G., Xu, L., Hou, D., Wang, J., Liu, X., Yang, T., et al. (2022) 'Disrupted mitochondrial homeostasis coupled with mitotic arrest generates antineoplastic oxidative stress.' *Oncogene*, 41(3) pp. 427-443.

Haselager, M. V., Kielbassa, K., ter Burg, J., Bax, D. J. C., Fernandes, S. M., Borst, J., Tam, C., Forconi, F., et al. (2020) 'Changes in Bcl-2 members after ibrutinib or venetoclax uncover functional hierarchy in determining resistance to venetoclax in CLL.' *Blood*, 136(25) pp. 2918-2926.

Hattori, N., Saito, T., Yagyu, T., Jiang, B. H., Kitagawa, K. and Inagaki, C. (2001) 'GH, GH receptor, GH secretagogue receptor, and Ghrelin expression in human T cells, B cells, and neutrophils.' *Journal of Clinical Endocrinology and Metabolism*, 86(9) pp. 4284-4291.

Hayward, D., Alfonso-Perez, T. and Gruneberg, U. (2019) 'Orchestration of the spindle assembly checkpoint by CDK1-cyclin B1.' *FEBS Letters*, 593(20) pp. 2889-2907.

He, Y., Sun, M. M., Zhang, G. G., Yang, J., Chen, K. S., Xu, W. W. and Li, B. (2021) 'Targeting PI3K/Akt signal transduction for cancer therapy.' *Signal Transduction and Targeted Therapy*, 6(1) p. 425.

Hein, J. B., Garvanska, D. H., Nasa, I., Kettenbach, A. N. and Nilsson, J. (2021) 'Coupling of Cdc20 inhibition and activation by BubR1.' *Journal of Cell Biology*, 220(5) p. e202012081.

Hellemans, J., Mortier, G., De Paepe, A., Speleman, F. and Vandesompele, J. (2007) 'qBase relative quantification framework and software for management and automated analysis of real-time quantitative PCR data.' *Genome Biology*, 8(2) p. R19.

Himi, K., Takeichi, O., Imai, K., Hatori, K., Tamura, T. and Ogiso, B. (2020) 'Epstein–Barr virus reactivation by persistent apical periodontal pathogens.' *International Endodontic Journal*, 53(4) pp. 492-505.

Holder, J., Poser, E. and Barr, F. A. (2019) 'Getting out of mitosis: spatial and temporal control of mitotic exit and cytokinesis by PP1 and PP2A.' *FEBS Letters*, 593(20) pp. 2908-2924.

Horiguchi-Yamada, J., Iwase, S., Kawano, T. and Yamada, H. (2005) 'Pretreatment with interferon-alpha radiosensitizes Daudi cells modulating gene expression and biomarkers.' *Anticancer Research*, 25(4) pp. 2631-2638.

Hoster, E., Dreyling, M., Klapper, W., Gisselbrecht, C., van Hoof, A., Kluin-Nelemans, H. C., Pfreundschuh, M., Reiser, M., et al. (2008) 'A new prognostic index (MIPI) for patients with advanced-stage mantle cell lymphoma.' *Blood*, 111(2) pp. 558–565.

Hsu, J. L., Leu, W. J., Hsu, L. C., Ho, C. H., Liu, S. P. and Guh, J. H. (2020) 'Phosphodiesterase Type 5 Inhibitors Synergize Vincristine in Killing Castration-Resistant Prostate Cancer Through Amplifying Mitotic Arrest Signaling.' *Frontiers in Oncology*, 10 p. 1274.

Hu, R., Mukhina, G. L., Brodsky, R. A., Jones, R. J., Brown, P., Sharkis, S. J., Lee, S. H., Englund, P. T., et al. (2009) 'Silencing of genes required for glycosylphosphatidylinositol anchor biosynthesis in Burkitt lymphoma.' *Experimental Hematology*, 37(4) pp. 423–434.

Huang, B.-B., Gao, Q.-M., Liang, W., Xiu, B., Zhang, W.-J. and Liang, A.-B. (2012) 'Down-regulation of SENP1 expression increases apoptosis of Burkitt lymphoma cells.' *Asian Pacific Journal of Cancer Prevention : APJCP*, 13(5) pp. 2045-2049.

Huang, X., Liu, H., Ye, H., Du, M. Q., Lin, S., Gao, Z., Zhang, Z., Chuang, S. S., et al. (2003) 'T(11;18)(q21;q21) in gastric MALT lymphoma and diffuse large B-cell lymphoma of Chinese patients.' *Hematology Journal*, 4(5) pp. 342-345.

Huerta-Garcia, C. S., Perez, D. J., Velazquez-Martinez, C. A., Tabatabaei Dakhili, S. A., Romo-Mancillas, A., Castillo, R. and Hernandez-Campos, A. (2022) 'Structure-Activity Relationship of N-Phenylthieno[2,3-b]pyridine-2-carboxamide Derivatives Designed as Forkhead Box M1 Inhibitors: The Effect of Electron-Withdrawing and Donating Substituents on the Phenyl Ring.' *Pharmaceuticals*, 15(3) p. 283.

Huggett, J., Dheda, K., Bustin, S. and Zumla, A. (2005) 'Real-time RT-PCR normalisation; strategies and considerations.' *Genes and Immunity*, 6(4) pp. 279-284.

Hung, J. M., Arabshahi, H. J., Leung, E., Reynisson, J. and Barker, D. (2014) 'Synthesis and cytotoxicity of thieno[2,3-b]pyridine and furo[2,3-b]pyridine derivatives.' *European Journal of Medicinal Chemistry*, 86 pp. 420-437.

Ichinohasama, R., Oji, Y., Yokoyama, H., Takeuchi, K., Fujiwara, T., Ishizawa, K., Taniguchi, O., Tsuboi, A., et al. (2010) 'Sensitive immunohistochemical detection of WT1 protein in tumors with anti-WT1 antibody against WT1 235 peptide.' *Cancer Science*, 101(5) pp. 1089-1092.

Istasi, D., Martinet, M., Maitre, E., Salaun, V., Chantepie, S. and Troussard, X. (2017) 'SOX11 and CD43 biomarkers in mantle cell lymphoma.' *Blood*, 130(Supplement 1) p. 2739.

Izawa, D. and Pines, J. (2015) 'The mitotic checkpoint complex binds a second CDC20 to inhibit active APC/C.' *Nature*, 517(7536) pp. 631-634.

Jacob, F., Guertler, R., Naim, S., Nixdorf, S., Fedier, A., Hacker, N. F. and Heinzelmann-Schwarz, V. (2013) 'Careful selection of reference genes is required for reliable performance of RT-qPCR in human normal and cancer cell lines.' *PLOS One*, 8(3) p. e59180.

Jahid, M., Rehan Ul, H., Avasthi, R. and Ahmed, R. S. (2018) 'Interleukin10-1082 A/G polymorphism: Allele frequency, correlation with disease markers, messenger RNA and serum levels in North Indian rheumatoid arthritis patients.' *Clinical Biochemistry*, 55 pp. 80-85.

Jain, N. and O'Brien, S. (2016) 'Targeted therapies for CLL: Practical issues with the changing treatment paradigm.' *Blood Reviews*, 30(3) pp. 233-244.

Jasinski-Bergner, S., Buttner, M., Kielstein, H., Quandt, D. and Seliger, B. (2018) 'Adiponectin and Its Receptors Are Differentially Expressed in Human Tissues and Cell Lines of Distinct Origin.' *Obesity Facts*, 10(6) pp. 569-583.

Jeon, S. M., Chandel, N. S. and Hay, N. (2012) 'AMPK regulates NADPH homeostasis to promote tumour cell survival during energy stress.' *Nature*, 485(7400) pp. 661-665.

Jeruzalska, E. and Mazur, A. J. (2023) 'The Role of non-muscle actin paralogs in cell cycle progression and proliferation.' *European Journal of Cell Biology*, 102(2) p. 151315.

Jha, S., Dhooria, A., Naidu, G., Kumar, R., Jain, S., Sharma, A., Singh, J., Minz, R., et al. (2019) 'BAFF and APRIL gene expression in patients with ANCA associated vasculitis.' *Annals of the Rheumatic Diseases*, 78 p. 821.

Jiang, B., Hattori, N., Liu, B., Kitagawa, K. and Inagaki, C. (2002) 'Expression of swelling- and/or pH-regulated chloride channels (ClC-2, 3, 4 and 5) in human leukemic and normal immune cells.' *Life Sciences*, 70(12) pp. 1383-1394.

Jin, F., Bokros, M. and Wang, Y. (2017) 'Premature Silencing of the Spindle Assembly Checkpoint Is Prevented by the Bub1-H2A-Sgo1-PP2A Axis in Saccharomyces cerevisiae.' *Genetics*, 205(3) pp. 1169-1178.

Johnson, A. and Skotheim, J. M. (2013) 'Start and the restriction point.' *Current Opinion in Cell Biology*, 25(6) pp. 717-723.

Johnson, A. S., Dubeau, L., White, R. J. and Johnson, D. L. (2003) 'The TATA Binding Protein as a Regulator of Cellular Transformation.' *Cell Cycle*, 2(5) pp. 440-442.

Jones, S. E., Grozea, P. N., Metz, E. N., Haut, A., Stephens, R. L., Morrison, F. S., Butler, J. J., Byrne, J. G. E., et al. (1979) 'Superiority of adriamycin-containing combination chemotherapy in the treatment of diffuse lymphoma: a Southwest Oncology Group study.' *Cancer*, 43(2) pp. 417-425.

Jordan, A., Hadfield, J. A., Lawrence, N. J. and McGown, A. T. (1998) 'Tubulin as a target for anticancer drugs: Agents which interact with the mitotic spindle.' *Medicinal Research Reviews*, 18(4) pp. 259-296.

Jordan, M. A. (2002) 'Mechanism of action of antitumor drugs that interact with microtubules and tubulin.' *Current Medicinal Chemistry - Anti-Cancer Agents*, 2(1) pp. 1-17.

Jordan, M. A. and Wilson, L. (2004) 'Microtubules as a target for anticancer drugs.' *Nature Reviews Cancer*, 4 pp. 253–265.

Jordan, M. A., Thrower, D. and Wilson, L. (1991) 'Mechanism of Inhibition of Cell Proliferation by Vinca Alkaloids.' *Cancer Research*, 51(8) pp. 2212-2222.

Jordan, M. A., Thrower, D. and Wilson, L. (1992) 'Effects of vinblastine, podophyllotoxin and nocodazole on mitotic spindles. Implications for the role of microtubule dynamics in mitosis.' *Journal of Cell Science*, 102 pp. 401-416.

Jordan, M. A., Toso, R. J., Thrower, D. and Wilson, L. (1993) 'Mechanism of Mitotic Block and Inhibition of Cell Proliferation by Taxol at Low concentrations.' *Proceedings of the National Academy of Sciences of the United States of America*, 90(20) pp. 9552-9556.

Juliusson, G. and Gahrton, G. (1993) '5 Cytogenetics in CLL and related disorders.' *Baillière's Clinical Haematology*, 6(4) pp. 821-848.

Kalathil, D., John, S. and Nair, A. S. (2020) 'FOXM1 and Cancer: Faulty Cellular Signaling Derails Homeostasis.' *Frontiers in Oncology*, 10 p. 626836.

Kami Reddy, K. R., Dasari, C., Vandavasi, S., Natani, S., Supriya, B., Jadav, S. S., Sai Ram, N., Kumar, J. M., et al. (2019) 'Novel Cellularly Active Inhibitor Regresses DDAH1 Induced Prostate Tumor Growth by Restraining Tumor Angiogenesis through Targeting DDAH1/ADMA/NOS Pathway.' *ACS Combinatorial Science*, 21(4) pp. 241-256.

Kapanidou, M., Curtis, N. L. and Bolanos-Garcia, V. M. (2017) 'Cdc20: At the Crossroads between Chromosome Segregation and Mitotic Exit.' *Trends in Biochemical Sciences*, 42(3) pp. 193-205.

Kapoor, T. M. (2017) 'Metaphase Spindle Assembly.' *Biology (Basel)*, 6(1) p. 8.

Kastan, M. B. and Bartek, J. (2004) 'Cell-cycle checkpoints and cancer.' *Nature*, 432 pp. 316-323.

Katritch, V., Jaakola, V. P., Lane, J. R., Lin, J., Ijzerman, A. P., Yeager, M., Kufareva, I., Stevens, R. C., et al. (2010) 'Structure-based discovery of novel chemotypes for adenosine A(2A) receptor antagonists.' *Journal of Medicinal Chemistry*, 53(4) pp. 1799-1809.

Kavallaris, M. (2010) 'Microtubules and resistance to tubulin-binding agents.' *Nature Reviews Cancer*, 10 pp. 194-204.

Kernan, J., Bonacci, T. and Emanuele, M. J. (2018) 'Who guards the guardian? Mechanisms that restrain APC/C during the cell cycle.' *BBA - Molecular Cell Research*, 1865(12), Dec, 20181002, pp. 1924-1933.

Kim, S., Chen, J., Cheng, T., Gindulyte, A., He, J., He, S., Li, Q., Shoemaker, B. A., et al. (2023) 'PubChem 2023 update.' *Nucleic Acids Research*, 51(D1) pp. D1373-D1380.

Kim, Y. J., Kim, N., Nam, C. H., Lee, M. K., Choi, H. J. and Baek, H. J. (2010) 'Overexpression and unique rearrangement of VH2 transcripts in immunoglobulin variable heavy chain genes in ankylosing spondylitis patients.' *Experimental and Molecular Medicine*, 42(5) pp. 319-326.

Kishimoto, T. (2015) 'Entry into mitosis: a solution to the decades-long enigma of MPF.' *Chromosoma*, 124(4) pp. 417-428.

Kiyomitsu, T. (2016) 'Analyzing Spindle Positioning Dynamics in Cultured Cells.' *Methods in Molecular Biology*, 1413 pp. 239-252.

Klemm, L. H. and Zell, R. (1968) 'Chemistry of thienopyridines. IV. Syntheses of 5-substituted thieno[2,3-b] pyridines.' *Journal of Heterocyclic Chemistry*, 5(6) pp. 773-778.

Koike, R., Nodomi, K., Watanabe, N., Ogata, Y., Takeichi, O., Takei, M., Kaneko, T., Tonogi, M., et al. (2020) 'Butyric Acid in Saliva of Chronic Periodontitis Patients Induces Transcription of the EBV Lytic Switch Activator BZLF1: A Pilot Study.' *In vivo (Athens, Greece)*, 34(2) pp. 587-594.

Konecna, M., Abbasi Sani, S. and Anger, M. (2023) 'Separase and Roads to Disengage Sister Chromatids during Anaphase.' *International Journal of Molecular Sciences*, 24(5) p. 4604.

Kops, G. J. P. L., Weaver, B. A. and Cleveland, D. W. (2005) 'On the road to cancer: aneuploidy and the mitotic checkpoint.' *Nature Reviews Cancer*, 5(10) pp. 773-785.

Korycka-Wołowiec, A., Wołowiec, D. and Robak, T. (2015) 'Ofatumumab for treating chronic lymphocytic leukemia: a safety profile.' *Expert Opinion on Drug Safety*, 14(12) pp. 1945-1959.

Kovalevska, L. and Kashuba, E. (2020) 'Expression pattern of MRPS18 family genes in malignantly transformed B-cells.' *Experimental Oncology*, 42(4) pp. 295-299.

Kozmus, C. E. P. and Potočnik, U. (2015) 'Reference genes for real-time qPCR in leukocytes from asthmatic patients before and after anti-asthma treatment.' *Gene*, 570(1) pp. 71-77.

Krauze, A., Grinberga, S., Krasnova, L., Adlere, I., Sokolova, E., Domracheva, I., Shestakova, I., Andzans, Z., et al. (2014) 'Thieno[2,3-b]pyridines--a new class of multidrug resistance (MDR) modulators.' *Bioorganic & Medicinal Chemistry*, 22(21) pp. 5860-5870.

Kristensen, I. B., Haaber, J., Knudsen, L. M., Abildgaard, N., Lyng, M., Ditzel, H., Klausen, T. W., Rasmussen, T., et al. (2011a) 'Multiple myeloma plasma cell (MM PC) co-expression of hepatocyte growth factor (HGF) isoforms and of the receptor cmet is associated with overall survival (OS) in mm patients.' *Haematologica*, 96

Kristensen, I. B., Haaber, J., Knudsen, L. M., Abildgaard, N., Lyng, M., Ditzel, H., Klausen, T. W., Rasmussen, T., et al. (2011b) 'Association between the expression of secreted frizzled related protein 3 (SFRP3), dickkopf1 (DKK1), and the osteolytic bone disease (OBD) in multiple myeloma (MM).' *Haematologica*, 96

Kristensen, L., Kristensen, T., Abildgaard, N., Thomassen, M., Frederiksen, M., Mourits-Andersen, T. and Møller, M. B. (2015) 'High expression of PI3K core complex genes is associated with poor prognosis in chronic lymphocytic leukemia.' *Leukemia Research*, 39(6) pp. 555-560.

Krumbholz, M., Meinl, I., Kumpfel, T., Hohlfeld, R. and Meinl, E. (2008) 'Natalizumab disproportionately increases circulating pre-B and B cells in multiple sclerosis.' *Neurology*, 71(17) pp. 1350-1354.

Kuo, H. H., Su, Z. R., Chuang, J. Y. and Yih, L. H. (2021) 'Heat shock factor 1 suppression induces spindle abnormalities and sensitizes cells to antimitotic drugs.' *Cell Division*, 16(1) p. 8.

Kuszynski, D. S. and Lauver, D. A. (2022) 'Pleiotropic effects of clopidogrel.' *Purinergic Signal*, 18(3) pp. 253-265.

Lanz, M. C., Dibitetto, D. and Smolka, M. B. (2019) 'DNA damage kinase signaling: checkpoint and repair at 30 years.' *EMBO J*, 38(18) p. e101801.

Lara-Gonzalez, P., Pines, J. and Desai, A. (2021) 'Spindle assembly checkpoint activation and silencing at kinetochores.' *Seminars in Cell and Developmental Biology*, 117 pp. 86-98.

Lara-Gonzalez, P., Moyle, M. W., Budrewicz, J., Mendoza-Lopez, J., Oegema, K. and Desai, A. (2019) 'The G2-to-M Transition Is Ensured by a Dual Mechanism that Protects Cyclin B from Degradation by Cdc20-Activated APC/C.' *Developmental Cell*, 51(3) pp. 313-325 e310.

Laudette, M., Coluccia, A., Sainte-Marie, Y., Solari, A., Fazal, L., Sicard, P., Silvestri, R., Mialet-Perez, J., et al. (2019) 'Identification of a pharmacological inhibitor of Epac1 that protects the heart against acute and chronic models of cardiac stress.' *Cardiovascular Research* 115(12) pp. 1766-1777.

Lee, J. C. and Timasheff, S. N. (1977) 'In vitro reconstitution of calf brain microtubules: effects of solution variables.' *Biochemistry*, 16(8) pp. 1754-1764.

Lemonnier, T., Dupre, A. and Jessus, C. (2020) 'The G2-to-M transition from a phosphatase perspective: a new vision of the meiotic division.' *Cell Division*, 15 p. 9.

Leung, E., Hung, J. M., Barker, D. and Reynisson, J. (2014) 'The effect of a thieno[2,3-b]pyridine PLC-[gamma] inhibitor on the proliferation, morphology, migration and cell cycle of breast cancer cells.' *MedChemComm*, 5(1) pp. 99-106.

Leung, E., Pilkington, L. I., van Rensburg, M., Jeon, C. Y., Song, M., Arabshahi, H. J., De Zoysa, G. H., Sarojini, V., et al. (2016) 'Synthesis and cytotoxicity of thieno[2,3-b]quinoline-2-carboxamide and cycloalkyl[b]thieno[3,2-e]pyridine-2-carboxamide derivatives.' *Bioorganic & Medicinal Chemistry*, 24(5) pp. 1142-1154.

Leung, E., Patel, J., Hollywood, J. A., Zafar, A., Tomek, P., Barker, D., Pilkington, L. I., van Rensburg, M., et al. (2021) 'Validating TDP1 as an Inhibition Target for the Development of Chemosensitizers for Camptothecin-Based Chemotherapy Drugs.' *Oncology and Therapy*, 9(2) pp. 541-556.

Li, L. J., Chai, Y., Guo, X.-J., Chu, S. L. and Zhang, L. S. (2017) 'The effects of the long non-coding RNA MALAT-1 regulated autophagy-related signaling pathway on chemotherapy resistance in diffuse large B-cell lymphoma.' *Biomedicine and Pharmacotherapy*, 89 pp. 939-948.

Liang, H., Lim, H. H., Venkitaraman, A. and Surana, U. (2012) 'Cdk1 promotes kinetochore bi-orientation and regulates Cdc20 expression during recovery from spindle checkpoint arrest.' *The EMBO Journal*, 31(2) pp. 403-416.

Liao, Y., Luo, D., Peng, K. and Zeng, Y. (2021) 'Cyclophilin A: a key player for etiological agent infection.' *Applied Microbiology and Biotechnology*, 105(4) pp. 1365-1377.

Limas, J. C. and Cook, J. G. (2019) 'Preparation for DNA replication: the key to a successful S phase.' *FEBS Letters*, 593(20) pp. 2853-2867.

Lister, T. A., Crowther, D., Sutcliffe, S. B., Glatstein, E., Canellos, G. P., Young, R. C., Rosenberg, S. A., Coltman, C. A., et al. (1989) 'Report of a committee convened to discuss the evaluation and staging of patients with Hodgkin's disease: Cotswolds meeting.' *Journal of Clinical Oncology*, 7(11) pp. 1630-1636.

Liu, R., Chen, Y., Liu, G., Li, C., Song, Y., Cao, Z., Li, W., Hu, J., et al. (2020) 'PI3K/AKT pathway as a key link modulates the multidrug resistance of cancers.' *Cell Death and Disease*, 11(9) p. 797.

Liu, T.-M., Woyach, J. A., Zhong, Y., Lozanski, A., Lozanski, G., Dong, S., Strattan, E., Lehman, A., et al. (2015) 'Hypermorphic mutation of phospholipase C, γ2 acquired in ibrutinib-resistant CLL confers BTK independency upon B-cell receptor activation.' *Blood*, 126(1) pp. 61-68.

Liu, X., Zhang, Y., Han, Y., Lu, W., Yang, J., Tian, J., Sun, P., Hu, Y., et al. (2020) 'Overexpression of GLT1D1 induces immunosuppression through glycosylation of PD-L1 and predicts poor prognosis in B-cell lymphoma.' *Molecular Oncology*, 14(5) pp. 1028-1044.

Liu, Y.-C., Margolskee, E., Allan, J. N., Mathew, S., Bhavsar, E., Casano, J., Orazi, A., Furman, R. R., et al. (2020) 'Chronic lymphocytic leukemia with TP53 gene alterations: a detailed clinicopathologic analysis.' *Modern Pathology*, 33(3) pp. 344-353.

Liu, Y. M., Zhai, X. M. and Wu, Y. W. (2016) 'Biological correlation between glucose transporters, Ki-67 and 2-deoxy-2-[18F]-fluoro-D-glucose uptake in diffuse large B-cell lymphoma and natural killer/T-cell lymphoma.' *Genetics and Molecular Research*, 15(2) p. gmr.15027242.

Livak, K. J. and Schmittgen, T. D. (2001) 'Analysis of relative gene expression data using real-time quantitative PCR and the 2(-Delta Delta C(T)) Method.' *Methods*, 25(4) pp. 402-408.

London, N. and Biggins, S. (2014) 'Signalling dynamics in the spindle checkpoint response.' *Nature Reviews Molecular Cell Biology*, 15(11) pp. 736-747.

Lopes, F. A. C., Fernandes, A. V. F., Rodrigues, J. M., Queiroz, M. R. P., Almeida, B. G., Pires, A., Pereira, A. M., Araujo, J. P., et al. (2022) 'Magnetoliposomes Containing Multicore Nanoparticles and a New Antitumor Thienopyridine Compound with Potential Application in Chemo/Thermotherapy.' *Biomedicines*, 10(7) p. 1547.

Lopus, M., Oroudjev, E., Wilson, L., Wilhelm, S., Widdison, W., Chari, R. and Jordan, M. A. (2010) 'Maytansine and cellular metabolites of antibody-maytansinoid conjugates strongly suppress microtubule dynamics by binding to microtubules.' *Molecular Cancer Therapeutics*, 9(10) pp. 2689-2699.

Lou, J., Wang, Y., Chen, J., Ju, L., Yu, M., Jiang, Z., Feng, L., Jin, L., et al. (2015) 'Effects of soluble and particulate Cr(VI) on genome-wide DNA methylation in human B lymphoblastoid cells.' *Mutation Research - Genetic Toxicology and Environmental Mutagenesis*, 792 pp. 12-18.

Lowe, J., Joseph, R. E. and Andreotti, A. H. (2022) 'Conformational switches that control the TEC kinase - PLCgamma signaling axis.' *Journal of Structural Biology: X*, 6 p. 100061.

Lu, P., Wang, S., Franzen, C. A., Venkataraman, G., McClure, R., Li, L., Wu, W., Niu, N., et al. (2021) 'Ibrutinib and venetoclax target distinct subpopulations of CLL cells: implication for residual disease eradication.' *Blood Cancer Journal*, 11(2) p. 39.

Lukinavicius, G., Reymond, L., D'Este, E., Masharina, A., Gottfert, F., Ta, H., Guther, A., Fournier, M., et al. (2014) 'Fluorogenic probes for live-cell imaging of the cytoskeleton.' *Nature Methods*, 11(7) pp. 731-733.

Luo, C., Wu, G., Huang, X., Ma, Y., Zhang, Y., Song, Q., Xie, M., Sun, Y., et al. (2021) 'Efficacy and safety of new anti-CD20 monoclonal antibodies versus rituximab for induction therapy of CD20(+) B-cell non-Hodgkin lymphomas: a systematic review and meta-analysis.' *Scientific Reports*, 11(1) p. 3255.

Luo, G., Lin, X., Vega-Medina, A., Xiao, M., Li, G., Wei, H., Velazquez-Martinez, C. A. and Xiang, H. (2021) 'Targeting of the FOXM1 Oncoprotein by E3 Ligase-Assisted Degradation.' *Journal of Medicinal Chemistry*, 64(23) pp. 17098-17114.

Ma, F., Zhu, L., Wang, Y., Zhao, F., Shi, G., Li, B., Li, G., Zhang, S., et al. (2000) 'Cloning and characterization of a cDNA encoding human differentiation antigen 5D4.' *Science in China. Series C, Life sciences*, 43(4) pp. 442-448.

Ma, F., Liu, J., Zhou, T., Lei, M., Chen, J., Wang, X., Zhang, Y., Shen, X., et al. (2018) 'Discovery and structure-activity relationships study of thieno[2,3-b]pyridine analogues as hepatic gluconeogenesis inhibitors.' *European Journal of Medicinal Chemistry*, 152 pp. 307-317.

Ma, H. T. and Poon, R. Y. C. (2016) 'TRIP13 Regulates Both the Activation and Inactivation of the Spindle-Assembly Checkpoint.' *Cell Reports*, 14(5) pp. 1086-1099.

Ma, H. T. and Poon, R. Y. C. (2020) 'Aurora kinases and DNA damage response.' *Mutation Research*, 821 p. 111716.

Ma, M., Zhao, L., Sun, G., Zhang, C., Liu, L., Du, Y., Yang, X. and Shan, B. (2016) 'Mda-7/IL-24 enhances sensitivity of B cell lymphoma to chemotherapy drugs.' *Oncology Reports*, 35(5) pp. 3122-3130.

Magne, J., Donzel, A., Jego, L., Aral, B., Guy, J., Nadal, N., Callier, P., Jenvrin, A., et al. (2018) 'Potential added value of a RT-qPCR method of SOX 11 expression, in the context of a multidisciplinary diagnostic assessment of B cell malignancies.' *Experimental Hematology and Oncology*, 7(1) p. 5.

Makino, K., Takeichi, O., Imai, K., Inoue, H., Hatori, K., Himi, K., Saito, I., Ochiai, K., et al. (2018) 'Porphyromonas endodontalis reactivates latent Epstein–Barr virus.' *International Endodontic Journal*, 51(12) pp. 1410-1419.

Malumbres, M. (2014) 'Cyclin-dependent kinases.' *Genome Biology*, 15(122) pp. 1-10.

Malumbres, M. and Barbacid, M. (2007) 'Cell cycle kinases in cancer.' *Current Opinion in Genetics & Development*, 17(1) pp. 60-65.

Malumbres, M. and Barbacid, M. (2009) 'Cell cycle, CDKs and cancer a changing paradigm.' *Nature Reviews Cancer*, 9 pp. 153-166.

Mansour, A., Bachelot-Loza, C., Nesseler, N., Gaussem, P. and Gouin-Thibault, I. (2020) 'P2Y(12) Inhibition beyond Thrombosis: Effects on Inflammation.' *International Journal of Molecular Sciences*, 21(4) p. 1391.

Mao, S., Jin, J., Li, Z. and Yang, W. (2021) 'Knockdown of long non-coding RNA ANRIL inhibits the proliferation and promotes the apoptosis of Burkitt lymphoma cells through the TGF-beta1 signaling pathway.' *Molecular Medicine Reports*, 23(2)

Marijan, S., Markotic, A., Mastelic, A., Rezic-Muzinic, N., Pilkington, L. I., Reynisson, J. and Culic, V. C. (2020) 'Glycosphingolipid expression at breast cancer stem cells after novel thieno[2,3-b]pyridine anticancer compound treatment.' *Scientific Reports*, 10(1) p. 11876.

Marino, G., Niso-Santano, M., Baehrecke, E. H. and Kroemer, G. (2014) 'Self-consumption: the interplay of autophagy and apoptosis.' *Nature Reviews Molecular Cell Biology*, 15(2) pp. 81-94.

Martinez-Alonso, D. and Malumbres, M. (2020) 'Mammalian cell cycle cyclins.' *Seminars in Cell & Developmental Biology*, 107 pp. 28-35.

Masch, A. and Kunick, C. (2015) 'Selective inhibitors of Plasmodium falciparum glycogen synthase-3 (PfGSK-3): New antimalarial agents?' *Biochimica et Biophysica Acta*, 1854(10 Pt B) pp. 1644-1649.

Masch, A., Nasereddin, A., Alder, A., Bird, M. J., Schweda, S. I., Preu, L., Doerig, C., Dzikowski, R., et al. (2019) 'Structure-activity relationships in a series of antiplasmodial thieno[2,3-b]pyridines.' *Malaria Journal*, 18(1) p. 89.

Mastelic, A., Cikes Culic, V., Rezic Muzinic, N., Vuica-Ross, M., Barker, D., Leung, E. Y., Reynisson, J. and Markotic, A. (2017) 'Glycophenotype of breast and prostate cancer stem cells treated with thieno[2,3-b]pyridine anticancer compound.' *Drug Design, Development and Therapy*, 11 pp. 759-769.

Mato, A. R., Meghan, T., John, N. A., Danielle, M. B., John, M. P., Chaitra, S. U., Brian, T. H., Nicole, L., et al. (2018) 'Real-world outcomes and management strategies for venetoclax-treated chronic lymphocytic leukemia patients in the United States.' *Haematologica*, 103(9) pp. 1511-1517.

Matou-Nasri, S., Rabhan, Z., Al-Baijan, H., Al-Eidi, H., Yahya, W. B., Al Abdulrahman, A., Almobadel, N., Alsubeai, M., et al. (2017) 'CD95-mediated apoptosis in Burkitt's lymphoma B-cells is associated with Pim-1 down-regulation.' *Biochimica et Biophysica Acta - Molecular Basis of Disease*, 1863(1) pp. 239-252.

Matsui, Y., Nakayama, Y., Okamoto, M., Fukumoto, Y. and Yamaguchi, N. (2012) 'Enrichment of cell populations in metaphase, anaphase, and telophase by synchronization using nocodazole and blebbistatin: a novel method suitable for examining dynamic changes in proteins during mitotic progression.' *European Journal of Cell Biology*, 91(5) pp. 413-419.

Matthews, H. K., Bertoli, C. and de Bruin, R. A. M. (2022) 'Cell cycle control in cancer.' *Nature Reviews Molecular Cell Biology*, 23(1) pp. 74-88.

McAinsh, A. D. and Kops, G. J. P. L. (2023) 'Principles and dynamics of spindle assembly checkpoint signalling.' *Nature Reviews Molecular Cell Biology*,

McCubrey, J. A., Steelman, L. S., Chappell, W. H., Abrams, S. L., Wong, E. W., Chang, F., Lehmann, B., Terrian, D. M., et al. (2007) 'Roles of the Raf/MEK/ERK pathway in cell growth,

malignant transformation and drug resistance.' *Biochimica et Biophysica Acta*, 1773(8) pp. 1263-1284.

McKay, P., Leach, M., Jackson, R., Cook, G. and Rule, S. (2012) 'Guidelines for the investigation and management of mantle cell lymphoma.' *British Journal of Haematology*, 159(4) pp. 405-426.

McNamara, C., Davies, J., Dyer, M., Hoskin, P., Illidge, T., Lyttelton, M., Marcus, R., Montoto, S., et al. (2012) 'Guidelines on the investigation and management of follicular lymphoma.' *British Journal of Haematology*, 156(4) pp. 446-467.

Meadows, J. C., Shepperd, L. A., Vanoosthuyse, V., Lancaster, T. C., Sochaj, A. M., Buttrick, G. J., Hardwick, K. G. and Millar, J. B. (2011) 'Spindle checkpoint silencing requires association of PP1 to both Spc7 and kinesin-8 motors.' *Developmental Cell*, 20(6) pp. 739-750.

Melarangi, T., Zhuang, J., Lin, K., Rockliffe, N., Bosanquet, A. G., Oates, M., Slupsky, J. R. and Pettitt, A. R. (2012) 'Glucocorticoid resistance in chronic lymphocytic leukaemia is associated with a failure of upregulated Bim/Bcl-2 complexes to activate Bax and Bak.' *Cell Death & Disease*, 3(8) pp. e372-e372.

Mena, A. L., Lam, E. W. and Chatterjee, S. (2010) 'Sustained spindle-assembly checkpoint response requires de novo transcription and translation of cyclin B1.' *PLoS One*, 5(9) p. e13037.

Menyhart, O., Harami-Papp, H., Sukumar, S., Schafer, R., Magnani, L., de Barrios, O. and Gyorffy, B. (2016) 'Guidelines for the selection of functional assays to evaluate the hallmarks of cancer.' *Biochimica et Biophysica Acta*, 1866(2) pp. 300-319.

Merino-Cortés, S. V., Gardeta1, S. R., Roman-Garcia, S., Martínez-Riaño, A., Pineau, J., Rosa Liebana, R., Isabel Merida, I., Dumenil, A. L., et al. (2020) 'Diacylglycerol kinase ζ promotes actin cytoskeleton remodeling and mechanical forces at the B cell immune synapse.' *Science Signaling*, 13(627) p. eaaw8214.

Miao, T. T., Tao, X. B., Li, D. D., Chen, H., Jin, X. Y., Geng, Y., Wang, S. F. and Gu, W. (2018) 'Synthesis and biological evaluation of 2-aryl-benzimidazole derivatives of dehydroabietic acid as novel tubulin polymerization inhibitors.' *RSC Advances*, 8(31) pp. 17511-17526.

Milletti, G., Colicchia, V. and Cecconi, F. (2023) 'Cyclers' kinases in cell division: from molecules to cancer therapy.' *Cell Death & Differentiation*, 30(9) pp. 2035-2052.

Mishal, R. and Luna-Arias, J. P. (2022) 'Role of the TATA-box binding protein (TBP) and associated family members in transcription regulation.' *Gene*, 833 p. 146581.

Mizushima, N., Levine, B., Cuervo, A. M. and Klionsky, D. J. (2008) 'Autophagy fights disease through cellular self-digestion.' *Nature*, 451(7182) pp. 1069-1075.

Mohareb, R. M. and Ibrahim, R. A. (2017) 'Design, cytotoxicity and toxicity of new thiophene and thieno [2,3-b] pyridine derivatives.' *Medicinal Chemistry Research*, 26(3) pp. 587-602.

Moher, D., Shamseer, L., Clarke, M., Ghersi, D., Liberati, A., Petticrew, M., Shekelle, P., Stewart, L. A., et al. (2015) 'Preferred reporting items for systematic review and meta-analysis protocols (PRISMA-P) 2015 statement.' *Systematic Reviews*, 4(1)

Mohi El-Deen, E. M., Anwar, M. M., Abd El-Gwaad, A. A., Karam, E. A., El-Ashrey, M. K. and Kassab, R. R. (2022) 'Design and synthesis of some novel pyridothienopyrimidine derivatives and their biological evaluation as antimicrobial and anticancer agents targeting EGFR enzyme.' *Arabian Journal of Chemistry*, 15(4) p. 103751.

Moloney, J. N. and Cotter, T. G. (2018) 'ROS signalling in the biology of cancer.' *Seminars in Cell & Developmental Biology*, 80 pp. 50-64.

Morelon, E., Dodelet, V., Lavery, P., Cashman, N. R. and Loertscher, R. (2001) 'The failure of Daudi cells to express the cellular prion protein is caused by a lack of glycosyl-phosphatidylinositol anchor formation.' *Immunology*, 102(2) pp. 242-247.

Moreno, C., Greil, R., Demirkan, F., Tedeschi, A., Anz, B., Larratt, L., Simkovic, M., Samoilova, O., et al. (2019) 'Ibrutinib plus obinutuzumab versus chlorambucil plus obinutuzumab in first-line treatment of chronic lymphocytic leukaemia (iLLUMINATE): a multicentre, randomised, open-label, phase 3 trial.' *The Lancet Oncology*, 20(1) pp. 43-56.

Mossman, T. (1983) 'Rapid colorimetric assay for cellular growth and survival: Application to proliferation and cytotoxicity assays.' *Journal of Immunological Methods*, 65(1-2) pp. 55–63.

Muller, M. R. and Rao, A. (2010) 'NFAT, immunity and cancer a transcription factor comes of age.' *Nature Reviews: Immunology*, 10(9) pp. 645-656.

Murphy, D., Parker, J., Zhou, M., Fadlelmola, F. M., Steidl, C., Karsan, A., Gascoyne, R. D., Chen, H., et al. (2010) 'Constitutively overexpressed 21 kDa protein in Hodgkin lymphoma and aggressive non-Hodgkin lymphomas identified as cytochrome B5b (CYB5B).' *Molecular Cancer*, 9 p. 14.

Murphy, P. T., Lynch, G., Bergin, S., Quinn, J., Glavey, S., Murphy, P. W. and Kennedy, P. (2016) 'Strong correlation between CTLA-4 and LEF1 gene expression levels in CLL: Targeting of the Wnt/beta-catenin pathway may adversely affect CTLA-4 expression and function.' *Blood*, 128(22) p. 5571.

Murray, A. (2004) 'Recycling the Cell Cycle: Cyclins Revisited.' *Cell*, 116 pp. 221–234.

Musacchio, A. (2015) 'The Molecular Biology of Spindle Assembly Checkpoint Signaling Dynamics.' *Current Biology*, 25(20) pp. R1002-1018.

Musacchio, A. and Salmon, E. D. (2007) 'The spindle-assembly checkpoint in space and time.' *Nature Reviews Molecular Cell Biology*, 8(5) pp. 379-393.

Naaz, F., Haider, M. R., Shafi, S. and Yar, M. S. (2019) 'Anti-tubulin agents of natural origin: Targeting taxol, vinca, and colchicine binding domains.' *European Journal of Medicinal Chemistry*, 171 pp. 310-331.

Nadeem, A. and Ahmad, S. F. (2023) 'Point mutations in the gene encoding IP3 receptor subtype 3 cause impairment in T-cell and B-cell immune responses via dysfunctional Ca(2+) mobilization.' *Cellular & Molecular Immunology*, 20(2) pp. 214-216.

Naguib, B. H. and El-Nassan, H. B. (2016) 'Synthesis of new thieno[2,3-b]pyridine derivatives as pim-1 inhibitors.' *Journal of Enzyme Inhibition and Medicinal Chemistry*, 31(6) pp. 1718-1725.

Nakamura, R. L., Burlingame, M. A., Yang, S., Crosby, D. C., Talbot, D. J., Chui, K., Frankel, A. D. and Renslo, A. R. (2017) 'Identification and Optimization of Thienopyridine Carboxamides as Inhibitors of HIV Regulatory Complexes.' *Antimicrobial Agents and Chemotherapy*, 61(7) pp. e02366-02316.

Nakatogawa, H., Suzuki, K., Kamada, Y. and Ohsumi, Y. (2009) 'Dynamics and diversity in autophagy mechanisms: lessons from yeast.' *Nature Reviews Molecular Cell Biology*, 10(7) pp. 458-467.

Naso, F. D., Polverino, F., Cilluffo, D., Latini, L., Stagni, V., Asteriti, I. A., Rosa, A., Soddu, S., et al. (2024) 'AurkA/TPX2 co-overexpression in nontransformed cells promotes genome instability through induction of chromosome mis-segregation and attenuation of the p53 signalling pathway.' *BBA - Molecular Basis of Disease*, 1870(4) p. 167116.

Nath, S., Banerjee, T., Sen, D., Das, T. and Roychoudhury, S. (2011) 'Spindle assembly checkpoint protein Cdc20 transcriptionally activates expression of ubiquitin carrier protein UbcH10.' *Journal of Biological Chemistry*, 286(18) pp. 15666-15677.

Naves, R., Jacobelli, S., Gonzalez, A., Reyes, L. I., Rosemblatt, M. and Bono, M. R. (2006) 'Lymphoid B cells induce NF-kappaB activation in high endothelial cells from human tonsils.' *International Immunology*, 18(2) pp. 259-267.

Neizer-Ashun, F. and Bhattacharya, R. (2021) 'Reality CHEK: Understanding the biology and clinical potential of CHK1.' *Cancer Letters*, 497 pp. 202-211.

Neumann, J., Van Nieuwenhove, E., Terry, L. E., Staels, F., Knebel, T. R., Welkenhuyzen, K., Ahmadzadeh, K., Baker, M. R., et al. (2023) 'Disrupted Ca(2+) homeostasis and immunodeficiency in patients with functional IP(3) receptor subtype 3 defects.' *Cellular & Molecular Immunology*, 20(1) pp. 11-25.

Nigro, P., Pompilio, G. and Capogrossi, M. C. (2013) 'Cyclophilin A: a key player for human disease.' *Cell Death and Disease*, 4(10) p. e888.

Nikitin, E. A., Malakho, S. G., Biderman, B. V., Baranova, A. V., Lorie, Y. Y., Shevelev, A. Y., Peklo, M. M., Vlasik, T. N., et al. (2007) 'Expression level of lipoprotein lipase and dystrophin genes predict survival in B-cell chronic lymphocytic leukemia.' *Leukemia & Lymphoma*, 48(5) pp. 912-922.

Nishimura, Y., Kitagishi, Y., Yoshida, H., Okumura, N. and Matsuda, S. (2011) 'Ethanol extracts of black pepper or turmeric down-regulated SIRT1 protein expression in Daudi culture cells.' *Molecular Medicine Reports*, 4(4) pp. 727-730.

Nkomba, G., Terre'Blanche, G., Janse van Rensburg, H. D. and Legoabe, L. J. (2022) 'Design, synthesis and evaluation of amino-3,5-dicyanopyridines and thieno[2,3-b]pyridines as ligands of adenosine A(1) receptors for the potential treatment of epilepsy.' *Medicinal Chemistry Research*, 31(8) pp. 1277-1297.

Nolan, T., Hands, R. E. and Bustin, S. A. (2006) 'Quantification of mRNA using real-time RT-PCR.' *Nature Protocols*, 1(3) pp. 1559-1582.

Odeya, D., Galila, A. and Lilah, T. (2018) 'The observed alteration in BCL2 expression following lithium treatment is influenced by the choice of normalization method.' *Scientific Reports*, 8(1) p. 6399.

Okumura, N., Yoshida, H., Nishimura, Y., Murakami, M., Kitagishi, Y. and Matsuda, S. (2012) 'Genistein downregulates presenilin 1 and ubiquilin 1 expression.' *Molecular Medicine Reports*, 5(2) pp. 559-561.

Oshima, K., Yanase, N., Mizuguchi, J., Ibukiyama, C., Yamashina, A., Kayagaki, N. and Yagita, H. (2001) 'Involvement of TRAIL/TRAIL-R interaction in IFN-alpha-induced apoptosis of Daudi B lymphoma cells.' *Cytokine*, 14(4) pp. 193-201.

Oturai, D. B., Søndergaard, H. B., Börnsen, L., Sellebjerg, F. and Christensen, J. R. (2016) 'Identification of Suitable Reference Genes for Peripheral Blood Mononuclear Cell Subset Studies in Multiple Sclerosis.' *Scandinavian Journal of Immunology*, 83(1) pp. 72-80.

Ovejero, S., Bueno, A. and Sacristan, M. P. (2020) 'Working on Genomic Stability: From the S-Phase to Mitosis.' *Genes (Basel)*, 11(2) p. 225.

Page, M. J., Moher, D., Bossuyt, P. M., Boutron, I., Hoffmann, T. C., Mulrow, C. D., Shamseer, L., Tetzlaff, J. M., et al. (2021a) 'PRISMA 2020 explanation and elaboration: updated guidance and exemplars for reporting systematic reviews.' *BMJ*, 372 p. n160.

Page, M. J., McKenzie, J. E., Bossuyt, P. M., Boutron, I., Hoffmann, T. C., Mulrow, C. D., Shamseer, L., Tetzlaff, J. M., et al. (2021b) 'The PRISMA 2020 statement: an updated guideline for reporting systematic reviews.' *BMJ*, 372 p. n71.

Pan, Y.-R., Chen, C.-C., Chan, Y.-T., Wang, H.-J., Chien, F.-T., Chen, Y.-L., Liu, J.-L. and Yang, M.-H. (2018) 'STAT3-coordinated migration facilitates the dissemination of diffuse large B-cell lymphomas.' *Nature Communications*, 9(1) p. 3696.

Papakonstantinou, N., Ntoufa, S., Touloumenidou, T., Anagnostopoulos, A., Stamatopoulos, K. and Belessi, C. (2013) 'Increased expression of the EZH2 methyltransferase and evidence of functionality in CLL subgoups with aggressive clinicobiological profiles.' *Haematologica*, 98 p. 44.

Pasquier, E. and Kavallaris, M. (2008) 'Microtubules: a dynamic target in cancer therapy.' *IUBMB Life*, 60(3) pp. 165-170.

Pastuszak-Lewandoska, D., Domańska-Senderowska, D., Kiszałkiewicz, J., Szmigielska, P., Snochowska, A., Ratkowski, W., Spieszny, M., Klocek, T., et al. (2020) 'Expression levels of selected cytokines and microRNAs in response to vitamin D supplementation in ultra-marathon runners.' *European Journal of Sport Science*, 20(2) pp. 219-228.

Patel, V. M., Balakrishnan, K., Douglas, M., Tibbitts, T., Xu, E. Y., Kutok, J. L., Ayers, M., Sarkar, A., et al. (2017) 'Duvelisib treatment is associated with altered expression of apoptotic regulators that helps in sensitization of chronic lymphocytic leukemia cells to venetoclax (ABT-199).' *Leukemia*, 31(9) pp. 1872-1881.

Pavani, M., Chiroli, E., Cancrini, C., Gross, F., Bonaiuti, P., Villa, S., Giavazzi, F., Matafora, V., et al. (2023) 'Triap1 upregulation promotes escape from mitotic-slippage-induced G1 arrest.' *Cell Reports*, 42(3) p. 112215.

Pede, V., Rombout, A., Vermeire, J., Naessens, E., Mestdagh, P., Robberecht, N., Vanderstraeten, H., Van Roy, N., et al. (2013) 'CLL Cells Respond to B-Cell Receptor Stimulation with a MicroRNA/mRNA Signature Associated with MYC Activation and Cell Cycle Progression.' *PLOS ONE*, 8(4) p. e60275.

Pennycook, B. R. and Barr, A. R. (2020) 'Restriction point regulation at the crossroads between quiescence and cell proliferation.' *FEBS Letters*, (594) pp. 2046–2060.

Perez-Chacon, G., Zapata, J. M. and De Los Rios, C. (2014) 'Indole-3-carbinol induces cMYC and IAP-family downmodulation and promotes apoptosis of Epstein-Barr virus (EBV)-positive

but not of EBV-negative Burkitt's lymphoma cell lines.' *Pharmacological Research*, 89 pp. 46-56.

Pérez-Pérez, M.-J., Priego, E.-M., Bueno, O., Martins, M. S., Canela, M.-D. and Liekens, S. (2016) 'Blocking Blood Flow to Solid Tumors by Destabilizing Tubulin: An Approach to Targeting Tumor Growth.' *Journal of Medicinal Chemistry*, 59(19) pp. 8685-8711.

Pervan, M., Marijan, S., Markotic, A., Pilkington, L. I., Haverkate, N. A., Barker, D., Reynisson, J., Meic, L., et al. (2022) 'Novel Thieno [2,3-b]pyridine Anticancer Compound Lowers Cancer Stem Cell Fraction Inducing Shift of Lipid to Glucose Metabolism.' *International Journal of Molecular Sciences*, 23(19) p. 11457.

Petry, S. (2016) 'Mechanisms of Mitotic Spindle Assembly.' *Annual Review of Biochemistry*, 85 pp. 659-683.

Pfaffl, M. W. (2001) 'A new mathematical model for relative quantification in real-time RT–PCR.' *Nucleic Acids Research*, 29(9) pp. 2002-2007.

Pfaffl, M. W., Tichopad, A., Prgomet, C. and Neuvians, T. P. (2004) 'Determination of stable housekeeping genes, differentially regulated target genes and sample integrity BestKeeper.' *Biotechnology Letters*, 26 pp. 505-515.

Pierce, S. K. and Liu, W. (2010) 'The tipping points in the initiation of B cell signalling: how small changes make big differences.' *Nature Reviews Immunology*, 10(11) pp. 767-777.

Pierobon, D., Bosco, M. C., Blengio, F., Raggi, F., Eva, A., Filippi, M., Musso, T., Novelli, F., et al. (2013) 'Chronic hypoxia reprograms human immature dendritic cells by inducing a proinflammatory phenotype and TREM-1 expression.' *European Journal of Immunology*, 43(4) pp. 949-966.

Pira, G., Piras, G., Uras, A., Murineddu, M., Palmas, A. D., Monne, M. and Latte, G. C. (2012) 'Pattern of expression of BCL11A in hematological malignancies.' *Haematologica*, 97 p. 560.

Poehlmann, A., Habold, C., Walluscheck, D., Reissig, K., Bajbouj, K., Ullrich, O., Hartig, R., Gali-Muhtasib, H., et al. (2011) 'Cutting edge: Chk1 directs senescence and mitotic catastrophe in recovery from G(2) checkpoint arrest.' *Journal of Cellular and Molecular Medicine*, 15(7) pp. 1528-1541.

Pop, L. M., Barman, S., Shao, C., Poe, J. C., Venturi, G. M., Shelton, J. M., Pop, I. V., Gerber, D. E., et al. (2014) 'A Reevaluation of CD22 Expression in Human Lung Cancer.' *Cancer Research*, 74(1) pp. 263-271.

Potashnikova, D., Gladkikh, A. and Vorobjev, I. A. (2015) 'Selection of superior reference genes'combination for quantitative real-time PCR in B-cell lymphomas.' *Annals of Clinical and Laboratory Science*, 45(1) pp. 64-72.

Potashnikova, D., Gladkikh, A., Gretsov, E., Vorobjev, I. and Barteneva, N. (2012) 'Expression of BCR-associated signaling components in sorted B-CLL cells.' *Cytometry Part B - Clinical Cytometry*, 82B(4) pp. o1–o17.

Pozarowski, P. and Darzynkiewicz, Z. (2004) 'Analysis of Cell Cycle by Flow Cytometry.' *In* Schönthal, A. H. (ed.) *Checkpoint Controls and Cancer: Volume 2: Activation and Regulation Protocols*. Totowa, NJ: Humana Press, pp. 301-311. https://doi.org/10.1385/1-59259-811-0:301

Prica, A. and Crump, M. (2019) 'Improving CD20 antibody therapy: obinutuzumab in lymphoproliferative disorders.' *Leukemia & Lymphoma*, 60(3) pp. 573-582.

Project, T. I. N.-H. s. L. P. F. (1993) 'A Predictive Model for Aggressive Non-Hodgkin's Lymphoma.' *New England Journal of Medicine*, 329(14) pp. 987-994.

Przybyl, J., Kozak, K., Kosela, H., Falkowski, S., Switaj, T., Lugowska, I., Szumera-Cieckiewicz, A., Ptaszynski, K., et al. (2014) 'Gene expression profiling of peripheral blood cells: new insights into Ewing sarcoma biology and clinical applications.' *Medical Oncology*, 31(8) p. 109.

Puyo, S., Montaudon, D. and Pourquier, P. (2014) 'From old alkylating agents to new minor groove binders.' *Critical Reviews in Oncology/Hematology*, 89(1) pp. 43-61.

Quer, J., Cos, J., Murillo, P., Esteban, J. I., Esteban, R. and Guardia, J. (2005) 'Improved attachment of natural HCV isolate to Daudi cells upon elimination of immune complexes and close pH control.' *Intervirology*, 48(5) pp. 285-291.

Raab, C. A., Raab, M., Becker, S. and Strebhardt, K. (2021) 'Non-mitotic functions of polo-like kinases in cancer cells.' *BBA - Reviews on Cancer*, 1875(1) p. 188467.

Rao, X., Huang, X., Zhao, Z. and Lin, Z. (2013) 'An improvement of the 2ˆ(–delta delta CT) method for quantitative real-time polymerase chain reaction data analysis.pdf>.' *Biostatistics, Bioinformatics and Biomathematics*, 3(3) pp. 71-85.

Rasola, A. and Geuna, M. (2001) 'A Flow Cytometry Assay Simultaneously Detects Independent Apoptotic Parameters.' *Cytometry*, 45 pp. 151-157.

Ravelli, R. B. G., Gigant, B., Curmi, P. A., Jourdain, I., Lachkar, S., Sobel, A. and Knossow, M. (2004) 'Insight into tubulin regulation from a complex with colchicine and a stathmin-like domain.' *Nature*, 428(6979) pp. 198-202.

Reinhardt, H. C. and Yaffe, M. B. (2009) 'Kinases that control the cell cycle in response to DNA damage: Chk1, Chk2, and MK2.' *Current Opinion in Cell Biology*, 21(2) pp. 245-255.

Rene, C., Lozano, C., Eliaou, J. F. and Villalba, M. (2015) '5' and 3' untranslated regions contribute to the differential expression of specific HLA-A alleles.' *European Journal of Immunology*, 45(12) pp. 3454-3463.

Reynisson, J., Jaiswal, J. K., ., Barker, D., D'mello, S. A. N., Denny, W. A., Baguley, B. C. and Leung, E. Y. (2016) 'Evidence that phospholipase C is involved in the antitumour action of NSC768313, a new thieno[2,3-b]pyridine derivative.' *Cancer Cell International*, 16(1) p. 18.

Reynisson, J., Court, W., O'Neill, C., Day, J., Patterson, L., McDonald, E., Workman, P., Katan, M., et al. (2009) 'The identification of novel PLC-gamma inhibitors using virtual high throughput screening.' *Bioorganic & Medicinal Chemistry*, 17(8) pp. 3169-3176.

Ribeiro, B. C., Alvarez, C. A. R., Alves, B. C., Rodrigues, J. M., Queiroz, M., Almeida, B. G., Pires, A., Pereira, A. M., et al. (2022) 'Development of Thermo- and pH-Sensitive Liposomal Magnetic Carriers for New Potential Antitumor Thienopyridine Derivatives.' *Materials (Basel)*, 15(5) p. 1737.

Riedel, G., Rudrich, U., Fekete-Drimusz, N., Manns, M. P., Vondran, F. W. and Bock, M. (2014) 'An extended DeltaCT-method facilitating normalisation with multiple reference genes suited for quantitative RT-PCR analyses of human hepatocyte-like cells.' *PLoS One*, 9(3) p. e93031.

Ritz, O., Rommel, K., Dorsch, K., Kelsch, E., Melzner, J., Buck, M., Leroy, K., Papadopoulou, V., et al. (2013) 'STAT6-mediated BCL6 repression in primary mediastinal B-cell lymphoma (PMBL).' *Oncotarget*, 4(7) pp. 1093-1102.

Rizk, O. H., Teleb, M., Abu-Serie, M. M. and Shaaban, O. G. (2019) 'Dual VEGFR-2/PIM-1 kinase inhibition towards surmounting the resistance to antiangiogenic agents via hybrid pyridine and thienopyridine-based scaffolds: Design, synthesis and biological evaluation.' *Bioorganic Chemistry*, 92 p. 103189.

Rizzelli, F., Malabarba, M. G., Sigismund, S. and Mapelli, M. (2020) 'The crosstalk between microtubules, actin and membranes shapes cell division.' *Open Biology*, 10(3) p. 190314.

Roberts, A. W., Davids, M. S., Pagel, J. M., Kahl, B. S., Puvvada, S. D., Gerecitano, J. F., Kipps, T. J., Anderson, M. A., et al. (2016) 'Targeting BCL2 with Venetoclax in Relapsed Chronic Lymphocytic Leukemia.' *New England Journal of Medicine*, 374(4) pp. 311-322.

Rocci, A., Gambella, M., Aschero, S., Cavallo, F., Larocca, A., Omede, P., Drandi, D., Ladetto, M., et al. (2010a) 'High expression of mRNA and gene amplification of Met in myeloma plasma cells characterize a more aggressive disease.' *Blood*, 116(21)

Rocci, A., Gambella, M., Gay, F., Aschero, S., Magarotto, V., Gilestro, M., Boccadoro, M., Palumbo, A., et al. (2010b) 'MET mRNA value predicts outcome in multiple myeloma patients.' *Haematologica*, 95

Roisman, A., Slavutsky, I., Metrebian, F., Narbaitz, M., Kohan, D., Garcia Rivello, H., Campo, E. and Hernandez, L. (2015) 'Expression of soxc cluster and miR-17-92 polycistron in mantle cell lymphoma patients.' *Haematologica*, 100 pp. 554-555.

Romagnoli, R., Baraldi, P. G., Kimatrai Salvador, M., Preti, D., Aghazadeh Tabrizi, M., Bassetto, M., Brancale, A., Hamel, E., et al. (2013) 'Synthesis and biological evaluation of 2-(alkoxycarbonyl)-3-anilinobenzo[b]thiophenes and thieno[2,3-b]pyridines as new potent anticancer agents.' *Journal of Medicinal Chemistry*, 56(6) pp. 2606-2618.

Roos, W. P. and Kaina, B. (2013) 'DNA damage-induced cell death: from specific DNA lesions to the DNA damage response and apoptosis.' *Cancer Letters*, 332(2) pp. 237-248.

Rosenberg, J. S., Cross, F. R. and Funabiki, H. (2011) 'KNL1/Spc105 recruits PP1 to silence the spindle assembly checkpoint.' *Current Biology*, 21(11) pp. 942-947.

Routledge, D. J. M. and Bloor, A. J. C. (2016) 'Recent advances in therapy of chronic lymphocytic leukaemia.' *British Journal of Haematology*, 174(3) pp. 351-367.

Roy, J. G., McElhaney, J. E. and Verschoor, C. P. (2020) 'Reliable reference genes for the quantification of mRNA in human T-cells and PBMCs stimulated with live influenza virus.' *BMC Immunology*, 21(1) p. 4.

Rozman, C. and Montserrat, E. (1995) 'Chronic Lymphocytic Leukemia.' *New England Journal of Medicine*, 333(16) pp. 1052-1057.

Rubin, S. M., Sage, J. and Skotheim, J. M. (2020) 'Integrating Old and New Paradigms of G1/S Control.' *Molecular Cell*, 80(2) pp. 183-192.

Rudenskaya, G. E. and Zakharova, E. Y. (2017) 'Adult-onset leukoencephalopathy with vanishing white matter.' *Human Physiology*, 43(8) pp. 898–903.

Ryynänen, J., Seuter, S., Campbell, M. J. and Carlberg, C. (2013) 'Gene Regulatory Scenarios of Primary 1,25-Dihydroxyvitamin D3 Target Genes in a Human Myeloid Leukemia Cell Line.' *Cancers*, 5(4) pp. 1221-1241.

Saeedi, M., Safavi, M., Allahabadi, E., Rastegari, A., Hariri, R., Jafari, S., Bukhari, S. N. A., Mirfazli, S. S., et al. (2020) 'Thieno[2,3-b]pyridine amines: Synthesis and evaluation of tacrine analogs against biological activities related to Alzheimer's disease.' *Archiv der Pharmazie (Weinheim)*, 353(10) p. e2000101.

Saito, K., Shinozuka, T., Nakao, A., Kunikata, T., Nakai, D., Nagai, Y. and Naito, S. (2021) 'Discovery of 3-amino-4-(3S)-3-[(2-ethoxyethoxy)methyl]piperidin-1-ylthieno[2,3-b]pyridine-2-carboxamide (DS96432529): A potent and orally active bone anabolic agent.' *Bioorganic & Medicinal Chemistry Letters*, 54 p. 128440.

Saldivar, J. C., Cortez, D. and Cimprich, K. A. (2017) 'The essential kinase ATR: ensuring faithful duplication of a challenging genome.' *Nature Reviews Molecular Cell Biology*, 18(10) pp. 622-636.

Salles, G., Barrett, M., Foà, R., Maurer, J., O'Brien, S., Valente, N., Wenger, M. and Maloney, D. G. (2017) 'Rituximab in B-Cell Hematologic Malignancies: A Review of 20 Years of Clinical Experience.' *Advances in Therapy*, 34(10) pp. 2232-2273.

Sampath, D. and Plunkett, W. (2007) 'The role of DNA repair in chronic lymphocytic leukemia pathogenesis and chemotherapy resistance.' *Current Oncology Reports*, 9(5) pp. 361-367.

Sancar, A., Lindsey-Boltz, L. A., Unsal-Kacmaz, K. and Linn, S. (2004) 'Molecular mechanisms of mammalian DNA repair and the DNA damage checkpoints.' *Annual Review of Biochemistry*, 73 pp. 39-85.

Sánchez-Espiridión, B., Sánchez-Aguilera, A., Montalbán, C., Martin, C., Martinez, R., González-Carrero, J. n., Poderos, C. n., Bellas, C., et al. (2009) 'A TaqMan Low-Density Array to Predict Outcome in Advanced Hodgkin's Lymphoma Using Paraffin-Embedded Samples.' *Clinical Cancer Research*, 15(4) pp. 1367-1375.

Sanchez, A. D. and Feldman, J. L. (2017) 'Microtubule-organizing centers: from the centrosome to non-centrosomal sites.' *Current Opinion in Cell Biology*, 44 pp. 93-101.

Schmeisser, H., Mejido, J., Balinsky, C. A., Morrow, A. N., Clark, C. R., Zhao, T. and Zoon, K. C. (2010) 'Identification of alpha interferon-induced genes associated with antiviral activity in Daudi cells and characterization of IFIT3 as a novel antiviral gene.' *Journal of Virology*, 84(20) pp. 10671-10680.

Schmidt, S., Rainer, J., Ploner, C., Presul, E., Riml, S. and Kofler, R. (2004) 'Glucocorticoid-induced apoptosis and glucocorticoid resistance: molecular mechanisms and clinical relevance.' *Cell Death And Differentiation*, 11 p. S45.

Seiter, K. and Mamorska-Dyga, A. (2015) 'Obinutuzumab treatment in the elderly patient with chronic lymphocytic leukemia.' *Clinical Interventions in Aging*, 10 pp. 951-961.

Sevinc, M., Eskazan, A. E., Gulturk, E., Salihoglu, A., Aydin, S. O., Baslar, Z., Ferhanoglu, A. B., Aydin, Y., et al. (2011) 'CLLU1 gene expression level as a prognostic parameter in patients with chronic lymphocytic leukemia.' *Blood*, 118(21) p. 4603.

Seymour, J. F., Mobasher, M. and Kater, A. P. (2018) 'Venetoclax–Rituximab in Chronic Lymphocytic Leukemia.' *New England Journal of Medicine*, 378(22) pp. 2141-2144.

Shamseer, L., Moher, D., Clarke, M., Ghersi, D., Liberati, A., Petticrew, M., Shekelle, P., Stewart, L. A., et al. (2015) 'Preferred reporting items for systematic review and meta-analysis protocols (PRISMA-P) 2015: elaboration and explanation.' *BMJ*, 350 p. g7647.

Shankey, T. V., Rabinovitch, P. S., Bagwell, B., Bauer, K. D., Cox, C., Duque, R. E., Hedley, D. W., Mayall, B. H., et al. (1993) 'Guidelines for the implementation of clinical DNA cytometry.' *Breast Cancer Research and Treatment*, 28(1) pp. 61-68.

Sharman, J. P., Egyed, M., Jurczak, W., Skarbnik, A., Pagel, J. M., Flinn, I. W., Kamdar, M., Munir, T., et al. (2020) 'Acalabrutinib with or without obinutuzumab versus chlorambucil and obinutuzumab for treatment-naive chronic lymphocytic leukaemia (ELEVATE-TN): a randomised, controlled, phase 3 trial.' *The Lancet*, 395(10232) pp. 1278-1291.

Shelanski, M. L., Gaskin, F. and Cantor, C. R. (1973) 'Microtubule Assembly in the Absence of Added Nucleotides.' *Proceedings of the National Academy of Sciences of the United States of America*, 70(3) pp. 765–768.

Shlapatska, L. M., Kovalevska, L. M., Gordiienko, I. M. and Sidorenko, S. P. (2014) 'Intrinsic defect in B-lymphoblastoid cell lines from patients with X-linked lymphoproliferative disease type 1. II. Receptor-mediated Akt/PKB and ERK1/2 activation and transcription factors expression profile.' *Experimental Oncology*, 36(3) pp. 162-169.

Shoemaker, R. H. (2006) 'The NCI60 human tumour cell line anticancer drug screen.' *Nature Reviews Cancer*, 6 pp. 813–823.

Silva, P. M., Ribeiro, N., Lima, R. T., Andrade, C., Diogo, V., Teixeira, J., Florindo, C., Tavares, A., et al. (2017) 'Suppression of spindly delays mitotic exit and exacerbates cell death response of cancer cells treated with low doses of paclitaxel.' *Cancer Letters*, 394 pp. 33-42.

Singh, A., Spitzer, M. H., Joy, J. P., Kaileh, M., Qiu, X., Nolan, G. P. and Sen, R. (2022) 'Postmitotic G1 phase survivin drives mitogen-independent cell division of B lymphocytes.' *Proceedings of the National Academy of Sciences of the United States of America*, 119(18) p. e2115567119.

Singh, P. and Lim, B. (2022) 'Targeting Apoptosis in Cancer.' *Current Oncology Reports*, 24(3) pp. 273-284.

Smith, L. K. and Cidlowski, J. A. (2010) 'Chapter 1 - Glucocorticoid-Induced Apoptosis of Healthy and Malignant Lymphocytes.' *In* Martini, L. (ed.) *Progress in Brain Research*. Vol. 182. Elsevier, pp. 1-30. http://www.sciencedirect.com/science/article/pii/S0079612310820011

Smith, R. J., Cordeiro, M. H., Davey, N. E., Vallardi, G., Ciliberto, A., Gross, F. and Saurin, A. T. (2019) 'PP1 and PP2A Use Opposite Phospho-dependencies to Control Distinct Processes at the Kinetochore.' *Cell Reports*, 28(8) pp. 2206-2219 e2208.

Solal-Céligny, P., Roy, P., Colombat, P., White, J., Armitage, J. O., Arranz-Saez, R., Au, W. Y., Bellei, M., et al. (2004) 'Follicular Lymphoma International Prognostic Index.' *Blood*, 104(5) p. 1258.

Sorigue, M. and Sancho, J.-M. (2018) 'Current prognostic and predictive factors in follicular lymphoma.' *Annals of Hematology*, 97(2) pp. 209-227.

Srinivasan, L., Sasaki, Y., Calado, D. P., Zhang, B., Paik, J. H., DePinho, R. A., Kutok, J. L., Kearney, J. F., et al. (2009) 'PI3 kinase signals BCR-dependent mature B cell survival.' *Cell*, 139(3) pp. 573-586.

Staff, N. P., Grisold, A., Grisold, W. and Windebank, A. J. (2017) 'Chemotherapy-induced peripheral neuropathy: A current review.' *Annals of Neurology*, 81(6) pp. 772-781.

Steinmetz, M. O. and Prota, A. E. (2018) 'Microtubule-Targeting Agents: Strategies To Hijack the Cytoskeleton.' *Trends in Cell Biology*, 28(10) pp. 776-792.

Stewart, C. M., Michaud, L., Whiting, K., Nakajima, R., Nichols, C., De Frank, S., Hamlin, P. A., Jr, Matasar, M. J., et al. (2022) 'Phase I/Ib Study of the Efficacy and Safety of Buparlisib and Ibrutinib Therapy in MCL, FL, and DLBCL with Serial Cell-Free DNA Monitoring.' *Clinical Cancer Research*, 28(1) pp. 45-56.

Stewart, Z. A., Westfall, M. D. and Pietenpol, J. A. (2003) 'Cell-cycle dysregulation and anticancer therapy.' *Trends in Pharmacological Science*, 24(3) pp. 139-145.

Stilgenbauer, S., Eichhorst, B., Schetelig, J., Coutre, S., Seymour, J. F., Munir, T., Puvvada, S. D., Wendtner, C. M., et al. (2016) 'Venetoclax in relapsed or refractory chronic lymphocytic leukaemia with 17p deletion: a multicentre, open-label, phase 2 study.' *Lancet Oncology*, 17(6) pp. 768-778.

Suzuki, S., Tsutsumi, S., Chen, Y., Ozeki, C., Okabe, A., Kawase, T., Aburatani, H. and Ohki, R. (2020) 'Identification and characterization of the binding sequences and target genes of p53 lacking the 1st transactivation domain.' *Cancer Science*, 111(2) pp. 451-466.

Swerdlow, S. H., Campo, E., Pileri, S. A., Harris, N. L., Stein, H., Siebert, R., Advani, R., Ghielmini, M., et al. (2016) 'The 2016 revision of the World Health Organization classification of lymphoid neoplasms.' *Blood*, 127(20) pp. 2375-2390.

Syed, N., Smith, P., Sullivan, A., Spender, L. C., Dyer, M., Karran, L., O'Nions, J., Allday, M., et al. (2006) 'Transcriptional silencing of Polo-like kinase 2(SNK/PLK2)is a frequent event in B-cell malignancies.' *Blood*, 107(1) pp. 250-256.

Tacar, O., Sriamornsak, P. and Dass Crispin, R. (2012) 'Doxorubicin: an update on anticancer molecular action, toxicity and novel drug delivery systems.' *Journal of Pharmacy and Pharmacology*, 65(2) pp. 157-170.

Tajeddine, N., Gailly, P., Millard, I. and Gala, J. L. (2006) 'Real-time RT-PCR quantification of PRAME gene expression for monitoring minimal residual disease in acute myeloblastic leukaemia.' *Clinical Chemistry and Laboratory Medicine*, 44(5) pp. 548-555.

Taylor, S. C., Nadeau, K., Abbasi, M., Lachance, C., Nguyen, M. and Fenrich, J. (2019) 'The Ultimate qPCR Experiment: Producing Publication Quality, Reproducible Data the First Time.' *Trends in Biotechnology*, 37(7) pp. 761-774.

Techer, H., Koundrioukoff, S., Nicolas, A. and Debatisse, M. (2017) 'The impact of replication stress on replication dynamics and DNA damage in vertebrate cells.' *Nature Reviews Genetics*, 18(9) pp. 535-550.

Teicher, B. A. (2008) 'Newer Cytotoxic Agents: Attacking Cancer Broadly.' *Clinical Cancer Research*, 14(6) pp. 1610-1617.

Thomas, M. R., Outteridge, S. N., Ajjan, R. A., Phoenix, F., Sangha, G. K., Faulkner, R. E., Ecob, R., Judge, H. M., et al. (2015) 'Platelet P2Y12 Inhibitors Reduce Systemic Inflammation and Its Prothrombotic Effects in an Experimental Human Model.' *Arteriosclerosis, Thrombosis, and Vascular Biology*, 35(12) pp. 2562-2570.

Tilly, H., Gomes da Silva, M., Vitolo, U., Jack, A., Meignan, M., Lopez-Guillermo, A., Walewski, J., André, M., et al. (2015) 'Diffuse large B-cell lymphoma (DLBCL): ESMO Clinical Practice Guidelines for diagnosis, treatment and follow-up†.' *Annals of Oncology*, 26(suppl_5) pp. v116-v125.

Torrance, H. D. T., Longbottom, E. R., Vivian, M. E., Lalabekyan, B., Abbott, T. E. F., Ackland, G. L., Hinds, C. J., Pearse, R. M., et al. (2018) 'Post-operative immune suppression is mediated via reversible, Interleukin-10 dependent pathways in circulating monocytes following major abdominal surgery.' *PLOS ONE*, 13(9) p. e0203795.

Torun, E. S., Aday, A. and Nalcaci, M. (2021) 'Activation Induced Cytidine Deaminase Expression in Patients with Myelodysplastic Syndrome and its Relationship with Prognosis and Treatment.' *Turkish Journal of Medical Sciences*, 51(4) pp. 2451-2460.

Urrutia, A., Duffy, D., Rouilly, V., Posseme, C., Djebali, R., Illanes, G., Libri, V., Albaud, B., et al. (2016) 'Standardized Whole-Blood Transcriptional Profiling Enables the Deconvolution of Complex Induced Immune Responses.' *Cell Reports*, 16(10) pp. 2777-2791.

Usarek, E., Barańczyk-Kuźma, A., Kaźmierczak, B., Gajewska, B. and Kuźma-Kozakiewicz, M. (2017) 'Validation of qPCR reference genes in lymphocytes from patients with amyotrophic lateral sclerosis.' *PLOS ONE*, 12(3) p. e0174317.

Valceckiene, V., Kontenyte, R., Jakubauskas, A. and Griskevicius, L. (2010) 'Selection of reference genes for quantitative polymerase chain reaction studies in purified B cells from B cell chronic lymphocytic leukaemia patients.' *British Journal of Haematology*, 151(3) pp. 232-238.

van Engeland, M., Ramaekers, F. C. S., Shutte, B. and Reutelingsperger, C. P. M. (1996) 'A novel assay to measure loss of plasma membrane asymmetry during apoptosis of adherant cells in culture.' *Cytometry*, 24 pp. 131-139.

van Rensburg, M., Leung, E., Haverkate, N. A., Eurtivong, C., Pilkington, L. I., Reynisson, J. and Barker, D. (2017) 'Synthesis and antiproliferative activity of 2-chlorophenyl carboxamide thienopyridines.' *Bioorganic & Medicinal Chemistry Letters*, 27(2) pp. 135-138.

Vandesompele, J., De Preter, K., Pattyn, F., Poppe, B., Van Roy, N., De Paepe, A. and Speleman, F. (2002) 'Accurate normalization of real-time quantitative RT-PCR data by geometric averaging of multiple internal control genes.' *Genome Biology*, 3(7) pp. research0034.0031–0034.0011.

Vasquez, R. J., Howell, B., Yvon, A. M., Wadsworth, P. and Cassimeris, L. (1997) 'Nanomolar concentrations of nocodazole alter microtubule dynamic instability in vivo and in vitro.' *Molecular Biology of the Cell*, 8 pp. 973 - 985.

Velasco-González, R. and Coffeen, U. (2022) 'Neurophysiopathological Aspects of Paclitaxel-induced Peripheral Neuropathy.' *Neurotoxicity Research*, 40(6) pp. 1673-1689.

Vermes, I., Haanen, C., Steffens-Nakken, H. and Reutellingsperger, C. (1995) 'A novel assay for apoptosis Flow cytometric detection of phosphatidylserine expression on early apoptotic cells using fluorescein labelled Annexin V.' *Journal of Immunological Methods*, 184(1) pp. 39-51.

Vilpo, J. A., Koski, T. and Vilpo, L. M. (2000) 'Selective toxicity of vincristine against chronic lymphocytic leukemia cells in vitro.' *European Journal of Haematology*, 65(6) pp. 370-378.

Vivanco, I. and Sawyers, C. L. (2002) 'The phosphatidylinositol 3-Kinase AKT pathway in human cancer.' *Nature Reviews Cancer*, 2(7) pp. 489-501.

Vukić, M., Neme, A., Seuter, S., Saksa, N., de Mello, V. D. F., Nurmi, T., Uusitupa, M., Tuomainen, T.-P., et al. (2015) 'Relevance of Vitamin D Receptor Target Genes for Monitoring the Vitamin D Responsiveness of Primary Human Cells.' *PLOS ONE*, 10(4) p. e0124339.

Walewska, R., Parry-Jones, N., Eyre, T. A., Follows, G., Martinez-Calle, N., McCarthy, H., Parry, H., Patten, P. E. M., et al. (2022) 'Guideline for the treatment of chronic lymphocytic leukaemia.' *British Journal of Haematology*, 197(5) pp. 544-557.

Wang, G., Liu, W., Gong, Z., Huang, Y., Li, Y. and Peng, Z. (2020) 'Design, synthesis, biological evaluation and molecular docking studies of new chalcone derivatives containing diaryl ether moiety as potential anticancer agents and tubulin polymerization inhibitors.' *Bioorganic Chemistry*, 95 p. 103565.

Wang, G., Liu, W., Fan, M., He, M., Li, Y. and Peng, Z. (2021) 'Design, synthesis and biological evaluation of novel thiazole-naphthalene derivatives as potential anticancer agents and tubulin polymerisation inhibitors.' *Journal of Enzyme Inhibition and Medicinal Chemistry*, 36(1) pp. 1694-1702.

Wang, J., Luo, C., Shan, C., You, Q., Lu, J., Elf, S., Zhou, Y., Wen, Y., et al. (2015) 'Inhibition of human copper trafficking by a small molecule significantly attenuates cancer cell proliferation.' *Nature Chemistry*, 7(12) pp. 968-979.

Wang, P. and Heitman, J. (2005) 'The cyclophilins.' *Genome Biology*, 6(7) p. 226.

Wang, Y., Zhang, H., Gigant, B., Yu, Y., Wu, Y. L., Chen, X., Lai, Q., Yang, Z., et al. (2016) 'Structures of a diverse set of colchicine binding site inhibitors in complex with tubulin provide a rationale for drug discovery.' *The FEBS Journal*, 283(1) pp. 102-111.

Wang, Y. L., Zhao, W. W., Bai, S. M., Ma, Y., Yin, X. K., Feng, L. L., Zeng, G. D., Wang, F., et al. (2022) 'DNA damage-induced paraspeckle formation enhances DNA repair and tumor radioresistance by recruiting ribosomal protein P0.' *Cell Death and Disease*, 13(8) p. 709.

Watanabe, S., Iga, J., Nishi, A., Numata, S., Kinoshita, M., Kikuchi, K., Nakataki, M. and Ohmori, T. (2014) 'Microarray analysis of global gene expression in leukocytes following lithium treatment.' *Human Psychopharmacology: Clinical and Experimental*, 29(2) pp. 190-198.

Weaver, B. A. (2014) 'How Taxol/paclitaxel kills cancer cells.' *Molecular Biology of the Cell*, 25(18) pp. 2677-2681.

Wheeler, M. L., Dong, M. B., Brink, R., Zhong, X.-P. and De Franco, A. L. (2013) 'DGK limited B cell antigen receptor-dependend activation of ERK signalling to inhibit early antibody responses.' *Science Signaling*, 6(297) p. ra91.

Wolach, O., Rabizadeh, E., Raanani, P., Shpilberg, O., Lederfein, D., Binkovski, N. and Inbal, A. (2012) 'Increased activity of prothrombinase FGL-2 in peripheral blood mononuclear cells of patients with B-cell lymphoma.' *Blood*, 120(21) p. 2665.

Woyach, J. A., Furman, R. R., Liu, T. M., Ozer, H. G., Zapatka, M., Ruppert, A. S., Xue, L., Li, D. H., et al. (2014) 'Resistance mechanisms for the Bruton's tyrosine kinase inhibitor ibrutinib.' *New England Journal of Medicine*, 370(24) pp. 2286-2294.

Wu, F., Sun, Y., Chen, J., Li, H., Yao, K., Liu, Y., Liu, Q. and Lu, J. (2021) 'The Oncogenic Role of APC/C Activator Protein Cdc20 by an Integrated Pan-Cancer Analysis in Human Tumors.' *Frontiers in Oncology*, 11 p. 721797.

Wu, H., Jing, S., Wang, Z., Xi, J., Yan, C., Song, J., Wang, L., Zhao, C., et al. (2020) 'Therapeutic and Immunoregulatory Effects of Tacrolimus in Patients with Refractory Generalized Myasthenia Gravis.' *European Neurology*, 83(5) pp. 500-507.

Wu, R. Y., Chiang, H., Hu, G. L., Zeng, Q. L. and Bao, J. L. (2000) 'The effect of 50 Hz magnetic field on GCSmRNA expression in lymphoma B cell by mRNA differential display.' *Journal of Cellular Biochemistry*, 79(3) pp. 460-470.

Yan, W. H., Jiang, X. N., Wang, W. G., Zhou, X. Y., Li, X. Q., Cao, J. N., Hong, X. N., Sun, Y. F., et al. (2020) 'Cell-of-Origin Subtyping of Diffuse Large B-Cell Lymphoma by Using a qPCR-based Gene Expression Assay on Formalin-Fixed Paraffin-Embedded Tissues.' *Frontiers in Oncology*, 10 p. 803.

Yan, Y., Gao, Y.-Y., Liu, B.-Q., Niu, X.-F., Zhuang, Y. and Wang, H.-Q. (2010) 'Resveratrol-induced cytotoxicity in human Burkitt's lymphoma cells is coupled to the unfolded protein response.' *BMC Cancer*, 10 p. 445.

Yang, E. V., Webster Marketon, J. I., Chen, M., Kim, S. J., Glaser, R. and Lo, K. W. (2010) 'Glucocorticoids activate Epstein Barr virus lytic replication through the upregulation of immediate early BZLF1 gene expression.' *Brain, Behavior, and Immunity*, 24(7) pp. 1089-1096.

Yang, J., Nie, J., Ma, X., Wei, Y., Peng, Y. and Wei, X. (2019) 'Targeting PI3K in cancer: mechanisms and advances in clinical trials.' *Molecular Cancer*, 18(1) p. 26.

Ye, J., Coulouris, G., Zaretskaya, I., Cutcutache, I., Rozen, S. and Madden, T. L. (2012) 'Primer-BLAST a tool to design target-specific primers for PCR.' *BMC Bioinformatics*, 13(134) p. 134.

Yousefi, Z., Sharifzadeh, S., Yar-Ahmadi, V., Andalib, A. and Eskandari, N. (2019) 'Fc Receptor-Like 1 as a Promising Target for Immunotherapeutic Interventions of B-Cell-Related Disorders.' *Biomarker Insights*, 14 pp. 1-19.

Yu, M., Chen, Y., Zeng, H., Zheng, Y., Fu, G., Zhu, W., Broeckel, U., Aggarwal, P., et al. (2017) 'PLCgamma-dependent mTOR signalling controls IL-7-mediated early B cell development.' *Nature Communications*, 8(1) p. 1457.

Yu, Y., Rabinowitz, R., Schlesinger, M., Polliack, A. and Ben-Bassat, H. (2000) 'B-lymphocytes in CLL and NHL differ in the mRNA splicing pattern of the CD45 molecule.' *European Journal of Haematology*, 64(6) pp. 376-384.

Zaki, Y. H., El-Gendey, M. S., Fouad, S. A., Mohamed, H. S. and Amer, H. H. (2022) 'Utility of Pyrimidine Thione Derivatives in the Synthesis of Biologically Active Heterocyclic Compounds.' *Polycyclic Aromatic Compounds*, pp. 1-26.

Zavridou, M., Strati, A. and Lianidou, E. (2018) 'Evaluation of pre-analytical conditions for gene expression studies in CTCs.' *Clinical and Experimental Metastasis*, 35(3) pp. 211-212.

Zhang, F. F. and Li, J. (2015) 'Inhibitory effect of chloroquine derivatives on presenilin 1 and ubiquilin 1 expression in Alzheimer's disease.' *International Journal of Clinical and Experimental Pathology*, 8(6) pp. 7640-7643.

Zhang, R., Zhu, H., Yuan, Y., Wang, Y. and Tian, Z. (2020) 'SPAG6 promotes cell proliferation and inhibits apoptosis through the PTEN/PI3K/AKT pathway in Burkitt lymphoma.' *Oncology Reports*, 44(5) pp. 2021-2030.

Zhang, X., Yang, W., Wang, X., Zhang, X., Tian, H., Deng, H., Zhang, L. and Gao, G. (2018) 'Identification of new type I interferon-stimulated genes and investigation of their involvement in IFN-β activation.' *Protein & Cell*, 9(9) pp. 799-807.

Zhao, Y., Li, M., Li, B., Zhang, S., Su, A., Xing, Y., Ge, Z., Li, R., et al. (2019) 'Discovery and optimization of thienopyridine derivatives as novel urea transporter inhibitors.' *European Journal of Medicinal Chemistry*, 172 pp. 131-142.

Zhong, Y., Arnoldo, A., Kowalski, P. E., Somers, G. R., Hawkins, C., Beimnet, K., Alli, Z. and Abdelhaleem, M. (2020) 'Multiplexed Digital Detection of B-Cell Acute Lymphoblastic Leukemia Fusion Transcripts Using the NanoString nCounter System.' *Journal of Molecular Diagnostics*, 22(1) pp. 72-80.

Zhou, X., Liu, J., Meng, J., Fu, Y., Wu, Z., Ouyang, G. and Wang, Z. (2021) 'Discovery of facile amides-functionalized rhodanine-3-acetic acid derivatives as potential anticancer agents by disrupting microtubule dynamics.' *Journal of Enzyme Inhibition and Medicinal Chemistry*, 36(1) pp. 1996-2009.

Zhou, X., Fu, Y. H., Zou, Y. Y., Meng, J., Ou-Yang, G. P., Ge, Q. S. and Wang, Z. C. (2022) 'Discovery of Simple Diacylhydrazine-Functionalized Cinnamic Acid Derivatives as Potential Microtubule Stabilizers.' *International Journal of Molecular Sciences*, 23(20) p. 12365.

Zieve, G. W., Turnbull, D., Mullins, J. M. and McIntosh, J. R. (1980) 'Production of large numbers of mitotic mammalian cells by use of the reversible microtubule inhibitor Nocodazole Nocodazole accumulated mitotic cells.' *Experimental Cell Research*, 126(2) pp. 397–405.